

**Alma Mater Studiorum – Università di Bologna**

**DOTTORATO DI RICERCA IN**

**Meccanica e Scienze Avanzate dell'Ingegneria**

**Ciclo XXXI**

**Settore Concorsuale: 09-C1**

**Settore Scientifico Disciplinare: ING-IND/08**

**Powertrain Architectures and Technologies  
for New Emission and Fuel Consumption Standards**

**Presentata da: Ing. Matteo De Cesare**

**Coordinatore Dottorato**

**Prof. Ing. Marco Carricato**

**Supervisore**

**Prof. Ing. Nicolò Cavina**

**Esame finale anno 2019**



# Preface

The realization of my research activity was made possible by the contribution of many people who I'd wish to thank.

First, I'm very thankful to Prof. Ing. Nicolò Cavina, who has encouraged me to start my PhD study and supported me during the years.

Great acknowledges go, also, to Prof. Fabrizio Ponti, Prof. Vittorio Ravaglioli, Prof. Enrico Corti and Prof. Davide Moro for the helpful cooperation in these years.

My gratitude also goes to all PhD colleagues, who have cooperated in some research activities.

Then I would like to thank Magneti Marelli, which has been the sponsor of this activity, and my colleagues, who have given their precious contribution to some research activities.

Finally, I would like to thank all my family, and in particular my wife Paola and my daughters Francesca and Chiara for their great support, understanding and patience in these years.

# Contents

Preface .....	2
Abstract .....	8
List of Publications .....	11
Abbreviations - Nomenclature .....	13
1. Introduction .....	16
1.1 Motivations .....	16
1.2 Research Objectives .....	17
1.3 Thesis Structure Overview .....	18
2. Factors Affecting Powertrain Evolution .....	20
2.1 Environmental Sustainability: Greenhouse Gas and Pollutant Regulations .....	22
2.1.1 CO <sub>2</sub> and Fuel Consumption Regulations .....	22
2.1.2 CO <sub>2</sub> and Fuel Consumption Regulation Issues .....	24
2.1.3 Pollutant Regulations .....	31
2.2 Car Buyers Needs/Wants .....	34
2.3 Smart, Connected and Autonomous Vehicles .....	36
2.4 The Power Generation Scenario .....	38
3. Description of Applied Methodology .....	41
3.1 Methodology Steps .....	43
3.2 Methods and Tools .....	44
3.2.1 Powertrain Quality Function Deployment and Requirement Management .....	44
3.2.2 Simulation in the Concept Process .....	45
3.2.3 Powertrain Architecture and Technology Evaluation .....	46
4. Powertrain Requirement Analysis and Basic Design .....	49
4.1 Deployment of Vehicle and Powertrain Requirements .....	50
4.2 Introduction to Hybrid Powertrain Architectures .....	53
4.3 Functions of Electric Hybrid Vehicles .....	54
4.4 Deployment of Powertrain Requirements .....	58



4.5	Evaluation of Powertrain Specifications to match Vehicle Requirements .....	59
4.5.1	Powertrain Features for Maximum Vehicle Speed.....	61
4.5.2	Energy Storage Capacity for Vehicle Autonomy .....	61
4.5.3	Vehicle and Powertrain Weight Evaluation .....	62
4.5.4	Powertrain Features to fulfill Vehicle Take-off Requirements .....	63
4.5.5	Powertrain Performances for Vehicle Acceleration Requirements .....	63
4.5.6	Powertrain Features to Recover Vehicle Kinetic Energy .....	63
4.5.7	Power and Torque Specifications for ICE and ETD Driveline .....	64
4.5.8	Transmission Specifications .....	65
4.5.9	Powertrain Features for Fuel Consumption and CO <sub>2</sub> Requirements .....	66
4.5.10	Powertrain Features for Pollutant Requirements .....	70
5.	Powertrain Architecture Options .....	71
5.1	Powertrain Architecture Classification and Energy Pathways .....	71
5.2	Electric Hybrid Powertrains Topologies and Classifications .....	73
5.3	Architecture Prioritization .....	79
6.	Technologies of ICE Based Powertrains .....	80
6.1	The state of arts of SI-ICEs .....	80
6.2	ICE Technologies Options to Improve Efficiency and Pollutions .....	81
6.3	New Technologies for GDI engine with stoichiometric combustion .....	82
6.4	Advanced Combustion Concepts .....	94
6.4.1	GDI Lean Combustion .....	94
6.4.2	Low Temperature Combustion Concepts .....	95
6.4.3	Premixed (PCCI) and Partially Premixed Compression Ignition (PPCI) Combustions .....	98
6.4.4	Spark Assisted HCCI Combustion .....	104
6.4.5	Reactivity Controlled Compression Ignition (RCCI) Combustion .....	106
6.4.6	Summary of Advanced Combustions Benefits and Drawbacks for ICE.....	109
6.5	Exhaust Gas After-treatment Technologies.....	109
6.6	Engine Technology Cost Analysis .....	113
6.7	Prioritization of Engine Air and Combustion Technologies .....	113
6.8	Focus on Water Injection Effects on Combustion of GDI TC Engine .....	116

6.9	Engine Waste Heat Recovery Systems.....	128
6.9.1	Engine Heat Recovery Technology Options .....	129
6.9.2	Other WHR Systems .....	134
6.9.3	WHR System Comparison and Prioritization.....	135
6.9.4	Focus on Rankine Cycle Systems.....	137
6.10	Transmission Technologies .....	144
7.	The Vehicle Electric Power Nets .....	146
7.1	Vehicle Voltage Architecture definition .....	148
7.2	The 48V Power Systems .....	149
8.	Technologies for Electric Propulsion .....	151
8.1	Electric Propulsion System Architecture.....	151
8.2	Electric Traction Drive Components.....	153
8.2.1	Electric Motors .....	153
8.2.2	Power Electronics.....	158
8.2.3	High Voltage vs. Low Voltage Electric Traction Drive Systems.....	159
8.3	Electric Energy Storage Devices .....	161
9.	Fuel Evolution: the Synthetic Fuels .....	169
9.1	Fuel Prioritization in transport sector: the e-Fuels .....	172
9.2	Production cycle of synthetic fuels: Power-to-Liquids .....	173
9.3	Technical and economic aspects of e-Fuels .....	175
9.4	Environmental benefits of PtL with renewable resources .....	176
10.	Models for Design and Technical-Economic Evaluations .....	178
10.1	Vehicle/Powertrain Simulator Structure.....	179
10.2	Vehicle and Powertrain Quasi-Static and Dynamic Models .....	180
10.3	Models of Vehicle Sub-systems .....	183
10.3.1	Driver.....	183
10.3.2	Longitudinal Vehicle Model.....	183
10.4	Models of Powertrain Sub-systems .....	185
10.4.1	Gearbox .....	185
10.4.2	Electric Axle.....	187

10.4.3	Torque/Power Split.....	187
10.4.4	Clutches .....	188
10.4.5	Internal Combustion Engine Model .....	189
10.4.6	Engine In-cylinder model - Willans Line Method.....	190
10.4.7	Electric Traction Drive Model.....	196
10.4.8	Battery Model.....	197
10.5	Vehicle and Powertrain Thermal Model .....	199
10.5.1	Temperature Model of Generic Component/Sub-system .....	200
10.5.2	Thermal Model of Vehicle Cabin.....	200
10.5.3	Engine Compartment Temperature .....	203
10.5.4	Engine Coolant Temperature.....	203
10.5.5	Gearbox Oil Temperature.....	206
10.5.6	Three Way Catalyst Temperature.....	206
10.6	Vehicle and Powertrain Model Validation .....	208
10.7	Modeling of Waste Heat Recovery Technologies .....	212
10.7.1	Rankine Cycle Modeling.....	212
10.8	Total Cost of Ownership Model.....	219
10.9	Lifecycle Cost Model for Hybrid Vehicle Architectures .....	222
11.	Powertrain Management and Controls .....	226
11.1	Gear-shift Model Based Strategy .....	226
11.2	Electric Hybrid Powertrain Energy Management .....	228
11.2.1	Model Based Energy Management .....	231
11.3	Powertrain Control based on Acoustic Sensing .....	233
11.3.1	Features of Acoustic Sensing System.....	233
11.3.2	Boost Pressure Control with support of Turbocharger Speed Sensing (Case Study).....	234
11.3.3	Knock Control of GDI Turbocharged Engine (Case Study) .....	251
11.4	Virtual Sensor of Combustion Indexes (Case Study).....	262
11.4.1	Indicated Torque and CA50 Evaluation via Crank-Shaft Speed Signal.....	266
11.4.2	SOC, ROHR Position and CA50 Evaluation via Accelerometer .....	274
11.4.3	Combustion Noise Control via Acoustic Emission Real-Time processing.....	279

11.5	Advanced Combustion Control: the case of RCCI.....	283
12.	Powertrain Architecture Definition and Selection.....	291
12.1	Conceptual Design and Analytic Assessment of E-Hybrid Powertrains towards 2025 regulations (Case Study) .....	291
12.2	Vehicle WTW and LCA Analysis towards post 2025 regulations (Case Study) .....	314
13.	Summary & Outlook .....	321
	References .....	327
	List of Figures .....	346
	List of Tables.....	358

# Abstract

Future emission regulations represent a great challenge for the automotive industry, however the definition of powertrain solutions has to take into account at the same time cost constraints and the end-user's requirements. The powertrain design is even more challenging because the legislations are focusing on real use of the vehicles. For these reasons new homologation procedures have been defined or are under evaluation in all main world countries.

To fulfill the requirements coming from the end-users and legislations, several powertrain architectures and engine technologies are possible, such as Spark Ignition (SI) or Compression Ignition (CI) engines, with many new technologies, new fuels, and different degree of electrification.

The definition of the more promising powertrain architectures, with proper technology mix, and the assessment of benefits and costs must be accurately evaluated by means of objective procedures and tools in order to choose among the best alternatives.

Moreover, the impacts on Greenhouse Gas (GHG) or energy consumption should be evaluated in term of powertrain Well-to-Wheel or Life Cycle and not only evaluating the Tank-to-Wheel, as many regulations are considering.

The original contributions of this study have been:

- the definition of a structured methodology to link constraints and end-user's requirements to powertrain technical features, in order to perform a conceptual basic design and an objective comparison of architectures and technologies;
- the development of a conceptual design procedure for the powertrain architectures, with a proper technology mix, with the aim of reducing the analysis to the more promising solutions;
- the analytic comparison of the defined powertrain architectures and technologies, considering their effectiveness vs. regulations and end-user requirements, the technological maturity and the impact on production costs;
- the analysis and investigations of the powertrain key technologies (e.g. Water Injection, Low Temperature Combustions, etc.);
- the definition of the possible powertrain technology pathways towards 2025 and a forecast for post-2025 timeframe.

The methodology adopted for the conceptual design, the analysis and the comparison of the main powertrain architectures and technologies is according to a System Engineering approach, based on the listed tools and methodologies:

- a modified QFD approach for the deployment of technical requirements;
- the deep technical literature analysis and experimental tests of the key technologies;
- vehicle and powertrain modelling, with different level of detail to support design and analysis;
- the technology cost analysis;
- the methodologies for technology selection and prioritization.

The basic powertrain areas to be improved are:

- the Internal Combustion Engine, with particular focus on combustion and heat recovery technologies and their controls;
- the reduction of fossil carbon contents in the fuel, with synthetic fuels produced by means of renewable energy and CO<sub>2</sub>;
- the powertrain electrification, with several architectures.

For each technology areas the priority solutions have been identified.

Focusing on ICE evolution, some of the key technologies to face the engine limits are: Water Injection (WI) during the combustion, Low Temperature Combustions (LTCs) and Waste Heat Recovery Systems (WHRS).

Water injection is a cost-effective solution to minimize knocking in turbocharged downsized gasoline engines, allowing at same time higher compression ratio. Furthermore the  $\lambda=1$  engine operation at high power is allowed, matching the new requirements of EU7 legislation, starting from 2023. This technology has been investigated in simulation and by means of experimental tests on a 1.4L TGD engine, confirming its potential.

The Low Temperature Combustion concepts are way to combine benefits of CI and SI engines, such as high efficiency and performance with easy pollution management, overcoming the limits of conventional engines. Different approaches are possible (e.g. PCCI, RCCI, GCI, etc.), but the main principle is to obtain a controlled homogeneous or partially homogeneous ignition of the air-fuel mixture, characterized by low local temperature and oxygen excess, that leads to high efficiency, low NO<sub>x</sub> and Soot generation. The main issue is the combustion instability, which can be overcome with a proper design of combustion, air and fuel systems, and by means of the closed loop control of the combustion process.

In this study the focus was on the approaches PCCI (Premixed Combustion Compression Ignition) and RCCI (Reactivity Controlled Compression Ignition), applying these concepts to a 1.3L diesel engines, equipped with an additional multi-point gasoline injection system, with the aim to develop an effective and affordable control system demonstrator.

The engine management was performed by means of an RCP system, that has allowed the development of an innovative combustion control, based on virtual sensors, and the investigation of key aspects of these innovative combustion modes. The control scheme is under study to manage the engine in Gasoline Compression Ignition (GCI) operation and it will be the object of future presentations.

The Waste Heat Recovery technologies have the aim of harvesting the engine waste energy. Packaging and costs are the limits to be overcome. Taking into account the technology maturity, the amount of recoverable energy, that increases the benefit/cost ratio (gCO<sub>2</sub>/€), the Rankine Cycle systems are the most promising. The evaluations for this technology have been performed by means of simulation models, investigating the achievable benefits in term of fuel consumption/CO<sub>2</sub> in different driving cycles, which can be representative of the real conditions.

For the effectiveness of the aforementioned technologies the proper control is fundamental. In some cases the state variables of the systems are not measurable, for cost and/or reliability of the sensors. This is the case of angular positioning of combustion for Low Temperature Combustions and engines adopting Water Injection. The use of virtual sensors based on grey-box models and sensors already present in the engine management system is an effective solution as confirmed in this study. However a novel multifunction sensor has been developed. It is based on acoustic sensing and allows to implement at affordable cost the

measurements of classic engine parameters (such as knock intensity and turbocharger speed) and new parameters (e.g. CN noise), for control and diagnosis purpose.

The cost and packaging issues of the electric drives and the electric energy storage systems are the main concerns to be overcome in order to allow a large application of electric propulsion systems. Among the technologies under development the Low Voltage (48V) propulsion systems are very promising solutions with good trade-off between benefits and costs, allowing the implementation of real “electric full hybrid” vehicle. The application of these low voltage systems at affordable cost is also favored by the power net evolution towards higher voltage than the current 12V, due to increase of electric devices on board the vehicle.

An important pathway towards clean powertrain is the fuel de-fossilization, especially in a long term scenario beyond 2030. Among the alternatives to fossil fuels, together with the renewable electricity, the so called e-Fuels are very promising options. By means of a process named “Power-to-Liquids” synthetic fuels can be produced from water, electric energy and CO<sub>2</sub>.

Using renewable electric energy and CO<sub>2</sub> extracted from the air the e-Fuels can significantly decrease the WTW CO<sub>2</sub> footprint of ICE based vehicles, taking into account a long term period, when the electric energy production is expected mainly from renewable sources, such as sun and wind. In this electric power generation scenario, the synthetic fuels are also promising options for large storage and simple local distribution of the energy, mitigating the discontinuity of the renewable sources. At the same time synthetic fuels can reduce up to four times the pollution production [PM/NO<sub>x</sub>] during the combustion process, decreasing the gap vs. pure electric propulsion. The main advantages compared with BioFuels are the negligible water demand and land use. The cost is the main challenge, but recent study forecast a price little higher than fossil fuel, considering future production technology improvements.

Finally, as case study, the concept methodology has been applied to define the powertrain architectures and the technology paths for a C-class vehicle and a SUV, which cover a large range of vehicle market. To fulfill customer requirements and future European legislations for the emissions, without any performance penalty, the following technologies mix can be implemented (in case of C-Segment Vehicle):

- the 2020 regulations (95 g/km CO<sub>2</sub> and EU6d final) can be fulfilled with a low grade of electrification, employing technologies to improve the ICE combustion and the gearbox automatization;
- for the 2025 legislations (82 g/km CO<sub>2</sub> and EU7) an higher electrification degree is needed, but low voltage (48V) traction systems can be a valid solutions to mitigate the cost increase;
- up to 2030 (61 g/km CO<sub>2</sub>), together with an higher electrification grade, vehicle weight reduction and further ICE improvements are needed, with the use of de-carbonized fuels (e.g. blend with bio-fuels or synthetic fuels over 20% ).

In a long term scenario, considering the WTW CO<sub>2</sub> footprint and pollutants towards zero, the adoption of de-fossilized fuel cannot be avoided. The BEVs are not the only solution, valid alternative can be HEVs, PHEVs and RE-EVs propelled with e-Fuels.

# List of Publications

1. Ponti, F., Ravaglioli, V., Stola, F., and De Cesare, M., "**Engine Acoustic Emission Used as a Control Input: Applications to Diesel Engines**", SAE Technical Paper 2016-01-0613, 2016, <https://doi.org/10.4271/2016-01-0613>.
2. Arsie, I., Cricchio, A., Pianese, C., Ricciardi, V., De Cesare, M., "**Modeling and Optimization of Organic Rankine Cycle for Waste Heat Recovery in Automotive Engines**", SAE Technical Paper 2016-01-0207, 2016, <https://doi.org/10.4271/2016-01-0207>.
3. Poggiani C., Cimarello A., Battistoni M., Grimaldi C., Dal Re M. A., De Cesare M., "**Optical Investigations on a Multiple Spark Ignition System for Lean Engine Operation**", SAE Technical Paper 2016-01-0711, 2016, <https://doi.org/10.4271/2016-01-0711>.
4. Cavina N., Businaro A., Rojo N., De Cesare M., Paiano L., "**Combustion and Intake/Exhaust Systems Diagnosis Based on Acoustic Emissions of a GDI TC Engine**", 71st Conference of the Italian Thermal Machines Engineering Association, ATI2016, 14-16 September 2016, Turin, Italy.
5. Ponti F., Ravaglioli V., De Cesare M., "**Real-time Processing of Engine Acoustic Emission for Diesel Injectors Diagnostic and Recentering**", ICEF2016-9470, Proceedings of the ASME 2016 Internal Combustion Fall Technical Conference.
6. Cavina, N., Businaro, A., De Cesare, M., Monti, F. et al., "**Application of Acoustic and Vibration-Based Knock Detection Techniques to a High Speed Engine**", SAE Technical Paper 2017-01-0786, 2017, <https://doi.org/10.4271/2017-01-0786>.
7. Cavina, N., Businaro, A., De Cesare, M., and Paiano, L., "**Knock Control Based on Engine Acoustic Emissions: Calibration and Implementation in an Engine Control Unit**", SAE Technical Paper 2017-01-0785, 2017, <https://doi.org/10.4271/2017-01-0785>.
8. Cavina, N., Ranuzzi, F., De Cesare, M., and Brugnioni, E., "**Individual Cylinder Air-Fuel Ratio Control for Engines with Unevenly Spaced Firing Order**", SAE Int. J. Engines 10(2):614-624, 2017, <https://doi.org/10.4271/2017-01-0610>.
9. De Cesare, M., Cavina, N., and Paiano, L., "**Technology Comparison for Spark Ignition Engines of New Generation**", SAE Int. J. Engines 10(5):2513-2534, 2017, <https://doi.org/10.4271/2017-24-0151>.
10. Cavina, N., Rojo, N., Businaro, A., Brusa, A., Corti, E., De Cesare, M., "**Investigation of Water Injection Effects on Combustion Characteristics of a GDI TC Engine**", SAE Int. J. Engines 10(4):2209-2218, 2017, <https://doi.org/10.4271/2017-24-0052>.
11. Battistoni, M., Grimaldi, C., Cruccolini, V., Discepoli, G., De Cesare, M., "**Assessment of Port Water Injection Strategies to Control Knock in a GDI Engine through Multi-Cycle CFD Simulations**", SAE Technical Paper 2017-24-0034, 2017, <https://doi.org/10.4271/2017-24-0034>.
12. Ravaglioli, V., Ponti, F., De Cesare, M., Stola, F. et al., "**Combustion Indexes for Innovative Combustion Control**", SAE Int. J. Engines 10(5):2371-2381, 2017, <https://doi.org/10.4271/2017-24-0079>.
13. De Cesare, M., "**Technology Overview for future Powertrains**", Keynote Speech, Automotive-International Conference of Electrical and Electronic Technologies for Automotive, 16 June 2017, Torino.



14. De Cesare, M., Covassin, F., Brugnoli, E., and Paiano, L., "**Boost Pressure Control in Transient Engine Load with Turbocharger Speed Sensing**", SAE Technical Paper 2017-24-0049, 2017, <https://doi.org/10.4271/2017-24-0049>.
15. I Ravaglioli, V., Stola, F., De Cesare, M., Ponti, F. et al., "**Injection Pattern Design for Real Time Control of Diesel Engine Acoustic Emission**", *SAE Int. J. Commer. Veh.* 10(1):308-316, 2017, <https://doi.org/10.4271/2017-01-0596>.
16. Ravaglioli, V., Carra, F., Moro, D., De Cesare, M. et al., "**Remote Sensing Methodology for the Closed-Loop Control of RCCI Dual Fuel Combustion**", SAE Technical Paper 2018-01-0253, 2018, <https://doi.org/10.4271/2018-01-0253>.
17. De Cesare M., "**Prospettive future del powertrain automobilistico**", Giornata di Studio "Giorgio Minelli" sui Motori a Combustione Interna, Bologna, 20-04-2018.
18. Zembi, M. Battistoni, F. Ranuzzi, N. Cavina and M. De Cesare "**CFD Simulations of Port Water Injection Benefits in a GDI Engine un-der Knock-Limited Conditions**", THIESEL 2018 Conference on Thermo- and Fluid Dynamic Processes in Direct Injection Engines
19. V. Ravaglioli, F. Ponti, F. Carra, M. De Cesare, "**Heat Release Experimental Analysis for RCCI Combustion Optimization**", Proceedings of the ASME 2018 Internal Combustion Fall Technical Conference, ICEF2018, November 4-7, 2018, San Diego, CA, USA.
20. De Cesare M., Cavina N., Brugnoli E., "**Conceptual Design & Analytic Assessment of 48V Electric Hybrid Powertrain Architectures for Passenger Cars**", SAE Technical Paper 2019-01-0353, 2019.
21. De Cesare M., Ravaglioli V., Carra, F., Stola F., "**Review of Combustion Indexes Remote Sensing Applied to Different Combustion Types**", SAE Technical Paper 2019-01-1132, 2019.
22. Ranuzzi F., Cavina N., Brusa A., De Cesare M., Panciroli M., "**Development and Software in the Loop Validation of a Model-based Water Injection Combustion Controller for a GDI TC Engine**", SAE Technical Paper 2019-01-1174, 2019.

# Abbreviations - Nomenclature

Acronym	Description
AD	Autonomous Driving
AFR	Air-Fuel Ratio
AHP	Adsorption Heat Pump
AMT	Automated Manual Transmission
APU	Auxiliary Power Unit
AT	Automatic Transmission
ATDC	After Top Dead Center
AWD	All Wheel Drive
BEV	Battery Electric Vehicle
BLDC	Brushless Direct Current Motor
BMEP	Brake Mean Effective Pressure
BSFC	Brake Specific Fuel Consumption
BTE	Brake Thermal Efficiency
BtL	Biomass-to-Liquid
CA50	Crank Angle at 50% Mass Fuel Burned
CA10	Crank Angle at 10% Mass Fuel Burned
CD	Charge Depleting
CF	Conformity Factor
CFD	Computational Fluid Dynamics
CI	Compression Ignition
CL	Closed Loop
CNG	Compressed Natural Gas
COP	Coefficient of Performance
COV	Common Rail
CR	Compression Ratio
CS	Charge Sustaining
CtL	Coal-to-Liquid
CVT	Continuously Variable Transmission
DCT	Dual Clutch Transmission
DOC	Diesel Oxidant Catalyst
DoE	Degree of Electrification
DME	Dimethyl ether
DP	Dynamic Programming
DPF	Diesel Particulate Filter
DWI	Direct Water Injection
EC	European Council
ECMS	Equivalent Consumption Minimization Strategy
ECU	Engine Control Unit
EEMS	Equivalent Emissions Minimization Strategy
EGR	Exhaust Gas Recirculation
EMG	Electric Motor-Generator
EMS	Energy Management Strategy
EREV	Extended Range Electric Vehicle
ETD	Electric Traction Drive
EU	Europe
EV	Electric Vehicle
FC	Fuel Consumption

FCEV	Fuel Cell Electric Vehicle
FF	Feed Forward
FGT	Fixed Geometry Turbine
FT	Fischer-Tropsch
FWD	Forward simulation
GB	Gearbox
GDI	Gasoline Direct Injection
GPF	Gasoline Particulate Filter
GT	Gas Turbine
GtL	Gas-to-Liquid
HCU	Hybrid Control Unit
HD	Human Driving
HEV	Hybrid Electric Vehicle
HiL	Hardware-in-the-Loop
HoQ	House of Quality
HR	Hybridization Ratio
HRR	Heat Release Rate
HV	High Voltage
ICE	Internal Combustion Engine
ICEV	Internal Combustion Engine Vehicle
IMEP	Indicated Mean Effective Pressure
ISFC	Indicated Specific Fuel Consumption
KER	Kinetic Energy Recovery
KL	Knock Limit
KLSA	Knock Limit Spark Advance
LCA	Life Cycle Assessment
LNG	Liquefied Natural Gas
LNT	Lean NO <sub>x</sub> Trap
LTC	Low Temperature Combustion
LV	Low Voltage
MAPO	Maximum Amplitude of Pressure Oscillation
MDL	Model
MFB50	Crank Angle at 50% Mass Fuel Burned
MVM	Mean Value Model
NEDC	New European Driving Cycle
nTC	Number of Turbo Charger revolutions per minute
OEM	Original Equipment Manufacturer
OL	Open Loop
ORC	Organic Rankine Cycle
PCCI	Premixed Combustion Compression Ignition
PMAX	Maximum in-cylinder pressure
PPCI	Partially Premixed Compression Ignition
PPRR	Peak Pressure Rise Rate
PtL	Power-to-Liquid
PTW	Pump-to-Wheel
PWI	Port Water Injection
QFD	Quality Function Deployment
QSS	Quasi-Static Simulation
RC	Rankine Cycle
RCCI	Reactivity Controlled Compression Ignition
RCP	Rapid Control Prototyping
REEV	Range Extender Electric Vehicle
ROHR	Rate of Heat Released
SA	Spark Advance
SAE	Society of Automotive Engineers
SI	Spark Ignition
SiC	Silicon Carbide

SMD	Sauter Mean droplet Diameter
SOC	Start of Combustion or State of Charge
SOEC	Solid Oxide Electrolysis Cell
STP	Standard Temperature and Pressure
TC	Turbocharger
TCO	Total Cost of Ownership
TDC	Top Dead Center
TEG	Thermoelectric Generator
TFP	Turbine Flow Parameter
TKI	Tabulated kinetics for ignition
TRL	Technology Readiness Levels
TTW	Tank-to-Wheel
TWC	Three Way Catalyst
US	United States
VCP	Volumetric Cooling Power
VGt	Variable Geometry Turbine
WHR	Waste Heat Recovery
WI	Water Injection
WLTC	World Light duty Test Cycle
WLTP	World Light duty Test Procedure
VOC	Voice of Customer
WOT	Wide Open Throttle
WTT	Well-to-Tank
WTW	Well-to-Wheel
ZT	Dimensionless figure of merit of thermoelectric performance

# 1.Introduction

In this chapter the main motivations and goals of the research activities carried out during the PhD program are clarified. Then the structure of the thesis is explained.

## 1.1 Motivations

The macro-trends that are shaping the evolution of powertrain technologies are:

- sustainability, namely the simultaneous reduction of CO<sub>2</sub>/ fuel consumption and emissions;
- autonomous driving;
- vehicle connectivity;
- powertrain electrification.

The definition of powertrain solutions has to take into account at the same time the sustainability constraints and the end-user requirements, see Figure 1-1. The powertrain design is even more challenging, because the legislations are focusing on the real use of vehicles. For this reason new homologation procedures have been defined in USA and recently in Europe with the introduction of WLTP [1,9,11] and Real Driving Emission (RDE) [1,9,10,11,104] procedures. Also new emerging countries are aligning to this regulation trends.

To fulfill the requirements coming from the end-users and legislations, several powertrain architectures and engine technologies are possible, such as Spark Ignition (SI) or Compression Ignition (CI) engines, with many new technologies, new fuels [4,69,70,71,72,73,74], and different degree of electrification [16,19,26,35,61,113,114,124,292].

The definition of the more promising powertrain architectures, with proper technology mix, and the assessment of benefits and costs must be accurately evaluated by means of objective procedures and tools in order to choose among the best alternatives.

Moreover, the impacts on Greenhouse Gas (GHG) or energy consumption should be evaluated in term of powertrain Well-to-Wheel path or Life Cycle [17,68,221,231,232,234,235] and not only evaluating the Tank-to-Wheel energy transformation, as many legislations are considering.

For these reasons the definition and evaluation of powertrain architectures and their subsystems technologies have to take into account the pathway of energy employed for the propulsion and to perform the auxiliary functions (e.g. AC, electric power supply, etc.) on board the vehicle.

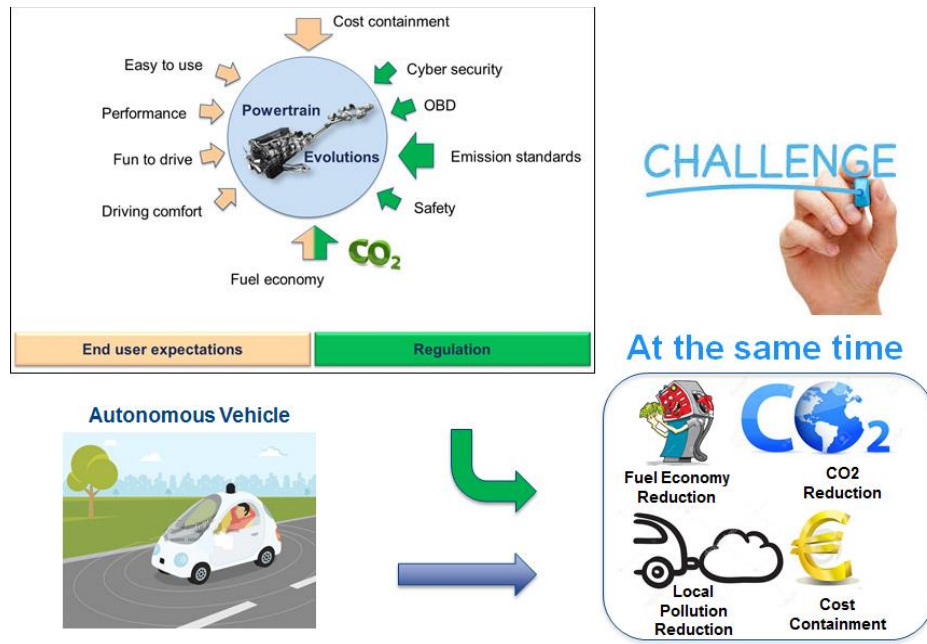


Figure 1-1 Powertrain design challenges

## 1.2 Research Objectives

PhD studies started from the previous research activities done to investigate new technologies and control methods for conventional powertrains, based on Compression Ignition engines [34,36,38,146,154,190,204,295,325] and Spark Ignition engines [149,189,211,212], with the purpose of improving emission, consumption and performances. New advanced technologies for ICEs (e.g. new combustion approaches) and powertrain electrification are needed to face the aforementioned complex scenario of requirements. Furthermore, the definition, selection and assessment of the new powertrain architectures and technologies have to be based on structured and objective methodologies, in order to guarantee affordable and effective solutions.

With these aims, the areas of original contribution and the main research goals of this work are summarized in the following list:

- the definition of a structured methodology to link constraints and end-user requirements to powertrain technical features, in order to perform a conceptual basic design and an objective comparison of architectures and technologies;
- the procedure definition for the conceptual design of the powertrain architectures, with a proper technology mix, with the aim of limiting the analysis to the more promising solutions;
- the conceptual comparison of the defined powertrain architectures and technologies, considering their effectiveness vs. standards and end-user requirements, the technological maturity and the impact on production costs;
- the analysis and investigations of the powertrain key technologies (e.g. Water Injection, Low Temperature Combustions, etc.);
- the definition of the possible powertrain technology pathways towards 2025 and a general forecast post-2025.

This work has also the objective of making available to the reader a very wide and accurate literature review on the topics discussed. The risk is that the dissertation is very long, but at the same time the expected benefit is that an interested reader may find in one single document all the relevant information.

## 1.3 Thesis Structure Overview

A brief introduction to each chapter is provided in this section. The structure of this work is presented in Figure 1-2 as a useful guide for the reader. The topics of each chapter are presented with task and purpose that supports the research goals outlined in previous paragraph #1.2.

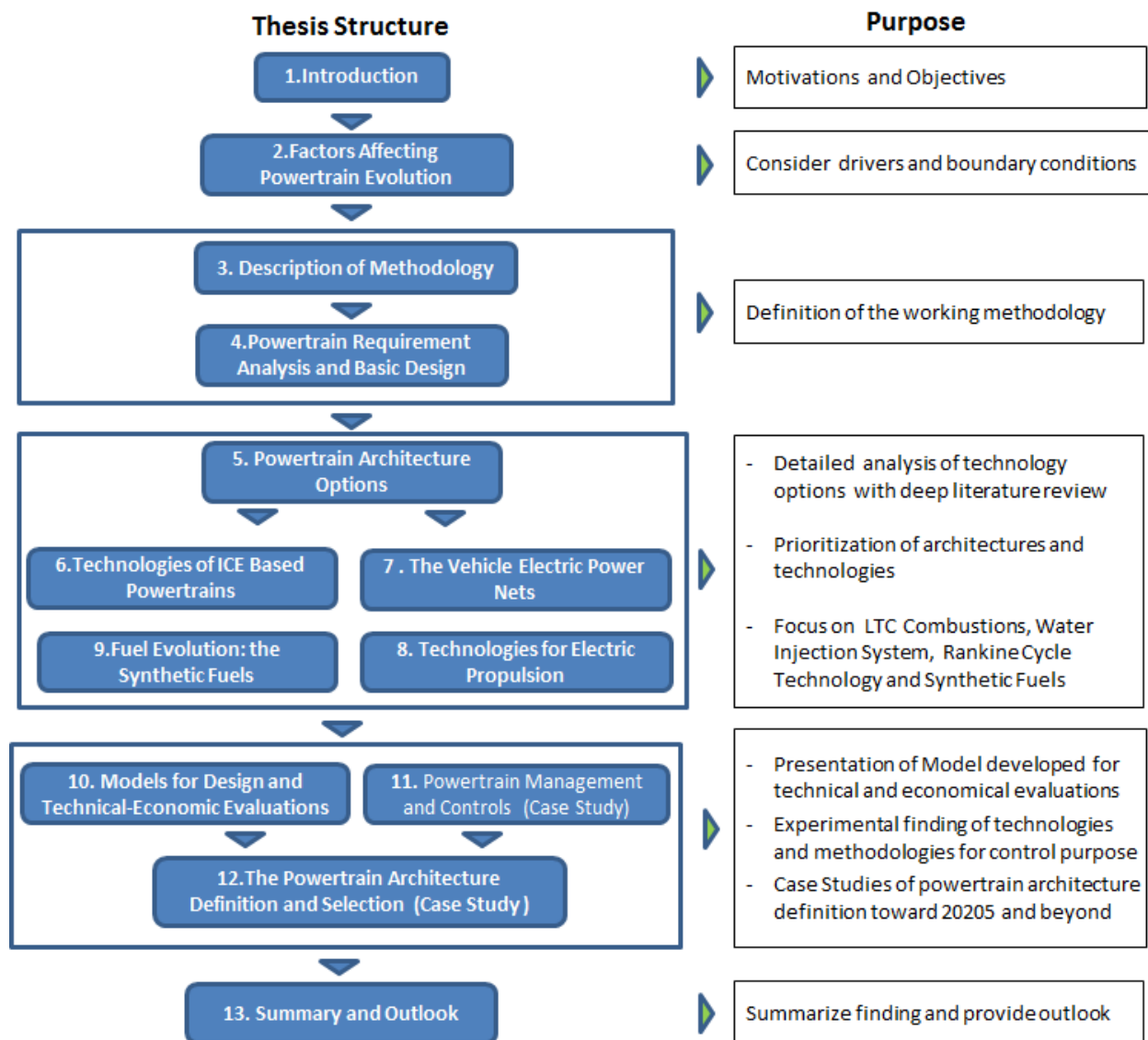


Figure 1-2 Thesis structural overview

The **Chapter #2** analyzes widely the factors affecting the powertrain evolution, such as regulation trends, automotive market drives, etc., highlighting how they impact on powertrain technologies.

The **Chapter#3** introduces the methodology used for requirement definition, conceptual design of powertrain architectures and the selection process of better solutions.

The subsequent **Chapter #4** presents a detailed analysis of the powertrain requirements, using the Quality Function Deployment (QFD) with a modified and personalized approach. Finally, the powertrain and sub-system specifications and the evaluation criteria for a quantitative comparison are defined.

The **Chapter #5** introduces the technology options of powertrain architectures, focusing on electric hybrid powertrains and their functions, features and drawbacks.

In the **Chapter #6** the different ICE technologies are described and critically analyzed, highlighting their effectiveness versus the main requirements. Such considerations are mainly based on the most significant technical and scientific literature. A deep focus has been done on water injection, advanced combustion approaches and waste heat recovery technologies, which were object of further investigations in the case studies presented in the following sections. Finally, the cost estimations of the main technologies are presented.

In the **Chapter #7** the evolution of vehicle electric power nets is presented. The voltage increasing, due to new vehicle functions offers an interesting synergy to introduce the electrification in the powertrain systems at affordable costs.

The **Chapter #8** describes the main devices for the electric propulsion and the key technology options, highlighting their features and effectiveness versus the main powertrain requirements.

In the **Chapter #9** the state-of-art of synthetic fuels (i.e. e-Fuels) from renewable energy sources and a comparison with other alternative fuels are presented.

The **Chapter #10** introduces the Powertrain and Vehicle models, which have been used to define, to optimize the subsystems and to assess analytically the relevant architectures and technologies selected in the previous sections.

In the **Chapter #11** the focus is on the study and experimental investigation to develop new sensors (e.g. acoustic based) and virtual sensors for the control of Low Temperature Combustions. Some case studies are presented. Then new model based approaches for Gearbox control and HEV powertrain energy management are explained. These algorithms are key for the architecture case study presented in the following sections.

In the **Chapter #12** examples of Powertrain Architecture definition and selections are presented, taking into account the horizon 2025 and the post-2025 scenario.

Finally in **Chapter #13** the summary of findings and the outlook are provided.



## 2. Factors Affecting Powertrain Evolution

Some macro-trends, shown in Figure 2-1, are shaping the future of the automotive industry and they have a considerable impact on the vehicle propulsion systems. The most significant ones are:

- sustainability, namely the simultaneous reduction of CO<sub>2</sub>/ fuel consumption [12,16,273,274] and pollutant emissions [3,5];
- autonomous driving;
- powertrain electrification.

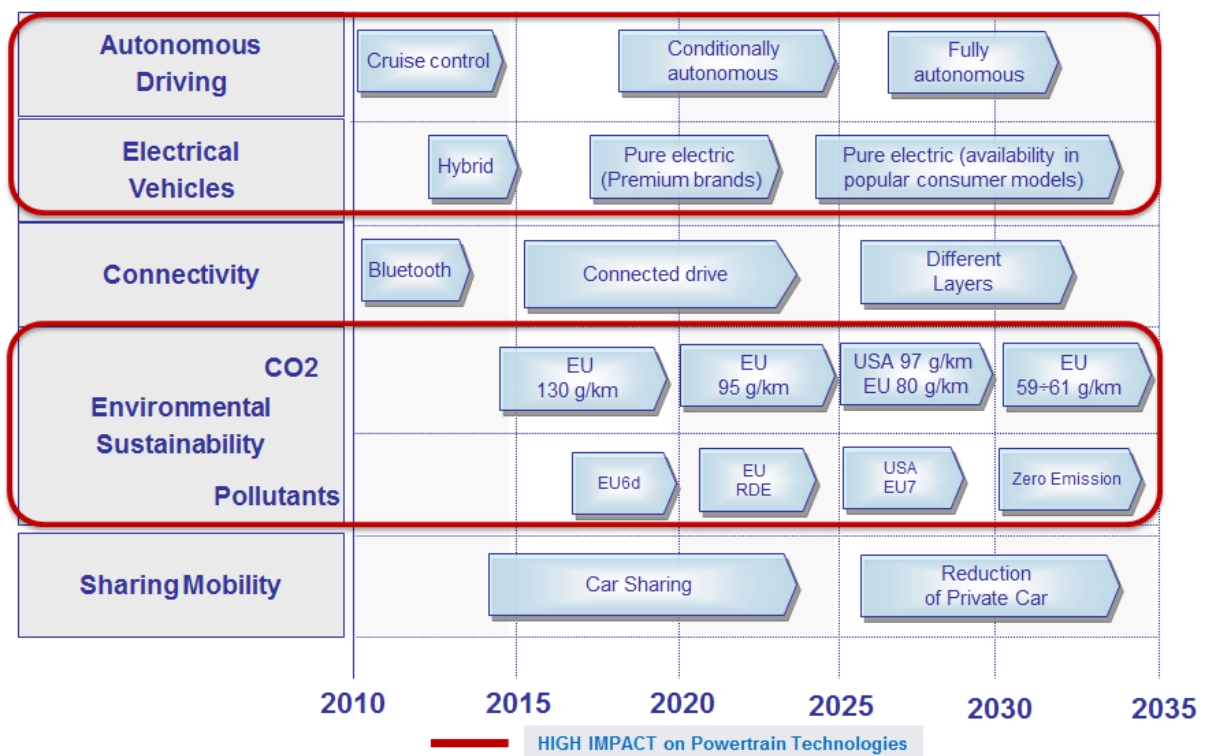


Figure 2-1 Automotive Technology Trends

In this scenario, as shown in Figure 2-2, internal combustion engines will still have a key role, as confirmed by many studies [6,275,276,277], in spite of different degrees of electrification will be necessary to fulfill the challenging requirements in term of sustainability and vehicle performances.

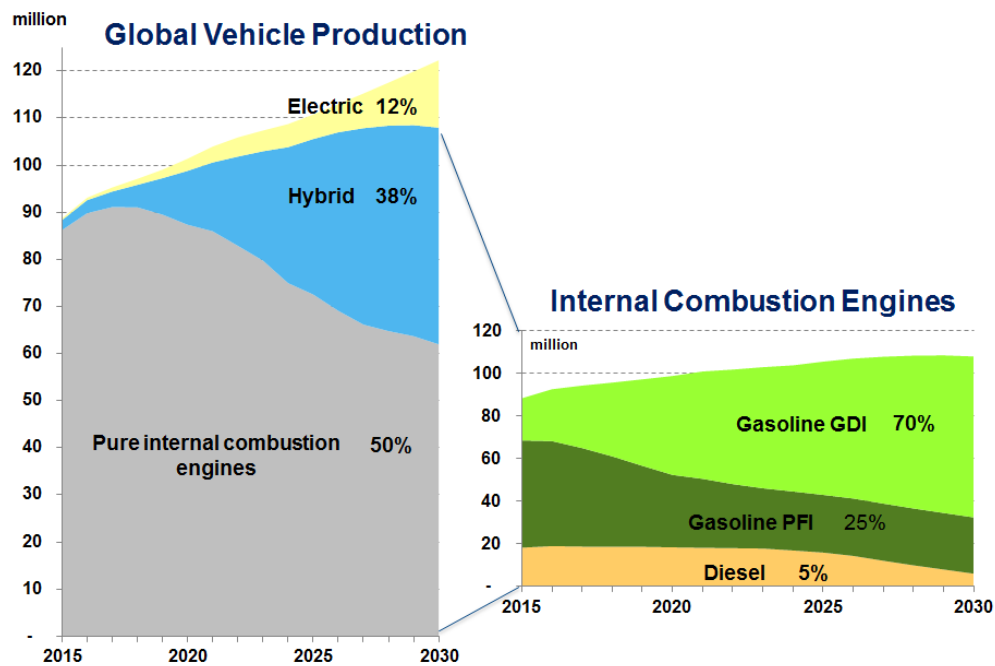


Figure 2-2 Passenger Cars and Light Duty Vehicle Powertrain market scenario, IHS data base

The importance of internal combustion engine can be also explained considering that it converts chemical energy stored in the fuel to support functions that are not closely related to propulsion, Figure 2-3:

- production of electricity for devices on board the vehicle;
- mechanical energy production for the air conditioning system [7,8,169];
- production of thermal energy to heat the passenger compartment.

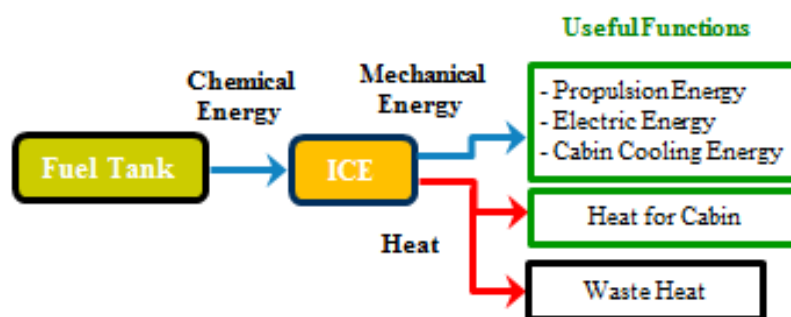


Figure 2-3 Energy flow and functions in an ICE based vehicle

In purely electric vehicles, with the absence of an internal combustion engine that converts chemical energy stored in the fuel, such additional functions [7,8] require an electrical energy storage on board

possibly much larger than what is necessary for traction only, with negative impacts on cost, weight, range and charging times.

## 2.1 Environmental Sustainability: Greenhouse Gas and Pollutant Regulations

Sustainability, namely the simultaneous reduction of CO<sub>2</sub>/ fuel consumption and pollutant emissions, which in all countries are defined by specific norms, updated periodically. The global trend is near-zero tailpipe emissions, considering more realistic conditions of use.

The last years have seen a continued emphasis on achieving reductions in pollutants and tailpipe CO<sub>2</sub> or fuel consumption, under dynamometer and real-world driving conditions. This section covers the major regulatory initiatives affecting the light-duty and passenger car vehicles.

### 2.1.1 CO<sub>2</sub> and Fuel Consumption Regulations

The EU has historically been a leader in implementing vehicle CO<sub>2</sub> emission standards. In recent years, however, most large economies have set converging CO<sub>2</sub> emission targets for new vehicles (see Figure 2-4). The European limit for 2030 is under discussion with a range between 67÷61 gCO<sub>2</sub>/km, 30÷35% lower than 2020 limit.

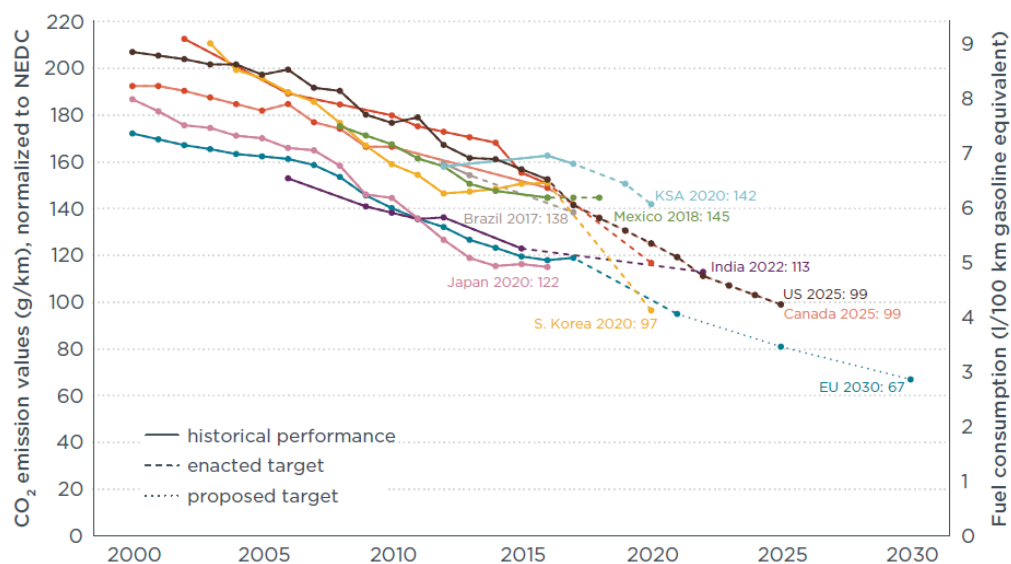


Figure 2-4 Comparison of global CO<sub>2</sub> regulations for new passenger cars (source: ICCT 2018)

Figure 2-5 summarizes the trends of the new standards shown in Figure 2-4: they will require a 3-6% reduction in tailpipe CO<sub>2</sub> per year to achieve the fleet-wide passenger car requirements. An overview of the regulations for the three main world areas (e.g. Europe, United States and China) is given in the next sections.

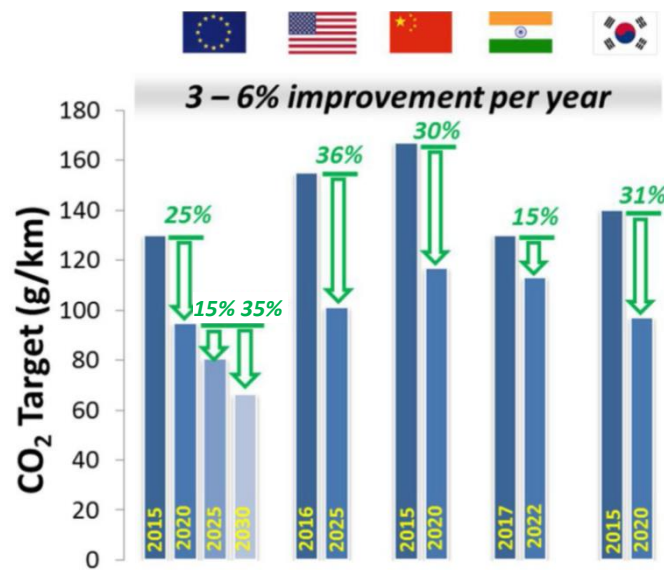


Figure 2-5 The major automotive regions will be requiring 3-6% reductions CO<sub>2</sub> per year, with Europe requiring the tightest standards

## Europe Standards

In Europe, the European Commission's strategy for low-emission mobility aims to limit transport related greenhouse gas (GHG) emissions by 2050 to be at least 60% lower than in 1990. In line with the strategy, the Commission adopted a legislative proposal in October 2018, targeting reductions in average fleet CO<sub>2</sub> emissions from new light-duty vehicles by 15% in 2025 and 30÷35% in 2030, compared to New European Drive Cycle (NEDC)-based CO<sub>2</sub> limits of 95 g/km for passenger cars and 145 g/km for light commercial vehicles in 2020 [273,274]. OEMs are provided with incentives to introduce zero- and low-emission vehicles, with emissions <50 g/km, via credits which can be applied to the fleet CO<sub>2</sub> targets. New CO<sub>2</sub> targets are challenging, especially as they are accompanied with changes to the measurement protocol (WLTP in 2021), born to overcome some issue of the norms, explained better below.

## United States Standards

In the US, the Environmental Protection Agency (EPA) re-opened the "Final Determination" on the need and feasibility of maintaining the current GHG standards for MY 2022-25 Light Duty vehicles [16,278], with revisions in 2018. California, while challenging the re-opening of the GHG standards, is now planning for more reductions in GHG emissions beyond 2025. Key strategy elements were listed to achieve a 40% reduction in overall GHG emissions over the 2020 levels by 2030. For the transportation sector, this includes a 50% reduction in black carbon (BC) and 40% reduction in methane emissions over 2013 levels. For electrification, the proposed targets are a cumulative 1.5 M zero emission vehicles (ZEVs) by 2025, which include plug-ins, fuel-cell vehicles and pure battery EVs. Sales in 2025 of actual ZEVs in California are mandated to be an estimated 145,000 vehicles or about 7% of new car sales [279] in 2025. For heavy duty, 2.5% and 10% ZEV trucks in the Class 3-7 sector in 2020 and 2025, respectively, are being considered.

## China Regulations

China has a broad industrial policy to decrease dependency on imported petroleum and lead the world in electric vehicles. In this regard, the Ministry of Industry and Information Technology (MIIT) finalized the New Energy Vehicle (NEV) mandate policy [280]. The policy, expands on California's ZEV credit

system, wherein vehicles get more credits for longer all-electric range, but China is the first to give more credit for higher efficiency vehicles. Auto manufacturers are required to generate 10% of NEV credits in 2019 and 12% in 2020. NEVs include plug-ins, full battery electric and fuel cell vehicles. Three credits on average per NEV could result in 4% adoption of NEVs in 2020 [281]. Excess credits can be traded to meet the NEV and also the corporate average fuel consumption requirements.

## 2.1.2 CO<sub>2</sub> and Fuel Consumption Regulation Issues

The current global legislations are even more stringent and challenging for car manufacturers, but there are some weaknesses to be improved with aim of reducing global emission footprint. These issues can be summarized as follow:

- gap between laboratory and test conditions for the type approval;
- using mass, as the utility parameter, disincentives vehicle light-weighting, specific problem of EU legislation and derivate regulations;
- the legislations take only into account Tank-to-Wheel emissions or energy consumption and not Well-to-Tank or LCA emissions of vehicles.

### Gap between laboratory and test conditions

Today, the car manufacturers are on track to meet the EU 2021 target of 95 g/km, as confirmed by a pictures of “Best in Class Vehicle for CO<sub>2</sub> Emission” in May 2016, see Figure 2-6. This rapid decline in CO<sub>2</sub> emission values seems to be a rousing success for CO<sub>2</sub> standards, but does not consider the real-world performance of vehicles.



Figure 2-6 Best in Class Vehicle for CO<sub>2</sub> Emission in NEDC Cycle, status at May 2016

Real world emissions are usually higher compared to those measured under laboratory conditions. The [14] reports that the difference between official and real world CO<sub>2</sub> emissions is as high as 30÷40%, and growing over the years. The data come on approximately 1.1 million vehicles from 14 data sources, including on-road, average estimates for private cars and company cars.

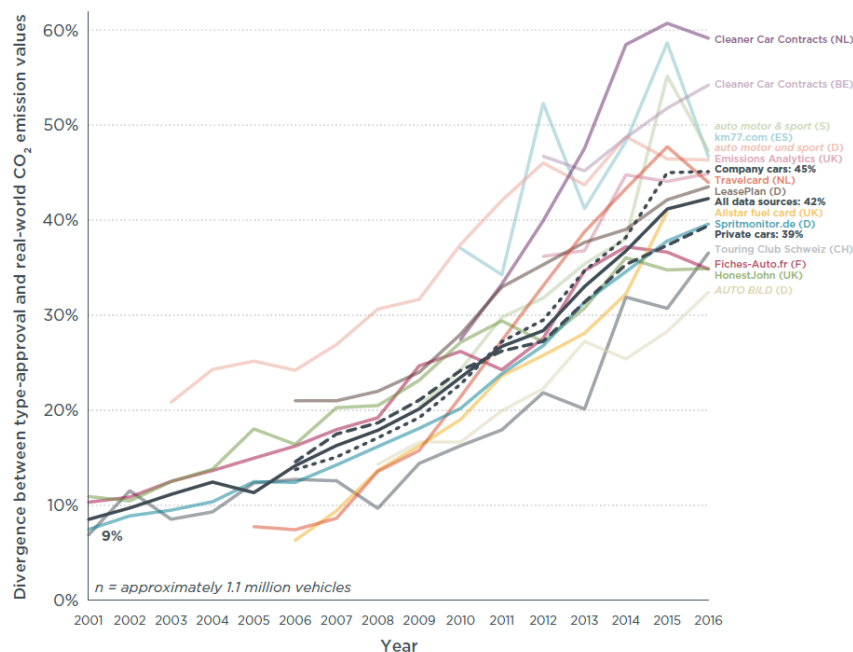


Figure 2-7 Divergence between real-world and manufacturers' type-approval CO<sub>2</sub> emission values (NEDC) for various on-road data sources, including average estimates for private cars, company cars, and all data sources

The same phenomena is confirmed in the six largest vehicle markets and nine of the top 11 have implemented standards to curb fuel consumption and greenhouse gas emissions of light-duty vehicles. While fuel efficiency standards thus sound like a success, there is evidence of a growing divergence (or “gap”) between official and real-world CO<sub>2</sub> values, implying that laboratory measurements are increasingly overestimating the fuel efficiency of cars.

Figure 2-8 from [15], based on more than 1.5 million passenger cars in the European Union (EU), the United States, China and Japan, indicates that the divergence between the official and real-world CO<sub>2</sub> Emission values has increased over time in all regions. The EU, which has used the New European Driving Cycle (NEDC) for vehicle testing, is the market with the steepest annual growth in the gap between 2001 and 2014, while Japan and the United States experienced smaller increases. Japan phased out the 10-15 mode cycle in the 2008–2011 timeframe, replacing it with the JC08 cycle. The United States is the only market with two sets of CO<sub>2</sub> values: the more limited two-cycle-based Corporate Average Fuel Economy (CAFE) values are used for regulatory purposes, while the U.S. Environmental Protection Agency (EPA) provides more inclusive five-cycle-based fuel economy label values to inform consumers about the real-world on-road performance of vehicles. The label values were found to offer the most realistic fuel consumption figures in the analysis. The label values are the basis for the adjustment factor used by U.S. regulators to convert CAFE values to real-world estimates during fuel economy standard rulemakings.



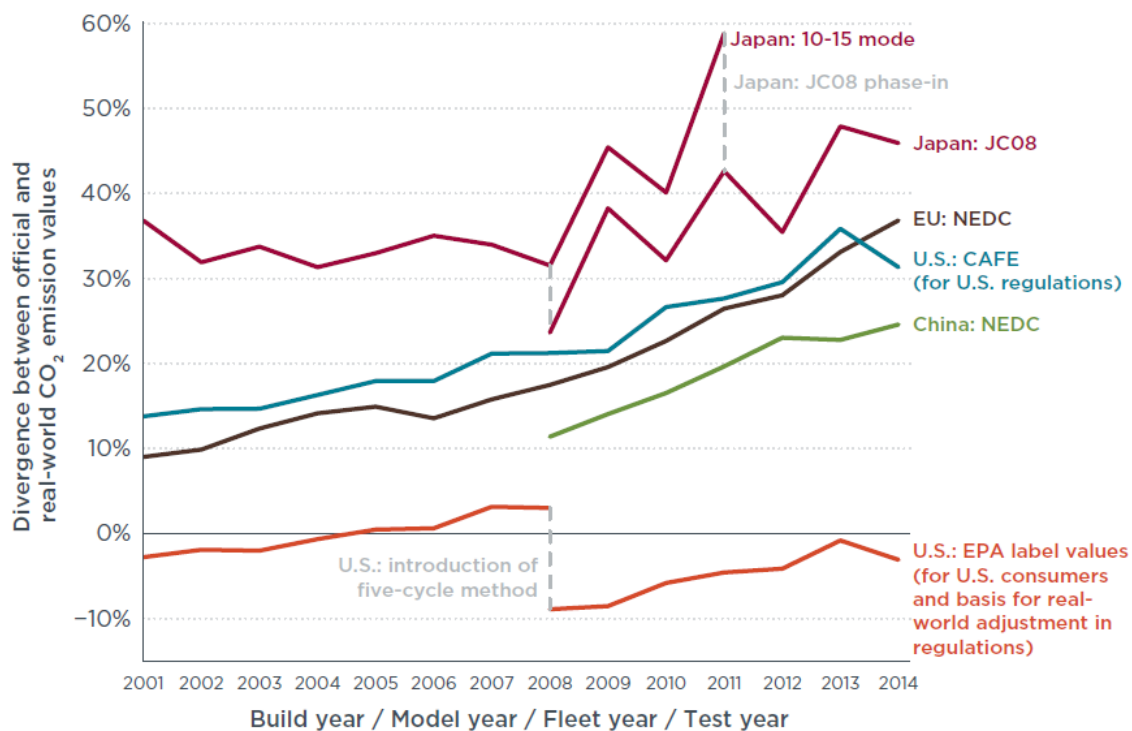


Figure 2-8 Divergence between official and real-world CO<sub>2</sub> emissions for new passenger cars in EU, United States, China, and Japan

The divergence is related to all vehicle types, both conventional ICE based and electric hybrid, as confirmed in Figure 2-9 from [14], that plots the average gap between type-approval and Travelcard CO<sub>2</sub> emission values by powertrain types in 2016.

Travelcard Nederland BV is a fuel card provider based in the Netherlands. Fuel cards are used as payment cards for fuel at gas stations and frequently are used by companies to track fuel expenses of their fleets. Travelcard passes are accepted in all Dutch fuel stations, as well as in more than 43,000 fuel stations across Europe. The company currently serves more than 200,000 vehicles registered in the Netherlands. The Travelcard fleet is a large, homogeneous group of drivers, who typically drive new cars and change vehicles every few years. Most cars are less than four years old.

Although vehicles with conventional powertrains and HEVs on average exceed type-approval CO<sub>2</sub> values by 45%, PHEVs stand out with a gap of 242%. This difference was observed in all build years, with PHEVs consistently exceeding the other power train types by more than 150 percentage points.

A possible explanation of this gap can be obtained analyzing the current ECE R 101 procedure for vehicles with multiple energy storage systems on board, e.g. PHEV, and different propulsion systems. The low use of electric operation of PHEVs, compared with the assumption of EU norms, is at the basis of higher CO<sub>2</sub> emissions than the type approval procedure.

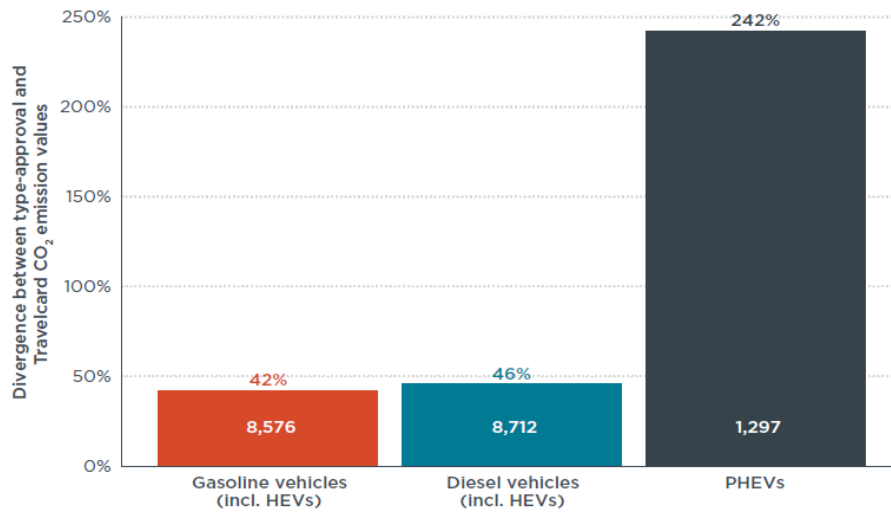


Figure 2-9 Divergence between type-approval and Travelcard Nederland BV CO<sub>2</sub> emission values by power train type in build year 2016. Number of vehicles per category presented at the base of each bar

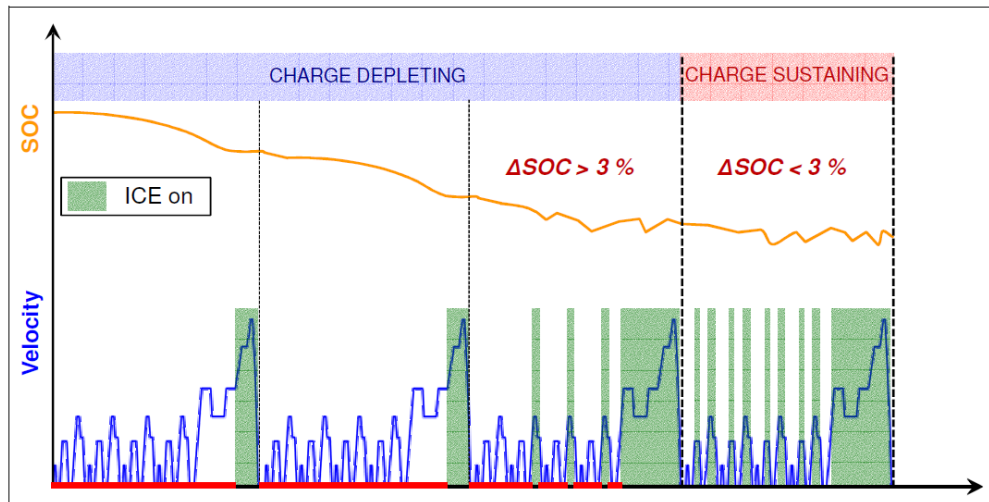


Figure 2-10 Evaluation of a PHEV fuel consumption based on the UN ECE R 101

The ECE R101 method evaluates the fuel consumption (FC) weighting the partial results of Charge Depleting (CD) and Charge Sustaining (CS) operation modes (see Figure 2-10) according to the following formula, from [282]:

$$FC = \frac{D_e \cdot FC_{CD} + D_{av} \cdot FC_{CS}}{D_e + D_{av}} \quad (2.1)$$

where

FC<sub>CD</sub>: Fuel Consumption during Charge Depleting

FC<sub>CS</sub>: Fuel Consumption during Charge Sustaining

D<sub>e</sub>: Total electric range during Charge Depleting (marked in red in Figure 2-10)



Dav: assumed mean distance between charging operations (= 25 km).

Thereby, CO<sub>2</sub> emissions are calculated from the determined fuel consumption, emissions from the provision of electric energy are not considered. The parameter Dav is typically 25 km, but if the interval increase the real FC and CO<sub>2</sub> emissions are higher than the certificated values.

To address some of the issues related to the testing procedure in EU, the CO<sub>2</sub> emissions testing will be done using the World-Harmonized Light-Vehicle Test Procedure (WLTP) starting in 2021 [283]. The change in test procedure is expected to increase the fleet wide CO<sub>2</sub> by 15-25% or 18÷30 g/km, referred to C-Class vehicle. In the meantime, the change in procedure for the pollutants has begun in September 2017, applying to type approvals for new vehicles, and extended to all vehicles in September 2018. Correlation of CO<sub>2</sub> emissions over WLTP and NEDC will be done using the CO2MPAS tool, developed by the European Commission's Joint Research Centre (JRC) [284]. The new test procedure reduces the gap with real conditions but it doesn't overcome the issue. More significant test conditions (e.g. with AC) should be needed.

To overcome these limit, in this work the analysis have been performed considering the EU cycles and other standard cycles (e.g. RTS95) that take into accounts the real use.

### Disincentives vehicle light weighting (EU standards)

The CO<sub>2</sub> target in EU regulations is an average value for the fleet of car manufacturers and it depends on average vehicle mass, the limit 95 g/km is related to 1380 kg. The Figure 2-11 from [13] shows the limit curve for 2025 and position of car manufacturers.

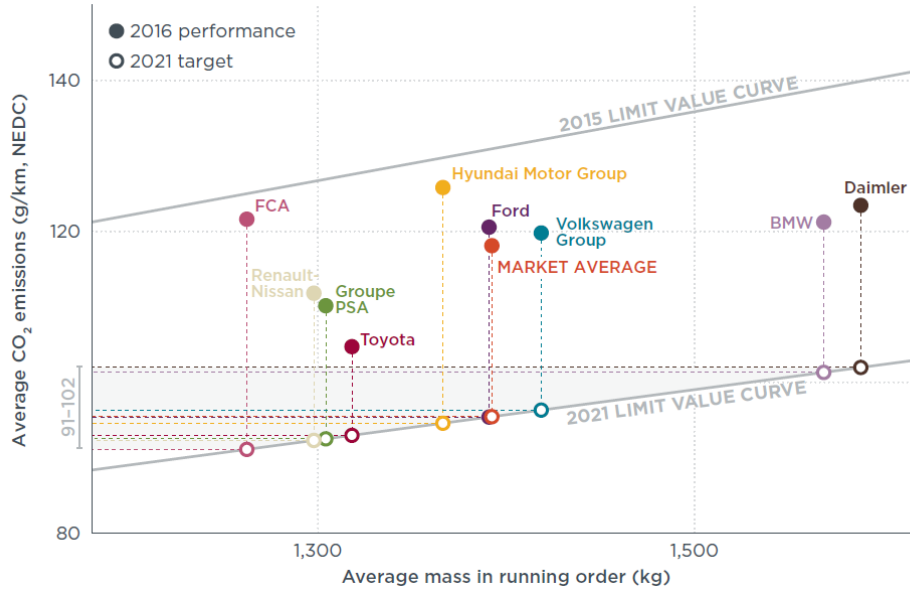


Figure 2-11 Average CO<sub>2</sub> emission values and vehicle mass of major manufacturer groups in 2016; hypothetical 2021 targets are based on average 2016 mass; limit value curve for 2015 included for reference

The formula to determine the CO<sub>2</sub> emission target for each individual manufacturer is

$$E = E_0 + sl \cdot (M - M_0) \quad (2.2)$$

with  $E_0$  being the fleet CO<sub>2</sub> target,  $sl$  the slope of the limit value curve,  $M$  the average mass of the manufacturer's vehicle fleet, and  $M_0$  the average mass of all manufacturers. Whereas slope  $sl$  is fixed for the entire duration of the regulation, the  $M_0$  parameter is updated every three years (every two years beginning in 2024) to account for changes in the average mass of the new vehicle fleet. This adjustment is done to ensure that, on average, the fleet target  $E_0$  is reached, even if the average mass of all manufacturers' vehicles increases. Irrespective of this (indirect) correction mechanism for the average mass of all manufacturers, it is the slope of the limit value curve that determines the disincentive for light-weighting.

As observed in Figure 2-12 the reduction of 100 kg in mass can lead, for instance, to a reduction of 4g/km of CO<sub>2</sub>, but it causes the contemporary limit reduction undermining the light-weighting. The steeper the limit value curve, the more CO<sub>2</sub> heavier vehicles are allowed to emit, and the higher the disincentive for light-weighting. A flatter slope could reduce the disincentive for light-weighting. The slope of the limit value curve is set based on the relationship between vehicle CO<sub>2</sub> emission values and vehicle mass, as observed on the market.

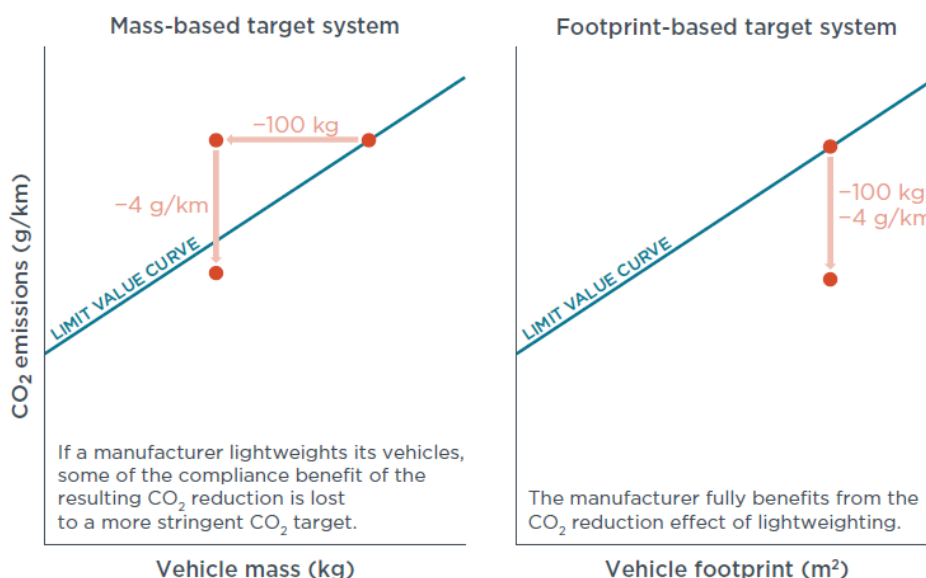


Figure 2-12 Mass reduction in a mass-based CO<sub>2</sub> target system (left) and in a footprint-based system (right)

The slope  $sl$  of the limit value curve was set at 0.0457 (g/km)/kg for the 2012÷2019 time period and at 0.0333 (g/km)/kg for the 2020÷2024 time period, reflecting a 27% reduction for all vehicle manufacturers (going from the 2015 target of 130 g/km of CO<sub>2</sub> to the 2021 target of 95 g/km of CO<sub>2</sub>).

Retaining mass as the utility parameter would not only require regular updates of the actual average fleet mass  $M_0$ , as is already the case in current regulation, but also of the slope  $sl$  of the limit value curve, in order to account for recent market developments and to avoid creating an incentive to increase vehicle mass.

For the 2025 and 2030 CO<sub>2</sub> standards, the European Parliament and European Council (EC) could deviate from the original EC proposal, remove the utility parameter, and switch to a fixed absolute CO<sub>2</sub> target value or a fixed CO<sub>2</sub> percentage reduction target for all manufacturers. That would simplify the regulation and increase the incentive for light-weighting. Alternatively, the European Parliament and Council could continue using a utility parameter but transition to vehicle footprint instead of mass. This transition would remove disincentives related to light-weighting and reduce overall compliance costs, but the standard would remain as complex as today.

## From Tank-to-Wheel to Well-to-Wheel or LCA emissions

The current automotive regulations defines the GHG limits only for the in use emissions, named Tank-to-Wheel (TTW) emissions, that takes into account the CO<sub>2</sub> or other gasses production due to process of fuel/energy conversion to energy to move the vehicle. These TTW emissions depend on vehicle energy needs and powertrain principle to generate energy for movement. In case of an ICE based vehicle, for a defined fuel, the CO<sub>2</sub> generation is strictly correlated to the fuel consumption. So an improvement of the TTW energy consumption means contemporary the TTW CO<sub>2</sub> reduction. This CO<sub>2</sub> metric is insufficient to compare impacts of Plug-in Hybrid (PHEV) and Battery Electric Vehicles (BEV), because the GHG of the upstream fuel and vehicle production are not considered. The Figure 2-13 helps to clarify the definitions introduced in this section.

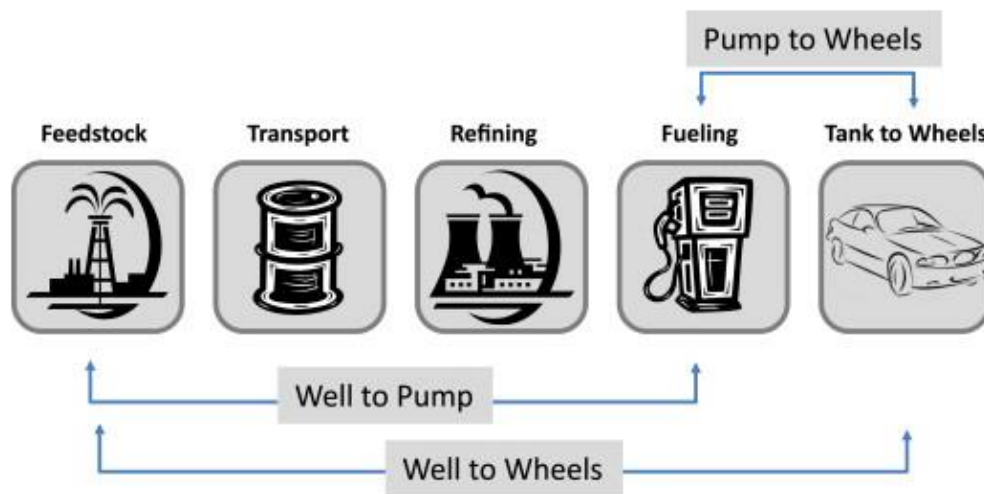


Figure 2-13 WTW, PTW and WTP definitions

In case of pure electric vehicle the in use emission of CO<sub>2</sub> is zero and the norms define only a way to measure the electric energy consumed from Pump-To-Wheels (PTW), including the battery charging consumption named Pump-To-Tank, and the vehicle consumption (TTW).

The previous definitions are not able to evaluate the global emission (or energy consumption) of a powertrain technology and of the related fuel or propulsion energy, considering its production, transport, and distribution. The footprint of energy supply processes is named Well-To-Tanks (WTT) emission (or energy consumption). The global footprint of a powertrain and the related propulsion energy is called Well-To-Wheels.

With this metric the global GHG footprint of BEV or PHEV depends on country electricity GHG intensity. To limit the global CO<sub>2</sub> emissions or to evaluate the global energy cost of a propulsion technology the legislation target should be defined by means of the WTW definition.

Life Cycle Assessment is a deeper measurement of powertrain technologies footprint than the WTW. It includes compiling inventories of the environmentally relevant flows (i.e. emissions, natural resources, material and energy, waste) related to all processes involved in the production, use, and end-of-life of a product and based on these, quantifying the associated cumulative life-cycle burdens [285]. The LCA methodology is based on international standards [286,287]. The complete LCA includes the WTW stages as well as the “equipment life cycle”, see Figure 2-14. The equipment life cycle covers production, manufacturing, maintenance and end-of-life of vehicle and road infrastructure.

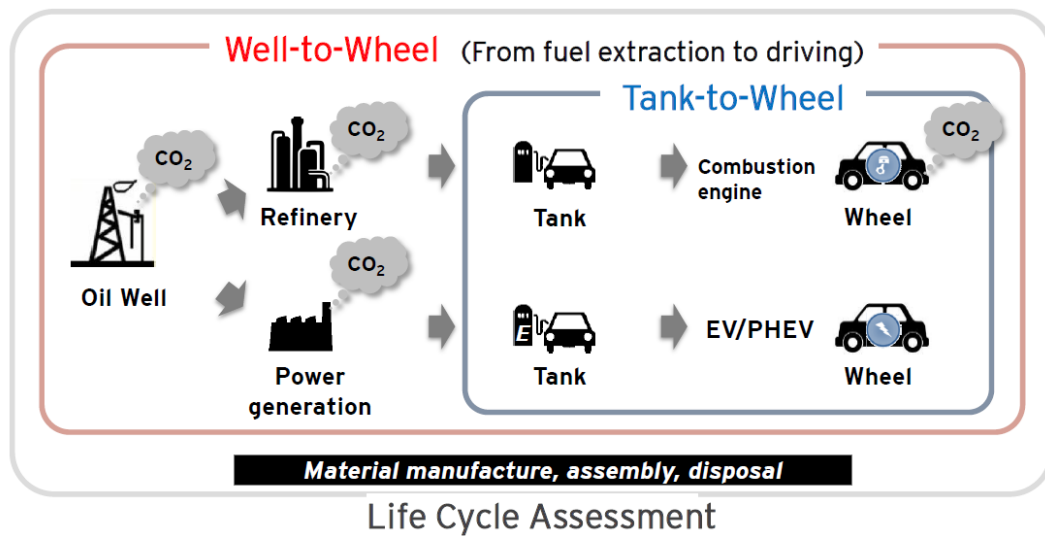


Figure 2-14 Simplified scheme of the scope of the LCA

In a long term scenario up to 2050, the vision of some manufacturers [18] defines a CO<sub>2</sub> Well-to-Wheel target 90% lower than the 2020 emission, very close the zero emission. This challenging target can be only faced with a system design approach of whole vehicle/powertrain and taking into account the proper energy carrier (e.g. fuel), as it will be explained in the next chapters.

### 2.1.3 Pollutant Regulations

The [5] summarizes the trend of pollutant regulation in main countries. The emission criteria are tighter for near-zero tailpipe emissions, considering more realistic conditions. These constraints are the main challenges confronting the design and development of new powertrains, together with safety, comfort, drivability/performance, and costs.





Years		2015	2016	2017	2018	2019	2020	2021	2022	2023	2024	2025
	EPA	Tier 2		Tier 3 (phase in)								
	CARB	LEV 3 phase in start PM < 3 mg/mi							all 3mg/mi Start 1mg/mi			
	Limit	EU6b GDI PN = 6 E+12 #/k			EU6d-TEMP GDI PN 6 E+11#/k		Eu6d		EU7 ? NOx < 40 mg CF=1 PN > 10 nm -7°C tests			
	Cycle	NEDC	monitor	WLTC	WLTC + RDE Cycle CF NOx =2.1, PN= 1.5		CF=1					
	Nation	China 4 (~ EU4)			China 5 (~ EU5)		CN6a GDI PN 6 E+11#/k RDE Monitor		CN6b RDE CF= 2.1			
	Beijing	Beijing 6			China 6b w/o RDE		RDE CF=2.1					
	Nation	BS III (~ EU3)			BS IV		BS VI (~ EU6b) RDE Introduction CF=?					
	12 Cities	BS IV (~ EU4)										

Figure 2-15 Criteria pollutants scenario

The comparison of trends for the main countries legislations are reported in the next Figure 2-16 and Figure 2-17, the details for the main countries are introduced following. In the figure the values for EU7 are not reported because under discussion.

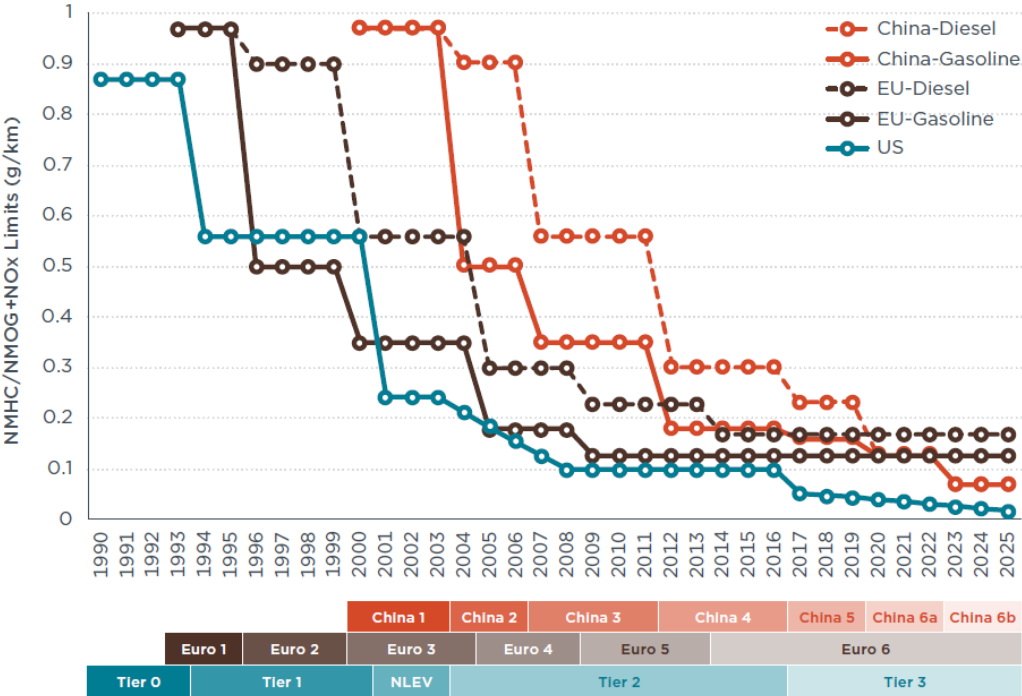


Figure 2-16 Comparison of NMOG/NMHC+NOX emission requirements in China, the European Union, and the United States during 1990 –2025 [257]

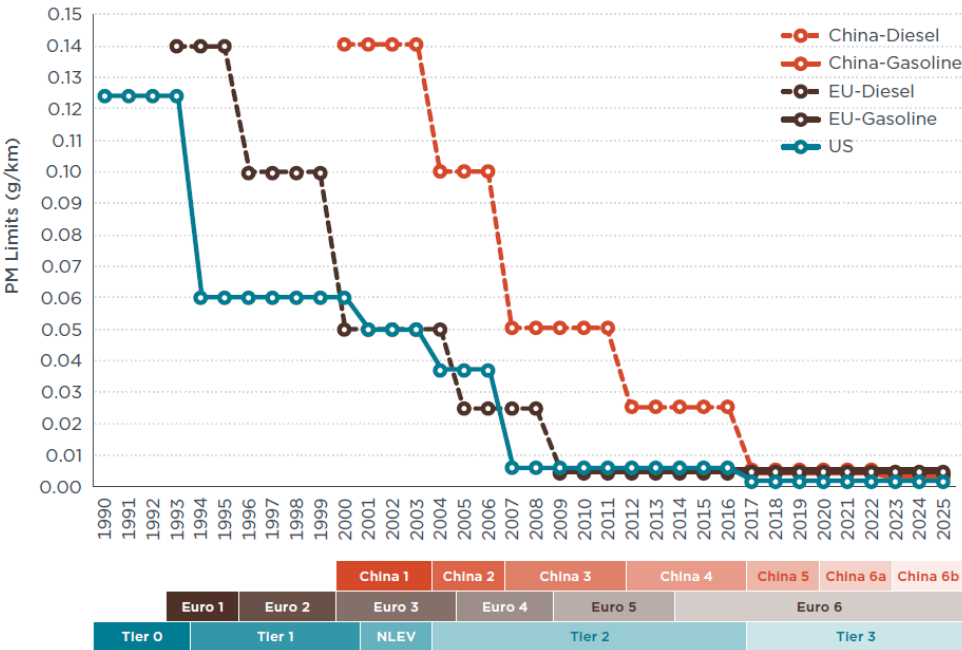
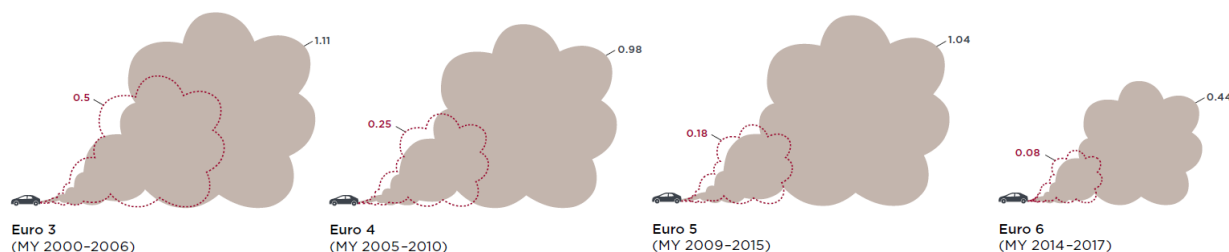


Figure 2-17 Comparison of PM emission requirements in China, the European Union, and the United States during 1990–2025 [257]

## Europe Standards

The main issue of EU legislation is the divergence of the type approval tests and real driving conditions, as reported in several studies [252, 288] and illustrated clearly in Figure 2-18, that highlights the gap for NO<sub>x</sub> emissions in diesel and gasoline cars.

**Diesel cars: Nitrogen oxide (NO<sub>x</sub>) emissions (in g/km)**



**Gasoline cars: Nitrogen oxide (NO<sub>x</sub>) emissions (in g/km)**

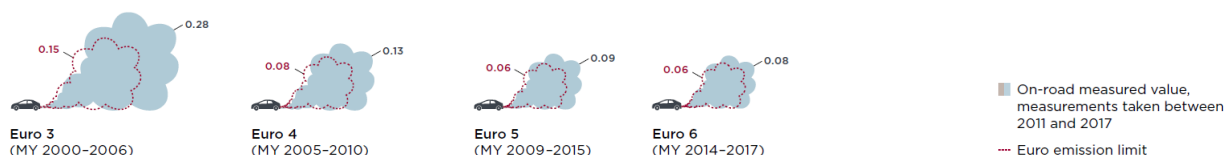


Figure 2-18 Gap between type approval and real emission for NO<sub>x</sub> (g/km) in Diesel and Gasoline cars

To overcome the problem new Real-Driving Emissions (RDE) requirements for Euro 6 passenger cars and vans was introduced starting Sept 1st, 2017. The draft version of the 3rd RDE package was officially published in June 2017 [13], and retains the key elements: Conformity factor (CF) of 1.5 for particulate number (PN), strengthening of the regulations by including the first 5 minutes of cold start emissions in the urban portion, and an emphasis on transparency with requirements that OEMs make public the maximum RDE NO<sub>x</sub> and PN values and provide an “extended documentation package” on auxiliary emission strategies. The regulatory package also sets the stage for inclusion of an evaluation that their RDE emission values are comparable with conventional vehicles.

The final method will be part of the fourth and final RDE package, expected to address in-service compliance and special provisions for light-commercial vehicles. Some changes are being considered to the RDE framework, such as inclusion of sub-23 nm particles.

RDE and WLTP are not perfect as there are still conditions in real world driving which are not captured in these tests. Emissions of both CO<sub>2</sub> and criteria pollutants are high during congested traffic, marked by more frequent start-stops and higher idling. [289] found significant increase in roadside emissions due to traffic congestion, attributed to both higher fuel consumption at low speeds as well as lower exhaust temperatures leading to low power and extensive idling. There is also criticism that the longer duration of the new cycles (compared to NEDC) actually diminishes the relative contributions of emissions from cold-starts.

There is a proposal under consideration to reform the vehicle type-approval process in Europe. The EU Commission will be authorized to carry out independent market checks, issue recalls and impose fines independent of the member states. Member states will be required to carry out periodic spot checks and

make results publicly available. In addition to the existing ban on defeat devices, the new rules require OEMs to provide access to software protocols.

### **China.**

China is moving quickly and taking bold steps to tackle its pollution issues. Notable updates in 2017 include:

- Provisions to increase the break-in allowance for the conformity of production (COP) tests from 300 to 3000 km if a gasoline particulate filter (GPF) is installed.
- Major cities may adopt the regulations earlier, in 2019. The details and timing are yet to be clarified.
- There is a greater emphasis on ensuring that vehicles meet the regulation on the road.

On-board diagnostics (OBD) will be used as a primary tool for conformity of production and ensuring in-use compliance, in addition to retaining full RDE testing as needed. The Ministry of Environmental Protection (MEP) also announced a national program to measure tailpipe emissions from in-use light- and heavy-duty diesel vehicles via remote sensing [290]. The regulation is aimed at screening highemitting vehicles with respect to NO and particulate matter emissions.

### **United States**

California Air Resource Board (CARB) is focusing on in-use compliance and ensuring that these limits are met under real-world conditions. Laboratory studies done at CARB have shown higher than anticipated cold start emissions from in-use LEV II ULEV and SULEV vehicles, and there is preliminary data which suggests that intermediate cold soaks could lead to higher emissions as compared to overnight soaks [291]. Particulate matter regulations are also being phased in, requiring vehicles to emit less than 3 mg/mi nationwide by 2021, and further tightening to 1 mg/mi in California starting in 2025.

## **2.2 Car Buyers Needs/Wants**

Most methods for product development recognize that customer input is essential in developing product requirements. These customer requirements shape the early product concept stages. It is critical for developers to consider what type of customers they will be serving. Is it a customer who lives mostly within a city, or does the person commute longer distances on highways? How much cargo space is needed? Does the customer have the ability to charge an electric car at home or at work? These and many other questions derive a catalog of requirements that help developers create concepts focused toward customer groups.

The problem facing developers is that customer input through traditional market research will rarely dictate a preference for futuristic technologies. Instead, the customer describes improvements from the established product and generates wishes that could lead to a product innovation.

The Quality Function Deployment (QFD) [248] methodology (also referred to as the House of Quality (HoQ)) is a tool that is utilized to translate customer requirements into technical requirements. In addition, this tool facilitates an assessment between competitors and the firm's own product. The procedural model can be incorporated throughout the development process to maintain the so called "voice of the customer" present in design decisions at each product development stage. More details of the tool and its application will be presented in the next chapters.



The “voice of the customer” translated to the “voice of the engineer” using the QFD/HoQ (see Figure 2-19) can be very useful in making improvements to generations of product families but has to be properly applied in its scope to seek out new technologies.

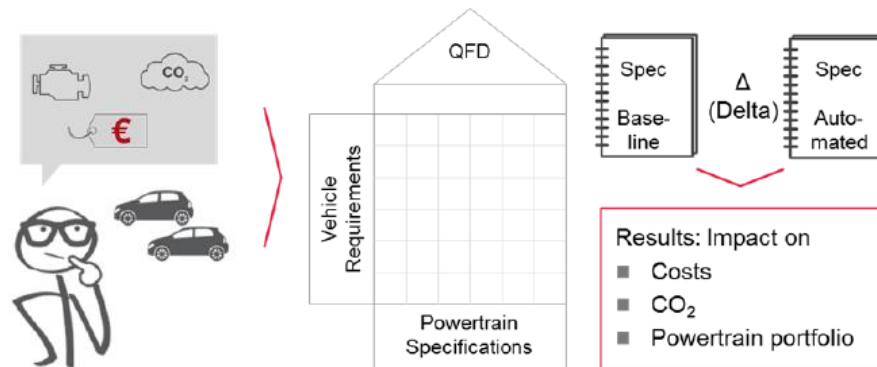


Figure 2-19 Vehicle requirements from Market survey to QFD methodology

## Identification of the Customer Needs

The auto industry uses a number of methodologies to extract customer feedback, some of which are shown in Table 2-1. The most part of these methodologies are effective to complement incremental product development innovations and most methodologies can be limited to address the initial purchase motivation of future vehicle architectures.

Table 2-1 Classic methodologies to determine future customer needs in the automotive industry from [134]

Methodology	Description
Customer Concept Clinic (Konzept-Klinik)	Selected customers satisfying the profiling requirements are invited to critique models or new car concepts
Auto Show/ Trade Fair Studies	Data is collected from auto show and trade fair visitors contemplating new car concepts or technologies to generate feedback from the market.
Customer Reviews from Market Research Studies / Virtual markets	Market Research agencies compare both subjective and objective product features that lead to purchase preferences. Data collection on particular customer and product groups are frequently collected. Virtual markets represent a new way of collecting consumer information.
Service Center Feedback	Service and Retail shops deliver feedback to developers on technical problems and special customer needs
Opinion leaders	Opinion leaders include technical press, consumer report journals and publications, celebrities and trendsetters
Benchmarking of Concept Cars and Lead User Innovations	The customer is influenced by competitors and niche player offerings in the market for new car architectures



Specific requirements for a future vehicle must take in consideration current and upcoming regulatory requirements, customer needs, competitor market offerings and the manufacturers own business strategy. An example of vehicle customer needs/wants evaluation and prioritization is presented in Table 2-2, adapted from [134]. The requirements are prioritized taking into account the end-user target. The final customer profile is a weighted average of different customer profiles (column of table). And each profiles is characterized by own preferences versus each requirement (row of table). The resulting priority is the input for the HoQ, that will be presented in the next chapters.

Table 2-2 Example of design requirements prioritization based on customer profile needs

Needs/Wants	Customer Profile Priority (0-Not Relevant, 1 - Low Priority, 2 - Priority, 3 - High Priority)								Overall Design Priority	
	Resource Conscious	Environm. Friendly	Thrifty	Trend- Setter	Driver (Sporty)	Practical Person	Inner City Customer	Outer City Customer	Score = $\Sigma (\text{Multiplier} \times \text{Priority}) / 8$	
Weight	1	3	1	1	1	3	2	3		
E-DriveUse Profile	3	3	3	2	1	2	3	3	5	High Priority
	3	3	3	2	0	0	1	2	3	Low Priority
	2	2	3	1	0	0	1	2	3	Low Priority
Performance (Low Velocity)	2	2	3	3	3	1	3	1	4	Priority
Performance (High Velocity)	1	1	1	3	3	1	1	2	3	Priority
Range	3	3	1	2	2	3	1	3	5	High Priority
Fuel Consumption & CO2 emission Standards	3	3	3	2	2	3	3	3	5	High Priority
Pollutant Emission Standards	0	3	0	0	0	0	3	2	3	Low Priority
Comfort	2	1	1	3	2	3	3	3	4	Priority
Costs	3	3	3	1	2	3	3	3	5	High Priority
Overall System Concept Quality	2	2	2	2	3	3	3	3	5	High Priority

## 2.3 Smart, Connected and Autonomous Vehicles

Driven by evolving customer behavior, regulations (e.g. "eCall") and a growing amount of connected services, vehicles are becoming more highly connected and smarter. FEV estimates that around 2027 nearly all vehicles on EU's roads are connected (see Figure 2-20).

Already today, intelligent powertrain applications exchange data with external resources to provide advanced eco-driving, predictive energy management, automated maintenance services, pay-as-you drive functionality and more. Looking forward, many additional onboard and aftermarket powertrain-related services will launch until 2030 using a mix of mobile, vehicle-to-vehicle and vehicle-to infrastructure communication.

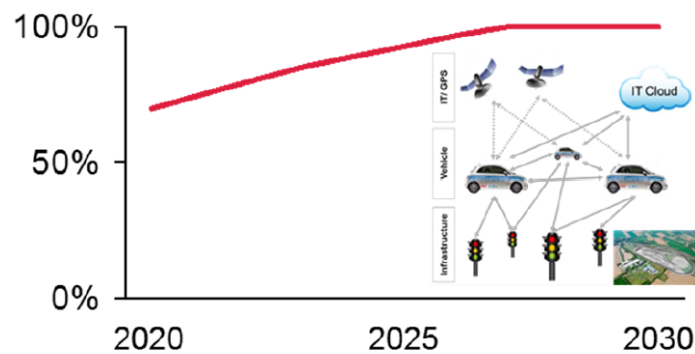


Figure 2-20 FEV forecast: connected vehicle penetration rate for EU market

FEV predicts that in 2030 about 10% of EU new vehicle sales are automated passenger vehicles according to SAE level 5 and about 85% are at SAE level 3&4 (see Figure 2-21 and Figure 2-22) [117]. On the journey to automated driving, major challenges such as refinement of prediction, decision-making algorithms, cyber security and efficient testing procedures need to be mastered.

SAE level	Name	Narrative definition	Control	Monitoring	Fallback	System capability
0	No Automation	Full-time performance by the <i>human driver</i> of all aspects of the <i>dynamic driving task</i>	Human driver	Human driver	Human driver	n/a
1	Driver Assistance	<i>Driving mode</i> -specific execution by a driver assistance system of either steering or acceleration/deceleration	Human driver and system	Human driver	Human driver	Some driving modes
2	Partial automation	The <i>driving mode</i> -specific execution by one or more driver assistance systems of both steering and acceleration/deceleration	System	Human driver	Human driver	Some driving modes
3	Conditional Automation	The <i>driving mode</i> -specific performance by an <i>automated driving system</i> of all aspects of the dynamic driving task. <i>Human driver</i> will respond appropriately to a <i>request to intervene</i>	System	System	Human driver	Some driving modes
4	High Automation	The <i>driving mode</i> -specific performance by an <i>automated driving system</i> of all aspects of the dynamic driving task	System	System	System	Some driving modes
5	Full Automation	The full-time performance by an <i>automated driving system</i> of all aspects of the <i>dynamic driving task</i> under all conditions	System	System	System	<b>All driving modes</b>

Figure 2-21 Levels of automated driving (Source: [117])

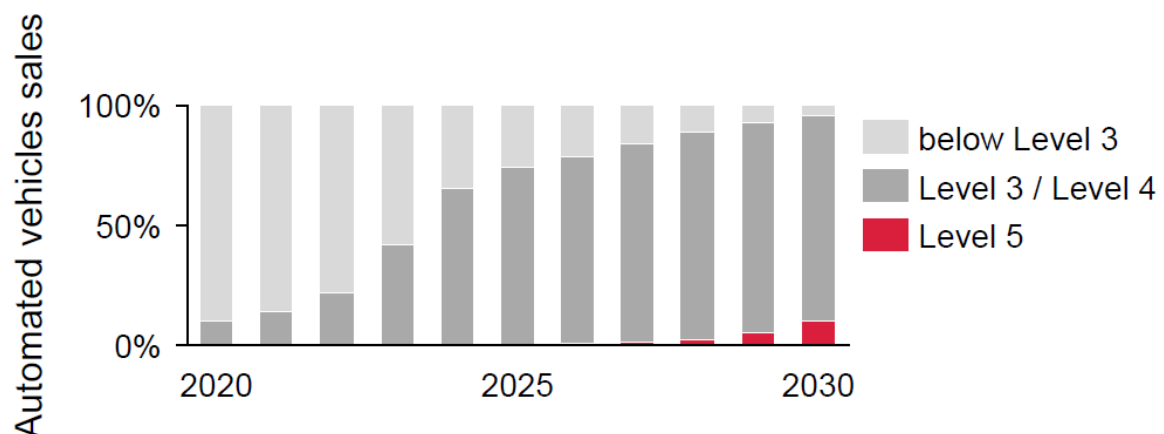


Figure 2-22 FEV forecast: automated vehicle sales in EU per SAE level

The work [117] presents an end-user survey study to evaluate the expectation in consideration of the aforementioned vehicles evolution. The market analysis shows the shifts in vehicle user needs/wants once vehicles become automated and highly connected. Survey participants had to answer how vehicle requirements and buying criteria of over several predefined characteristics change in terms of importance depending on the tuple characteristic, see Figure 2-23.

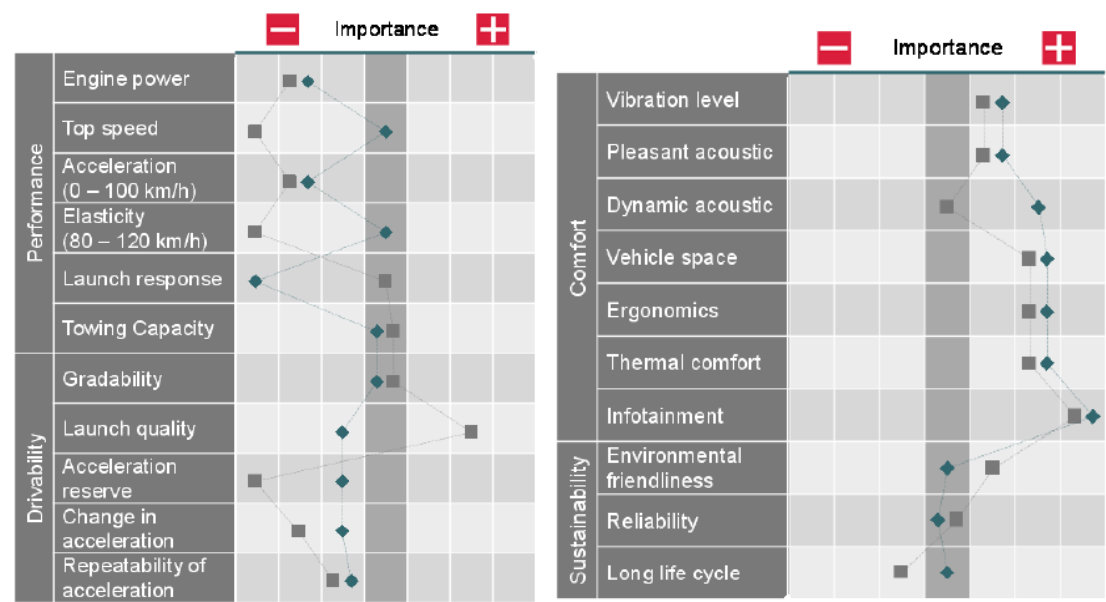


Figure 2-23 End-user requirement variation in case of Autonomous Driving for two different users:■ city driving with A-class vehicle; ♦ highway driving with C-Class vehicle (adapted from [117])

The results show that importance is significantly decreased for some requirements, in particular performance and drivability categories. In contrast to these outcomes, comfort aspects gain strongly in importance, especially the requirements infotainment, thermal comfort, vehicle space and ergonomics show a strong increase in importance.

As a consequence, in next sections the powertrain characteristics impacted by the survey results will be shown. Significant optimizations for powertrains of fully automated vehicles in terms of costs and fuel consumption are possible, depending on vehicle use.

## 2.4 The Power Generation Scenario

Focusing on European scenario, the European Commission is looking at cost-efficient ways to make the European economy more climate-friendly and less energy-consuming, to comply with 2015 Paris agreement.

Its low-carbon economy roadmap (see Figure 2-24) suggests that:

- By 2050, the EU should cut greenhouse gas emissions to 80% below 1990 levels;
- Milestones to achieve this are 40% emissions cuts by 2030 and 60% by 2040;
- All sectors need to contribute.

Action in all main sectors responsible for Europe's emissions – power generation, industry, transport, buildings, construction and agriculture – will be needed, but differences exist between sectors on the amount of reductions that can be expected.

Emissions from Transport could be reduced to more than 60% below 1990 levels by 2050 and the intermediate targets up to 2030 have been already presented in a previous section.

The Power sector has the biggest potential for cutting emissions. It can almost totally eliminate CO<sub>2</sub> emissions by 2050. Electricity could partially replace fossil fuels in transport and heating.

Electricity will come from renewable sources like wind, solar, water and biomass or other low-emission sources like nuclear power plants or fossil fuel power stations equipped with carbon capture & storage technology. This will also require strong investments in smart grids.

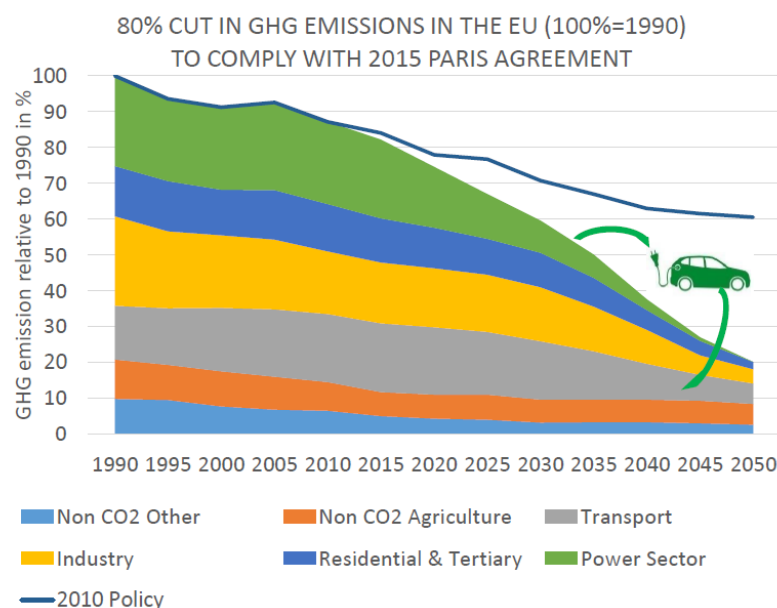


Figure 2-24 EU low-carbon economy road-map up to 2050 (source European Commission website)

The share of renewables is expected achieving at least 55% in gross final energy consumption in 2050. Renewable electricity generation systems are comprised of running water, biomass, geothermal, wind and solar energy. Wind and solar PV electricity are highly fluctuating while the others can be considered as much more stable with continuous production profiles

The fluctuating nature of the energy generated requires inevitably to store large amounts of electricity during times of excess production and to release electricity in times of production capacity shortage. These storage demands can be supplied by calculating time and power rating of the overage. The power requirements and required energy storage times (seconds to days or longer) will ultimately demand on the entire system dynamics. From the portfolio of the available energy storage options (see Figure 2-25) the most suitable option can be selected. In principle, the grid itself can be considered as a large electricity storage device, while potential users are connected. In times of insufficient grid capacity, though, additional electricity quantities cannot be fed into or via the grid.

The consequence is the necessity to implement solutions which can utilize the foreseeable increasing electricity generation capacities efficiently and economically. Supply gaps must be closed ideally by providing electricity quantities captured during times of capacity availability. Short term storages such as pumped hydro and increasingly batteries are becoming more common. Beyond about 50% renewable

electricity production, storage using Power-to-Gas (PtG) technologies will emerge as a strong addition to existing storage concepts, where the gas can be Hydrogen or Methane. The use of renewable sources for hydrogen or methane production by water electrolysis constitutes an effective linking of a clean energy economy and low carbon mobility. The use of wind power for hydrogen production has been object of many pilot projects with positive results and large scale plants are planned in next years [69]. The hydrogen transportation is the main issue of this technology.

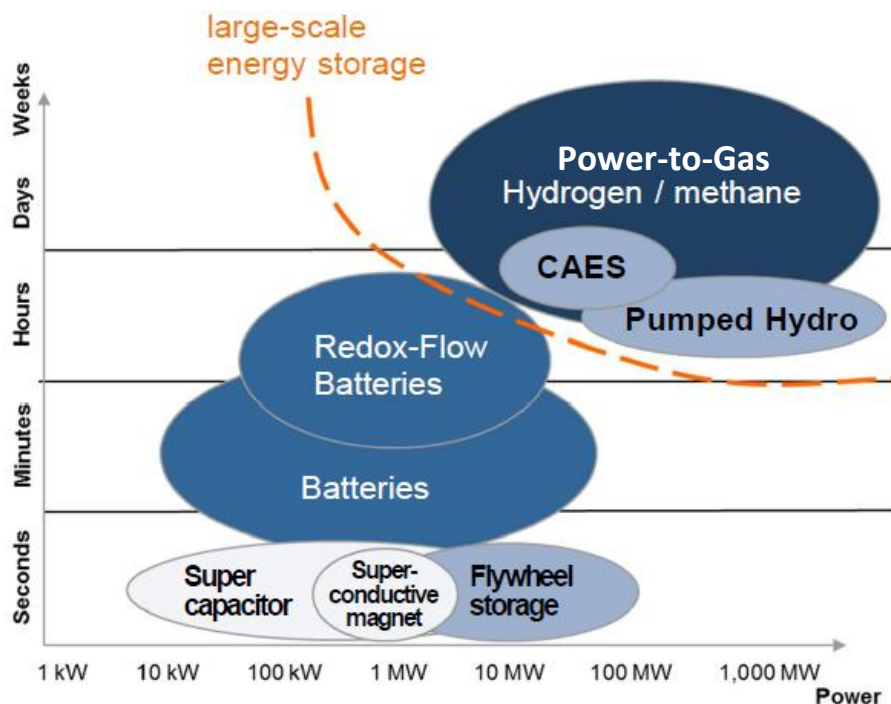


Figure 2-25 Segmentation of electrical energy storage, adapted from [256]

There are several pathways for transporting renewable energy from the point of generation to gas demand (refueling stations, stationary or backup fuel cells, and thermal power plants). Electricity could be transmitted via grid lines to local electrolyzers, but may cause additional grid strain with high current fluctuating with variable generation. A more attractive option, considering grid utilization, is large scale on-site gas production with transport by trucks or railways, and maybe even by pipelines, that for the hydrogen has to be dedicated to maintain high quality needed for the use in low temperature fuel cells.

In addition to charging infrastructure for battery electric vehicles, the gas technology provides an additional link between mobility, and electricity infrastructure. These stepwise improvements will accelerate progress towards an economically viable clean energy system.

An evolution of PtG approach is the Power-to- Liquid (PtL) process, that doesn't stop to methane production but it continues making liquid "e-fuels". These kinds of fuels can be used without any impact in current engines and have the great advantage of using current fuel distribution infrastructures. The aviation and marine transportation sectors are pushing the technology evolution of these fuels [4]. The use of wind power for eFuels production has been object of many pilot projects with positive results and large scale plants are planned in next years [69]. A focus on the eFuels is presented in the Chapter #9.

### 3.Description of Applied Methodology

The main objectives of this methodology are the definition, sizing and assessment, with a system engineering approach, of the global powertrain and its relevant sub-systems, adjusted on requirements. The methodology covers the first two phases of powertrain product development based on Systems Engineering V-Model (see steps of Figure 3-1 highlighted in red).

**Systems Engineering V-Model** – [2] The V-Model describes a methodology for the interdisciplinary development of complex systems and products. The V shape represents the two fundamental parts of the model. The left-hand side describes system deployment, whereas the right-hand side describes steps necessary in system integration and verification.

The depiction in Figure 3-1 shows an adaptation of the V-Model to the development of vehicles through the entire lifecycle of the product.

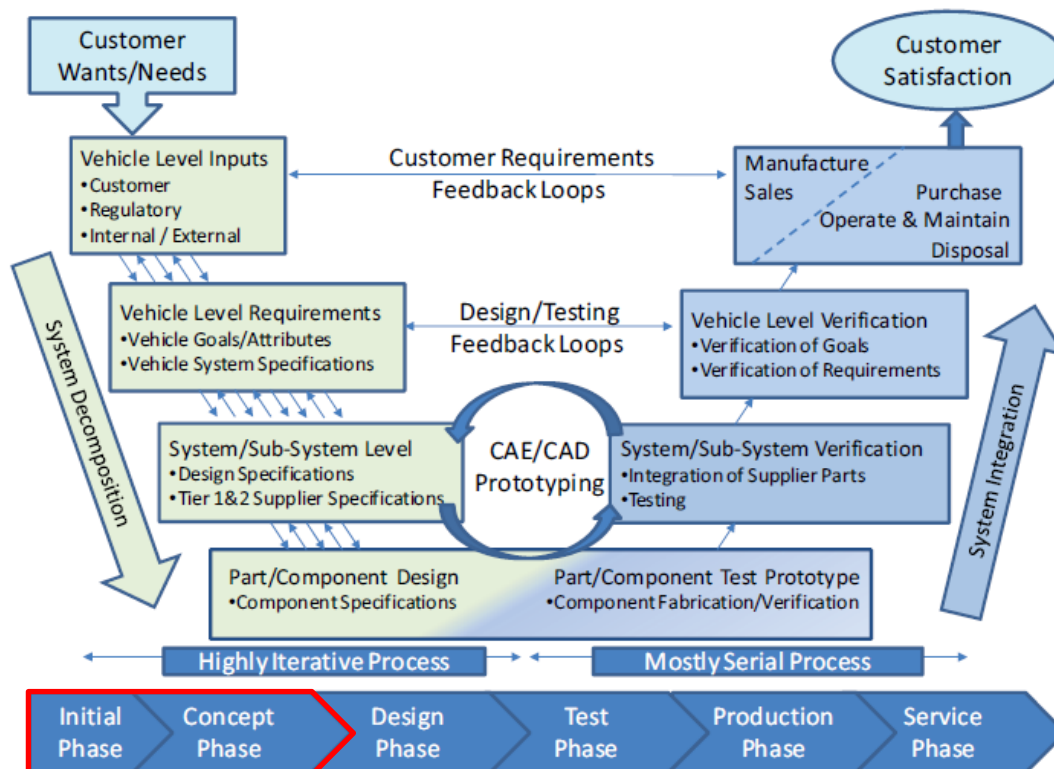


Figure 3-1 Systems Engineering V-Model to Vehicle Development

The V model starts with the customer needs and ends with customer satisfaction, implying that product/systems are built primarily for customer or user utility. The left hand side is highly iterative as the system is clarified and partitioned. The partitioning starts from gathering the vehicle level inputs from the customer, competitor's products, government regulations and the firm's own requirements. These inputs are formalized in vehicle requirements that are further broken down into vehicle sub-system requirements. Finally, the component solution search, selection and design occur at the bottom of the V-Model with the help of computer aided engineering, design models and prototyping.

Requirements develop in a cascading manner providing increasing resolution at each process step as more detailed requirement information. Likewise feasibility feedback acquired through the design causes iterations in the search for solutions as the project moves from the initial planning phase and on through the concept and design phase.

The right hand side of the V-model shows the integration and testing of the many system parts to make a functional whole. This process is mostly serial, meaning that iterations are greatly reduced. Inputs to the system verification side of the V-model come from the appropriate levels of abstraction on the left hand side. Once the component level design and prototype fabrication is worked out (bottom of the V-Model), the testing phase begins starting at the component level, working its way through assemblies of components, into the subsystem verification level and finally into the total vehicle verification. The production use and disposal of the vehicle is ensured at the top of the left hand side. These process steps show that the model extends throughout the lifecycle of the system or product.

The proposed methodology is necessary because the modern powertrain consists in complex systems with many sub-systems and components see Table 3-1, that means many possible solutions, with different degree of effectiveness and costs.

Table 3-1 Example of space of solutions for powertrain design

Drive Train Configuration		Conventional ICE		Serial Hybrid		Parallel Hybrid		Series-Parallel Hybrid		Power-Split Hybrid		Electric Vehicle	
Drive Train	Sub-Systems	Components											
Primary Drive	Primary Motor	Compression Ignition ICE		Spark Ignition ICE		Low Temperature ICE		Electrical Machine					
	Primary Energy Storage	Fuel Tank						Battery		Fuel Cell with Hydrogen Tank			
Secondary Drive	Secondary Motor	C.I. Engine	S.I. Engine	LTC Engine	Free Piston	Wankel	Gas Turbine	Hydraulic Motor	Electrical Machine				
	Secondary Energy Storage	Fuel Tank						Pneumatic Energy Storage	Battery	Fuell Cell with Hydrogen Tank	Electro-Mechanical Flyweel	Capacitor	
Connection to the Drive Shaft		Primary Motor			Secondary Motor					Switchover Gearbox		Transfer Gearbox	
Energy Charging system for the Main Drive Train		Liquid re-fuelling		Gas re-fuelling		Electric Plug-in Charging		Battery Electrolyte Substitution	Battery Swap Charging		Photovoltaic Solar Charging		

Especially considering an electric hybrid powertrain many alternative configurations of the drive train can exit, with different positioning and connection of the electric machines and different possible energy storage systems.



### 3.1 Methodology Steps

Following a System Engineering approach, the methodology used for the conceptual design, analysis and comparison of powertrain architectures and technologies is composed of the listed steps:

1. Evaluation and understanding of vehicle requirements, including pollution and GHG legislations, in a timeframe up to 2025 and beyond, to be considered as criteria for final assessment and selection of the solutions.
2. Identification of powertrain technical requirements, based on multi-level Quality Function Deployment (QFD), that allows the propagation of the needs by the users and the legislation constraints from the vehicle level to technical specifications at powertrain level, see Figure 3-4.
3. Quantitative definition of the technical specifications for powertrain and its main sub-systems.
4. Analysis of the powertrain architecture options, including the technologies for Internal Combustion Engines (ICEs) and Electric Traction Drive Syetms (ETDS); this phase is performed on the basis of technical literature, integrating missing data by means of powertrain and its sub-systems modelling and experimental tests on engine/vehicle.
5. Synthesis and dimensioning of key sub-systems and components.
6. Sensitive analysis versus technical specifications by means of Vehicle/Powertrain models and design refinement.
7. Evaluation of the powertrain architectures and technologies by means of Selection Matrix, using as criteria the technical features defined through the QFD.

Figure 3-2 illustrates the workflow of powertrain concept process described above.

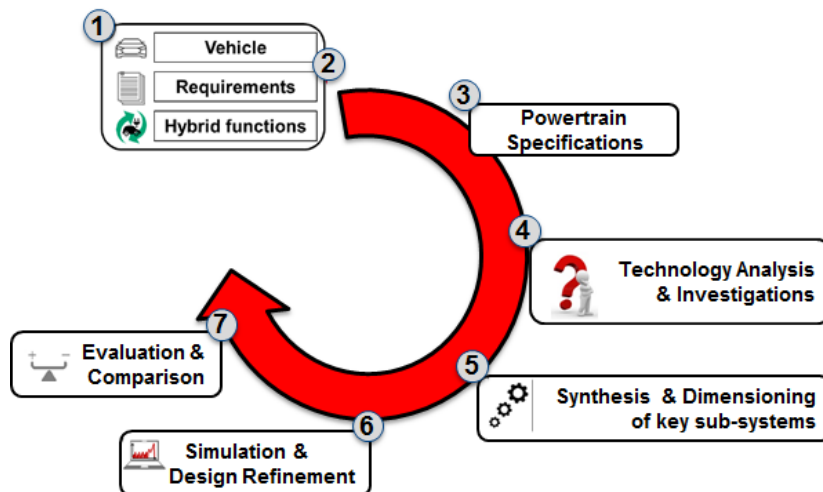


Figure 3-2 Scheme of powertrain concept process adapted from [247]



## 3.2 Methods and Tools

In the next paragraphs an overview of the main tools employed during the concept process is given.

### 3.2.1 Powertrain Quality Function Deployment and Requirement Management

The process of requirements and specification definition is supported by a multilevel QFD, that allows to translate the qualitative customer needs/wants (e.g. performance, etc.) in technical requirements for the vehicle and its subsystems, as explained in [216]. The single unit of the proposed method is the House of Quality (HoQ), see Figure 3-3, where by means of a matrix a correlation between the requirements (WHAT), on vertical axis, and technical features (HOW) is defined.

The HoQ is composed of the following “rooms” (Figure 3-3):

1. Customer attributes (CAs), the requirements; 2. Weightings of CAs; 3. Customer competitive analysis;
4. Engineering characteristics (ECs) in response to CAs; 5. Technical correlations between ECs;
6. Relationships between ECs and CAs; 7. Importance weightings of ECs; 8. Target values of ECs;
9. Technical competitiveness of ECs.

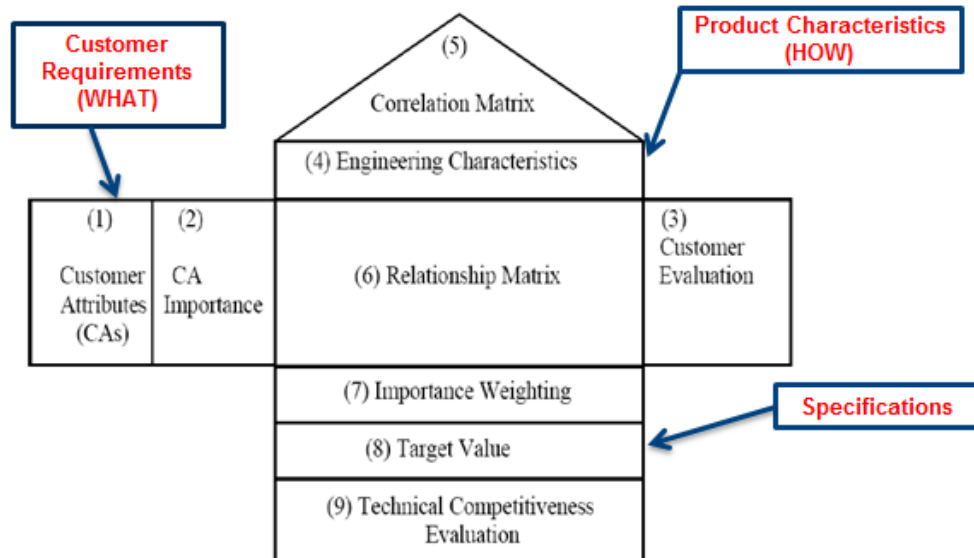


Figure 3-3 Scheme of House of Quality, adapted from [249]

In this work a modified approach is applied, considering a simplified HoQ with rooms (1), (2), (4), (6), (7), (8), but the HoQ use has been extended to different levels of vehicle and powertrain sub-systems. In this way a multi-level QFD has been obtained. This is a novel approach, only partially applied to the design of aviation gas turbine [116].

The Figure 3-4 describes the different levels of used QFD and the top-down propagation flow of the requirements and specifications. In particular in HoQ1 (level 1 of QFD), customer desires are defined and transformed in terms of vehicle requirements, allowing the definition of the global powertrain specifications (HoQ2), used for the powertrain architecture designing in a second phase.

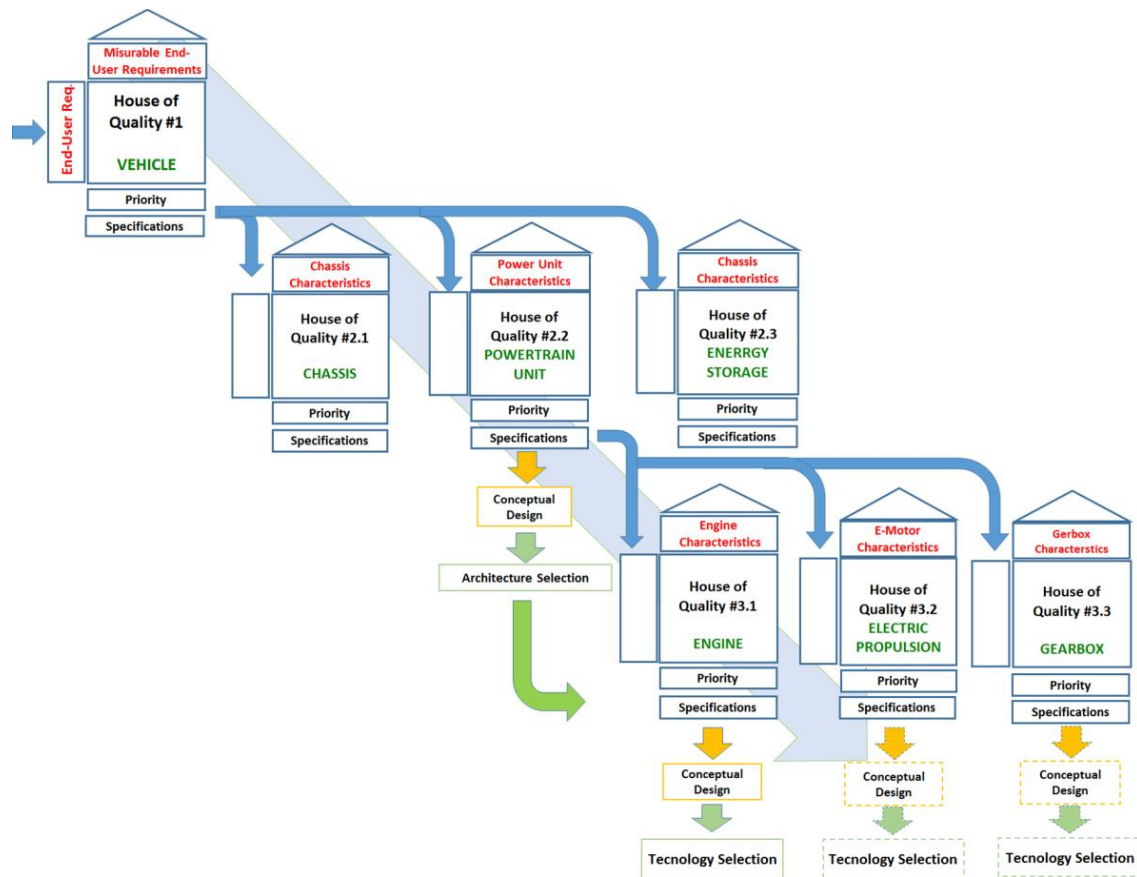


Figure 3-4 Multi-level QFD, from Needs/Wants of End-user to Powertrain Technical Characteristics, covers the first steps of V-Cycle

After the definition and ranking of technical features of powertrain in HoQ2 and subsystems in the HoQ3, the powertrain, energy storage and subsystem specifications are deduced from vehicle specifications by means of a simplified vehicle model. This phase will be detailed in the next chapter.

### 3.2.2 Simulation in the Concept Process

Known the global powertrain specifications, after technologies analysis performed by mean of literature review or experimental investigation, the more promising architectures among the possible ones are defined.

The simulation of the vehicle and powertrain is then a fundamental step to optimize and to evaluate the effectiveness of the technologies selected in the preliminary steps of conceptual design, see Figure 3-5.

Much information to evaluate new technologies relating to the powertrain can in fact be found in literature or with proper experimental tests, however, the effects due to the technology mixing and their application to different vehicle segments can be predicted only thanks to the simulation approach.

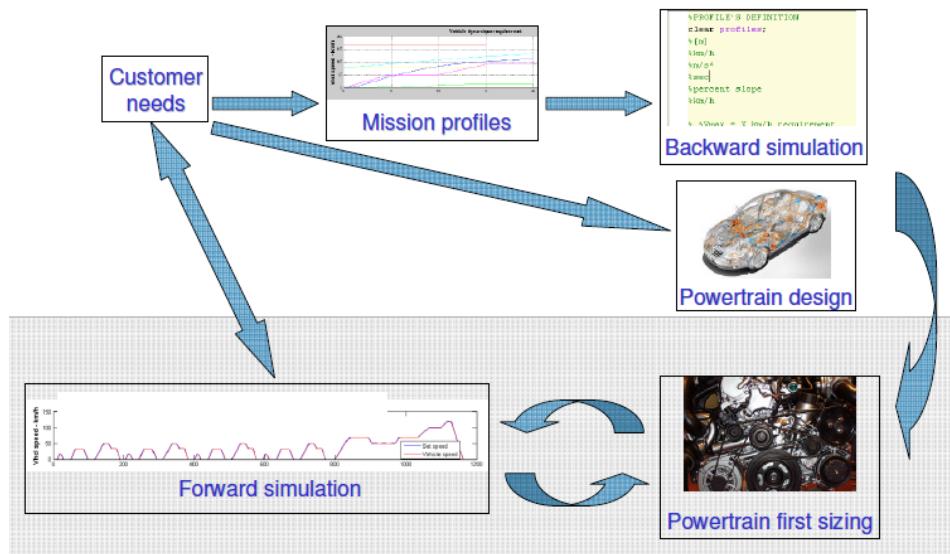


Figure 3-5 Simulation in the development process

The adopted models must be at the same time adequately accurate and fast, to carry out evaluations on long driving profiles and to be used for system optimization. Chapter #10 will present the models used in this study.

For every technically suitable configuration simulations by means of a Vehicle-Powertrain model can be performed considering different driving cycles, with aim to optimize and assess the performances and fuel consumption results.

Furthermore the configurations can be analyzed in regard of technical effects and parameter sensitivities. Beside the variation of parameters, the process of Powertrain Synthesis includes the systematic variation of characteristic for powertrain components. Already in the concept phase of development, the synthetic map approach allows the investigation of sensitivities for parameters and technologies regarding criteria like CO<sub>2</sub>-emissions, driving performance and powertrain costs. The objective assessment of various architectures and technologies variants is a key feature of Powertrain Synthesis. For the investigation of a wide spectrum of technologies and parameters, the generation of consumption maps is achieved by the combination of fast-running algorithms with fully calibrated and predictive 1-D models, as already introduced in [216]. These models are calibrated with test bench measurements of existing engines and make it possible to predict fuel consumption maps on the basis of geometric parameter.

### 3.2.3 Powertrain Architecture and Technology Evaluation

One of the final steps of the concept development is the scoring and selection of the generated solutions, as highlighted in the simplified process description in Figure 3-6.

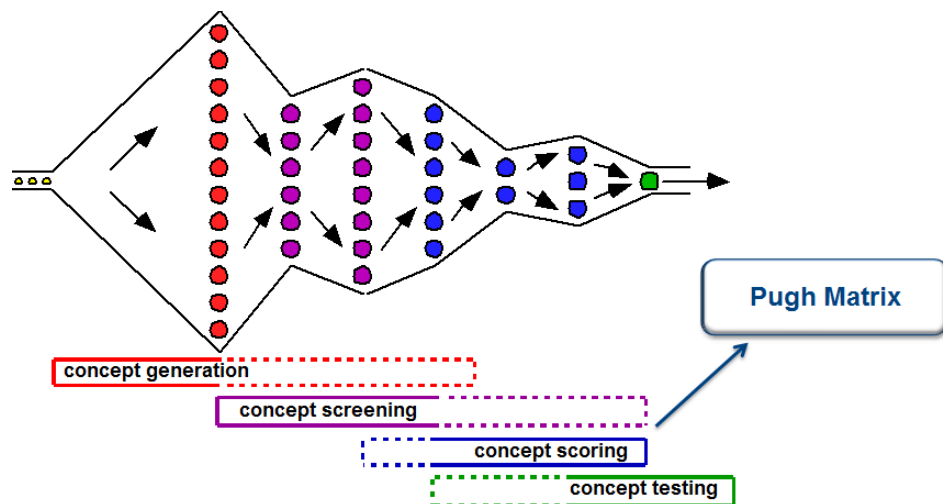


Figure 3-6 The funnel of concept definition: focus on scoring

The powertrain architectures and technologies defined with the processes and tools presented in the previous sections have to be compared in terms of fulfillment of the design criteria and priorities coming from HoQ1 and HoQ2.2 respectively, taking into account not only the GHG emission or fuel consumption but also other technical characteristics linked to the purchase reasons of the vehicle (e.g. performance, fun to drive, etc.). In addition to the individual technologies, some interesting combinations among them and some powertrain architectures can be considered. The comparison was made with a selection matrix (Pugh Matrix) shown in the following figure.

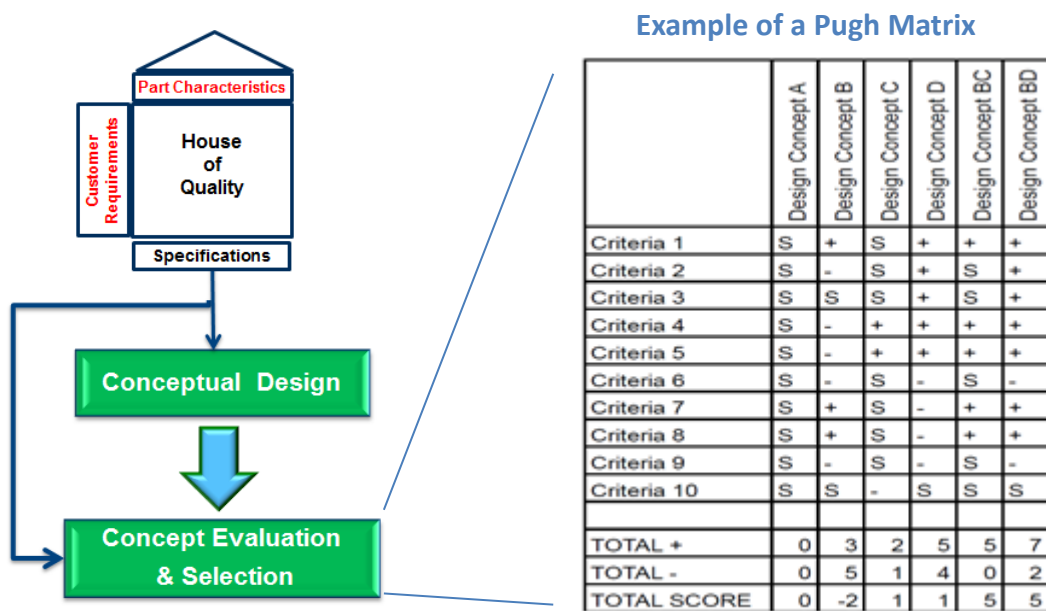


Figure 3-7 Technology selection process and Pugh Matrix structure

The values shown in the matrix depend on the technology or architectures effectiveness in satisfying the different design criteria. In the lower part of the matrix, the technology ranking can be found. The ranking expresses the effectiveness of the technology *Requirement Effectiveness* defined with following equation

$$Requirement\ Effectiveness = \frac{\sum_1^n W_i \cdot S_i}{\sum_1^n W_i \cdot S_{max}} \cdot 100 \quad (3.1)$$

where  $W_i$  is the priority [0÷100] of the technical requirements, coming from HoQ,  $S_i$  is the satisfaction degree of technical requirement by the considered technology and  $S_{max}$  the maximum value of  $S_i$ .

However, another essential aspect is the Value Analysis of the technology or architecture, defined as benefit/cost ratio, where the benefit is weighted by means of the costs defined after the powertrain architecture definition and subsystem sizing.

The parameter *Technology Value Ratio* describes the relationship between the satisfaction of the requirements (benefits) and the use of resources (costs), according to the equation:

$$Technology\ Value\ Ratio = \frac{Requirement\ Effectiveness}{Cost} \quad (3.2)$$

By this procedure, the *Technology Value Ratio*, for each technology or architecture and their combinations, can be obtained. In some case the ranking based on the two parameters above mentioned is different. The *Technology Value Ratio* has typically priority for the decision of a technology implementation in the product.

## 4. Powertrain Requirement Analysis and Basic Design

The bases of every development project are the product requirements. They include and define the customer, developer and manufacturer expectations of a potential new product. The product requirements represent the basic benchmark for the solution space and the evaluation of possible products. For this purpose, the product requirements have to be defined at the beginning of the development process based on the existing data. During the development phases, the different requirements will be adjusted, substantiated and expanded. The requirements for a development project and the final product are diverse, and can lead to conflicting objectives.

Within the powertrain development, the requirements come from the desired and necessary characteristics and functionalities of the powertrain and are not solely based on customer wishes and OEM specifications. The constraints are within the individual transport mode, and society, as well as the relevant regulations, already introduced in previous chapters. In the context of the early powertrain conceptual design, the focus is on driving performance criteria, powertrain manufacturing cost and environmental sustainability based on the emission regulations and the mobility demand and habits of the customer. The Figure 4-1 illustrates the main steps of powertrain conceptual sizing process, that is not linear, but circular with refinement loops.

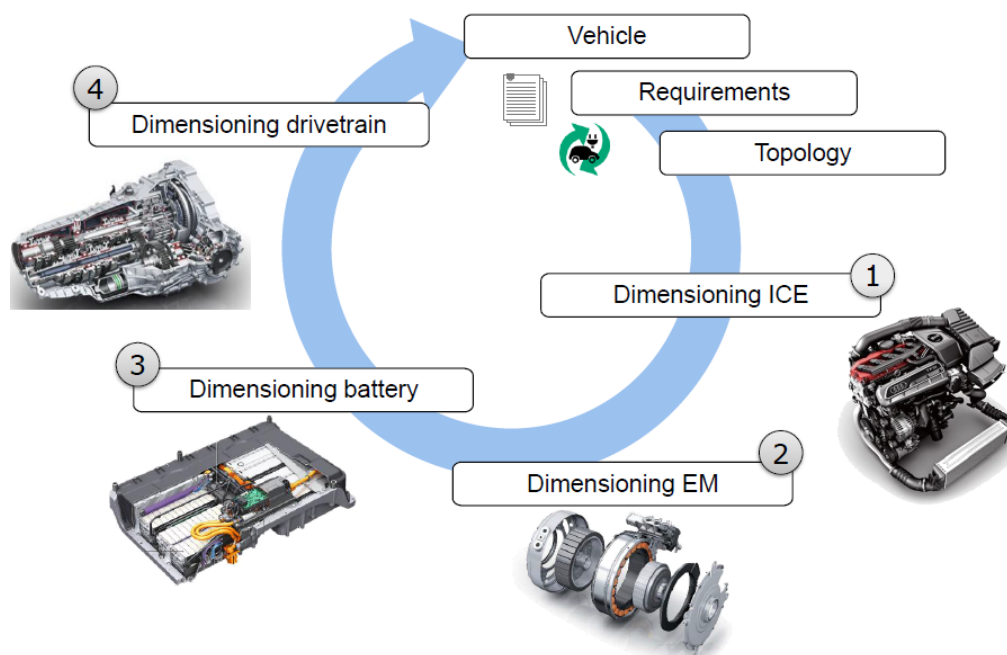


Figure 4-1 Conceptual sizing process of a Powertrain

In the next paragraphs the deployment of vehicle and powertrain requirements is described and a quantitative methodology to define the specifications of an electric hybrid powertrain is presented.

## 4.1 Deployment of Vehicle and Powertrain Requirements

The vehicle and powertrain requirements can be classified into three categories:

- explicit customer and societal requirements;
- legislative requirements, for instance CO<sub>2</sub> and pollutant emissions, characterized by combined emissions;
- boundary constraints.

The functionalities of vehicle and drivetrain have to be ensured in all possible scenarios, depending on the different markets. This includes especially comfort attributes, which can have a great impact on the energy converters and energy storage systems.

Legislation requirements are clearly of great importance because vehicle needs to fulfill them to be saleable. They are not explicitly considered by the user although their impact on customer's choice is becoming greater, due to the driving bans imposed in many cities to the vehicles complying with old legislations.

Before the conceptual phase of a development program can be started, it is essential to fully understand the requirements or needs/wants, which is referred to as the voice of customer (VOC), the standards and the manufacturer. In Chapter #2.2 we have seen the methodology for end-user desires collections and prioritization. As it has been introduced, the QFD is a tool to create a systematic approach to transfer the needs/wants (WHATs) into technical features (HOWs). Another main aspect of QFD is the improved communication resulting from the use of a common language between all involved organizations.

The final results of this methodology are summarized in technical specifications with a detailed description of all major powertrain subsystems. As introduced in the Chapter #3, a multilevel approach is defined and applied during this study (Figure 4-2): the Level-1 is related to the Vehicle, the Level 2 to the vehicle sub-systems, including the powertrain and Level 3 to the powertrain sub-systems (e.g. ICE, Transmission, etc.). Specifically, needs/wants are evaluated by the users at the vehicle high level, and propagated until the powertrain level is reached, where engine, electric motor and other powertrain components are considered. A brief illustration of the process and its application to powertrain technologies analysis was already given in [216].

Table 4-1 shows the House of Quality 1 for the vehicle. On the left side of HoQ1, the WHATs are listed to identify the requirements, expressed in qualitative way, with their rated importance, typically obtained from market research and analysis [216,227, 228]. The priority of User's desires and regulations is measured with a number (1-low, 7-high). On the top the vertical list is the HOWs, they represents the measurable technical features of the vehicle to fulfill the qualitative requirements. The relationship between the needs/wants and technical features indicates how they are working with each other, described as number rate between 1÷9.

Specifically, in HoQ1 (house of quality, level 1), driver's needs are evaluated in an objective way by means of engineering variables. For instance, the demand for high performances can be objectified by the maximum speed of vehicle, its acceleration (the time from 0 to 100 km/h) and so on.

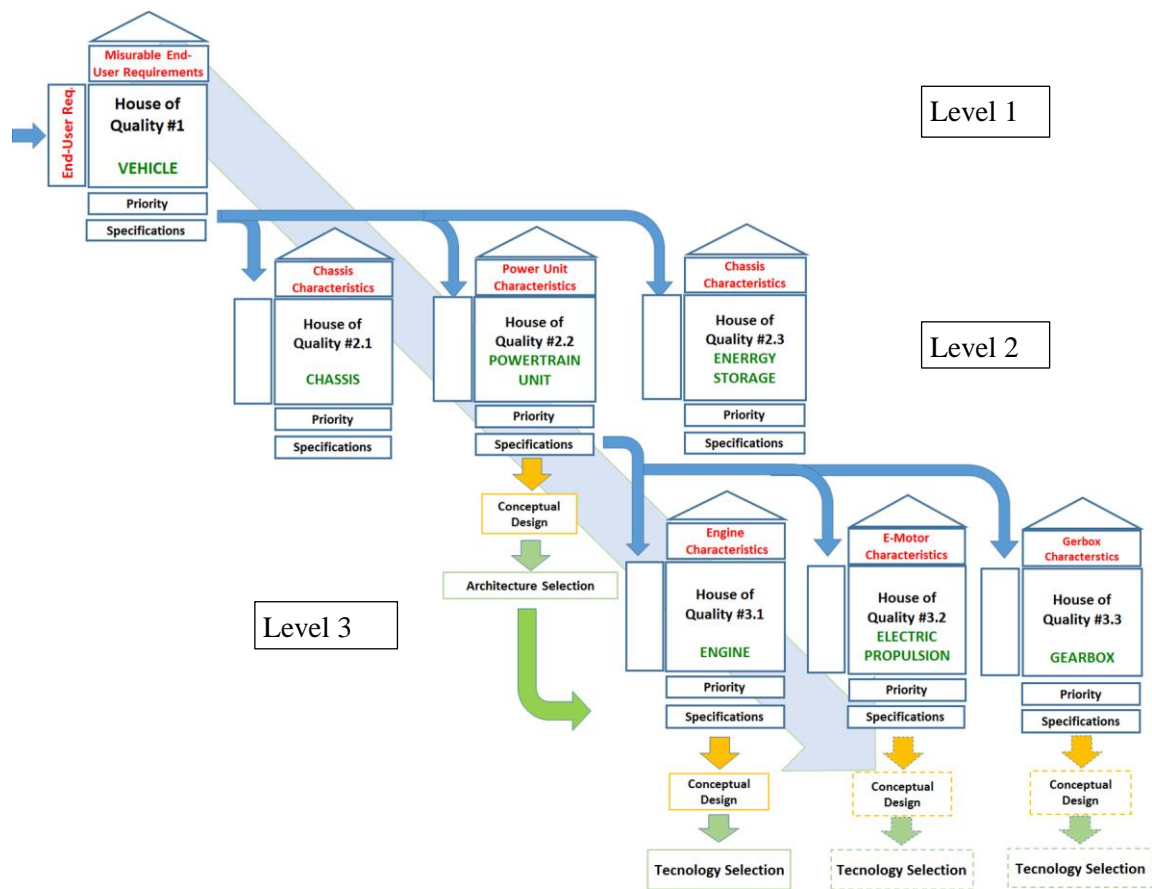


Figure 4-2 Multilevel QFD: User and Standard requirements deployment to technical features of Vehicle and Powertrain sub-systems

Table 4-1 shows the measurable requirements, which, in turn, represent the inputs for the second level, coming from regulation or driver's point of view.

The technical vehicle specifications, the columns of HoQ1, can be simplified as reported in Table 4-2, for each of them a target has to be assumed. For the application in the next chapters, this compact form will be used. In addition to prioritization for human driving vehicle, the priorities for the autonomous vehicle are considered, taking into account the considerations presented in Chapter #2.3.

Legislation requirements are clearly of great importance, because vehicle needs to fulfill them to be saleable. As already explained, they are not explicitly considered by the user, although their impact on customer's choice is becoming greater.

In case of autonomous vehicle, the requirements related to performances (such as vehicle speed or acceleration time) become less important. The opposite is true for those related to comfort, such as NVH, torque regularity, vibration. However, the constraints on CO<sub>2</sub> and pollutant emissions remain at high priority and are the main driver of the technological change requested to new vehicles and powertrains.



Table 4-1 Example of HoQ1

			VEHICLE TECHNICAL FEATURES																																	
			1	2	3	4	5	6	7	8	9	10	11	12	13	14	15	16	17	18	19	20	21	22	23	24	25	26	27	28	29	30	31			
Misurable End-User Requirements  HoQ 1			→ Noise Emission	→ Accel.Time 0 ->100 km/h	→ Accel.Time 80 ->120 km/h (elasticity)	→ Top Vehicle Speed	→ Max Amplitude of Jerking Oscillation	→ Accel.Time 0 ->50 km/h	→ Gradability	→ Time w/o acceleration during load request	→ Traction Control Response Time	→ Vehicle Speed Control Response Time	→ Vehicle Speed Control Accuracy	→ Cabin Comfort Response Time	→ Max Ambient Temperature for Cabin Comfort	→ Fuel Consumption (WLTC, NEDC)	→ Energy Refilling Autonomy	→ Re-fuelling Time	→ CO2 Tile Pipe (WLTC, RDE)	→ NOx Tile Pipe (WLTC, RDE)	→ HC Tile Pipe (WLTC, RDE)	→ CO Tile Pipe (WLTC, RDE)	→ PM Tile Pipe (WLTC, RDE)	→ PN Tile Pipe (WLTC, RDE)	→ Millage w/o Failure	→ Easy troubleshooting (Time to identify failure)	→ Easy serviceability (time to solve the problem)	→ Maintenance Cost per year	→ Maintenance Interval	→ Breaking Distance at 50 Km/h	→ Extra-Torque Recovery Time	→ Tempo di percorrenza su slalom normale, con pesi e ingombri differenti	→ Vehicle Weight/Size			
			→ [db]	→ [s]	→ [s]	→ [km/h]	→ [rpm]	→ [s]	→ [s]	→ [%]	→ [ms]	→ [ms]	→ [s]	→ [km/h]	→ [s]	→ [°C]	→ [L/100 km/h]	→ [km]	→ [min]	→ [g/km]	→ [mg/km]	→ [mg/km]	→ [mg/km]	→ [mg/km]	→ [mg/km]	→ [1000 Km]	→ [min]	→ [min]	→ [Euro]	→ [y or 1000 km]	→ [m]	→ [ms]	→ [s]	→ [kg]		
			E 1	High Performance	3	9	9	9	9	9	3	9	9	9	9	9	5	5	9	9	5	5	5	5	9	9	9					1	9	1	9	9
			E 2	High Comfort	4	3	9	9	9	9	9	9	1	9	9	9	9	9	9	9	9	9	9	9	9	3	3					3	1	3	3	3
			E 3	High Fuel Economy	4	3	3	3	3	3	3	3	3	3	3	3	5	9	9	9	9	9	9	9	3	3					3	5	5	5	5	
			I 4	Low CO2	7	3	3	3	3	3	3	3	3	3	3	3	5	9	9	9	9	9	9	9	1	1	1					3				9
			I 5	Low Pollution (EU6d/EU7 regulation)	7	3	3	9									5	9	9	9	9	9	9	9	9	9	3								3	
			I 6	High Relaiable	4	1											5	9									9	1								
			E 7	Easy to Repair	3	3											3	3										9	1							
E 8	High Safety	7	3	3	3									1	1										1	9					9	9	9	3		
E 9	Easy to use	4		1										3	5										9	1					5			9		
SPEC Target																																				
Technical Importance Rating			58	114	142	144	36	83	70	36	98	95	95	177	177	171	162	162	177	157	157	157	145	145	100	38	63	13	187	134	78	142	180			
Importance Relative Weight [0-100]			15	29	37	37	9	21	18	9	25	25	25	46	46	44	42	42	46	41	41	41	37	37	26	10	16	3	48	35	20	37	47			

Table 4-2 Measurable Vehicle Requirements and Priority, reported from HoQ1

	Needs/ Requests	Measurable Needs and Request (from HoQ1, Vehicle Level)	Priority from MR		Unit
			Vehicle Controlled by Driver	Autonomous Driving	
End-User	Low Noise	1 Noise Emission Level	4	5	[dB]
	High Performance	2 Accel.Time 0 -->100 Km/h (ICE/EV)	3	2	[sec]
		3 Accel.Time 80 -->120 Km/h (elasticity)	3	2	[sec]
		4 Max Vehicle Speed (ICE/EV)	3	2	[km/h]
	High Comfort	5 Accel. Time 0 -->50 Km/h (direct transmission)	4	2	[sec]
		6 Gradability	4	2	%
		7 Time w/o acceleration during load Req.	4	5	[ms]
		8 Low Vibration	4	5	[dB]
		9 Cabin Comfort (response and ambient Temp)	4	5	[sec] [°C]
	High Reliability	10 Mileage w/o failure	4	5	[kkm]
	Easy to use	11 Energy Refilling autonomy	5	5	[km]
		12 Maintenance intervall	4	5	[kkm]
		13 Energy Refilling Time	4	4	[min]
	Low Fuel Consumption	14 Fuel Economy	4	5	[km/l]
Standards	Low Emission	15 Toxic Emission according to Standard (WLTP and RDE)	7	7	[mg/km]
		16 EOBD/OBD2 compliance	7	7	[mg/km]
		17 CO2 according to Standard (NDEC)	7	7	[g/km]
	Safety	18 Mileage w/o critical event	7	7	[km]

The priorities and requirements targets in Table 4-1 and Table 4-2 depend on the vehicle segments as described in the Chapter #2.2 and [216,227,228], legislation standards and the manufacturer position among the competitors. Moreover, it is important to underline that costs are not considered here. The reason is that cost is one of the main requirements for the end-user and its weight would not be enough important if considered at this level. It instead the cost requirement will be considered by means of the *Technology Value Ratio*, as defined in the Chapter # 3.2.3.

## 4.2 Introduction to Hybrid Powertrain Architectures

Hybrid electric vehicle architectures are composed of two systems, a fuel (1) and an electric (2) power system. Figure 4-3 shows a generic representation of possible hybrid vehicle system configurations. In principle, parallel hybrid powertrain systems refer to additive systems that combine both drives, whereas the series hybrid powertrain system works in a sequential manner having the fuel based powertrain provide power to the electric powertrain, as seen in Figure 4-3 depicted by the red arrow path. The energy load refers to the energy needed in propelling the vehicle. The illustration allows for different operation energy flows based on the electrical and fuel based power systems. Vehicles that can mix features of both parallel and series hybrid operating modes are referred to as combined hybrid systems. Combined hybrid vehicles may either split the energy from the fuel converter into the series and parallel hybrid energy paths

simultaneously as in the case of “power split” hybrids. They may also have a distinct switch that allows for only parallel or series drives at once.

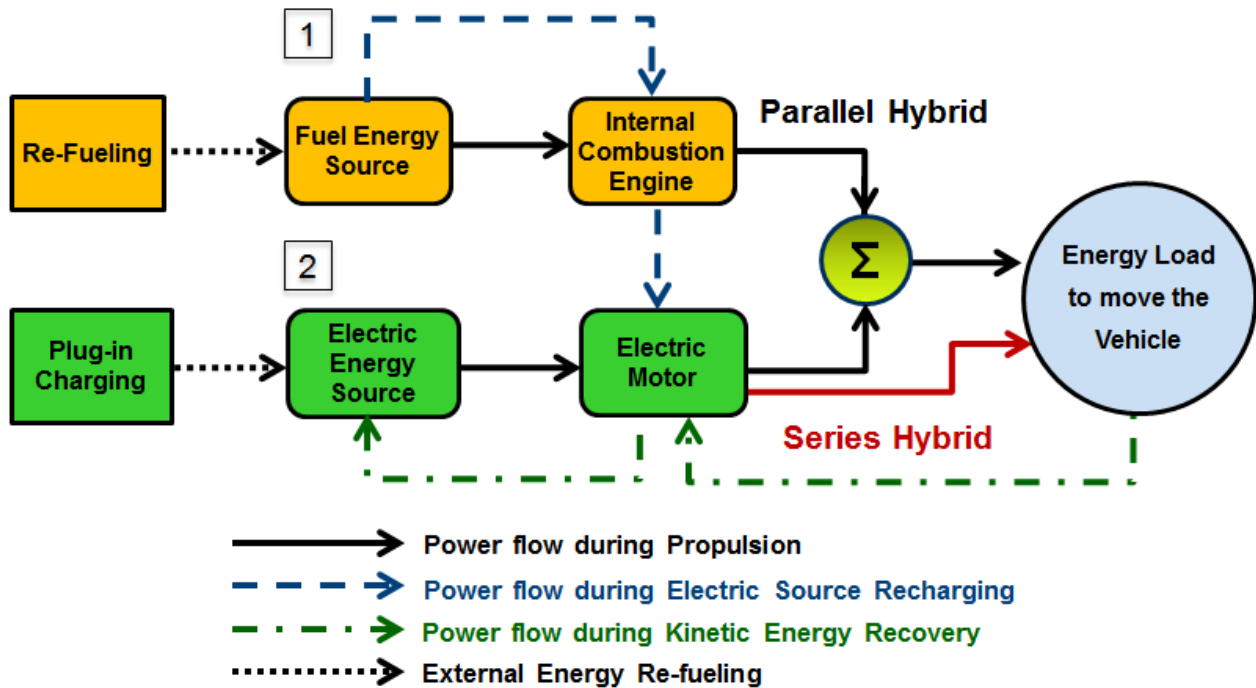


Figure 4-3 Principle scheme and power flows of a hybrid electric powertrain

The electric hybrid powertrain architectures can be described also in a two dimensional solution space of electrical driving range and degree of electrification as depicted in. The first dimension entails the electric distance the car can achieve with the electrical propulsion system alone, whereas the Degree of Electrification (DoE) is determined by the ratio of the cumulative peak electric motor power to the maximum combined electric and engine power, according to the following expression:

$$DoE = \frac{P_{peak,elect}}{P_{peak,elect} + P_{max,ice}} \quad (4.1)$$

A DoE equal to zero describes a conventional internal combustion engine vehicle with no electric propulsion system, whereas a DoE of one describes a battery electric vehicle with no internal combustion engine installed.

### 4.3 Functions of Electric Hybrid Vehicles

Some vehicle functions characterize electric hybrid powertrains and they are value added of electric hybrid systems for the customer. These functions pertain directly to the various operating modes presenting in Figure 4-3 and are explained briefly in this section. The main functions include:

- engine start & stop;

- sailing;
- regenerative braking;
- power boost;
- electric driving;
- battery charging by engine;
- torque gap filling during gear shifts;
- all wheel driving;
- torque vectoring;
- external battery charging.

The listed functions are briefly discussed below.

**Engine Start & Stop** – The engine start-stop function is a basic function found in all hybrid vehicle concepts. As soon as the hybrid control system senses that the vehicle will come to a complete stop, for example at a traffic light, the engine will shut off and be prevented from idling. The engine is restarted by means of an electrical motor or starter-generator as soon as there is a power requirement that merits it to start again. In micro hybrid systems that do not offer electric driving, the automatic start stop feature is able to start the engine and have it available for acceleration in less than a second. The driver's signal to start the engine is normally depressing the clutch for manual transmission cars or releasing the brake for automatic transmission cars. For architectures that have electric driving capability, the transition from rest to starting the engine can be delayed by using the electric driving mode as a first means of propulsion before starting the engine for additional power.

**Sailing** – The “sailing” function is somewhat trivial but never the less useful in optimizing a hybrid control strategy. The function refers to the decoupling of both the engine and the electric system from the wheels and using the force of gravity or the inertia to move the vehicle without friction losses of powertrain loads. Conventional vehicles can glide when placed in neutral during downhill operation. Hybrids however, must have the ability to rapidly connect the appropriate powertrain that best suits the driving situation moving in and out of a gliding operating environment.

**Regenerative Braking** – The term regenerative braking refers to the capturing of braking energy that would normally be lost to friction and heat in conventional car systems. It is most relevant function to achieve higher fuel economy and lower CO<sub>2</sub> emissions. Brake energy recuperation is achieved by setting the electric traction motor in a generative mode that serves as a counter force to the vehicle direction of movement. The energy obtained through regenerative braking can be directly stored in the traction battery and later used for boosting, electric driving or powering the electrical system components.

The use of electric motors as brakes could be sufficient for most braking situations. However, redundant friction braking systems are still required for safety purposes. Hybrids with enough power systems display a regenerative braking capability that can prolong the life of traditional friction brakes as an added benefit to the customer. As presented in Chapter #4.5.6, regenerative braking is limited by the battery system and motor ability to allow for impulse power storage in short time scales. Super capacitors have been proven to be well suited for regenerative braking in the case of micro and mild hybrid systems, where 2-3 seconds of high power inputs and outputs are used in charging and discharging from the capacitor device.

**Power Boost** – When the driver's situation requires excess acceleration power beyond what the combustion engine can deliver the electric motors provide additional torque to the wheels known as

boosting. Power boosting situations also include driving on inclines or towing use cases. In this mode, the battery charge is depleted and delivered through the electric motors as an additional source power.

Boosting is particularly effective in improving car acceleration specifications (e.g. 0-100km). Figure 4-4 shows that the electric motor delivers the highest torque starting from rest and low RPM values (0-900 RPMs), whereas the typical otto-cycle combustion engine achieves maximum power at higher RPM values (2000-2500 RPMs). In a typical hybrid car the resulting system performance is enhanced when accelerating from rest by initially using the torque that the electric motor supplies to the drive train.

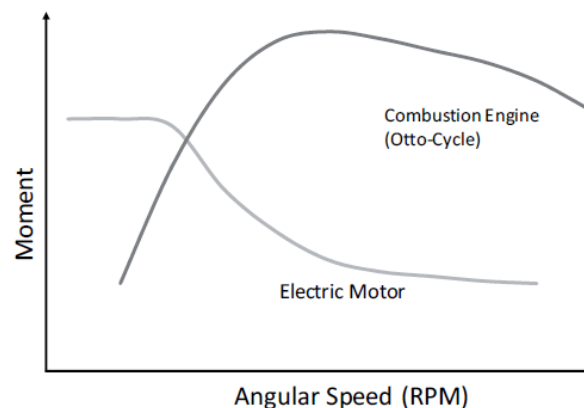


Figure 4-4 Example of Torque vs. Transmission Speed for an electric motor and combustion engine; Boosting function allows for additional torque for acceleration, especially when starting

**Electric Driving** – Electric driving is performed by using electric energy stored in the traction battery to power the propulsion motor that powers the wheels. During the electric driving mode, the combustion engine is decoupled from the powertrain. It is either shut-off or used to generate electric power. Electric driving is limited by the energy availability of the electrical storage system.

**Battery Charging by Engine** – Based on energy management logics the ICE is turned on to recharging the electric battery. In case of parallel hybrid powertrain the battery charging can be performed by the engine with the contemporary propulsion. In serial hybrid the engine is used only to recharge the battery with the aim to extend the electric traction operation. The battery energy management can be carried out in the following main modes: charge-depleting, charge-sustaining and blended operations.

Charge-depleting refers to a mode of vehicle operation that is dependent on the energy from the battery pack and is typical of pure electric vehicles. In charge-sustaining the battery state of charge (SOC) is maintained according to logics of energy management that alternate electric propulsion, engine propulsion and battery recharging modes, with the contemporary aim of minimizing fuel consumption. In case of plug-in hybrids blended charging modes are used. More details of battery energy management will be presented in Chapter #11.2.

**Torque Gap Filling during Gear Shift** - A typical issue of an Automated Manual Transmission (AMT) is the absence of traction during gear shifting, that is consequence of discomfort for the driver. The availability of an electric motor, positioned in the driveline downstream the gearbox (see P3 architecture in Chapter #5.2 ) or an electric driven axle (P4 architecture), allows to overcome the drawback. In this way the comfort of an AMT is comparable with other more expensive transmission systems (e.g. DCT and AT). The disadvantage of this function is the electric energy consumption, with negative impact on fuel consumption and electric autonomy.

**All Wheel Drive (AWD)** - By means of an axle electrification (see P4 architecture in in Chapter #5.2 ) is possible to implement the four wheels driving, without any changes on the conventional front/rear wheel drive powertrain of the vehicle. In this case the function is named e-AWD.

**Torque Vectoring** - Torque Vectoring (TV) is the ability to vary the torque delivered to each wheel. This function allows for the wheels to grip the road for better launch and handling. The TV function is typically performed by means of a mechanical differential on the same axle and a torque splitter between the front and rear axles, in case of AWD. These mechanical devices are electronic controlled in recent applications. The use of an electric driven axle to implement an AWD vehicle makes the TV function available too.

**External Battery Charging** – External battery charging differentiates plug-in hybrid concepts from all other hybrid vehicle concepts. In addition to the typical hybrid components, a battery charging unit can be added to the car with the possibility to plug into an external electrical grid. The possibilities of connecting hybrid and electric cars to the electrical grid opens up possibilities for night time charging when electricity is cheapest and the electric load capacity of local power stations are at their lowest level. Vehicle to grid studies within electric mobility research are complementary areas of study that have garnered recent attention.

## 4.4 Deployment of Powertrain Requirements

In the level two of QFD, in HoQ2.2, the requirements and priorities for the powertrain, described in Table 4-2, are mapped in Table 4-3 with its technical characteristics, with appropriate specifications in order to effectively satisfy the requirements.

Table 4-3 Example of House of Quality2.2

		HoQ2.2 Powertrain Level																												
Need/ Requests	Measurable Needs and Request (from HoQ1, Vehicle Level)	Priority	Unit	Traction Power Generation & Control										Emissions Control					HVAC			Energy Storage					KER	SW		
				Vehicle Controlled by Driver										Autonomous Driving					eGen.			Self-diagnosis								
				1	2	3	4	5	6	7	8	9	10	11	12	13	14	15	16	17	18	19	20	21	22	23			24	25
		[dB]	[e]	[Nm]	[rpm]	[kW]	[rpm]	[min]	[dB]	[%]	[%]	[g/kWh]	[g/kWh]	[g/kWh]	[g/kWh]	[kW]	[kW]	[kW]	[%]	[J]	[min]	[h]	[min]	[min]	[min]	[min]	[J]	[min]		
End-User	Low Noise	1	→	→	→	→	→	→	→	→	→	→	→	→	→	→	→	→	→	→	→	→	→	→	→	→	→	→		
		2	→	→	→	→	→	→	→	→	→	→	→	→	→	→	→	→	→	→	→	→	→	→	→	→	→	→		
	High Performance	3	→	→	→	→	→	→	→	→	→	→	→	→	→	→	→	→	→	→	→	→	→	→	→	→	→	→		
		4	→	→	→	→	→	→	→	→	→	→	→	→	→	→	→	→	→	→	→	→	→	→	→	→	→	→		
		5	→	→	→	→	→	→	→	→	→	→	→	→	→	→	→	→	→	→	→	→	→	→	→	→	→	→		
End-User	High Comfort	6	→	→	→	→	→	→	→	→	→	→	→	→	→	→	→	→	→	→	→	→	→	→	→	→	→	→		
		7	→	→	→	→	→	→	→	→	→	→	→	→	→	→	→	→	→	→	→	→	→	→	→	→	→	→		
		8	→	→	→	→	→	→	→	→	→	→	→	→	→	→	→	→	→	→	→	→	→	→	→	→	→	→		
	High Reliability	9	→	→	→	→	→	→	→	→	→	→	→	→	→	→	→	→	→	→	→	→	→	→	→	→	→	→		
		10	→	→	→	→	→	→	→	→	→	→	→	→	→	→	→	→	→	→	→	→	→	→	→	→	→	→		
End-User	Easy to use	11	→	→	→	→	→	→	→	→	→	→	→	→	→	→	→	→	→	→	→	→	→	→	→	→	→	→		
		12	→	→	→	→	→	→	→	→	→	→	→	→	→	→	→	→	→	→	→	→	→	→	→	→	→	→		
	Low Fuel Consumption	13	→	→	→	→	→	→	→	→	→	→	→	→	→	→	→	→	→	→	→	→	→	→	→	→	→	→		
		14	→	→	→	→	→	→	→	→	→	→	→	→	→	→	→	→	→	→	→	→	→	→	→	→	→	→		
		15	→	→	→	→	→	→	→	→	→	→	→	→	→	→	→	→	→	→	→	→	→	→	→	→	→	→		
Standards	Low Emission	16	→	→	→	→	→	→	→	→	→	→	→	→	→	→	→	→	→	→	→	→	→	→	→	→	→	→		
		17	→	→	→	→	→	→	→	→	→	→	→	→	→	→	→	→	→	→	→	→	→	→	→	→	→	→		
		18	→	→	→	→	→	→	→	→	→	→	→	→	→	→	→	→	→	→	→	→	→	→	→	→	→	→		
Safety			10	14	19	16	20	10	17	12	24	28	13	15	14	22	4	28	20	14	14	14	15	15	19	21	22	5	37	
Powertrain characteristic ranking - Human driving			13	9	14	9	13	11	15	16	22	23	16	17	16	19	5	23	18	12	12	12	15	17	17	22	25	21	8	34

The Table 4-4 reports the technical parameters in the column of Table 4-3, for an easy reading. The priority specifications are reported in case of driver or driverless vehicle. The relevance of the different characteristics in case of human driving is highlighted by the green histogram on the left. Among all, the powertrain weight, including the contribution of the energy storage system, represents the most important factor in addition to the energy generation efficiency for the propulsion. Among the technical characteristics with higher ranking, it must be noted that the energy refilling time is critical for pure electric powertrains but not for hybrid ones. Clearly, emissions still have a crucial role. In case of vehicle with autonomous driving, the powertrain characteristics related to the performances are less important, whereas the comfort features are more relevant. This is true in case of the vehicles being used exclusively in driverless mode.

Table 4-4 Powertrain Technical Characteristics and relevance from HoQ2.2

Relevance histogram (HD)	Powertrain Characteristics (from HoQ2.2)	Relevance (0÷100)		Unit
		Human Driving	Auton. Driving	
1	Powertrain Noise Level	10	13	[dB]
2	Powertrain Time to Full Power	14	9	[s]
3	Low-end Torque (at wheel)	19	14	[Nm]
4	Speed Range of High Torque	16	9	[rpm]
5	Maximum Power	20	13	[kW]
6	Max Amplitude of Jerking Oscillation	10	11	[rpm]
7	Time w/o Torque delivery during load Req.	17	15	[ms]
8	Powertrain Vibration	12	16	[dB]
9	Tank to Wheel Maximum Efficiency	24	22	[%]
10	Tank to Wheel Efficiency at part/low load	28	23	[%]
11	NOx Emission according to RDE	13	16	[g/Kwh]
12	HC/CO Emission according to RDE	15	17	[g/Kwh]
13	Soot/PN according to RDE	14	16	[PN]
14	CO2 on WLTC	22	19	[g/Kwh]
15	Heating Power	4	5	[kW]
16	Mech Power for Cooling	28	23	[kW]
17	Efficiency of Electric Power Gen.	20	18	[%]
18	Energy Storage Capacity	14	12	[J]
19	Energy Refilling Time	14	12	[min]
25	% Braking energy recovered	22	21	[%]
26	PWT Size	5	8	[Lit]
27	PWT Weight	37	34	[kg]

The reported characteristics and their targets are the inputs for the next phase of definition and selection of the powertrain architecture. In the following section a procedure to define the quantitative powertrain characteristics is presented.

## 4.5 Evaluation of Powertrain Specifications to match Vehicle Requirements

In this section the focus is on quantitative powertrain specifications of Table 4-4 deduced from the quantitative end-user requirements from Table 4-2. Solving the equation that describes the classical



vehicle longitudinal motion, it is possible to define power and torque specifications of the powertrain from vehicle performances, in particular:

- maximum vehicle speed;
- acceleration (time to go from 0 to 50 or 100 kph);
- take-off capabilities (to move off the vehicle on a 10÷35% slope).

Instead the CO<sub>2</sub> emission, fuel consumption and maximum vehicle range, especially in electric mode, are used to define the powertrain overall efficiency, kinetic recoverable energy and energy storage capacity. In particular, the electric energy storage system is specified to match with range requirements in electric mode.

User comfort and accessories, that influences the energy consumption of the vehicle, are considered constant in this work. The pollutant requirements impact mainly on combustion mode and after-treatment technologies.

To be consistent in the procedure, it is mandatory to integrate, at each step of the design process, a relevant vehicle mass evaluation.

Since the mass of powertrain and energy storage system affects highly the performance, emissions and autonomy of the vehicle, the masses of both systems are assumed for the preliminary definition of powertrain characteristic. Then they can be refined with re-calculation loop and, after the architecture selection, the final sizing are assessed with vehicle model simulation.

The work flow for the specification definition starting from the aforementioned vehicle requirements is illustrated in Figure 4-5. As it can be observed the process is not linear, but loops are possible to refine the specifications.

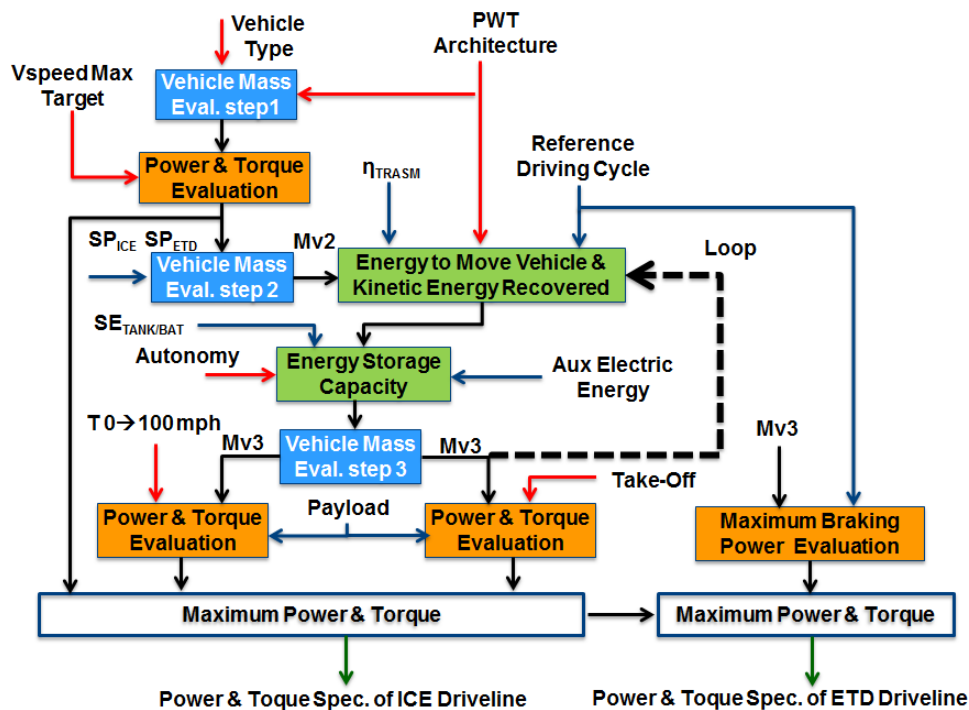


Figure 4-5 Block diagram of the specification workflow (SP =specific power, SE= specific energy)

The key formulas to define many powertrain parameters are obtained from vehicle longitudinal model. A vehicle is subject to different forces, correlated with the fundamental dynamic principle: the aerodynamic drag force, the rolling drag force, the gravitational force and the powertrain traction force.

Introducing the power in vehicle dynamic model, the powertrain traction power  $P_{trac}$  can be calculated with the following equation:

$$P_{trac} = M_V (a + C_r \cdot g + g \cdot p\%) \cdot V + \frac{1}{2} \cdot \rho \cdot C_x \cdot S_f \cdot V^3 \quad (4.2)$$

where  $M_V$  is the vehicle mass and  $a$  the acceleration,  $C_r$  represents the rolling coefficient,  $p$  the road slope (in percent),  $\rho$  the air density,  $C_x$  and  $S_f$  the aerodynamic drag coefficient and the vehicle frontal area respectively and  $V$  the vehicle speed.

From the equation (4.2), introducing the wheel radius  $r$ , the traction torque  $T_{trac}$  can be evaluated with following equation:

$$T_{trac} = (M_V (a + C_r \cdot g + g \cdot p\%) + \frac{1}{2} \cdot \rho \cdot C_x \cdot S_f \cdot V^2) \cdot r \quad (4.3)$$

To proceed with the calculation some vehicle parameters have to be assumed. According to the workflow in Figure 4-5 the power required for the top speed requirement is evaluated as first step.

The powertrain power obtained from vehicle maximum speed requirement is typically the maximum needed and it depends little on weight, so the uncertainty in the mass doesn't introduce significant error in the calculation.

### 4.5.1 Powertrain Features for Maximum Vehicle Speed

Assuming zero acceleration in the equations (4.2) and (4.3), and considering the required vehicle speed  $V_{max}$  from HoQ 1 (Table 4-2), the powertrain traction power and torque can be calculated:

$$P_{Vmax} = f_1(M_v, V_{max}) \quad (4.4)$$

$$T_{Vmax} = f_2(M_v, V_{max}) \quad (4.5)$$

The  $V_{max}$  is according to the target set in Table 4-2 and for the vehicle mass  $M_v$ , a preliminary weight from similar applications is considered.

### 4.5.2 Energy Storage Capacity for Vehicle Autonomy

Considering the vehicle speed profiles and the preliminary vehicle mass defined in the previous section, it is possible to define with equation (4.2) the power in the driving cycles to move and brake the vehicle and, as consequence, by means of an integration process the energies  $E_{MOV}$  needed to move the vehicle and dissipated  $E_{braking}$ .

To evaluate the battery capacity as a function of electric autonomy requested in Table 4-2, the following equations can be used.

The electric energy requested for the trip  $E_{trip}$  to be stored is calculated with the equation:

$$E_{trip} = \int_0^{t_{trip}} P_{bat} dt - E_{KER} \quad (4.6)$$

where the power  $P_{bat}$ , that the energy storage system has to be delivered, can be obtained from the following equation:

$$P_{bat} = P_{aux} + P_{trac} \cdot \eta^{-1} \quad (4.7)$$

where  $\eta$  is the efficiency, that takes into account the transmission and the electric traction drive losses.  $P_{aux}$  is the auxiliary power, considered constant during the trip. Re-writing equation (4.6) the following expression is obtained:

$$E_{trip} = \int_0^{t_{trip}} P_{bat} dt - E_{KER} = E_{MOV}/\eta + E_{aux} - E_{braking} \cdot \eta \quad (4.8)$$

The battery capacity  $E_{SS}$  is calculated with the subsequent equation

$$E_{stored} = \frac{E_{trip}}{\alpha \cdot \beta} \cdot \frac{Electric\ Autonomy}{Trip\ Distance} \quad (4.9)$$

in which  $E_{trip}$  is the value of NEDC with 20%÷40% of increasing, to take in to account the gap with realistic condition,  $\alpha$  is the factor used to estimate the useful energy of total battery energy capability, and  $\beta$  the factor that takes into account battery aging. From the energy need  $E_{SS}$ , considering the specific energy  $SE_{bat}$ , and packaging factor  $\gamma$ , the mass of battery pack  $M_{bat}$  is calculated:

$$M_{bat} = \frac{\gamma \cdot E_{SS}}{SE_{bat}} \quad (4.10)$$

### 4.5.3 Vehicle and Powertrain Weight Evaluation

The preliminary vehicle mass  $M_v$  can be updated with the equation

$$M_v = M_{chas} + M_{pwt} + M_{ess} + M_{driver} \quad (4.11)$$

where  $M_{chas}$  is the vehicle chassis mass, depending on vehicle segment and

$$M_{ess} = M_{fuel} + M_{bat} \quad (4.12)$$

with  $M_{bat}$  calculated as in the previous section and  $M_{fuel}$  the mass of fuel and tank assumed according typical value. The more critical parameter is the mass of the battery, that can vary among 10÷20 kg in an HEV and up to 70÷100 kg of in a Plug-in hybrid electric vehicle.

The powertrain mass  $M_{pwt}$  is composed of:

$$M_{pwt} = M_{trasm} + M_{ice} + M_{etds} \quad (4.13)$$

with  $M_{trasm}$ ,  $M_{ice}$ ,  $M_{etds}$ , respectively the masses of transmission, internal combustion engine and one or more Electric Traction Drive (ETD) systems, depending on the power of these subsystems.

The masses of powertrain elements can be assumed on the basis of similar vehicles or considering the power from equation (4.4) to reach the top vehicle speed and the typical value of the machine power density, as indicated in [63,229] and in next Chapter #8.2.

#### 4.5.4 Powertrain Features to fulfill Vehicle Take-off Requirements

The powertrain traction power and torque to achieve vehicle take-off requirements can be calculated with the equations (4.2) and (4.3), where the acceleration is defined as  $a = 1.6 - 0.08(p-10)$ , linking the vehicle target acceleration to the slope  $p$  [182], and the vehicle speed is assumed equal to 10 km/h. A payload  $M_{pload}$  is added to the vehicle mass.

$$P_{take-off} = f_3(M_v + M_{pload}, V_{tkoff}, a_{tkoff}) \quad (4.14)$$

$$T_{take-koff} = f_4(M_v + M_{pload}, V_{tkoff}, a_{tkoff}) \quad (4.15)$$

#### 4.5.5 Powertrain Performances for Vehicle Acceleration Requirements

Generally, vehicle acceleration requirements are defined by criteria such as time interval to go from 0 to 50 kph or 0 to 100 kph, with the target defined in Table 4-2. Analytically the power requested can be obtained from the integration of equation (4.2). Assuming that the traction power  $P_{trac}$  of the powertrain is constant, the calculation of the duration  $t_f$  to go from a zero speed to a final speed  $V_f$  can be carried out by solving the following equation:

$$t_f = \int_0^{V_f} \frac{M_v}{\frac{P_{acc}}{V} - M_v \cdot C_r \cdot g - \frac{1}{2} \cdot \rho \cdot C_x \cdot S_f \cdot V^2} dt \quad (4.16)$$

#### 4.5.6 Powertrain Features to Recover Vehicle Kinetic Energy

One of the main advantages of an electric hybrid powertrain is the capability to recover the vehicle kinetic energy during the driver braking request. The recovered energy can be used for vehicle propulsion,

allowing significant energy/fuel saving. The braking events are characterized by short duration and high amount of kinetic energy, that is typically dissipated by means of mechanical braking system. The harvested energy depends mainly on the braking power and the efficiencies of the electric machine and the battery.

The power can be evaluated using the equation (4.16) where the initial vehicle speed is the current speed  $V_c$  and the final is zero or a lower level  $V_l$  and  $t_{braking}$  the braking duration

$$t_{braking} = f_5(M_v, V_c, V_l, P_{braking}) \quad (4.17)$$

The recoverable energy is lower than the kinetic energy available, due to the efficiency of energy conversion in the transmission, electric motor and battery.

The maximum regenerative braking power has high impact on the performance of the battery too.

Table 4-5 shows as an example the maximum braking power  $P_{braking}$  in different standard cycles, for two different vehicles: it is higher in the cycles with fast transients and for vehicle with higher mass.

Table 4-5 Maximum braking power  $P_{braking}$  for different standard cycles

	Standard Cycles	C-Segment	SUV
<b>Maximum Braking Power</b> [kW]	NEDC	22	32
	WLTC	28	38
	RTS95	60	82
	FTP-75	23	32
	US06	47	65

To maximize the energy recovered  $E_{KER}$ , the Electric Traction Drive (ETD) and battery have to be designed having a peak power higher than the maximum peak of braking power  $P_{braking}$ , defined with the equation (4.17) and with efficiencies  $\eta_{etd}$  and  $\eta_{bat}$  as high as possible, as indicated in equation (4.18). Furthermore the proper definition of transmission ratio between the electric machine and the wheels is key to achieve high efficiency of energy recovery, because it influences the operation points and so the efficiency of the ETD. This aspect will be shown in a next section.

$$P_{KER} = P_{braking} \cdot \eta_{trasm} \cdot \eta_{etd} \cdot \eta_{bat} \quad (4.18)$$

$$E_{KER} = \int_0^{t_{trip}} P_{KER} dt \quad (4.19)$$

#### 4.5.7 Power and Torque Specifications for ICE and ETD Driveline

The powertrain maximum power  $P_{pwt}$  and torque  $T_{pwt}$  at vehicle wheel can be defined considering the maximum of the terms evaluated above, with the equations:

$$P_{pwt} = \max(P_{Vmax}, P_{take-off}, P_{acc}) \quad (4.20)$$

$$T_{pwt} = \max(T_{Vmax}, T_{take-off}, T_{acc}) \quad (4.21)$$

Typically the more demanding power request is due to the maximum vehicle speed, whereas the torque has the maximum value during the take-off with the slope of 25÷35%.

The equations (4.20) and (4.21) define the total outputs requested to the powertrain without any differentiation between electric motor and internal combustion engine.

In case of HEVs or P-HEVs, the above specifications are related to ICE mode operation, whereas specific requirements for the electric propulsion mode have to be considered.

Taking into account in addition the power for kinetic energy recovery, the specifications for the ETD driveline can be deduced, for the peak and continuous values:

$$P_{elect\ peak} = \max(P_{braking}, P_{e-take-off}, P_{e-acc}) \quad (4.22)$$

$$P_{elect\ cont} = P_{e-vmax} \quad (4.23)$$

$$T_{elect\ cont} = \max(T_{braking}, T_{e-take-off}, T_{e-acc}) \quad (4.24)$$

$$T_{elect\ cont} = T_{e-vmax} \quad (4.25)$$

The continuous Power and Torque specifications depend only on top speed target defined for the electric operation.

## 4.5.8 Transmission Specifications

The previous quantities for power and torque are the values at the wheels. To deduce the power and torque at engine and electric motor shafts, we need to consider the transmission that links the machines to wheels, introducing the gear ratio  $\tau$ , defined as

$$\tau = \frac{\omega_{mot}}{\omega_{wheel}} = \frac{\omega_{mot}}{V/r} \quad (4.26)$$

Considering also the efficiency of transmission  $\eta_{trasm}$ , the power and torque for the ETD become:

$$P_{etd} = \frac{P_{elct}}{\eta_{trasm}} \quad (4.27)$$

$$T_{etd} = \frac{T_{elct}}{\eta_{trasm} \cdot \tau} \quad (4.28)$$

The same equations can be used for the ICE. The gear ratio and transmission efficiency depend on the transmission type and the hybrid powertrain architecture. Furthermore the values of  $\tau$  have a significant

impact on powertrain performances and energy consumption, because of the great influence on the machine efficiency and sizing. A sensitivity analysis will be presented in the case study in Chapter #12.1.

#### 4.5.9 Powertrain Features for Fuel Consumption and CO<sub>2</sub> Requirements

The reduction of CO<sub>2</sub> produced by the vehicle can be achieved with two main actions, see Figure 4-6:

- the substitution of fuel used for the ICE propulsion, with its de-carbonization (e.g. CNG) or de-fossilization, for instance using bio-fuels or other energy carriers (e.g. electricity);
- decreasing the vehicle energy consumption.

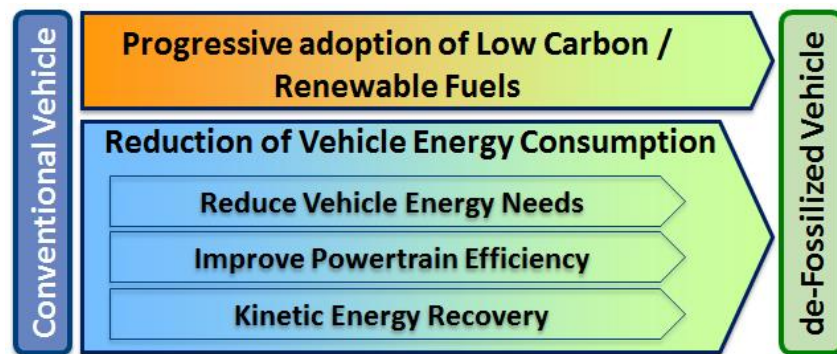


Figure 4-6 Pathway for a de-Fossilized Vehicle

The first item will be discussed in the Chapter #9, the second one is analyzed in this chapter.

The energy/fuel consumption and CO<sub>2</sub> targets in HoQ1 is the more challenging for the vehicle due to even more stringent norms, as presented previously. In the current legislation they are defined as integral Tank-to-Wheel targets on standard driving cycles (e.g. NEDC in EU). It is not immediate to transform these requirements in quantitative powertrain specifications,

To fulfil the fuel consumption and CO<sub>2</sub> requirements, a global system approach has to be employed for the vehicle design, with the following main actions, see Figure 4-6 and Figure 4-7:

- reducing the energy for the vehicle movement, that depends on mass, aerodynamic characteristics of the vehicle and wheel rolling resistance, according to equation (4.2);
- reducing the energy used on board by the accessories (e.g. AC, etc.) and other electric devices (e.g. heaters, lamps, etc.) or producing it in more efficient way;
- improving the energy conversion efficiency from fuel to mechanical energy for propulsion;
- recovering the vehicle kinetic energy, otherwise dissipated during braking.

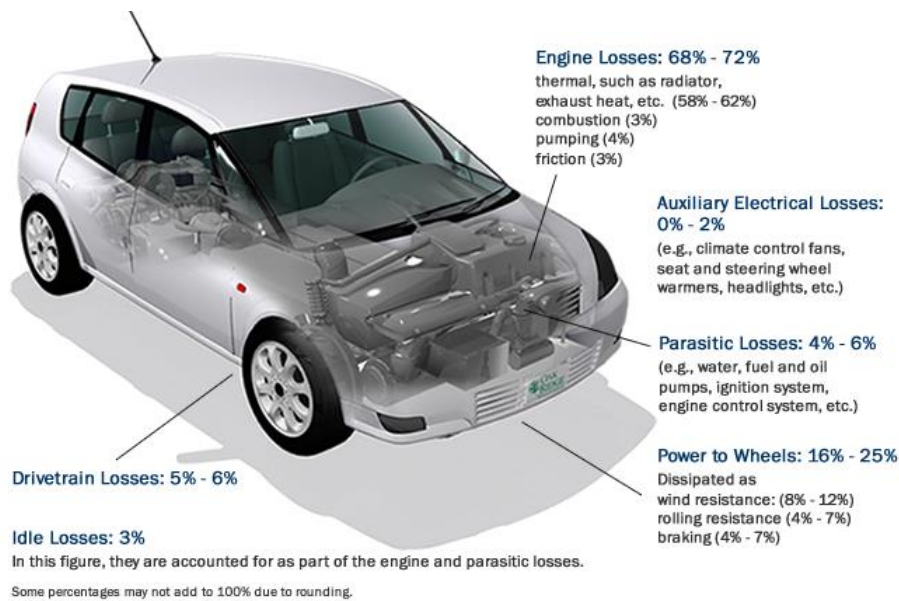


Figure 4-7 Energy requirements for vehicle with gasoline engine in US combined Highway/Driving cycle (source: [www.fueleconomy.org](http://www.fueleconomy.org)).

## Reduction of Vehicle Energy Needs for propulsion

The energy needs for the propulsion is mainly dependent on vehicle segment and chassis characteristics. The powertrain impact on energy needed to move the vehicle is due to the weight and volume. The second feature sets constraint for vehicle shape and aerodynamic resistance. Due to these reasons higher specific power and power density for the powertrain are preferred.

Furthermore the mass and volume of energy storage systems are particularly critics, especially in P-HEVs and BEVs, as already explained in the previous section.

The electric hybrid powertrains are disadvantage compared with pure ICE powertrains, since the mass increase causes fuel penalty, which reduces the electrification benefits.

## Reduction of Energy Needs for Auxiliary Functions

The reduction of energy not used for propulsion is another challenging item to improve the fuel economy and the CO<sub>2</sub> emission. In [21] the main technology options to face this point at vehicle level are presented. However the request of new vehicle functions, for instance autonomous driving and connectivity, implies the addition of many sensors and electric devices [24,25], that contrasts the improvements due to efficiency increase of the conventional electric systems on board the vehicle.

The vehicle energy needs not used for propulsion has an undirected impact on powertrain systems, and the following Figure 4-8 can clarify it.

For instance, the cabin heating is an important requirement for the end-user, that depends on engine features. In fact the high efficiency engines (e.g. Diesel ones), due to lower heat losses, cannot be able to perform the fast heat-up of cabin in worst cold conditions and electric heating systems or engine exhaust heat recovery systems have to be adopted, see Chapter #6.9.



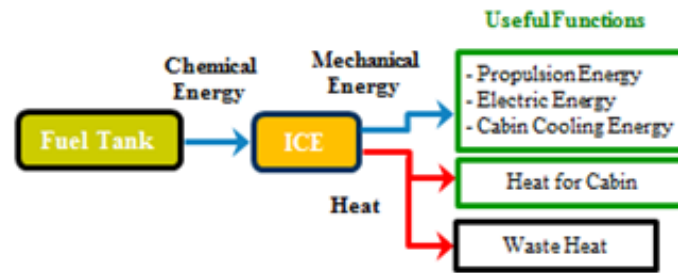


Figure 4-8 Energy flow and functions of an internal combustion engine in a vehicle

In the real use of vehicle, the AC system is another great energy consumer device. It can affect significantly the fuel consumption and vehicle autonomy. Focusing only on the aspect related to powertrain, that can improve the AC function, the heat to cooling energy conversion should have high advantage. In this field, the more promising technology is based on adsorption principle and it will be described with more details following.

### Vehicle Kinetic Energy Recovery

The recovery of braking energy is an important function to improve vehicle efficiency and it has great impact on powertrain architecture, because it forces to introduce devices that are able to harvest the braking energy of vehicle. Among the technology options (e.g. hydraulic based, etc.) the recovery based on an electric system is the most widely adopted solution, favored by the technological progress of the ETD and batteries in the last decades.

Table 4-6 shows the typical values of energy requested to move two different vehicles and the energy dissipated during braking, considering different driving cycles. It can be noted that 20÷35% of energy used during the trip is dissipated by means of the braking and as consequence its harvesting can lead to an important advantage in terms of fuel consumption and emission reduction.

Table 4-6 Energy for vehicle moving and dissipated during braking, considering two different vehicles

	Cycle	Trip Distance	C-Segment		SUV	
		[km]	[MJ]	[kwh]	[MJ]	[kwh]
Energy to move Vehicle [MJ or (kwh)]	NEDC	10.8	3.9	1.08	5.3	1.47
	WLTC	23.29	10	2.78	13.6	3.78
	RTS95	12.74	7.6	2.11	10.2	2.83
	US06	12.81	6.9	1.92	9.3	2.58
Braking Energy [MJ or (kwh)]	NEDC	10.8	1.2	0.33	1.6	0.44
	WLTC	23.29	2.7	0.75	3.7	1.03
	RTS95	12.74	2.6	0.72	3.2	0.89
	US06	12.81	1.5	0.42	1.8	0.50

### Improvement of Propulsion Efficiency

The last contribution affecting the fuel consumption and CO<sub>2</sub> emission is the conversion efficiency of fuel to mechanical energy for propulsion, known as Tank-to-Wheel efficiency of the engine/motor. With focus on the SI engines, favorable for lower cost of exhaust gas after-treatment, the study [216] analyzes the critical areas of engine to be improved, as shown in the engine operating map in Figure 4-9:

- pumping losses at partial loads in zone n.1;

- limited thermodynamic efficiency due to reduced compression ratio, to avoid knocking damages at high loads, mainly in zones 2 and 3;
- combustion chamber and exhaust system thermo-mechanical stresses at high loads in zone n.4, where the enrichment of the mixture is necessary to protect the engine components, such as the turbine.

In [5,216] and in Chapter #6 the engine technologies options are presented, showing that maximum Brake Thermal Efficiency (BTE) over 40÷45% can be achieved. High efficiency is needed in an area of the engine map as large as possible, especially to ensure low fuel consumption and CO<sub>2</sub> emission in real use conditions, where a wide area of operating conditions are involved.

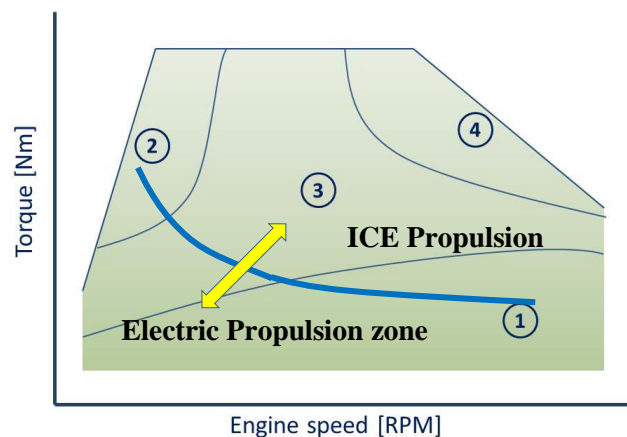


Figure 4-9 Strategic zones of improvements for SI Engine

The use of automated transmissions (e.g. DCT or AT) with high number of gears and proper shifting strategies can bring the engine to work in the most efficient area. The market penetration of automated transmission is expected to increase in the near future, to fulfil new comfort requirements and to allow the implementation of autonomous driving.

In addition to energy recovery, the electric propulsion helps to overcome the limit of engine at part load, below the blue line in Figure 4-9, reducing the engine operation points with low efficiency in zone 1 and shifting the engine operation at high load with higher efficiency. Considering the blue line as an iso-power curve, its position depends on the electric traction drive and the engine efficiency. The higher the efficiency gap among the electric system and the internal combustion engine, the higher is the power level where electric propulsion will be convenient.

However to fulfill the even more stringent requirements on fuel consumption and CO<sub>2</sub>, considering driving cycle with higher operating load (e.g. WLTC and in the near future maybe EU RDE cycles), the electrification of the powertrain doesn't allow to relax the specifications target for the engine. In Figure 4-10 this concept is clarified. The electric propulsion zone, considering its extension due to use of kinetic energy recovery, covers a lower part if the driving cycle load is extended, with lower benefits. To improve global powertrain efficiency, ICE has to increase its efficiency in area not covered by the electric propulsion.

As consequence of these considerations, the engine technologies that overcome the ICE limits in the zone 2, 3 and 4 have higher priority in the design and they will be presented in a following chapter. With simulation models, presented in the Chapter #10, it is possible to obtain a quantitative target for the efficiency of ICE, and to evaluate how much such area has to be extended.

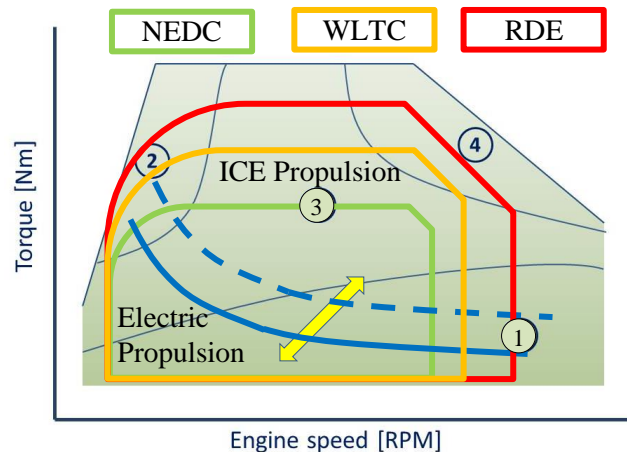


Figure 4-10 Operating points of WLTC and RDE cycles in SI Engine maps

#### 4.5.10 Powertrain Features for Pollutant Requirements

As already mentioned the trend of new emission standard is towards zero tailpipe pollutants in real conditions; this is the aim of new standard cycles. With focus on EU regulations, real conditions mean tests for type approval with higher load and colder conditions, for instance cycle starting at ambient temperature of  $-7^{\circ}\text{C}$  [5].

Higher load can lead engine to operate in zone 4 of Figure 4-9, characterized by thermo-mechanical stresses for the engine components, such as the turbine, that can be protected with dedicated cooling systems or by means of the enrichment of the mixture.

The first solution is not suitable for all components and in some cases not sufficient. The new EU7 standard forces to limit HC/CO and PM/PN emissions at high load, as consequence operation at  $\lambda=1$  is needed. To fulfill these technical requirements, avoiding performance or engine specific power reduction, some technologies are mandatory (e.g. EGR, Water Injection) and they will be discussed in a dedicated chapter for the ICE.

The monitoring of PM and PN in real conditions with lower limits forces the improvement of the GDI combustion process with higher fuel injection pressure ( $>350$  bar) and the adoption of dedicated exhaust after-treatment devices, like the Gasoline Particulate Filter. The support of electric motor during load transients can help to reduce the PM/PN production by the engine.

To cope with the cold start issue and avoiding the reduction of electric mode operation to warm-up the catalyst, faster catalyst light-off is requested. The main technological solution is the Electric Catalyst Heating that offers advantages in conventional powertrains, higher in case of electrification.

## 5. Powertrain Architecture Options

In this chapter the powertrain architecture classification and the relation with energy pathways are presented. Then the focus is on electric hybrid powertrains and their functions, highlighting features and drawbacks.

The right selection of powertrain architecture is key to obtain a tailored solution able to satisfy the powertrain requirements. The architecture has a great impact on ICE, Transmission and ETD technical features. As introduced in the previous chapter, the efficiency (Tank-to-Wheel) is one of the key specifications of the powertrain and the electrification is one of the most effective ways to improve it.

### 5.1 Powertrain Architecture Classification and Energy Pathways

Powertrain architecture refers to the linkage of components in a particular configuration to meet a desired set of functional goals or requirements. Understanding that the vehicle is a complex system consisting of multiple sub-systems and components, three types of powertrain architecture exist, considering the vehicle propulsion system dependence on external energy sources: monovalent, bivalent and multivalent architectures.

**Monovalent Architectures** – Vehicle with the propulsion system depends on one external energy source. Most vehicles today are monovalent cars that use an internal combustion engine (ICE) with a one liquid fuel such as gasoline or diesel. Hybrid vehicles that exhibit a secondary internal fuel source in form of an electric battery are also referred to be monovalent, as the powertrain remains dependent on one external fuel source.

**Bivalent Architectures** - Vehicles that exhibit a propulsion system with two external energy sources, as already presented in Chapter #4.2. An example of a bivalent vehicle, or fuel flexible car, is a plug-in hybrid electric vehicle, where two external energy sources are transferred and stored within the vehicle, electricity and fuel.

Advances in vehicle architecture are expected to evolve through various lines of development, otherwise known as “pathways.” The fuel pathways shown in Figure 5-1 present how energy is transformed from primary sources to a variety of energy carriers (fuels).

**Primary Energy Sources** - Primary energy sources include fossil fuels, nuclear, biomass and renewable sources. Fossil fuels are used as an input source of energy for making all other energy carriers, whereas renewable energy and nuclear sources are used mainly in the production of electricity. Biomass is a growing alternative to produce liquid and gaseous fuels.

**Energy Carriers** – Years of research and development have gone into developing “cleaner fuels” and experimenting with developing varying stoichiometric mixtures of hydrocarbons. In addition to the gasoline and diesel fuels derived from crude oil widely available around the world, liquid fuel compositions of similar content can be developed using process of synthesis from other energy sources.

Among synthetic fuels Biofuels blended with gasoline or diesel are today used mainly in Brazil and in Europe. The synthetic fuels are widely analyzed and compared each other in the Chapter #9. Among gaseous fuel compressed natural gas (CNG) needs particular attention because its use in ICE allows a significant reduction of CO<sub>2</sub>.

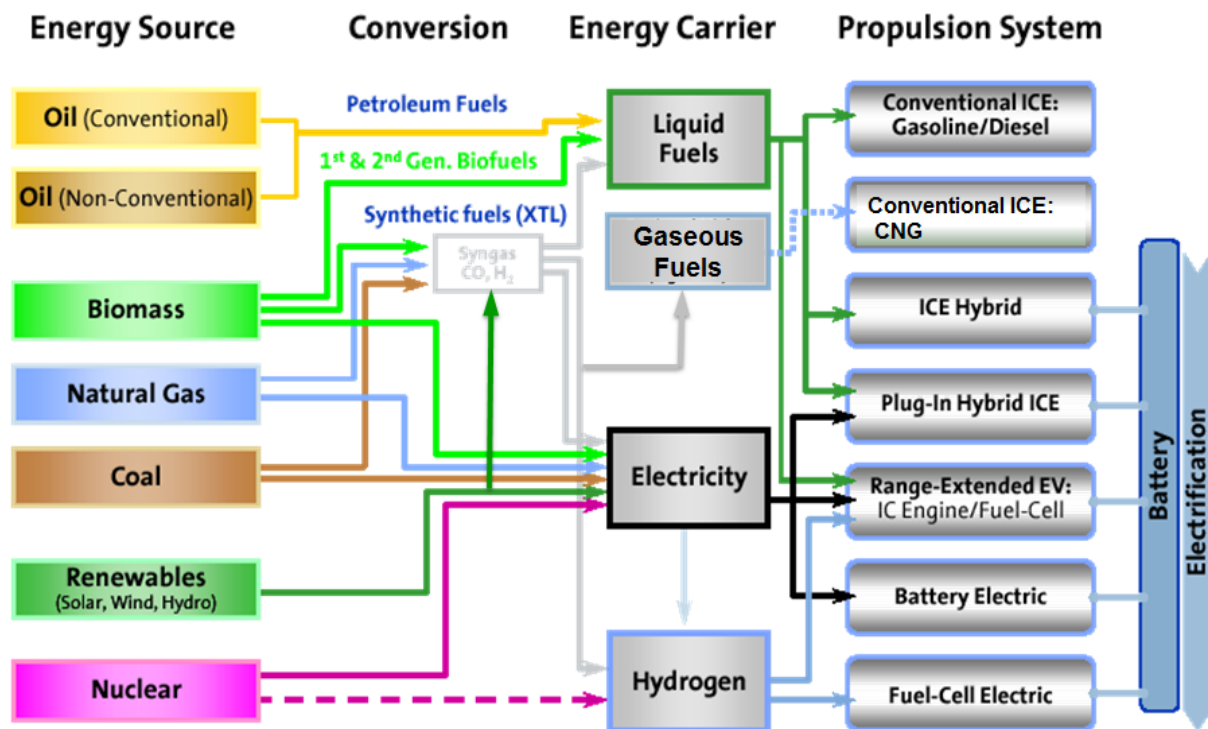


Figure 5-1 Propulsion energy pathways and vehicle powertrain architectures

Finally Hydrogen, by means of fuel cells, and electricity in Plug-in Electric Vehicles permit to achieve zero tail pipe emissions.

**Powertrain Architectures** – Four general powertrain architecture pathways are known to date. These include steam, internal combustion engine, battery, and fuel cell based architectures with multiple combinations thereof. Steam based architectures, which once dominated the early automotive market from approximately 1790 to 1906, have not seen successful commercialization at a large scale ever since. Attempts have been made and are under evaluation to combine the early steam concepts with internal combustion engine, using exhaust gasses to generate steam and consequently mechanical power. These kind of systems are Rankine Cycle based and they will be analyzed in Chapter #6.9.

Gasoline-powered spark ignition (SI) engines and diesel-powered compression ignition (CI) internal combustion engine (ICE) types are well known alternatives. Other combustion engine alternatives for vehicles, such as turbine engines, have also been studied but have failed to meet the equivalent performance in fuel consumption to SI and CI engines. New combustion concepts, named Low Temperature Combustions, have opened a new age for the internal combustion engines. These advanced approaches are key technologies studied in this research and will be presented in Chapter # 6.4, with focus on controls in Chapter # 11.5. The use of new synthetic fuels (see Chapter #9) from renewable sources can reduce significantly the GHG footprint of ICEs based vehicles, as shown in the Chapter #12.2.

Electrified powertrains are gaining favor, as environmental demands for the reduction of exhaust gasses in transportation have become a leading issue. Hybrid electric vehicles (HEVs) represent the first commercially available alternative to the conventional ICE. Initial hybrids feature small electric systems

that assist the internal combustion engine in delivering power to the wheels. The emission regulations are forcing to introduce larger battery electric architectures with external battery charging, as in the case of plug-in hybrid electric vehicles (PHEVs). Battery electric vehicles (BEVs) are gaining importance for city driving and thanks to battery cost reduction some models are able to achieve more than 250 km of autonomy. The large advantage of the battery based architecture pathway is the ability to reduce tailpipe emissions and gained flexibility in selecting less CO<sub>2</sub> emission intensive production of electricity from primary energy sources. The greatest limitation to battery-based architecture is the battery itself. Improvement in battery life, energy density limitations and costs are key factors to making the battery-based pathway a success.

Finally, the fuel cell architecture is considered an alternative solution to overcome autonomy limits and long re-charging time of the BEV. A Fuel Cell Electric Vehicle (FCEV), considered as technology reference, has been commercialized by Toyota in 2015, but there are some steps to improve the maturity and costs of the technology. FCEVs combine a large battery electric system and a fuel cell range extender with the ability to chemically convert fuel into electricity to be used in powering electric motors. Fuel cell powertrains may feature hydrogen as a fuel or a variety of liquid fuel carriers such as methanol.

## 5.2 Electric Hybrid Powertrains Topologies and Classifications

This section introduces the terminology used to describe vehicle architecture structures for the wide spectrum of hybrid and electric vehicles. Following the definition of vehicle architecture presented in previous section, the classification of vehicle architecture structures is primarily dependent on the functional concept of the system and the general configuration of key component subsystems such as the engine (or fuel converter), transmission, electric motors and energy storage devices, described in the following sections. Each configuration differs in the overall vehicle functionality achieved.

### Topology by the Operation Mode

The hybrid electric architectures can be classified by means of the operating mode, meaning mainly degree of electrification (DoE) and electric autonomy. The basic architecture types, that populate solution space, are: conventional ICE, micro hybrid, mild hybrid, full hybrid, plug in hybrid, range extender electric vehicle, the battery electric vehicle and fuel cell electric vehicle. The Figure 5-2 illustrates the main aforementioned powertrain architectures, and for each one the key sub-systems are highlighted.

For each architecture the main features are described below:

- **Conventional Internal Combustion Engine (ICE):** the conventional ICE is the current dominant architecture, characterized by a DoE and electric driving range equal to zero, without any electrical propulsion system installed.
- **Micro Hybrid Electric Vehicle:** Micro hybrids achieve propulsion exclusively by an ICE, but offer some functionality of hybrid vehicles; the most important is the engine Start&Stop function. The start-stop function of a micro hybrid can be achieved by a 12V electric battery system and requires a more robust starter generator system. Some micro hybrids also exhibit limited regenerative braking.
- **Mild Hybrid Electric Vehicle:** Mild hybrids differentiate themselves from micro hybrids in that they offer limited functionality in electric driving (some mild hybrids do not offer electric-only driving). Mild hybrids thus include the three key components of the electric drive system: a 48V or high voltage battery, an electric motor/generator for propulsion/electric generation and an Energy Management System that determines when the electric and the combustion engine systems works. Mild hybrids are

solely parallel systems as described in Figure 4-3 and offer additional functionality of motor assist and expanded regenerative braking.

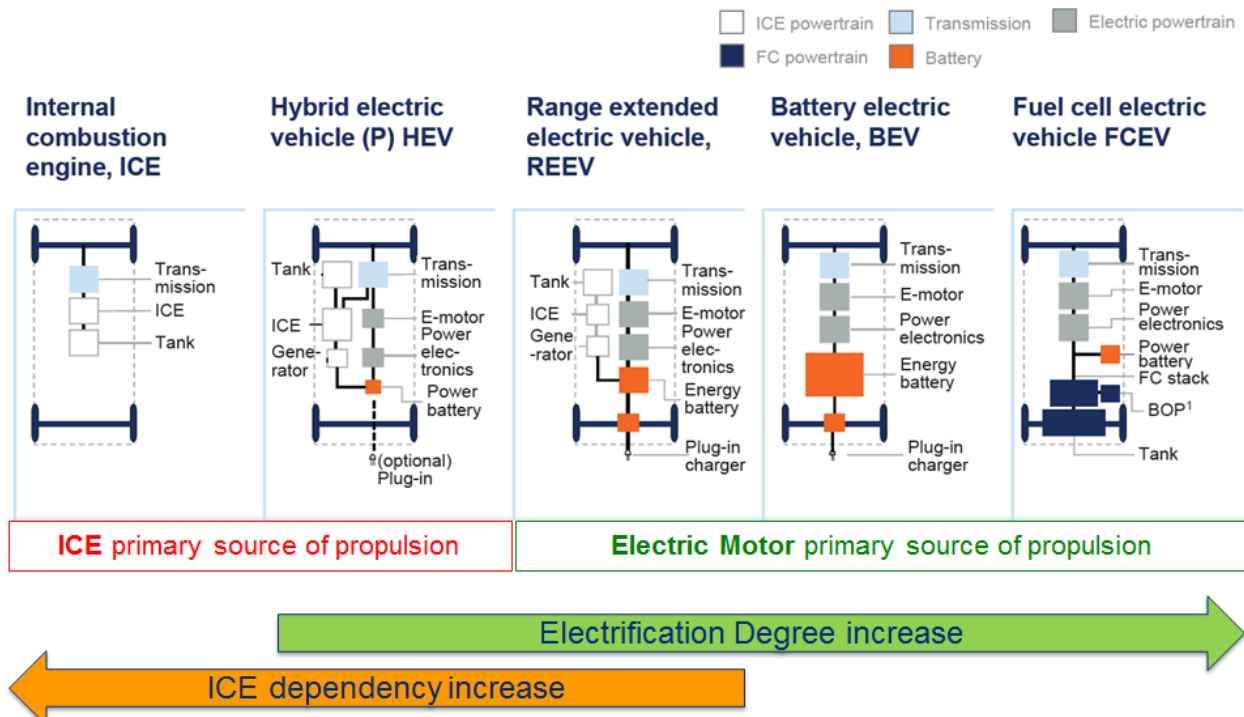


Figure 5-2 Main Electrified Powertrain Architectures

- **Full Hybrid Electric Vehicle (HEV):** Full hybrids display larger degree of electrification (10% ÷ 50%) than mild hybrids and are characterized by short electric driving distances (up to 5 ÷ 10 km). The primary propulsion system still remains with the internal combustion engine but the electric system can assist in providing power to the wheels. Most full hybrids exhibit parallel or combined configurations. Full hybrids exhibit all functions of mild hybrid and have a larger capacity for regenerative braking.
- **Plug In Hybrid Electric Vehicle (P-HEV):** Plug-in HEVs are differentiated from other HEV types by the ability to charge the traction battery externally through a battery charger and plug to an external energy source. PHEVs come in a wide range of architectures including parallel, series and combined configurations and offer extended electric driving ranges (> 25km). PHEVs offer a degree of electrification typically above 40%.
- **Range Extender Electric Vehicle (RE-EV):** This is a particular type of P-HEV with hybrid series architecture. The ICE is used to extend the vehicle range and can vary from large ICE power systems to small “limp home” emergency system IC engine. The DoE is equal to 1 and the pure electric autonomy is higher than 100 km.
- **Battery Electric Vehicle (BEV):** The battery electric vehicle falls outside of the HEV solution space with a DoE equal to one. BEVs have no internal combustion engine installed and are plug-in vehicles by definition, with the electricity the only energy source. The electric range of BEVs is dependent on the level of electrification installed and varies between 150 and 500 km.
- **Fuel Cell Electric Vehicle (FCEV):** Fuel cell cars exhibit an electrochemical cell that converts a source of fuel into an electrical current. FCEVs are primarily configured in a series architecture where the fuel cell power system provides energy to the electrical power system for propulsion.

The Figure 5-3 shows the positioning of electrified vehicles in the space of the electric range and of the electrification degree.

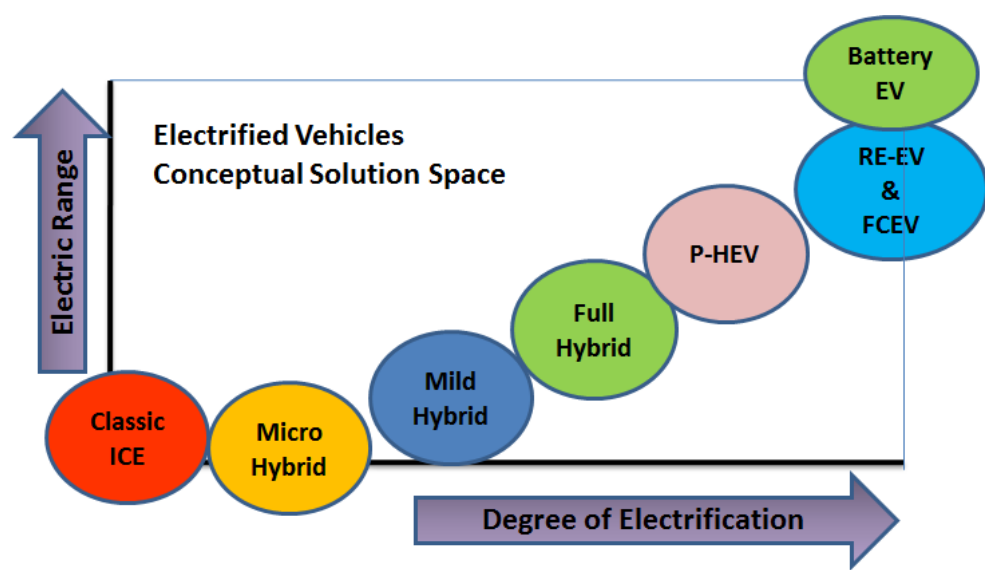


Figure 5-3 Positioning of electrified vehicles in the space of Electric Range and Degree of Electrification

### Topology by Electric Machine Position

Alternatively to DoE, the architectures of hybrid electric powertrain can be defined by means of the electric machine positioning, denoted by P0, P1, P2, P3 and P4 in the Figure 5-4.

In Figure 5-5, in addition to the electric machine positioning, the power flows between the main powertrain elements are presented.

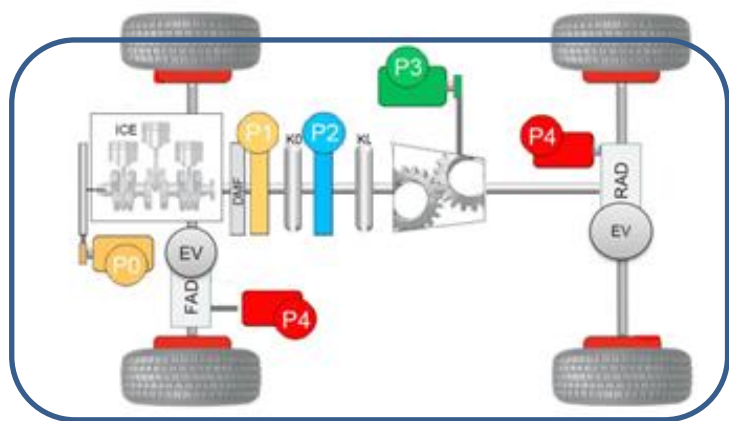


Figure 5-4 Electric machine positioning in HEVs

From B to F, the powertrain degree of electrification (DoE) increases, this implies a greater availability of electrical power with respect to the total power used for traction and a higher pure electric range.





- Due to the fact that the e-motor cannot be decoupled from the combustion engine, the recuperation potential is smaller and the hybrid functionality is reduced.
- The package is more challenging due to the fact that additional space between engine and transmission is required.

**P2-** in this configuration, the EM is located upstream the transmission between one or two clutches, in parallel to the ICE.

- P2 configuration allows the functionality of pure electric driving, with higher fuel consumption saving than P0/P1 architectures, because a clutch allows EM decoupling by the engine.
- The torque delivered by the EM is limited by the maximum torque of transmission; hence in case of contemporary use of ICE and EM, the gearbox must transmit the sum of the torques delivered by the two machines.
- Compared with other hybrid concepts such as P3 and P4 hybrids, the P2 hybrid concept has the advantage that, when the speed of the vehicle changes, the speed of the electric motor stays within the optimum efficiency range of the electric motor, because the transmission gears also act on the electric motor.
- The coaxial variant is often limited in powertrain length and the system complexity increases because of additional clutch control and hybrid functionality.
- The parallel e-motor can be driven by gear set and need less space in length, but some additional package space on the side of the powertrain.
- In case of two clutches, see Figure 5-4, the EM can also be used as generator and driver of the AC-compressor during the vehicle stop condition (e.g. in case of stop & start function), avoiding the addition of a generator in position P0 and of an electric compressor.

**P3-** the EM is connected in parallel to the ICE downstream, between the gearbox and the differential.

- The full hybrid functionality can be realized with such a concept. The powertrain can remain on the standard position. Due to additional gear set also a high speed e-motor is possible.
- The package space is often limited and the additional gear ratio from the transmission cannot be used in a concept like this.
- The e-motor cannot be used for engine start and to charge the battery during engine stops, therefore a BSG or ISG (>4kW) is recommended in addition.
- In case of AMT the EM can be used to reduce torque gap during gear-shift, with significant improvement on the comfort.

**P4-** electrical axle, installed rear and/or front vehicle.

- The full hybrid functionality is given including the potential for four wheel drive and torque vectoring. Single or multi speed can be realized in the e-axle.
- An additional BSG or ISG should be used for engine start and battery charging in idle.

- This configuration allows the integration into most vehicle platforms, especially on platforms with AWD-option, because the available space can be used. This keeps the integration efforts at a reasonable cost level.
- In addition no changes on the conventional combustion front wheel drive powertrain of the vehicle. This allows a cost effective modular approach of entry electrification as well as a free choice of additional internal combustion engine (ICE) and transmission measures to perfect the vehicle.

A mix of the previous architecture is possible, when more electric machines can be installed, in this case some drawbacks can be overcome.

**Power Split-** ICE is connected at the same time to the generator and the electric motor by a planetary gearbox, and the motor shaft is connected to the wheels with a final gear reduction.

- Power split concept combines features of both series and parallel hybrid.
- Full hybrid functionality can be obtained with the highest energy recuperation potential.

In [298] a comparison between Powerplit and P2 architectures is shown. The Power-Split layout is more efficient and flexible, but it pays the disadvantages in terms of costs and integration, because a redesign of driveline is needed.

According to this classification RE-EVs, FCEVs and BEVs are included in the P4 architecture. The architectures from C (only P2) to F in Figure 5-5 can be plug-in, with the possibility to recharge the battery like a pure electric vehicle. Considering the described architectures, the possible functions are summarized in Table 5-1.

Table 5-1 Functions in hybrid electric powertrains

Functions	ICE	P0/P1 12V	P0/P1 48V	P2/P3, Power Split	P4
Cold Start	Y		P	Y	Y
Stop & Start	Y	Y	Y	Y	Y
Coasting	Y*	Y	Y	Y	Y
High Efficiency Electric Power Generation		Y	Y	Y	Y
Regenerative Braking		P	Y	Y	Y
Torque Assist		P	Y	Y	Y
Electric Take-off			Y	Y	Y
Electric Driving				Y	Y
All Wheel Driving					Y
Torque Vectoring					Y

\* with e-clutch or AMT/DCT

Y=Yes P=Partially

The P2, P3, P4 and Power Split architectures are implemented with a minimal nominal voltage of 48V for the electric traction drives.

## 5.3 Architecture Prioritization

Taking into account the previous analysis, an objective prioritization of powertrain electrified architectures has been carried out on the basis of the ability to meet the targets defined in the HoQ1. With this aim, Table 5-2 shows a comparison of the architectures and their mix by means of an evaluation matrix that uses the technical specifications defined in the HoQ 2.2.

Table 5-2 Selection Matrix of electric hybrid architectures

			DoE increasing							
	POWERTRAIN ARCHITECTURES	Relevance (0-100)	1	2	2	2	3	4	5	6
			ICE GDI Turbo + DCT	Hybrid P2 48V	Hybrid P0/P4 48V	Hybrid P2/P4 48V	Hybrid P2 HV	Hybrid Power Split HV	Hybrid P2/Power Split Plug-in	Range Extender EV Plug-in
	Powertrain Characteristics (from HoQ2.2)	Human Driving								
1	Powertrain Noise Level	10	1	2	2	3	3	5	7	7
2	Powertrain Time to Full Power	14	3	5	5	7	7	9	9	9
3	Low-end Torque (at wheel)	19	3	5	7	7	7	9	9	9
4	Speed Range of High Torque	16	3	5	7	7	7	9	9	9
5	Maximum Power	20	7	9	9	9	9	9	9	9
7	Time w/o Torque delivery during load Req.	17	5	7	7	7	7	9	9	9
8	Powertrain Vibration	12	1	2	2	3	3	5	7	7
9	Tank to Wheel Maximum Efficiency	24	3	5	5	7	7	9	9	9
10	Tank to Wheel Efficiency at part/low load	28	3	7	7	9	9	9	9	9
11	NOx Emission according to RDE	13	1	3	3	5	5	5	7	9
12	HC/CO Emission according to RDE	15	3	5	7	7	7	7	7	9
13	Soot/PN according to RDE	14	1	3	3	5	5	5	5	5
14	CO2 on WLTC	22	3	5	7	7	7	7	9	9
15	Heating Power	4	9	9	9	9	9	9	9	7
17	Efficiency of Electric Power Gen.	20	3	5	5	5	5	7	7	9
18	Energy Storage Capacity	14	7	7	7	7	7	7	7	7
19	Energy Refilling Time	14	9	9	9	9	9	9	5	3
25	% Braking energy recovered	22	0	5	5	7	7	7	7	7
26	PWT Size	5	7	5	5	3	5	3	3	3
27	PWT Weight	37	7	5	5	3	5	3	3	3
PWT Architecture Ranking [0+100]			47	67	72	78	81	88	90	92
			Effectiveness increasing							
			Cost decreasing							

The ranking of architectures, and consequently their effectiveness, increases with the electrification degree. Focusing on the analysis targets (i.e. EU 2025 standards) and taking into account the cost target, the preferable architectures are the intermediate ones; in particular P2, P0+P4 and P2+P4, and their application will be presented in the Chapter #12.

## 6. Technologies of ICE Based Powertrains

As previously presented, lower CO<sub>2</sub> emissions may be achieved by reducing fuel consumption, or by using fuels with smaller carbon content, such as bio-fuels or natural gas [68]. Furthermore, the efficiency increase should proceed in parallel with the reduction of pollutant emissions, both during regulated driving cycles and real driving conditions [10]. These constraints are the main challenges confronting the design and development of new internal combustion engines (ICE), together with safety, comfort, drivability, performance, and costs.

Among ICEs, new gasoline engines, operating with stoichiometric mixture, appear particularly promising for the simultaneous reduction of fuel consumption and pollutant emissions. The Three-Way-Catalytic converter is a well-proven, affordable and very efficient after-treatment system. Diesel engines are more efficient, but NO<sub>x</sub> and PM reduction is much more complex, expensive and potentially highly impacting on end user use. In fact the SCR system will be used more frequently to respect the new NO<sub>x</sub> limits under real driving conditions, thus requiring urea refills more often [83,84]. Alternatively to SI and CI engines, “advance combustion” concepts have been analyzed. They are very promising to overcome the drawbacks of the two engine families, joining their advantages.

This chapter presents a conceptual comparison among the most promising technologies for the Internal Combustion Engines (i.e. spark ignited and with advanced combustions types), considering their effectiveness, technological maturity and impact on powertrain production costs. With this aim a deep review of technical literature related to the engine technologies has been carried out and some promising technologies were investigated with more detailed research activities (e.g. Water Injection and Low Temperature Combustion concepts). The technology mix has been evaluated with models presented in Chapter #10, also taking into account the application in electric hybrid powertrain, and then a prioritization with technical criteria from QFD is carried out. The considered timeframe horizon is up to 2025, with an overview beyond.

The last part of chapter is dedicated to the analysis of ICE waste heat recovery technologies, with focus on the most relevant ones.

### 6.1 The state of arts of SI-ICEs

Downsizing concepts, including turbocharging in combination with direct injection, have significantly contributed to the recent improvements of internal combustion engines [79,80,102]. Among these, gasoline engines, operated with stoichiometric mixture. Nonetheless, SI engine efficiency is still to be significantly increased to respect the next and future CO<sub>2</sub> regulations. To better identify and understand the most effective technologies that could be introduced or adopted, one should firstly focus on the main limiting factors affecting efficiency and transient response. Referring to Figure 6-1 and [86,87]:

- pumping losses at partial loads in zone n.1;

- limited thermodynamic efficiency, due to reduced compression ratio, to avoid knocking damages at high loads, mainly in zones 2 and 3;
- combustion chamber and exhaust system thermo-mechanical stresses at high loads in zone n.4, where an enrichment of the mixture is necessary to protect the engine components such as the turbine;
- turbo-lag for turbo-downsized engines, in zone n.2 where scavenging strategies should be adopted with negative effects on the Three-Way Catalyst (TWC).

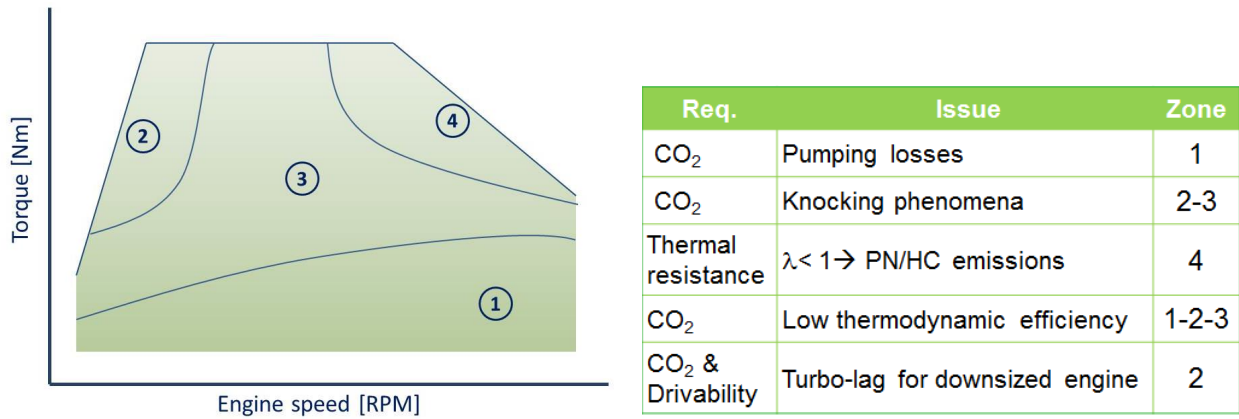


Figure 6-1 Engine requirements and issues of SI engines

## 6.2 ICE Technologies Options to Improve Efficiency and Pollutions

This section summarizes the most relevant technologies for SI-ICE, highlighting their advantages and the main drawbacks, considering a GDI turbocharged engine as baseline. The considered technologies can be classified according to working principle and sub-systems, as described in the Figure 6-2.

The aforementioned technologies have been chosen for their degree of maturity with respect to the horizon of year 2025; moreover, they are considered the most effective for overcoming the limits of SI-ICEs, exposed previously.

Furthermore, the technologies to reduce ICE mechanical friction and the power from auxiliaries, especially in the type approval cycles when the system starts from cold conditions, can be considered already state-of-art in many applications. They can be summarized as follows:

- electrification of coolant and lubricating systems, allowing to optimize pumping requirements for the coolant and oil, depending on the real needs of the engine, in contrast with non-variable mechanical pumps; furthermore, the combination of the electrification with split cooling, allows the engine to achieve warm conditions sooner, while the charge air cooler is kept colder in order to keep the filling efficiency at an appropriate level;
- crankshaft offset adjustments, bearings design or steel pistons (instead of aluminum).

After-treatment systems are presented with focus on of stoichiometric combustion, and in particular PM/PN reduction and cold condition management. In case of engines with Advanced Combustions, if the NO<sub>x</sub> emission are not enough low, another catalyst to reduce NO<sub>x</sub>, such as SCR or LNT must be added, following the development on going for diesel engine.

Furthermore, the benefits achievable with alternative fuels (e.g. biofuels) will be illustrated in Chapter #9.

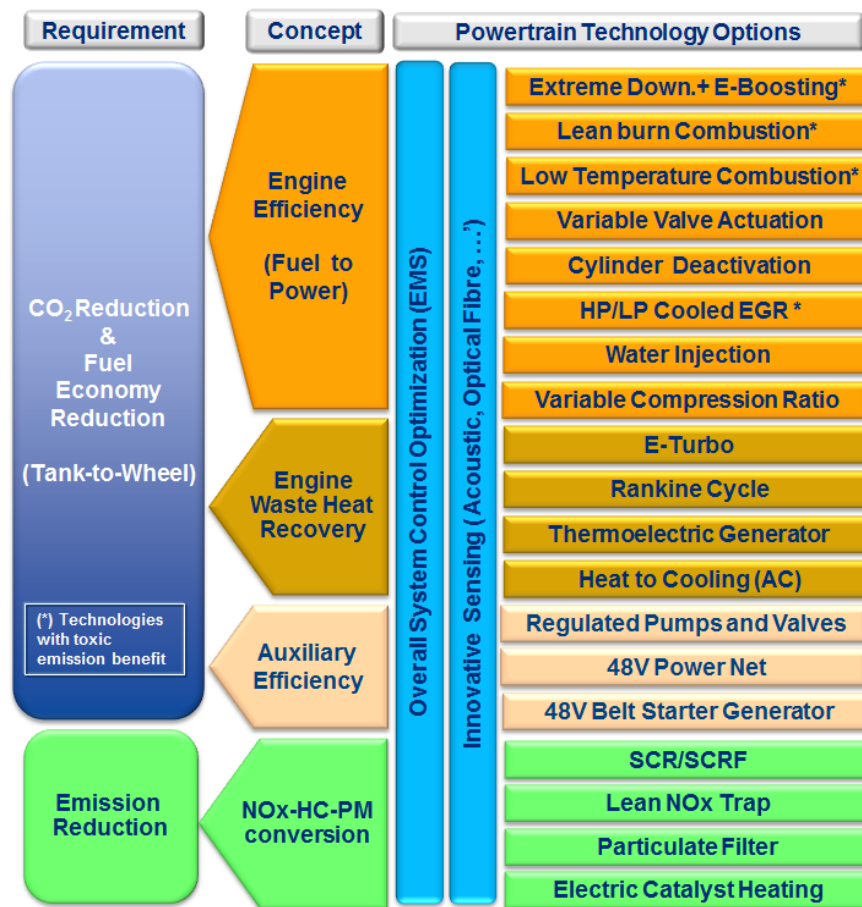


Figure 6-2 Technologies to improve ICE based powertrains

## 6.3 New Technologies for GDI engine with stoichiometric combustion

In this section the analysis of technologies to improve GDI engine, based on stoichiometric combustion, are presented. However, these technologies can be added also to new combustion approaches that will be illustrated in paragraph #6.4. The considered technologies can be classified according to the engine subsystems, as described in the following table:

Engine Subsystem	Technologies
Combustion System	Miller/Atkinson Cycle Variable Compression Ratio Water Injection Cylinder Deactivation
Air System	External EGR Multistage Air Charging

## Miller/Atkinson Cycle

Miller-Cycle describes a combustion system with early or late intake valve closing [86,87,88,89,90,91]. Figure 6-3 illustrates the two possibilities used to perform the Miller cycle.

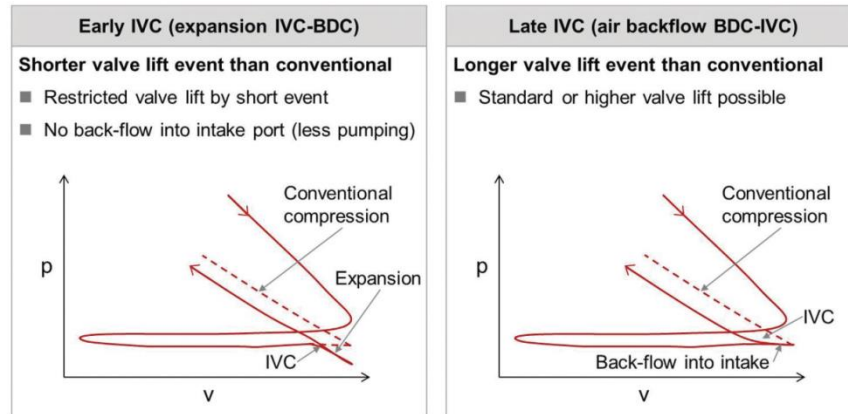


Figure 6-3 Miller cycle: Early and Late Intake Valve Closing (IVC). (Source: FEV 2015)

Miller cycle is based on Otto cycle, having an expansion stroke which is longer than the compression stroke. In late intake valve closing Miller cycle (LIVC), the intake valve is kept open during a significant part of the piston movement during compression, so that part of the mixture contained in the cylinder is sent back to the inlet manifold, allowing the reduction of mixture mass that is “trapped” in the cylinder. Moreover, pumping losses are reduced, and the volume of the ‘trapped’ mixture corresponds to the cylinder volume at the closure of the intake valve. In early intake valve closing Miller cycle (EIVC), the descent of the piston creates a vacuum inside the cylinder, achieving the manifold pressure somewhere during compression, near the position where the intake valve was closed on the downward movement of the piston.

The major benefits of Miller cycle can be obtained in combination with boosting and charge air cooling, with a higher compression ratio (which increases part load operation efficiency). Moreover, in medium load conditions, lower peak pressure and temperature are reached, leading to a lower knock tendency.

Atkinson-Cycle is instead a combustion system with increased expansion stroke realized by a different crank train, which involves a system redesign. Atkinson, as Miller, has a lower effective compression ratio compared to the expansion ratio.

On the other hand, both for Miller and Atkinson cycles, depending on the gasoline engine configuration, a turbocharger upgrading or installation might be necessary to ensure the specific power and the low-end torque. In naturally aspirated engines, the lower engine power and torque might also be compensated by an increased displacement which in turns increases the friction losses.

In [86], FEV estimates that the Miller cycle reduces fuel consumption by 3.9%÷5.7% over a baseline, 1.0 L downsized turbocharged engine with variable valve lift and timing. Part of the efficiency increase is due to the increase of geometric compression ratio from 10:1 to 12:1.

VW recently implemented the Miller cycle concept in EA211 1.5L TSI EVO engine family [89] and the claimed average efficiency improvement is 10% compared with the previous generation engine (1.4L TSI), including also a VGT (variable geometry turbocharger), cylinder deactivation and other in-cylinder improvements to increase engine efficiency. However, the reduction of BSFC, due to the Miller cycle implementation, was estimated to be at least half of the overall benefit. The new engine shows a reduction in fuel consumption between 5÷10%, compared to the previous generation over most of its engine map.



Furthermore, for a significant portion of the low loads region, Miller cycle enables 10-30% reduction in fuel consumption.

In [90], Audi shows a significant fuel economy improvement for the 2.0L TFSI with Miller cycle, implemented by means of the EIVC, in which, some additional gas expansion occurs, which helps reducing in-cylinder temperatures. In this configuration, engine compression ratio was increased from 9.6:1 to 11.7:1. Compared to the previous generation, fuel consumption is reduced up to 21% (on the NEDC), while power output is increased up to 25%.

In [92], Hyundai presents its fully variable VVL system and evaluates its benefits in 1.6L 4-cylinder gasoline engines, both NA PFI and TC DI. VVL, by the combination of four valve timings (IVO, IVC, EVO, and EVC), has the potential to improve the fuel efficiency by 4 to 5 %. Low speed torque, in the NA PFI engine, is increased by more than 5 to 10%, while in the TC DI engine, it is increased by more than 10%.

### **Variable Compression Ratio**

Increasing the Compression Ratio (CR) is an effective way to improve the engine efficiency, as clearly stated by equation (10.37) in Chapter #10.4.5. However, this solution is limited by high peak cylinder pressures and temperatures, which affect the powertrain design (friction and materials) as well as increasing knocking tendency in gasoline engines. Alternatively, the reduction of compression ratio helps solving the problems mentioned before, reducing the overall friction, but also getting some improved powertrain efficiency at full load operation. However, this possibly leads to cold start problems, combustion stability issues and worse efficiency at part load.

Currently, in the market, both tendencies of increasing and decreasing the compression ratio can be found, requiring different side measures, as shown in Figure 6-4. To get the best from both trends, a Variable Compression Ratio (VCR) system should be employed, using a higher CR at engine part load operations and a lower CR at higher loads.

. Two possible VCR technical solutions have been recently developed:

- a 2-step compression ratio [87, 93], that improves full load performance, reducing emissions and friction with lower compression ratios, while it increases the thermodynamic efficiency at lower loads with higher compression ratio;
- a fully variable VCR [87, 94, 95], that allows adjusting the optimal CR for each operating point, using the full potential of this technology.

In addition, there are no significant disadvantageous interdependencies with other technologies. Compared to the fully variable VCR, the cost of the 2-step VCR is much lower [93], and at the same time more than 80% of the fuel consumption reduction potential of the continuous system can be achieved in gasoline engines.

Moreover, in 2-step VCR, the compression ratio can be maximized at lower loads without redesigning the different systems which are subjected to high stresses, e.g. piston or crankshaft, with important advantages in terms of packaging, modification of production and friction. Clearly, theoretical potential will not be fully available; indeed, due to the piston design for maximum compression ratio, disadvantages in the combustion efficiency and knock limit arise. Moreover, the modified conrod is usually heavier than the original one.

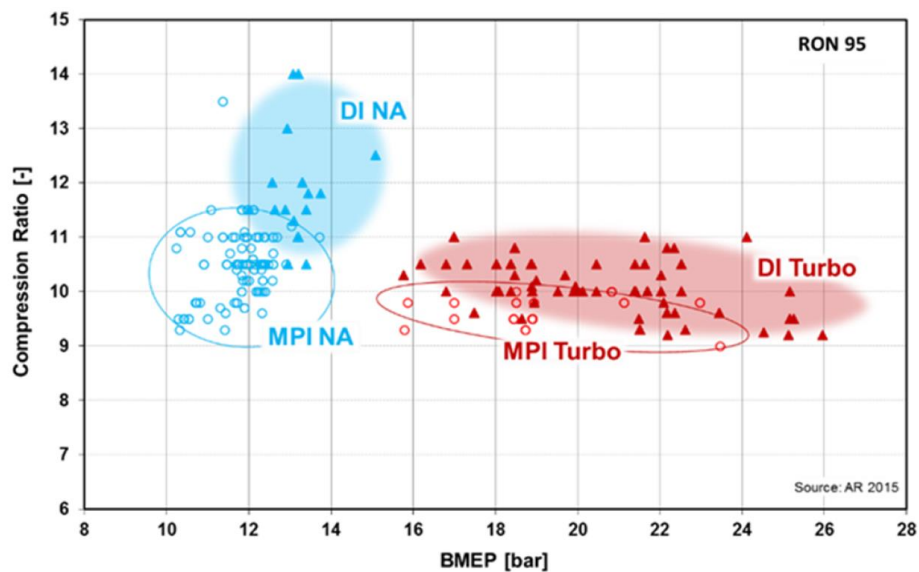


Figure 6-4 Relationship between maximum BMEP and geometric compression ratio, series gasoline engines MY 2015/16 (Source: [93])

In [93], AVL presents its 2-stage VCR system based on the connecting rod length variation. The concept allows modular integration in the existing engine architecture without significant modifications, with only minor adaption of the production lines and thus it represents a highly attractive solution with respect to costs. Depending on the vehicle class, the load profile and the power rating, a CO<sub>2</sub> reduction between 5% and 9% in the WLTC is achievable.

## Water Injection

Water injection (WI) is a cost-effective solution to minimize knocking in (downsized) gasoline engines, especially with high compression ratio, and to lower the exhaust gas temperature in engine high power region. This technology is already well-known because it has been used in motorsports and aviation industry. The current trends in legislation related to the automotive sector make it particularly relevant for serial production in passenger vehicles. Water injection can be exploited as a solution to reduce fuel consumption and CO<sub>2</sub> emissions, especially at medium and high load, as well as to increase the engine power output [76,81,96,97]. The main concept is to inject water and to use its high latent heat of vaporization to reduce gas temperatures before their combustion. In fact, the addition of vaporized water would result in an efficiency decrease due to the reduction of  $cp/cv$  ratio. However, the evaporation of water results in a significant temperature reduction of the mixture of air or air/fuel and water, permitting the adoption of a higher spark advance, thus possibly reaching the optimum MFB<sub>50</sub> position. This effect can overcompensate the efficiency decrease expected when adding gaseous water. At the same time, the dilution of the mixture with water and the reduced temperature level in the combustion chamber have minor influences on the losses due to unburned fuel and the losses due to heat transfer.

Furthermore, the cooling effect may be utilized in different ways according to the desired benefits:

- knock tendency reduction → higher compression ratio enabled/ advanced spark ignition permitted → fuel efficiency increase at the same desired brake torque;
- reduction of exhaust temperatures under full load operation → mixture enrichment can be avoided → fuel efficiency increases at the same desired brake torque;

- knock tendency reduction → advanced spark ignition → torque increase at the same fuel consumption.

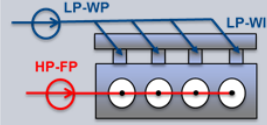
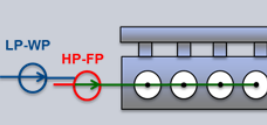
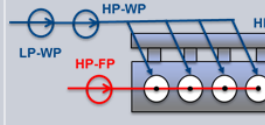
The ability of WI to lower the exhaust gas temperature is also of interest, since it can allow the engine operation at  $\lambda=1$  in all engine area, avoiding mixture enrichment, and it may be used as an enabler for employing turbochargers with variable geometry turbines (VGT) even in gasoline engines, thus allowing further downsizing potential. Alternatively, it may be used to reduce material costs on the turbochargers, due to reduced thermal stresses on the component.

As shown in Figure 6-5, three different implementations of water injection systems are possible:

1. **Port Water Injection (PWI).** In this approach, water is injected on the inlet side with a low-pressure system (5 ÷ 20 bar). The advantage of this solution is its simplicity because it includes a simple pressure supply with an electrically driven water pump. Furthermore, corrosion and freezing issues caused by water are relatively easy to handle.
2. **Direct Water Injection Mixture (DWI-M).** Water is mixed with gasoline and it is directly injected via a modified high-pressure injector. Water quantity is metered based on the intake air mass measurement; the water-fuel mixture is compressed to an emulsion by the high-pressure pump after which it is injected via the high-pressure water-fuel injectors directly into the combustion chamber. While the amount of water required is slightly lower than PWI, the system suffers from several technical challenges and risks. Firstly, the presence of high-strength steels in such high-pressure systems is not trivial and thus magnifies the challenges associated with corrosion damage. This implies a major and complete overhaul of the existing high-pressure fuel system. Secondly, to enable a quick availability of water in the system, the connecting pipes and components need to have small cross-sectional areas and volumes, respectively. This creates high pressure pulsations and thus high-pressure peaks in the injectors and in the high-pressure pump. Therefore, a completely new and complex high-pressure system is required, which has a negative effect on costs and risks. Furthermore, when the engine is stopped, water needs to be removed from the fuel system by running the engine and flushing it with pure gasoline. This makes the solution less effective when used together with hybrid powertrain solutions and start-stop technology. Finally, the challenges associated with freezing and corrosion are magnified in such a high-pressure system.
3. **Direct Water Injection Separate (DWI-S).** A high-pressure water injection system is installed in parallel to the existing high-pressure fuel injection system requiring additional high pressure direct water injectors to be integrated in increasingly smaller and complex cylinder heads. Component costs are then higher than the equivalent low-pressure variant. As in the previous case, the presence of high-strength steels magnifies the problem of corrosion damage, while keeping the robustness against freezing, i.e. due to anomalous water expansion. In addition, reversing the flow through the high pressure mechanical pump is achieved only with additional valves and a high system complexity which adversely affects weight and costs.

As a result of the previous considerations, the Port Water Injection concept is the best candidate for series production. Its main drawback with respect to the other possible solution is the higher water consumption.

The general limit of WI is the availability of good quality of water (deionized) on-board the vehicle. Three main solutions are under investigation: refilling by the user, A/C condensation and rainwater harvesting, exhaust gas condensation. The first one is the most promising because it is cheap and accepted by the end-customer, as reported in the survey [76]. The other solutions are considered to be developed to minimize the end-user impact and refilling costs.

	Port Water Injection	Direct Water Injection - Mixture	Direct Water Injection - Separate
			
<b>Comb. Benefits</b>	Good	Good	Good
<b>Cost</b>	Low	High	High
<b>Robustness</b>	High	Complex (reversible HP Pump)	Complex (reversible HP Pump)
<b>Packaging</b>	Modular and Compact	Non-modular	Extra HP circuit for Water
<b>Energy Efficien.</b>	Low Energy demand	High energy demand	High energy demand
<b>Water Consumption</b>	Higher Water consumption	Lower water consumption	Lower water consumption

LP-WP= Low Pressure Water Pump      HP-WP= High Pressure Water Pump

HP-FP= High Pressure Fuel Pump

LP-WI= Low Pressure Water Injector      HP-WI= High Pressure Water Injector

Figure 6-5 Description and comparison of possible implementations for a water injection system

In [76], the benefits of PWI with a CR increased by 2 points were studied, resulting in 4% of fuel saving on WLTC, 13% in real word conditions and up to 20% in full load. Water rate related to fuel was up to 60%, with a water consumption under real world driving conditions between 1.3-2.8 L/100 km, considering a large family car equipped with a turbo GDI engine with 115÷130 kW rated power.

In [81], the DWI-S technology combined with Miller cycle, cooled exhaust gas recirculation and variable compression ratio was investigated. After a single cylinder experimental investigation, driving cycle simulations were carried out in order to understand both the fuel and water reduction potentials. The combination of water injection with the Miller cycle and cooled EGR has allowed to improve the indicated specific fuel consumption up to 197 g/kWh together with a significant enhancement of the region of very attractive efficiency values, especially at low engine speeds and high loads. Increasing the VCR up to 10.7/14.7 from 9.5/13, the resulting fuel consumption benefit in WLTP was up to 6.7 %. At the same time, water consumption was up to 3 l/100km. Therefore, onboard water generation or, at least, the utilization of tap water for a refill tank are required, in order to ensure an affordable cost also from the ownership's perception.

The WI technology has been also investigated with dedicated research activities presented in different publications [216,217,218,225] and the main results will be presented in the next sections.

## Cylinder Deactivation

Cylinder Deactivation (CD) allows a significant reduction of the pumping as well as heat transfer losses at lower engine loads, by reducing the number of active operating cylinders [98,99,100]. The active displacement is reduced, increasing manifold pressure and reducing pumping losses. The requested load on the cylinder (BMEP) is also increased, which reduces the relative heat transfer to the cylinder walls

with respect to the available heat. Since other technologies (e.g. downsizing or VVT) can reduce pumping and friction losses, the coupling of CD with other technologies could be not so effective.

There are two possible main solutions to implement cylinder deactivation:

1. A variable valvetrain is used to shutoff the intake and exhaust valves of the deactivated cylinders.
2. Electronic Cylinder Deactivation, in which, the exhaust system is duplicated (for instance, each cylinder pair 1-4 and 2-3 has a dedicated exhaust line) and the injection is switched off for one cylinder group.

The second mode is an alternative method without the need for additional flexibility in the valve train and it additionally offers the chance to utilize the deactivated cylinders with the characteristic sound of the engine. The main drawback is the packaging impact of the exhaust line.

The conventional cylinder deactivation, the first solution, is normally applied only to large engines with an even number of cylinders. In this way, the cylinders are deactivated symmetrically in order to avoid intense torque fluctuations and vibrations. Furthermore, higher improvements can be attained with the dynamic deactivation of individual cylinders. Regarding this particular technology, many systems are being currently developed. These systems continually change the active cylinders and have many potential advantages over conventional cylinder deactivation, such as:

- maintaining uniform engine operation temperatures;
- allowing the throttle to remain nearly fully open by controlling the engine power by varying the firing cylinders;
- handling noise, vibration and harshness by dynamically controlling the active cylinders, allowing the adoption of cylinder deactivation at lower engine rpm;
- expanding the range of applicability to smaller engines, even to 3-cylinder engines or with an odd number of cylinders.

An example of this new CD system is the DSF (Dynamic Skip Fire) system, described in [100], that claims to achieve a fuel benefit between 10÷20%, depending on engine type.

In [98], the benefits achievable with the Electronic Cylinder Deactivation in a 4 Cyl 1.4L TC GDI engine are shown. In the NEDC cycle, fuel consumption improvements are up to 7%, with small penalty in comparison with a 2 Cyl 0.9L TC GDI engine.

## **External EGR**

The external Exhaust Gas Recirculation (EGR) [80, 85, 87, 97] is an alternative to the internal one, made using VVA systems. It can be carried out according to the three layouts described in Figure 6-6:

- High Pressure (HP-EGR);
- Low Pressure (LP-EGR);
- Dedicated EGR (D-EGR).

High pressure and low-pressure split is also possible. In the HP-EGR solution, exhaust gases are recycled from upstream the turbine to the intake manifold; in the LP-EGR version, exhaust gases are recycled from downstream the catalyst to the compressor intake. In both cases, gas is cooled with an air/water cooler before entering the control valve, typically driven by a DC-motor. For the LP-EGR case, a lower pressure ratio for the gas flow is available, however, the main advantage is the lower temperature in the manifold

[112]. Indeed, exhaust gases are cooled both in the LP-Cooler and in the turbocharger intercooler, which is designed for the maximum engine power, a faraway condition from the operating area of LP-EGR. Furthermore, LP-EGR leads the compressor to work in an area with greater efficiency, with benefits on fuel consumption for the lower exhaust pressure at turbine upstream due to the reduced compressor requested power. In SI engines, EGR can be used for the reduction of  $\text{NO}_x$  emissions, the de-throttling at partial loads and knock mitigation. An additional benefit is at high engine power, thanks to the avoiding of the enrichment of the mixture with advantages on BSFC and PN production.

The main EGR drawbacks are the reduction of maximum power with a given turbocharger layout and the negative impact on transient response at low engine speeds, because of the increased turbocharger size to compensate for maximum power loss with EGR. Furthermore, cooling capacity of the engine cooling system as well as for the charge air intercooler (for LP-EGR) has to be adapted and integrated to the front end of the vehicle.

In [85], the following advantages with the adoption of LP-EGR are shown:

- 1% BSFC improvement at partial loads;
- more than 4% BSFC improvement, with the same PN-emission, by shifting the 50% MFB50 to the optimum in knock limited engine operating points.

In [105], an extreme downsizing from a 3.7L V6 NA engine to a I4, 2.5L turbocharged engine is allowed by a cooled HP-EGR in combination with scavenging, achieving an increase in the low-end torque and maximum efficiency by more than 30%, as well as a significant weight and size reduction.

The third variant for the external EGR is called “dedicated EGR”, as shown in Figure 6-6. The dilution of the intake charge with the traditional EGR provides benefits in terms of cycle efficiency and knock resistance. However, it also poses challenges in terms of combustion stability, condensation and power density.

With D-EGR [38,106], one cylinder, which operates in rich condition, produces EGR for all four cylinders of the engine, introducing reformates such as CO and  $\text{H}_2$  into the intake charge by means of a mixer installed upstream the intake manifold, bringing back some of the stability lost for EGR dilution, leading to a higher ratio of specific heats and a benefit on effective RON of the fuel. To enable the technology, in addition to the high-pressure EGR loop and EGR cooler, a supercharger with a bypass valve and an after-cooler is used. A cold start valve is installed as alternative path for exhaust gases when the EGR valve is closed. A PFI injector can be added to the intake manifold which allows flexibility in the way the extra fuel to the 4th cylinder is delivered.

In [106], D-EGR improves the knock resistance of a 2.L GDI engine allowing a compression ratio equal to 11.7. In this configuration, the improvement in engine efficiency was at least 10% across the whole performance map, with substantially higher improvements for certain engine operating points. For instance, BSFC @ 2000 rpm/ 2 bar BMEP improved from 385 g/kWh to 330 g/kWh and the lowest BSFC in the engine map was 212 g/kWh compared to 236 g/kWh of the original engine. The addition of 2-stage boosting also allowed the engine to meet its BMEP target of 17 bar from 1500 to 5500 rpm while maintaining good transient response and low engine-out emissions. The main drawbacks of D-EGR are the need to control combustion stability and the complexity due to a second stage of air boosting to recover the power loss at high loads.

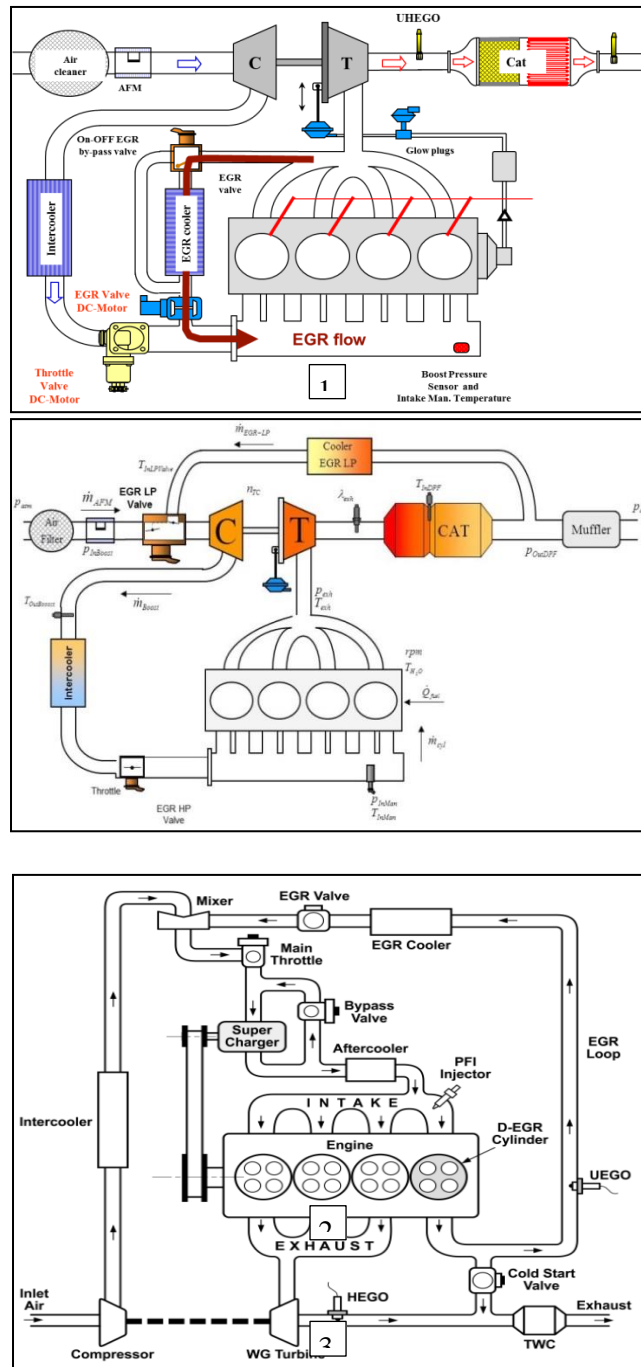


Figure 6-6 External EGR System Layouts: 1. HP-EGR, 2. LP-EGR, 3. Dedicated EGR (Source SwRI)

## Multistage Air Charging

The most effective way to reach a higher specific power output is increasing the boost pressure. This allows more air (oxygen) into the cylinders. Furthermore, increased boost pressure is necessary in combination with increased EGR and the application of Miller Cycle to avoid reduced volumetric efficiency and reduced full load torque.

The extension of boosting operative range can increase the low-end torque, which is a critical issue especially in extreme downsized engines [97], with fun to drive benefits and/or possibility to implement down-speeding strategies. Furthermore, the use of complex charging systems is necessary to fulfill the new European emission standards, where scavenging strategy will not be implementable, because it can cause the decrease of TWC efficiency.

The extension of the boosting range is possible employing a VGT turbocharger, as long as exhaust gas temperature is low enough, however better results can be attained employing multistage charging layouts, according to two main solutions (see Figure 6-7):

- 2-stage turbocharger;
- mechanical supercharger or electric turbocharger in addition to the first turbocharger stage.

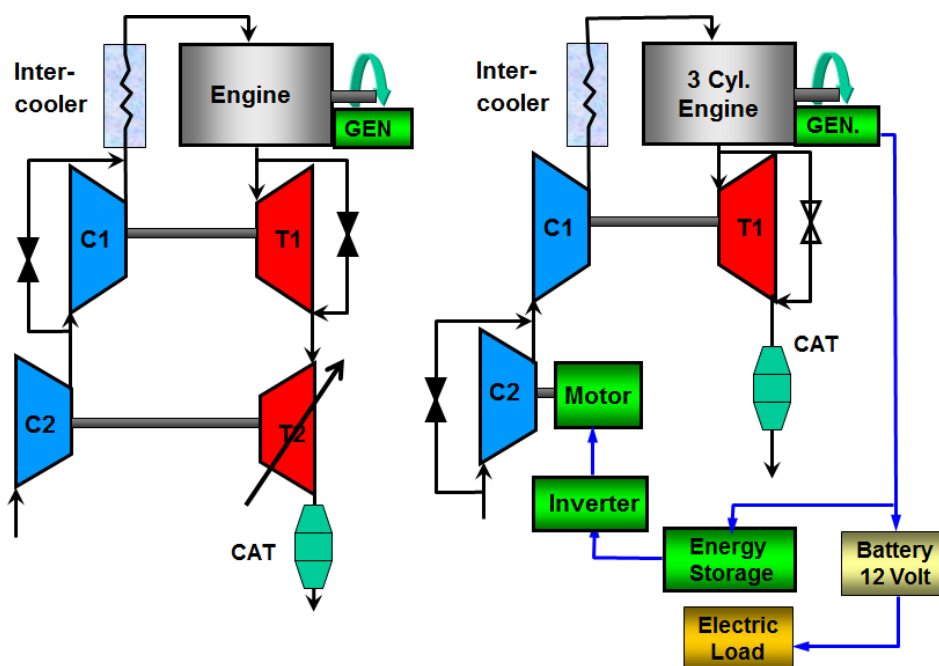


Figure 6-7 2-Multistage air boosting systems: 2stage turbocharger and electric supercharger in addition to the turbocharger

In the first solution, two differently sized turbochargers are used and chosen to be operative in different areas of the engine map. This solution has huge impact on cost and layout. In the second solution, the tendency is to use an electric turbocharger (or an e-booster only), that can deliver air at maximum boosting pressure within 300-1000 ms [107,108]. This technology is particularly suitable when used in conjunction with a 48 Volt power net and a Belt Starter Generator (P0 architecture in Chapter #5.2), allowing to achieve a fuel economy improvement over 10% and a significant gain in the fun to drive, as shown in [79, 107,108].

### Summary of Technology benefits and drawbacks for GDI engines

The technology impact on the GDI engine features, obtained from literature analysis, is summarized in Table 6-1. The focus is on advantages in terms of efficiency improvement and CO<sub>2</sub> benefits on normed test cycle. This data will be used as reference to validate the vehicle and powertrain models presented in Chapter #10.



Table 6-1 Summary of technology impact from literature analysis

Analyzed Technology	Reference Work	Vehicle Segment	Engine Reference	Other Engine Modification	Engine Characteristics					
					Low-end Torque Improvement	$\Delta$ Maximum Power	$\Delta$ Tank-to-Wheel Maximum Efficiency	$\Delta$ Tank-to-Wheel Efficiency at part/low load	CO <sub>2</sub> Benefit in WLTC	CO <sub>2</sub> Benefit in NEDC
					[%]	[%]	[%]	[%]	[%]	[%]
Port Water Injection	76		TC,GDI, 130 Kw	CR=+2			13		4	
	96		1.0L,TC,GDI, CR=11.6	SA optimizatin			1.8			
Direct Water Injection	81	E	1.6L,TC,GDI, VCR 13/9.5 AT 8-speed	VCR 14.7/10.7					6.7	4.4
GDI Lean	22	D	2.0 L, TC, GDI, 200kW						12	14
Miller Cycle	86	C	1.0L,TC,GDI, VVL,CR=10	CR=12					3.9	4.4
	89		1.4L,TC,GDI	1.5L,CR=12.5, VGT,CD			5	10÷30	10	
	90	D	2.0 L, TC, CR= 9.6	CR=11.7		25				21
	80	D	2.0L,TC,GDI ,4cyl, CR= 10.5	CR=13.1, 4 Cyl, Supercharger CR=13.1, 3Cyl, Supercharger				1.8÷9.4 5.3÷21.8	6.3 12.5	
	92	C	1.4L,TC,GDI RC=10,S/B=1.17	1.6L, CR=13, S/B=1.35, Friction Reduction			2			
LP-EGR	85	C	1.2L,TC,GDI RC= 10.5					1	4	
Dedicated EGR	106		2.0 L, TC	Supercharger added, CR=11.7			10			
HP-EGR	105	SUV	3.7L,V6, NA, CR=13	2.5L,TC,Scav. GDI,CR=10	30		30			
Variable Compression Ratio	93		2.0L,TC, GDI, CR=9.5	Miller, 2step VCR=9.5/14					5÷9	
	95		1.6L,TC,GDI,CR=10	Continuous VCR=11	10			4÷5		
	87		CR=13.1	2 step VCR=12.1					4.2÷6.2	
Cylinder Deactivation	98	C	1.4L,TC,GDI	Electronic Cylinder Deactivation						7
	100			Dynamic Skip Fire						10÷20
48V BSG	80								5.1÷6.2	
	108	B	NA,PFI						4	
	80									10
48V BSG + eBooster	80	C	2.0 L, 4 cyl, PFI	1.0l, 3 Cyl, TC, GDI						50
	80	C	1.0l, 3 Cyl, TC, GDI	Combustion & Thermal optimization						17
	80			1.75L,TC, GDI				200 g/kwh		
	80		TC, GDI							
	108	Sport	TC, GDI, AT			50			6	15

Moreover the evaluated technology benefits, drawbacks and the influences in the main zones of engine map referring to Figure 6-1 are illustrated in Table 6-2.

Focusing on new EU7 standard that forces to limit HC/CO and PM/PN emissions at high load, the enrichment engine operation must be avoided, as consequence the combustion operation at  $\lambda=1$  is needed. To fulfill these technical requirements, avoiding performance reduction or engine specific power reduction, some of the aforementioned technologies can be employed (e.g. EGR, Water Injection).

In [109] a comparison of the possible technologies to achieve engine  $\lambda=1$  operation is presented. The analysis has been carried out for two different GDI base engines, with specific power outputs of 110 kW/L and 90 kW/L, named respectively “A” and “B”. Both specific power values are typical for the current gasoline engine market. The base engine A is a high power variant with a large turbocharger (TC) and an integrated exhaust manifold (IEM). To reach the specific power of 110 kW/l, a strong fuel enrichment (approximately  $\lambda = 0.7$ ) is necessary. In contrast, with a smaller TC, higher compression ratio and less enrichment for component protection (approximately  $\lambda = 0.8$ ), base engine B only reaches 90 kW/l.

Table 6-2 Summary of Technology benefits and drawbacks for GDI engines

ICE Technology	Advantages	Influenced Engine Zones	Drawbacks
Miller/Atkinson Cycle	<ul style="list-style-type: none"> <li>- Pumping losses reduction at low loads</li> <li>- Higher geometric CR enabled</li> <li>- Knock mitigation</li> <li>- Lower peak pressure and temperature</li> <li>- VGT enabling with higher cylinder displacement</li> </ul>	All engine operating area with higher impact on 1 and 2	<ul style="list-style-type: none"> <li>- Lower volumetric efficiency, more boosting required</li> <li>- Displacement needs to be increased to recover the engine power leading to higher friction losses</li> </ul>
Variable Compression Ratio	<ul style="list-style-type: none"> <li>- Higher efficiency at low loads, due to the high Compression Ratio (CR)</li> <li>- Very effective coupling with Miller</li> </ul>	Zones 1 and 3	<ul style="list-style-type: none"> <li>- High cost and complexity</li> <li>- Complex handling during switching from high CR to low CR</li> </ul>
Water Injection	<ul style="list-style-type: none"> <li>- Very effective way to mitigate knock phenomena</li> <li>- CR can be increased</li> <li>- Lower exhaust temperature in full load avoiding enrichment and enabling VGT</li> </ul>	Zones 2,3 and 4. If higher CR is adopted, the impact is on the whole engine operative area	<ul style="list-style-type: none"> <li>- Water consumption leads to the need of producing it on board</li> <li>- Corrosion needs to be handled</li> </ul>
Cylinder Deactivation	<ul style="list-style-type: none"> <li>- Pumping and heat losses reduction</li> <li>- Higher efficiency at low loads</li> </ul>	Zone 1	<ul style="list-style-type: none"> <li>- Torque fluctuation, vibrations and noise to be handled</li> <li>- Low effectiveness in coupling with other technologies</li> <li>- Cost and packaging impact</li> </ul>
External EGR (HP/LP)	<ul style="list-style-type: none"> <li>- Knock mitigation</li> <li>- Lower heat losses</li> <li>- De-throttling at partial loads</li> </ul>	Zone 2,3 and 4	<ul style="list-style-type: none"> <li>- Reduction of maximum power with a given turbocharger layout</li> <li>- Negative impact on transient response</li> </ul>
2-Stage Air Charging	<ul style="list-style-type: none"> <li>- Low end torque increase</li> <li>- Downsizing and down-speeding enabler</li> <li>- Scavenging reduction or elimination</li> </ul>	All the engine operative area	<ul style="list-style-type: none"> <li>- Cost and packaging impact</li> <li>- Added complexity for the engine control</li> </ul>

The next Figure 6-8 shows the technology options to obtain  $\lambda=1$  combustion. The Water Injection is the most effective technology to fulfill the technical requirement of  $\lambda=1$  combustion. Indeed only the Water Injection is able to ensure stoichiometric combustion, without any reduction of engine specific power. The cooling power of the WI at high load is confirmed also by the PhD activity research presented in a next section of this work.

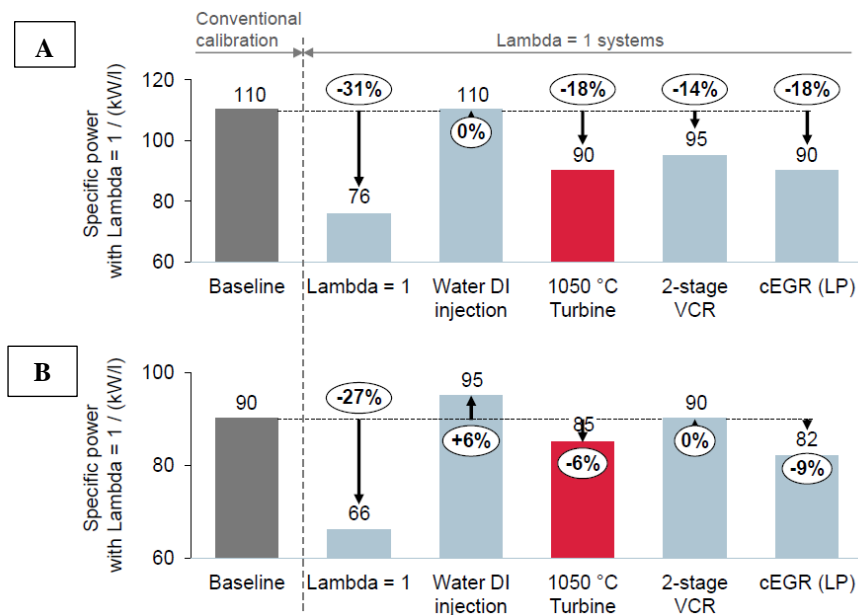


Figure 6-8 Comparison of engine technologies for  $\lambda=1$  combustion for two different base engines

## 6.4 Advanced Combustion Concepts

The conventional SI combustion has the aforementioned limits; alternatively the CI combustion is characterized by high efficiency, but due to lean operation NO<sub>x</sub> is not easy to reduce in the exhaust after-treatment systems and the diffusive combustion generates high Soot quantity. The Figure 6-9 compares the main combustion features of SI and CI engines.

In several studies new combustion concepts have been investigated to overcoming the problems of these combustion approaches. For SI engine the main investigated field was the GDI stratified lean combustion and at end of the '90s some engines were launched in production by some car manufacturers. For cost reason, mainly due to the exhaust aftertreatment, the SI lean technology was abandoned, but recently the interest is come back, due to even more strict requirements on CO<sub>2</sub> and the technological improvements of engine management systems.

For CI engines many technologies have significantly reduced the Soot (e.g. High pressure fuel injection, over 2200 bar) and NO<sub>x</sub> (e.g. EGR-HP and LP) generated in cylinder, but the recent emission regulations have forced the introduction of complex and expensive after-treatment systems, with DPF, LNT and SCR catalysts.

The more promising combustion technologies, object of many studies, are the Low Temperature Combustions, that will be analyzed in the next sections.

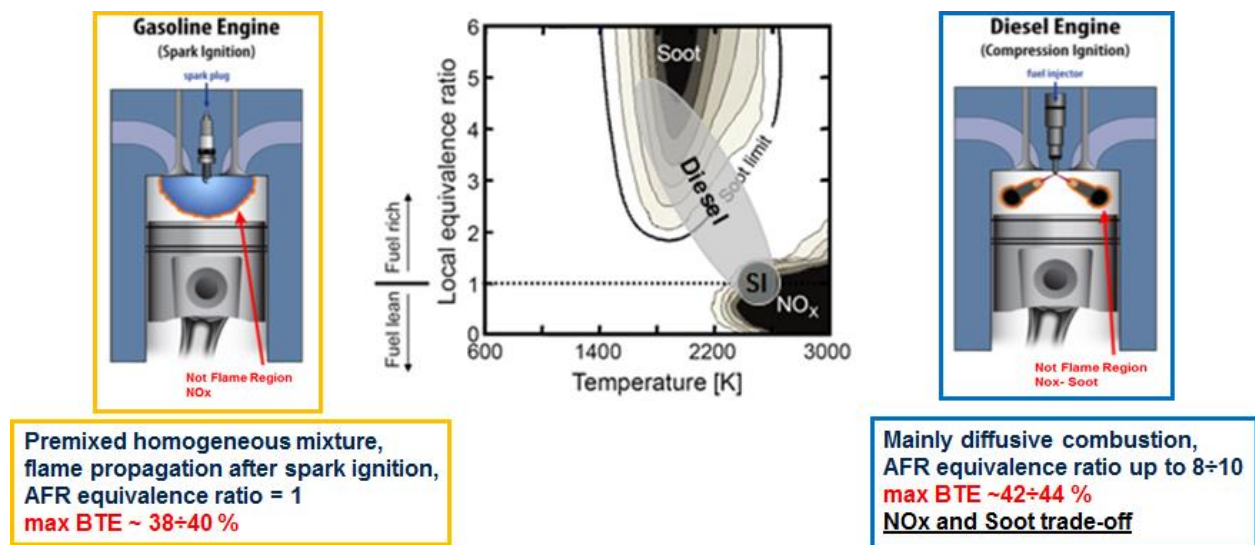


Figure 6-9 Comparison of the SI and CI combustion features

### 6.4.1 GDI Lean Combustion

Lean combustion in gasoline engine has proven to significantly increase the overall efficiency [86]. Unfortunately, like diesel engine, an expensive exhaust after-treatment is necessary because the three-way catalyst cannot reduce NO<sub>x</sub> in case of excess of oxygen in the exhaust gas. To mitigate the catalyst cost increase, engine has to operate in extreme lean conditions (e.g.  $\lambda > 1.8$ ), thus obtaining a drastic reduction of engine out NO<sub>x</sub> emissions and further engine efficiency improvement, thanks to the higher ratio of specific heats and lower heat losses to the cylinder walls. Figure 6-10, from [22], is an example of

the operating modes of a lean concept in the engine working points, highlighting the operating range in the WLTC cycle.

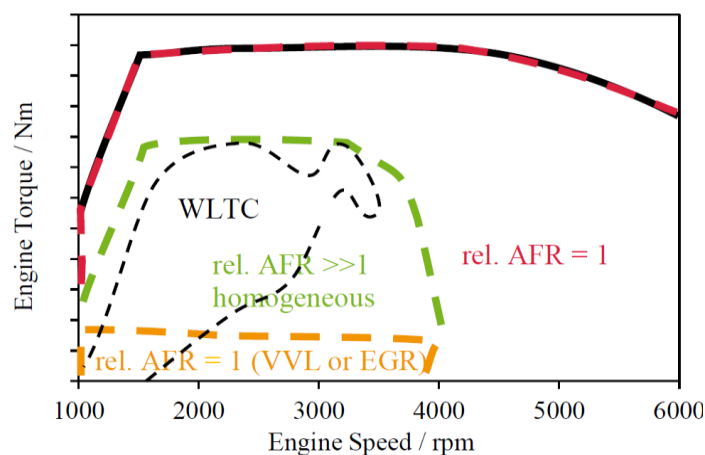


Figure 6-10 Lean concept operating modes in engine working points (Source: [22])

In addition to the increased demand on the air charging system, further challenges arise with the extreme lean operation. The ignition of the diluted mixture is strongly hindered by the poor thermal boundary conditions that might lead to misfiring, therefore ignition system technology development is often required [208]. An additional limitation under lean conditions is the increased cycle-to-cycle variations (*CoV*) due to the slower combustion. *CoV* can be minimized with higher turbulent combustion velocity by enhancing the in-cylinder charge motion. Hence, port and combustion chamber design as well as the spray pattern layout play a key role in the development of extreme lean combustion concepts. Furthermore, the transient operations including the switching between operating modes, e.g. from stoichiometric to lean air/fuel ratios or vice-versa, have to be properly managed. As for all lean gasoline engines, the control of  $\text{NO}_x$  emissions remains a challenge, therefore Lean  $\text{NO}_x$  Trap (LNT) or SCR solutions are needed. LNT was already employed at end of the '90s in the first vehicles (Toyota, Mitsubishi, VW) equipped with GDI lean engines, and in the recent years it has been widely adopted in diesel engine applications.

In [23], Ricardo shows a lean burn combustion concept that uses spray guided lean stratified operation.  $\text{NO}_x$  emissions control is carried out by means of a LNT catalyst. The study highlights the BSFC improvement achievable in stratified lean burn conditions (2.0 L turbo, 200 kW rated power) for a D-segment vehicle. Over NEDC, the solution has been simulated producing a 14% reduction of  $\text{CO}_2$  emissions compared with the equivalent stoichiometric turbocharged GDI engine, considering LNT regeneration. Over WLTC, the fuel consumption reduction is 12%.

## 6.4.2 Low Temperature Combustion Concepts

The aim of these type of combustions is to increase fuel conversion efficiency ensuring at same time low emissions, in particular Soot/PN and  $\text{NO}_x$ , overcoming the limits of both gasoline engine and diesel engine. These results are achieved performing a fast ignition of mixture air-fuel. The ideal ignition occurs for compression in a wide area of combustion chamber with high excess of oxygen, the Figure 6-11 and Figure 6-12 show the comparison of SI and Homogeneous Charge Compression Ignition (HCCI) combustion principles. The main features and advantages of LTC engines are:

- the heat release is fast, lowering the heat exchange with cylinder walls;
- the local temperature is low, preventing  $\text{NO}_x$  formation;

- Soot/PN is low because the higher oxygen concentration guarantees the absence of local rich points;
- no trade-off between NO<sub>x</sub> and Soot affects the combustion;
- de-throttling, due to ultra-lean operation, with benefit on pumping loss reduction and fast transient load responsiveness;
- flexibility of fuel use, including gasoline, diesel, bio-fuels and others synthetic fuels.

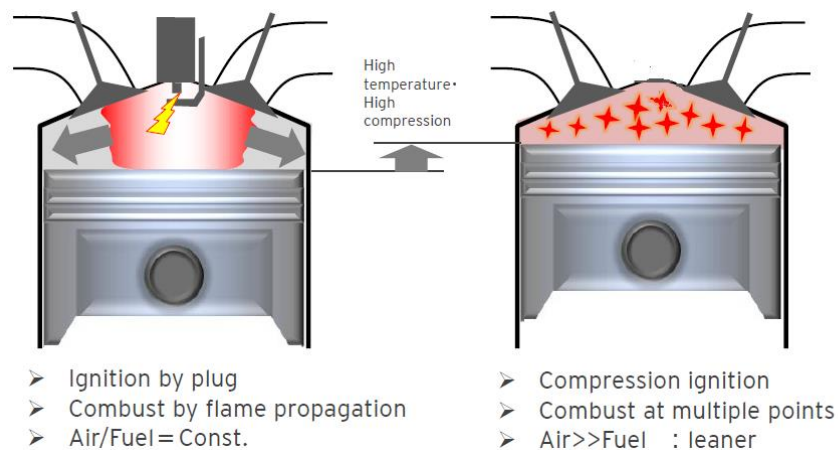


Figure 6-11 SI and Homogeneous Charge Compression Ignition (HCCI) combustion principles

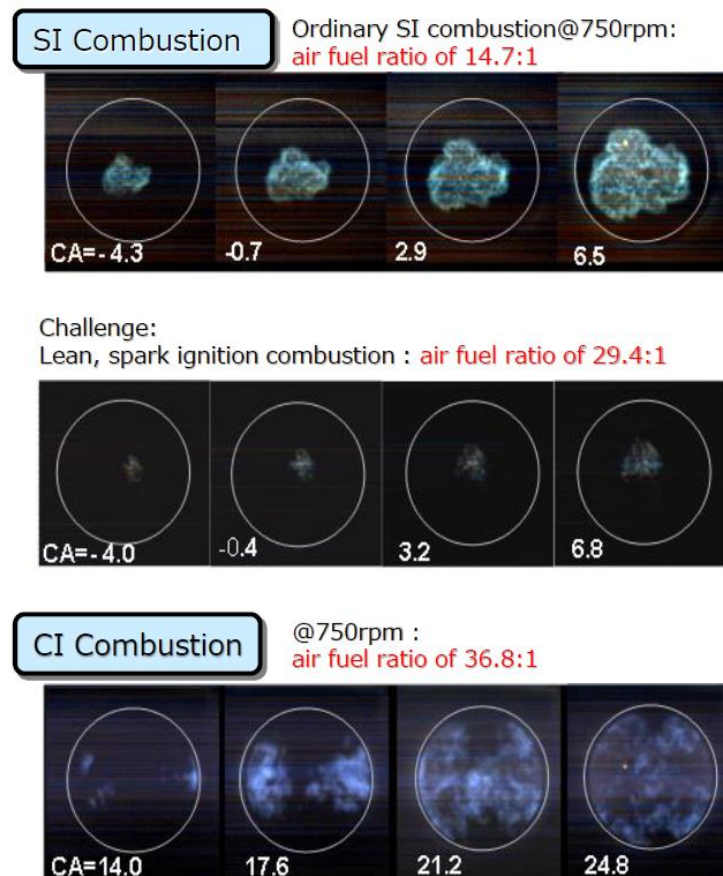


Figure 6-12 Comparison of SI conventional combustion with lean (misfired) and HCCI combustion



The main concerns [40, 41, 42, 47, 219, 223, 226] of these combustions are:

- load limitations, typically low-to-medium loads, thus for real-world application transition between LTC and conventional operation has to be managed, see Figure 6-13;
- the instability, due to difficulty in controlling combustion timing and high sensitivity to air and chamber thermal state;
- lower in-cylinder temperature impedes post-oxidation of HCs and conversion of CO to CO<sub>2</sub>; thus, LTC basically suffers from the problem of high HC and CO emissions.

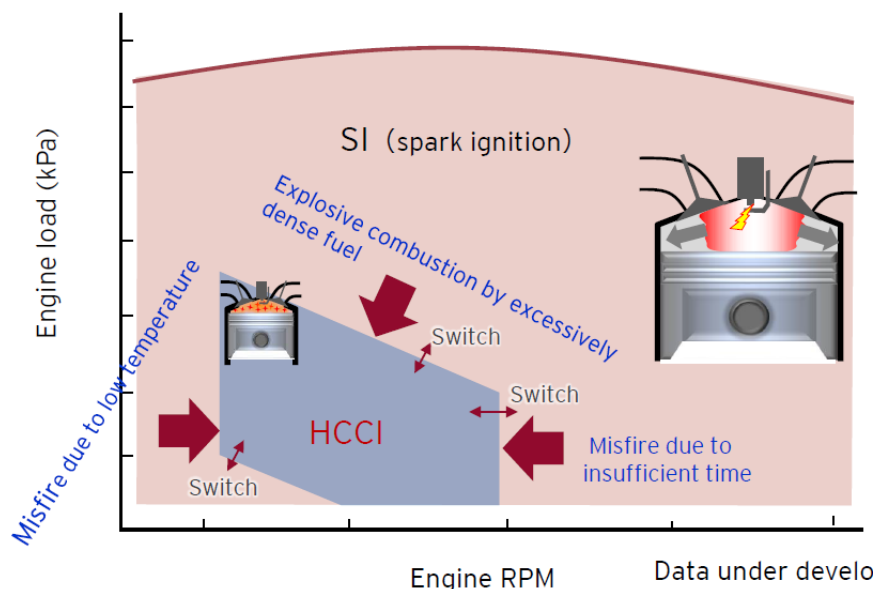


Figure 6-13 Issues with the HCCI combustions

High accuracy in air and fuel delivery and a closed loop control of combustion are mandatory to overcome the issues. As introduced LTC engines generally suffer from high levels of carbon monoxide (CO) and unburnt hydrocarbon (UHC) emissions, but, in recent years, several researchers have demonstrated that boosted LT combustions can exhibit nearly 100 per cent combustion efficiency [250, 308]. These improvements come through the use of piston designs featuring minimum crevice volumes, as well as use of high intake pressures.

The Figure 6-14 summarizes the alternative approaches to implement the Low Temperature Combustion concepts with a mapping on used fuel characteristics.

Between the different solutions investigated in last decade the more promising, born to overcome the drawback of the HCCI combustion, are:

- the PCCI (Premixed Charge Compression Ignition) or the variant PPCI (Partially Premixed Compression Ignition), implemented using diesel or gasoline fuel; in last case the acronyms of GCI (Gasoline Compression Ignition) or GDCI (Gasoline Direct Compression Ignition)[45,46] are also used;
- the spark assisted HCCI;
- the RCCI (Reactivity Controlled Compression Ignition), based on dual fuel to obtained the proper fuel with chemical characteristic useful for the combustion.

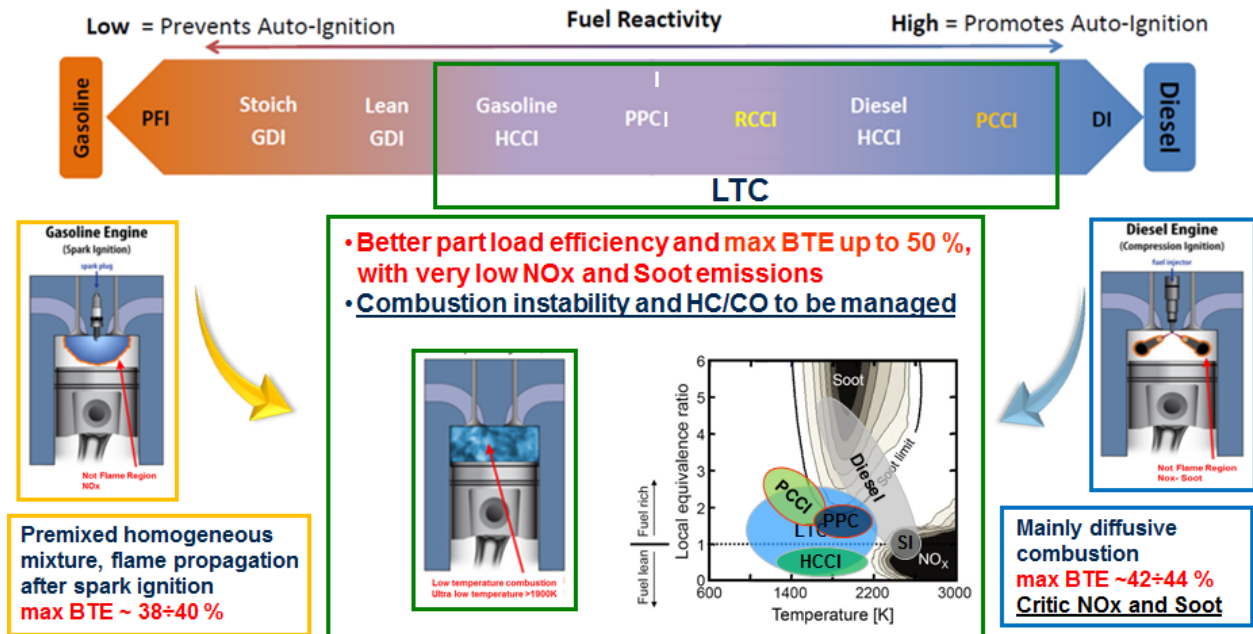


Figure 6-14 Low Temperature Combustion concepts

### 6.4.3 Premixed (PCCI) and Partially Premixed Compression Ignition (PPCI) Combustions

These combustion approaches are evolutions of HCCI combustion to improve combustion stability. The control over combustion events with direct injection strategy is retained and a greater percentage of the total charge is premixed prior to ignition relative to conventional diesel combustion. Depending on the level of homogeneity of the air-fuel mixture, PCCI combustion strategy uses early direct injection while PPCI applies late direct injection of fuel to prepare partially premixed mixture of air and fuel. In both engines, fuel is injected at an intermediate timing between that of HCCI and conventional CI engine. This results in a partially premixed fuel-air mixture, which auto-ignites similar to HCCI combustion mode. PCCI and PPCI combustion seem better compared to HCCI combustion, due to the better control over the combustion events, which leads to relatively superior engine performance.

Various injection strategies are available for PCCI combustion, but commonly advanced injection timings are used to increase fuel-air mixing time. Despite the charge not being completely premixed (homogeneous), the same principles are applied to obtain low emissions as with HCCI.

The factors used to promote combustion conditions toward the PCCI mode of operation are primarily the injection strategy and EGR rate. PCCI combustion is a single-stage combustion technique in which most fuel is burnt in premixed combustion phase. There is very small or practically no fuel remaining in the combustion chamber for diffusion combustion, which results in a relatively lower bulk temperature inside the combustion chamber. PCCI engines at high loads are facilitated with high boost pressure [250], which helps in oxidation of fuel resulting in relatively lower CO and HC emissions. Therefore, PCCI engine not only offers benefits of LTC with lower NOx and PM emissions but also results in lower HC and CO emissions.

One of the major challenges of PCCI combustion is to prepare the premixed charge (highly diluted fuel-air mixture to give reasonable burn rates) before auto-ignition temperature is attained and combustion

starts in the combustion chamber. In PCCI combustion engines, effective mixture preparation technique is required for achieving high efficiency, low HC, and PM emissions and preventing lubricating oil dilution. There are several techniques employed for charge preparation in PCCI combustion engines, depending on test fuel properties and control strategies being used.

For any combustion mode, combustion characteristics inside the combustion chamber affect overall performance parameters of the engine such as power output, emissions. Considering the fluid mechanics, PCCI combustion can be divided into three distinct phases, namely pre combustion, combustion, and post-combustion Figure 6-15 Low Temperature Combustion phases.

- Pre-combustion: flow dominates; small change in species.
- Combustion: chemistry dominates; heat release occurs so rapidly and globally that turbulent mixing does not have time to be a significant influence.
- Post-combustion: chemistry and turbulent mixing are likely to have some coupling, but no chemical heat release occurs.

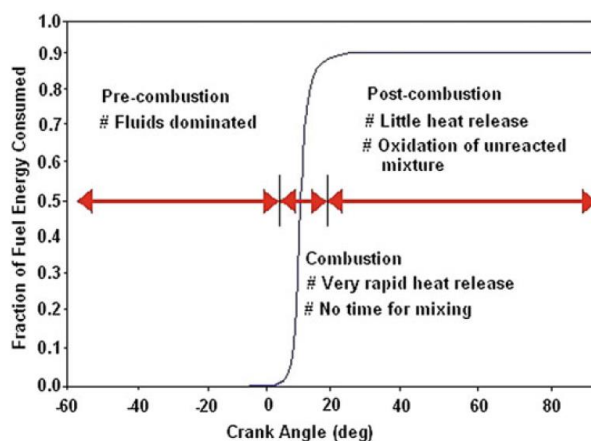


Figure 6-15 Low Temperature Combustion phases

Figure 6-16 presents the comparison of the emissions between a Conventional Diesel Combustion (CDC) and a PCCI combustion, obtained in the experimental tests, during research activities, with a 1.3L Common Rail diesel engine, installed on engine dyno in University of Bologna. The engine operation point is at 2000 rpm and 3 bar of BMEP. The CDC was characterized by 2 Pilot Injections of 1 mm<sup>3</sup>/stroke, in addition to a Main injection of 8 mm<sup>3</sup>/stroke. The PCCI combustion has been obtained by means of a single pilot injection of 4 mm<sup>3</sup>/stroke anticipated of 10 CA deg compared with the CDC and rail pressure increase from 550 bar up to 900 bar. The premixed combustion is characterized by lower NO<sub>x</sub> and Soot, with slight increase of HC and CO and approximately the same fuel consumption.

## Control Parameters of PCCI Combustion

Stable and efficient operation of LTC engines need accurate controlled combustion timings. One of the main challenges in LTC engines is the combustion control since onset of combustion depends on in-cylinder temperature, pressure, and fuel–air mixing inside the combustion chamber, and there is no direct control for initiating the combustion. When combustion control is not fast enough, too advanced or too retarded combustion can take place in the engine. Too advanced combustion can yield unacceptable RoPR or unacceptable peak cylinder pressure, thus causing excessive noise and potentially damage of the engine.



Additionally, NO<sub>x</sub> emissions from the engine tend to increase with ignition advance [309]. Another driver for an effective closed-loop combustion control is the fact that late combustion timing leads to incomplete combustion and increasing emissions of CO and HC. The worst case of “too late combustion” leads to a complete misfire, which if repeated, can cause the engine to stall. The main combustion control parameters are explained following.

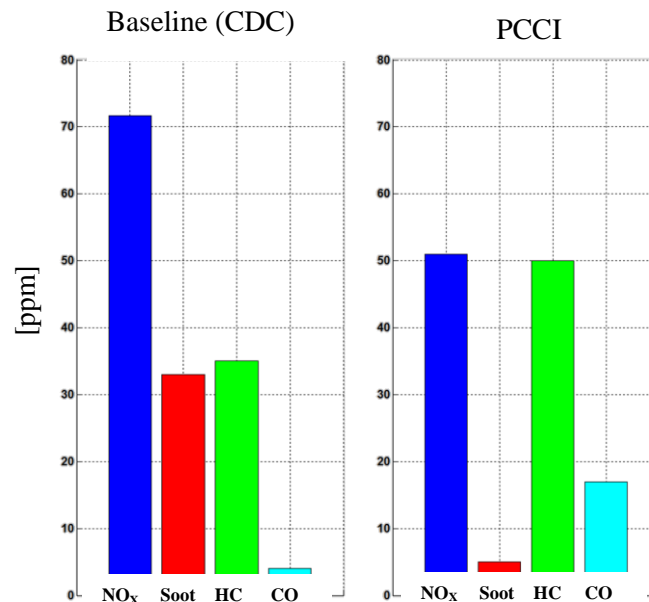


Figure 6-16 Comparison of CDC and PCCI combustion in 1.3L diesel engine (Smoke [FSN] and CO [% vol] have been multiplied by 100)

**EGR** is essential to achieve simultaneous reduction in Soot and NO<sub>x</sub> emissions from LTC without prohibitively high fuel consumption penalties due to poor combustion phasing. Tuning the amount of EGR is the most commonly used technique to adjust the in-cylinder temperature, which controls the SOC [302]. LTC is achieved by varying the inlet air temperature and EGR fraction over a range of equivalence ratios. High heat capacity constituents of EGR are CO<sub>2</sub>, H<sub>2</sub>O, N<sub>2</sub>, O<sub>2</sub>, CO, PM, HC, NO<sub>x</sub>, and other intermediate species of combustion reactions which control the LTC. These constituents showed following four effects on the combustion and emissions:

- First was the preheating effect, in which the inlet charge temperature increased when hot EGR was mixed with the fuel–air mixture.
- Second was the dilution effect, where by the introduction of EGR led to substantial reduction in oxygen concentration.
- Third was the heat capacity effect, in which total heat capacity of the mixture of EGR, air, and fuel would be higher owing to higher heat capacity of CO<sub>2</sub> and water vapor. This would lead to a reduction in gas temperature at the end of the compression stroke.
- Fourth and final was the chemical effect, where unburnt combustion products in the EGR would take part in chemical reactions. HC, CO, CO<sub>2</sub>, NO, H<sub>2</sub>O, etc., in the EGR take part in chemical reactions and lead to a moderate effect on the reaction rates.

Integrating all these effects, SOC during the LTC and combustion duration can be controlled by regulating the EGR quantity. Therefore, EGR makes it possible to suppress the excessively advanced SOC by low-

temperature reactions in the LTC phase. This excessively advanced and rapid combustion causes knocking, which limits the operating range of LTC. EGR use can be internal EGR and external one, as presented in Chapter #6.3. Internal EGR rate can be controlled by changing the valve overlap period and the external EGR rate can be adjusted by the combined effect of the exhaust backpressure and EGR valve. Cooled external EGR reduces the fuel–air mixture temperature in the compression stroke and hence delays the SOC of high cetane fuels such as biodiesel.

However, the research studies also pointed out the need to control dilution ratios because maximum fuel conversion efficiency was obtained at moderate charge dilution levels. Over-dilution leads to poor trade-off between work conversion efficiency and combustion efficiency, thus reducing fuel conversion efficiency. Another advantage of charge dilution is increased ignition delay, which can improve IMEP and COV. Asad et al. [303] performed LTC experiments using different EGR rates to postpone SOC by increasing the ignition delay and to reduce the severity of high RoPR. They stated that EGR was effective in delaying combustion phasing toward higher thermal efficiency window by withholding the cylinder charge from early ignition. Figure 6-17 shows that increasing EGR rate results in stable combustion. It was concluded that combustion efficiency reduced with increasing EGR, which was compensated by improvement in combustion phasing. This trade-off between combustion efficiency and emissions showed the importance of EGR in LTC engines.

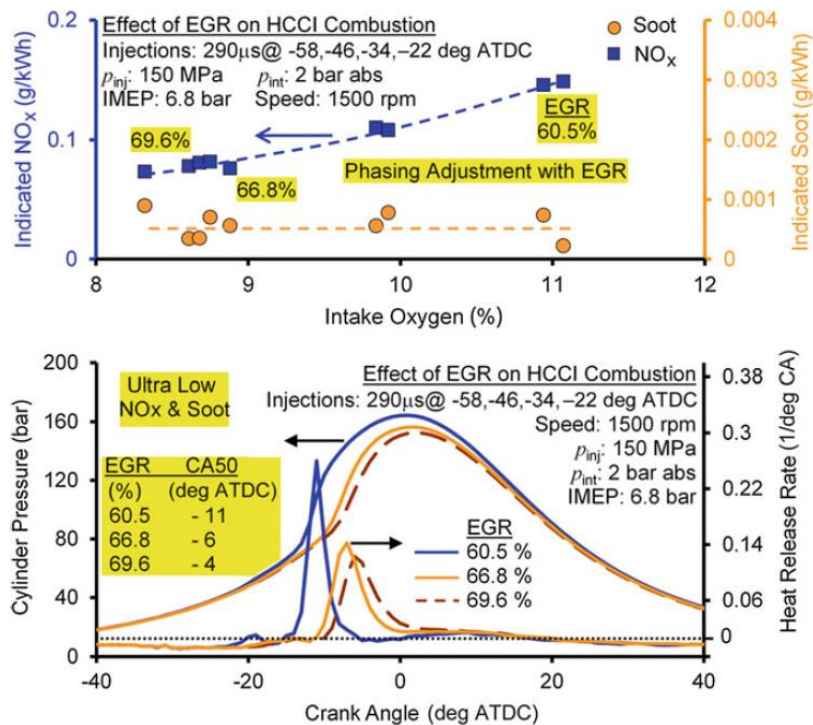


Figure 6-17 Effect of EGR on HCCI combustion and emissions [302]

**Injection Pattern** - Early injection can lead to impingement of fuel on the cylinder walls, particularly at high BMEPs. Single-injection LTC is applicable to limiting conditions, where tighter controls on operating conditions are required compared to conventional CI combustion. Issues of LTC such as high HRR and uncontrolled combustion can be resolved by using split fuel injection strategy. Major quantity of fuel was injected early in the compression stroke (100° BTDC) to prepare premixed charge, and the remaining quantity was injected near TDC to control SOC. This resulted in better combustion characteristics, precise control of SOC, and higher BMEP.

Results clearly showed that NO<sub>x</sub> emissions from PCCI combustion were much lower compared to CI combustion and advanced pilot injection (from 100° BTDC to 150° BTDC) showed further reduction in NO<sub>x</sub>. The effect of split injection strategy on emission formation in a PCCI diesel engine was investigated in [310,311].

The researchers realized that higher thermal efficiency and lower NO<sub>x</sub> emissions at moderate loads could be achieved by single-injection strategy; however, they experienced problem of very high RoPR. In case of split injection strategy, a small quantity of pilot injection helped in suppressing higher RoPR. The application of early pilot injection resulted in a significant improvement in thermal efficiency and reduction in engine noise and emissions by optimizing SOI timings and EGR rate. They later dealt mainly with effect of pilot injection on engine noise and performance. Engine noise remained one of the major factors governing combustion and performance characteristics. They reported a reduction in BMEP with an increase in pilot quantity above 40%. Further, relatively higher engine noise was observed for almost all early single-injection timings, mainly due to very high RoPR. The inclusion of pilot injection proved to be very effective in reducing noise, but it also led to reduction in BMEP.

Neely et al. [304] investigated the effect of number of pilot injections (up to 3) to achieve PCCI combustion in order to reduce NO<sub>x</sub> in light-duty and heavy-duty vehicles. They stated that an early single pilot injection was effective for ~14% NO<sub>x</sub> reduction, but it was at the expense of higher CO and BSFC. However, CO and BSFC penalty significantly reduced along with NO<sub>x</sub> by employing multiple pilot injections at lower loads. This was mainly due to superior fuel–air mixing. For heavy-duty vehicles, multiple pilot injections proved to be ineffective in reducing NO<sub>x</sub> compared to single pilot injection. In addition, multiple pilot injections also led to higher HC and CO emissions. Asad et al. [303] performed HCCI experiments and suggested that optimized SOI of the multiple injections could assist in preparation of a near-homogeneous charge that resulted in near-zero soot emissions.

Following the more interesting studies on PPCI engines with alternative fuels to diesel (e.g. Gasoline and Naphtha) are presented.

### Gasoline Direct Compression Ignition (GDCI) Engine

One of the more interesting studies on PPCI engine with gasoline fuel is carried out by Delphi, which is at the third generation of its GDCI engine [46]. Key objectives of this demonstrator engine include diesel-like fuel efficiency, extremely low tailpipe emissions on-cycle and off-cycle, to meet US 2025 CAFE and Tier 3 Emissions, and robust GDCI combustion with good transient control. The following picture shows the engine architecture. The powertrain main features are: optimized GDI fuel injection system, advanced boost, thermal management, EGR, and exhaust gas after-treatment systems that meet packaging requirements for a D-class passenger car.

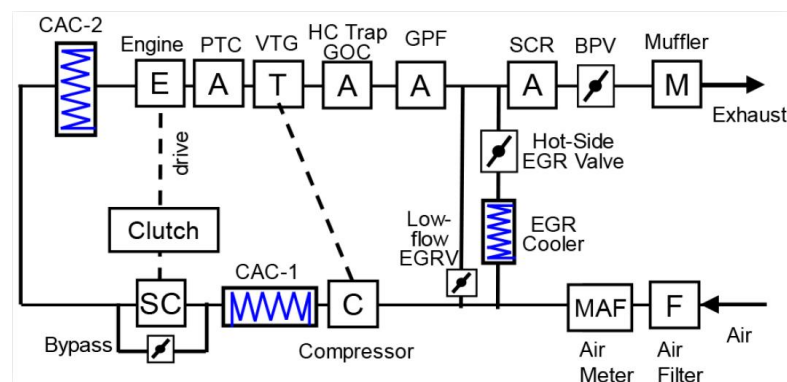


Figure 6-18 Architecture of GDCI engine

The engine can operate with a range of gasoline fuels including less-processed, low-octane gasoline and higher-octane, high sensitivity gasoline. The test results using RON91 fuel indicated very low fuel consumption, while meeting targets for engine out NO<sub>x</sub> and PM emissions, combustion noise and stability. BSFC at the 2000 rpm and 2 bar BMEP global test point was 250 g/kWh. Minimum BSFC was measured at 205 g/kWh with inert catalysts over a wide range of medium loads where customers regularly drive. The exhaust gas after-treatment system exhibited high exhaust temperatures and high conversion efficiency for HC and CO emissions. Preliminary tests at cold cranking conditions indicated robust first-cycle combustion with the potential for fast catalyst light-off.

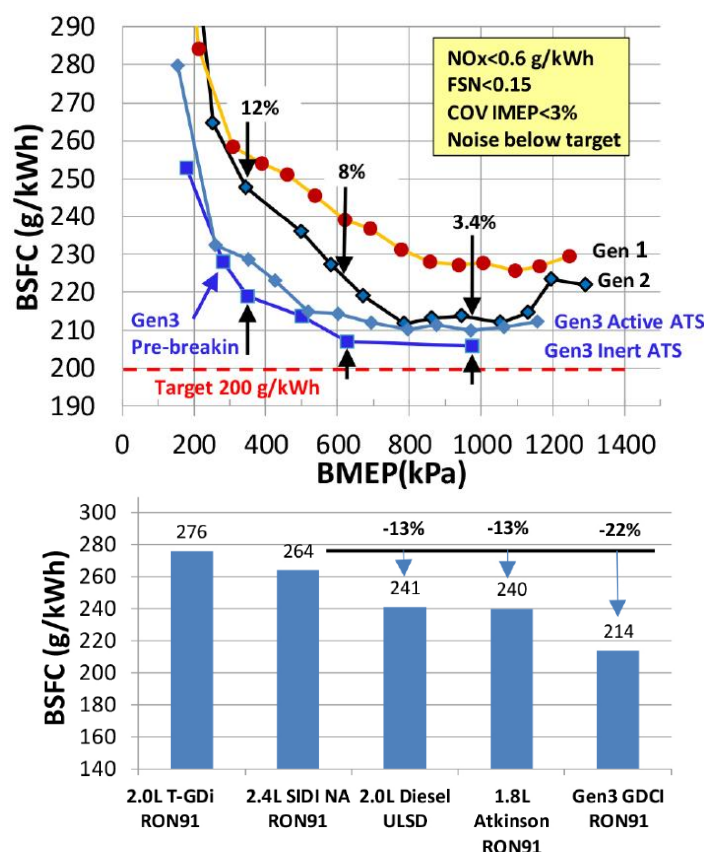


Figure 6-19 BSFC at 1500 rpm as a function of load for the three generations of the GDCI and comparison of the Gen.3 engine at 6 bar IMEP with various competitive engines

The Figure 6-19 shows the evaluation and the assessment of BSFC data at 1500 rpm and 6 bar IMEP compared with variety of class leading powertrains including a 2.0L turbo Spark Ignited (SI) engine, a 2.4L naturally aspirated SI engine, a 2.0 L turbo diesel engine, and a 3rd-generation Prius Atkinson-cycle engine. The Gen.3 GDCI engine exhibited the lowest BSFC of 214 g/kWh of the group, and was approximately 11 percent lower than the 2.0 L diesel.

### Gasoline Compression Ignition (GCI) Engine

This engine is based on PPCI combustion and characterized by the use of less processed fuel compared to diesel or gasoline, and hence easier to manufacture, with “low quality”, i.e. RON between 65 and 85 (Cetane number less than 25) and no strict requirement on volatility. In [110] the benefits of the GCI approach were investigate by means of a single cylinder GDI engine in the most significate point of FTP

cycle. The main future of the engine were: Compression Ratio 14, piston bowl like diesel, central mounted outwardly open injector up to 150 bar, and an exhaust rebreathing strategy to trap the exhaust gas (35-45% internal residual at part load when intake and exhaust manifold pressure difference about 15kPa). A single and double pulse strategy for the injection is used with Light naphtha fuel (RON 68, DCN 31, Evaporation T90 70 °C).

Compared with conventional stoichiometric SI operation, over a range of part load operating points representative of the federal test FTP, an average 26% of improvement was achieved, whit engine out ISNOx below 0.3 g/kwh and PM below 0.2 FSN, see Figure 6-20 with the complete engine maps.

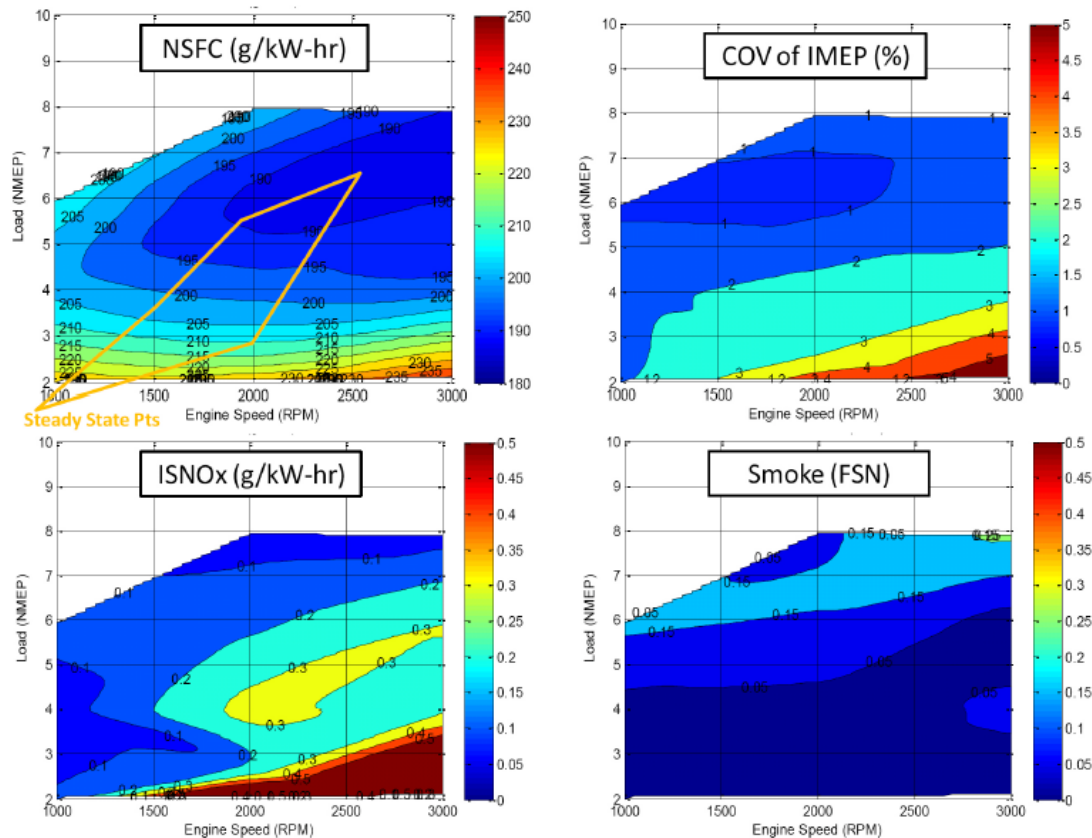


Figure 6-20 Engine Load-Speed Contour Plots with light naphtha + CR 14 piston configuration: High load line is limited by maximum pressure rise rate (5bar/°crank) and low load line is limited by COV of IMEP.

#### 6.4.4 Spark Assisted HCCI Combustion

This approach was proposed by Mazda to overcome the controllability problem of HCCI combustion and they named this kind of combustion system SPCCI (Spark Controlled Compression Ignition) and the engine “Skyactiv-X”, as reported in [47]. The implementation is claimed for production at beginning of 2019 and the new engine is the convergence of the first generation PCCI engines, named “Skyactiv-D” and “Skyactiv-G”, respectively diesel and gasoline engines [48, 105]. In the SPCCI combustion the spark plug is used as control factor of the compression ignition. The fire ball, generated with spark, increases the in cylinder pressure causing the simultaneous ignition in many places of combustion chamber in high lean condition ( $\lambda$  up to 2.5) burn in, see Figure 6-21. In this way the compression ratio can be maintained around 16 limiting knock issues at high loads.

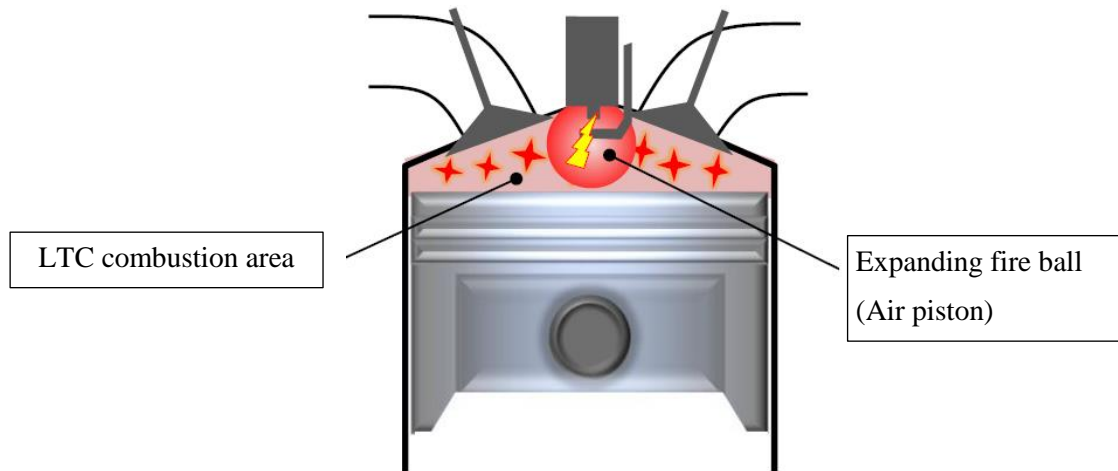


Figure 6-21 SPCCI basic concept

As presented in [47] the SPCCI works over a wide range of engine speed and loads and allows stable switching between HCCI and SI combustions, performed at high engine speed and load. The engine in LTC mode operates in high lean condition with cold EGR and de-throttling. The performance at high load is supported by a mechanical compressor, allowing good EGR tolerance to contrast the knock and fast responsiveness. The Figure 6-22 illustrates the improvement of output Torque curve for Mazda's SPCCI engine with previous generations, considering two different gasoline fuels.

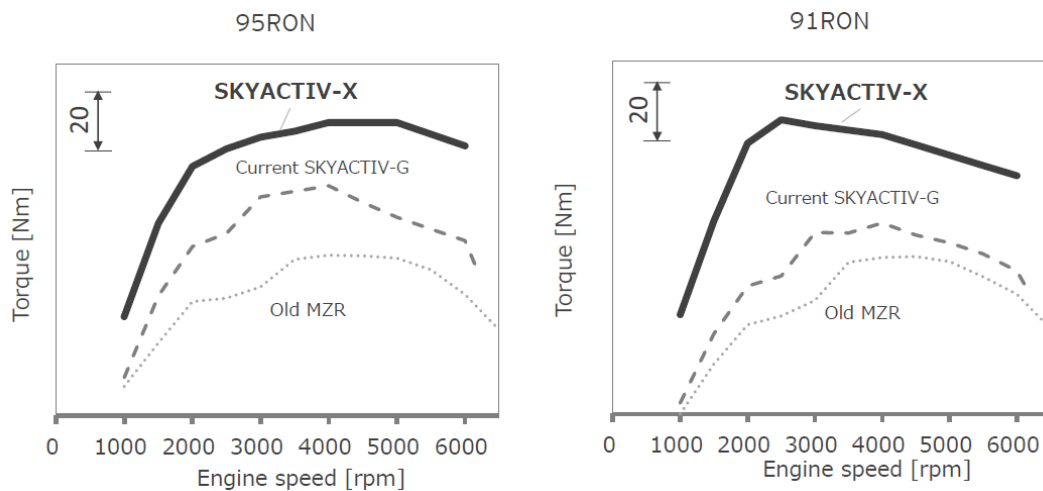


Figure 6-22 Comparison of output Torque curve for SPCCI engine of Mazda with previous generations

In [48] the efficiency of previous Mazda's engines, based on PCCI combustion, was assessed. The benchmark-by means of engine testing performed by EPA shows the better performance in significant engine points, see Figure 12-16.



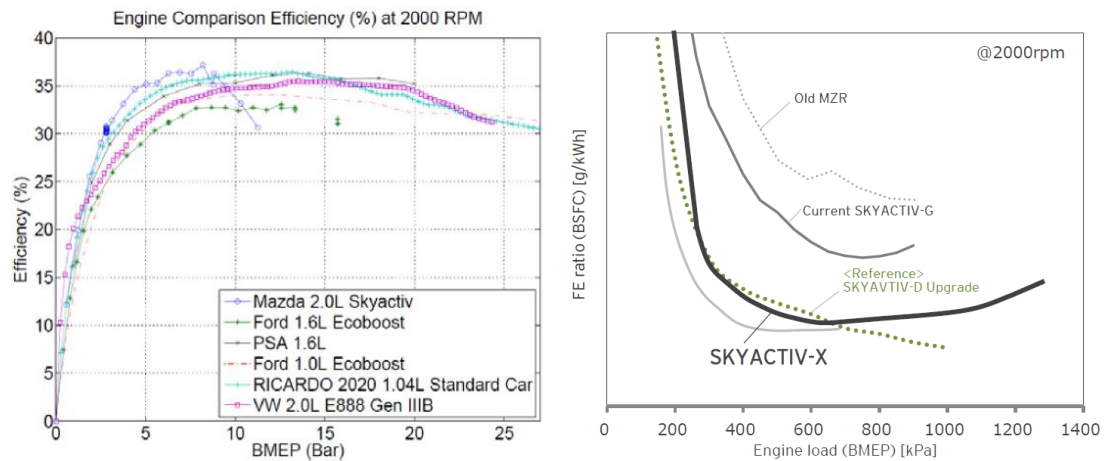


Figure 6-23 BTE comparison of Mazda's engine (SkyActiv-G) with other competitors and the BSFC evolution of new SkyActiv-X vs. SkyActiv-G

Another important feature of the SPCCI engine of Mazda is the flat BSFC curve, see Figure 6-24, that allows little difference in fuel economy performance in the real world. Driving pleasure as combination of performance & efficiency is the global achievement of Mazda approach.

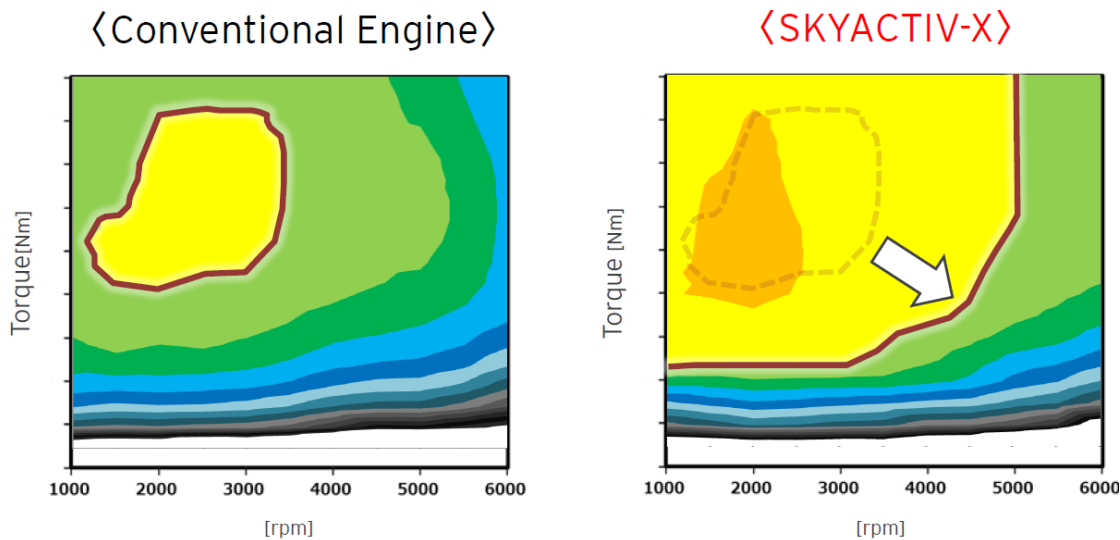


Figure 6-24 Comparison of BSFC curve for Mazda's SPCCI engine with conventional engine

## 6.4.5 Reactivity Controlled Compression Ignition (RCCI) Combustion

LTC dual-fuel combustion is commonly referred to as RCCI combustion and has been demonstrated extensively for diesel–gasoline and diesel–ethanol blends. In this LTC approach, two fuels with different auto-ignition properties are used. The system would have a main fuel with a high octane number and a secondary fuel with low octane number, that is use to ignite the air-fuel mixture. Different auto-ignition properties of dual-fuel systems are used to control the combustion phasing in LTC as blending two fuels in

different proportions changes their auto-ignition properties. In [41] a wide review of this combustion approach is presented by Rietz et al. Between the analysis reported, the main results obtained by his research group has been presented. Focusing on passenger cars, the experimental activities were carried out on 1.9L diesel Common Rail engine, with a rated power of 110kW and compression ratio equal to 17.5. A port fuel injection system was retrofitted. The engine was used to investigated the combustion phenomena in RCCI mode, using different fuel mixture, including biofuels, and different engine control parameters, such as SOI, injection pattern, and intake temperature and pressure. The experimental activities have been supported by CFD analysis that led to combustion chamber optimization, modifying the piston bowl compared with diesel engine.

A comparison in term of engine outputs between a Conventional Diesel Combustion (CDC) and the RCCI combustion performed with gasoline and a mixture E85 has been presented in [41] with more details in [236]. From Figure 6-25 it can be seen that the BTE of RCCI is higher than CDC at higher load.

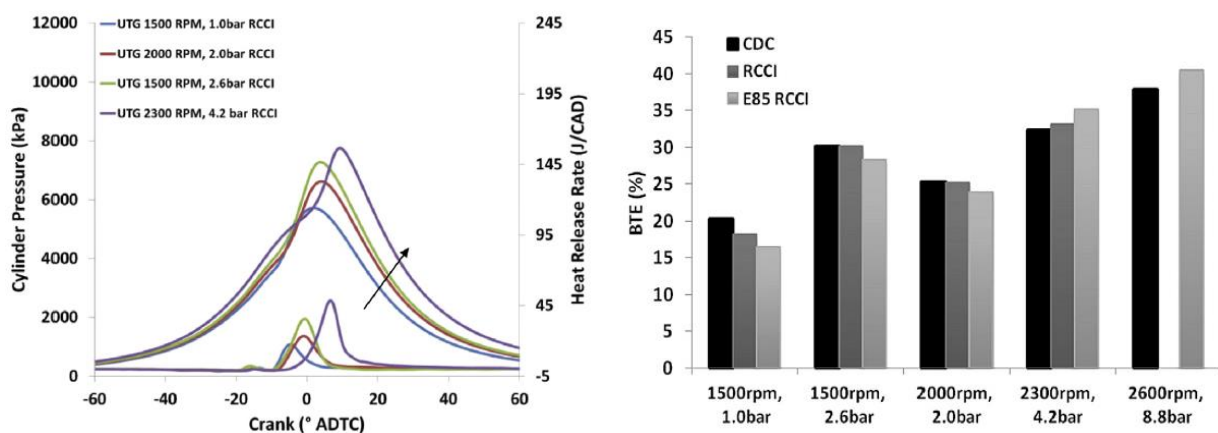


Figure 6-25 Pressure and HRR in RCCI with gasoline (left), BTE for Gasoline and E85 compared to CDC (right)

The NO<sub>x</sub> emissions of RCCI operation with E85 are lower than CDC operation, especially at high speed, as depicted in Figure 6-26. In the same figure PM emissions of RCCI operation were nearly zero. The soot concentration was estimated by correlation with the filter smoke number (FSN).

The hydrocarbon emissions for G/D RCCI and E85/D RCCI were higher than for CDC operation (see Figure 6-27). RCCI with E85 provided decreased HC emissions compared to RCCI with gasoline and this decrease in HC was observed with increases in load and speed.

The CO emissions followed the same trends as seen for the HC emissions, as shown in Figure 6-27. At lower load, CO emissions for RCCI with E85 were higher than RCCI with gasoline and vice versa at the higher load, but at all the loads and speed CO emissions of RCCI with both the PFI fuels were higher than with CDC operation.

The exhaust temperatures as measured at the turbocharger outlet are shown in Figure 6-28. The exhaust temperatures for RCCI operation range from 22% to 35% lower than that of CDC operation. This aspect is a critical issue for the catalyst operation and has to be properly managed.

Moreover in [41] a sensitivity analysis of HCCI, PCCI and RCCI versus intake pressure and temperature has been presented, resulting in a high impact on combustion of these parameters variations. These facts confirm the need of a combustion closed loop control to compensate the dependence on mixture thermal variations.



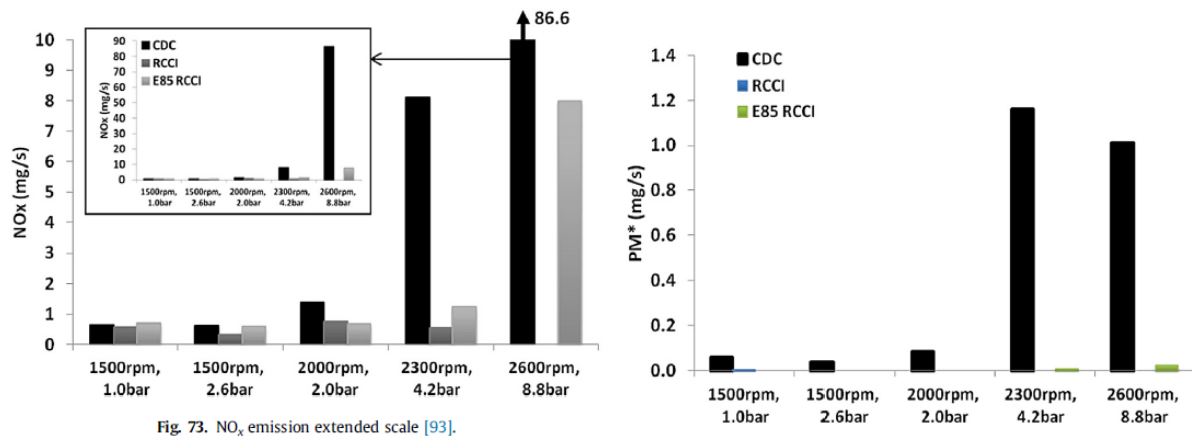


Fig. 73. NO<sub>x</sub> emission extended scale [93].

Figure 6-26 NO<sub>x</sub> emission (left) and PM emission (right) in RCCI vs. CDC

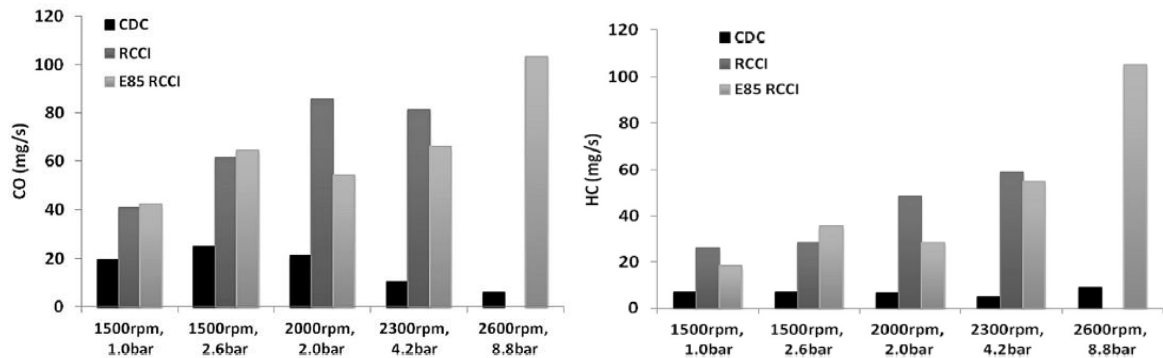


Figure 6-27 CO emission (left) and HC emission (right) in RCCI vs. CDC

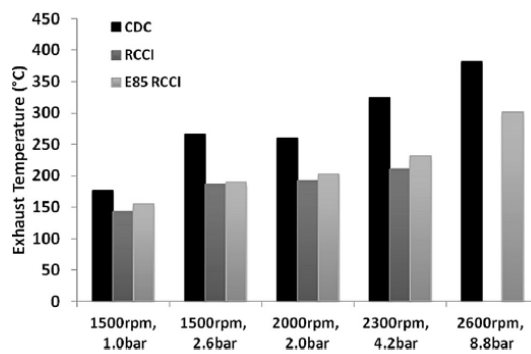


Figure 6-28 Exhaust gas temperatures in RCCI vs. CDC

The LTC Control is one object of investigation in this PhD study and the main finding are illustrated in the Chapter #11.5 and published in [209,223,226]. Since the RCCI concept has shown to provide better control of combustion in more wide area of engine operations, without complex engine modifications compared to other approaches, the research activity was focused on it.

## 6.4.6 Summary of Advanced Combustions Benefits and Drawbacks for ICE

The main features of the advanced combustion approaches are summarized in the following Table 6-3. The references are GDI turbocharged and Diesel Common Rail Turbocharged engines.

Table 6-3 Summary of Advanced Combustion technologies benefits and drawbacks

ICE Technology	Advantages	Influenced Engine Zones	Drawbacks
<b>GDI lean Combustion</b>	<ul style="list-style-type: none"> <li>- Pumping losses reduction at low loads</li> <li>- Higher ratio of specific heats</li> <li>- Knock mitigation</li> <li>- Lower heat losses towards cylinder walls</li> <li>- Operation in stoichiometric mode allows the TWC use at high engine power</li> </ul>	All engine operating area with higher impact on 1, 2 and 3	<ul style="list-style-type: none"> <li>- Expensive exhaust after-treatment for NOx reduction</li> <li>- Higher cycle-to-cycle variation</li> <li>- Higher Boosting demand</li> <li>- Combustion chamber and piston re-design</li> <li>- Advanced ignition system requirements</li> </ul>
<b>HCCI Combustion</b>	<ul style="list-style-type: none"> <li>- Pumping losses reduction at low loads</li> <li>- Higher ratio of specific heats</li> <li>- Lower heat losses towards cylinder walls</li> <li>- Lower PN/PM than Diesel and GDI</li> </ul>	All engine operating area with higher impact on 1, 2 and 3	<ul style="list-style-type: none"> <li>- Low controllability and unstability of combustion</li> <li>- Combustion Noise to be managed</li> <li>- Higher EGR rate and Boosting demand</li> <li>- Combustion chamber and piston re-design</li> <li>- Cold start to be managed</li> <li>- Limited engine operation area</li> <li>- Difficult stoichiometric operation</li> </ul>
<b>PCCI/PPCI Combustion</b>	<ul style="list-style-type: none"> <li>- Pumping losses reduction at low loads</li> <li>- Higher ratio of specific heats</li> <li>- Lower heat losses towards cylinder walls</li> <li>- Lower PN/PM than Diesel and GDI</li> <li>- More controllability than HCCI</li> <li>- Wider engine operation area than HCCI</li> </ul>	All engine operating area with higher impact on 1, 2 and 3	<ul style="list-style-type: none"> <li>- Unstable combustion to be managed with closed loop control and higher fuel injection accuracy</li> <li>- Combustion Noise to be managed</li> <li>- Higher EGR rate and Boosting demand</li> <li>- Combustion chamber and piston re-design for gasoline use</li> <li>- Cold start to be managed</li> <li>- Engine operation up to middle load</li> <li>- Proper fuel use in case of GCI</li> <li>- Difficult stoichiometric operation</li> </ul>
<b>RCCI Combustion</b>	<ul style="list-style-type: none"> <li>- Pumping losses reduction at low loads</li> <li>- Higher ratio of specific heats</li> <li>- Lower heat losses towards cylinder walls</li> <li>- Lower PN/PM than Diesel and GDI</li> <li>- Highest controllability among LT combustions</li> <li>- Widest engine operation among LT combustions</li> </ul>	All engine operating area with higher impact on 1, 2 and 3	<ul style="list-style-type: none"> <li>- Complexity and Cost, due to dual fuel use (gasoline/ethanol and diesel)</li> <li>- Unstable combustion to be managed with closed loop control</li> <li>- Combustion Noise to be managed</li> <li>- Higher EGR rate and Boosting demand</li> <li>- Combustion chamber and piston optimization</li> <li>- Operation like Diesel engine at high power with high NOx production</li> </ul>
<b>Spark Assisted HCCI Combustion</b>	<ul style="list-style-type: none"> <li>- Pumping losses reduction at low loads</li> <li>- Higher ratio of specific heats</li> <li>- Lower heat losses towards cylinder walls</li> <li>- Lower PN/PM than Diesel and GDI</li> <li>- More controllability than HCCI</li> <li>- Wider engine operation area than HCCI</li> <li>- Operation in stoichiometric mode allows the TWC use at high engine power</li> </ul>	All engine operating area with higher impact on 1, 2 and 3	<ul style="list-style-type: none"> <li>- Unstable combustion to be managed with closed loop control and higher fuel injection accuracy</li> <li>- Combustion Noise to be managed</li> <li>- Higher EGR rate and Boosting demand</li> <li>- Combustion chamber and piston re-design for gasoline use</li> <li>- Cold start to be managed</li> <li>- Engine operation up to middle load</li> </ul>

The RCCI allows a wider engine operation area, but it is weak in terms of cost and easy use for the end-user. Indeed, in addition to dual fuel refilling, a de-NOx after-treatment device is needed in high power condition, due to lean operation like a diesel engine. The Spark Assisted HCCI combustion seems to be the better trade-off between benefits and costs. In addition to the part load advantages, like other LTC approaches, the s-HCCI can operate in stoichiometric mode allowing the use of Three Way Catalyst, especially in high power conditions, avoiding expensive after-treatment for the NOx.

## 6.5 Exhaust Gas After-treatment Technologies

As mentioned the trend of new emission standards is towards zero tailpipe pollutant in real conditions; this is the aim of new standard cycles. With focus on EU regulations, the real conditions are verified for type

approval with higher load and colder conditions, for instance the test cycle starting at ambient temperature-7°C [5].

Focusing on SI engines, higher load can lead the engine to operate in a zone characterized by thermo-mechanical stresses for the engine components, such as the turbine, that can be protected with dedicated cooling systems or by means of the enrichment of the mixture.

The first solution is not suitable for all components and in some cases not sufficient. The new EU7 standard forces to limit HC/CO and PM/PN emissions at high load, as a consequence the operation at  $\lambda=1$  is needed. To fulfill this technical requirement, avoiding performance reduction or engine specific power reduction, some technologies are mandatory (e.g. EGR, Water Injection) and they have been discussed in a previous section.

The monitoring of PM and PN, in real conditions with lower limits, forces the improvement of the GDI combustion process with higher fuel injection pressure (>300 bar) [305, 320, 321] and the adoption of dedicated exhaust after-treatment devices, like the Gasoline Particulate Filter (GPF) [321]. The support of an electric motor during load transient can help to reduce the PM/PN production by the engine in hybrid electric vehicles, but it can not avoid the GPF application.

### Gasoline Particulate Filter

The GPF is an exhaust after-treatment device with the purpose of trapping particulate within its porous honeycomb ceramic substrate (wall-flow filter). Pores generally have a diameter in the range of  $10\ \mu\text{m} \div 30\ \mu\text{m}$ , trapping bigger particles and being passed through by the gaseous components. Ceramic is used for the substrates due to high temperatures which the GPF is exposed to, via extruding a porous ceramic material in order to obtain a monolithic cylinder. Blind parallel channels are made in the substrate, being alternately open/close at their upstream and downstream extremities, forcing gases to pass through the porous walls and to deposit suspended particles, see Figure 6-29. Particle agglomerates cumulate on the filtering surfaces, enhancing GPF capability to trap increasingly smaller particles, but also rising back-pressure.

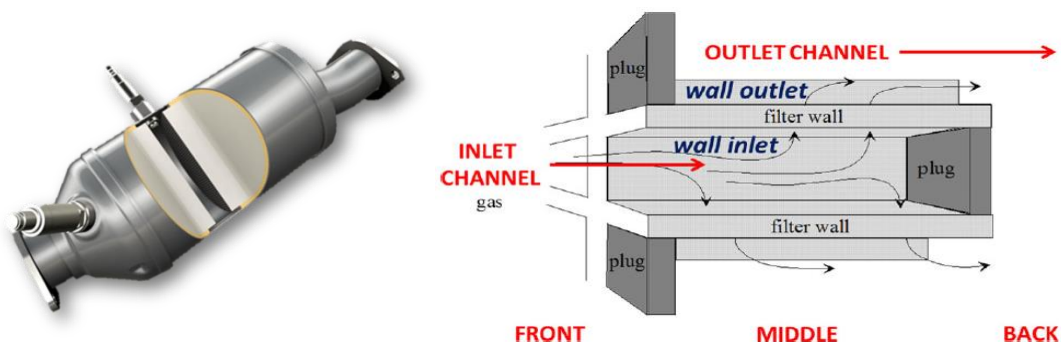


Figure 6-29 GPF assembly and filtering scheme inside its channels

The GPF is periodically cleaned through an oxidation of the deposits by means a procedure called «regeneration». Two different kinds of regeneration can be performed, depending on  $\text{O}_2$  availability and the temperature conditions:

- **Passive Regeneration**, the GPF is capable of auto-regeneration, in case of sufficiently high temperature, without external energy contribution.
- **Active Regeneration**, external energy contribution is needed to reach temperature for GPF regeneration (e.g. expansion injection of fuel to keep the combustion during the exhaust stroke).

The GPF technology is derived by Diesel Particulate Filter (DPF). The following Table 6-4 illustrates a comparison of the main features and summarizes the data published in [237,238].

Table 6-4 Differences between GPF and DPF (V<sub>eng</sub>: engine displacement)

	DPF	GPF
<b>Main requirements</b>	<ul style="list-style-type: none"> <li>Filtration efficiency</li> <li>Back-pressure with soot</li> <li>Resistance to gradient thermal shock</li> </ul>	<ul style="list-style-type: none"> <li>Filtration efficiency</li> <li>Back-pressure without soot</li> <li>Resistance to peak thermal shock</li> </ul>
<b>Filtration Efficiency</b>	>99% ← Periodic regeneration	60% ÷ 90% ← “Continuous” regeneration
<b>Back-pressure</b>	Similar trends with soot loading	
<b>Layout</b>	Trend of integration with other after-treatment devices	
<b>Materials &amp; Size</b>	SiC/AlTi, 1.5 V <sub>eng</sub> ÷ 2.0 V <sub>eng</sub> , 600 ÷ 800 g/l	Cordierite, ≈ V <sub>eng</sub> , 300 ÷ 400 g/l
<b>Cell Structure</b>	Layout: Asymmetric inlet/outlet channels Cell density: 200 ÷ 300 cpsi Wall thickness: 12 ÷ 15 mm  To accommodate more ashes, <b>asymmetric substrates</b> (different size for inlet/outlet channels) were created for DPFs, causing back-pressure to increase without soot, but to decrease with soot due to the larger filtration surface	Layout: Symmetric inlet/outlet channels Cell density: 200 ÷ 350 cpsi Wall thickness: 6 ÷ 12 mm  For GPFs, the main constraints are the back-pressure without soot and the substrate mechanical strength, thus the <b>symmetric substrate</b> is the best choice
	V <sub>eng</sub> = engine displacement	cpsi = cells per square inch

The higher DPF efficiency can be explained with the soot cake formation [238]. In GPF the soot cake is easily eliminated due to passive regeneration, favored by higher temperature during fuel cut-off events. There are a number of options for the positioning of GPF in the exhaust system, see Figure 6-30 from [239]: in the underfloor position, in a position close to the engine and behind a TWC or in a CC1 (Closed Coupled 1) position close to engine. All concepts respectively offer different advantages and disadvantages and impose various requirements on the coating which are contrasted below.

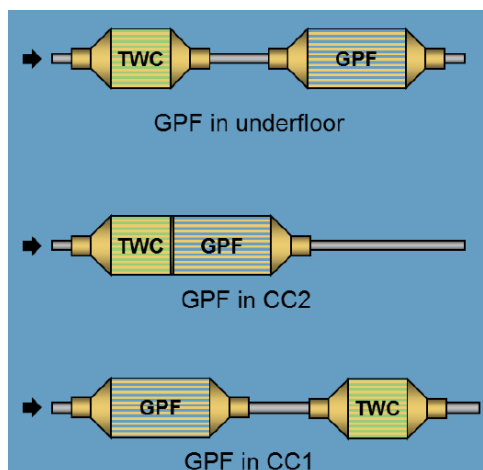


Figure 6-30 Overview of the possible positioning of the GPF with the integrated TWC functionality in the exhaust system

- GPF in the underfloor structure behind a TWC* allows the GPF to be used as an “add-on” solution in many applications. The configuration of the application close to the engine can remain unchanged and the diagnosis of TWC in the CC position must not be changed either. A challenge

for using the GPF in the underfloor position is the soot regeneration of the filter. It must not only be guaranteed that the necessary temperature for the combustion of the soot is generated, but the necessary oxygen must be provided as well.

- *GPF in the CC2 position behind a TWC* is characterized by good temperature for easy passive regeneration. The packaging is the main challenge, due to the positioning in engine compartment close to the engine. For this reason compact solution can be adopted, with negative effect on the backpressure.
- *GPF in the CC1 position* is a closed-coupled position as the first catalytic component in the exhaust system offers the best conditions with respect to soot regeneration. The filter must have a low light-off temperature even after severe ageing to ensure the emission in cold start, in the relevant cycles as well as under all RDE conditions. This low light-off temperature is primarily important because the filter substrate has a higher thermal mass than a conventional three-way catalytic converter discharge substrate and therefore has disadvantages during cold start. Another challenge is that the complete on-board diagnosis (OBD) must take place using the GPF since the GPF is installed at the CC1 position. This poses special requirements for the oxygen storage capacity of the GPF. For the diagnosis, it must be ensured that an adequate amount of oxygen storage capacity is available after relevant ageing, while the amount in fresh state must not be too high. These prerequisites for the coated GPF make it necessary to develop a special coating that can fulfil the requirements of positioning in CC1.

## Electric Heating Catalyst

To cope with the cold start issue, a faster light-off of catalyst is requested. The main technological solution is the Electric Heating Catalyst (EHC), which offers advantages in conventional powertrain and higher electrification ones. In fact in HEVs, in cold starts condition, the thermal engine is maintained on until the catalyst reaches the operation temperature, delaying the pure electric mode operation. The EHC can accelerate the catalyst warm-up and maintaining it warm, extending the electric mode operation.

The EHC system can be enabled by the introduction of 48V power net on board the vehicle, that can easily support the needed peak of power over 4 kW.

In the EHC an electric coil is installed in a metal catalyst, and supplied and heated with energy from the traction battery. The electric catalyst is a thin catalyst disc directly followed by another, often ceramic, catalyst [147]. The resulting heat energy of the first catalyst disc is transported through the complete catalyst by secondary air or the exhaust gas flow. In this way the whole exhaust system is finally heated. The electrically heated catalyst is already being used in series in some high performance cars. This technology benefits from the increasing electrification of the powertrain, because higher voltages (> 12 V) allow a sufficient heating level (> 4 kW) and higher battery capacity from traction batteries can be used.

As already proven in some studies [147,148], this technology allows a fuel saving versus the conventional light-off management, as illustrated in Figure 6-31.

A similar temperature level can be achieved using electric heating or engine-based catalyst heating, even if the energy used in the EHC is much lower. This is predominantly the effect of the lower mass flow rate in EHC based catalyst heating than engine-based catalyst heating. Temperatures and mass flows at the catalyst using a range of different heating processes. This means that in engine-based catalyst heating the energy needed consists of two contributions: the first one is the energy needed to heat up the mass flow from the temperature reached during normal operation to the desired temperature.

The second is the energy needed to heat up the additional mass flow to the desired temperature. This second contribution is needed to heat up the catalytic converter as fast as possible. Therefore, in order to achieve a defined catalyst temperature, an energy level that is almost three times as high as with electric heating will be necessary (Figure 6-31). Thus, in the context of modern automotive architectures, the EHC appears particularly interesting from the energy requirement point of view.

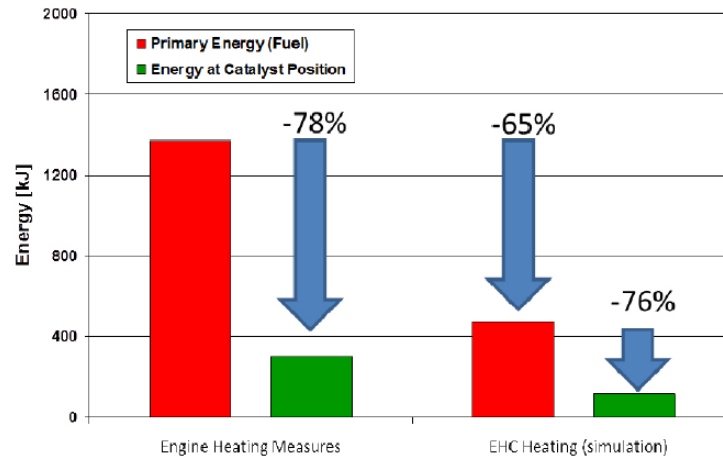


Figure 6-31 Comparison of primary energy used and resulting energy at the catalyst in the first 100s for identical emissions level using both heating processes [147]

## 6.6 Engine Technology Cost Analysis

Cost estimations for the powertrain manufacturers, during the early phase of technologies investigation or product development, are subject to several uncertainties. These uncertainties are related to information concerning the product and the production, including the production process and its resources. Nevertheless, especially when developing a new technology, the assumed product costs must be tracked in order to lead the product to a successful market introduction. The sources of technology costs are [80,87, 93, 99]. Information coming from these works was reviewed, and the estimated costs at 2025 of the main technologies are summarized in the following Table 6-5. The baseline is a 4 cylinders Turbocharged GDI engine.

Table 6-5 Costs of analyzed technologies

Technology	Baseline	$\Delta$ Average Cost [€]	Remark
GDI Lean	1-stage TC, GDI, 4 Cyl	385	including LNT catalyst
Miller Cycle	1-stage TC, GDI, 4 Cyl, VVA	200	considering a 2st of TC or displacement increasing
VCR- 2stages	1-stage TC, GDI, 4 Cyl	125	
VCR- Continuous	1-stage TC, GDI, 4 Cyl	350	
Port Water Injection	1-stage TC, GDI, 4 Cyl	95	
DWI - Separate	1-stage TC, GDI, 4 Cyl	180	
DWI - Mixture	1-stage TC, GDI, 4 Cyl	130	
Electronic Cyl Deact.	1-stage TC, GDI, 4 Cyl	100	
Cylinder Deactivation	1-stage TC, GDI, 4 Cyl, VVA	200	
LP-EGR	1-stage TC, GDI, 4 Cyl	115	
HP-EGR	1-stage TC, GDI, 4 Cyl	115	
2stages-Turbo	1-stage TC, GDI, 4 Cyl	200	
eBooster	1-stage TC, GDI, 4 Cyl	400	including Li battery
BSG	1-stage TC, GDI, 4 Cyl	700	including Li battery
BSG+eBooster	1-stage TC, GDI, 4 Cyl	1000	including Li battery

## 6.7 Prioritization of Engine Air and Combustion Technologies

The engine technologies analyzed in the previous chapters by means of the literature review and using the models that will be presented in Chapter #10, can be compared both in terms of CO<sub>2</sub>/energy consumption



on the reference cycles and, in a more effective and complete way, in terms of fulfillment of the design criteria and priorities coming from HoQ2.2, taking into account not only the GHG emission or fuel consumption, but also other technical characteristics linked to the purchase reasons of the vehicle (e.g. performance, fun to drive, etc.). In addition to the individual technologies, some interesting combinations among them and some powertrain architectures listed in the previous chapter are considered in this work. The combinations and architectures have been chosen considering the time horizon of 2025 and certain assumptions on the emission legislation. The comparison was made with the selection matrix shown in Table 6-6. The values shown in the matrix depend on the technology effectiveness in satisfying the different design criteria. In the lower part of the matrix, the technology ranking can be found. The ranking expresses the effectiveness of the technology and it is graphically summarized by the green and light blue histograms for human and autonomous driving, respectively.

As it is clearly shown, the powertrain characteristics that impact on CO<sub>2</sub> and emissions are still the most important both for human and autonomous driven vehicles. Conversely, the characteristics linked to the performances are more relevant for the human driven vehicles. The most effective technology combinations include a mix able to improve the limits of gasoline engines shown in the previous chapters. In particular, the downsizing from 4 to 3 cylinders, with a second turbocharger stage (e.g. electric type), in conjunction with Miller and port water injection is a particularly interesting solution. This best engine configuration has been optimized and assessed in terms of CO<sub>2</sub> reduction by means of modelling simulations, obtaining the results shown in Chapter #12.1.

Table 6-6 Selection Matrix of Technologies to ICE improvement (2025 timeframe)

			SELECTION MATRIX															
			COMBUSTION TECHNOLOGIES								AIR DELIVERY TECHS.				TECHS. MIX			
			1	2	3	4	5	6	7	8	9	10	11	12	13	14	15	16
			Port Water Injection	DWL- Separate	DWL- Mixture	GDI Lean	Miller/Atkinson Cycle	LP-EGR	HP-EGR	Variable CR	3cyl + 2-stage TC (BMEP 27 bar)	3cyl + 2-stage TC (BMEP 35 bar)	Cylinder Deact. (VVA)	Electronic CD	1+9+11	1+5+9	5+6+8+9	4+6+9
ENGINE ARCHITECTURES	Relevance (0-100)																	
Powertrain Characteristics (from HoQ2.1)	Human Driving	Auton. Driving																
1 Powertrain Noise Level	10	13									-1	-1	-1		-1	-1	-1	-1
2 Powertrain Time to Full Power	15	9	3	3	3	5		-1	-1	1	3	3	-1		5	7	5	5
3 Low-end Torque (at wheel)	20	14	7	7	7		-1	3	3	5	5	7			7	7	5	5
4 Speed Range of High Torque	16	9	3	3	3			1	1		3	7			5	5	5	5
5 Maximum Power	21	14	7	7	7		7			3	7	9			7	5	5	5
7 Time w/o Torque delivery during load Req.	18	15									1	3				1		
8 Powertrain Vibration	13	16											-1		-1	-1	-1	-1
9 Tank to Wheel Maximum Efficiency	25	22	5	5	5	3	9	3	3	5			5	5	5	9	9	5
10 Tank to Wheel Efficiency at part/low load	29	24	3	3	3	7	7	3	3	5	7	9	9	9	7	7	7	7
11 NOx Emission according to RDE	14	16	3	3	3	-1	1	3	3	1					3	3	3	
12 HC/CO Emission according to RDE	16	18				3							1	1	1	1		
13 Soot/PN according to RDE	15	17				1	-1	-1	-1		1	1			1	1	1	1
14 CO2 on WLTC	23	19	5	5	5	7	9	1	1	5	7	9	5	5	7	7	5	5
15 Heating Power	5	5																
26 PWT Size	5	8	-1	-1	-1	-3	-5	-3	-1	-1				-1	-1	-1	-1	-3
27 PWT Weight	38	35				-1	-1	-1	-1	-1		-3	-1	-1	-1	-1	-1	-1
Technology Ranking [0÷100] - Human D.			25	25	25	17	25	8	8	18	25	31	15	16	32	37	31	25
Technology Ranking [0÷100] - Auton. D.			21	21	21	15	22	6	7	16	20	24	14	15	26	31	25	20

However, another essential aspect is the value analysis (benefit/cost), where the benefit is weighted by means of the costs, summarized in the previous chapter. The *Technology Value Ratio* describes the relationship between the satisfaction of a requirement (benefits) and the use of resources (costs), according to the equation (3.2).

For this aim, the function effectiveness is measured by means of the ranking in the selection matrix, Table 6-6, whereas the costs are evaluated according to Table 6-5. By this procedure, the function/cost value, for each technology and their combinations, can be obtained.

In Figure 6-32, the comparison of the technologies is shown both in terms of ranking from the selection matrix and of *Technology Value Ratio*. According to the last index, water injection, Miller cycle and cylinder deactivation are very promising technologies. However, to achieve the CO<sub>2</sub> emission target a mix of engine technologies are needed even if these combinations (right side of figure) have a lower value, showing a growing powertrain cost in order to meet the legislation limits.

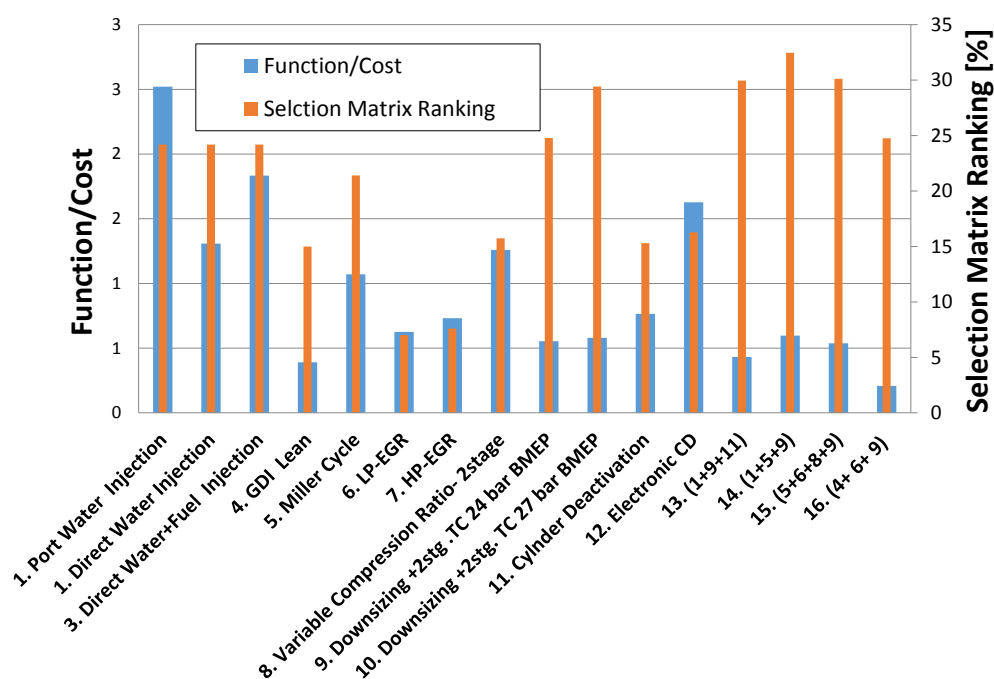


Figure 6-32 Comparison of Technologies (Ranking and TechnologyValue Ratio)

Alternatively, the technologies value can be defined as ratio between the percentage of CO<sub>2</sub> savings and cost. This evaluation is depicted in Figure 6-33. Assuming that 1% of CO<sub>2</sub> saving is slightly above 1 g/km, considering the baseline SI engine (125 g/km), it can be observed that all technologies and their mix are below the cost of the penalty (95€ /g) foreseen by the legislation. It is also important to remark that the affordable cost per gram of CO<sub>2</sub> saving depends on the distance of the powertrain emissions from the legislation limit. This means that the application of the technologies at higher cost could be mandatory to achieve the legislation limits, as long as the cost itself remains lower than the legislation penalty.



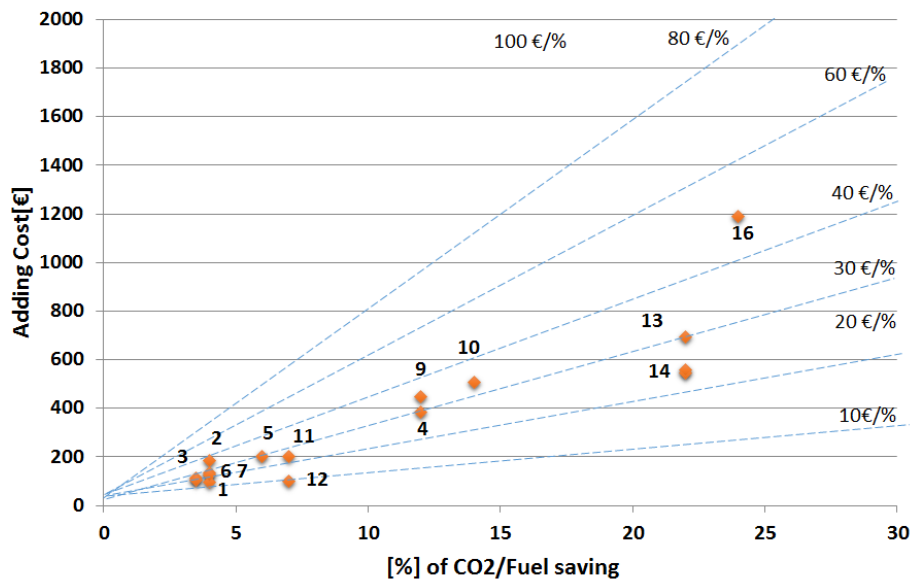


Figure 6-33 Value Analysis of GDI engine Technologies [Cost/% CO2 Saving]

## 6.8 Focus on Water Injection Effects on Combustion of GDI TC Engine

The outcomes of the SI engine technology comparison have highlighted the high potentiality of the WI technology, and a deep investigation has been carried out in the research activity by means of :

- experimental tests on engine dyno with a 4 cylinder Turbocharged GDI engine, equipped with a PWI system [217];
- CFD simulations, to support the experimental activities and to enlarge the understanding of phenomena in the intake manifold and in the combustion chamber [218,225];
- system analysis, to evaluate the achievements in terms of fuel economy and CO2 reduction [216].

An overview of the main results obtained by means of the first two activities is presented in this section, whereas the system analysis will be presented in Chapter #12.

### Experimental Tests

Experimental tests have been conducted on a prototype Gasoline Direct Injection (GDI) turbocharged engine (Table 6-7), whose intake system has been modified in order to install port water injectors and rail.

Table 6-7 Specification of engine tested with PWI system

Displaced Volume	1390 cm <sup>3</sup>
Bore	76.5 mm
Stroke	75.6 mm
Compression Ratio	10.1
Architecture	L4, firing order 1-3-4-2
Number of valves	4 per cylinder
Exhaust Valve Open	580° BTDC @ 0.1 mm lift
Exhaust Valve Close	356° BTDC @ 0.1 mm lift
Intake Valve Open	358° BTDC @ 0.1 mm lift
Intake Valve Close	132° BTDC @ 0.1 mm lift
Maximum Torque	220 Nm @ 1500 ÷ 4000 rpm
Maximum Power	103 kW @ 6000 rpm

In Figure 6-34 and Figure 6-35 the modified intake manifold water rail and injectors position are visible. Water injectors location is as close as possible to the intake valves, according to the CFD indication about water evaporation dynamics [218]. Prototype water injectors and pump were developed by Magneti Marelli and are controlled by a RCP (Rapid Control Prototyping) system developed by the research group in collaboration with Alma Automotive, controlling injection timing and rail pressure, with great flexibility.



Figure 6-34 Detail of the experimental setup: modified intake manifold (red arrow) and water rail (green arrow) are visible. Water injectors are highlighted with blue circles.

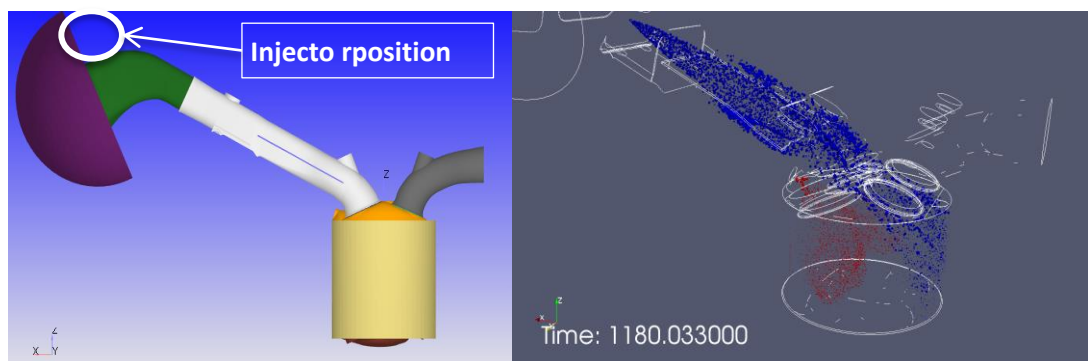


Figure 6-35 Images of water injector position in intake manifold and spray targeting

Experimental data here presented have been obtained with constant injection pressure and timing, 10 bar and 360°CA ATDC (beginning of the intake stroke), respectively. Such values have the results of

preliminary sensitivity analysis. Engine operating point as an example is 3000 rpm, 1.5 bar of intake manifold pressure, and stoichiometric mixture. Additional information about operating conditions are collected in Table 6-8.

Table 6-8 Operating conditions for tests

<b>r</b>	<b>In Cylinder Air</b> [mg/cycle/cylinder]	<b>Fuel Mas</b> [mg/cycle/cylinder]	<b>Water Mass</b> [mg/cycle/injector]
0	519.17	35.56	0
0.2	495.38	33.93	6.78
0.4	504.86	34.58	13.83
0.6	500.63	34.29	20.57

where  $r$  is defined as

$$r = \frac{\text{Water Mass}}{\text{Fuel Mass}} \quad (6.1)$$

### Combustion phasing

Figure 6-36 confirms the significant water injection effects on combustion timing and larger markers identify maximum efficiency points. Another effect of the water injection is the shift towards lower values of CA50%MFB corresponding to maximum efficiency, as water quantity increases. In Figure 6-36 such value goes from about 11°CA ATDC for  $r = 0$  to about 6°CA ATDC for  $r = 0.6$ .

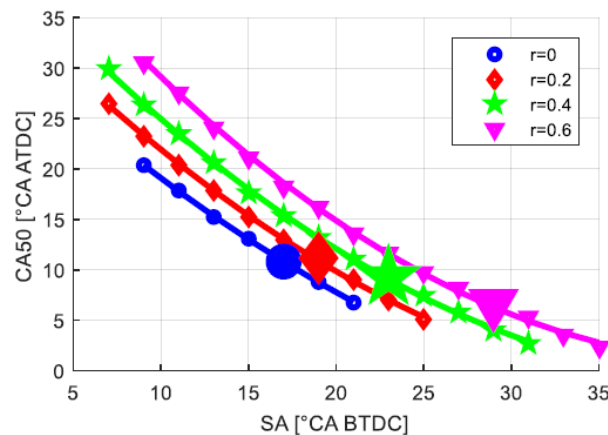


Figure 6-36 Effect of water injection on combustion phasing

### Indicated Mean Effective Pressure

Figure 6-37 shows IMEP (Indicated Mean Effective Pressure) values. It results a slight reduction in the maximum IMEP achievable as water is injected. Larger markers identify maximum IMEP (and efficiency) points.

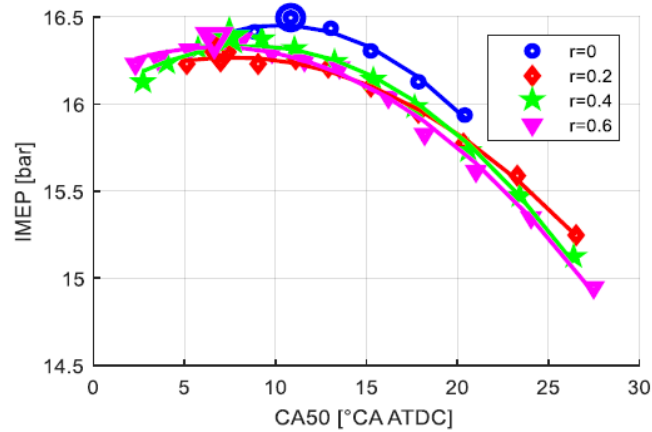


Figure 6-37 Measured IMEP as a function of CA50%MFB, for different water quantities; larger markers identify maximum IMEP (and efficiency) points

### Exhaust temperature

Exhaust temperature reduction, should be evaluated (at least in a first analysis) at maximum efficiency points (highlighted in Figure 6-38 by larger markers). In fact, because of water injection effect on combustion duration, exhaust temperature slightly increases as water mass increases, for the same spark advance angle.

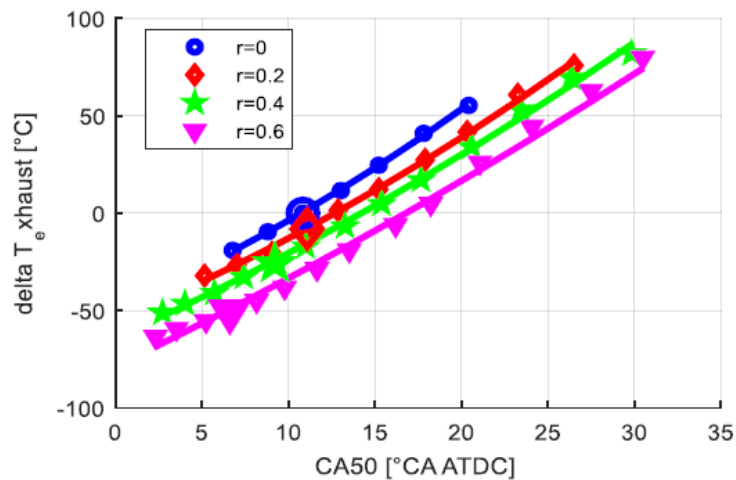


Figure 6-38 Measured exhaust temperature reduction, depending on water ratio; bigger markers correspond to MBT. A reduction of about 50°C is achieved with 60% of water ratio

Supposing the highlighted point for  $r = 0$  as knock limited (i.e., supposing knock intensity to be above the admissible threshold), the achievable gain in terms of exhaust temperature reduction is even greater than 50 °C.

### Knock

Experimental knock intensities is shown in Figure 6-39. The knock intensity is evaluated by means of 98th MAPO percentile. The Knock Limit (KL) indicated in figure is based on the empirical relationship:  $KL = \text{Engine Speed}/2000$ . What is particularly interesting is the knock intensity reduction for the maximum efficiency points (larger markers) as water mass increases. Inconsistently, for  $r = 0.2$ , knock intensity at maximum efficiency is greater than for  $r = 0$ . This is probably due to an ambiguous identification of the

maximum efficiency spark advance value. The selected operating point (1500 rpm, 1.5 bar) is not considered to be knock limited, and further investigation on higher load operation is required. Anyway, a slight reduction on knock intensity as injected water mass increases is verified.

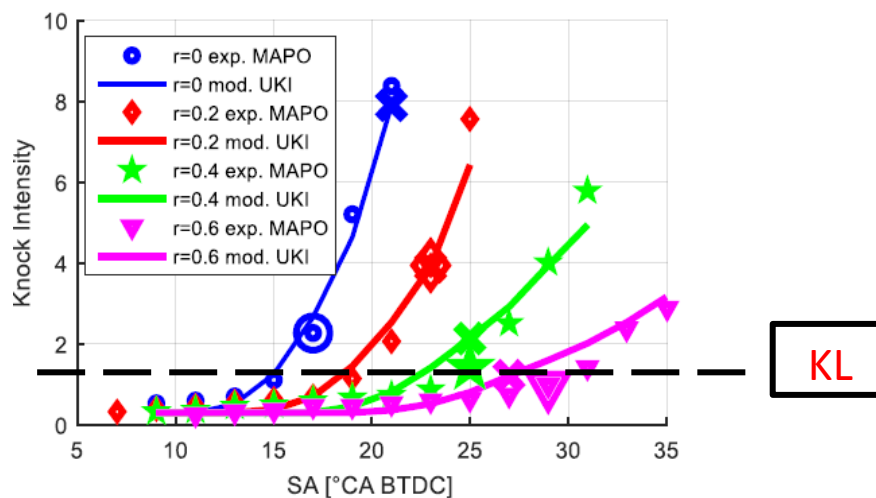


Figure 6-39 Comparison of knock intensity at different values of water/fuel mass; bigger markers correspond to MBT

Last analysis is on Brake Specific Fuel Consumption (Figure 6-40). Basically, investigated water quantities do not affect engine efficiency, confirming that effectively water enables an extension of the engine operation, with no compromises. In particular with  $r=0.4$  and an higher SA then baseline ( $r=0$ ), a quite BSFC reduction has been observed ( $\sim 2\%$ ), with lower sensitivity MAPO/SA.

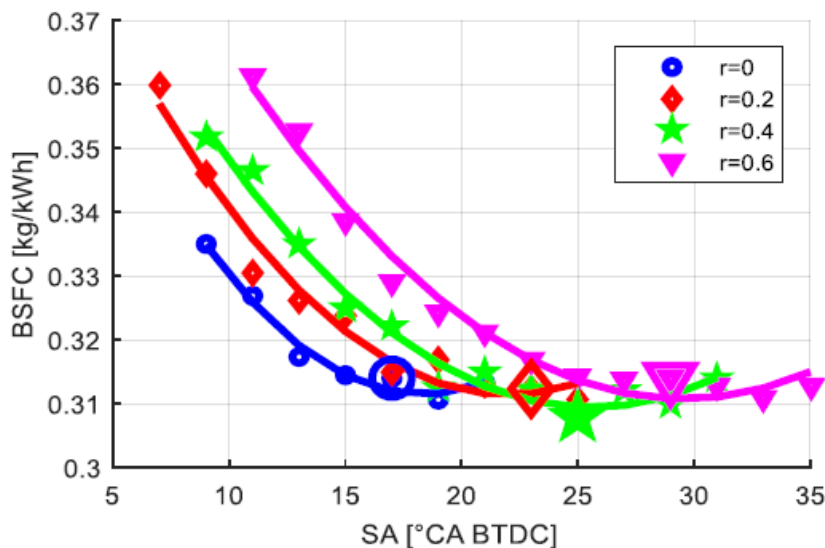


Figure 6-40 Measured Brake Specific Fuel Consumption trends for different water ratio values

## CFD Simulations

Numerical simulations can assist in designing water injection systems and in understanding the intertwined phenomena occurring from the water spray to the combustion. Some examples of CFD stud-

ies have been presented recently in the literature [218, 269]. Two aspects combine: the realistic modeling of the water injection process and the robust knock risk prediction. Spray model validations are mandatory, for a proper description of the water and fuel distribution in the ports and in the cylinders.

Concerning SI combustion modeling, it has been clearly shown that large eddy simulation (LES) is the proper method to account for all statistical phenomena from flame propagation to autoignition [270], at the expense of costly multi-cycle simulations. Using tabulated kinetics for ignition (TKI) combined with the extended coherent flamelet (ECFM) combustion model, the authors showed high accuracy in capturing knock frequency of occurrence and intensity, over a range of conditions.

However, RANS is still the method of choice for large number of design space explorations [218, 269]. Some authors are proposing new advanced models with presumed probability distribution functions to include knock statistics upfront in RANS [271,272].

In this section we first show validations of an overall engine model, then we investigate how port water injection affects combustion, and lastly, we quantify the IMEP gain that can be achieved adding water and re-optimizing the spark timing. The main purpose is a fundamental study on water injection behavior using CFD. The water wall film dynamics in the intake ports is of the utmost importance in this problem, and several engine cycles are needed to reach a converged behavior. Due to the costly method requiring multi-cycle simulations because of the port injection, we limited our range of investigation to a single engine baseline point, under a KLSA operating condition. We explored different water injection timings and pressures to assess the effectiveness of a fixed amount of water. A well validated G-equation combustion model was used to simulate multiple-cycles efficiently. Spark sweeps were then carried out by simply restarting the simulations on the last cycle slightly before the ignition, and adopting the ECFM model for the combustion coupled with TKI to add autoignition prediction capability. The CFD simulations showed to be very useful for estimating the charge cooling effect, the reduction of the burning rate and ultimately the power increase under the same KLSA criterion.

## Computational setup

The engine used for the investigation is the same of the experimental activities, see Table 6-7, as well as the engine operating point, 1.5 bar of intake pressure and 2500 rpm of engine speed.

The CFD model is built for a single-cylinder configuration, cutting out just one cylinder from the original 4-cylinder geometry, as already presented in [218]. Figure 6-41 shows the geometry and how the CFD analyses were setup. Water injector and gasoline injector locations are highlighted with white cones in Figure 6-41.a and an example of spray patterns is shown with blue and red parcels, respectively, in Figure 6-41.b. The airbox has been replaced by the hemispherical region positioned at the inlet of the single runner configuration. Being aware that during the closed valve period some water droplets could travel backwards toward the inlet boundary, because of convection or pressure waves, we checked simulation results and verified that no water mass was lost in any analyzed case. Therefore, the adopted inlet region (grey in Figure 6-41.a) is considered adequate for the scope of this work. The CONVERGE CFD solver has been used in this study, which uses a modified cut-cell Cartesian gridding method to automate the creation of the mesh at runtime (Figure 6-41.c). Various fixed and adaptive meshing refinement strategies were used, ad-hoc temporally and spatially activated, to achieve 0.75 mm cell size in sprays and combustion areas. Around spark a resolution of 0.1875 mm was used. More details about computational set-up are provided in the published work [225].

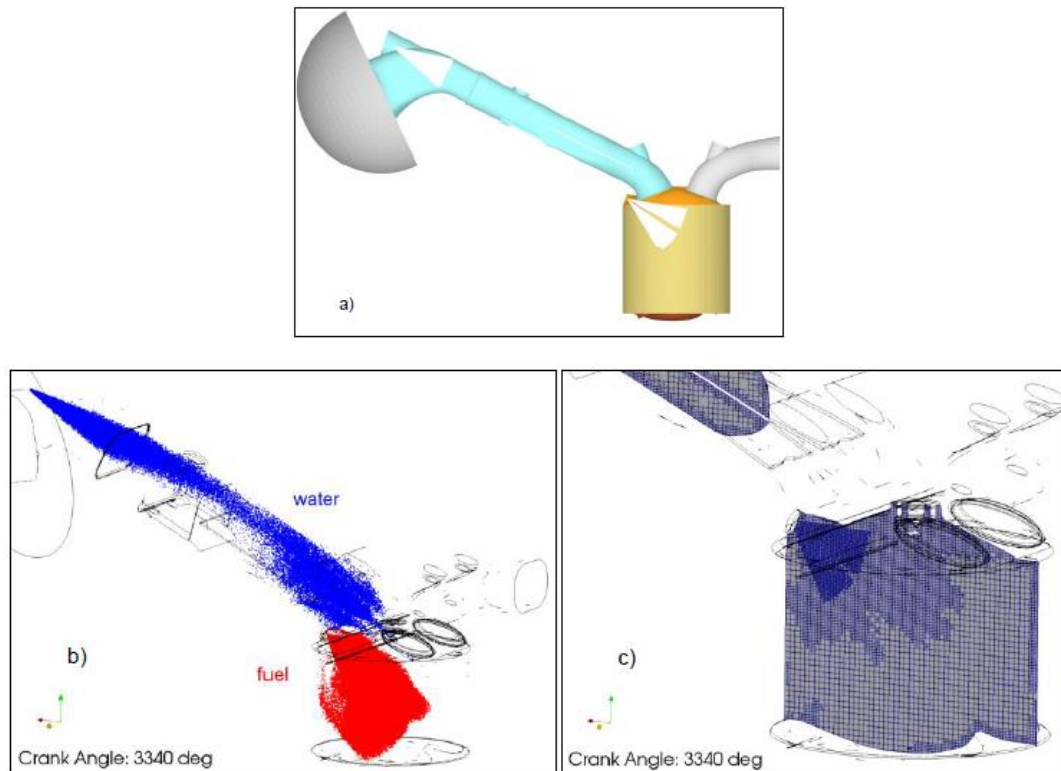


Figure 6-41 CFD engine model: geometry with injector locations (a); water and gasoline spray visualization (b); mesh (c)

## Spray Validation

In order to build a reliable engine model, the preliminary focus was on the accurate setup and validation of the spray sub-models. Magneti Marelli is the manufacturer of both water and gasoline injectors and provided experimental data collected in a constant volume vessel.

The water injector features a three-hole nozzle, with almost parallel and interacting jets lying on the same plane. All the three holes have been modeled so that the global asymmetric spray morphology is naturally reproduced. Injection rates and a population of atomized droplets based on RR distributions are prescribed as boundary conditions. Three injection pressures have been explored, namely 3, 6, and 9 bar, with an initial Sauter mean droplet diameter (SMD) of 74, 65, 60  $\mu\text{m}$ , respectively. These values have been selected after a preliminary calibration based on the comparison of the simulated spray droplet sizes against measurements.

As an example, the validation results for the 6 bar case are following illustrated. The water injected is 8.39 mg at fluid temperature of 296 K in a chamber at 1bar and 373 K. Results are shown in Figure 6-42. Figure 6-43 shows a comparison of the measured and predicted SMD ( $=D_{32}$ ) and average diameter ( $=D_{10}$ ), at 15 mm from the injector tip (z direction). Simulations are able to reproduce experimental trends and values in a satisfactory manner. Only minor differences can be observed, as the experimental curves show a mild peak in the center that is less evident in the simulations.



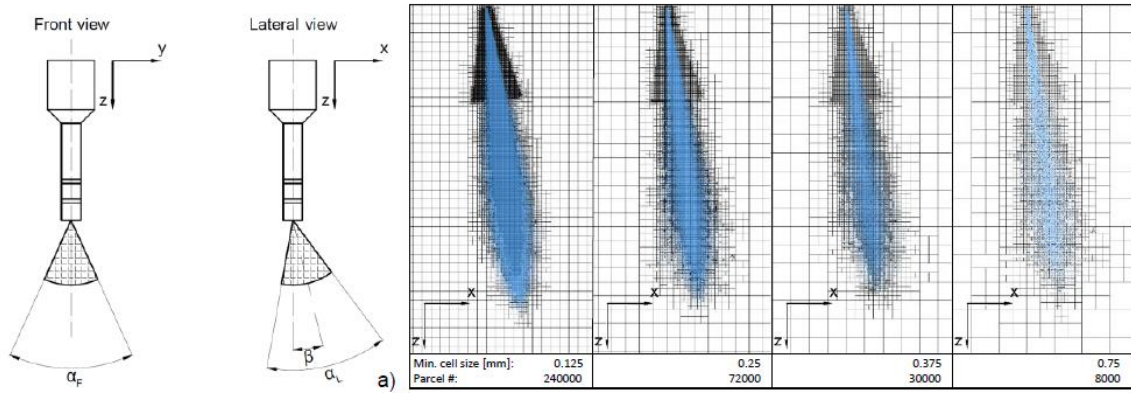


Figure 6-42 (a) Spray angles definition; (b) Grid size effects on spray patterns and on tip penetration

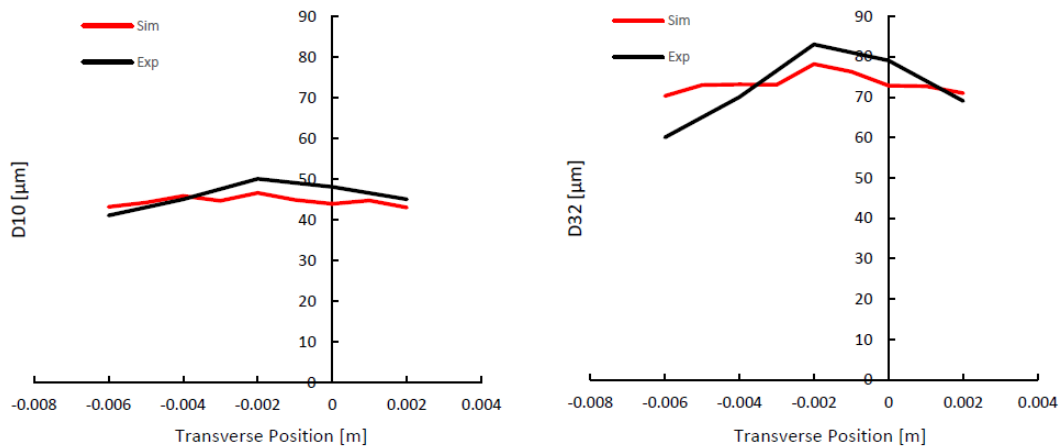


Figure 6-43 Comparison of simulated and measured droplet diameters at various transverse locations at 15 mm from the tip

Similarly, the model of 5 holes GDI injector has been validated considering as test liquid Exxsol-D40. More details are provided in the published work [225].

## PWI Multi-Cycle Simulations

The PWI injection generally causes impingement on the port walls or on the valves, and complex film dynamics is generated. Multiple cycles are required to model these phenomena. In the current implementation of the ECMF combustion model it is not possible to handle more than one liquid species, therefore multicycle analyses have been conducted using the G-equation combustion model which has no restrictions in this regard and allows to have two different injectors with different liquids. The baseline SA of 14 CAD before top dead center firing (bTDCf) is knock-free, hence calculations with G-equation are correct. Within this framework, the focus of the first part of the work is on the amount of in-cylinder trapped water, on the amount of charge cooling due to evaporation, and on the peak pressure reduction with fixed SA. Later, in the second part of the study, we will switch to the ECMF+TKI combustion model to investigate knock occurrence by varying spark advance.

Water injection cases that have been analyzed are specified in Figure 6-44.a. Five water SOI timings are considered at 3 bar injection pressure, ranging from 0 CAD to 540 CAD after top dead center firing (aTDCf). In addition, two pressures with equal SOI of 300 CAD aTDCf are investigated, namely 3 vs. 9 bar cases, to assess the effect of injection pressure. Water mass is fixed at a 0.3 water-to-fuel ratio, and injection temperature is set to 308 K. Special care was devoted to prescribing wall temperatures for the



critical part of the intake port and runner surfaces. After a preliminary exploration of conditions assessed against available measurements, we set a spatially varying condition of the wall temperatures, with a linear variation from 330 K in the upstream part of the duct up to 420 K just before the intake valve.

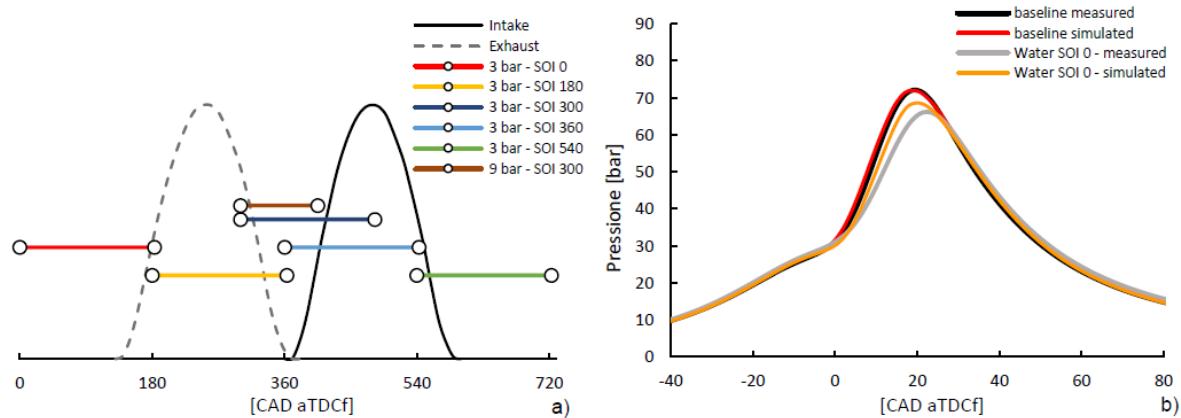


Figure 6-44 Timing and duration of each water injection case (a), and comparison of measured pressure vs. simulated in-cylinder pressure (b)

Figure 6-44.b shows the comparison between the computed in-cylinder pressure and the experimental trace for the baseline case and for a case with water injected at 3 bar and SOI = 0 CAD aTDCf. It can be observed that the reduction of peak pressure due to water injection is to some extent underestimated. The main reason is attributed to the specific dynamics of the wall film accumulation and will be discussed further in next section.

### Water spray dynamics in the intake runner and ports

Focusing on the intake runner and ports, results of the liquid water dynamics for each simulation are presented in Figure 6-45. In each chart three curves are shown: the cumulated injected water mass, in red; the cumulated mass of the water that reaches the cylinder in liquid form, in light blue; and the accumulated wall film mass, in green. Vapor phase is not shown for clarity, as it can be easily inferred from the information on the liquid phase. First, we notice that none of the cases under investigation leads to null wall film mass, meaning that the conditions are not sufficient for vaporizing or stripping off the total amount of water impinging on the walls. Also, none of the cases after ten cycles reached a steady state amount of accumulated wall film mass. Therefore, part of the water mass sticks to the walls and will not contribute to the anticipated scopes on the combustion mitigation. It is likely that in the engine point under consideration, longer times are needed to reach fully developed wall films and quasi-steady engine behaviors, which unfortunately means long and costly runs. In all the simulated cases, the water mass entering the cylinder is noticeably lower than the injected mass, decreasing the overall effectiveness and leading to an underestimation of the peak pressure reduction (cf. Figure 6-44.b). This effect can be further investigated in the future, also considering higher load points with higher operating temperatures to reduce the time scale of the phenomena. The results of all simulated conditions are provided in Figure 6-46, which shows the percentages, with respect to the injected mass, of the liquid entering the cylinder and of the liquid remaining on the wall.

In conclusion, we observe that, from the point of view of spray dynamics, the most effective timing at 3 bar injection pressure is the SOI = 180 CAD aTDCf, which produces the lower amount of wall film and the largest amount of liquid water reaching the cylinder.

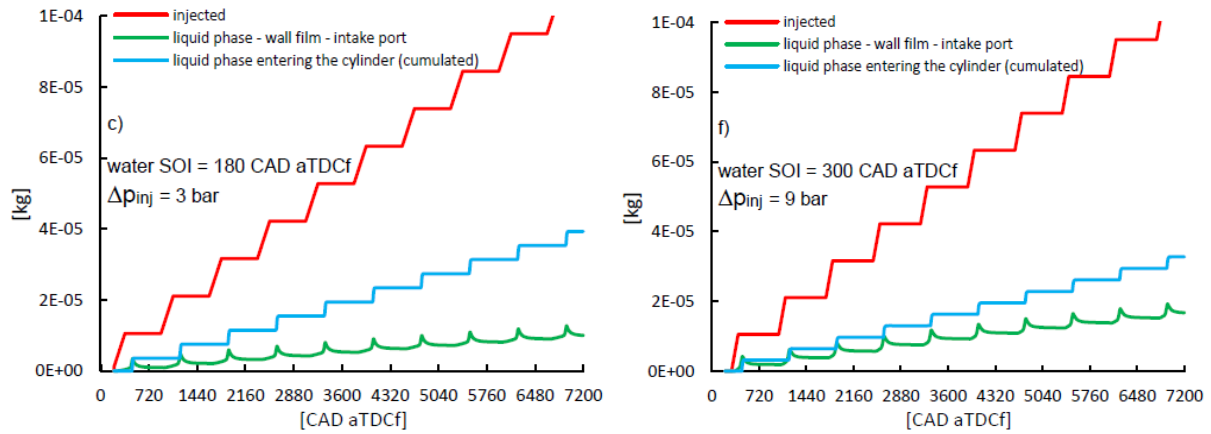


Figure 6-45 Dynamics of liquid water in the ports and runner, focus on case (c) and (f), see the following Figure 6-46

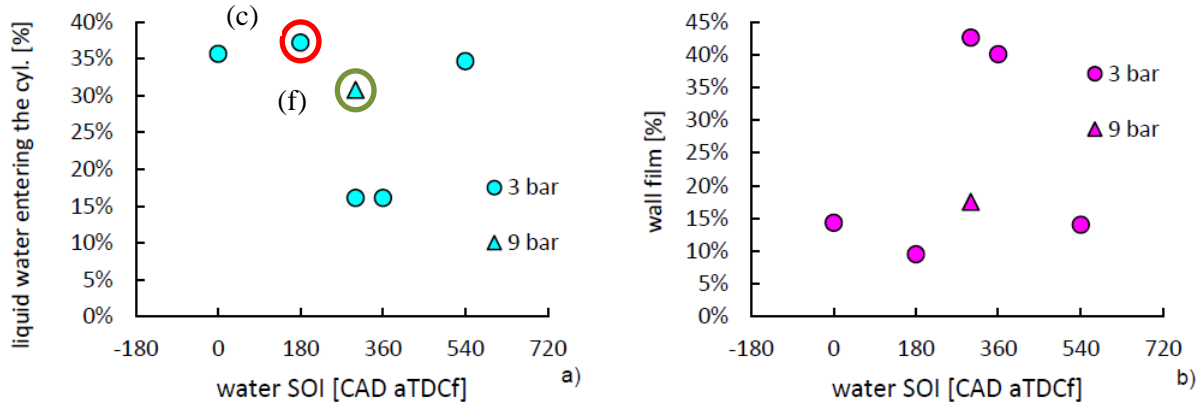


Figure 6-46 Liquid water balance in the ports and runner; percentages refer to the injected water mass

When comparing the 9 bar injection pressure case against the low pressure case, at 300 CAD aTDCf SOI, we observe a rather effective reduction of the wall film (about 0.4x) and an increase of the in-cylinder trapped liquid water (about 2x). This is in agreement with what has been already observed in the previous published work [218] spanning various injection timings, suggesting that better atomization and shorter timings are potentially beneficial. Using higher injection pressure, the mass of liquid water entering the cylinder and evaporating with less wall contact increases substantially, therefore a larger impact is expected on the combustion.

### Impact on combustion

Ultimately, the goal of water injection is to affect combustion. A comprehensive view of the water impact for the various cases is presented in Figure 6-47. The top left chart shows the reduction of the peak pressure caused by the water, normalized with respect to the baseline case without water, for all cases compared to measurements. The top right chart quantifies how much the combustion is slowed down in terms of MFB50 (crank angle of 50% mass fraction burned). The bottom chart reports the charge cooling effect, before spark, as the decrease of in-cylinder temperature w.r.t. the no-water case.

The reduction of peak pressure which is achieved is in the order of 4÷6% according to the simulations, while measurements suggest a reduction of about 7÷8%, depending on the pressure. Experimental data were acquired for several injection timings, but a clear trend was not observed, and an overall data scatter and uncertainty of about  $\pm 2\%$  was observed. We previously noted that the accumulated water wall film mass in the simulation is not quasi-steady after 10 cycles, therefore this can explain the reduced

effectiveness provided by the model. Focusing on the effect of the injection pressure, we observe that due to improved atomization level, at constant SOI timing, the charge cooling effect increases, the peak pressure reduction is more significant, and the combustion slows down more, consistently. A reduction of about 2% in the peak pressure is observed in the simulations switching from 3 bar to 9 bar injection pressure, which correlates with measurements.

Concerning the effect of the injection timing, at 3 bar, we observe that the ~300 CAD aTDCf cases behave as the worst, as the peak pressure is less reduced and the MFB50 is less retarded, in agreement with the previous conclusions on the spray dynamics (see results in Figure 6-46). The case at SOI = 0 CAD aTDCf does not strictly follow this criterion though, and despite the trapped water was not the highest, it produces the strongest impact on the combustion. This can be explained including other combined side effects. In particular, the amount of vapor being formed in the ports decreases the volu-metric efficiency and alters the average equivalence ratio. In this case, being  $\phi = 1$  in the baseline case, in the water cases the mixture tends to be slightly rich (injected fuel is kept constant) because of lack of oxygen replaced by vaporized water. This is more pronounced at 0 CAD aTDCf SOI and it explains the reduction of the combustion rate. In addition, as visible in Figure Figure 6-47.c, the effect of charge cooling for this case is not the largest at 3 bar, so the peak reduction is a result of a slight decrease of combustion efficiency, as the air-fuel ratio variations are not compensated in the models.

## Results under similar KLSA

Because water slows down the burn rate, the comparison in terms of performance must be made after the spark timing is re-adjusted to the same knock risk margin. As mentioned in the introduction, to do this we used the ECFM combustion model with tabulated autoignition data. We run several spark sweeps mapping the flow variables from the last available cycle and restart-ing the calculations with different SA timings to cover the combustion. Starting from -14 CAD aTDCf, spark is advanced up to -28 CAD aTDCf. Results are shown in Figure 6-48, in terms of heat release rate (HRR), maximum amplitude of pressure oscillation (MAPO), and lastly in terms of cylinder pressure under the same knock margin. MAPO is calculated by taking the difference of point pressure (in the most severe knock occurrence location identified) and average in-cylinder pressure, rectifying and taking the maximum, examples were documented in the published work [218].

As these simulations are run within the RANS framework, without any model for predicting the statistical occurrence of knock, we only expect the results to be representative of an ensemble average behavior. Knock is clearly non-linear and stochastic, but we are not modeling the likelihood of few cycles exhibiting knock. Therefore, results might not be comparable in absolute terms to experiments or ex-pensive multi-cycle LES calculations, as to the capability of predicting the correct knock onset as SA is varied. However, the spark sweeps for various cases provide a consistent indication of the benefits achievable with water injection.

With this in mind, the results for the case with water SOI = 360 CAD aTDCf, which is the most conservative in terms of benefits, show that sensible autoignition starts to take place at -20 CAD aTDCf, as visible from the HRR curve, while the knee on the MAPO vs. SA curve occurs at -24 CAD aTDCf. A slight advantage is observed for the case with water SOI = 0 CAD aTDCf, which was more effective on slowing down combustion (see previous section). In this case at -24 CAD aTDCf, the MAPO level is still very small, but the onset is sharp as well.

Considering that the MAPO knee was located at about -22 CAD aTDCf for the baseline no-water case, we conclude from these comparisons that about 2 CAD of spark advance are gained in this engine point, using port water injection with a 0.3 water-to-fuel ratio. The value found here is in good agreement with engine measurements already reported in [217], for the same engine point, which indicated a shift of about 3 CAD for the same water-to-fuel ratio. Again, the underestimation could be linked to the time scale of the water wall-film accumulation already discussed. The benefits of a KLSA shift of 2 CAD are shown in

Figure 6-48.c, comparing in-cylinder pressure curves. The IMEP is 1.8% higher when water is used, therefore this improvement is also achieved in terms of overall thermal efficiency.

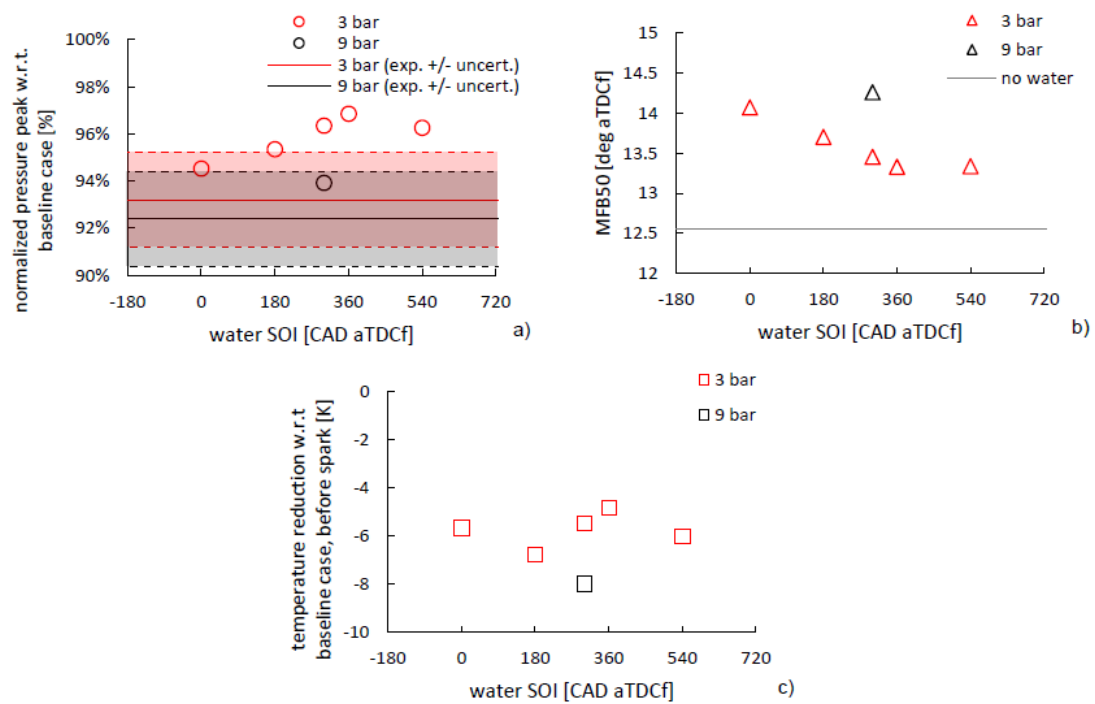


Figure 6-47 Water effect on (a) peak pressure, (b) combustion phasing, and (c) charge cooling before spark, at -20 CAD aTDCf. Spark timing is fixed at SA = -14 CAD aTDCf

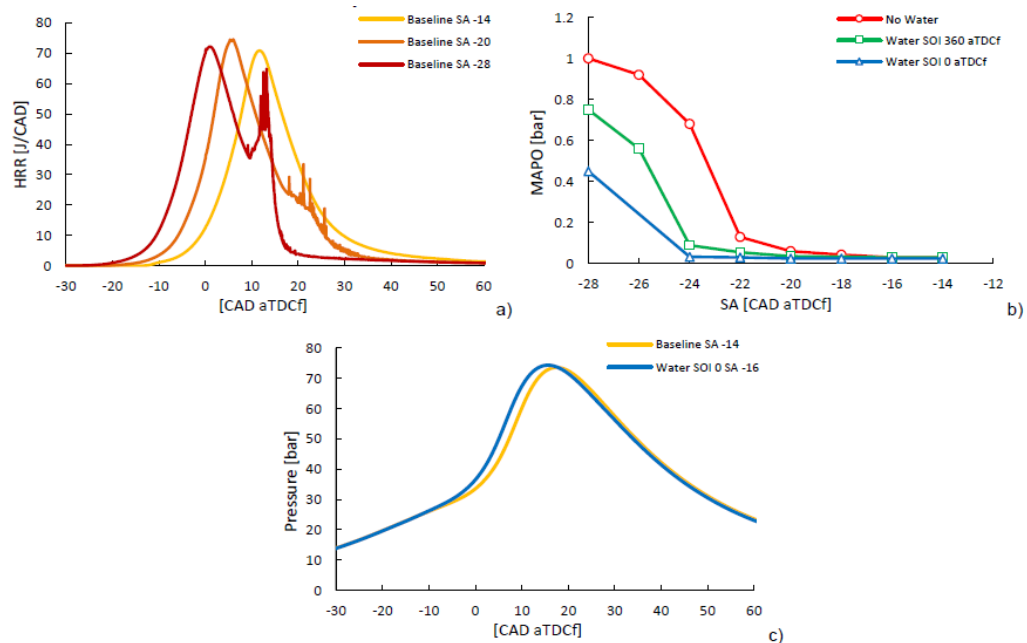


Figure 6-48 Effect of spark timing variation; Heat Release Rates at 3 bar injection pressure and water SOI = 360 CAD aTDCf (a). MAPO vs. SA at 3 bar and SOI = 0 CAD and 360 CAD aTDCf (b); in-cylinder pressure curves, with and w/o water, under the same knock margin (c)

## Summary

The work has discussed the effects of PWI in a boosted GDI engine at medium speed and mid-load, under incipient knocking conditions, and it has used CFD models to analyze the impact and benefits of various water injection strategies. The work has investigated the effect of water injection timing and pressure, providing quantitative results for water spray dynamics and charge cooling effects, which are rather difficult to assess experimentally. Also, the results compare favorably with available measurements in a specific engine point in terms of combustion behavior and efficiency gain.

Useful predictions can be achieved using a detailed CFD model, which can assist the design, development and optimization of water injectors and system architectures. Water injection timing clearly needs to be optimized, for a specific port installation position and operating conditions. In addition, the water atomization quality has been found to be a tangible parameter for optimum effectiveness of WI. The study has shown that an increase of the water injection pressure can lead to substantial benefits.

Future work will be devoted to more extensive validation in multiple engine points, also considering different installation locations and injector designs, as well as different water-to-fuel ratios.

## 6.9 Engine Waste Heat Recovery Systems

A great amount of the energy in an internal combustion engine is discharged in the exhaust gas, in the cooling system and in the environmental, see Figure 6-49. The partial recovery of this energy can improve in significant manner the powertrain efficiency.

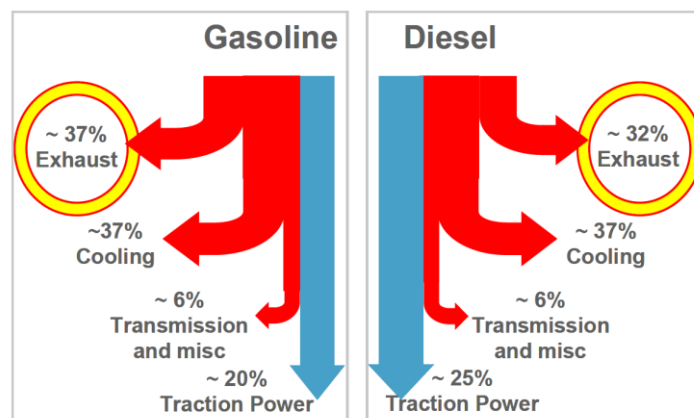


Figure 6-49 In average conditions, about 2/3 of the energy stored in the fuel is lost through the exhaust and cooling systems of an ICE

Engine Waste Heat Recovery (WHR) systems are a set of technologies that can increase overall efficiency of ICE based powertrains, bringing the maximum BTE over 50%.

The energy can be harvested from engine cooling and exhaust gas and employed:

- to accelerate the warm-up of the engine or the other sub-systems;
- to generate mechanical energy, used to reduce the engine load for the propulsion;

- to produce electric power, that reduces the alternator load or can be use for the electric propulsion;
- to cool the cabin in alternative to the conventional A/C system, based on compression cycle.

The next Figure 6-50 adapted from [130] shows an example of the potential benefits of the heat recovery systems in a sedan vehicle equipped with a 4 cylinders 1.6 liter Turbo GDI engine. Up to 10% of fuel economy can be achieved, depending on the driving cycle and the employed technology. In addition to kinetic energy recovery systems, with WHR systems a great part of fuel losses can be recovered.

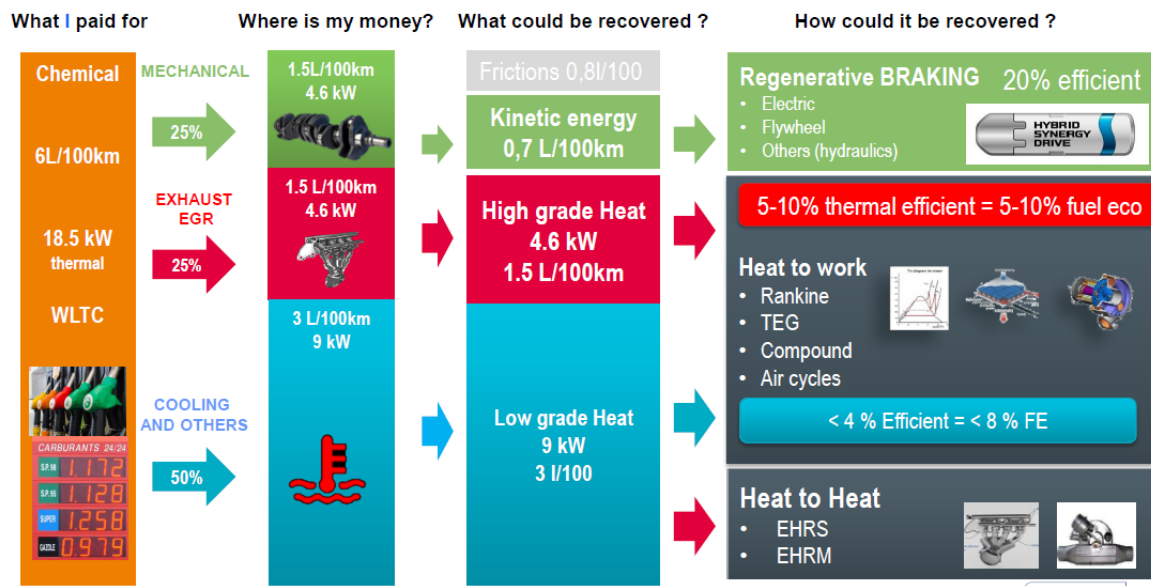


Figure 6-50 Simplified energy balance in vehicle with GDI engine and waste recoverable energy [130]

## 6.9.1 Engine Heat Recovery Technology Options

The WHR systems can be divided in two main families and an overview is presented in Figure 6-51. The classification depends on the form in which the harvested heat is converted:

- **Heat to Heat** systems, that transfers the heat from exhaust gas or engine coolant to another fluid (oil, coolant, etc.); the main technologies based on this principle are:
  - Fast Warm-up system for engine, trasmission and cabin fast heating.
  - Adsorption Heat Pump (AHP), that converts heat to energy for cabin cooling.
- **Heat to Power** systems, where the heat is converted in mechanical or electric power; the main technologies are:
  - Thermo Electric Generator (TEG), based on Seebeck effect the heat is transformed in electric energy.
  - Turbo-compound, that generates mechanical or electric power by means of a turbine driven by engine exhaust gas.

- Rankine Cycle (RC) system, that generates mechanical or electric power by means of a proper working fluid in a closed thermodynamic cycle.
- Stirling Engine, that generates mechanical or electric power.

The main features for each technology are illustrated following, highlighting the working principle, the main benefits and technical challenges.

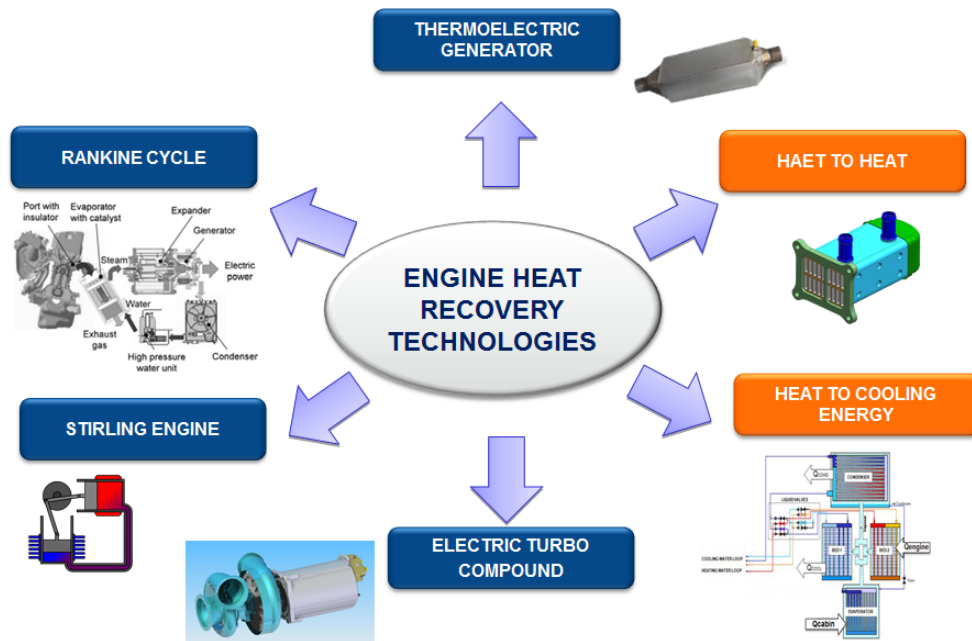


Figure 6-51 Engine Heat Recovery systems: Heat to Power technologies highlighted in blue and Heat to Heat in orange

**Fast Warm-up system** - An heat exchanger (see Figure 6-52), installed typically downstream the catalyst, transfers heat from exhausts gas to a fluid, oil or coolant for engine, transmission and vehicle cabin. The exchanger is bypassed when the warm up is finished or to reduce exhaust back pressure at high engine exhaust mass flow rate.

The technology is suitable for Hybrid Vehicles [27,28], reducing engine utilization to maintain coolant temperature (thermal management) and improving the cabin comfort in winter conditions (faster coolant warm-up).

The technology constraints are the managing of exhaust pressure drop and the avoiding of fluid boiling. The Fast Warm-up technology is considered key also in this study and its benefit will be shown in the case study in Chapter #12.1.



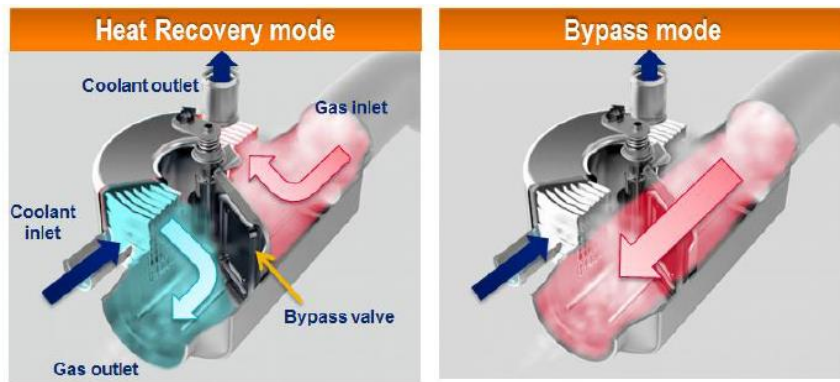


Figure 6-52 Description of Fast Warm-up operating modes

**Adsorption Heat Pump (AHP)** – The cooling cycle is performed without the mechanical compressor, which is replaced by a “thermal compressor”, the BED1 and BED2 in the Figure 6-53, that alternatively exchange heat with cabin and engine (exhaust gas or coolant). The working fluid is typical water or  $\text{NH}_3$  and the adsorption material used in the two beds are Silica Gel or Zeolite.

The capability to work also with waste heat at low temperature below  $100^\circ\text{C}$  is a promising feature for automotive applications. The system can be used for the cabin air conditioning or as a refrigerant. The main challenge are the system inertia and the maturity of the technology. The Volumetric Cooling Power (VCP) achievable is around  $1000 \text{ W/Liter}$ , comparable with electric compressor cycle, and the Coefficient of Performance (COP) is in the range  $0.4\div 0.6$ , as reported in [29, 30].

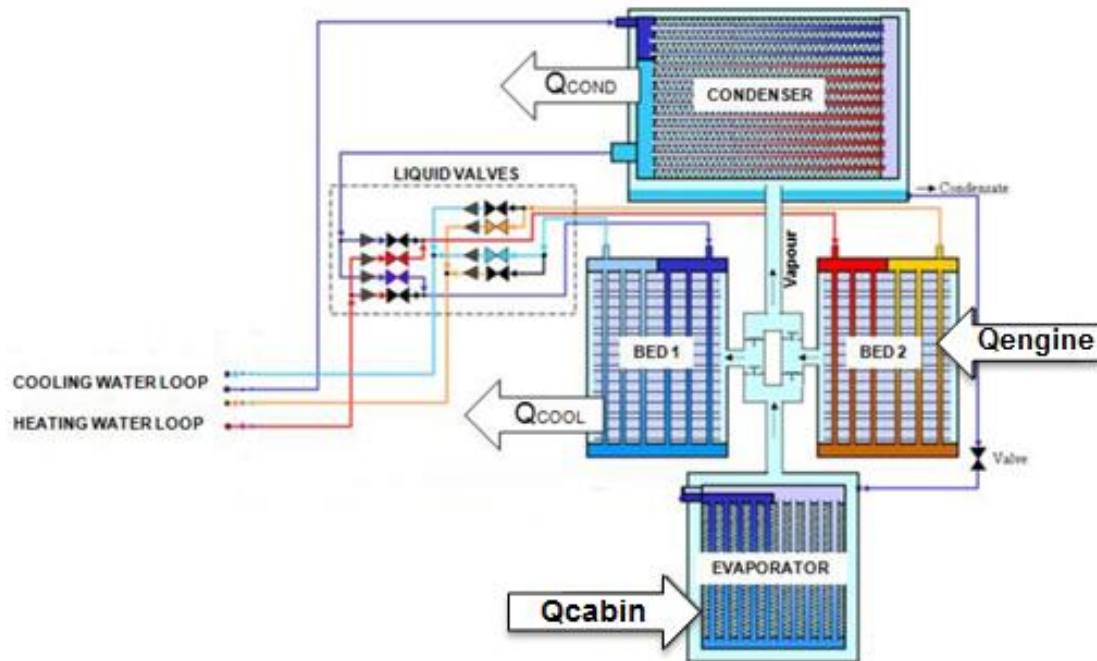


Figure 6-53 Scheme of an AHP system



**Turbo-compound** - An additional turbine, installed downstream turbocharger turbine, generates power output either electrical or mechanical (Figure 6-54, case a). It can be used as power boost or as a fuel saving component.

In an alternative layout an electric moto-generator is integrated on turbocharger shaft (Figure 6-54, case b), named typically e-Turbo. In this case, in addition to the energy recovery, the compressor assist is possible, allowing turbo lag compensation. The technical challenges of this system are:

- the engine back-pressure, that reduces the advantage of the energy recovery;
- the lowering of exhaust gas temperature, in case of the preferred installation upstream the catalyst, with negative impact on the catalyst performance;
- the complexity of system in case of mechanical solution;
- the reliability of electric motor, mainly due to high speed and thermal stress.

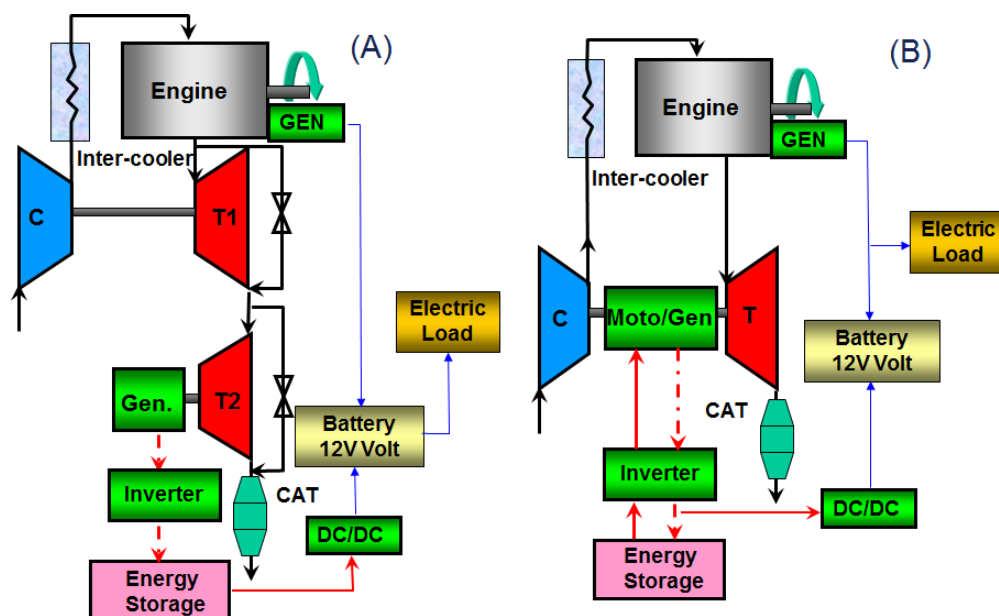


Figure 6-54 Main layouts for the Electric Turbo-compound

This technology allows fuel saving up to 4÷6 % in standard cycles, if it is used only for the energy recovery. This achievement is confirmed by some studies [33], among these one [38] of the thesis author. In case of architecture (b), the air boosting assist enables an higher degree of engine downsizing, that allows a fuel economy improvement up to 10%.

The design and integration of motor/generator with the turbocharger are the key aspects of the electric turbo-compound. In Table 6-9 a comparison of the possible electric machines is presented, indicating a measurement of their features versus the technical requirements. In the published studies and demonstrators the preferred solutions are the Brushless Direct Current (BLDC-PM) motor [240, 241] and the Variable Reluctance motors [107], both synchronous and switched: the first one for its performance and lower noise, the second ones for their benefit/cost ratio and reliability.

Table 6-9 Comparison of the electric machines for Electric Turbo-compound

E-Turbo Specifications		Electric Motor Type vs. E-Turbo Specifications			
Technical Criteria	Weight	Brushless DC	Induction	Synchronous Reluctance	Switched Reluctance
Low Noise	5	5	5	4	3
High Power Density	5	5	3	3	3
High Speed Capability	5	3	4	5	5
Low Ripple	3	5	4	3	2
Low Inertia	5	4	3	4	5
Control Complexity	3	4	3	3	3
Robustness/ Thermal Sensitivity	5	2	3	5	5
Ranking (Effectiveness)	[%]	78.7	71.6	79.4	77.4
High Cost [1-5]	[adim]	4	3	2	2
Technology Value	[%/adim]	19.7	23.9	39.7	38.7

**Thermo-Electric Generator (TEG)** – It works using an heat exchanger with thermoelectric generators layers between exhaust gases and engine coolant. The temperature difference between plates produces electron circulation (electric current), according to Seebeck effect. The electric production is performed with only one component and no moving parts, that is the main advantage of the technology. The used materials are different and in continuous evolution, the preferred ones are Bi2Te2 (Bismute Tellurure), Mg2Si and CoSb3 (skatterudite). The efficiency depends on a generating performance index of the material ZT according the following equation

$$\eta_{\max} = \frac{T_{\text{hot}} - T_{\text{cold}}}{T_{\text{hot}}} \frac{\sqrt{1 + ZT} - 1}{\sqrt{1 + ZT} + \frac{T_{\text{cold}}}{T_{\text{hot}}}}$$

Carnot                      TE Materials

(6.2)

For the typical materials ZT has a value between 0.2 and 1.4, depending on the temperature. The back pressure introduced in the exhaust line is negligible compared with the turbo-compound system. The technology challenges of TEGs are:

- the efficiency, low with actual materials (<8% thermal efficiency);
- the heat exchanger sizing (wall thermal resistance and conductance) and packaging;
- the material costs, that lead to 1÷1.5 €/W for the over all system.

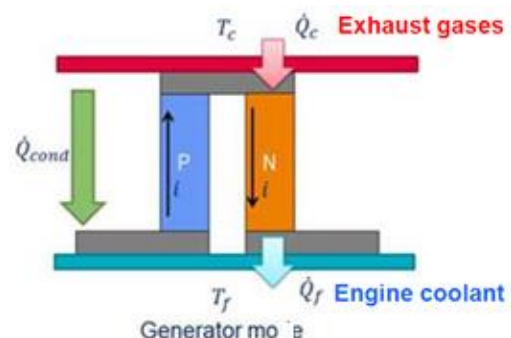


Figure 6-55 TEG packaging and principle scheme of Seebeck cell

This technology allow fuel saving up to 1÷5 % in standard cycles, as confirmed by some studies [31,32,33], among these one [34] of the thesis author.

The costs and the limited power density are the main barriers for this technology application in mass production. But many researches on new material can improve significantly the TEG systems.

**Rankine Cycle (RC) System** – The system works with thermodynamic cycle based on Rankine process. The system (see Figure 6-56) is composed of the following parts:

- the Pump, that feeds the evaporator with high pressure liquid;
- the Evaporator, that generates high temperature vapor with exhaust heat;
- the Expander, that expands vapor to produce mechanical work;
- the Condenser, that turns low pressure vapor back into liquid.

High fuel saving can be achieved up to 10% in real conditions. The back-pressure introduced by the evaporator in the exhaust line is lower compared with the turbo-compound system and it can be installed downstream the catalyst. These are the key advantages of this technology, that is very promising for ICE based powertrain, especially electric hybrid ones.

The technical challenges to be managed are the proper matching of the system with the engine (heat exchange sizing, working fluid and expander), the system complexity and mainly the packaging. For the high potential benefits and synergy with electric hybrid powertrain a deep analysis of the technology is presented following.

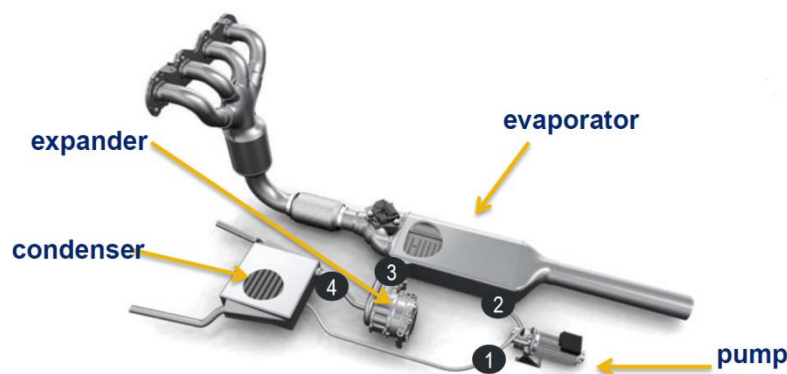


Figure 6-56 Rankine Cycle system components [130]

## 6.9.2 Other WHR Systems

Systems based on other thermodynamic cycles such as Stirling or Joule cycles are also among possible waste heat recovery technologies. The Stirling cycle engine doesn't seem favorable for automotive or truck integration since it has been evaluated to be very heavy and not compact [242], therefore, few literature on automotive or truck integration is available. The Joule cycle engine presents also huge drawbacks for mobile applications of waste heat recovery. The Joule cycle engine has a gas-gas heat exchanger that requires a huge heat transfer area in order to achieve an high efficiency. This conclusion was reached by the only researchers that worked on a Joule cycle system for a mobile application in the open literature [243].

Other more exotic technologies have been investigated. As an example, a prototype vehicle moved with a thermophotovoltaic generator has been built [244]. This technology is based on the conversion of heat into photons that will produce electricity afterwards. However, this requires a very high temperature since the photon production is proportional to the temperature to the power.

### 6.9.3 WHR System Comparison and Prioritization

To summarize this state of the art review, it can be concluded that waste heat recovery technologies could be helpful in reducing CO<sub>2</sub> emissions and three of them are emerging: Rankine Cycle systems, Turbo-compounding and Thermoelectric Generators. This conclusion is also shared by different authors [33,129, 130,131].

In particular [131] and the next Figure 6-57 present the comparison of the WHR technologies according to the two key technical parameters: the package and the heat recovery effectiveness. From figure the RC system has the better trade-off between the heat utilization and packaging.

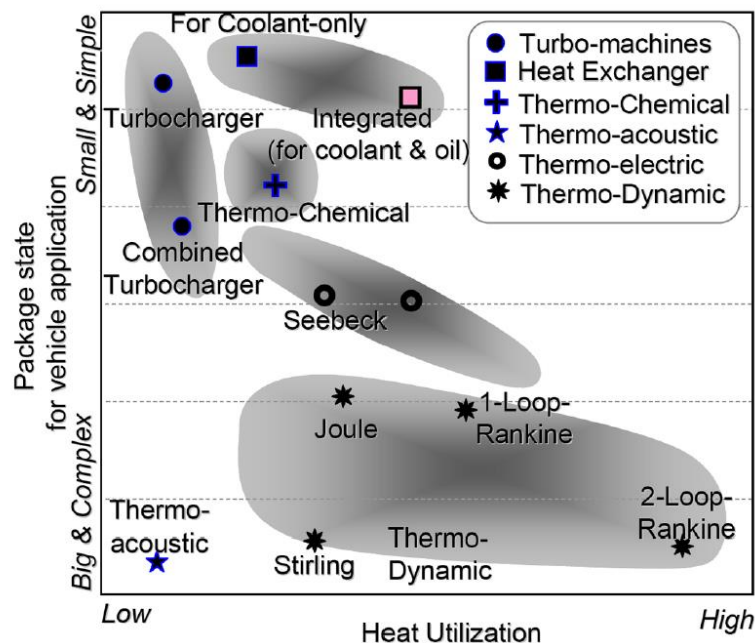


Figure 6-57 Energy utilization vs. package space of several heat recovery systems [131]

Another important indicator for a passenger car application is the weight-to-power ratio. According to different information provided in the literature, Figure 6-58 has been drawn and introduces weight-to-power ratio for the aforementioned waste heat recovery technologies. No data have been found however for the Joule cycle engine. For all other technologies, data comes from mobile applications and in priority from passenger car applications. For thermoacoustic generators, figures could not be found for car applications and data from a space probe has been used. Moreover mechanical turbocompound systems for cars does not exist and an additional weight of 5 kg to the electric turbocompound has been added to take into account the weight of the reduction gearbox. Figure 6-58 clearly shows the advantage of turbocompound units followed by Rankine cycle ones.

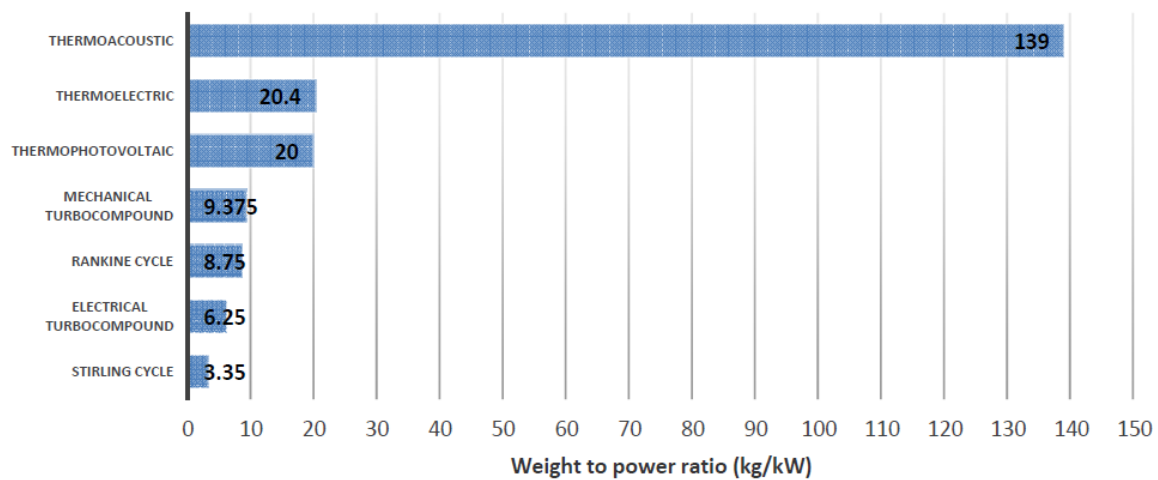


Figure 6-58 Weight to power ratio for different waste heat recovery technologies on a mobile application [33]

The studies [34,38,133], where the author of this thesis has been involved, evaluate the benefits in terms of CO<sub>2</sub> of the TEG, the Electric Turbo Compound (ETC) and the Organic Rankine Cycle (ORC) system in passenger cars, by means of simulations. The TEG and the ETC were applied to a B-class vehicle equipped with 1.3L 70 kW CR Diesel engine. The achieved benefits in NEDC were 1.38 % for TEG and 4.19% for ETC. The ORC was evaluated in C-class vehicle equipped with a 1.4L Turbocharged SI engine, resulting a CO<sub>2</sub> saving of 3.7% in the NEDC and 4% in the WLTC. In all the case studies an electric load of 350 W was assumed, thus the advantages in terms of emissions were derived by the alternator load reduction. The achieved results are aligned with the analysis presented in [33].

As a conclusion of the technology analysis, it should be noted that the indicators presented in Figure 6-57, Figure 6-58 and the CO<sub>2</sub> benefits are not the only parameters to take into account in the choice of a waste heat recovery technology.

Integrating the previous analysis, an objective comparison is performed by the following selection matrix, where the effectiveness of the technologies is compared with technical specification coming from the Level 3 of QFD and cost index based on the information coming from technical literature [87,129,135,175, 130].

Table 6-10 Selection Matrix of Exhaust Heat Recovery Technologies

HoQ 3.1		WHR Technologies					
Technical Criteria	Weight	Fast Warm-up	Mechanical Turbocompounding	Electrical Turbocompounding	Rankine Cycle	Thermoelectric	Stirling
Thermal Efficiency	5	5	3	3	4	2	4
High Power Density	5	4	2	4	2	3	1
High Specific Power	4	4	4	4	4	2	5
Low Engine Back-Pressure	5	4	2	2	4	4	4
Low Aftertreatment Impact ( $\Delta T$ )	5	5	2	2	5	5	5
Packaging	5	5	2	3	2	4	1
Low Complexity	4	5	2	4	3	4	2
Real Driving Operating Conditions	5	3	3	3	4	3	4
Ranking (Effectiveness) [0÷100]		87	49	62	70	68	65
Costs [1÷5]		3	3	4	4	5	4
Technology Value		29.1	16.5	15.4	17.5	13.6	16.2

According to the technical and economic criteria (*Technology Value*) calculated in the selection matrix, the Fast Warm up and Rankine Cycle systems are preferable technologies for passenger car application and for these reasons a detailed focus will be presented in the next paragraphs.

### 6.9.4 Focus on Rankine Cycle Systems

The implementation of the RC for vehicle waste heat recovery was originally considered in relation to heavy-duty long-haul diesel trucks. Cummins in 2014 showed the “Super Truck” program, sponsored by the US Department of Energy, where made much progress. The test results on road by a RC system installed on a diesel engine showed that the brake efficiency of diesel engine was increased from 47.5% to over 51%. Recently, a greater number of research groups [132,133,135] and vehicle manufacturers (e.g. Toyota, Honda, BMW, etc. [129,131]) are investigating RC applications to passenger vehicles and an increased application potential has been shown.

#### RC System Architectures

Different layouts are possible depending on the heat source: engine coolant and exhaust gas (including EGR), which carry a quite similar amount of thermal energy. However, exhaust gas shows a much greater recovery potential in terms of exergy because of a much higher temperature range. The preferred architectures for passenger car applications are mainly three:

- Architecture 1 - the RC system utilizes the exhaust gas as the only heat source to evaporate the working fluid (Figure 6-59).
- Architecture 2 - compared to the previous RC layout a recuperator is added before the evaporator, using the steam from the expander to preheat the working fluid (Figure 6-60).
- Architecture 3 - in the RC system the waste heat from the engine coolant is used to preheat the working fluid (Figure 6-61).

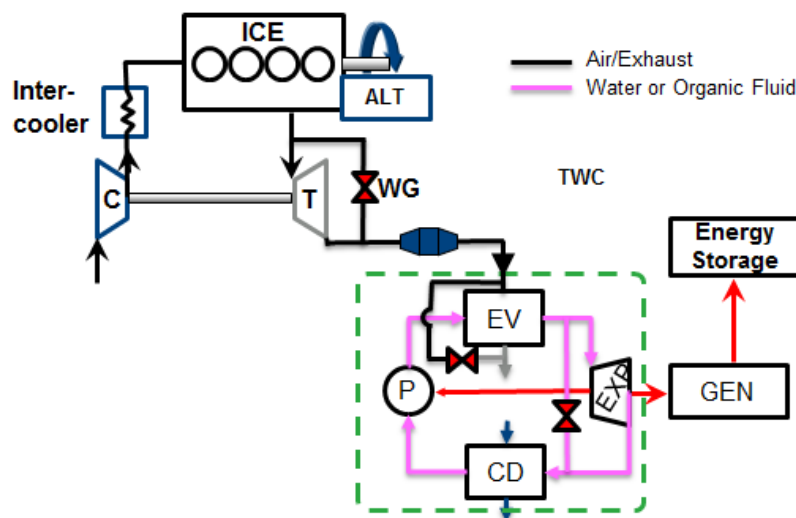


Figure 6-59 Architecture 1- the RC system utilizes the exhaust gas as the only heat source to evaporate the working fluid.

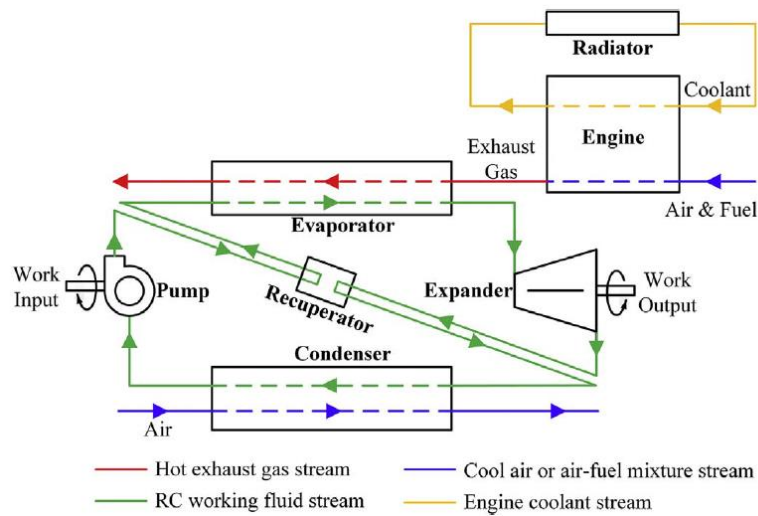


Figure 6-60 Architecture 2 of the RC in which a recuperator is added before the evaporator using the steam from the expander to preheat the working fluid

Other layouts are possible, for instance with dual loops using exhaust and cooling sources (see [132]), but for cost, complexity and packaging issues they are not preferred for passenger cars. The regenerative preheating of the architecture 2 requires a very complex liquid-gas heat exchanger with high surface area, while the preheater in architecture 3 is only required. For some working fluids, e.g. organic fluids, architecture 2 (with a recuperator) is needed to cool down the vapor exiting from the expander, which is still superheated, to reduce the cooling load of the condenser.

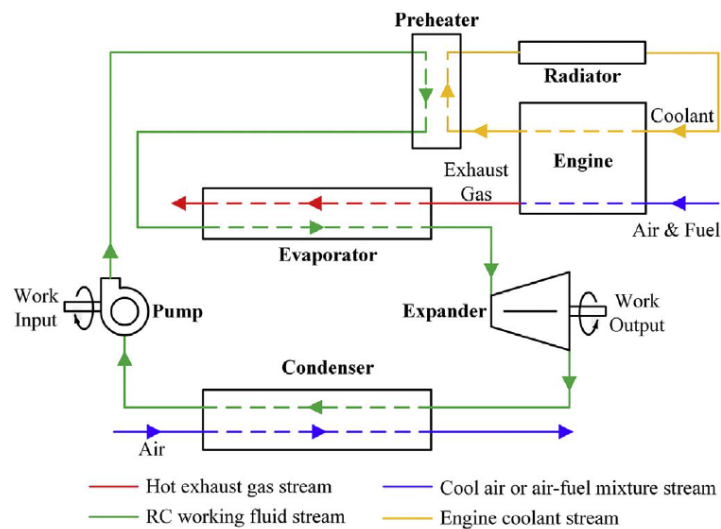


Figure 6-61 Architecture 3- in the RC system waste heat from the engine coolant is used to preheat the working fluid

A novel integration of the RC is proposed and analyzed in this research activity, see Figure 6-62, with the aim to overcome the packaging and cost issues. In case of electric hybrid powertrain, the expander is linked to electric moto-generator (e.g. BSG) by means of the clutch CLT1. GB is a gearbox the can be used in case of high speed expander (e.g. Turbine). The clutch CLT2 connects the electric machine with engine shaft. In this architecture the Motor/Generator performs multiple functions, without the addition of a specific electric generator for the RC system.



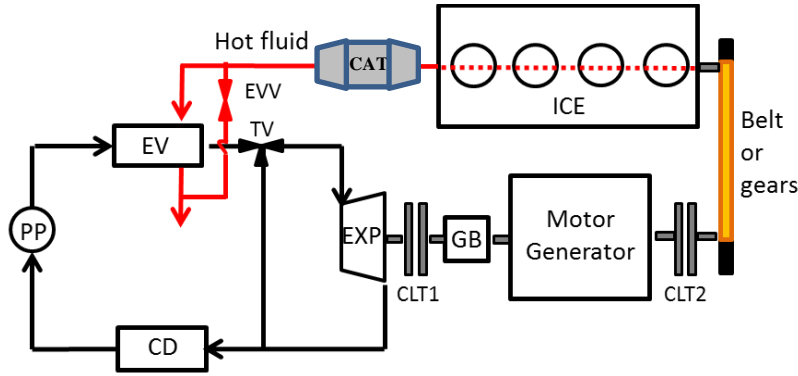


Figure 6-62 Proposed RC system integration in electric hybrid powertrain

Different operation modes are possible by means of the command of the clutches:

- with CLT1 and CLT2 closed the mechanical power from expander is transmitted to the wheel in parallel to engine or alternative both thermal machines generate electric power;
- with CLT1 closed and CLT2 open the power from RC system is used to generate only electric power, for instance if the energy harvested is higher than the load requested for the traction;
- with CLT1 open and CLT2 closed the motor is used to deliver power without the inertia of RC system, for instance during boosting maneuvers.

The benefits of this architecture will be studied by means of simulation on standard cycle and presented in Chapter #12.

## RC efficiency

The thermodynamic efficiency of RC system can be expressed with the following equation:

$$\eta_{RC} = \frac{\dot{W}_{exp} - \dot{W}_{pump}}{\dot{Q}_{in}} \quad (6.3)$$

where  $\dot{W}_{exp}$  is the power from expander,  $\dot{W}_{pump}$  the power consumed by the pump to recirculate and pressurize the working fluid and  $\dot{Q}_{in}$  is the heat power delivered by the exhaust gas to the evaporator. Introducing the evaporator efficiency:

$$\eta_{evap} = \frac{\dot{Q}_{evap}}{\dot{Q}_{in}} \quad (6.4)$$

and thermodynamic efficiency

$$\eta_{th,RC} = \frac{\dot{W}_{exp} - \dot{W}_{pump}}{\dot{Q}_{evap}} \quad (6.5)$$

the RC system efficiency can be obtained as a function of the  $\eta_{evap}$  and  $\eta_{th,RC}$ :

$$\eta_{RC} = \eta_{evap} \cdot \eta_{th,RC} \quad (6.6)$$



The following Figure 6-63 clarifies the meaning of the variables in the  $\eta_{RC}$  definition and it illustrates the typical values of the power flows.

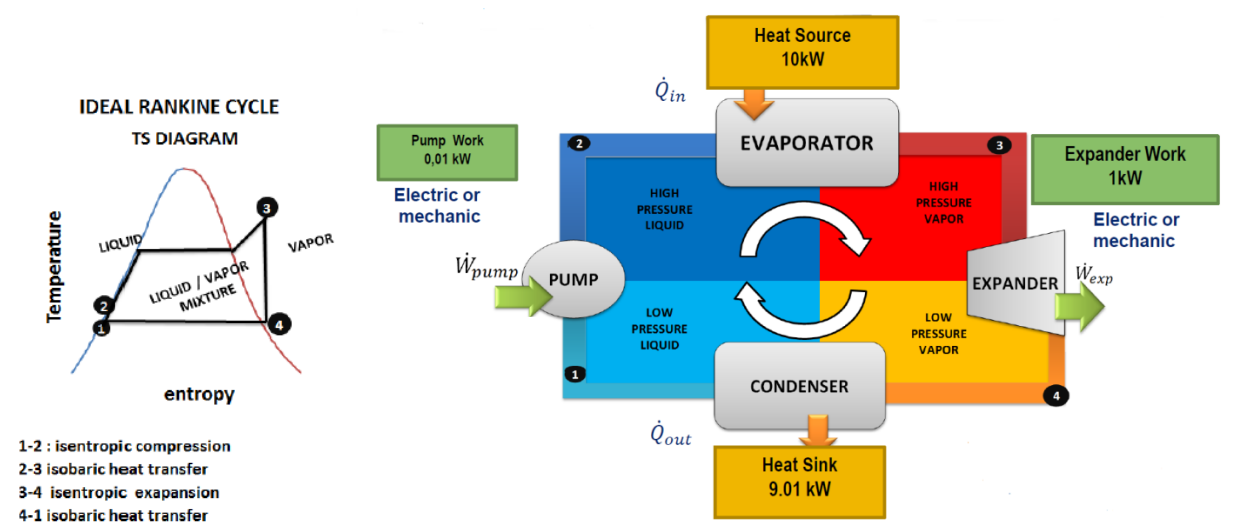


Figure 6-63 Example of Energy balance in RC System, adapted from [130]

In Figure 6-64 the comparison between an ideal and a real RC cycle is illustrated. The main not ideality causes are:

- the finite size of the evaporator, that limits its efficiency;
- the evaporator pressure drop and maximum pressure/temperature constraints;
- the expander losses;
- the condenser pressure drop, size and low pressure constraints.

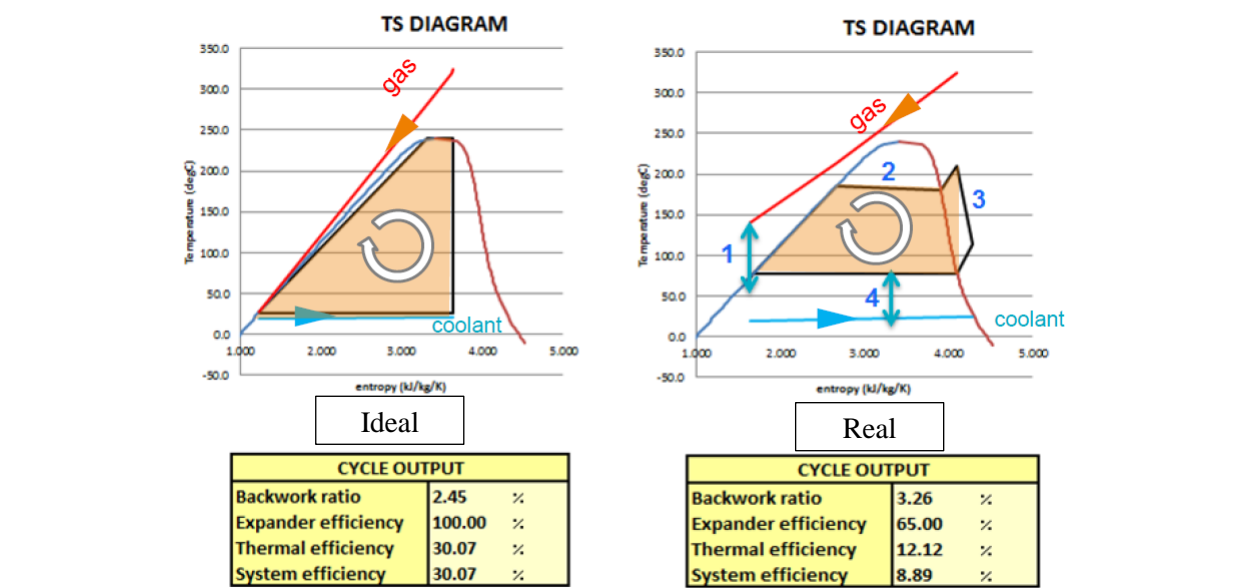


Figure 6-64 Ideal vs. real RC cycle in TS diagram

Another way to measure the effectiveness of RC system in passenger cars, commonly used in the literature is the thermal efficiency  $\eta_{th}$  defined by the equation

$$\eta_{th} = \frac{\dot{W}_{exp}}{\dot{m}_{fuel} \cdot LHV} \quad (6.7)$$

in which  $\dot{m}_{fuel}$  is the engine fuel consumption rate and  $LHV$  is the fuel low heating value. Table 6-11 summarizes the pros and cons of the three different RC architectures and the typical ranges of RC thermal efficiency  $\eta_{th}$  for passenger vehicle applications, as presented in [132].

Table 6-11 Comparison among the RC architectures

RC Architecture	Pros	Cons	$\eta_{th}$
<b>Architecture 1</b>	Simple structure	Only recover exhaust gas waste heat	1÷5%
<b>Architecture 2</b>	- Reutilize waste heat of vapor from expander; - Reduce the cooling load of the condenser	An extra liquid-gas heat exchanger	1.5÷5.5%
<b>Architecture 3</b>	Recover part of waste heat from engine coolant	- An extra liquid-liquid heat exchanger; - Single working fluid to match two heat sources at different temperatures	1÷7%

## RC Component Features

In the considered architectures the *evaporator* can be installed on the engine exhaust line or EGR path. The back-pressure introduced by the evaporator in the exhaust line is lower than the turbo-compound system, but it has to be limited with a proper design, taking into account also the impact on weight increase of vehicle. In [301] an experimental characterization of back-pressure and its impact on LCV diesel engine is presented, demonstrating that with a proper RC sizing it can be contained.

**Working Fluid** -When designing an RC system, special attention should also be paid to the working fluid selection, according to the heat source temperature, which has a significant effect on the system thermal and exergetic efficiency. The choice of the working fluid used in the RC depends on a number of factors including thermodynamic efficiency, environmental, safety, and process-related economic issues. For safety reason, alcohols and hydrocarbons, in spite of their good thermodynamic efficiencies, are not ideal candidates. Instead, refrigerants, which are used in automotive air conditioning systems, are usually better options. Generally, according to the slope of the saturation curve, the working fluid may be categorized into three different types: 1) wet fluid, 2) dry fluid and 3) isentropic fluid, see Figure 6-65.

Water is a preferable working fluid for high exhaust gas temperatures ranging from 500 to 800 °C, for this motive it is suitable for SI engines. In terms of the disadvantages of water, there is the requirement for superheating to avoid turbine blade erosion if such a machine is selected for the expander. Also, the high degree of superheating makes water less practical for automotive applications due to the variation of exhaust temperature at different load conditions. Also, water high freezing point (0 °C) cannot meet the standard automotive working temperature range (−40 ÷ 85 °C). Therefore, practical solutions to solve these issues need to be developed if water is chosen as the working fluid for RC vehicle applications.

Most organic fluids are either dry fluids (e.g. R113, R245fa, R245ca, etc.) or isentropic fluids (e.g. R11, R134a, R123, etc.). Associated CFCs/ HCFCs have been rejected due to environmental concerns and phased out according to international protocols. Dry/isentropic refrigerants are widely used in small-scale RC applications because of their good heat transfer properties, excellent thermal stability and low viscosity. They are generally non-flammable, which is a great advantage for automotive application and

compatible with most materials. Under low temperature ambient conditions ( $-40 \div 0$  °C) they also do not freeze, which is a major benefit relative to water.

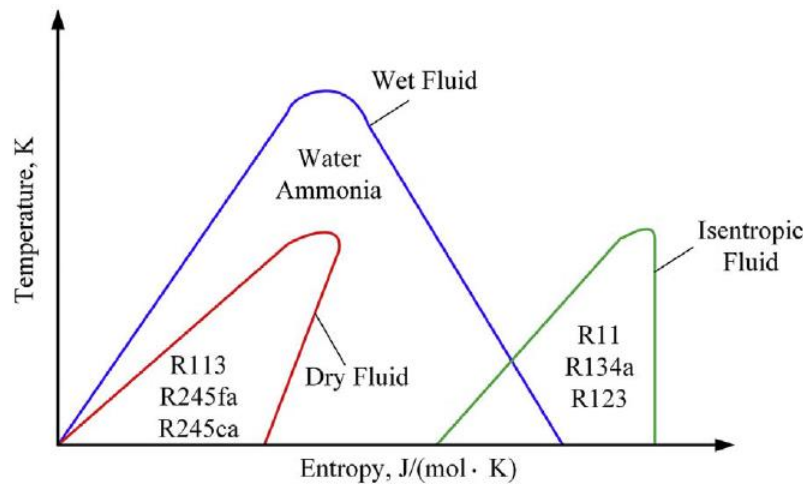


Figure 6-65 Three types of working fluid: dry fluid, wet fluid, and isentropic fluid.

It was also found that the heat exchanger effectiveness for R123 and R245fa is higher than that for water, and consequently when the exhaust temperature is relatively low, organic fluids can be considered appropriate for vehicle RC application. Organic fluids usually exhibit a lower power output than water, require an extra recuperator to reduce the cooling load of the condenser, have relatively low thermal instability temperatures. The selection of working fluid should be considered together with the expander for the specific vehicle RC application.

**Expander** - The *expander* can be mechanically plugged to the engine or connected to an electric generator or to both, as illustrated in Figure 6-62. In the case of connection with engine the harvested energy is used with high efficiency, without other conversions, but the system doesn't allow a versatile energy management, furthermore the expander speed is linked to the engine with not optimal operation. The four main types of expanders (turbine, scroll, screw and piston types) have their own advantages and disadvantages for passenger vehicle applications.

The turbine expander has a compact structure, is light weight, and has high efficiency. However, design and manufacturing is very difficult, thus leading to a higher cost. The turbine expander also has lower efficiency under off-design conditions and cannot tolerate two-phase conditions. For the high rotational speed ( $50 \div 100$  krpm), the turbine requires a gearbox for the direct connection and it can more suitable to combine with electrical generators for energy conversion.

The scroll expander is characterized by lower flow rates, higher pressure ratios and much lower rotational speeds than turbomachines. It has a compact structure, fewer moving parts, lower levels of noise and vibration, and the most cost efficient design.

A screw expander is highly efficient in off-design conditions. However, lubrication is required to avoid direct contact while achieving a seal between the lobes of the two rotors; this feature makes the screw expander relatively more expensive to fabricate than scroll expanders.

Piston expanders have larger built-in volume ratio, high achievable operating pressures and temperatures, and low rotational speeds. All of the three displacement types of expanders (scroll, screw, and piston types) have the ability to tolerate two-phase flow. Table 6-12 from [132] summarizes the advantages and disadvantages of the different types of expanders for RC application to passenger vehicles.

Table 6-12 Comparison of different types of expanders for RC application to passenger vehicles

Expander	Advantages	Disadvantages
Turbine expander	Compact structure, light weight, high efficiency, mature manufacturability	Difficult to design and fabricate, high cost, low off-design efficiency, cannot bear two-phase, high rotational speed
Scroll expander	Compact structure, high reliability, fewer moving parts, lower rotate speed and lower level of noise and vibration, can handle two-phase flow	Leakage of the working fluid leads to low efficiency, low capacity, require lubrication
Screw expander	Tolerate two-phase flow, low rotate speed and efficient in off design conditions	Mostly adopted in RC plants, require seal to prevent internal leakage, lubrication is required
Reciprocating piston expander	Larger built-in volume ratio, higher achievable operating pressures and temperatures, tolerate two-phase flow, low rotational speeds	Heavy weight, have valves and torque impulse, many moving parts

**Heat Sink-** The heat sink can be the engine coolant or the ambient air. The first one is the most stable source in temperature ( $80\div 100^{\circ}\text{C}$ ) and capacity flow ( $3\div 10\text{kW/K}$ ), whereas air as heat sink allows lower temperatures, but higher temperature drops. The state-of-arts of RC systems is presented in the review study [132], from which the following Table 6-13 is extracted.

Table 6-13 Summary of the works about the application of Rankine Cycle to passenger vehicles

Ref.	Year	Vehicle/Engine	Heat Source	Architecture	Expander	Working fluid	RC $\eta_{th}$ [%]	RC $\eta_m$ [%]	Research method
[312]	2005	HEV, SI-ICE 1.4L L4 NA	Exhaust (high pressure) Exhaust Low pressure) Exhaust (ORC)	Structure 1 Structure 1 Structure 1	Turbine Turbine Turbine	Water Water R-245ca	2+4 1.3+3 4+5	/	Numerical Numerical Numerical
[313,314]	2007	HEV, SI-ICE 1.4L NA 1.3L and 2.0L	Exhaust	Structure 1	Axial Piston	Water	3.8	/	Experiment
[131]	2009	SI-ICE 1.4L NA	Exhaust	Structure 3	Turbine	Ethanol	3.2		Experiment
[315]	2009	HEV-Prius	Exhaust + Coolant	Structure 1 and 3	Piston Expander	Water		9	Numerical
[316]	2012	Series 5	Exhaust	Structure 1	Impulse Turbine	Water		6	Experiment
[317,318]	2012	SI-ICE 1.8L L4 NA	Exhaust Coolant Exhaust+Coolant	Structure 2 Structure 2 Structure 2		245fa	3.4 1.7 5.1	/	Numerical Numerical Numerical
[319]	2013	SI-ICE 2.8L VR6	Exhaust	Structure 1	Turbine	Water R245fa	2.64 6.96	/	Numerical Experiment
[326]	2013	SI-ICE 1.3L L4 NA 67kW	Exhaust	Structure 1	Turbine	Water	3+8	/	Experiment + Numerical
[301]	2015	TDI-ICE 3.0L L4 130 kW	Exhaust	Structure 2	Sliding Vane Rotary	R236fa	5.5	/	Experiment
[327]	2015	SI-ICE 2.0L L4 NA 153kW	Exhaust + Coolant	Structure 3	Piston Expander	Ethanol	1.2	/	Experiment

## Rankine Cycle System Cost Estimation

The economic evaluation is derived from data reported in [87,135,175] and it is based on estimations for the cost of the utility components: pump, expander, heat exchangers (condenser and evaporator).

The cost value for every component is coming from the cost analysis of parts already known and with a large scale application in the automotive industry. The reference elements for the pump and the heat

exchangers are the components used for the air cooling installation in the vehicle, engine cooling and EGR. For the expander cost the engine turbo machines are benchmarked.

The total utility cost is defined by the following equation:

$$\text{Cost}_{\text{RC}} = \text{Cost}_{\text{condenser}} + \text{Cost}_{\text{evaporator}} + \text{Cost}_{\text{pump}} + \text{Cost}_{\text{expander}} + \text{Cost}_{\text{pipes}} + \text{Cost}_{\text{fluid}} \quad \text{in [€]} \quad (6.8)$$

The following table summarizes the range of cost for each components considering a system in a range of power 5÷10 kW.

Table 6-14 Cost breakdown of RC system

Rankine Element	Cost Range [€]	
Pump	30	45
Expander	160	200
Evaporator	80	100
Condenser	30	40
Pipes	25	30
Working Fluid	25	30
Total Cost [€]	350	445

## 6.10 Transmission Technologies

The task of the transmission is to transfer the power of the ICE and the ETD to the traction wheels at a proper speed. The transmission reduces the high propulsion machine speed to the lower wheel speed by increasing the torque. The use of automated transmission is key to implement management logics that lead the engine and electric motor to operate in high efficiency points and it will be mandatory for the autonomous driving implementation.

### *Transmission Technology Options*

Three technologies are the main options for the future ICE based powertrains: the Automatic Transmission, the Dual Clutch Transmission and the Continuous Variable Transmissions.

The Automated Manual Transmission (AMT) is applied in low cost market and is not considered of wide diffusion due to the issue of the torque gap during gear-shift and the limit in number of implementable gears.

**Automatic Transmission (AT)** - This is a (globally) wide-spread solution for the pickup and SUV segment, due to torque overshoot at start-up. The gear ratios of an automatic transmission are realized via planetary gears. Synchronization is realized via multi-plate clutch, multi-disk brakes, etc. The start-up element is usually a torque converter.

The main benefits are: good launch at vehicle take-off and the comfort, by means of a smooth ride. These transmissions are widespread for the heavier vehicles, especially in the US-market. It also enhances hybridization potential.

**Dual Clutch Transmission (DCT)** - It combines almost the comfort of a conventional AT with the dynamics of a Manual Transmission (MT). The DCT comprises two independent and separate transmissions. The dual clutch connects both transmissions with the engine via two driving shafts in a force-locking manner. Furthermore, shift events are realized without interruption of traction. The

transmission management is operated via a mechatronic module (incl. ECU, sensors, etc.). For the smaller segments which require less power needs, a dry dual clutch is enough (no oil requirements), while higher power versions require a hydraulic system realizing a “wet” dual clutch.

The main DCT benefits are modern and sportive reputation, increased fuel efficiency, less emission, high potential for hybridization and the combination of fuel economy, sport and automatic mode.

***Continuous Variable Transmissions (CVT)*** - Continuous variable transmissions use a variator in combination with a torque converter to realize fully variable gear ratios in a wide range. A torque converter is required for the drive away.

The advantage of the CVT is the optimization of the engine operation points for optimal efficiency. With the CVT the engine can be operated on the maximum efficiency curve with the highest efficiency for each output power.

The disadvantage is the relative low efficiency of the transmission in comparison to manual transmissions, dual clutch transmissions or automatic transmission.

Higher number of gears for DCT and AT, respectively up to 8 and 10, reduces the gap versus CVT in term of engine efficiency. For this reason the DCT and AT are preferred in the next analysis. The number of speed and the selection of transmission ratio for each gear are fundamental to achieve the performance and the efficiency targets of the powertrain.

For the electric motors a single transmission ratio is typical used in the architecture from P0 to P3. In case of P4 configuration a single speed or multi-speed up to 4 with automated gear shifting can be employed. The multi-speed transmission is employed to allow the electric motor operation in high efficiency points.

As for the engine, the electric motor performance and efficiency are highly affected by the proper selection of transmission ratios.

## 7. The Vehicle Electric Power Nets

The electronic control of accessory loads of powertrain, such as pumps and valves [24,36,57], has the benefits in relation to improved component operating efficiency, improved control, or reduced (parasitic) power loads. These components applied to conventional and alternative propulsion technologies, as illustrated in [36,57], allow the reduction of the real auxiliary power for engine operating. The powertrain electrification can take advantage from synergy with a general trend of electrical load increase, due to new vehicle functions and features desired by the end-user, for instance navigation systems, infotainment systems, etc. The next generation of vehicles are expected to have more vehicle electronics, which will push the threshold of the power source output over 3 kW, the present day limit for 12V power net. Next to 12V, an increased onboard power net voltage such as the 48V is expected to rise the output power threshold by 4 times compared to today 12V power net, thereby not only better managing higher power requirements but also reducing the electrical current levels.

Remaining at level of vehicle functions, the Automated Driving, with the enormity of electrical assist and electronic controls needed, is expected to peak current demands that a 12V alternator will be unable to satisfy, as highlighted in [24, 25] and Figure 7-1.

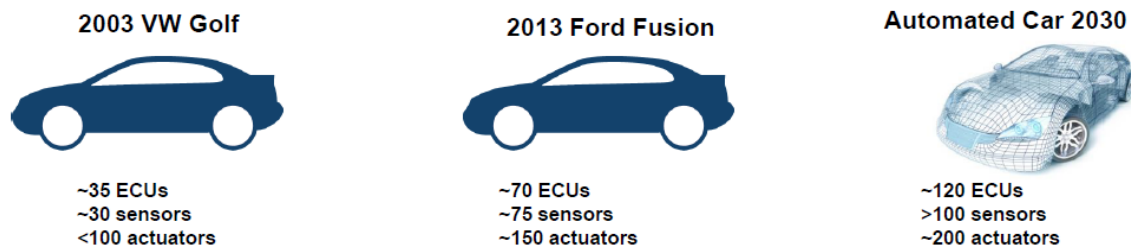


Figure 7-1 Expected impact of the Automated Driving on electric and electronic architectures [24]

The passage of high electric loads from 12V power net system to the 48V system has also benefits in term of vehicle mass and weight.

In line with the reduced electrical current level, the size of wire harnesses will also reduce, thereby directly contributing to the total weight and mass reduction of a vehicle.

48V also facilitates the switch from hydraulic and mechanical belt-driven systems to electrically powered systems, thereby eliminating the use of hydraulic pumps, belts, and hoses, thus further reducing the mass and volume at a vehicle level.


The availability of 48V power net contributes to application of electric components at powertrain level, like the electric Supercharging, the 48V Electric Traction Drive and the Electric Heating Catalyst system, because the cost of battery and its management system can be shared among vehicle and powertrain subsystems.

Furthermore in ICE based vehicles, up to 15% of the energy produced by the engine is used by other devices. Transferring auxiliary load from 12V to higher voltage (e.g. 48V) enables a better optimization in terms of fuel efficiency and emissions.



The following Table 7-1 shows the power estimation of the main onboard vehicle electric loads, considering the conventional loads and new electrified components (e.g. electric AC compressor). To estimate the maximum continuous load for the alternator a probability of use is defined, with the meaning of a contemporary factor. The estimation of electric load probability has been performed for a Compact vehicle on the basis of activation time in a WLTC driving, considering an increasing of 30% to take into account the realistic condition. The load of the electric Supercharging (e-Booster) is obtained from [268], whereas that of the EHC from [147,148]. The electric A/C compressor and the fan are considered active only during the stop phase of the driving cycle. The new electronic devices for the automated driving are only partially considered, because the technology is in continuous evolution and electric loads depends on level of autonomy (see Chapter #2.3).

Table 7-1 Vehicle electric load evaluation for conventional and new electric devices

 Electric Load	Peak Power (W)	Probability of load begin on	Power Probability (W)
Engine Starter	900	0.1	90
e-Booster	4000	0.2	800
E-Heating Catalyst	4000	0.15	600
E-Water Pump	200	1	200
E-Oil Pump	200	1	200
Others E-Actuators	300	1	300
A/C Fan	900	0.3	270
E-A/C Compressor	1650	0.3	495
E- Power Steering	1680	0.1	168
Vacuum Pump	200	0.5	100
Wipers	70	0.1	7
Headlamps	140	0.5	70
Tail lamps	70	0.5	35
Radio	50	0.9	45
ECUs/Cluster	500	1	500
<b>Total</b>	<b>14860</b>		<b>3880</b>

The results in the table confirm the needed of power higher than the current systems. The electrification of the accessories is an opportunity to simplify the base engine, compensating the cost of new electric devices. Table 7-2 adjusted from [57] summarizes the impact of the new electric components considered in Table 7-1.

Table 7-2 Powertrain impact of the new electrified devices

Electric Device	Effect on performance	Effect on FC & Efficiency	Pollutant Emission	Comfort	Package	Complexity reduction
Generator/E-machine	+	+	+	+	O	+
E-Water pump	O	+	+	O	+	+
E-Oil pump	O	+	+	O	+	+
E-AC compressor	O	O	O	+	+	+
Vacuum pump	O	+	O	+	+	+
E-Cam phaser	+	+	+	O	+	O
E-Booster	+	+	+	+	O	O
E-Catalyst	O	+	+	O	O	O
+ Advantage	O No advantage					



## 7.1 Vehicle Voltage Architecture definition

Depending on voltage levels different power net architectures are possible.

### Single Voltage Architecture

A single voltage vehicle system includes only one voltage level as found in current vehicles, such as a complete 12V system. All the loads and actuators work with a unique supply standard, see Figure 7-2. The battery typically is a Lead-Acid type and the alternator is a synchronous machine able to generate only electric power, with a rate below 3kW.

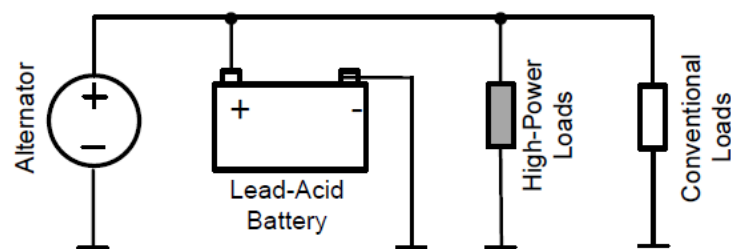


Figure 7-2 Single Voltage and Single-Battery standard architecture (12V)

### Dual Voltage Architecture

A dual voltage system includes two separate voltage systems, such as a 12V/48V or 12V/ HV system, see Figure 7-3. The battery typically is a Li-ion type and depending on the application, it can be substituted or supported by a super-capacitor. The electric energy is produced at 48V or HV and a DC/DC converter is used to transfer energy from 48V (or HV) side to 12V net. The electric machine is typically a Belt Starter Generator (P0 architecture) able to delivery also mechanical power to start and assist the ICE. This electric architecture is typical of Hybrid Electric Vehicles.

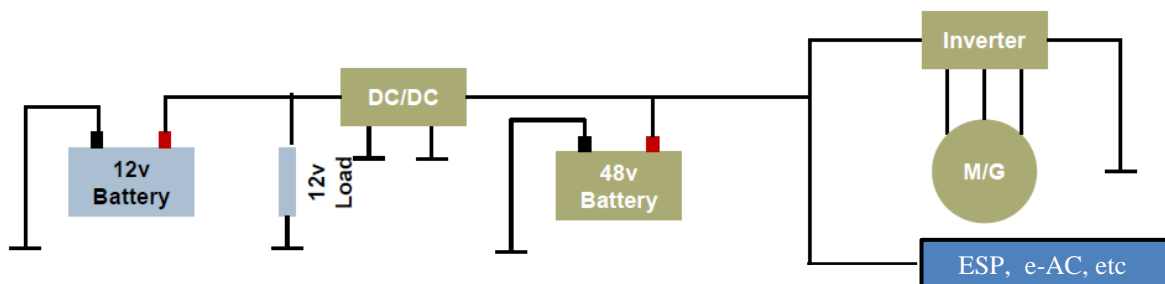


Figure 7-3 Dual Voltage architecture (12V/48V), typical of BSG (P0) application

High power consuming applications in the range of 500 watts to 5kW, such as EPS and e-AC compressor, are soon expected to follow once a 48V power net is installed in a vehicle.

## Multi-Voltage Architecture

A multi-voltage system is capable of generating three or more voltages. Voltage changes depending on the application and they are typically including at least an high voltage level, 48V and 12V, see Figure 7-4. It is typical of full Hybrid Electrical Vehicles, with voltage up to 800V, which requires a higher level of protection against electrical shocks.

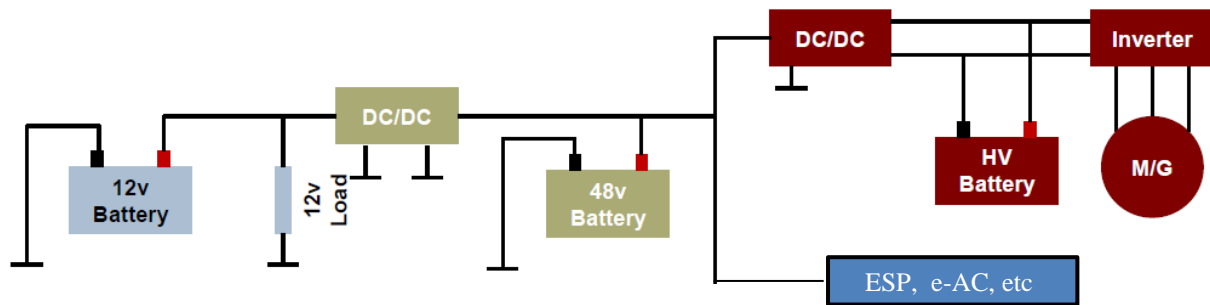


Figure 7-4 Multi-Voltage architecture (12V/48V/HV)

## 7.2 The 48V Power Systems

48V systems typically use dual voltage architecture, including a 12V net linked to the 48V net via a DC/DC converter as illustrated in Figure 7-3.

Here in Figure 7-5 an example of a 48V system including a BSG and an electric supercharger is presented. 48V standard has also a strong convenience in terms of electric system lower complexity (compared to HV systems) for vehicle hybridization and consequently lower system cost.

48V systems are defined Low Voltage systems because classified as a Class-A component (<60 V DC & < 30V AC) according to standard ISO 6469-1. The systems advantages related to this classification can be summarized following:

- No need for electrical shock protection for users, such as galvanic isolation, interlock safety system, isolation monitoring functions.
- No need for waterproof connector, class IP6X.
- No need for creepage gap inside Power Board and internal components isolation.
- Use of MOSFET transistor with enhanced low power efficiency.
- No need of special licenses for service operators as for HV.

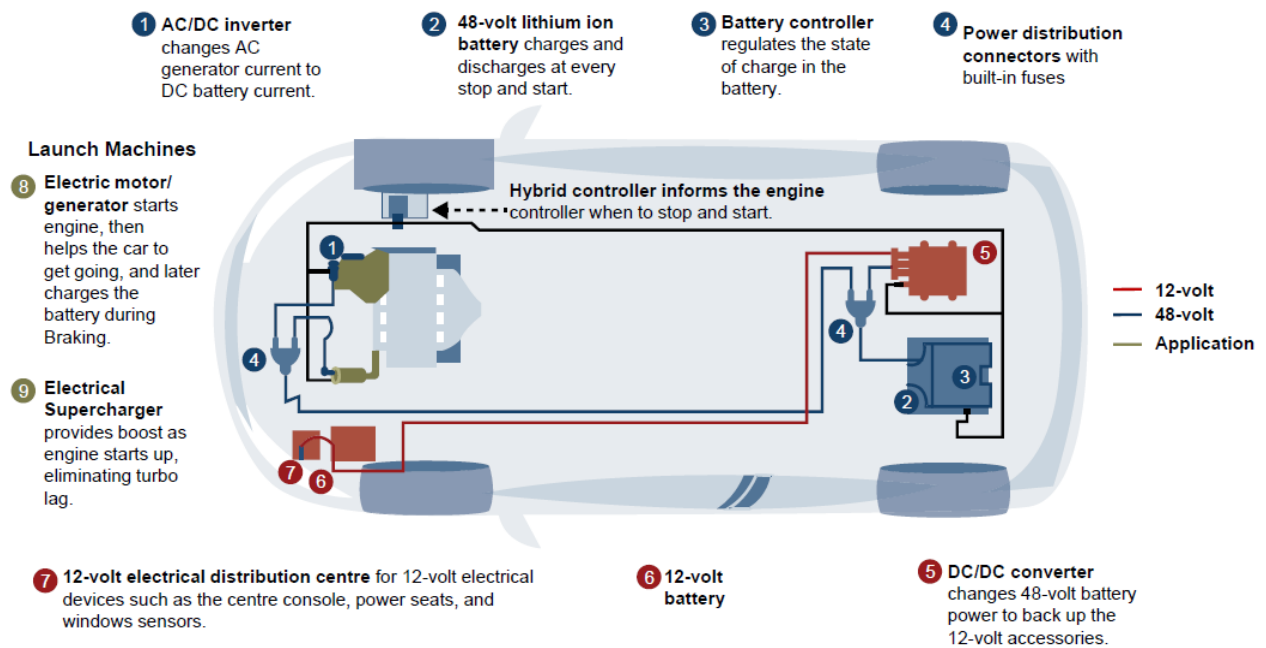


Figure 7-5 Example of dual voltage 48V/12V electric power net architecture

The following Table 7-3 summarizes the evolution of the vehicle power net in the near future taking into account the above analysis and considerations. The Dual Voltage architecture 48V/12V will see a large adoption to support the increasing electrification process of the powertrain and vehicle functions.

Table 7-3 Power –net evolution in the near future

Parameter	Present	Future
<b>Redundancies</b>	1 per safety –critical function	Several for each safety-critical functions
<b>Driving module</b>	Electrically assisted and electronically controlled steering, throttle, gearshift.	Steer, throttle, and shift-by-wire systems
<b>Power rating</b>	3kW alternator	> 10kW generator
<b>Power source</b>	1 lead-acid 12V power net	Minimum 2 batteries—one on 48v Li-ion and one on 12v (chemistry depends on OEM preference)
<b>Communication protocol</b>	Primarily CAN & LIN, with some limited applications using FlexRay, Ethernet/IP	Primarily CAN & Ethernet/IP, with limited applications using LIN and FlexRay
<b>Potential weight reduction</b>	Present day 12v system offers little to no potential for weight reduction.	Using a 48v power-net allows for component and wire harness downsizing with mass, volume, and packaging advantage, thereby positively impacting CO2 emission

## 8. Technologies for Electric Propulsion

### 8.1 Electric Propulsion System Architecture

The conceptual typology of an Electric Traction Drive (ETD) system is depicted with blue blocs in the following Figure 8-1. The subsystem is integrated with other devices on-board the vehicle and it is powered by the electric battery, that can be recharged by the external power net in a plug-in vehicle.

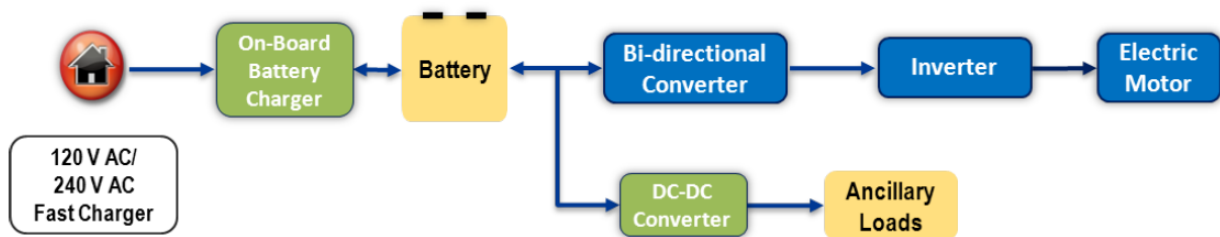


Figure 8-1 Electric Propulsion System Architecture

The ETD systems can be classified for the electric machine type or for the supply voltage, as detailed in next paragraph. Many HEVs in production use ETD with a voltage up to  $350 \div 450\text{V}$  [55,56, 177,229] and new high performance vehicles are expected with voltage up to 800V. But the technical options under evaluation in many studies and demonstrators [57, 114,58,60] use a nominal supply voltage of 48V, named Low Voltage (LV).

An objective comparison of the Electric Traction Drive systems has to taking into account the main key technical parameters defined in the HoQ3.2. In addition to **Power** and **Torque**, instantaneous and continuous, the parameters described below have to be considered:

**Power Density** – The power density is an extremely important feature due to limited space “under the hood” and in the vehicle. Packaging constraints vary with the different types of electric drive applications, but can be of greatest concern in vehicle types that have the most potential for reducing the vehicle fuel usage.

**Specific Power** – The vehicle mass directly affects overall fuel efficiency and the benefits of the additional ETD can be greatly reduced if the mass is not carefully managed. Additionally, increasing vehicle mass complicates and may even prevent integrating ETD systems into vehicles.

**Efficiency** - System efficiency is important, not only for the direct effect on fuel consumption, but equally important is that the losses (inefficiencies) are converted to heat, which must be removed with a thermal management system, that carries added cost, weight, volume, and system complexity.

**Integration** – Specific Power and Power Density, obviously affect the integration, with different impact depending on the ETD position. Another critical parameter is the supply voltage, because to ensure safety standards with high voltage system the electrical architecture increase significantly the complexity.

The relevance of the ETD key technical and economical features in each electric hybrid powertrain is summarized in the following Table 8-1.

As expected, the power and torque increase with electrification degree, as well as the efficiency importance, due to its impact on electric autonomy, whereas the integration is more critical for hybrid architectures. In general the specific power is highly relevant for all the systems, because of its impact on weight and energy consumption.

Table 8-1 Key Features of Electric Traction Drives vs. powertrain architectures

ETDS Key Features	Rilevance vs. Powertrain Architecture			
	Middle HEV	HEV	PHEV	RE-EV,BEV or FCEV
ETD Usage	Electric traction ability depending on power	Multiple modes of operation for each motor through trasmissions, clutches and planetary gear sets, variable gear ratio	Multiple modes of operation for each motor through trasmissions, clutches and planetary gear sets, variable gear ratio	Full speed range electric traction
Number of Electric Motors and PIMs Required	up to 2, 1 for traction and 1 generation	up to 2, 1 for traction and 1 generation	up to 2 for traction and 1 for generation	up to 4
Peak Mechanical Output Power (kW)	10 ÷ 40	50÷85 (traction), 40÷ 60 (generator)	70÷110 (traction), 45÷55 (generator)	110÷150
Continuous Mechanical Output Power (kW)	6 ÷15	20÷30 (traction) 20÷30 (generator)	35÷85 (traction) 20÷40 (generator)	65
Specific Power and Torque	High	High	High	High
Power and Torque Density	High	High	High	Medium
Wide High-Efficiency Area around Maximum Continuous Power	Medium	High	High	High
High Efficiency @ Maximum Peak Power Levels	Medium	Medium	High	High
Efficiency over wide input Voltage Ranges	High	High (narrower voltage range)	Medium (depends on battery control strategy)	High
Motor Cooling – Current Options	Ethylene Glycol water jacket	Trasmission oil Spray	Trasmission oil Spray	Ethylene Glycol Water Jacket or Trasmission Oil Spray
Inverter Cooling – Current Options	Ethylene Glycol	Ethylene Glycol (105°C or 75°C)	Ethylene Glycol (105°C or 75°C)	Ethylene Glycol (Low temp. loop 75°C)
Integration	High	High	Medium High	Medium High
Cost (relative to overall system)	High	High	Medium	Medium High

## 8.2 Electric Traction Drive Components

In the following paragraphs an overview of the ETD components is presented, with state of the art and some highlights on the next developments.

### 8.2.1 Electric Motors

Electric motors are energy converters that take in electrical energy as input and convert it to a mechanical power output. Electric motors have the benefit of being reversible when functioning as generators, hence mechanical power can be transformed to electrical power and stored in a battery. The best efficiency operating points of electric motor/generators are much better than ICEs, ranging from 75-96% depending on motor construction.

The following Figure 8-2 shows the typical characteristic of an electric motor, with three regions: constant torque, constant power and reduced power. The nominal angular speed is known also “base speed”. The maximum speed can be the same of critical speed in case of the absence of the third region. Similar power and torque curves can be depicted for continuous and peak operation, see Figure 8-3. The peak outputs can be maintained for 30÷60 seconds and they are 1.5÷2 times higher than continuous values, depending on the motor type and power electronic capability.

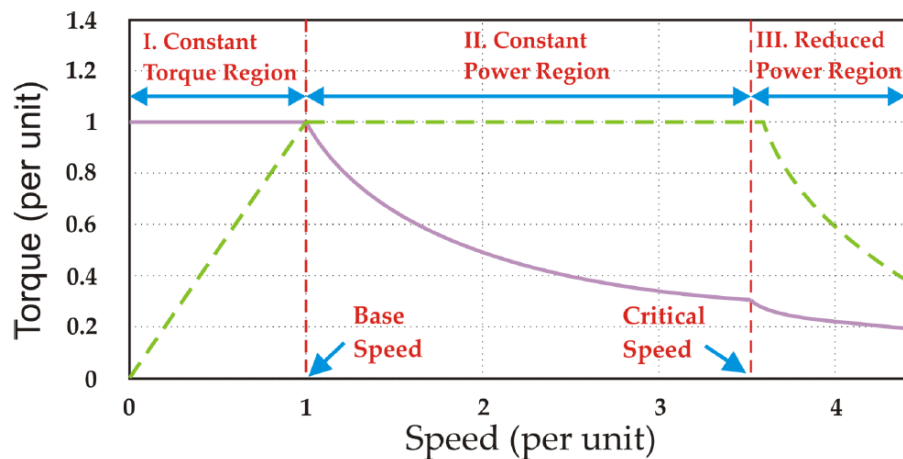


Figure 8-2 Normalized Torque and Power characteristic vs. speed of an electric motor

The ETD technical specifications defined in Chapter #4.5 impact on the key points of the motor characteristic highlighted in Figure 8-3. In pure electric traction the vehicle requires a constant-torque operating region at low speed for starting and up-hill march and then a constant power speed range at higher vehicle speed. The continuous power at maximum speed determines the maximum speed of the vehicle on flat (F red square, for Flat). The continuous stall torque determines the maximum slope that the vehicle can climb continuously (U red square, for Uphill). Transient overload torque and power are limited by the inverter current rating ( $i_0$ ), and the combination of voltage and current limits ( $v_0$ ,  $i_0$ ), respectively.

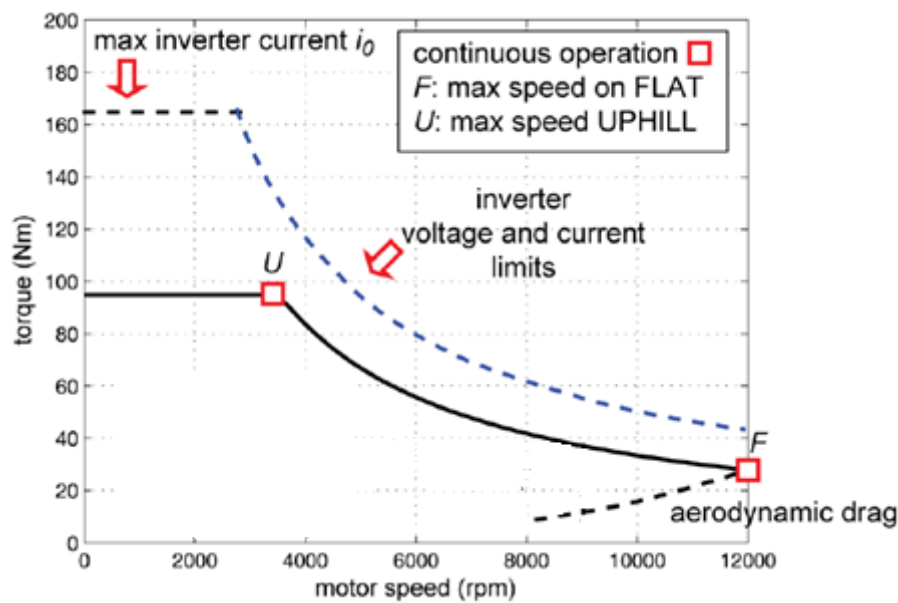


Figure 8-3 Example of target specification for an electric vehicle adapted from [ 178]

The electric motors can be classified in different ways. The typical classification takes into account the type of electric power supply according to Figure 8-4. In Figure 8-5 simplified cross sections of rotor (center rotating shaft) for the main motor types are depicted, giving an idea of the constructive features.

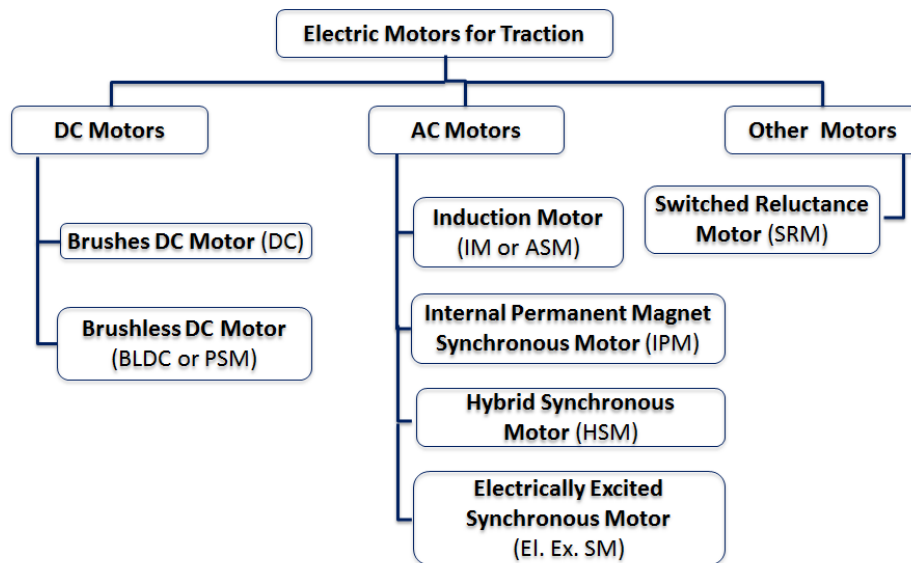


Figure 8-4 Classification of electric motor types based on electric power supply

Following the main features of the relevant motors for the car propulsion are summarized:

**DC- Motors** - During the early 1900s the first electric cars featured direct current (DC) brush motors, due to the easy of transferring electricity from and to the DC batteries to power the wheels without great transformation efforts. DC motors have ever been prominent in electric propulsion, also because their torque-speed characteristics suit traction requirements well and their speed controls are simple. However, DC motor drives have bulky construction, low efficiency, low reliability and need of maintenance, mainly due to the presence of the mechanical commutator (brush), even if interesting progress have been done in



slippy contacts. Moreover, the development of rugged solid-state power semiconductors made it increasingly practical to introduce AC Induction and Synchronous motor drives that are mature to replace DC motor drive in traction applications. In fact, the commutatorless motors are attractive as high reliability and maintenance-free operation are prime considerations for electric propulsion.

Today many automotive DC motors are brushless DC motors (BLDC), where the commutation of the current is performed electronically, which reduce friction losses, improve efficiency and are used in many automotive applications already, for example as servo motors. DC Motors are best suited for high moment at low shaft speeds and are limited by efficiency losses at high RPM values. Motors with permanent magnet rotors exhibit high cost for the magnet materials.



Figure 8-5 Simplified cross sections of rotor for different motor types (red and green are the permanent magnets)

**AC Motors** include a greater variety of motors for hybrid and electric powertrains, including types that reduce the need for expensive magnet materials. In this motor family the more relevant are the Internal Permanent Magnet Motors (IPM), the Induction Motors (IM) and Hybrid Synchronous Motors (HSM).

**Induction Motors** - Cage induction motors are widely accepted as one of the suitable solution for the electric propulsion of HEVs according to their reliability, ruggedness, low maintenance, low cost, and ability to operate in hostile environments. In the past, induction motor drives were facing a number of drawbacks that pushed them out from HEVs electric propulsion. These drawbacks are mainly: high loss, low efficiency, low power factor, and low inverter usage factor, which is more serious for high speed and large power motor. These drawbacks have been overcome with an evolution of control technique based on sinusoidal PWM strategy. Today, induction motor drive is the most mature technology among various commutator-less motor drives.

**Internal Permanent Magnet Motors** - The IPM motors are the most diffuse for the electric propulsion of HEVs. These motors have a number of advantages, which are: (a) overall weight and volume significantly reduced for a given output power (high power density), (b) higher efficiency as mentioned above and (c) heat efficiently dissipated to surroundings. However, these motors inherently have a short constant power region. In order to increase the speed range and improve the efficiency, the conduction angle of the power converter can be controlled at above the base speed. The speed range may be extended three to four times over the base speed. However, at very high-speed range the efficiency may drop, the motor may suffer from demagnetization.

**Hybrid Synchronous Motors** – The HSMs are variants of the IPM motors with reduced quantity of magnet and a structure of the rotor similar to the variable reluctance motor. HSMs offer wider speed range and higher overall efficiency but more complex construction.

In the family of alternative motors the more relevant one is the Switched Reluctance Motor (SRM).

**Switched Reluctance Motors** – SRMs are gaining much interest and are recognized to have potential for HEV applications, mainly for their magnet free operation. These motors have the definite advantages of simple and rugged construction, fault-tolerant operation, simple control, and outstanding torque-speed



characteristics. A SRM can inherently operate with extremely long constant power range. There are, however, several disadvantages, which for many applications outweigh the advantages. Among these disadvantages, acoustic noise generation, torque ripple, special converter topology, excessive bus current ripple, electromagnetic interference (EMI) noise generation. All of the above advantages as well as the disadvantages are quite critical for vehicle applications. Acceptable solutions to the above disadvantages are needed to get a viable SRM based HEV. Nevertheless, the SRM is a solution that is actually envisaged for light and heavy HEV applications.

## Electric Machine Comparison

The magnet rich IPM motors display higher torque and power at lower speeds, whereas the HSM and IM motors have the ability to offer sustained power at higher speeds. A property of all electric motors is that they produce the highest torque during the first two seconds of operation and can sustain a relative high level of power for the first 30-seconds. After the vertex point the power and torque properties taper off with motor speed as losses are encountered during continuous operation.

A negative torque is induced during braking. This torque is subject to losses when changing electric polarity of the stator. Losses are more pronounced in motors with high permanent magnet content such as the IPM. The HSM and IM configurations thus have a marked advantage in switching from positive to negative torque and are better suited for continuous electrical driving. As support for the comparison, the Torque and Power curves for the different motor typology are illustrated in Figure 8-6. The speed is normalized with the respect to base speed.

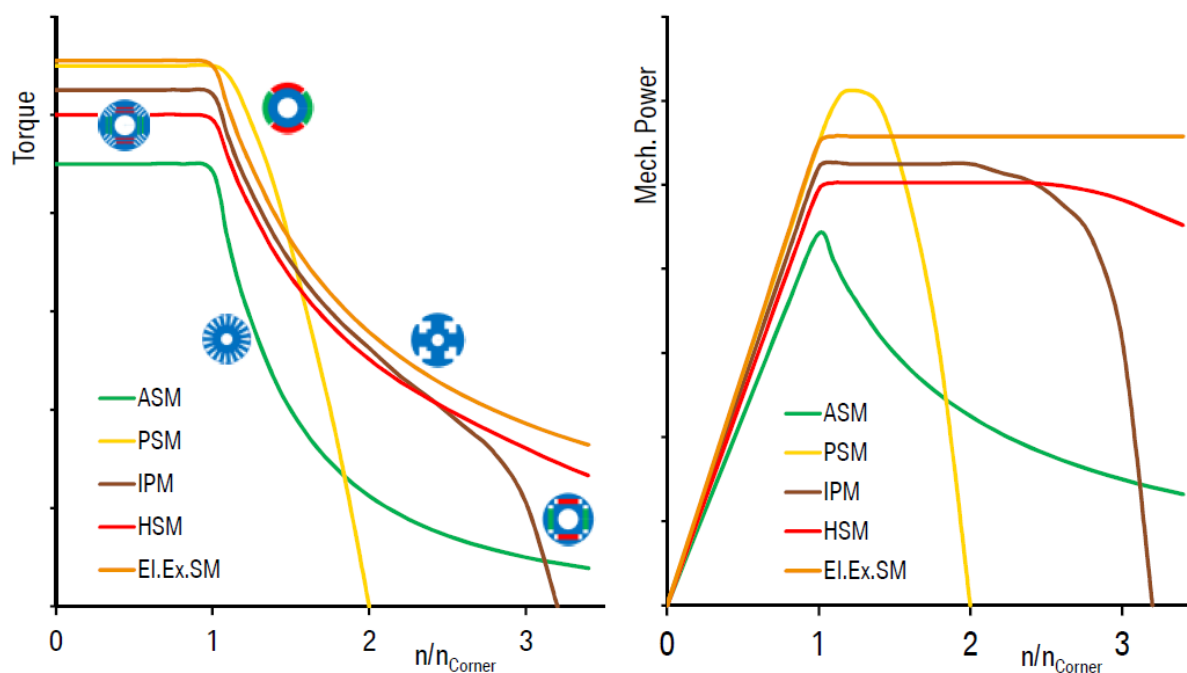


Figure 8-6 Comparison of different machine topologies for limited stator current, adapted from [56]

In Figure 8-7 the exemplary efficiency map of different machine types is depicted. The lines are equipotential lines, that surround the range of an efficiency  $\eta > 85\%$ . The PMSM (IPM) has its best efficiency at low speed whereas the induction machine and the SRM have their best efficiency at higher speeds and over a wider speed range. In this case the PMSM (IPM) would be the best choice. But if most

of the operation points are at higher speeds or over a wide speed range, the IM and SRM should be preferred.

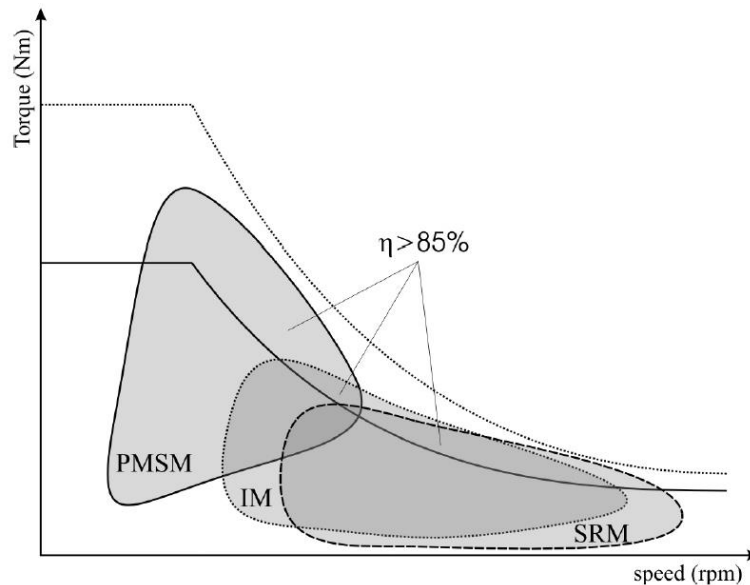


Figure 8-7 Exemplary efficiency maps of different machines with constant power [179]

In the Selection Matrix in Table 8-2 a comparison of the electric motors for vehicle propulsion is presented. For power hybrid systems dimensioned to assist the internal combustion engine, IPM motors offer the best capability in terms of efficiency and low rotor losses at lower speeds. For hybrids that feature sustained electric driving hybrid synchronous motors (HSM) offer better performance characteristics in terms of power to weight and efficiency combining the benefits of IPM and IM configurations.

Table 8-2 Selection Matrix with comparison of the electric motors for vehicle propulsion

E-Motor Specifications		Electric Motor Type vs. Specifications				
Technical Criteria	Weight	Brushed DC Motor	Internal Permanent Magnet	Hybrid Synchronous Motor	Induction	Switched Reluctance
Low Noise	5	3.5	5.0	5.0	5.0	3.0
High Specific Power/Torque	5	2.5	5.0	4.5	3.5	3.5
High Power/Torque Density	5	2.5	5.0	4.5	3.5	3.5
Efficiency	5	2.0	5.0	4.5	4.0	4.5
High Speed Capability	3	2.0	4.0	4.5	5.0	5.0
Low Ripple	2	4.0	5.0	5.0	4.0	2.0
Low Inertia	3	3.0	3.0	4.0	3.0	5.0
Controllability	5	5.0	5.0	5.0	5.0	4.0
Reliability	5	2.5	4.0	5.0	5.0	5.0
Ranking (Effectiveness)	[%]	59.5	92.6	93.7	85.3	79.7
High Cost [1-5]	1	2	5	3.5	3	3
Technology Value	[%/adim]	29.7	18.5	26.8	28.4	26.6

As a rule of thumb, when magnet material is replaced with windings the more complex and costly the electric control system and AC/DC inverter becomes. Asynchronous AC motors (IM) offer ferromagnetic

material savings and good efficiency for very high speed and power applications at the expense of a larger volume, more complex electronics and efficiency reduction for high torque loads.

### 8.2.2 Power Electronics

**Inverter** -The inverter is a device that converts the high voltage DC electrical power from the high voltage battery into AC power used to power the electric motor/generator, see Figure 8-8. This functionality can be reversed during regenerative braking as the inverter rectifies the input current from the generator to charge the DC battery.

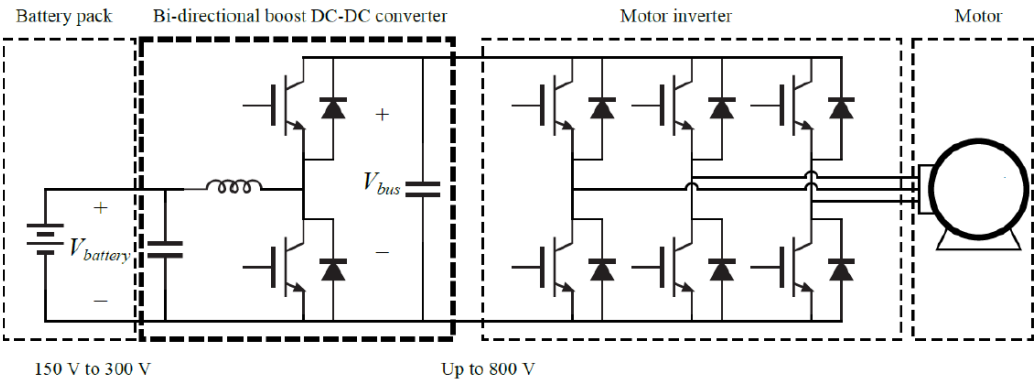


Figure 8-8 Simplified scheme of 3-phase power Inverter with a DC/DC converter between it and the battery

The inverter is typically a 3-phase converter, and it can be used to drive all AC motors and the BLDC motors. The difference among the machine driving is in the control technique adopted. Typically the Inverter includes the logic HW and SW to perform the electric machine control, as the scheme depicted in the following Figure 8-9.

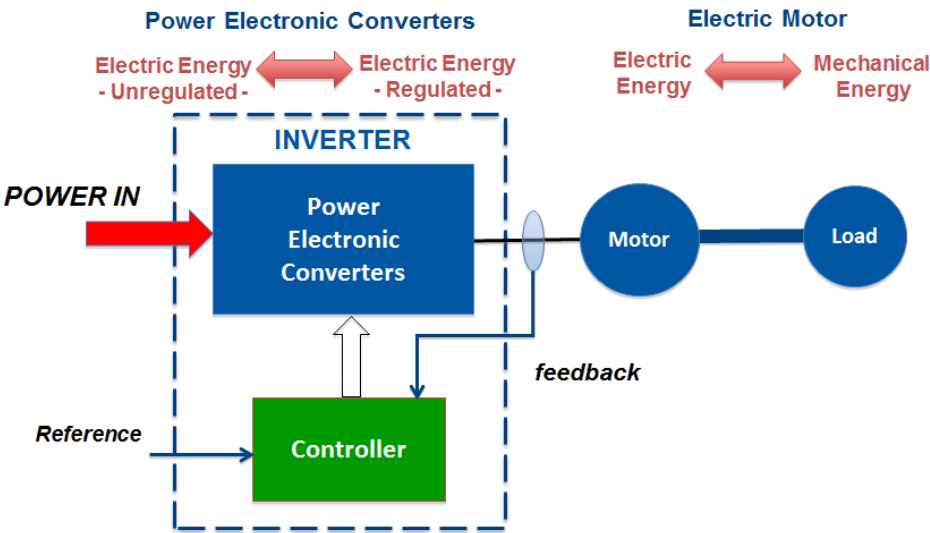


Figure 8-9 Scheme of an Electric Traction Drive controller

Focusing on power electronic components, the power modules inside the inverter use transistors MOSFET or IGBT based on silicon (Si) technology. The first type of transistor is employed for high switching frequency, necessary for high motor speed, up to medium power. For high power application typically the IGBT transistor is used, with limit on switching frequency. New power electronic device based on SiC technology are under development. A new generation of MOSFET is able to operate at high power maintaining its previous advantages, see Table 8-3 adapted from [181], with benefits on efficiency and power density.

Table 8-3 Comparison between SiC MOSFET and Si IGBT

Parameter	Si IGBT	SiC MOSFET
Switching principle	Normally -Off	Normally -Off
Control parameter	Voltage	Voltage
Control power	Low	Low
Control circuit	Simple	Simple
On-resistance	Low	Low
Switching speed	Medium	Fast
Switching loss	Medium	Extremely low
Efficiency at low current	Low	High
Operating junction temperature	Up to 175°C	>200°C

### 8.2.3 High Voltage vs. Low Voltage Electric Traction Drive Systems

From the review of the technical literature on ETD is evident an interesting evolution of the 48V systems. From the first ETD systems characterized by low peak power up to 5kW, obtained as an evolution of classic alternator technology, the 48V electric drives have become even more power, achieving peak power up to 35 kW. With this evolution P2 and P4 architectures have been object of concept and demonstrator with the aim to implement not only mild hybrid vehicle but also full hybrid and plug-in vehicles. A detailed analysis on this potentiality will be presented in the next Chapter #12.1.

In Table 8-4 the High Voltage and Low Voltage electric traction drive systems are compared, indicating the typical parameter values in technical literature. The comparison of HV and LV Electric Traction Drive systems has to take into account the main key technical parameters of HoQ3.2, presented in the previous paragraph #8.1. The state of arte of electric traction drive shows that 48V ETD systems are comparable with HV in term Specific Power/Torque and Efficiency.

**Cost Target** - Cost is a dominant factor to select the proper ETD system. Hybrid and electric vehicles should cost no more than comparable ICE vehicles. The cost targets allow for a small price premium, but the cost difference should be no greater than that which could be recovered from the fuel savings in 3 years [229].

The 48V ETD systems are favored to achieve the target cost, because they have less safety devices requested by the standards. Furthermore the lower electric complexity of LV systems is an advantage for ETD system integration in vehicle too. In [58] a comparison of HV and LV system costs are reported, see Figure 8-10.

Table 8-4 Comparison of High Voltage and Low Voltage (48V) Electric Traction Drive Systems

Key Parameters (HoQ3.2)	High Voltage (> 350 V)	Low Voltage (48 V)
Peak/Continuous Mechanical Output Power/Gen. [kW]	110(9795) [55] 125/75 [56]	25/na [57] 14.7/na [114] 30/20 [58] na/20 [59] 25/na [60]
Peak/Continuous Mechanical Output Torque [Nm]	320(3283)/na [55] 250/na [56]	50/na [114] 110/80 [57] 20/na [60]
Rated Speed [rpm]	9795 [55] 11400 [56]	16 000 [114] 16 500 [57] 50 000 [60]
Specific Power/Torque [kW/kg]	2.5/5 [56]	3.2/4 [60]
Efficiency @ Maximum Continuous Power		96÷97 % [57]
Efficiency @ Maximum Peak Power Levels	97 [56]	90÷94% [57]
Machine Type	PM [55] PM-HSM [56]	PM [57] IM [114] PM [58] PM [59] PM [60]
Cooling Options	water cooled [55] water cooled [56]	water cooled [57] water cooled [60] water cooled [114]
Integration	Demanding safety requirements	Low safety requirements

It can be noted that the price of LV systems is convenient compared with HV ones up to 60 kW. Further advantages in terms of costs can be obtained if we consider the aforementioned synergy with introduction of 48V power net.

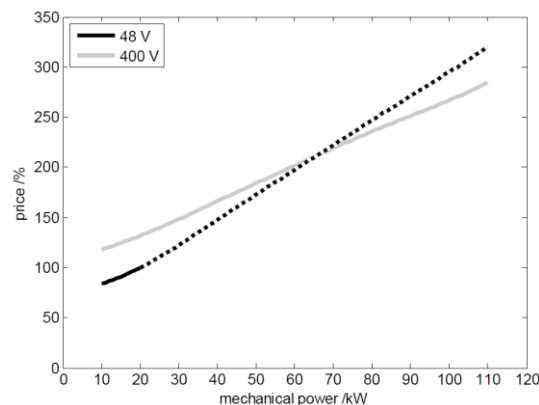


Figure 8-10- Comparison of the cost relative by system power and supply voltage [58]

## 8.3 Electric Energy Storage Devices

Energy storage devices used in hybrid electric cars include the fuel tank for the internal combustion engine, the high voltage batteries (>12V) and super capacitors for the electrical system. The focus in this section lies on the electrical system storage devices, for which Lithium Ion and super capacitors will be discussed as the leading storage devices being developed for use in hybrid electric vehicles. An overview on new battery technologies is presented too.

Perhaps the biggest hurdle for electric mobility is the fact that battery systems today offer so little volumetric energy density and specific energy. Table 8-5 shows how transportation liquid fuels are more than an order of magnitude higher in energy density over leading battery systems.

Table 8-5 Energy content for various energy sources by mass and volume [86,182,183]

Energy Source	Energy Density [Wh/l]	Specific Energy [Wh/kg]
Diesel Fuel	10 700	12 700
Heating Oil	10 400	12 800
Gasoline	9 700	12 200
Butane	7 800	13 600
LNG (-160 °C)	7 216	12 100
Propane	6 600	13 900
Ethanol	6 100	7 850
Methanol	4 600	6 400
250 Bar Natural Gas	3 100	12 100
Liquid Hydrogen	2 600	39 000
Hydrogen (compressed at 700 bar)	2550	39 000
150 Bar Natural Gas	405	39 000
NiMH Battery	280	100
Li-Ion Battery	200	150
Lead-Acid Battery	40	25
STP Propane	26	13 900
STP Natural Gas	11	12 100
STP Hydrogen	3	39 000

**Electric Traction Batteries** – The electric battery for traction transforms electrical energy into chemical energy functioning as an energy storage device during load level increase and regenerative braking. For plug-in hybrid and electric vehicles the battery serves as an energy reservoir for electric energy supplied from an electric power source outside the vehicle.

Energy stored in the electric battery can be readily used for powering the electrical onboard networks, as presents in Chapter #7.1, and to fulfill electric only driving or boosting by means of the electric motor converting electrical energy into mechanical energy. The battery pack itself is composed of battery modules of battery cells, see Figure 8-11. The various battery types differentiate themselves by battery chemistry of the anode and cathode, battery shape (cylindrical, prismatic, pouch or button), quantity of modules and number of cells.

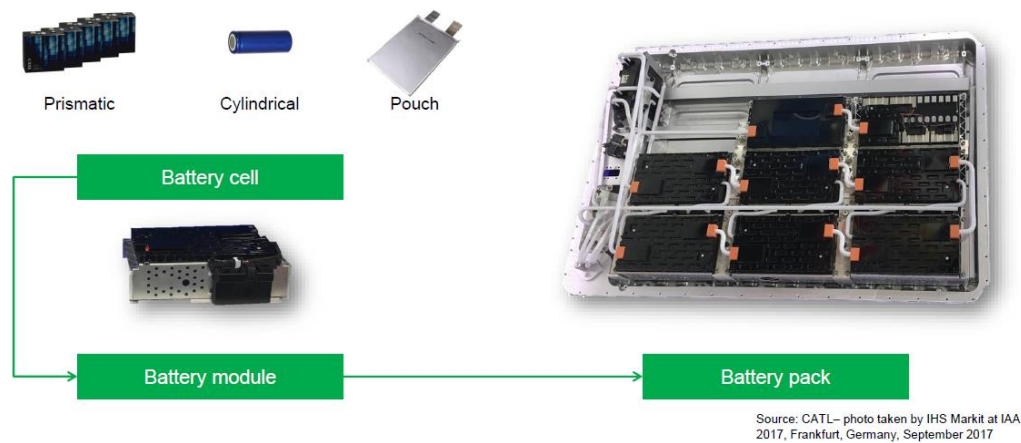


Figure 8-11 Battery pack breakdown [184]

Batteries are normally compared by specific power (W/kg) and specific energy content (Wh/kg). Figure 8-12 shows the tradeoff between specific power versus specific energy of commercially available battery types according to [184]. Specific power is plotted in the vertical axis on a logarithmic scale. Specific energy is represented on the x-axis for a specified discharge rate say C/1 (full discharge in one hour). The light gray bands represent the power and energy capabilities of Lead-acid, Nickel-cadmium, ZEBRA (Na/NiCl<sub>2</sub>) and Lithium – polymer chemistries. Highlighted in green is the super capacitor band, in blue the nickel metal hydrate band and in red the variety of Lithium-ion chemistries.

The appropriate cell chemistry for a particular hybrid car is dependent on the power and energy requirements of the electric propulsion system. Super capacitors offer high power discharge but very limited specific energy, whereas Lithium-ion batteries offer the broadest range of specific energy and power packaging.

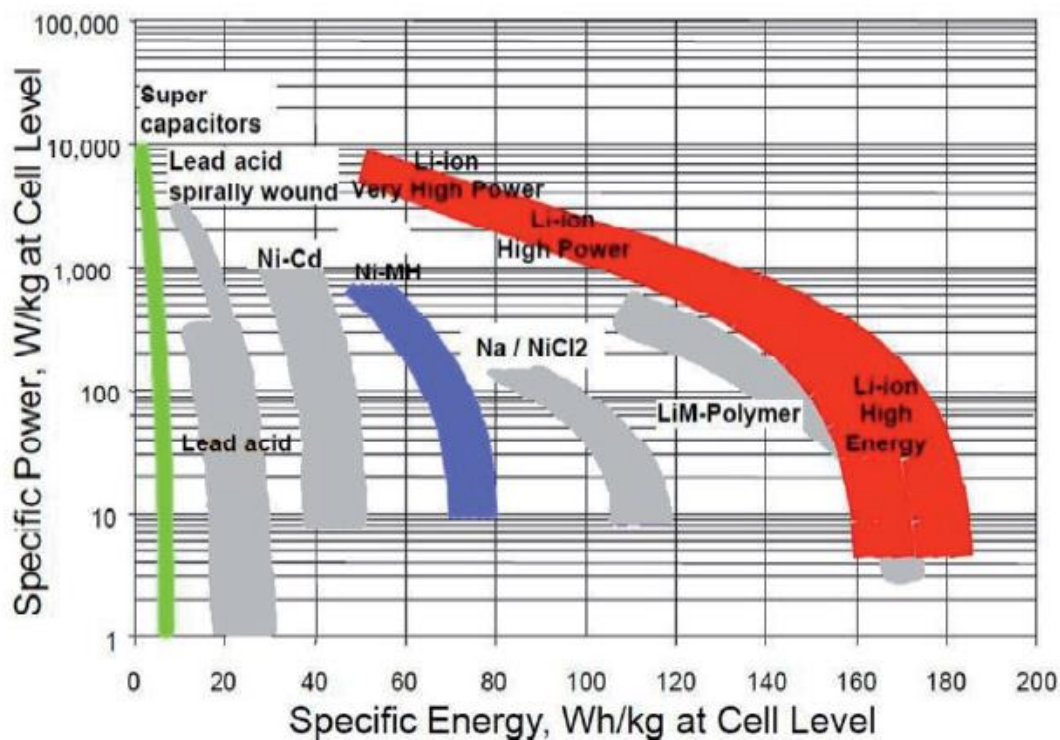


Figure 8-12 Specific Power vs. Specific Energy for various cell types from [185]



At the moment, Lithium-ion batteries represent the most widely used battery type for commercial applications of hybrid vehicles for their proven performance and safety improvement. Automakers will continue using Li-ion batteries in electric vehicles (EVs) for at least a decade as alternative technologies are still in the development phase.

**Lithium-ion Battery** – Lithium-ion technologies display the greatest flexibility in selecting the optimal power to energy placement for the wide spectrum of hybrid electric vehicle applications from micro hybrids to plug-in hybrids and electric vehicles. Lithium is the lightest of metals and has the greatest electrochemical potential which makes it one of the most reactive of metals. It is for this reason that the typical cathode material does not use free lithium but rather a lithium compound. The anode material is typically made from graphite or silicon/carbon composites.

Finally, the electrolyte is usually based on a Lithium salt in an organic solvent or a gel polymer with a porous separator. New batteries based on solid-state electrolytes are under study and development [322,323,324], with the aim of improving costs, safety and energy density (up to 2.5x compared with current battery based on liquid electrolyte). Table 8-6 applies for a Lithium-Cobalt oxide battery commonly used for laptop battery applications and consumer electronic products. Lithium-ion batteries containing cobalt are expensive for the high material cost of this metal.

Table 8-6 Chemical Reaction for a Lithium-Cobalt Oxide Battery (for  $0 < x < 1$ )

	Charge	↔	Discharge
Positive Electrode	$Li_{(1-x)}CoO_2 + x Li^+ + x e^-$	↔	$Li_xCoO_2$
Negative Electrode	$Li_xC_6$	↔	$C_6 + x Li^+ + x e^-$
Cell Reaction	$Li_{(1-x)}CoO_2 + Li_xC_6$	↔	$Li_xCoO_2 + C_6$

The selection of cathode and anode material chemistries results in a tradeoff between voltage potential (V) and specific cell capacity (Ah/kg) as shown in Figure 8-13. Power cells use carbon or graphite based anodes along with high voltage cathodes, whereas energy cell configurations tend to use silicon-carbon composites. The voltage potential for Lithium-ion battery cells lies between 1.25V - 4.2V. For use in automotive applications Lithium-Manganese oxide ( $LiMn_2O_4$ ) and Lithium-Iron-Phosphate ( $LiFePO_4$ ) are particularly interesting for their lower cost potential due to the use of less expensive metals. The latter is particularly favorable for its light weight, low cost and ability to eliminate explosive reactions during crash testing. Alternatively, NMC batteries are used for the high specific energy.

Safety is perhaps the most important consideration for automotive considerations as lithium-ion cells can experience uncontrolled reactions during overcharging that can lead to cell damage and short circuit battery discharge burn out.

The following Table 8-7, adapted from [183], summarizes and compares the proprieties of current Li-ion different types of families.



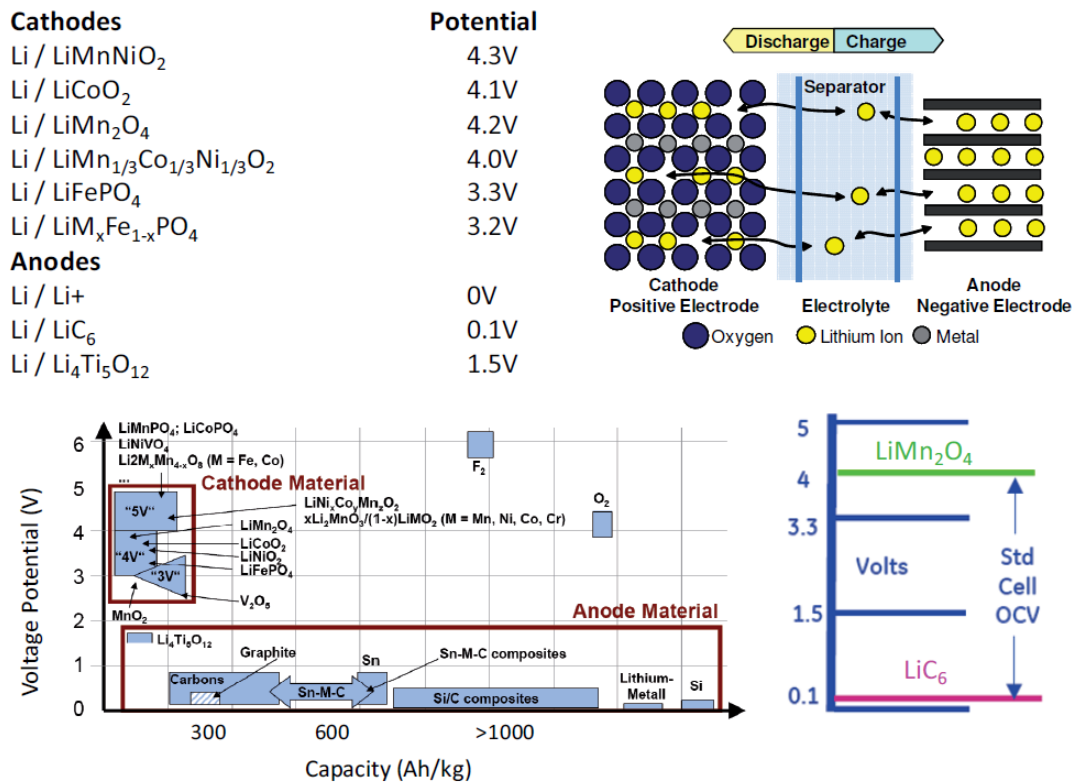


Figure 8-13 Common chemistries of Lithium-ion battery electrodes and their open circuit voltage(top left); bottom tradeoff between voltage potential and capacity (bottom left); schematic of Lithium-ion battery structure (top right); example of standard cell open current voltage (OCV) potential (bottom right), from [134]

Table 8-7 Properties and comparison of Li-ion batteries (0 means average performance, + advantage, - disadvantage)

Type	LCO	LNO	NCA	NMC	LMO	LFP	LTO
Items	Lithium Cobalt Oxide	Lithium Nickel Oxide	Lithium Nickel Cobalt Aluminum Oxide	Lithium Nickel Manganese Cobalt Oxide	Lithium Manganese Spinel	Lithium Iron Phosphate	Lithium Titanate
<b>Cathode</b>	LiCoO <sub>2</sub>	LiNiO <sub>2</sub>	Li(Ni <sub>0.85</sub> Co <sub>0.1</sub> Al <sub>0.05</sub> )O <sub>2</sub>	Li(Ni <sub>0.33</sub> Mn <sub>0.33</sub> Co <sub>0.33</sub> )O <sub>2</sub>	LiMn <sub>2</sub> O <sub>4</sub>	LiFePO <sub>4</sub>	LMO, NCA,
<b>Anode</b>	Graphite	Graphite	Graphite	Graphite	Graphite	Graphite	Li <sub>4</sub> Ti <sub>5</sub> O <sub>12</sub>
<b>Cell Voltage</b>	3.7V – 3.9V	3.6V	3.65V	3.8-4.0V	4.0V	3.3V	2.3-2.5V
<b>Energy Density</b>	150mAh/g	150Wh/kg	130Wh/kg	170Wh/kg	120Wh/kg	130Wh/kg	85Wh/kg
<b>Power</b>	+	0	+	0	+	+	++
<b>Safety</b>	-	0	0	0	+	++	++
<b>Lifetime</b>	-	0	+	0	0	+	+++
<b>Cost</b>	--	+	0	0	+	+	0

The main issue of the Li-ion batteries is the availability of the raw material used. The Figure 8-14 shows the mass of raw materials used in Li-ion battery of BEV and PHEV. Due to deposits concentration in limited areas of the world and taking into account the market increasing of electric propulsion systems, cost rising of battery materials is waited.

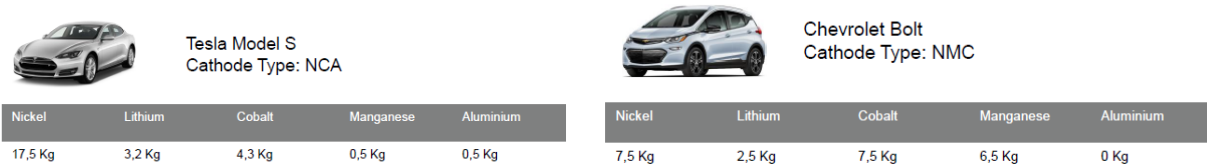


Figure 8-14 Mass of raw material used in Li-ion battery of two electrified vehicle from [184]

Taking into account the future requirements of electrified vehicles, substantial developments are shaping up to decrease energy consumption and weight while increasing range for all types of vehicles.

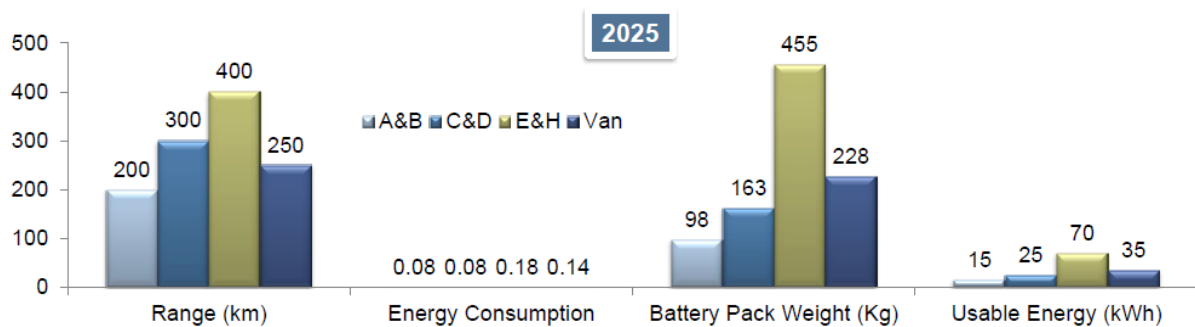


Figure 8-15 New battery requirements at 2025 [184]

The material availability and costs and the requirements of higher density and specific energy are pushing the research towards batteries based on alternative technologies.

## Future Battery Chemistry

Advanced Li-ion technologies [322,323,324], Li-air, Li-S, and Zn-air batteries are expected to be the most promising alternatives to the existing batteries in terms of energy density, safety, cost, and life cycle.

Figure 8-16 from [183] summarizes the working principle of new batteries in research phase, whereas Figure 8-17 shows the comparison of specific energy and volumetric energy in comparison with the current Li-ion battery.

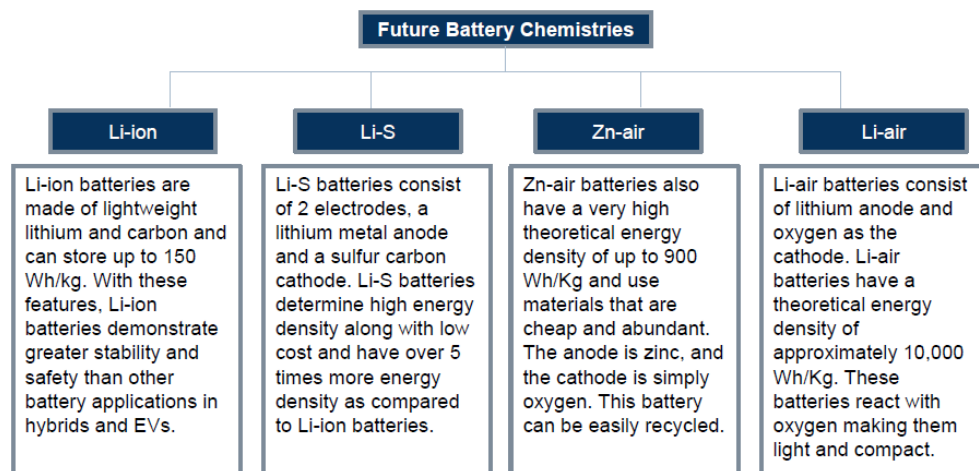


Figure 8-16- Future battery chemistry

As all the technology developers are focusing on developing a battery that should be lighter and smaller with high energy density.

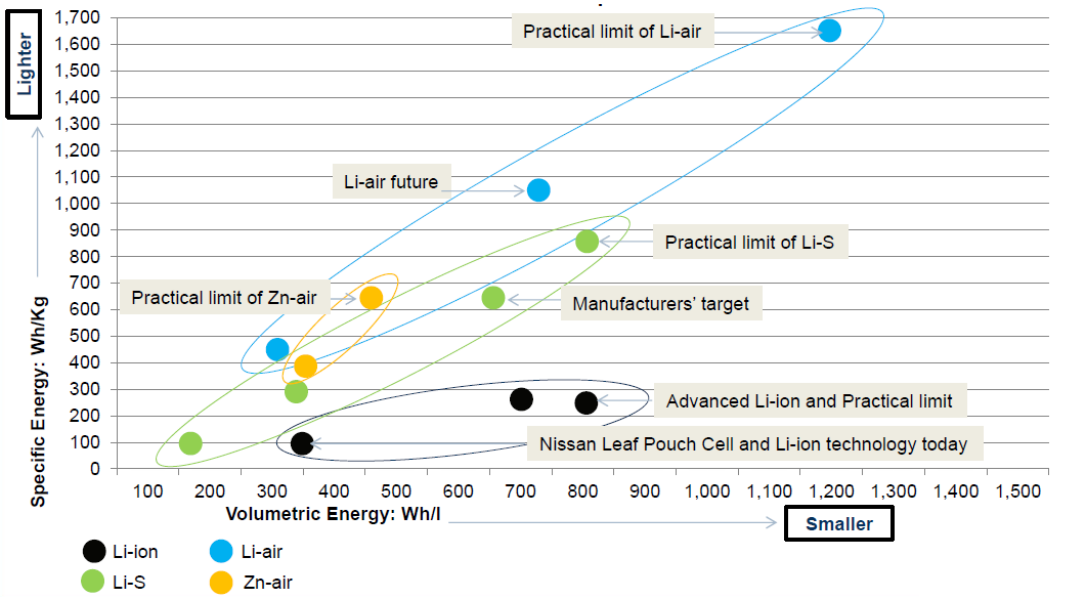


Figure 8-17 Specific Energy and Energy Density of new batteries in comparison with current Li-ion [183]

The summary of the comparative analysis between the current Li-ion battery based on liquid electrolyte and new emerging technologies is illustrated in the next Table 8-8 and in Figure 8-18. All battery types, including Li-ion, are facing safety concerns, which have become the prime challenge.

Table 8-8 Comparative analysis of new batteries in comparison with current Li-ion, adapted from [183, 322]

Comparative Analysis	Specific Energy [Wh/kg]	Challenges	R&D Needs
Li-ion	110÷280	<ul style="list-style-type: none"> <li>- Cold cranking</li> <li>- Specific energy density for high voltage automotive cell</li> <li>- Charge acceptance at lower temperatures</li> </ul>	Development required for anode, cathode and electrolyte for high voltage and low temperature performance
Li-air	500÷600	<ul style="list-style-type: none"> <li>- Charging efficiency</li> <li>- High impedance during discharge</li> <li>- System integration similar to fuel cell</li> <li>- Ageing effects by electrolyte loss</li> </ul>	<ul style="list-style-type: none"> <li>- Necessity to resolve the efficiency losses and life-anode</li> <li>- Protection passivation from lithium hydrolysis</li> </ul>
Li-S	400	<ul style="list-style-type: none"> <li>- High self discharge</li> <li>- Charging efficiency via polysulfide solubility</li> <li>- High charge and discharge power</li> <li>- High cycle life at high power rates</li> </ul>	<ul style="list-style-type: none"> <li>- Improvement of power density-cathode and electrolyte improvements</li> <li>- Improvement of cycle life-anode, cathode, and electrolyte</li> </ul>
Zn-air	380	<ul style="list-style-type: none"> <li>- Lifetime</li> <li>- Power density limited by cathode</li> <li>- Low voltage</li> </ul>	<ul style="list-style-type: none"> <li>- Stable anion electrolytes</li> <li>- High efficiency air cathode</li> <li>- Dimensionally stable zinc electrodes</li> </ul>

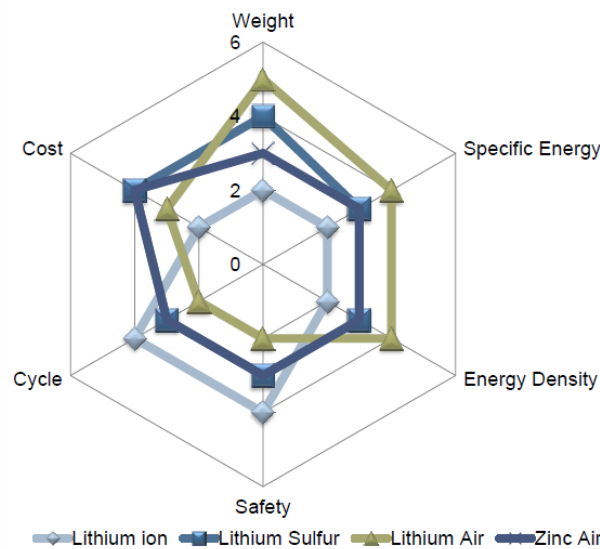


Figure 8-18- Comparative radar chart of new batteries in comparison with current Li-ion [183,322]

Li-ion technology is the most promising solution for BEVs, due to the characteristics mentioned in the radar chart and the future improvements expected with solid-state electrolytes [322,323,324], that reduce the gaps with other technologies in terms of specific energy and costs. However, Li-S batteries are expected to be the safest alternative technology and they are far more promising than Li-ion in the long term in terms of specific energy and density. Li-air batteries have the highest energy density across all chemistries, but practicality and adoption are factors still far in the future.

Zn-air batteries have been suitable for consumer applications, and they are being developed for implementation in EVs. Zn-air technology is likely to be the most cost-effective solution due to the wide availability of materials.

Summarizing, Li-S and Zn-air are likely to be adopted as future battery types in the next 5÷10 years, but Li-ion batteries will equally compete in the long run due to technological maturity and advancements of the chemistry.

**Super Capacitors and dual storage systems** – Double layer capacitors, super capacitors or ultra-capacitors have been long considered as an ideal storage medium for micro and mild hybrid systems that only use energy for acceleration boosting, regenerative braking and the engine start-stop function. These storage systems offer high specific power for short periods of time (i.e. 3÷10 seconds). Capacitors have the benefits of better temperature operating ranges over batteries, and lower costs to manufacture [182]. The cell voltage of a capacitor is determined by the circuit application, and is not limited by the cell chemistry as with batteries. Very high cell voltages are possible; however, there is a trade-off with capacity.

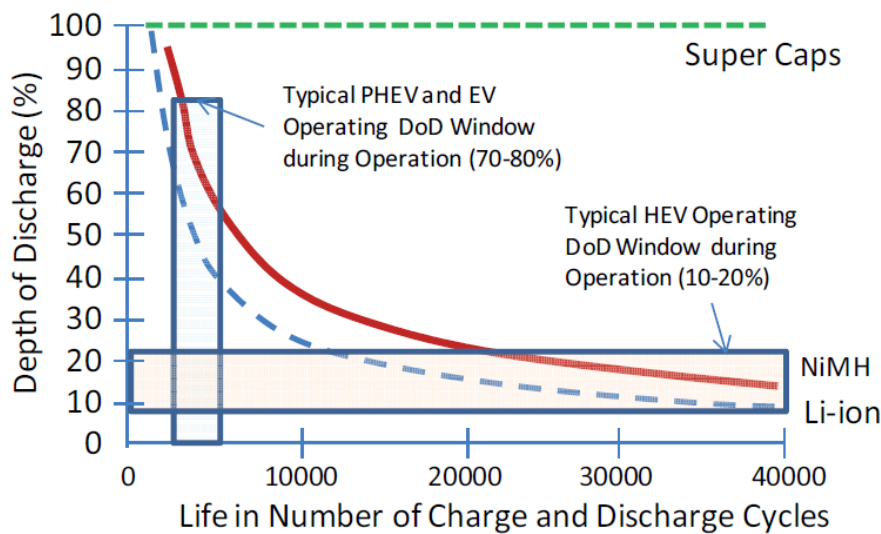


Figure 8-19 Battery Cycle Life comparison [134]

In comparing battery lifecycle between the three electric energy storage concepts, the advantages of the super capacitors stand out. Figure 8-19 displays the tradeoff between battery depth of discharge allowed by the control system and battery life measured in number of cycles. In order to increase the life of NiMH and Li-ion batteries, auto manufacturers limit the allowable depth of discharge window. For high power applications such as in HEVs the typical discharge window is limited to 20% allowing for a considerable life extension of the high voltage battery. In contrast in high energy applications such as with PHEVs and EVs, the depth of discharge window is set at 70÷80% to fulfill the all-electric range of the vehicle at the expense of battery life.

Super capacitors can be combined with a primary battery system to provide an effective short duration peak power boost allowing the prime battery to be downsized. However, since the capacitor is normally connected in parallel with the battery in these applications, it can only be charged up to the battery upper voltage level and it can only be discharged down to the battery lower discharge level, leaving considerable unusable charge in the capacitor, thus limiting its effective or useful energy storage capacity and adding weight and bulk of the system,

Disadvantages of super capacitors are in the low energy density and rapid self-discharge. During discharge capacitors tend to have a linear voltage drop that can pose a challenge in using all available energy. These shortcomings render super capacitors unsuitable as primary power source for EV and HEV applications.

## 9. Fuel Evolution: the Synthetic Fuels

One of the pathways to move the powertrain of light duty vehicles towards the zero GHG emissions is the adoption of de-fossilized fuels, see Figure 9-1.

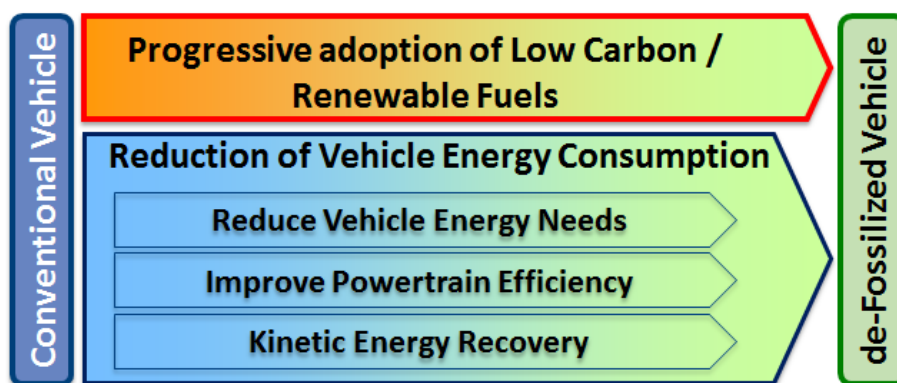


Figure 9-1 Pathways towards a de-fossilization of the powertrain: focus on de-fossilized fuels

The fuel analysis has to consider the complete fuel pathways from the production to the use, according to WTW approach. Figure 9-2 presents how the energy is transformed from primary sources to a variety of energy carriers (fuels) to be used in the different powertrains to move the vehicle.

### Primary Energy Sources

At the moment, fossil fuels are used as the main input source of energy for making all other energy carriers, whereas renewable energy and nuclear sources are used mainly in the production of electricity.

The biomass alternative has been effective in countries that have the land and resources available. Methanol, ethanol and biodiesel blends are created from biomass for standalone utilization or to mix with gasoline or diesel fuels. Biomass can also be used to produce Compressed Natural Gas (CNG), Liquefied Petrol Gas (LPG) or hydrogen. Countries like Brazil have been successful in developing a biomass infrastructure used to support an alternative vehicle auto industry.

In last years the renewable electric power generation has been object of technological improvements, allowing short returns on investments. For this reason, in many countries the installation rate of power plant based on sun and wind generation has overcome the conventional plants.

The main issue of this kind of technologies is the discontinuity of power generation and the lack of infrastructure to distribute the energy from big power plant to users.

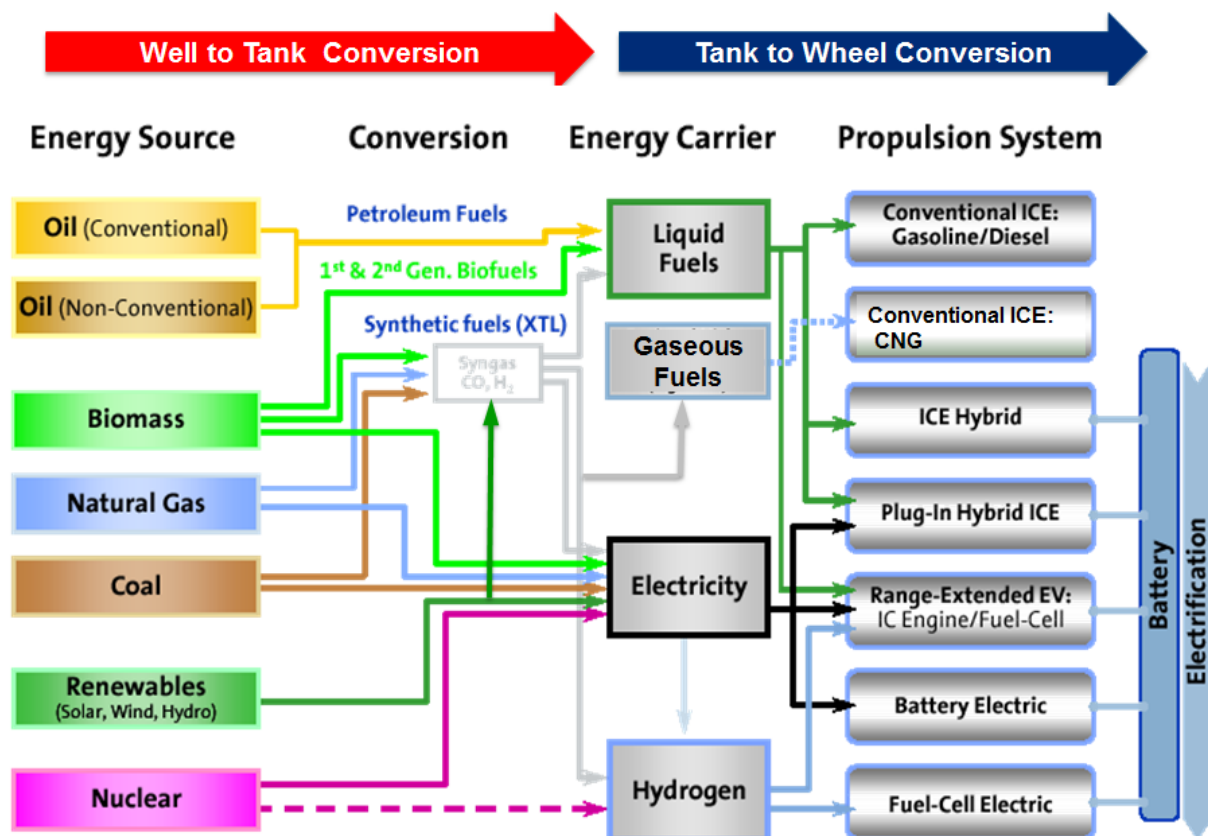


Figure 9-2 Energy to vehicle powertrains pathways

## Energy Carriers

Years of research and development have gone into developing “cleaner fuels” and experimenting with developing varying stoichiometric mixtures of hydrocarbons [86]. In addition to the gasoline and diesel fuels derived from crude oil widely available around the world, liquid fuel compositions of similar content can be developed using Biomass-to-Liquid and Power-to-Liquids chemical processes.

Among gaseous fuel Compressed Natural Gas (CNG) needs particular attention, because its use in ICE allows a significant reduction of CO<sub>2</sub>. Finally Hydrogen and electricity are alternative energy carriers that can be produced with several methods and with different impacts in terms of GHG.

**Biofuels** - They are blends of gasoline or diesel with alcohol-based liquid fuels produced from biomass. Examples of ethanol biofuels are designated by the letter “E” along with the percent of ethanol blended in. For instance, E85 is a blend of 85% ethanol and 15% conventional gasoline. A known problem with biofuels is the competition for use of farm lands for fuel versus food production. New methods of producing “advanced” biofuels are being researched that decouple their production from that of food. Two such methods are the conversion of lignocellulosic material to fuel components via the use of enzymes and biomass gasification followed by a Fischer-Tropsch process, also known as Biomass-to-Liquid (BTL) [186, 187]. The latter process can use a range of biomass feedstocks from agricultural or municipal waste. Successful scaling of these processes can reduce the price of biomass-sourced fuels to the levels of common gasoline and diesel fuel [188].

**CNG** – This kind of fuel is methane stored at high pressure, typically 20-25 MPa, and it can be easily used in the current engines and it can lead to a reduction of CO<sub>2</sub> emission, due to low content of carbon inside it

molecule. To facilitate the transport and the storage, the methane can be liquefied lowering the temperature below  $-162^{\circ}\text{C}$ , obtaining the so called Liquefied Natural Gas (LNG). This kind of fuels is object of interest for long distance transport (shipping and trucks), as volumetric energy density is approximately 2.5÷3 times that of CNG. The CNG can be produced also with synthetic processes from Biomass or from electricity with the so named Power-to-Gas processes. The last ones are similar to Power-to-Liquid processes presented in the following sections.

The lower efficiency of the engine and the higher impact of  $\text{CH}_4$  slip as GHG (25 times higher than  $\text{CO}_2$ ), reducing strongly the advantages. A recent study [259] highlights that emissions due to leakage in the supply chain can be relevant. For this reason CNG/LNG well-to-wheel impacts are comparable with diesel cars [258]. Furthermore investment in adequate delivery infrastructure is the biggest barrier to mainstream adoption for the methane fuel.

**LPG** - it is expected to generate enough demand to attract a viable infrastructure. LPG is comparable to gasoline with the added benefit of producing lower conventional pollutants. LPG is expected to remain a niche product within major markets as use is limited but still growing and fueling points are relatively inexpensive to install.

**Hydrogen** –This energy carrier has the benefit of offering zero tail pipe emissions. However, currently the production of hydrogen is mainly based on steam methane reforming of natural gas, resulting in higher emissions than most other fuels when the entire production and delivery  $\text{CO}_2$  emissions are considered [230,231]. An alternative Hydrogen production method is from electrolysis. The energy required in separating hydrogen and oxygen in water molecules is larger than the amount of energy released in burning the produced hydrogen fuel. Electrolysis is also not a carbon neutral process and depends on the primary energy sources used in generating the electricity used. However, when hydrogen is produced with electricity stemming from nuclear or renewable energy sources the fuel takes on close to no  $\text{CO}_2$  footprint.

Perhaps the most difficult problem of hydrogen fuel is the inability to contain the fuel for large periods of time. The hydrogen molecule is small enough to find its way out of a solid fuel container after several weeks. Technology advances in hydrogen production, distribution and storage will be necessary for successful broad commercialization.

**Electricity**- It is as an energy carrier has the advantage of having multiple sources of production from primary sources. Electricity enjoys the advantage of having a well-established distribution infrastructure in most developed countries. Due to its wide availability and flexibility, it can directly compete with widely available fuel carriers such as gasoline and diesel for transportation purposes. The greatest limitations for electricity using for personal transportation is the lack of infrastructure of charging.

**e-Fuels** - Promising carbon free energy carriers, alternative to hydrogen and electricity, are the synthetic fuels named “e-Fuels” or “Power-to-Liquid” fuels. They use as primary energy source renewable energy (from power and wind, etc.), that is transformed by means of  $\text{CO}_2$  and Water in liquid fuels, like gasoline, naphtha and etc. Another key advantage of e-Fuels is the use as valid mean to store and distribute renewable electricity, employing existent infrastructure.

Vehicle technologies are commercially available for most of the fuels, with some limitation for hydrogen fuel cells. The commercial infrastructure for transportation is available only for the leading liquid fuels. Hydrogen is the only fuel with safety limitations as its highly reactive small molecule size is hard to contain. For refueling time and storage capability, liquid fuels are most practical with gaseous fuels and batteries showing considerable limitations. The energy used to produce each fuel and the “Well to Tank” emissions are based on a joint industry study for Europe [230]. In these last two categories the assessment particularly on electricity and hydrogen depend on whether the fuel is produced using renewable energy; the better assessments assume the use of renewable energy. Table 9-1 provides a comparison summary of the energy carriers based on the thesis author’s assessment.



Table 9-1 Energy carrier comparisons, based on research findings presented in this section (0 means average performance, + advantage, - disadvantage)

Energy Carriers	Vehicle technology Availability	Commercial Infrastructure	Safety	Refueling Time	Storage Capability	Energy Requirements to Produce	GHG Well to Tank Emissions
Gasoline	+	+	0	+	+	+	-
Diesel	+	+	0	+	+	+	-
FT Gasoline	+	--	0	+	+	--	--
FT Diesel	+	--	0	+	+	--	--
BioDiesel	+	-	0	+	+	-/0	0
Methanol	0	0	0	+	+	-	--/+
Ethanol	+	0	0	+	+	-	0
DME	0	--	0	0	-	-	--/-
CNG	+	--	0	0	-	+	--
LPG	+	0	0	+	-	+	-
Hydrogen	-	--	--	-	--	-	--/+
Electricity	+	+	0	--	-	-/0	--/'++
e-Fuels	+	--	0	+	+	-	--/+

## 9.1 Fuel Prioritization in transport sector: the e-Fuels

Different energy carriers for transportation require different primary energy consumption and have diverse technology requirements for their implementation. Fuels have been prioritized according to the above characteristics. Direct electrification is the most energy efficient form of transport and is the main priority in all scenarios. Electrification can provide energy security, as it can be generated by a wide variety of means. Unfortunately, many transport subsectors are not suitable for electrification and will continue to rely on liquid fuels as a result of limited energy storage, power and weight issues: for example in long distance transportation such as trucks, aviation and maritime transport [4]. The powertrain electrification for personal transportation is also critical for the lack of charging infrastructures.

Apart from electrification, the only other proposed solution for achieving a 100% renewable transport sector has, so far, been the use of biofuels. However, there are a number of concerns relating to biofuel production in 100% renewable energy systems, such as the availability of adequate land. Even though this problem is well reported [4], many biofuel technologies are well established on the market, primarily because they can be used directly or with slight modifications in the existing combustion engines that are available on the market today. Many biofuels are subsidized to encourage a 10% penetration in the transport sector by 2020, in line with European Union targets, blending the conventional fossil fuels. All EU members have either quota obligations and/or tax exemptions for implementing biofuels. There are some concerns about the extent to which biofuels really influence emission reductions.

The conversion of electricity into liquid fuels via electrolysis could be beneficial in the future transport sector because output gas can be catalyzed into various types of fuels. Synthetic fuels based on renewable energy, so called e-Fuels, will be an important pillar for future fuel supply. Transportable and easy to store chemical energy carriers are beneficial to solve the target triangle of energy policy: environmental impact, economic viability and security of energy supply.

Synthetic fuels overcome land-use problems, have no interference with the food supply, and provide solution for supply related issues of conventional fuels and biofuels. Methanol and DME are chosen as the

most promising types of fuels, primarily due to the well-known chemical synthesis for producing these kinds of fuels and since they can be used in existing internal combustion engines with relatively few modifications. Where possible, the produced fuel from syngas is assumed to be the methanol, because it is the simplest and lightest alcohol. It is also possible to use methanol as a petrol substitute in Otto engines due to its high octane rating, and methanol cars are a well-known technology. For example, methanol flexible fuel vehicles were available in the United States from the mid-1980s to the late 1990s. Today, China is the leader in using methanol for transportation with five different methanol gasoline mixtures available on the market e M5, M10, M15, M85 and M100.

Moreover, methanol is a platform chemical used to produce a range of other chemicals and fuels so it is a flexible solution, see the next paragraph.

DME can be used as an alternative to conventional diesel, and it is often characterized as one of the most promising alternative automotive fuel solutions due to the more efficient diesel engines. The first DME fueled heavy vehicle was developed by Volvo as a part of the development plan in the period from 1996 to 1998. The conversion losses during dehydration of methanol to DME are gained due to the higher efficiencies of diesel engines compared to petrol engines. Therefore, the results for methanol and DME are similar and no distinction was made. It was assumed that methanol/DME could be used directly in all modes of transport except aviation.

Methane is often considered as the easiest fuel to produce with synthetic processes, but the application of methane is too expensive since the existing transport fuel infrastructure is designed for liquid fuels.

## 9.2 Production cycle of synthetic fuels: Power-to-Liquids

The production cycle of synthetic fuels is named as Power-to-Liquids (PtL): electric energy, water and CO<sub>2</sub> resources are converted in liquid hydrocarbons, as described in principle scheme of Figure 9-3 from [4]. PtL production comprises three main steps:

1. Hydrogen production from renewable electricity using the electrolysis of water.
2. Provision of renewable CO<sub>2</sub> and conversion.
3. Synthesis to liquid hydrocarbons with subsequent upgrading/conversion to refined fuels.

PtL production results in a mix of gasoline, kerosene, diesel, and other fuel products.

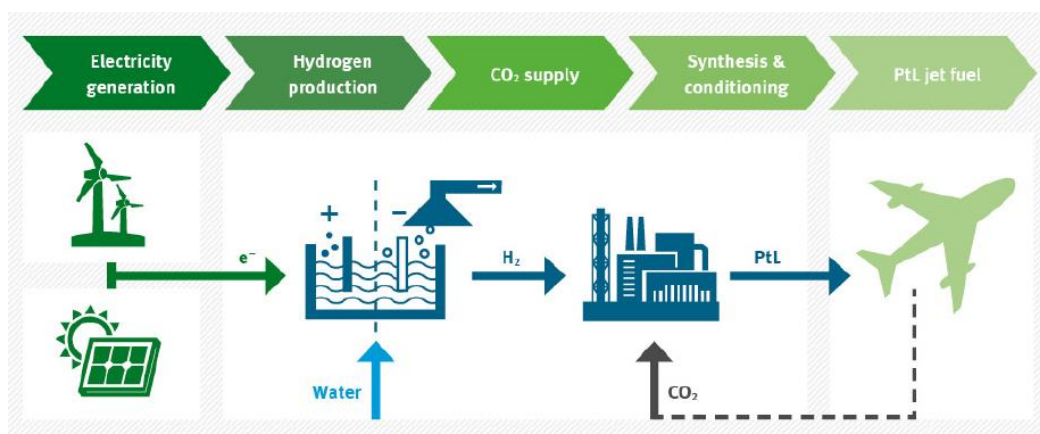


Figure 9-3 Power-to-Liquids production, principle scheme from [4]

There are two principle pathways to produce the renewable PtL e-Fuels:

- Fischer-Tropsch (FT) synthesis and upgrading.
- Methanol (MeOH) synthesis and conversion.

### Fischer-Tropsch pathway

The Fischer-Tropsch process to synthetic fuel is commonly used in biomass-to-liquid (BtL), gas-to-liquid (GtL) and coal-to-liquid (CtL) processes. Instead of biomass, natural gas, and coal, respectively, hydrogen from water electrolysis is used (Figure 9-4).

The Fischer-Tropsch synthesis requires carbon monoxide. In synthesis pathways like BtL and CtL, this is provided from the gasification of biomass and coal respectively. In the FT for PtL case, CO<sub>2</sub> from concentrated sources or extracted from the air is used. The CO<sub>2</sub> is converted to CO via an inverse CO-shift reaction using the reverse water gas shift process. The electricity demand for high-temperature steam electrolysis using a Solid Oxide Electrolysis Cell (SOEC) is significantly lower compared to the electricity demand for low-temperature electrolysis of water.

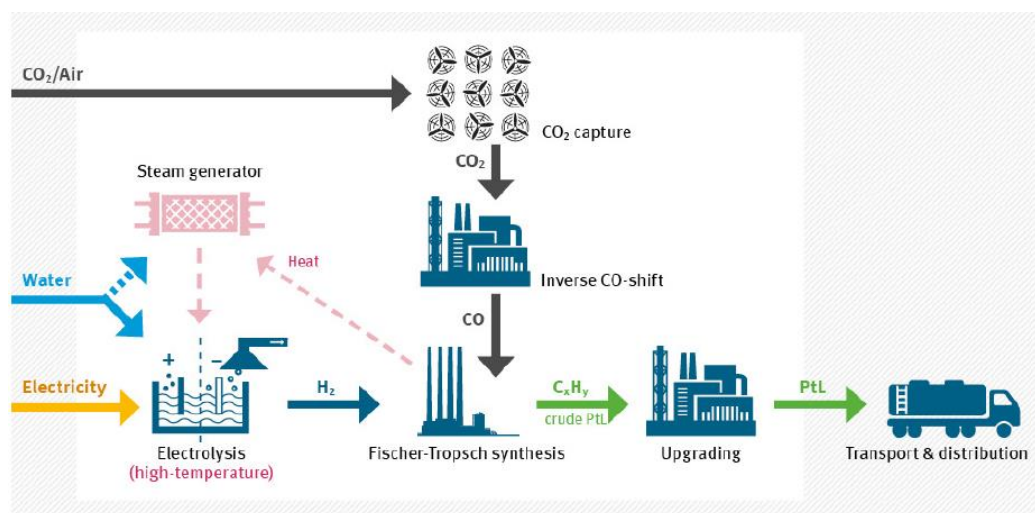


Figure 9-4 PtL production via Fischer-Tropsch pathway (high temperature electrolysis optional) [4]

In the case of high-temperature electrolysis, waste heat (220÷250°C) from the exothermic Fischer-Tropsch synthesis is used for steam generation, thus lowering the electricity demand. High-temperature electrolysis may furthermore allow for co-electrolysis of steam and CO<sub>2</sub>, producing hydrogen and carbon monoxide in a single step. In this case, an inverse CO-shift process step is not needed. Upgrading the FT-derived crude product to jet fuel and other hydrocarbons comprises several process steps, notably hydrocracking, isomerization, and distillation. These processes are commonly used today at largescale in crude oil refineries as well as in CtL and GtL plants. The share of products from the Fischer-Tropsch synthesis suitable for fuel use is about 50 to 60 % (by energy).

## Methanol pathway

An alternative pathway for the production of liquid hydrocarbons is via the intermediate product methanol. The pathway can build on industrially proven processes which have already been used for decades in various large-scale applications, such as natural gas reforming and synthesis to methanol (including methanol-to-gasoline conversion in some cases). The production pathway for the PtL methanol pathway is depicted in Figure 9-5 [4].

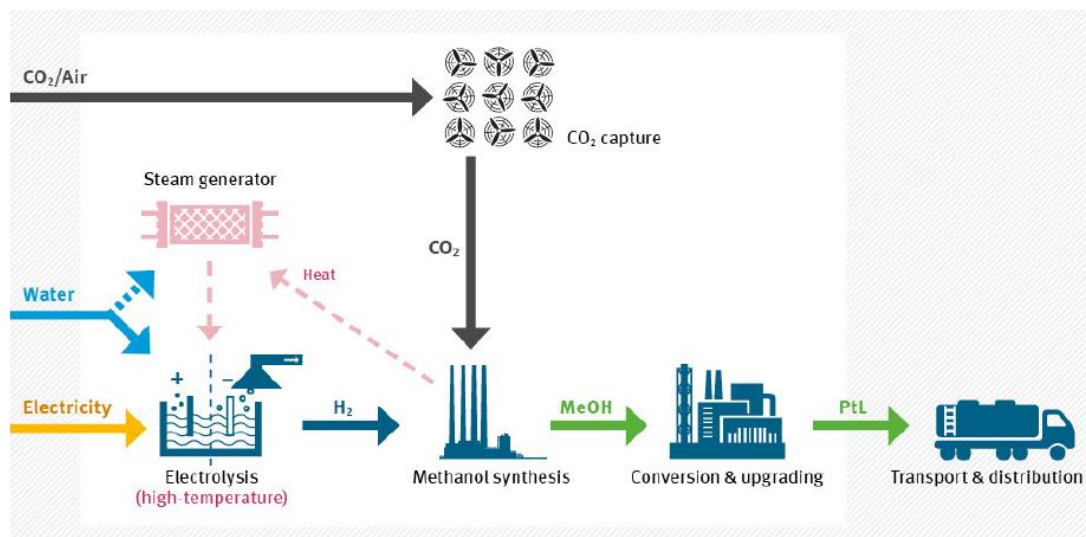


Figure 9-5 PtL production via methanol pathway (high temperature electrolysis optional) [4]

If high temperature steam electrolysis is applied, the heat from the exothermal methanol formation and other synthesis reactions in the production pathway can be used for steam generation, analogous to the Fischer-Tropsch pathway. The electricity input for hydrogen production is lowered significantly and the overall power-to-fuel conversion efficiency increased. For the synthesis reaction to methanol both CO and CO<sub>2</sub> can be used. A reverse water gas shift process or co-electrolysis of steam and CO<sub>2</sub>, as in case of the FT pathway, is consequently not a necessity.

Conversion and upgrading of methanol to fuel comprises several process steps, notably DME synthesis, olefin synthesis, oligomerization, and hydrotreating. Gasoline produced via the methanol pathway is compatible to conventional gasoline used in cars.

## 9.3 Technical and economic aspects of e-Fuels

### Technology Readiness of PtL Production

Both PtL pathways (via Fischer-Tropsch or methanol) offer a high level of technology readiness. PtL can be produced from concentrated CO<sub>2</sub> sources, using established industrial-scale processes with Technology Readiness Levels (TRL) between 8 and 9 [4]. While individual processes have been deployed at large scale, PtL full system integration is currently significantly progressed with the Fischer-Tropsch pathway demonstration plant by Sunfire in Dresden, Germany [69]. Improved processes for CO<sub>2</sub> extraction from air (TRL 6) and high-temperature electrolysis (TRL 5) increase the production potential and efficiency, respectively [4]. Renewable electricity costs have dropped significantly in recent years, meriting a fresh look at Power-to-Liquids pathways.

The Aviation is the main transportation sector that is pushing the e-Fuel developments.

### Energy Efficiency of e-Fuel Production

The energy efficiency (the energy effort required to produce a unit of fuel) of the Fischer-Tropsch and the Methanol pathway are about the same. Both processes are highly sensitive regarding how well waste heat from syntheses can be recuperated and used in, e.g. electrolysis or CO<sub>2</sub> provision. Table 9-2 from [4] summarizes the production efficiencies “gate-to-gate” (fuel output vs. electric input) of the PtL pathways.

Table 9-2 PtL production efficiencies “gate-to-gate” (fuel output vs. electric input)

Pathway	PtL production efficiency today → improved, using CO <sub>2</sub> from different sources		
	Air	Exhaust gas (e. g. wood burner)	Fermentation (e.g. biogas upgrading)
PtL with low-temperature elettrolysis	38% → 41%	47% → 51%	48% → 53%
PtL with high-temperature elettrolysis	45% → 46%	60% → 61%	62% → 63%

The energy efficiencies of PtL production pathways investigated in [4] can be as low as 38 % and as high as 63 % ‘well-to-tank’, subject to the combination of CO<sub>2</sub> source and electrolyzer technology.

### Costs and Price

e-Fuel costs are mainly determined by the renewable electricity costs (photovoltaic already < 3US Ct/kWh), in [74] the market price estimation is 2.0÷2.5 EUR per liter, representing a low and high taxation scenario.

## 9.4 Environmental benefits of PtL with renewable resources

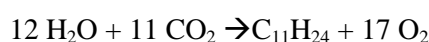
The environmental benefits of PtL are evident when using electricity, CO<sub>2</sub>, and water from renewable sources.

### Greenhouse Gas Emissions

Greenhouse gas emissions of PtL can be made near carbon-neutral “well-to- wheel”, when using renewable electricity and CO<sub>2</sub> from biomass sources or the air. According to [230] the overall greenhouse gas emissions for production, transportation, distribution and dispensing of PtL from renewable electricity and CO<sub>2</sub> are about 1 g CO<sub>2</sub> equivalent per MJ of final fuel. Since renewable electricity and CO<sub>2</sub> are used for vehicle fuel production, greenhouse gas emissions only occur at transportation, distribution and dispensing.

### Water Demand

The amount of water needed can be estimated based on the overall process stoichiometry. Liquid fuel consists of hydrocarbons with a carbon number distribution between 8 and 16 (8÷16 carbon atoms per molecule). Assuming an average carbon number of 11 (corresponding to e.g. undecane, C<sub>11</sub>H<sub>24</sub>) results in the following net reaction for fuel production via PtL:



This net reaction is valid for both the Fischer-Tropsch and the Methanol pathway.

Introducing the lower heating value of fuel amounts to about approximately 43 MJ per kg, the translation of energy into theoretical water demand is of 0.032 m<sup>3</sup> per GJ of fuel. Considering the real process of fuel production, this value becomes 0.040 m<sup>3</sup> of water per GJ of fuel, that means 1.4 liters of water per liter of fuel are required.

PtL water demand is almost negligible compared with biofuels. The following Figure 9-6 from [4] gives indications on the comparative sustainability performance of PtL.

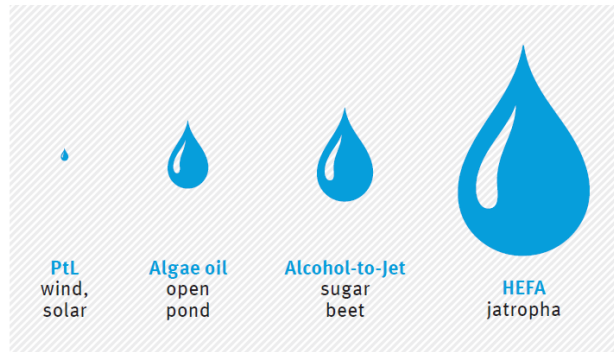


Figure 9-6 PtL water demand compared to selected biofuels (volume representation, PtL water demand  $\sim 1.4$   $L_{H_2O}/L_{fuel}$ )

## Land use

Considering the utilization in the aviation sector, [4] estimates a land use ten times lower than biofuel average.

## Pollutant emissions

As a synthetic fuel, PtL offers improved combustion with less pollutants than conventional fossil fuels.. According to [73] a proper fuel design can lead to a significant reduction of ICE emissions. In Figure 9-7 the effect of synthetic fuel in a diesel engine is shown. The utilization of a Fischer-Tropsch-Diesel, and thus reducing the aromatic content of the fuel, already improves the typical Soot/NO<sub>x</sub> trade-off. If then the fuel features increased oxygen content (e.g. 1-decanol), the trade-off becomes even more beneficial. In the investigated operative engine point a contemporary reduction of NO<sub>x</sub> and Soot of about four times are achievable compared with standard diesel fuel.

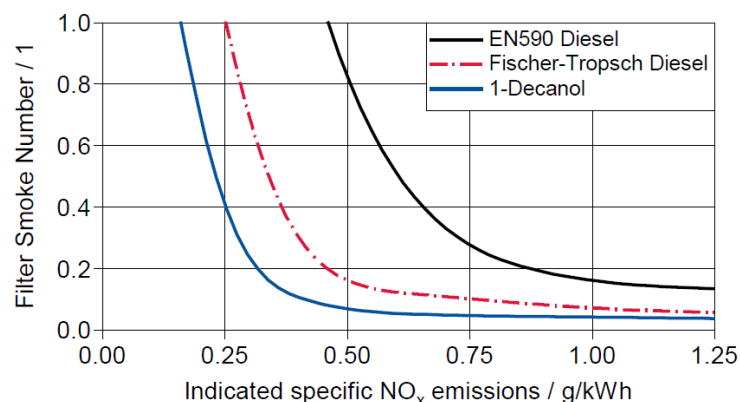


Figure 9-7 Soot/NO<sub>x</sub> trade-off for different fuels at engine speed 2280 rpm and IMEP 9.4 bar



## 10. Models for Design and Technical-Economic Evaluations

The simulation of the Vehicle and the Powertrain is a fundamental step to optimize and to evaluate the effectiveness of the technologies selected in the preliminary steps of design, presented in the previous chapters. Much information to evaluate new technologies relating to the powertrain can be found in literature or with proper experimental tests; however, the effects due to the technology mixing and their application to different vehicle segments can be predicted only thanks to the simulation approach.

The adopted models must be at the same time adequately accurate and fast, to carry out evaluations on long driving profiles and to be used for system optimization. The author of this thesis has already presented in different previous studies vehicle and powertrain models with two main aims: system analysis and control design purpose. The models had different levels of complexity from MVM in Matlab/Simulink [36,133,145,146,154,155] to 1-D model in GT-Suite and AMESim [36,149]. Another application of these kinds of models will be illustrated in the Chapter #11.3.2, where the problem of control design is approached with co-simulation of Simulink and GT- Suite.

The chapter presents a model that integrates the contributions of the previous and recent works. Furthermore some new subsystems and components have been modelled (e.g. cabin temperature and other powertrain components). The main purposes were the technical and economic evaluations to support the conceptual design and selection of the powertrain architectures and technologies, and the study of the energy management of the complex propulsion systems. To perform simulations and optimizations in long driving cycle, the low execution time (faster than reality) has been a primary requirement, researching a proper level of modelling to avoid lack of accuracy. The last point has been achieved using more complex models (e.g. 1-D/3-D) to generated date used in the simplified models.

The following table summarizes the model classification according to their aim and their features, taken into account in the presented research activities.

Table 10-1 Features of Model employed in this thesis

Aim	Model Type	Description	Pro/Cons
- System Analysis, Definition and Optimization - Supervisor Strategies	Quasi-Static model or 0-D Dynamic model	Black-box or grey box model	- Fast, suitable for complex system simulation - Many data for identification - Limited provisional features
- Sub-system design - Control Strategies definition	1-D model or Mean Value Model	Physical and grey box model	- Medium simulation time - Limited data for identification - Good provisional features
Component Design	3-D model	Physical model	- High computational time - Few data for identification - High provisional features
ECU on board model for control strategies	Simplified MVM or QS	Black-box or grey box model	- Real-time simulation of simplified sub-systems -Acceptable provisional features

## 10.1 Vehicle/Powertrain Simulator Structure

The simulator is based on 0-D models, whose scheme is depicted in Figure 10-1. Two main approaches are applied:

- Quasi-Static Simulation (QSS) or backward-facing approach.
- Dynamic simulation or forward-facing approach.

The high level model outputs are: fuel consumption, emissions and performance, evaluated on different driving profiles (e.g. NEDC, WLTC, etc.).

In addition, the vehicle Total Cost of Ownership and Life Cycle indicators for the CO<sub>2</sub> and the Energy are provided.

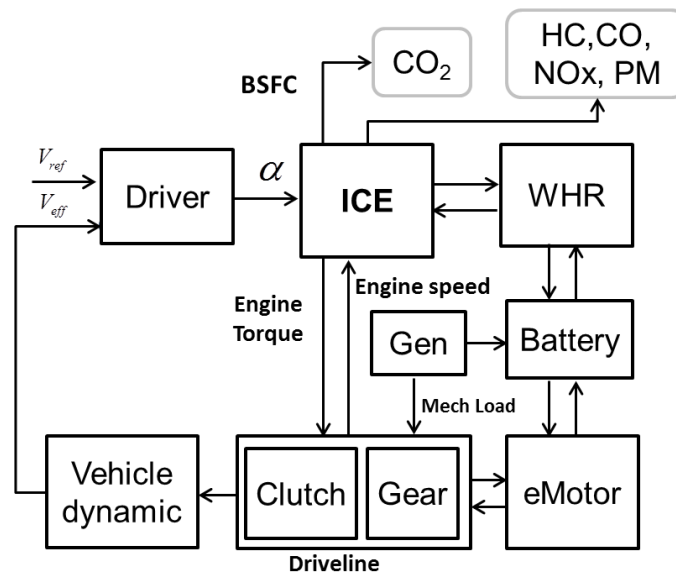


Figure 10-1 Scheme of 0-D model used for the powertrain system concept definition and analysis

The main areas of work compared with the model baseline presented in previous works are:

- Structure evolution, to simulate faster and with flexibility complex hybrid electric powertrain architectures (e.g. multiple electric machines and different transmissions).
- Update of the ICE and Electric Motor maps generated by means of Willans method, to take into account the specifications defined in the preliminary design phase (Chapter #4).
- Enhancement of the friction model of Engine and Gearbox.
- Enhancement of thermal model for each sub-system and addition of new components (e.g. vehicle cabin, TWC with EHC, etc.).
- Better integration of thermal flows between the powertrain subsystems.
- Introduction of the Total Cost of Owner and LCA models.
- Definition of Gear-shift logics and Energy management logics with model based approach.



Finally, a graphical interface allows configuring of the Vehicle and Powertrain systems, including their control logics, selected between the pre-set available systems.

The following sections provide an overview of the main sub-models.

## 10.2 Vehicle and Powertrain Quasi-Static and Dynamic Models

The QSS models, described in [150,151, 152], assume that the vehicle always perfectly meets the required speed trace, calculating the required force to accelerate it at each time step. The vehicle speed is translated into rotational speed while the traction/braking force is converted to torque assuming some components efficiencies. The computation flows upstream, from the wheels to the prime movers, against the physical power flow. The main advantages of the latter backward-facing approach can be summarized as follows:

- experimental efficiency tables (maps) are often computed in terms of speed and torque or power, so that they can be directly implemented within this approach;
- it allows very simple integration routines (i.e. Euler) to be implemented with large time steps (typically 1s);
- quick execution.

The major disadvantages that can be encountered due to the implementation of a QSS approach are:

- it is not suitable for "best effort" performance simulations, since it requires the theoretical speed profile to be always perfectly matched;
- since the energy use is estimated by means of quasi-static steady-state experimental maps, its use does not take into account dynamic effects;
- it is not based directly on relevant control signals for the vehicle (e.g. the throttle position and the brake pedal position).

If the purpose of the simulator is to develop an appropriate and realistic description of the real control signals, for control hardware and software development, dynamic forward-facing models are needed [152]. They include a driver model that provides appropriate accelerator and brake pedal signals. The calculation proceeds from the prime movers through the transmission to the wheels, finally computing the vehicle acceleration. The main paybacks are:

- measurable and realistic control signals and torques are used;
- dynamic models and high frequency effects (i.e. elasticity and dampers) can be included;
- WOT events can be simulated.

Conversely, some of the major drawbacks are:

- Lower simulation speed caused by the need of integration for vehicle components speed. They are executed at smaller time steps to provide stability and accuracy of the higher order integration scheme applied.

- The implementation of a PI driver model is not suitable for the integration of dynamic models into an optimization procedure based on dynamic programming (DP), since the latter proceeds backward in time.

To overcome the disadvantages of both the QSS and the Dynamic Modeling paradigms, mixed forward/backward approaches have been investigated. The authors of [153] developed an extended backward-facing parametric library that is enhanced by additional forward-facing features, e.g. correction loops for the consideration of physical limitations of the machines, the wheels slip etc.

In the next chapters, both backward and forward approaches are adopted. The key idea beyond both methodologies is that only the longitudinal vehicle dynamics is relevant to achieve the goal of optimal control strategies of interest.

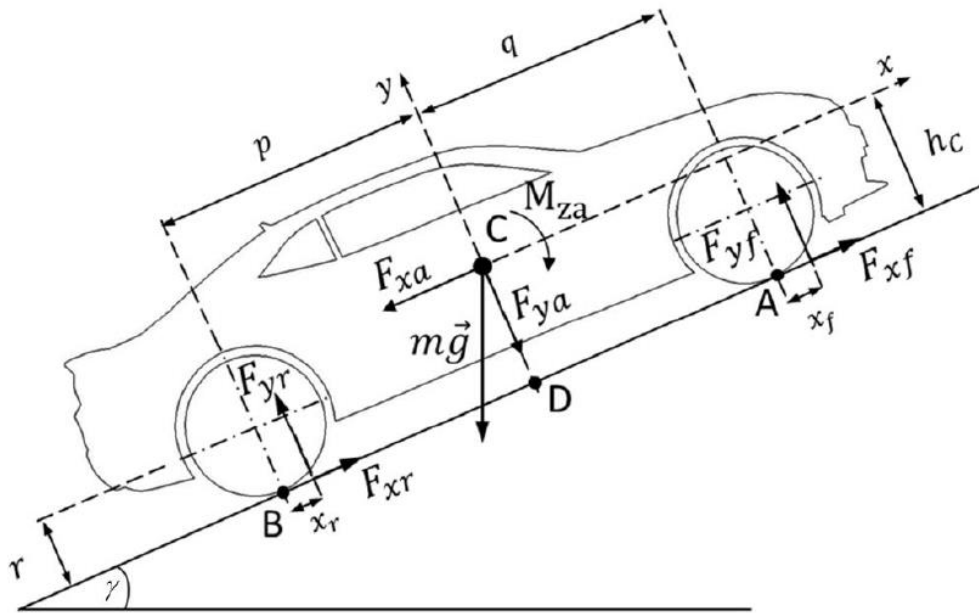


Figure 10-2 Forces acting on a vehicle on a road grade, see [136]

In the next sections, a detailed description of the equations used to model the vehicle and powertrain behavior is provided for each component. The main difference between QSS and Dynamic approaches lies in the physical causality of the signal routing.

Although the basic balance equations employed are the same, in many cases the input/output criterion is the opposite. Figure 10-3 depicts the schematic QSS model for the parallel HEV, REEV and BEV in study, while Figure 10-4 offers a representation of the dynamic input/output causality for the same electrified vehicle architectures. The powertrain model is flexible and can represent all the architectures presented in the previous Chapter #5. It can be observed that a major difference between the above QSS and the Dynamic model below lies in the causality of torques and speeds for the energy converters (machines and mechanical transmissions) and in the presence of a Driver, who tackles the desired speed, imposed by the Driving Cycle profile (DC).



The following sections provide a full mathematical description of all powertrain components included in the vehicle models adopted.

## 10.3 Models of Vehicle Sub-systems

The equations reported in the next sections are valid for each vehicle model, both for the QSS and for the Dynamic approach, following the distinction in terms of physical input/output causality previously introduced.

### 10.3.1 Driver

The driver block consists of a PI controller that is aimed at reducing the error between the actual vehicle speed  $v(t)$  and the reference value  $v_{ref}(t)$ , adapting the theoretical extended throttle  $\alpha_t(t)$  as follows:

$$\tilde{\alpha}_t(t) = k_{p,D} \cdot (v_{ref}(t) - v(t)) + \frac{1}{T_{i,D}} \cdot \int_0^t (v_{ref}(t) - v(t)) dt \quad (10.1)$$

The theoretical throttle  $\alpha_t(t)$  equals the physical throttle position in case of positive torque demand and corresponds to the brake pedal position when its value is negative. The theoretical value must be saturated as the following equations express:

$$\alpha_t(t) = \begin{cases} 100 & \text{if } \tilde{\alpha}_t(t) > 100 \\ \tilde{\alpha}_t & \text{if } -100 \leq \tilde{\alpha}_t(t) \leq 100 \\ -100 & \text{if } \tilde{\alpha}_t(t) < -100 \end{cases} \quad (10.2)$$

The driver model is only included in forward-facing modeling approaches. In case of parallel hybrid vehicles, this signal is transmitted to the PMS block, where the actual split factor is computed and the desired torques  $T_{req}(t)$  or powers  $P_{req}(t)$  are converted into ICE/EMGs commands.

### 10.3.2 Longitudinal Vehicle Model

The total traction force necessary to accelerate the vehicle can be split into four contributions, already presented in the chapter of powertrain conceptual design:

$$F_t(t) = F_i(t) + F_a(t) + F_r(t) + F_g(t) \quad (10.3)$$

They represent the inertial  $F_i$ , the air drag  $F_a$ , the rolling friction  $F_r$  and the slope  $F_g$  forces. They can be calculated by means of the equations below:

$$\begin{aligned}
F_i(t) &= (M_v + M_{re}) \cdot \dot{V}(t) \\
F_a(t) &= \frac{1}{2} \cdot \rho_{air} \cdot C_x \cdot S_f \cdot V(t)^2 \\
F_r &= M_v \cdot C_r \cdot g \cdot \cos \gamma(t) \\
F_g &= M_v \cdot g \cdot \sin \gamma(t)
\end{aligned}
\tag{10.4}$$

where the vehicle mass  $M_v$  is the sum of chassis, powertrain, energy storage and payload masses according to the equation (4.11), that for easy reading is below reported:

$$M_v = M_{chas} + M_{pwt} + M_{ess} + M_{payload} \tag{4.11}$$

The  $M_{re}$  includes all equivalent masses related to rotating elements of relevant inertia. For the parallel HEV, where the electric motor is always linked to the GB primary shaft, its value would be written as follows:

$$M_{re} = \frac{J_w}{r^2} + \frac{J_M \cdot \tau_g^2(u_g(t))}{r^2} \tag{10.5}$$

where the major inertias always connected to the driveline are the wheels and the electric motor, whose equivalent mass depends on the gear ratio  $\tau_g$ , that is as a function of the gearshift command  $u_g(t)$ .  $J_w$  and  $J_M$  are respectively the wheel and electric motor inertias. Angular speed and acceleration of the wheels depend on the wheel radius  $r$ :

$$\begin{aligned}
\omega_w(t) &= \frac{v(t)}{r} \\
\dot{\omega}_w(t) &= \frac{\dot{v}(t)}{r}
\end{aligned}
\tag{10.6}$$

The wheel torque can be computed using the following rotational balance expression:

$$T_w(t) = F_t \cdot r + J_w \cdot \dot{\omega}_w(t) \tag{10.7}$$

If the forward-facing modeling approach is chosen, the causality of the considered block is inverted. For the vehicle dynamics block, the vehicle acceleration is an output and is computed by the equation (10.8).

$$\dot{V}(t) = \frac{1}{M_v} \cdot \left( \frac{T_w(t)}{r} - F_a - F_r - F_g \right) \tag{10.8}$$

Similar considerations concerning differences between the input/output of QSS and Dynamic models are valid for the blocks described in the next sections. They will be omitted since the equations are suitable for both modeling paradigms.

## 10.4 Models of Powertrain Sub-systems

This section presents the model of powertrain sub-systems and components.

### 10.4.1 Gearbox

The task of the gearbox block is to provide the current selected gear as a function of discrete input gearshift command  $u_g(t)$ , so that torques and speeds at the primary shaft, where the propulsion machines are installed, can be calculated by means of the corresponding overall gear ratio  $\tau_g$ . The latter comprises the final drive gear ratio.

As explained in the next Chapter, in case automated transmission (DCT, AT, etc.) a gearshift strategy is included in the PMS, to enhance the optimal gear selection. The gearshift command is then expressed as a function of vehicle speed and power requested as:

$$u_g(t) = f_g(V(t), P_{req}(t)) \quad (10.9)$$

Once the resulting overall gear ratio  $\tau_g(u_g(t))$  is known, the angular speed and acceleration at the torque link on the primary shaft can be computed.

$$\begin{aligned} \omega_g(t) &= \omega_w(t) \cdot \tau_g(u_g(t)) \\ \dot{\omega}_g(t) &= \dot{\omega}_w(t) \cdot \tau_g(u_g(t)) \end{aligned} \quad (10.10)$$

The torque and power at primary shaft of the gearbox GB can be calculated as follows:

$$T_g(t) = \frac{T_{w2}(t)}{\tau_g(u_g(t)) \cdot \eta_g} \quad (10.11)$$

$$P_g(t) = \frac{P_{w2}(t)}{\eta_g} \quad (10.12)$$

where  $T_{w2}(t)$  and  $P_{w2}(t)$  are equal to  $T_w(t)$  and  $P_w(t)$  respectively, in case of the propulsion through single axle.  $\eta_g$  is the GB efficiency as a function of the gears and oil temperature  $T_{og}(t)$ , to take into account the friction losses and their dependence on variation of lubricant viscosity.

$$\eta_g(t) = f_{\eta g}(u_g(t), P_w(t), T_{og}(t)) \quad (10.13)$$

The function  $f_{\eta g}$  is implemented by means of look-up tables and experimental data that can be collected applying the procedure presented in [137,138].

The assumption of  $\eta_g$  as a constant can lead to significant model error in cold and warm conditions, due to its high variability, as confirmed in [138] for an AT (see Figure 10-5) and in [139] for a wet DCT (see Figure 10-6) employed for high performance powertrains.

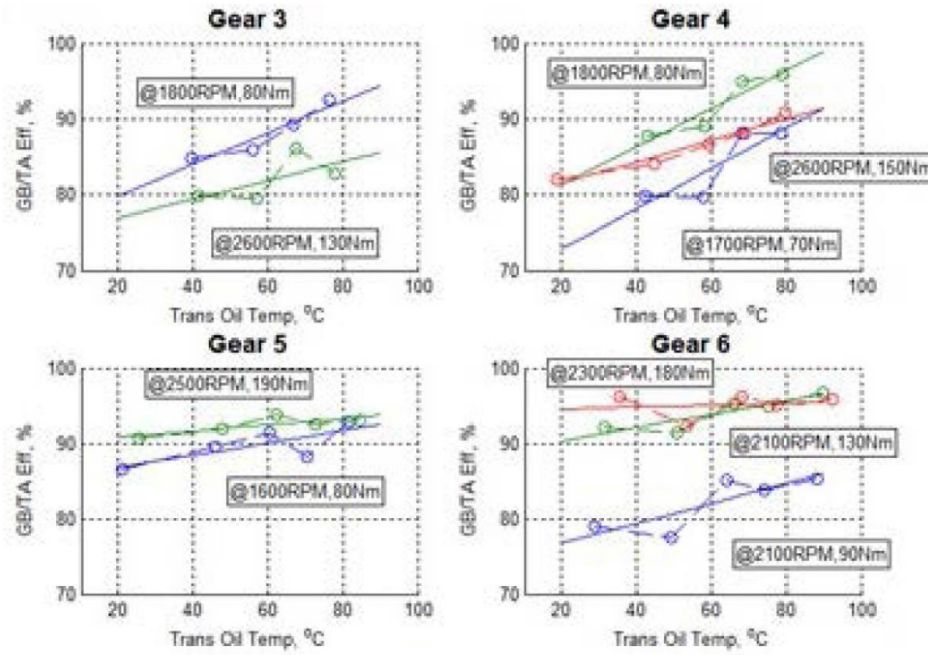


Figure 10-5 Ford Fusion thermally sensitive simplified transmission model, gear efficiency as a function of lubricant temperature [138]

The energy losses in wet DCT are caused by the wet clutch related components and they can exceed 40% of the total transmission energy dissipations. To overcome this issue, for lower performance vehicles, the dry clutch is employed achieving the same efficiency of a MT gearbox.

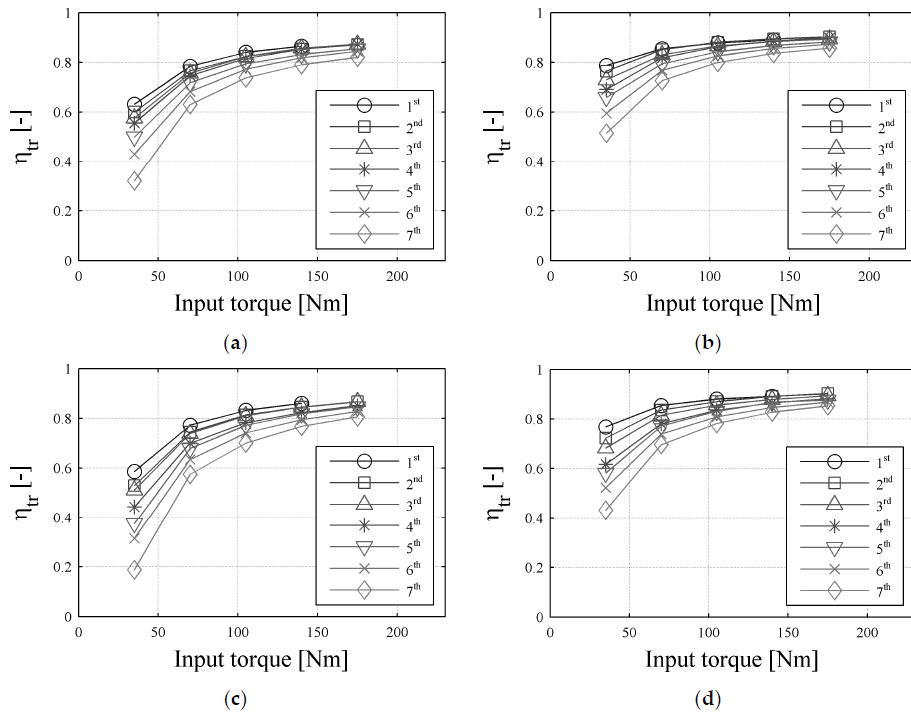


Figure 10-6 Sample of the experimentally measured DCT efficiency values as functions of input torque and different transmission temperature: (a)  $\omega_{in} = 1000$  rpm,  $T = 30$  °C; (b)  $\omega_{in} = 1000$  rpm,  $T = 70$  °C; (c)  $\omega_{in} = 2000$  rpm,  $T = 30$  °C; (d)  $\omega_{in} = 2000$  rpm,  $T = 70$  °C [139]

The gearbox oil temperature  $T_{og}$  is obtained by means of a grey-box model based on thermal energy balance of the gearbox and is presented following. The Fast Warm-up system can speed-up the oil heating, with benefit on vehicle fuel economy, as illustrated in the next sections.

### 10.4.2 Electric Axle

The equations (10.11) and (10.12) are valid also for torque  $T_{m1}$  and power  $P_{m1}$  of the electric motor M1 in P4 configuration, for HEV, REEV and BEV:

$$T_{m1}(t) = \frac{T_{w1}(t)}{\tau_{emt}(u_{emt}(t)) \cdot \eta_{emt}} \quad (10.14)$$

$$P_{m1}(t) = \frac{P_w(t)}{\eta_{emt}} \quad (10.15)$$

where  $u_{emt}(t)$  is the command on axle transmission, that typically has one or two gears,  $\tau_{emt}$  is gear ratio and  $\eta_{emt}$  the efficiency, for which the same consideration aforementioned are valid.

In case of propulsion through a single electric machine  $T_{w1}(t)$  is equal to  $T_w(t)$ , otherwise, in case of two electric machines, the totoal torque to the wheels  $T_w(t)$  is splitted according the factor  $u_{ts1}(t)$ , defined with the following equation (10.19).

### 10.4.3 Torque/Power Split

In case of HEV, in the torque/power split link (mechanical link upstream the gearbox) the torque/ power balance leads to the following equation, that distibuities the power/torque between the ICE and the electric machine M2:

$$T_g(t) = T_{ice}(t) + T_{m2}(t) \quad (10.16)$$

$$P_g(t) = P_{ice}(t) + P_{m2}(t) \quad (10.17)$$

The control input of the PMS is the torque split factor  $u_{ts}(t)$  and it is expressed by the equation below:

$$u_{ts2}(t) = \frac{T_{m2}(t)}{T_{ice}(t) + T_{m2}(t)} \quad (10.18)$$

This definition can be expressed alternatively in terms of power ratio and is valid only for the architectures where ICE and EM are connected upstream the gearbox (i.e. P0, P1 and P2 configurations).



In case of HEVs or BEVs architectures with two or more electric machines (e.g. P4+P2), that can generate torque/power contemporary linked to different axles (i.e. front and rear axles), another split factor is introduced to take into account the split between the two different drivelines:

$$u_{ts1}(t) = \frac{T_{w1}(t)}{T_w(t)} = \frac{T_{w1}(t)}{T_{w1}(t) + T_{w2}(t)} \quad (10.19)$$

where the torque are referred to the wheel shafts. In the next chapter the logic for the splitting will be presented.

### 10.4.4 Clutches

The torques coming from the clutch blocks depend on the current status of the clutches, which can be a simple discrete on/off command or an accurate signal describing the realistic command of the clutch actuator, capable of describing both stick and slip phases. In the present dissertation the slipping of the clutch is not considered.

In both QSS and forward-facing models utilized in the simulations described in the next chapters, the clutch command is a discrete variable, identifying the engaged and the disengaged status as follows:

$$u_c(t) = \begin{cases} 1 & \Rightarrow T_{c,i}(t) = T_i(t) \text{ and } \omega_{c,i}(t) = \omega_i(t) = \omega_g(t) \\ 0 & \Rightarrow T_{c,i}(t) = 0 \quad \text{and} \quad \omega_{c,i}(t) = \omega_g(t) \end{cases} \quad (10.20)$$

When the clutch is engaged and sticking, the following equations describe the identity of input/output torques and speed:

$$\begin{aligned} T_c(t) &= T_i(t) = T_o(t) \\ \omega_i(t) &= \omega_o(t) \end{aligned} \quad (10.21)$$

The following Figure 10-7 helps to describe the clutch model.

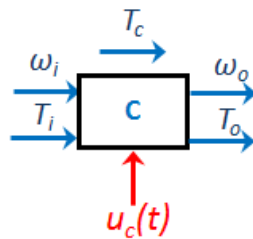


Figure 10-7 QSS schematic representation of a friction clutch element block

## 10.4.5 Internal Combustion Engine Model

The representation of ICE models aimed at system analysis and optimization or definition of the energy management supervisory are often a simple experimental steady-state maps or black box model, based on polynomial model or neural networks [154,155].

### Fuel Consumption

An example of Brake Specific Fuel Consumption (BSFC) for a SI engine is illustrated in Figure 10-8. It is related to a 4 cylinders 1.4L Turbo GDI engine, that is the baseline engine for the analysis of the C-Segment vehicles in this work.

If the engine is mechanically connected to the driveline, an internal engine torque and power can be computed, considering its inertial term  $J_e$  :

$$\begin{aligned} T_e(t) &= T_{ice}(t) + J_e \cdot \dot{\omega}_e \\ P_e(t) &= P_{ice}(t) + J_e \cdot \dot{\omega}_e \cdot \omega_e \end{aligned} \quad (10.22)$$

Once the net engine torque is known, the fuel mass flow is done by means of the previously introduced BSFC map, based on the current operating point, with the well-known expression:

$$\dot{m}_{fuel}(t) = P_e(t) \cdot BSFC(BMEP, \omega_e) \quad (10.23)$$

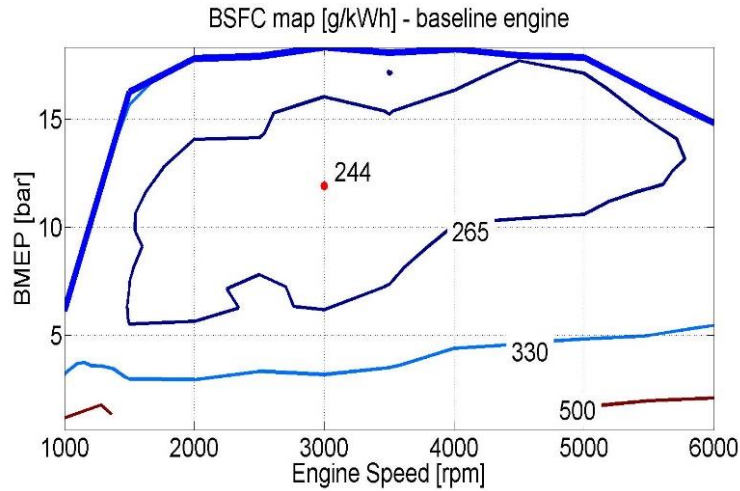


Figure 10-8 BSFC map of 1.4L Turbo GDI engine (baseline)

where the  $BMEP$  is easily obtained from the torque  $T_e(t)$  and engine displacement  $V_d$ . Normally the BSFC map is obtained by means of engine dyno tests in steady state conditions and with an engine coolant temperature above 80°C. To simulate cold conditions and warm-up phase of the engine, a correction term has been introduced, depending on estimated engine coolant temperature. As a consequence in the equation (10.23) the  $P_e$  is replaced with the corrected value:

$$P_{e,cor}(t) = P_e(t) + f_1(TH2O, \omega_e) + f_2(TH2O, BMEP) \quad (10.24)$$

where the  $f_1$  and  $f_2$  are correction maps deduced from experimental data.

The coolant temperature  $TH2O$  is obtained by means of a mean value grey-box model based on thermal energy balance of the engine coolant system and it is presented following.

The Fast Warm-up system can speed-up the engine coolant heating with benefit on vehicle fuel economy, as illustrated in the next section.

### CO2 Emission

The CO<sub>2</sub> emissions in [g/km] are evaluated converting the fuel consumption in [L/100km] deduced from the fuel mass flow of the equation (10.23) and the covered distance by the vehicle:

$$CO2 = Fuel\ Consumption \cdot k_{FtoCO2} \quad (10.25)$$

where  $k_{FtoCO2}$  is a constant equal to 23.2 for gasoline and 26.5 for diesel fuels.

### Engine Exhaust Temperature

The temperature model of the exhaust gas is a black-box model by means of a regression with following structure:

$$Texh(t) = f_1(BMEP, \omega_e) + f_2(TH2O) \quad (10.26)$$

### Emission Model

As the other engine outputs a black box approach is used by means of look-up tables, alternatively neural networks can be used. Both approaches have been already presented by the author of this thesis in [145,146,154,155].

## 10.4.6 Engine In-cylinder model - Willans Line Method

The map based modelling of the engine is possible when the experimental data are available. In alternative the map of the specific fuel consumption can be generated starting from data of a known engine with Willans line approach. This approach is powerful for the analysis of new technologies, not present in available engine. With the Willans line method [156, 297], the in-cylinder processes and friction losses of the ICE are modelled by a parametric approach. Willans line approach consists of an affine representation relating the available energy (i.e. the energy theoretically available for conversion) to the useful energy that is actually present at the output of the energy converter. There are many advantages of adopting such a formulation to describe both conventional and hybrid vehicles. Among others the most important are: the ability to make the model independent of the power rating or displacement of the device, thus permitting easy scaling; the compactness of the model, requiring only two parameters; its straightforward definition

and implementation; and the ability to easily compose models, thanks to the unified method of representation.

Nevertheless, some drawbacks should be considered when applying such an affine relationship to modern powertrain configurations, such as those featuring turbocharging, downsizing or both advanced design solutions.

The Willans line modeling technique was initially applied to describe the relationship, approximately linear, linking mean effective pressure to brake and engine fuel consumption. Rizzoni et al. in [157] extended this model to describe the energy converters, such as engines and electric machines.

In fact, in stationary conditions, it is possible to estimate the efficiency of a new machine belonging to the same category, using a scaling approach [158]. Furthermore, this approach is well-suited for immediate and approximate assessment of new design configurations and new engineering solutions for those classes of prototype machines or, in general, for those machines for which there are not enough data on efficiencies.

The key factor of this unique representation is that for a fixed speed, there is a linear relationship between output and input variables. That method suggests a close correlation between the total available energy (the fuel chemical energy) and the real used energy (the energy available at the crankshaft). The resulting representation is described by two factors: the slope, or intrinsic energy conversion efficiency  $e$ , and the vertical axis intercept  $P_{loss}$ , which represents the losses due to mechanical friction, alternator, auxiliaries etc., as shown in Figure 10-9.

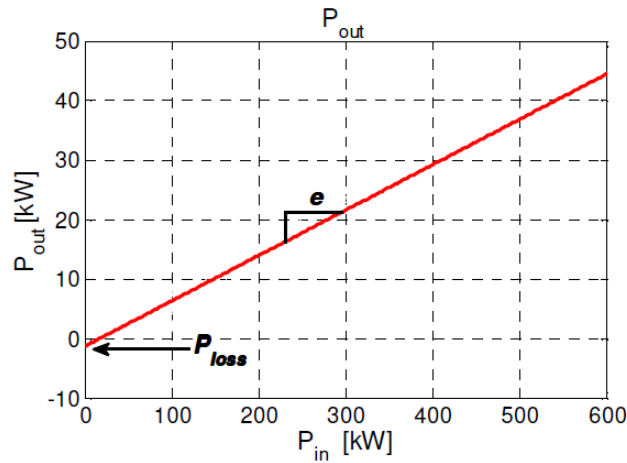


Figure 10-9 Linear relation between  $P_{out}$  and  $P_{in}$  at constant speed, adapted from [157]

The energy conversion efficiency and the relationship between input and output powers are thus expressed by the following equation:

$$P_{out} = e \cdot P_{in} - P_{loss} \quad (10.27)$$

where  $e$  has been considered obtained as the product of thermodynamic  $\eta_t$  and combustion  $\eta_b$  efficiencies. This means that  $e$  already accounts for losses due to pumping work. Equation (10.27) can also be expressed in terms of torque:

$$T_e = e \cdot H_{LHV} \cdot \frac{\dot{m}_f}{\omega} - T_{loss} = e \cdot T_a - T_{loss} \quad (10.28)$$

with  $T_a$  the available torque,  $H_{LHV}$  as the fuel lower heating value,  $\dot{m}_f$  the fuel flow rate and  $T_{loss}$  loss torque due to frictions.

To achieve scalable relations, it is necessary to introduce the concept of mean effective pressure *BMEP* (which can also be seen as the engine's ability to provide mechanical work), the available mean effective pressure *AMEP* (that represents the available chemical energy by fuel supply) and the average piston speed  $v_{pist}$ , corresponding respectively to the output torque, the available torque and engine speed. For a four stroke engine, they can be obtained:

$$\begin{cases} BMEP = T_e \cdot \left(\frac{4\pi}{V_d}\right) \\ AMEP = H_{LHV} \cdot \left(\frac{4\pi}{V_d}\right) \cdot \frac{\dot{m}_f}{\omega} \\ v_{pist} = \left(\frac{S}{\pi}\right) \cdot \omega \end{cases} \quad (10.29)$$

Where  $V_d$  is the engine displacement and  $S$  is the piston stroke. The engine efficiency can then be defined as follows:

$$\eta_{ICE} = \frac{P_{out}}{P_{in}} = \frac{T_e \cdot \omega}{\dot{m}_f \cdot H_{LHV}} \quad (10.30)$$

By means of the relationships given by equations (10.29) and substituting them into equations (10.28) and (10.30), the definition of engine dimensionless efficiency is

$$BMEP = e \cdot AMEP - FMEP \Rightarrow \eta_{ICE} = \frac{BMEP}{AMEP} \quad (10.31)$$

where *FMEP* is the mean effective pressure lost and is defined in a similar way to *BMEP* and *AMEP*. Parameters  $e$  and *FMEP* are functions of load and piston average speed. The following parameters, selected by referring to Willans line parameter correlations proposed in [157], were experimentally validated on different engines.

$$e = e_0(v_{pist}) - e_1(v_{pist}) \cdot AMEP$$

$$e_0 = e_{00} + e_{01} \cdot v_{pist} + e_{02} \cdot v_{pist}^2$$

$$e_1 = e_{10} + e_{11} \cdot v_{pist}$$

$$(10.32)$$

$$FMEP = FMEP_0 + FMEP_2 \cdot v_{pist}^2$$

$$(10.33)$$

It is worth mentioning here that the efficiency-related parameters listed in equations (10.32) and (10.33) were curve-fitted as a multi-linear regression model, here obtained by substituting such equations in equation (10.31). As aforementioned, the pumping work produces losses that are considered into the

efficiency term  $e$ . For several applications, it needs to decouple the pumping losses from the other members of the equation (10.31), and the result is expressed by the following equation:

$$BMEP = e \cdot AMEP - FMEP - PMEP \quad (10.34)$$

where the pumping losses are defined from the difference between the exhaust manifold and intake manifold pressures:

$$PMEP = p_{pumping} = p_{exh} - p_{intake} \quad (10.35)$$

This splitting of the several contributions of losses allows accounting for the effect of additional turbocharging or of other devices and technologies that could affect the backpressure and the boosting of the engine. The efficiency related parameters should be adapted in such a way as to decouple purely thermodynamic from turbocharging effects.

Starting from the equation (10.34) the torque delivered can be re-calculated with following equation, by splitting the terms related to both mechanical and pumping losses from the available torque generated by the fuel:

$$T_e = k_e \cdot e \cdot \eta_{idc} \cdot H_{LHV} \cdot \frac{\dot{m}_f}{\omega} - k_f \cdot p_{loss} \cdot \frac{V_d}{4\pi} - k_p \cdot p_{loss} \cdot \frac{(p_{exh} - p_{intake}) \cdot V_d}{4\pi} \quad (10.36)$$

where the coefficients  $k_e$ ,  $k_f$  and  $k_p$  have been introduced to consider the effects linked to the different engine technologies presented in the previous Chapter # 6.

In particular  $k_e$  takes into account the correction on the thermodynamic efficiency (e.g. for lower/higher heat losses, MFB50 position, knock phenomena),  $k_f$  is the correction for the friction losses (e.g. for heavier/lighter crank-train, bigger/smaller bearings, etc.),  $k_p$  is the correction for the pumping losses (e.g. for part load operations throttle adoption or not, turbocharger improvements, VGT or WG adoption, etc.).

Moreover, the coefficient  $e$  of equation (10.34) is re-formulated highlighting the ideal thermodynamic efficiency  $\eta_{idc}$ , dependent on compression ratio. In this work, a further modification to theoretical efficiency has been introduced to take into account the Miller cycle, as proposed in [88]:

$$\eta_{idc} = 1 - \frac{1}{r_g^{\gamma-1}} \cdot f(\sigma) \quad (10.37)$$

where  $\sigma = r_g/r_{tr}$  is the expansion – compression ratio, with  $r_g$  geometrical and  $r_{tr}$  trapped compression ratio, respectively. Moreover,  $f(\sigma)$  takes into the account the effect of the Miller cycle on the theoretical efficiency and in [88] is evaluated as:

$$f(\sigma) = \frac{\sigma^\gamma \cdot (\gamma - 1) - \gamma \cdot \sigma^{\gamma-1} + 1}{(\gamma - 1) \cdot \sigma^{\gamma-1} \cdot B} \quad (10.38)$$

with

$$B = \frac{H_{LHV}}{R \cdot T_{air} \cdot (1 + AFR)}$$

where  $AFR$  is the air to fuel ratio and  $T_{air}$  the temperature of intake air. Finally the equation (10.36) can be re-written introducing the parameter  $\lambda$ , the volumetric efficiency  $\eta_v$  and the air density  $\rho$  as:

$$T_e = k_e \cdot e \cdot \eta_{idc} \cdot \eta_v \cdot \frac{\rho \cdot V_d}{\lambda \cdot 14.56} \cdot H_{LHV} - k_f \cdot p_{loss} \cdot \frac{V_d}{4\pi} - k_p \cdot p_{loss} \cdot \frac{(p_{exh} - p_{intake}) \cdot V_d}{4\pi} \quad (10.39)$$

Summarizing, Willans line main concepts and applications are:

- to scale engine characteristics from a reference one, with the constraints that they should belong to the same engine class, such as SI engines or CI engines, either aspirated or turbocharged;
- since they aim at generating scale coefficients, the curves should adapt to a wide range of  $v_{pist}$  values, to avoid extrapolation when Willans-based engine model is scaled up/down or used for other engine configurations;
- to evaluate the impact of additional technologies on the engine efficiency.

### Analysis of Technologies to improve a Turbo GDI Engine

The equation (10.39) has been used to evaluate the achievable improvement on BSFC of 1.4L 4 cylinder, Turbo GDI engine, with a VVT and Compression Ratio (CR) equal to 10, chosen as baseline engine.

The corrective parameters  $k_f$ ,  $k_e$  and  $k_p$  have been evaluated starting from literature analysis and by means of a 1-D engine model, calibrated and validated against experimental data, as described in a published work dedicated to activity research on WI system [217]. Specifically, the 1-D model contains, in addition to the air path with turbocharger and supercharger, a predictive combustion modelling, which can also predict MAPO statistical distribution. In case of water injection, as an example, the corrective parameters can be found by firstly establishing a trade-off between MAPO percentile and indicated efficiency for knock limited engine operating points [76]. Subsequently, water injection is simulated and the new trade-off can be defined;  $k_e$  is therefore calculated and extrapolated for the nearest points, obtaining the static map to be used in the 0-D model. In Table 10-2, the effects of the ICE investigated technologies on the parameters are illustrated:

Table 10-2 ICE technologies and main parameters

ICE Technology	Linked Parameter
Cylinder deactivation (VVA)	$V_d, k_f, k_p$ in part load operations
Cylinder deactivation (2 CATs)	$V_d, k_f, k_p$ in part load operations
Miller/Atkinson Cycle	$\sigma$ and therefore $\eta_{idc}, k_p$ in the part load operations, $\eta_v, k_e$ depending on the strategies used
External EGR	$k_e$ for the lower heat losses and knock mitigation, $k_p, \gamma$
Lean Combustion	$\gamma, k_e, k_p$ especially at part low operations and knock resistance
Water Injection	$k_e, \gamma$ and knock resistance $\rightarrow$ higher $r_g$ allowed $\rightarrow$ higher $\eta_{idc}$
Variable Compression R.	$\eta_{idc}, k_f$
2stage-Air Charging	Extreme downsizing $\rightarrow V_d$ and $pme_{req}$

In Figure 10-10 and Figure 10-11, the *BSFC* map and the correlations between measured and estimated values of *BMEP* and *BSFC* for the baseline engine are shown, demonstrating the feasibility of the approach.

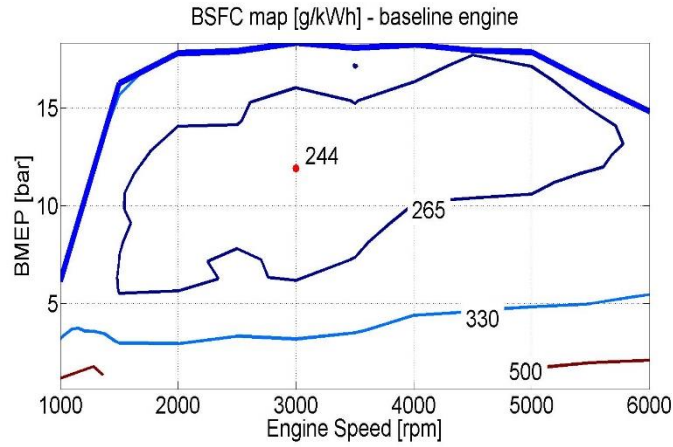


Figure 10-10 BSFC evaluation for 1.4L Turbo GDI engine (baseline)

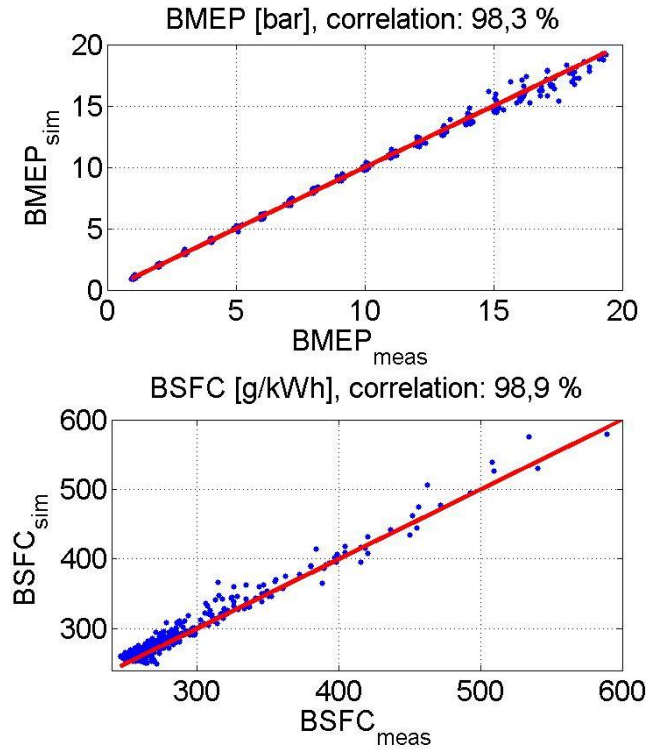


Figure 10-11 Correlation of BMEP and BSFC estimated vs. measured

The advantage of the approach is its modularity. Indeed, from the baseline case, the *BSFC* curve derived for any combination of technologies can be estimated. As an example, Figure 10-12 shows the *BSFC* map for the baseline case, adding the Miller cycle with an increased CR (12.5), cylinder displacement 1.5L and friction reduction of 20%. The results are quite similar than those shown in Figure 10-13, describing the measured *BSFC* map of the baseline engine improved with the previous technologies, as investigated in [159].



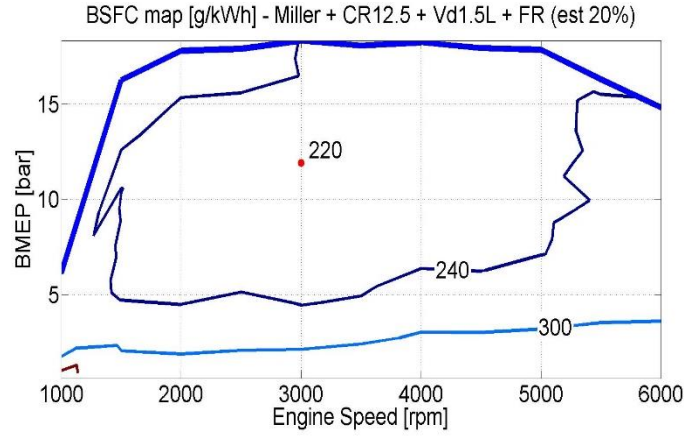


Figure 10-12 Simulated BSFC of 1.5L Turbo GDI with Miller cycle

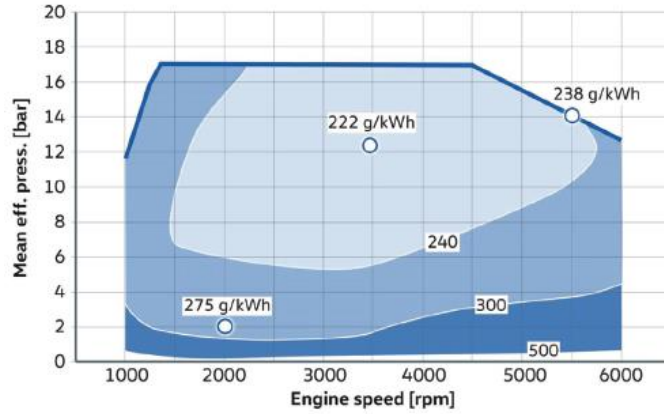


Figure 10-13 Measured BSFC map from [159] of the engine used for demonstrating the approach feasibility; the results are similar to the ones shown in Figure 10-12 obtained from the model

### 10.4.7 Electric Traction Drive Model

Detailed dynamic models of electric machines for HEVs are described in literature [160]. However, simple steady-state maps can be implemented even in forward-facing approaches. Figure 10-14 illustrates the global electric traction drive efficiency and maximum/minimum torques map, for a 48V propulsion system. Typically the efficiency includes the power electronic and electric machine efficiency and it is expressed as a function of inner motor torque  $T_{i,m}(t)$  and motor angular speed  $\omega_m(t)$ :

$$\eta_m(t) = f(T_{i,m}(t), \omega_m(t)) \quad (10.40)$$

The inner motor torque is evaluated by the equation:

$$T_{i,m}(t) = T_m(t) + J_m \cdot \dot{\omega}_m(t) \quad (10.41)$$

Speed and torque limitations must hold at every simulation step:

$$\begin{aligned}
 0 &\leq \omega_m(t) \leq \omega_{m,max} \\
 T_{m,min}(\omega_m(t)) &\leq T_{i,m}(t) \leq T_{m,max}(\omega_m(t))
 \end{aligned}
 \tag{10.42}$$

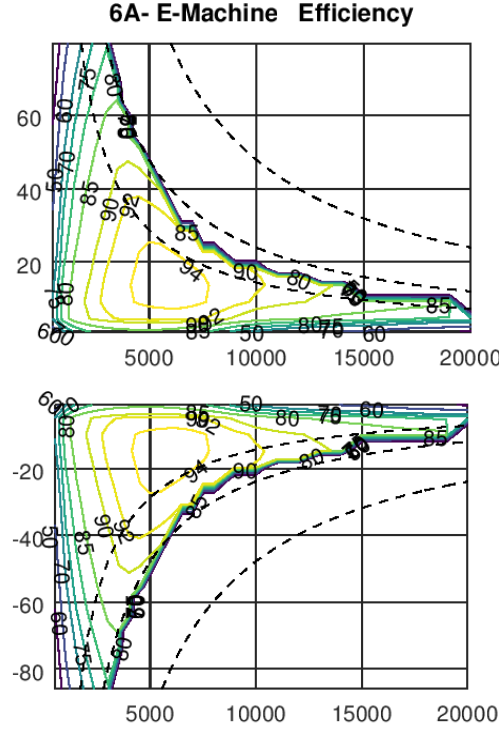


Figure 10-14 ETD steady-state efficiency and max./min. torque maps

The electric power depends on the operating point, as follows

$$P_m(t) = T_{i,m}(t) \cdot \omega_m(t) \tag{10.43}$$

It can be noted that the efficiency and the torque limits in generator/motor modes may differ.

### 10.4.8 Battery Model

At the electric power link, the power balance must be respected, considering a possible electric auxiliary power system request  $P_{e,aux}(t)$  and the power of electric motors.

$$P_b(t) = P_{m1}(t) + P_{m1}(t) + P_{e,aux}(t) \tag{10.44}$$

Hence, a model for the battery is required to compute the variation at each time step. Several modeling techniques have been investigated, both for batteries and super-capacitors [161,162]. Some of them focus on lead-acid batteries, others on Ni-MH batteries or on Li-Ion technologies. The main difference between

the modeling approaches lies in the choice of the physical details represented. Advanced physical models [163] are used to represent high transient dynamics, while simplified models are useful and reliable representations in standard operating conditions [164,165].

Another task regarding battery modeling is related to the determination of its most relevant parameter, i.e. the State-of-Charge (SOC). The authors of [166] present a review of possible methodologies for the on-line estimation of the SOC, while the authors of [167] focus on Kalman's filter technique, considered the most effective one. Other important aspects that should be taken into account are the battery ageing phenomena and the battery thermal behavior [168]. Throughout the present dissertation, neither temperature dependencies nor ageing phenomena are treated, and the batteries are modeled by means of a resistive equivalent circuit, as illustrated in Figure 10-15.

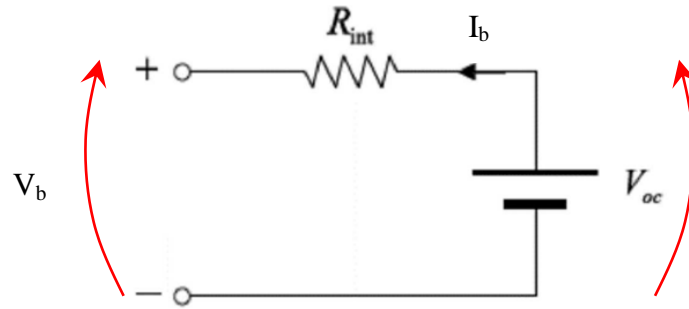


Figure 10-15 Equivalent resistive circuit of a battery, Kirchoff law-based approach

The battery electric power is expressed by:

$$P_b(t) = V_b(t) \cdot I_b(t) \quad (10.45)$$

The voltage at the battery clamps  $V_b(t)$  depends on the inner (open-circuit) voltage  $V_{OC}(SOC(t))$  and on the internal resistance  $R_{int}$ , which is also as a function of the current  $I_b$  direction and of the SOC. The equation below describes such relationships.

$$V_b(t) = V_{OC}(SOC(t)) - R_{int}(SOC(t), sign(I_b(t))) \cdot I_b(t) \quad (10.46)$$

The next Figure 10-16 shows the  $V_{OC}$  dependence on the SOC for a LiFePO<sub>4</sub> battery cell at 23 °C from [141].

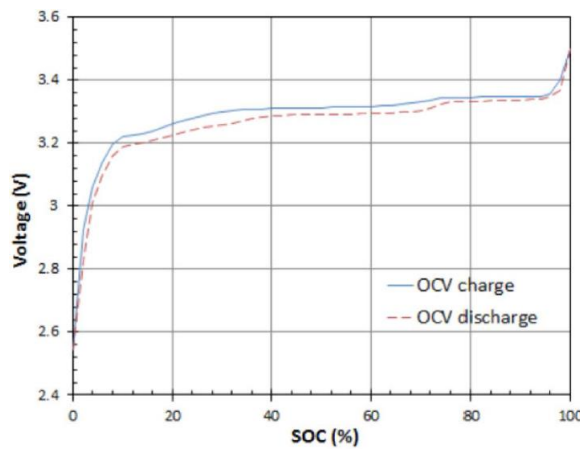


Figure 10-16 Open Circuit Voltage ( $V_{OC}$ ) of LiFePO<sub>4</sub> Battery Cell at 23 °C [141]

The current flowing from or to the battery can be modeled through the following equation:

$$I_b(t) = \frac{V_{oc}(\cdot) - \sqrt{V_{oc}^2(\cdot) - 4R_{int}(\cdot) \cdot P_b(t)}}{2R_{int}(\cdot)} \quad (10.47)$$

The state-of-charge can be found, once the battery maximum charge capacity  $Q_o$  is known:

$$\begin{aligned} SOC(t) &= \frac{Q(t)}{Q_o} \\ \frac{dSOC(t)}{dt} &= -\frac{I_b(t)}{Q_o} \end{aligned} \quad (10.48)$$

Constraints can be active both on SOC range and on maximum/minimum current limitations:

$$\begin{aligned} SOC_{min} &\leq SOC(t) \leq SOC_{max} \\ I_{b,min} &\leq I_b(t) \leq I_{b,max} \end{aligned} \quad (10.49)$$

## 10.5 Vehicle and Powertrain Thermal Model

The vehicle and powertrain thermal models are dynamic models composed of Mean Value Models of the main components. Both QSS and Dynamic models for fuel consumption and emission evaluations receive as input the thermal status of each component evaluated in parallel. Below in Figure 10-17 the scheme of the block connections is presented.

The main flows between the sub-systems are depicted. The thermal source at higher temperature is the internal combustion engine, whereas the lower temperature sink is the ambient. The Fast Warm-up system is positioned upstream the power heat recovery system (RC or TEG) and it delivers heat to engine and vehicle cabin.

The TWC can be heated by means of an electric heating (EHC) to speed up the light-off. The WI tank is de-frozen by means of engine coolant and/or an electric heater. The cabin can be heated/cooled by means of the waste heat from engine and heat/cooled by means of a compressor heat pump, mechanical or electric. In the next section the thermal model of each component is presented.

The structure of the model for each sub-system or component is similar and it is described following. After that for each component the specific terms are illustrated.

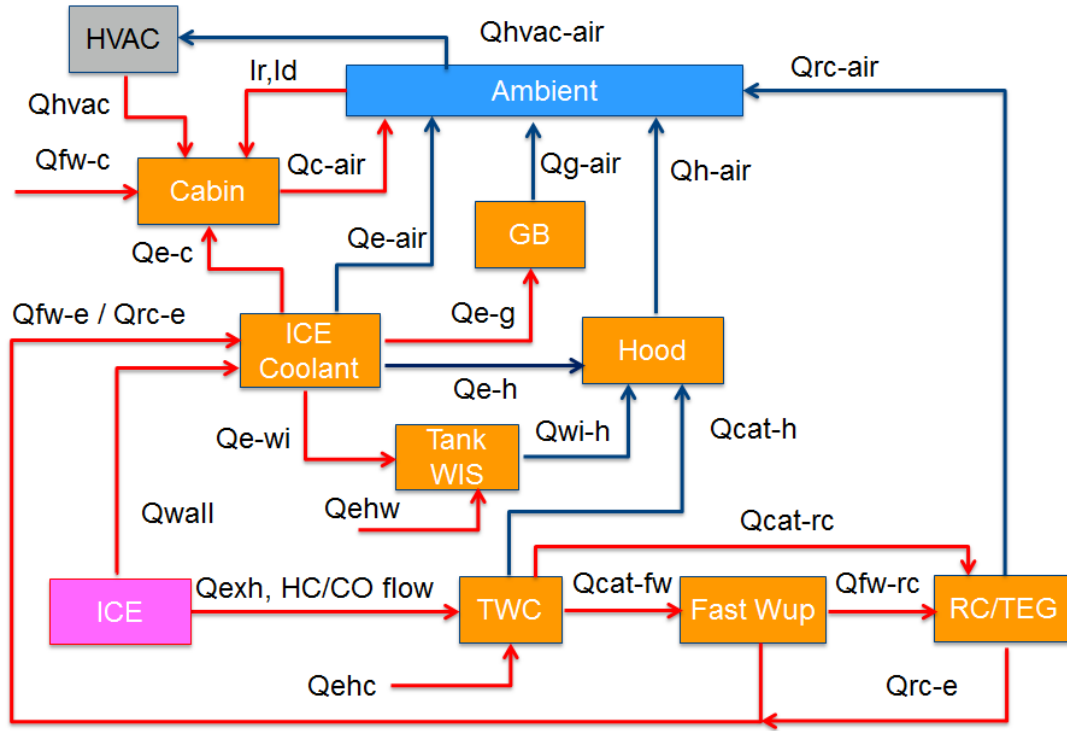


Figure 10-17 Simplified scheme of heat flows between the vehicle and powertrain sub-systems

### 10.5.1 Temperature Model of Generic Component/Sub-system

The temperature  $T_i(t)$  related to the key parameter of each component is obtained by means of a grey-box model, based on thermal energy balance:

$$T_i(t) = T_i(t_0) + \frac{1}{c_{p,i} \cdot M_i} \cdot \int_{t_0}^t (\dot{Q}_{gen,i}(t) + \dot{Q}_{eh,i}(t) - \dot{Q}_{exch,i}(t)) dt \quad (10.50)$$

where  $c_{p,i}$  and  $M_i$  are respectively the equivalent specific heating and mass of the generic element.

The  $\dot{Q}_{gen,i}(t)$  is the heating power generated inside the component, for instance the chemical reaction in TWC, the  $\dot{Q}_{eh,i}(t)$  is the heat flow due to an external source (e.g. electric heating) and the  $\dot{Q}_{exch,i}(t)$  is the heat flow exchanged with an external environment, typically the ambient. The last term is as a function of delta temperature between the component and the environment. The description of the terms in equation (10.50) for each component is reported following.

### 10.5.2 Thermal Model of Vehicle Cabin

The model goals are the system analysis of the technologies in the powertrain domain, that can impact on the thermal comfort of the driver, and the evaluation of the cabin conditioning influence on energy consumption [169,169]. Considering the trade-off between estimation performance and calculation time,

the proposed model is a MVM that is only suitable to give an average value of the cabin temperature  $T_c$ . It is important point out that the driver comfort is the results of many physical parameters (e.g. temperature, humidity, etc.) and their distribution in the space, therefore only a 3-D model is able to evaluate the real status in term of cabin comfort. The [140] are the reference works for the implemented model, from which many sub-models were deduced.

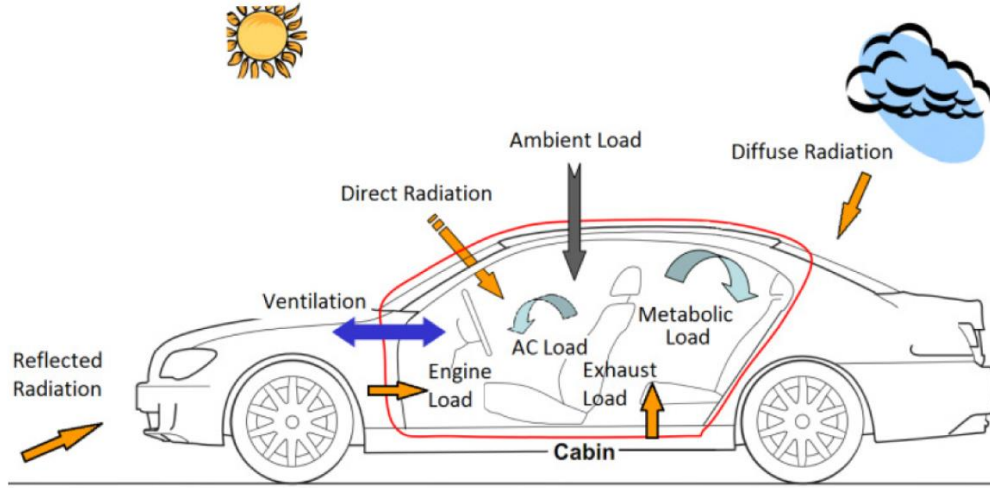


Figure 10-18 Schematic representation of thermal loads in a typical vehicle cabin

The equivalent thermal capacity of cabin is calculated by means of the equation:

$$c_c \cdot M_c = c_a \cdot m_a + DTM \quad (10.51)$$

where DTM is the sum of all the deep thermal masses, i.e. the overall thermal inertia of all objects other than air present inside the cabin. These objects include the seat structures, the dash, the dash components, etc., which are combined with the cabin air in the lumped model and  $m_a$  is the cabin air mass and  $c_a$  is the air specific heat.

The heat flow exchanged with the external environment  $\dot{Q}_{exch,c}(t)$  is the  $\dot{Q}_{amb}(t)$  and it is the contribution of the thermal load transferred to the cabin air due to temperature difference between the ambient and cabin air. Exterior convection, conduction through body panels, and interior convection are involved in the total heat transfer between the ambient and the cabin. The equation (10.52) shows the general form of the ambient load model.

$$\dot{Q}_{exch,c}(t) = \dot{Q}_{amb}(t) = \sum_{surfaces} S \cdot U \cdot (T_c(t) - T_a) \quad (10.52)$$

where  $U$  is the overall heat transfer coefficient between the surface elements.  $U$  has different components consisting of the inside convection, conduction through the surface, and outside convection. It can be written in the form

$$U = \frac{1}{R} \text{ where } R = \frac{1}{h_0} + \frac{l}{k} + \frac{1}{h_i} \quad (10.53)$$

where  $R$  is the net thermal resistance for a unit surface area.  $h_o$  and  $h_i$  are the outside and inside convection coefficients,  $k$  is the surface thermal conductivity, and  $l$  is the thickness of the surface element. The thermal conductivity and thickness of the vehicle surface can be measured rather easily. The convection coefficients  $h_o$  and  $h_i$  depend on the orientation of the surface and the air velocity. Here, the following estimation is used to estimate the convection heat transfer coefficients as a function of vehicle speed [171].

$$h_c = h_{c1} + h_{c2} \cdot \sqrt{V} \quad (10.54)$$

where  $h_c$  is the convection heat transfer coefficient in  $\text{W/m}^2\text{K}$  and  $V$  is the vehicle speed in  $\text{m/s}$ . Despite its simplicity, this correlation is applicable in all practical automotive instances [171]. The cabin air is assumed stationary and the ambient air velocity is considered equal to the vehicle velocity. Numerical simulations can also be used to provide the model with convection coefficients that have higher accuracy and take into account the different orientation and position of every surface component.

The  $\dot{Q}_{gen,c}(t)$  is due to passengers in the car and it is named metabolic load  $\dot{Q}_{Met}(t)$ . The metabolic activities inside human body constantly create heat and humidity (i.e. perspiration), for details see [140].

The heating flow due to external source  $\dot{Q}_{eh,c}(t)$  is the results of three terms:

- the heat gain due to solar radiation  $\dot{Q}_{rad}(t)$ , that is a significant part of heating power of the cabin; according to [172], solar radiation heat load can be categorized into direct, diffuse, and reflected radiation loads;
- the ventilation load  $\dot{Q}_{ven}(t)$ , the minimum flow of fresh air that should be supplied into the cabin to maintain the air quality for passengers; for a small sedan car at a pressure difference of 10 Pa, a leakage of 0.02  $\text{m}^3/\text{s}$  is typical [173];
- the air conditioning system power  $\dot{Q}_{hvac}(t)$  to compensate for other thermal loads so that the cabin temperature remains within the acceptable comfort range.

The deep description of first two terms is reported in [140], whereas the third term depends on air conditioning system type. In the developed model four options have been considered:

- a. heating by means of an engine coolant heat exchanger, the conventional solution used for the cabin heating during winter in an ICE based vehicle, see Figure 10-19;
- b. cooling by a conventional mechanical compressor cycle;
- c. an electric heat pump for heating and cooling, typically used in BEV;
- d. an adsorption heat pump for cooling and a Fast warm-up system for heating by means of engine waste heat recovery.

The desired temperature is controlled using a PI controller that defines the conditioning power  $\dot{Q}_{hvac}(t)$ . From this heat power, assuming a Coefficient of Performance (COP) for the selected HVAC system, the power to be delivered to the conditioning system is evaluated:

$$P_{hvac}(t) = \frac{\dot{Q}_{hvac}(t)}{COP} \quad (10.55)$$

The  $P_{hvac}(t)$  for each case is:

- case a, the heat of engine cooling with  $COP=0.6 \div 0.75$ ;
- case b, the mechanical power delivered by the engine with  $COP = 2.5 \div 4$  [296];
- case c, electric power from battery with  $COP = 3 \div 4$ ;
- Case d, engine exhaust gas or cooling with  $COP=0.3 \div 0.6$  [29,30].

The model is validate comparing the temperature and conditioning power presented in [140] and [142], where the air conditioning of an ICE based vehicle and a BEV was studied.

### 10.5.3 Engine Compartment Temperature

The engine compartment temperature is used to model with better accuracy, the engine coolant, TWC and water tank temperatures. These components exchange part of the heat with engine compartment, which has a temperature dynamic depending on the layout, engine thermal status, external ambient temperature and vehicle speed.

The mean value model of engine compartment temperature  $T_{hood}$  is based on equation (10.50) and its terms are calculated as following.

The equivalent thermal capacity of engine compartment is calculated as  $c_{p,air} \cdot M_{hood}$ , considering an equivalent mass identified by means of experimental data.

The heat flow received by the engine  $\dot{Q}_{eng,hood}(t)$  is described with the expression:

$$\dot{Q}_{eng,hood}(t) = S_{eng,hood} \cdot h_{eng,hood} \cdot (T_{eng}(t) - T_{hood}(t)) \quad (10.56)$$

where term  $S_{eng,hood} \cdot h_{eng,hood}$  is assumed constant.

The heat flow  $\dot{Q}_{hood,amb}(t)$  released by the hood to external environment is obtained with:

$$\dot{Q}_{hood,amb}(t) = S_{hood,amb} \cdot h_{hood,amb}(t) \cdot (T_{hood}(t) - T_a) \quad (10.57)$$

in which

$$h_{hood,amb} = h_{h1} + h_{h2} \cdot \sqrt{V} \quad (10.58)$$

### 10.5.4 Engine Coolant Temperature

The mean value model of engine coolant  $T_{eng}$  is based on equation (10.50) and its terms are calculated as following. For an easy understanding of the model the scheme of a typical thermal management system for a spark ignition engine is illustrated in Figure 10-19.



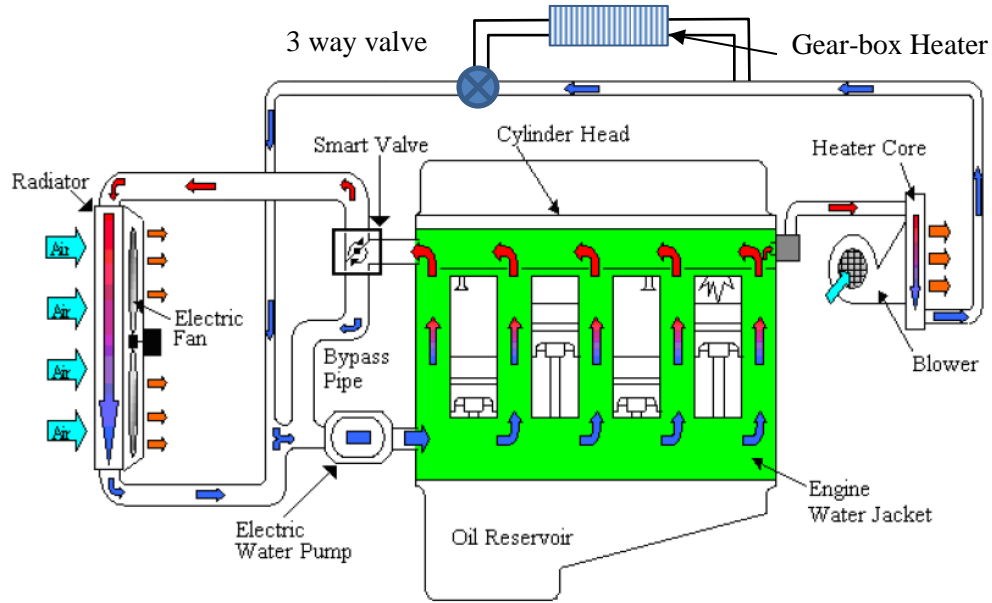


Figure 10-19 Example of thermal management system architecture for a spark ignition engine [143]

The equivalent thermal capacity of engine coolant is calculated considering the coolant mass and engine block mass by means of the equation:

$$C_{eng} \cdot M_{eng} = c_{coolant} \cdot m_{coolant} + c_{eng\ block} \cdot m_{eng\ block} \quad (10.59)$$

where  $c_{coolant}$  and  $c_{eng\ block}$  are the specific heat of the cooling fluid and the engine block, typically in aluminum. The heat flow  $\dot{Q}_{exch,eng}(t)$  exchanged with external environment and other vehicle devices is the results of four terms, see equation (10.60):

- the heat towards the ambient by means of the radiator  $\dot{Q}_{eng,rad}$ ;
- the heat re to the engine compartment  $\dot{Q}_{eng,hood}$ ;
- the heat used for cabin heating  $\dot{Q}_{eng,cab}$ ;
- the heat to warm the gearbox oil  $\dot{Q}_{eng,gbox}$ .

$$\dot{Q}_{exch,eng}(t) = \dot{Q}_{eng,rad}(t) + \dot{Q}_{eng,hood}(t) + \dot{Q}_{eng,cab}(t) + \dot{Q}_{eng,gbox}(t) \quad (10.60)$$

where

$$\dot{Q}_{eng,rad}(t) = (1 - EngCoolValvCmd(t)) \cdot S_{rad} \cdot h_{eng}(t) \cdot (T_{eng}(t) - T_a) \quad (10.61)$$

with  $S_{rad}$  the equivalent surface of the radiator, that can be scaled considering as a proportional function of engine maximum power, and  $h_{eng}$  the heat transfer coefficient, depending on vehicle speed with the mathematical relation:

$$h_{eng} = h_{e1} + h_{e2} \cdot \sqrt{V} \quad (10.62)$$

The *EngCoolValvCmd* is the command to the smart thermostat, defined by a PI controller to achieve the desired coolant temperature.

The heat flow  $\dot{Q}_{eng,hood}(t)$  released to the hood is described in the relative model, see equation (10.56).

The term  $\dot{Q}_{eng,cab}(t)$  is calculated with equation (10.55).

The thermal power  $\dot{Q}_{eng,gbox}(t)$  to warm the gearbox oil is estimated with the formula:

$$\dot{Q}_{eng,gbox}(t) = Wup3wValvCmd \cdot SU_{eng,gbox} \cdot (Tu_{cab,heater}(t) - T_{oilg}(t)) \quad (10.63)$$

with  $SU_{eng,gbox}$  the equivalent conductivity of heat exchange between engine coolant circuit and gearbox lubricant circuit, *Wup3wayValvCmd* the on/off command of the 3 way by-pass valve and  $Tu_{cab,heater}(t)$  the coolant temperature downstream cabin heater obtained from the equation:

$$Tu_{cab,heater}(t) = T_{eng}(t) - \frac{\dot{Q}_{eng,cab}(t)}{SU_{eng,cab}} \quad (10.64)$$

In case of the Water Injection system the engine coolant can be used to thaw the water stored in a specific tank, through a liquid-liquid heat exchanger installed inside the tank. The water heating is activated by an on/off valve, when the engine coolant temperature overcome a defined threshold (e.g. 60 °C) and is turned-off when the water is completely thawed. In this case the estimation of the heat provided to water tank has to be added to equation (10.60).

The heat flow due to external sources  $\dot{Q}_{eh,eng}(t)$  is received from Fast Warm-up system  $\dot{Q}_{fwu,eng}$ .

The heating flow  $\dot{Q}_{fwu,eng}(t)$  is the thermal power coming from Fast Warm-up system, that harvests energy from exhaust gas and its estimation is carried out with a simplified model:

$$\dot{Q}_{fwu,eng}(t) = FWupValvCmd \cdot Eff_{FWU} \cdot cp_{exh} \cdot \dot{m}_{exh} \cdot (T_{cat,out}(t) - T_{eng}(t)) \quad (10.65)$$

where *FWupValvCmd* is the command of the on/off valve that can by-pass the heat recovery system; the term  $Eff_{FWU}$  is the efficiency of the system, that is assumed constant in a range between 0.7÷0.85, on the basis of tests in Magneti Marelli. The catalyst outlet temperature  $T_{cat,out}(t)$  is estimated with equation (10.78).

The  $\dot{Q}_{gen,eng}(t)$  is the heat released during the combustion to cylinder walls and is evaluated with the expression:

$$\dot{Q}_{gen,eng}(t) = k \cdot (1 - \eta_{eng}) \cdot \dot{m}_{fuel} \cdot LHV \quad (10.66)$$

with an empirical coefficient  $k$  as a function of engine speed and load. The first attempt average value is 0.5, with the assumption that 50% of fuel dissipated energy is discharged in the engine coolant.

### 10.5.5 Gearbox Oil Temperature

The equivalent thermal capacity for temperature model of gearbox oil is calculated considering the oil mass and transmission mass by means of the equation:

$$c_{gbox} \cdot M_{gbox} = c_{oilg} \cdot m_{oilg} + c_{trasm} \cdot m_{transm} \quad (10.67)$$

where  $c_{oilg}$  and  $c_{trasm}$  are the specific heat of the transmission lubricant and block, typically in steel. The heat flow  $\dot{Q}_{exch,gbox}(t)$  exchanged with external ambient is evaluated with the expression

$$\dot{Q}_{exch,gbox}(t) = S_{gbox} \cdot h_{gbox}(t) \cdot (T_{oilg}(t) - Ta) \quad (10.68)$$

with  $S_{gbox}$  the equivalent surface of gearbox exposed to external air flow, and  $h_{gbox}$  the heat transfer coefficient, depending on vehicle speed with the mathematical relation

$$h_{gbox} = h_{gb1} + h_{gb2} \cdot \sqrt{V} \quad (10.69)$$

The  $\dot{Q}_{gen,gbox}(t)$  takes into account the mechanical power dissipated in the transmission and it is calculated as a function of the power input in the gearbox and the mapped transmission efficiency, depending on gear engaged:

$$\dot{Q}_{gen,gbox}(t) = k_{gbox} \cdot \left(1 - \eta_g(\tau_g(t))\right) \cdot (Pe + P_{m2}) \quad (10.70)$$

In hybrid P2 architecture the mechanical power is the sum of electric motor and ICE power. The model has been validated comparing the oil temperature presented in [144] and [138], considering ICE based vehicles in different driving cycles.

### 10.5.6 Three Way Catalyst Temperature

The temperature model  $T_{cat}$  of the catalyst is already present in other previous works [145,146] of the thesis author. Herein the model is summarized with the addition of the electric heating catalyst modelling.

The thermal capacity of catalyst,  $c_{cat} \cdot M_{cat}$ , is obtained by data of catalyst manufacturer. The catalyst mass is scalable as a function of engine displacement  $V_d$ .

The heat flow  $\dot{Q}_{exch,cat}(t)$  exchanged with engine compartment is calculated with the expression:

$$\dot{Q}_{exch,cat}(t) = \dot{Q}_{cat,hood}(t) = S_{cat,ezt} \cdot h_{cat,ext}(t) \cdot (T_{cat}(t) - T_{hood}(t)) \quad (10.71)$$

with  $S_{cat,ext}$  the external surface of catalyst, and  $h_{cat,ext}$  the heat transfer coefficient, depending on vehicle speed with the mathematical relation:

$$h_{cat,ext} = h_{ce1} + h_{ce2} \cdot \sqrt{V} \quad (10.72)$$

The  $\dot{Q}_{gen,cat}(t)$  is the result of chemical exothermal reactions of HC/CO oxidation in the catalyst and can be estimated with the following equation:

$$\dot{Q}_{gen,cat}(t) = \dot{m}_{HC} \cdot LHV_{HC} + \dot{m}_{CO} \cdot LHV_{CO} \quad (10.73)$$

where the  $\dot{m}_{HC}$  and  $\dot{m}_{CO}$  are estimated with look-up tables or a neural network with inputs the engine exhaust mass flow rate,  $BMEP$ , engine speed and engine coolant temperature.

The heating flow due to external source  $\dot{Q}_{eh,cat}(t)$  is the results of two terms: the heat gain due to exhaust gas  $\dot{Q}_{egas,cat}(t)$  and the thermal power due to catalyst light-off management  $\dot{Q}_{cat,ligoff}(t)$ .

The first contribution is estimated with the formula:

$$\dot{Q}_{egas,cat}(t) = S_{cat,int} \cdot h_{cat,int}(t) \cdot (T_{exh}(t) - T_{cat}(t)) \quad (10.74)$$

with  $T_{exh}(t)$  the engine exhaust gas temperature estimate with equation (10.26),  $S_{cat,int}$  the equivalent internal surface of catalyst, and  $h_{cat,int}$  the heat transfer coefficient, depending on engine exhaust gas mass flow rate with the mathematical relation:

$$h_{cat,int} = h_{ci1} + h_{ci2} \cdot \sqrt{\dot{m}_{exh}} \quad (10.75)$$

The light-off thermal power  $\dot{Q}_{cat,ligoff}(t)$  is defined by a PI controller to achieve the minimal desired catalyst temperature (180÷200 °C). This heat flow is converted in fuel flow, in case of conventional light-off, where combustion is degraded to increase exhaust gas temperature, or in electrical heating power through the following equations

$$\dot{m}_{fuel,ligoff}(t) = \frac{\dot{Q}_{cat,ligoff}}{k_{ligoff} \cdot LHV} \quad (10.76)$$

where  $k_{ligoff}$  (0.2÷0.3) takes into account the efficiency of the fuel conversion in useful heat for heating, according to the analysis carried out in [147]. In case of Electric Heating Catalyst the electric power needed to support the light-off phase is evaluated with the formula:

$$P_{e,ligoff}(t) = \frac{\dot{Q}_{cat,ligoff}}{k_{e-ligoff}} \quad (10.77)$$

where  $k_{e-ligoff}$  (0.7÷0.8) according to [147].

In the catalyst thermal model the temperature of the exhaust gas outlet catalyst is evaluated as input for downstream WHR systems:

$$T_{cat,out}(t) = T_{exh}(t) - \frac{\dot{Q}_{egas,cat}(t)}{cp_{exh} \cdot \dot{m}_{exh}} \quad (10.78)$$

with  $cp_{exh}$  the specific heat of exhaust gas. The model of electric catalyst heating has been validate comparing the cat temperature presented in [147] and [148] for ICE based vehicles in different driving cycles.

## 10.6 Vehicle and Powertrain Model Validation

The models have been validated comparing the performance, fuel consumption and CO<sub>2</sub> emission of different vehicle segments with the claimed values. The considered vehicles have been ICE based (gasoline and diesel) and pure electric types.

The available efficiency maps of the engines and of the electric motors have been scaled through the Willans approach to obtain the missing data of the powertrains used for the validation.

The machine features used as baseline are listed below:

- 4 cylinder 1.4L Turbo GDI engine, 130 HP, see Figure 10-10 for the BSFC;
- 4 cylinder 2.0L Turbo GDI engine, 280 HP;
- 4 cylinder 2.2L Turbo CR diesel engine, 150 HP;
- Synchronous IPM electric traction drive, 48V 25 kW.

The aerodynamic characteristics, the masses of vehicles and the transmission data have been obtained from technical datasheets of vehicles.

The following table summarizes the results of the QSS model versus the claimed data of the car manufacturers. The maximum error for the acceleration time is lower than 3%, whereas the errors for the Fuel Consumption (FC) and CO<sub>2</sub> emission of ICEVs is below 4% and the energy consumption of BEVs is lower than 2%.

Table 10-3 Vehicle and Powertrain Model validation with different vehicle/powertrain architectures

		C-Segment		D-Segment		SUV	
Vehicles with ICE-GDI		Engine 1.5 TGDI 130 HP		Engine 2.0 GDI 200 HP		Engine 2.0 TGDI 280 HP	
Requirements	Unit	Claimed	Simulation	Claimed	Simulation	Claimed	Simulation
CO <sub>2</sub> in NEDC	g/km	113	115.4	138	138.8	161	161.8
FC in NEDC	L/100km	4.9	5.1	6	6.1	7.0	7.0
FC on ECE	L/100km	6.2	6.3	8	8.2	8.9	8.7
FC on EUDC	L/100km	4.2	4.3	5	4.9	5.9	6.0
Time 0-100 Km/h	sec	9.1	8.9	6.6	6.5	5.7	5.6
Vehicles with ICE-Diesel CR		Engine 1.6 TDI CR 150 HP		Engine 2.2 TDI CR 180 HP		Engine 2.2 TDI CR 210 HP	
CO <sub>2</sub> in NEDC	g/km	102	99.4	109	110.5	127.0	124.0
FC in NEDC	L/100km	3.9	3.8	4.2	4.2	4.8	4.7
FC on ECE	L/100km	4.1	4.0	5.3	5.1	5.5	5.3
FC on EUDC	L/100km	3.8	3.7	3.5	3.7	4.4	4.3
Time 0-100 Km/h	sec	8.6	8.5	7.1	7.2	6.6	6.5
Electric Vehicles		Nissan Leaf 2016				Tesla X 90 PD	
Requirements	Unit	Claimed	Model			Claimed	Model
Range NEDC	km	250	245			467	458
Consumption NEDC	kwh/100 km	14.7	14.5			19.3	19.6
Time 0-100 Km/h	sec	11.3	10.9			3.9	4.0

Figure 10-20 illustrates the model simulations of Fuel Consumption, Power and the engine operating point of a SUV equipped with a 280 HP TGDI engine in NEDC.

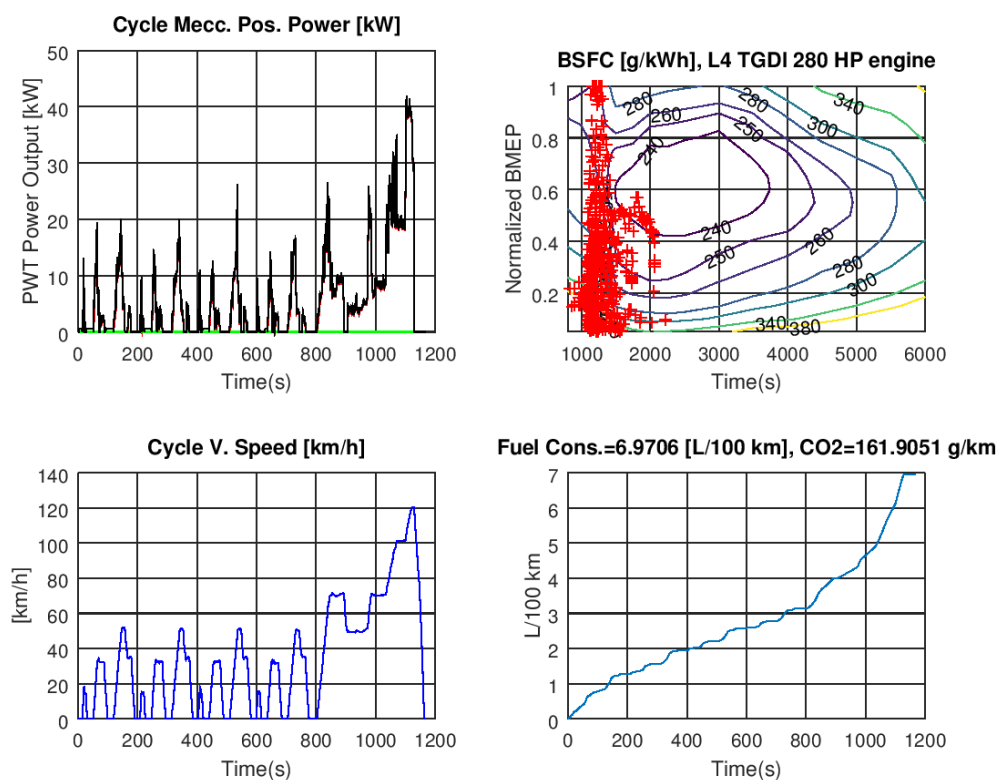


Figure 10-20 NEDC Simulation of SUV equipped with 2.0L TGDI engine

Furthermore, Figure 10-21 and Figure 10-22 illustrate the comparison of simulated and measured values of fuel mass flow rate and engine coolant temperature during NEDC. The results show a good agreement of the model and experimental data.

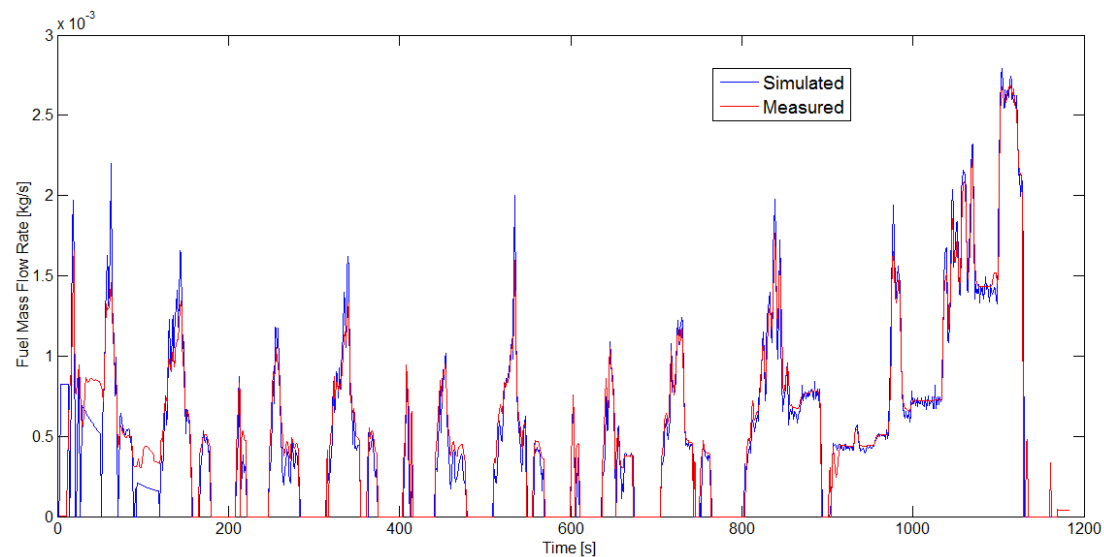


Figure 10-21 Results of Fuel mass flow rate simulation in a SUV equipped with 2.0L TGDI engine during NEDC

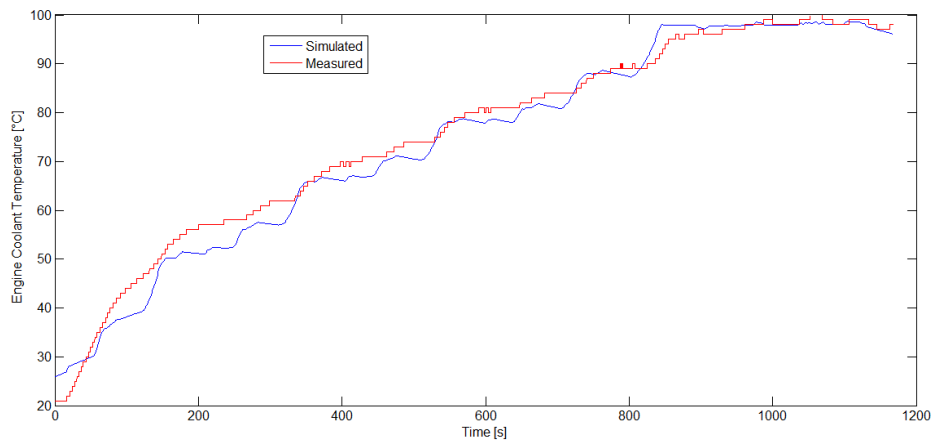


Figure 10-22 Results of Engine coolant simulation in a SUV equipped with 2.0L TGD engine during NEDC

For BEV the measurements were not available, but only the claimed data. Figure 10-23 shows the simulation of Energy consumption, the operating points of the electric motor and the battery SOC in NEDC for a C-Class BEV (Nissan Leaf), equipped with a 80 kW electric motor and a battery of 30 kWh.

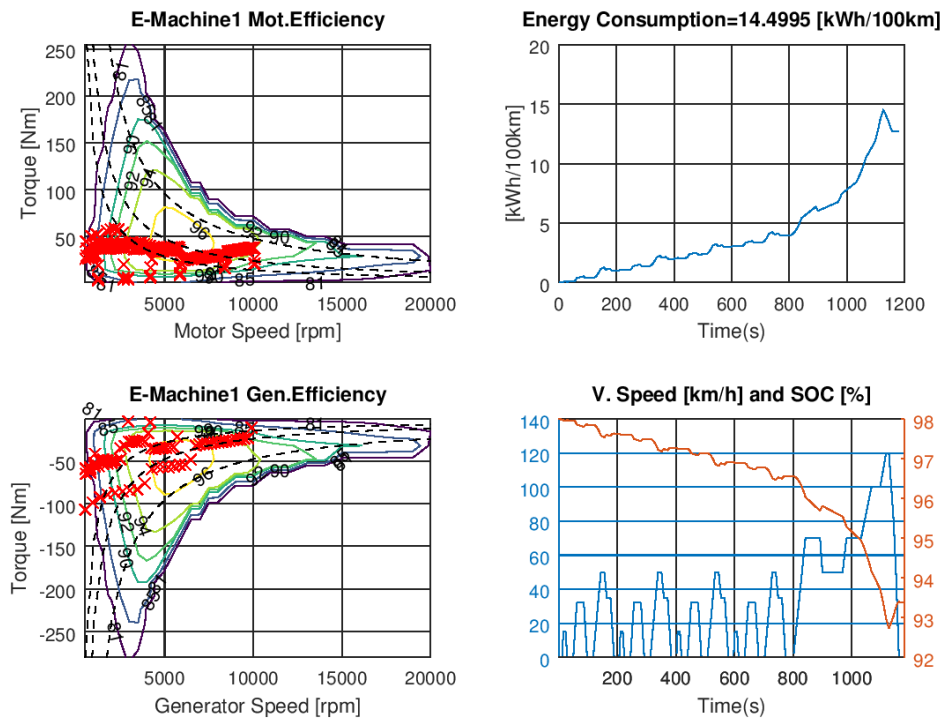


Figure 10-23 NEDC Simulation of C-Class BEV (Nissan Leaf) equipped with a 80 kW electric motor and a battery of 30 kWh

A further validation of the model has been performed with regard to the CO<sub>2</sub> impact of ICE technologies presented in the Chapter #6.3, by means of the comparison with literature review outcomes, see Table 6-1. The cumulative trends in fuel consumption on NEDC cycle for a C-segment vehicle equipped with the a 1.4L TGD engine and with some of the technologies presented in Chapter #6.3 are shown in Figure 10-24; moreover, in Table 10-4, all the most meaningful technologies and their combinations are analyzed; their savings in fuel/CO<sub>2</sub> both in NEDC and WLTC are shown. The CO<sub>2</sub> estimation through the model is 125 g/km in NEDC cycle against 123 g/km of the real emission concerning the baseline vehicle.

The mass of the baseline vehicle (only ICE) was considered equal to 1350 kg, whereas it has been increased by 40 kg for a 48 Volt 22kW hybrid in P2 configuration and 1 kWh of battery capacity.

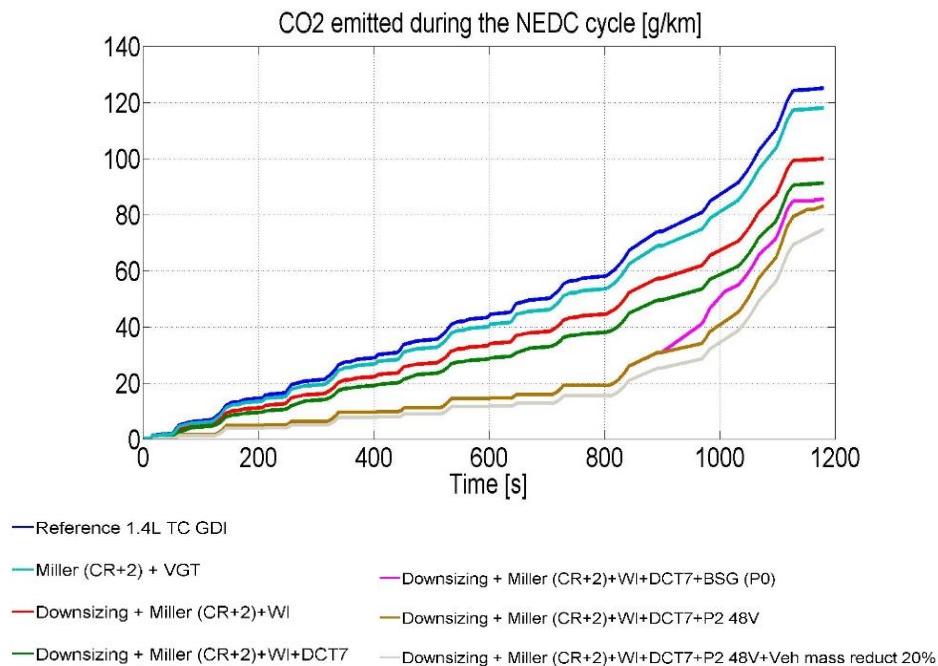


Figure 10-24 CO<sub>2</sub> evaluation on NEDC for different technology mix

From Figure 10-24 and Table 10-4, it is clearly shown that the benefits given by each technology are not additive and that the contribution of the electrification decreases with increasing the efficiency of ICE, especially in the WLTC cycle which is characterized by a higher average load. As it can be observed, the estimation of the improvements related to the analyzed technologies is aligned with the values highlighted in the bibliography.

Table 10-4 Fuel benefit of ICE technologies vs. baseline engine estimated and from literature data

Technology	CO <sub>2</sub> /Fuel Saving in NEDC [%]		CO <sub>2</sub> /Fuel Saving in WLTC [%]	
	Model	Literature	Model	Literature
BaselineTC, GDI, S&S	1.4L, 4Cyl	1.0L+2.0L, TC, 3/4 Cyl	1.4L 4Cyl	1.0L+2.0L, TC, 3/4 Cyl
Miller Cycle (CR +2)	6	5+12	5	5+12
2stage VCR (CR +2)	4	4+9	5.5	4+9
Port Water Inj. (CR +2)	4	4.4	6.0	4+6.5
Electronic Cyl Deactivation	5	7	5	
Cylinder Deactivation	7	-	6	10
LP-EGR/ HP-EGR	3.5	-	3	3+4
Miller Cycle+ WI	10	-	9	-
Miller Cycle+VCR	10	-	9	5+9
2st.-Turbo (3cyl + downsp)	12	12+18	12	-
eBooster (3cyl + downsp)	12	12+18	12	-
BSG	8	5 + 10	6	5+6
BSG+eBooster+ 3 cyl+ downspeeding	14	12+18	10	6
BSG+eBooster+WI (CR +2) 3 cyl+ downspeeding	15	-	12	-
P2 48Volt 22kw	20	15+20	18	-
P2 48V 22kw +Miller +WI	28	-	24	-



## 10.7 Modeling of Waste Heat Recovery Technologies

In Chapter #6.9, comparing the WHR technologies, the Fast Warmup and Rankine Cycle systems have received the preference in terms of effectiveness and costs. In this section the focus on the modelling of the RC system is presented. Moreover, the TEG [34] and Electric Turbo-Compound [38] models and their application to 1.3L Diesel engine were illustrated in previous published works with University of Salerno. The Fast Warm up system model can be considered as a sub-case of the evaporator or condenser model in the RC system, considering the proper properties of the fluids in the heat exchanger.

### 10.7.1 Rankine Cycle Modeling

The reference plant, whose scheme is depicted in Figure 10-25, considers a Rankine Cycle system thermally coupled to the engine exhaust pipe and mechanically to an electric generator. In HEVs the expander can be considered linked in parallel to P0, P1 or P2 machine by means of a clutch CLT1 for the decoupling of the machines. A second clutch CLT2 allows to generate electric power only with RC system.

The evaporator is placed downstream the catalyst in exhaust line, thus the exhaust gases downstream the catalyst is considered as hot fluid for the evaporator and environmental air the cold fluid for the condenser. The evaporator of the RC system is described through a grey-box model that takes in account the equations describing both thermodynamic and heat exchange phenomena. The data for model definition and validation was derived from [174]. The components (pump, expander and condenser) are modeled through a black-box approach. Moreover, an optimal sizing for all components is needed in order to obtain the best results with reference to vehicle application.

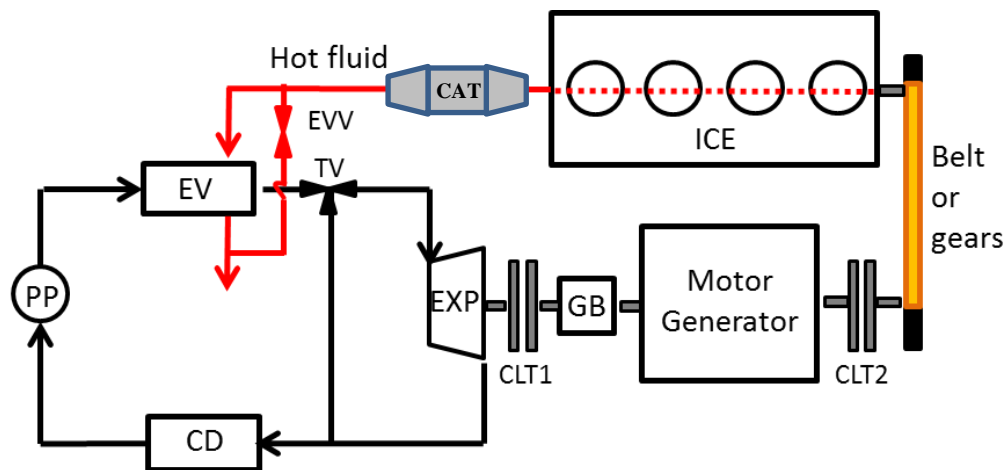


Figure 10-25 Scheme of RC system utilizes the exhaust gas as heat source and integration with hybrid powertrain

As aforementioned, a Rankine Cycle is aimed at harvesting the waste heat from the engine by the heat exchange between a working fluid and engine exhaust flow. The operating fluid follows an evaporation process within the heat exchanger, afterwards it evolves as superheated vapor in a volumetric expander (e.g. Scroll) directly coupled to electric machine and/or the engine. The electrical energy is stored into a battery pack and used to feed auxiliaries and/or the electric traction drive, in case of HEVs. The Figure 10-26 shows the relationships among the system components.

The input variables of the RC system are the pump rotational speed, which sets the organic fluid flow rate, and the expander rotational speed, which influences the evaporation temperature. These control variables

are managed in order to optimize the cycle efficiency, for each engine working conditions. Furthermore, the following hypotheses are assumed: i) the condensation pressure is set constant; ii) the cooling of the working fluid in liquid phase into the condenser is set constant; iii) the outlet temperatures of pump and expander are evaluated through a polytropic process [133]. In the following paragraphs, the sub-models of the RC system components are described.

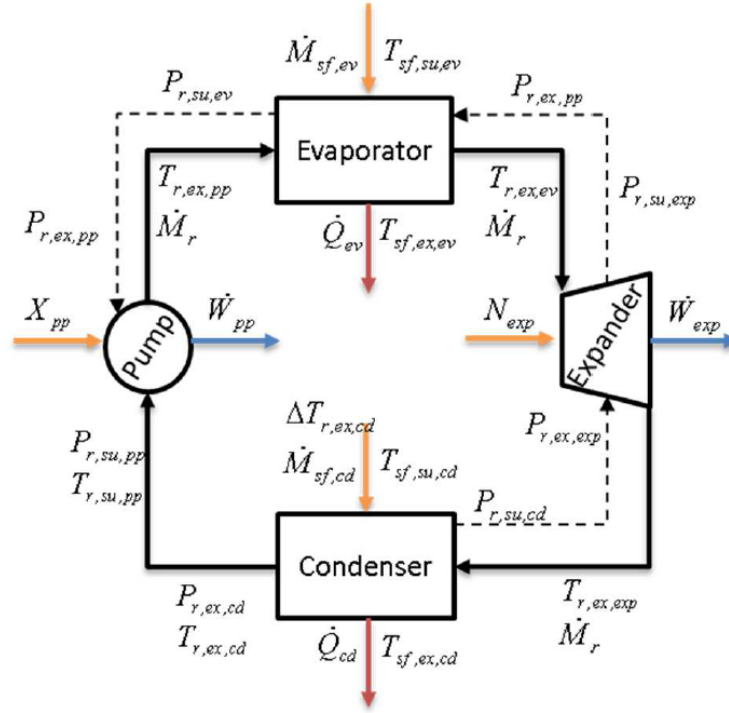


Figure 10-26 Scheme of the Rankine Cycle plant model

### Pump model

The volumetric pump considered for the RC system has been modeled through a black-box approach that implies the characterization of isentropic efficiency as a function of working fluid mass flow rate and enthalpies in the suction and exhaust sections [133]. The mass flow through the pump  $\dot{m}_r$  was evaluated by the following equation:

$$\dot{m}_r = \frac{X_{pp} \cdot \dot{V}_{pp,max}}{v_{in,p}} \quad (10.79)$$

where  $X_{pp}$  is the pump volumetric fraction, linked to the operating frequency,  $\dot{V}_{pp,max}$  is the maximum pump flow rate and  $v_{in,p}$  is the specific volume of the working fluid in the suction section. The pump power  $\dot{W}_{pp}$  was then evaluated by the equation:

$$\dot{W}_{pp} = \frac{\dot{m}_r \cdot (h_{ex,p,is} - h_{in,p})}{\eta_{pp}} \quad (10.80)$$

where  $\eta_{pp}$  is the pump efficiency,  $h_{ex,p,is}$  and  $h_{in,p}$  are the exhaust isentropic and inlet pump enthalpy, respectively.

## Evaporator model

The evaporator is a countercurrent type and it is divided into three zones, each one is representative of the working fluid physic state. The purpose of this model is to evaluate the outlet heat exchanger temperature of both fluids by considering the transferred heat and neglecting the pressure drop along the pipes. The exhaust engine flow rate represents the hot fluid while the RC working fluid is the cold one. The evaporator was firstly modelled by means of a grey-box approach, afterwards a black-box model has been developed to achieve lower computational burden. The scheme of the countercurrent evaporator is reported.

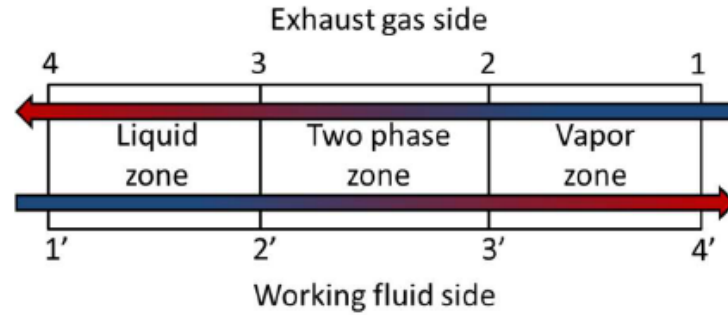


Figure 10-27 Scheme of the countercurrent evaporator [133]

### Grey-box model

The grey-box model assumes as input variables the flow rates and the inlet temperatures of both the working and the hot fluid, the evaporating pressure, the thermal transmittance for each zone and the total exchanging area. The total area was evaluated with the following equation

$$A_l + A_v + A_{tp} = (N_p - 2) \cdot L \cdot W \quad (10.81)$$

where  $A$  represents the exchanging area of the several zones of the evaporator,  $N_p$  the numbers of plates of the heat exchanger,  $L$  and  $W$  the length and the width of the heat exchanger plates, respectively. The thermal transmittance  $U$  for each zone is evaluated by means of the following equation

$$\frac{1}{U} = \frac{1}{h_r} + \frac{1}{h_{sf}} \quad (10.82)$$

where  $h_r$  and  $h_{sf}$  are the convective resistances of organic and secondary fluid respectively. In case of a single phase zone, these parameters are dependent on fluid speed and viscosity by means of Reynolds, Prandtl and Nusselt numbers. On the other hand, in case of two phases, as during boiling and condensation processes, the parameters are calculated by the Hsieh and Kuo correlations, respectively [174]. By applying the thermal energy equation for each zone, the following set of nonlinear equations is obtained

$$\begin{aligned} \dot{Q}_l &= m_{hf} c_{p,hf} (T_3 - T_4) \\ \dot{Q}_{lat} &= m_{hf} c_{p,hf} (T_2 - T_3) \\ \dot{Q}_{surr} &= m_r c_{p,r} (T_{4'} - T_{3'}) = m_{hf} c_{p,hf} (T_1 - T_2) \end{aligned}$$

$$\begin{aligned}
\dot{Q}_l &= A_l U_l \left( -\left( \frac{T_{1'} + T_{2'}}{2} \right) + \left( \frac{T_4 + T_3}{2} \right) \right) \\
\dot{Q}_{lat} &= A_{tp} U_{tp} \left( \left( \frac{T_2 + T_3}{2} \right) - T_{2'} \right) \\
\dot{Q}_{surr} &= m_r c_{p,r} (T_{4'} - T_{3'}) = A_v U_v \left( \left( \frac{T_2 + T_1}{2} \right) - \left( \frac{T_{3'} + T_{4'}}{2} \right) \right) \\
A_l + A_v + A_{tp} &= (N_p - 1) \cdot L \cdot W
\end{aligned} \tag{10.83}$$

The model outputs are the areas of each zone and the outlet temperatures of organic and secondary fluids. The grey-box model is applied to evaluate the heat exchanger efficiency vs. the engine operating conditions, in order to calibrate the black-box model parameters [133].

### **Black-box model**

The black-box model is based on synthetic functional relationships with the aim to speed-up the computational time for potential real-time application [133]. The model parameters are calibrated by a set of data, generated by exploiting the grey-box model in a wide engine operating range.

The modeling approach used for the countercurrent evaporator is known in literature as  $\varepsilon$ -NTU method. The total transferred heat within the evaporator was calculated through the following equation

$$\dot{Q}_{ev} = \varepsilon \cdot c_{min} \cdot \Delta T_{max} \tag{10.84}$$

where,  $\varepsilon$  is the efficiency of the exchanger,  $c_{min}$  is the minimum thermal flow among the fluids and  $\Delta T_{max}$  is the maximum temperature difference over the exchanger and is evaluated by subtracting the inlet organic fluid temperature  $T_{1'}$  from the inlet hot fluid temperature  $T_1$ . The exchanger efficiency was previously characterized as a function of the fluids flow rates and  $\Delta T_{max}$ . The outlet hot fluid temperature  $T_4$  is the result of the equation (10.84) by considering the power balance over the hot fluid.

$$\dot{Q}_{ev} = \varepsilon \cdot c_{min} \cdot \Delta T_{max} = m_{hf} \cdot c_{p,hf} \cdot (T_4 - T_1) \Rightarrow T_4 \tag{10.85}$$

By imposing the equality between the equation (10.84) and the sum of liquid phase heating  $\dot{Q}_l$ , latent heat  $\dot{Q}_{lat}$  and vapor phase superheating  $\dot{Q}_{surr}$ , the outlet cold fluid temperature  $T_{4'}$  was evaluated

$$\dot{Q}_{ev} = \varepsilon \cdot c_{min} \cdot \Delta T_{max} = \dot{Q}_l + \dot{Q}_{lat} + \dot{Q}_{surr} \Rightarrow T_{4'} \tag{10.86}$$

### **Scroll expander model**

The Scroll expander is the tread-off between efficiency, reliability and cost, as already explained in previous chapter. For this reason is preferred in this study.

The Scroll expander model evaluates the adiabatic efficiency and the filling factor, both expressed as function of the RC fluid density in the expander inlet, expander rotational speed and expansion ratio. The inlet fluid specific volume  $v_{in,exp}$  can be determined by using the filling factor  $\phi$ , previously identified on experimental data [174].

$$v_{in,exp} = \frac{\phi \cdot \dot{V}_{s,exp}}{\dot{m}_r} \quad (10.87)$$

Thus, the inlet expander pressure can be evaluated once the inlet density and temperature are known. The expansion was modeled as a two-step process: an adiabatic reversible expansion and a constant volume expansion, as reported in the following equation

$$\dot{W}_{exp} = \dot{m}_r \cdot [(h_{in,exp} - h_{m,is,exp}) + v_{in,exp} \cdot (P_{m,exp} - P_{ex,exp})] \quad (10.88)$$

### Condenser model

The condenser model is based on the same black-box approach of the evaporator. The exchanger efficiency is expressed as a function of the RC fluid flow rate and the inlet temperature of both working fluid and cold fluid (i.e. ambient air). This model is used to evaluate the cold fluid outlet temperature while the working fluid outlet temperature is considered constant by imposing either the condensation pressure and the liquid cooling.

### RC model validation

The models of the RC components were validated against literature experimental data [174]. A good correlation is obtained for each model, ranging from 0.85 to 0.98. The graphs in Figure 10-28 show the comparison between predicted and measured adiabatic efficiency of the pump, thermal power of evaporator and condenser and expander power, evidencing very good fittings.

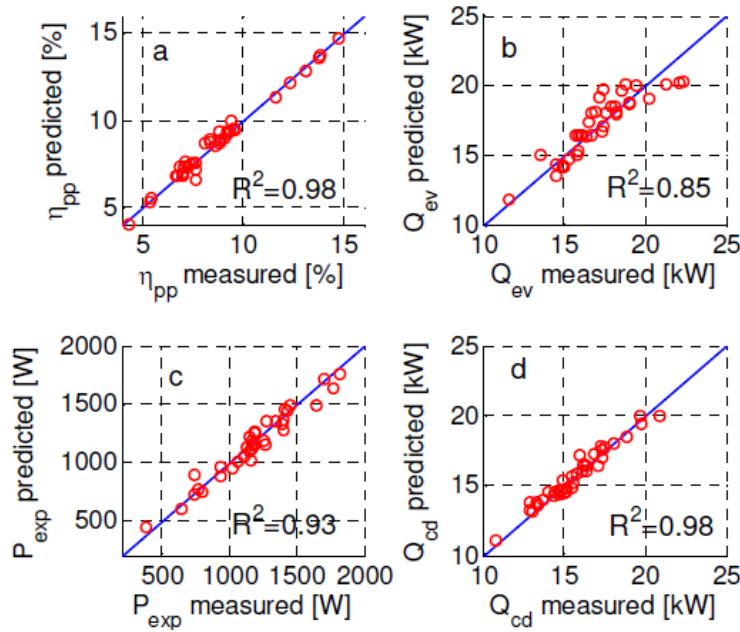


Figure 10-28 Validation results of the RC components models, with respect to literature experimental data: a) pump isentropic efficiency, b) evaporator power, c) expander power, d) condenser power

## RC Component sizing and Control

The pump displacement has to be defined according to the engine working conditions (i.e. exhaust temperature and flow rate), to obtain a balanced heat flow from the exhausted gases towards the working fluid.

The countercurrent evaporator is composed of  $N$  plates with a specific size. The exchanging area sizing can be assessed through a sensitivity analysis on the grey-box model in order to obtain, in the worst conditions, a title equal to 1 at the exchanger outlet. A similar approach can be used for the condenser; particularly, the exchanging area is chosen to have an optimal condensation pressure. A further analysis can be carried out, taking into account the possibility to use the engine coolant fluid in the condenser, against the ambient air. This choice results in higher coolant temperature (323 K with respect to 296 K assumed for the ambient air), but a more compact condenser size, due to the higher heat exchange coefficient of coolant fluid than the ambient air.

The Scroll expander volume is defined by means of a sensitivity analysis in order to maximize the RC output power according to engine operating conditions. Therefore, the expander displacement is set to be suitable for the pump characteristics.

The RC system presents two control variables, namely pump and expander rotational speed, and two external inputs corresponding to the exhaust gas flow rate and temperature. The evaporation temperature (and pressure) is controlled through the expander rotational speed, while the overheating is imposed by regulating the coolant mass flow rate, operating on the pump working frequency. In order to maximize the RC thermodynamic efficiency along the vehicle driving transient, an optimization analysis has to be carried out to evaluate the reference values of evaporation temperature ( $T_{ev}^*$ ) and overheating ( $\Delta T_{3'4}^*$ ). The optimization process has to consider the following constraints on:

- i) the maximum working fluid temperature, that must be lower than the critical temperature;
- ii) the exhaust gas temperature downstream the evaporator, that must be maintained within a suitable range to guarantee efficient catalyst operation.

For the RC system control, both reference evaporation temperature and overheating are expressed as function of the engine exhaust flow rate and temperature. It is worth noting that the most efficient working condition can be identified through the following path:

- i) reduction of the minimum temperature and pressure of the organic fluid;
- ii) decrease of the evaporator overheating;
- iii) identification of the optimal evaporation temperature and pressure, see Figure 10-29.

This latter task has to be pursued by considering the following opposite effects: on the one hand, an increase of the evaporation temperature results in better cycle efficiency and greater expander specific work, due to the higher pressure ratio; on the other hand, it leads to lower adiabatic efficiency of the expander, due to the major losses.

The RC system control (see Figure 10-30) is performed by applying two PI controllers to the pump frequency and the expander rotational speed: the first one operates adapting the working fluid overheating to the reference value, the latter works on the error between the effective and the reference evaporation temperature.

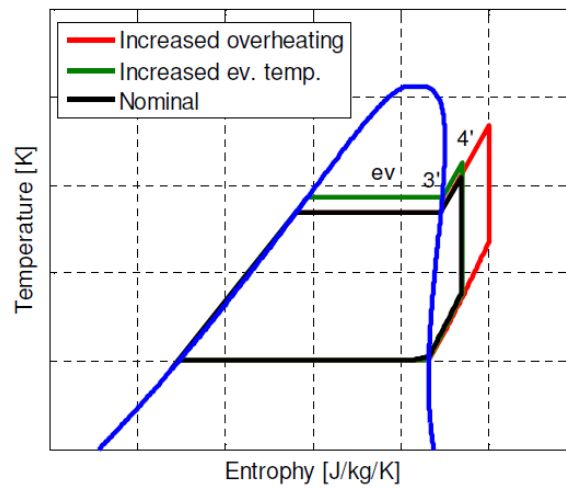


Figure 10-29 Qualitative representation of the RC on T-s diagram in nominal condition (black curve) against the cycles obtained with variation of overheating (red curve) and evaporation temperature (green curve) [133]

An increase of the working fluid flow rate, due to a high pump speed, results in a lower heat exchange and in increased intake expander pressure and density with enhanced expander efficiency and output power. A reduction of the expander speed, at constant flow rate, leads to increased evaporation pressure and, consequently, thermodynamic cycle efficiency [133].

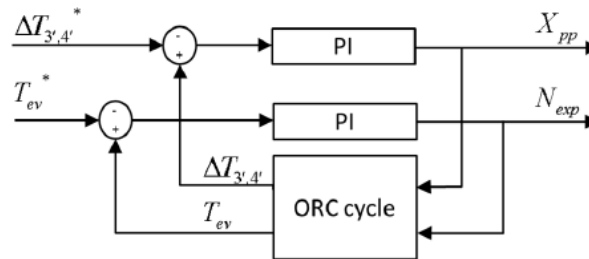


Figure 10-30 Scheme of the RC system control [133]

## 10.8 Total Cost of Ownership Model

The cost is a fundamental aspect to evaluate a technology from industrial point of view. Indeed the engineering value of a technology, that is an indicator of the market penetration, depends on costs as already presented in equation (3.2).

Following an economic model to estimate the vehicle cost from the end-user point of view, with focus on powertrain, is presented. The next Figure 10-31 can help to clarify the model.

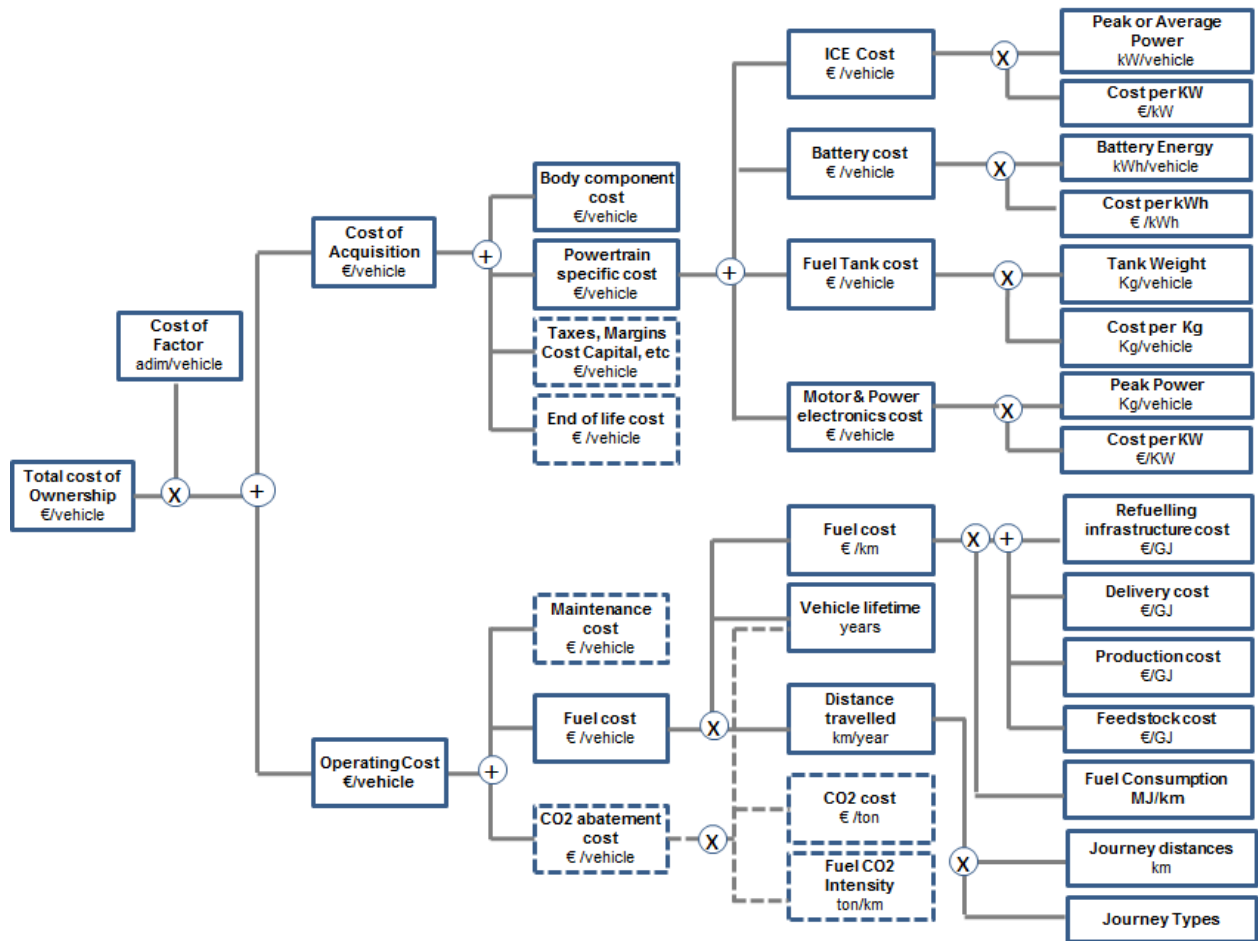


Figure 10-31 Scheme of model to evaluate vehicle Total Cost of Ownership

The vehicle Total Cost of Ownership is the result of two main terms:

$$TCO = CoA + CoO \quad (10.89)$$

where CoA and CoO are respectively the Cost of Acquisition and the Operating Cost, expressed in [€/vehicle].



### Vehicle Cost of Acquisition

The first term of equation (10.89) can be divided in cost of vehicle body  $Cost_{Body}$  and powertrain cost  $Cost_{PWT}$ , neglecting the potential cost coming from capital and end of life, reported in Figure 10-31.

$$CoA = (Cost_{Body} + Cost_{PWT}) \cdot CostFact \quad (10.90)$$

The CoA depends on technical factors, car manufacturers costs, margin and business strategy. These aspects are considered with an average factor  $CostFact$ , that can vary in the range 1.5÷1.8.

For the analysis the  $Cost_{Body}$  is assumed depending on vehicle segment and, considering an average market value of vehicle from which is subtracting the powertrain cost, it is determined according the following formula

$$Cost_{Body} = \frac{Vehicle\ Cost\ in\ Market}{CostFact} - Cost_{PWT, Ref} \quad (10.91)$$

where the  $Cost_{PWT, Ref}$  is equal to ICE cost, since the reference vehicle is typically equipped with thermal combustion engine, and it is calculated as

$$Cost_{PWT, Ref} = Cost_{ICE, Ref} = UnitPowerCost_{ICE} \cdot P_{ICE} \quad (10.92)$$

in which the cost of engine for unit power  $UnitPowerCost_{ICE}$  is in  $\left[\frac{\text{€}}{\text{kW}}\right]$  and the ICE power  $P_{ICE}$  is expressed in [kW]. [176] indicates an average unit power cost for the ICE equal to 15 €/kW.

To consider the introduction of new powertrain technologies, the  $Cost_{PWT}$  is the result of

$$Cost_{PWT} = Cost_{ICE} + Cost_{ETD} + Cost_{ETD,Transm} + Cost_{BAT} \quad (10.93)$$

where

$$Cost_{ICE} = Cost_{ICE, Ref} + \Delta Cost_{ICE Techs} \quad (10.94)$$

with  $\Delta Cost_{ICE Techs}$  evaluated by means of Table 6-5. The cost due to the fuel tank is included in the ICE cost, in case of liquid fuel.

The ETD cost is evaluated with the expression:

$$Cost_{ETD} = UnitPowerCost_{ETD} \cdot P_{ETD} \quad (10.95)$$

in which the cost of ETD for unit power  $UnitPowerCost_{ETD}$  is in  $\left[\frac{\text{€}}{\text{kW}}\right]$  and the ETD power  $P_{ETD}$  is expressed in [kW]. [67,176 ,229] indicate the unit power cost for the ETD equal to 30€ today and ~ 20 €/kW expected in 2025.

The  $Cost_{ETD,Transm}$  is due to the transmission devices that connect ETD to the driveline. It depends on power and architecture, but a constant average value is assumed in the range 200÷400 €.

For the battery cost in [€], the following simplified estimation is used:

$$Cost_{BAT} = EnergUnitCost_{BAT} \cdot E_{BAT} \quad (10.96)$$

where  $E_{BAT}$  is the battery capacity in [kWh] and  $EnergUnitCost_{BAT}$  is the cost of battery per energy unit expressed in  $\left[\frac{€}{kWh}\right]$ . Considering Li-Ion technology [67,176] indicate a fork between 250÷350 €/kWh.

### **Vehicle Operating Cost**

The evaluation of vehicle operating cost CoO is the result of two terms

$$CoO = Cost_{Maintenance} + Cost_{Energy} \quad (10.97)$$

The maintenance cost depends on the life of the vehicle and it can be neglected for pure ICE powertrain compared with the energy cost. In case of electrified powertrain the maintenance cost is considered equal to the battery cost (10.96), due to the battery substitution when the vehicle overcomes a certain mileage.

The  $Cost_{Energy}$  is the sum of two terms:

$$Cost_{Energy} = Cost_{Fuel} + Cost_{Electricity} \quad (10.98)$$

where

$$Cost_{Fuel} = Cost_{Fuel/L} \cdot \frac{Fuel\ Consumption}{100} \cdot Distance_{ICE} \quad (10.99)$$

with  $Cost_{Fuel/L}$  in [€/L], the Fuel Consumption in [L/100km] and  $Distance_{ICE}$  the mileage covered with thermal engine in [km];

$$Cost_{Electricity} = Cost_{Electricity/kwh} \cdot \frac{Energy\ Consumption}{100} \cdot Distance_{ETD} \quad (10.100)$$

with  $Cost_{Electricity/kwh}$  in [€/kwh], the Energy Consumption in [kwh/100km] and  $Distance_{ETD}$  the mileage covered in electric mode in [km].

In case of HEV, the  $Cost_{Electricity}$  is zero because the primary source is only the fuel.

It can be noted that the fuel and energy cost decrease with the improvement of global vehicle efficiency.

The fuel and energy consumption are the output of vehicle/powertrain models presented in the previous sections of this chapter.

## Breakeven Distance

The Breakeven Distance indicates the value for which the TCO of a vehicle with the evaluated technologies becomes lower than TCO of a vehicle considered as baseline.

## 10.9 Lifecycle Cost Model for Hybrid Vehicle Architectures

Comprehensive objective evaluation of technologies can only be achieved under consideration of the entire product lifecycle. The CO<sub>2</sub>-equivalent (CO<sub>2</sub>e) emissions and energy consumption of different drivetrain technologies can be evaluated according the simplified scheme in Figure 10-32.

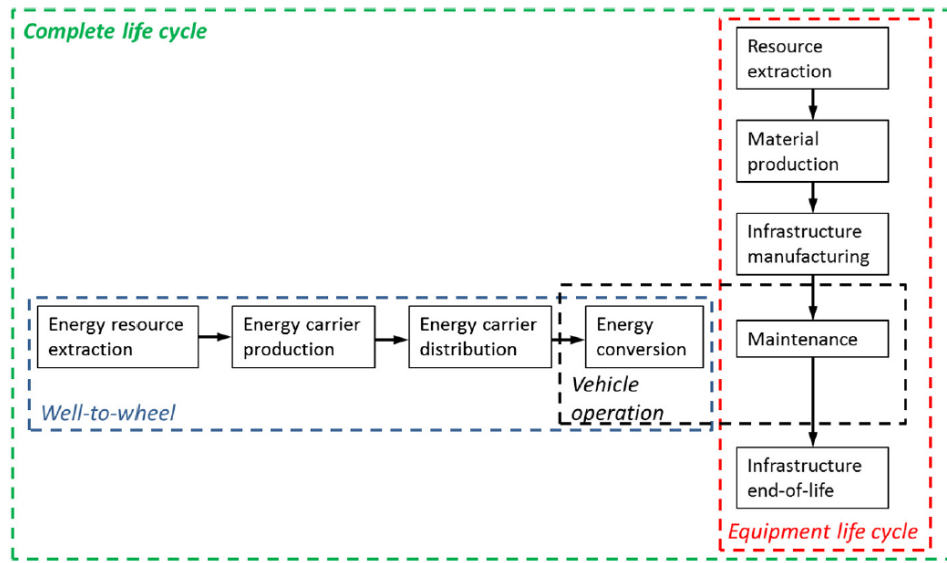


Figure 10-32 Simplified scheme of LCA scope adapted from [17]

The *Energy* consumption and *GHG* emission (*CO<sub>2</sub>e*), according to the complete Life Cycle approach, are the results of the following equations

$$\begin{aligned}
 Energy_{LC} &= Energy_{VEH,LC} + Energy_{WTW} \quad \text{in [MJ/km]} \\
 CO2_{LC} &= CO2_{VEH,LC} + CO2_{WTW} \quad \text{in [g CO}_2\text{eq/km]}
 \end{aligned}
 \tag{10.101}$$

where the  $CO2_{VEH,LC}$  is the equivalent CO<sub>2</sub> measured in [g CO<sub>2</sub>eq/km] and  $Energy_{VEH,LC}$  the energy consumed in [MJ/km] for the manufacturing, maintenance and re-cycling of the vehicle, including battery for HEVs and BEVs.

Well-to-Wheel evaluations for CO<sub>2</sub>e and for consumed energy cover the life cycle of energy source up to conversion in the vehicle (i.e. driving), according to the following equations

$$Energy_{WTW} = Energy_{TTW} \cdot (1 + Energy_{WTT}) \quad \text{in [MJ/km]}
 \tag{10.102}$$

where  $Energy_{WTT}$  is expressed in [MJ/MJ] and represents the total expended energy to produce and distribute 1 MJ of energy or fuel.  $Energy_{TTW}$  is the energy consumed to move the vehicle in [MJ/km] and take into account the global vehicle efficiency, including the powertrain.

$$CO2_{WTW} = CO2_{TTW} + (Energy_{TTW} \cdot CO2_{WTT}) \quad [\text{g CO}_2\text{eq/km}] \quad (10.103)$$

where  $CO2_{WTT}$  is expressed in [g CO<sub>2</sub>eq/MJ] and  $CO2_{TTW}$  is the CO<sub>2</sub> produced by the engine for 1 km of vehicle motion.

CO<sub>2</sub> emission and the energy consumption, according to Well-to-Tank evaluation, are the footprints of the whole energy supply processes (e.g extraction, production and distribution).

Whereas Tank-to-Wheel terms measure the efficiency of energy conversion and the CO<sub>2</sub> impacts to move the vehicle. These terms can be evaluated by means of the vehicle and powertrain models presented in the previous sections.

In case of pure electric vehicle the in use emission of CO<sub>2</sub> is zero and the norms define a way to measure the electric energy consumed from Pump-To-Wheels (PTW), including the battery charging consumption named Pump-To-Tank, and vehicle consumption (TTW). As consequence the PTW consumption is the results of two terms according the following equation:

$$Energy_{PTW} = Energy_{PTW} * Energy_{TTW} \quad \text{in [MJ/km]} \quad (10.104)$$

where  $Energy_{PTW}$  is expressed in [MJ/MJ].

In this study an alternative index to TTW is also proposed, with the aim of taking into account the other possible useful functions powered through the energy stored on board the vehicle.

The useful functions are not closely related to the propulsion, but they are auxiliary functions requested by the end-user related to comfort needs (priority in the HoQ1, in the Chapter #4.1), in particular:

- production of electricity for devices on board the vehicle;
- mechanical energy production for the air conditioning system;
- production of thermal energy to heat the passenger compartment.

Figure 10-33 shows the energy flows in three powertrain architectures. The case (A) is a conventional ICE based vehicle, where in addition to the main energy conversion chain to move the vehicle, waste heat is used for cabin heating. In case (B), in a BEV, the heating for the cabin is provided by the electric battery through heating devices. In the third case (C), in a RE-EV, the energy from fuel is used to recharge the battery and the waste heat for the battery and cabin heating. In the first and third architectures the waste heat from ICE performs useful functions that have to be considered to evaluate the global powertrain efficiency.

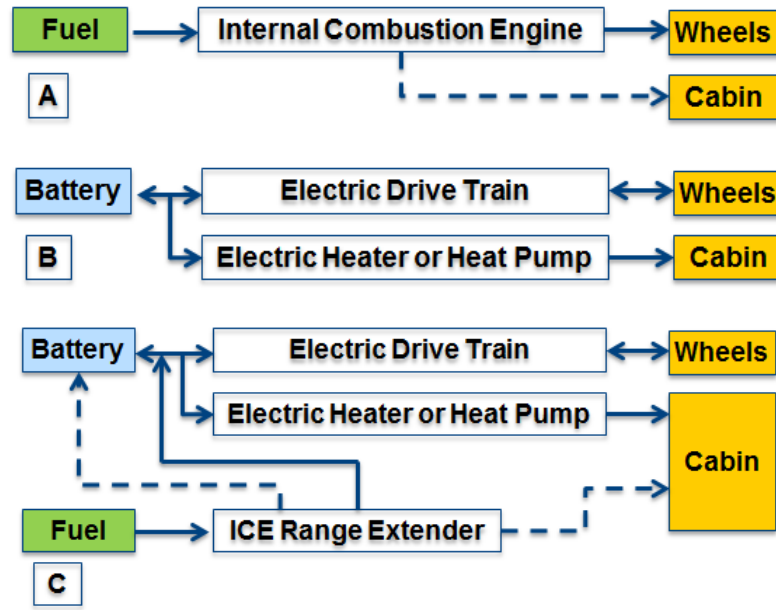


Figure 10-33 Energy flow in different powertrain architectures (dashed line waste heat): (A) ICE vehicle, (B) Battery Electric Vehicle, (C) Range Extender Electric Vehicle

For the aforementioned reasons TTW should include in addition the useful energy not used for traction, leading to a more significant index to evaluate vehicle efficiency. The new index is named Tank-To-Use (TTU) efficiency:

$$Energy_{TTU} = \frac{Energy\ Useful\ in\ Vehicle}{Energy\ Taken\ from\ Tank} \quad (10.105)$$

where

$$Energy\ Useful = Energy_{Propulsion} + Energy_{HVAC} + Energy_{Electric} \quad (10.106)$$

Employing the TTU index is possible to define the Well-to-Use (WTU) index, as an alternative to the WTW index:

$$Energy_{WTU} = Energy_{WTW} \cdot Energy_{TTU} \text{ in [MJ/MJ]} \quad (10.107)$$

with the meaning of the efficiency to obtain the useful energy from the primary source.

The workflow scheme to evaluate the LCA or WTW index is summarized in the Figure 10-34.

The vehicle and powertrain models presented in the previous sections of this chapter are used to evaluate the TTW or TTU indexes and then the WTW or the LCA results, whereas the fuel and vehicle data for the WTT evaluation are obtained from literature analysis, as it will be presented in the case study of Chapter #12.2.

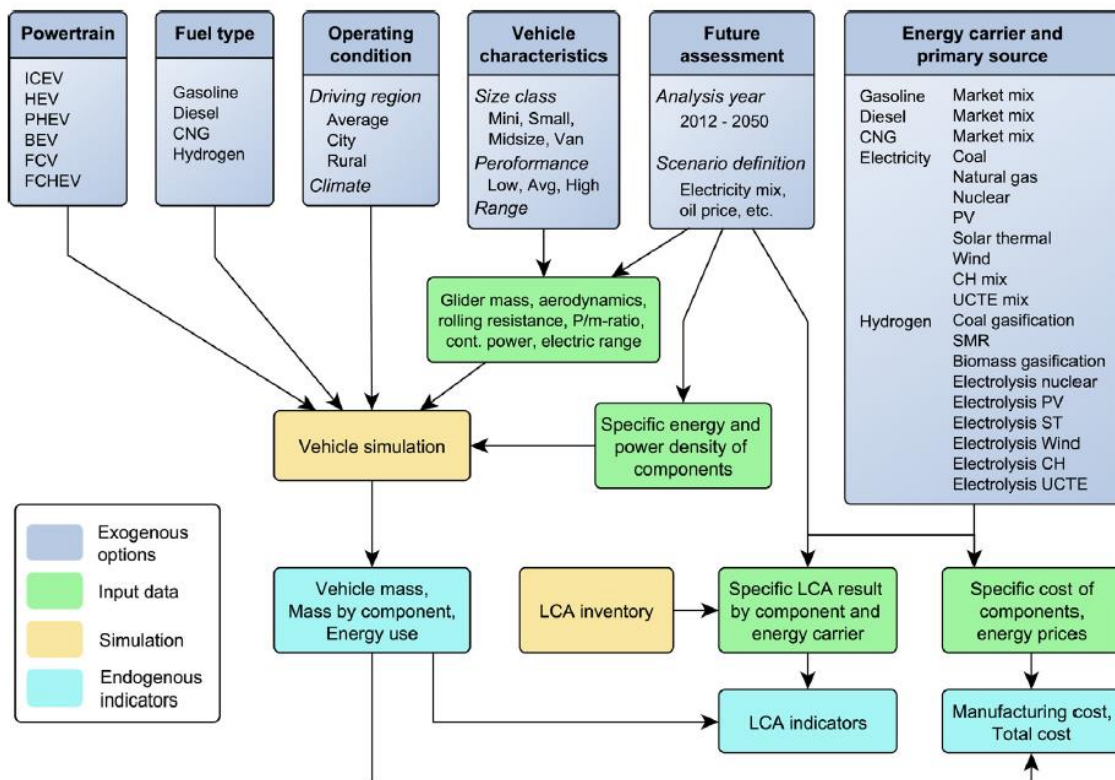


Figure 10-34 Workflow scheme for the LCA/WTW evaluation of Vehicle/Powertrain architectures, adapted from [17]

# 11. Powertrain Management and Controls

For the effectiveness and efficiency of the powertrain and its sub-system the proper management and control are fundamental. Therefore new sensors and sophisticated logics are needed. This trend is supported by an increasing of hardware resources in the new Electronic Control Units, which are able to manage a high number of I/O and run complex algorithms, using multi-core microprocessor architectures. In this context many control solutions can be implemented (e.g. physical based, multi-variable, adaptive controls, etc.).

In some cases the state variables of the systems are not measurable, for cost and/or reliability of the sensors. This is the case of the angular positioning of combustion for engines with Low Temperature approach and Water Injection technology. The use of virtual sensors based on grey-box models and sensors already presented in the engine management system is an effective solution, as confirmed in this study. However a novel multifunction sensor has been developed. It is based on acoustic sensing and allows to implement at affordable cost the measurements of classic engine parameters (such as knock intensity and turbocharger speed) and new parameters (e.g. CN noise), for control and diagnosis purpose.

In this chapter two main subsets of controls will be presented, at Powertrain level and Engine subsystem level.

In the first area, a model based Gear-Shift logic for automated transmissions and a model based Energy Management strategy for HEVs will be described. The main future of these logics is the easy tuning because they are based on the powertrain architecture description, including the engine and the electric machines. For instance, through the efficiency maps knowledge of the engine and electric motor, it is possible to define the command of transmission to obtain the better operating point of the machines.

The second area is related to innovative and virtual sensors used for the fine control and diagnosis of the some new engine technologies previously introduced (e.g. LTC).

## 11.1 Gear-shift Model Based Strategy

The automated transmissions have typically different logics of management that the driver can select. For instance, the transmission management can have priority to achieve high performance or low fuel consumption.

This section presents a model based logic to maximize engine or electric motor efficiency and, at the same time, guarantee the best dynamic performance. This logic has been used in the vehicle and powertrain models employed to design and check the performance of the analyzed powertrain architectures. The gear-shift management has the advantage of an “automatic” tuning, if the characteristic of the powertrain is modified. After the definition of gear number  $N_g$  and their transmission ratios and efficiency, the logic uses the efficiency map of the engine or the electric motor (e.g. in P2 architecture) to define the gear that maximize the energy conversion efficiency of the whole powertrain, without limiting the vehicle dynamic performance.

The following equations describe the workflow to define the optimal gear of a transmission with discrete ratios (not CVT): for each gear  $i$ -th the engine speed  $n_{eng}$  and the maximum wheel torque  $T_{whe}$  are calculated:

$$n_{eng,i} = \tau_i \cdot \tau_{FR} \cdot V_{veh} \cdot K_{wheel} \quad (11.1)$$

$$T_{whe,i} = \max[T_{eng}(n_{eng,i}, T_{oil})] \cdot \eta_{FR} \cdot \eta_i \cdot \tau_i \cdot \tau_{FR} \quad (11.2)$$

Then the maximum deliverable wheel torque

$$T_{whe,max} = \max(T_{whe,i}) \quad (11.3)$$

This value is used to define actual traction torque requested by driver:

$$T_{whe,req} = k_{driver} \cdot T_{whe,max} \quad (11.4)$$

The gears (or gear)  $i_g$  that guarantee the following conditions are found:

$$n_{eng,i_g} \geq n_{eng,idle} \ \& \ n_{eng,i_g} \leq n_{eng,revlim} \ \& \ T_{whe,i_g} \geq T_{whe,req} \quad (11.5)$$

For each of these the corresponding engine Brake Specific Fuel Consumption is calculated:

$$BSFC_{eng,i_g} = BSFC_{eng}(T_{eng,i_g}, n_{eng,i_g}, T_{oil}) \quad (11.6)$$

The optimal gear  $i_g$  is the one related to the minimum  $BSFC_{eng,i_g}$ .

The same logic can be used if the gearbox is linked to the electric motor instead of the internal combustion engine. In P2 architecture the transmission is the same of the ICE, in P4 there is a dedicated gearbox. For the electric motor the last equation become:

$$\eta_{em,i_g} = \eta_{em}(T_{em,i_g}, n_{em,i_g}, T_{em}) \quad (11.7)$$

and in the same manner the optimal gear  $i_g$  is that gives the minimum  $\eta_{em,i_g}$ .

If the transmission is a CVT, the previous calculus steps change slightly, while the core logic still remain the same. In particular, a gear ratio that respects CVT range and all condition written above has to be found.

The same logic can be used to optimize the kinetic energy recovery in HEVs or EVs with electric motor in P2 or P4 layouts. Also in this case, only gear ratios that guarantee motor speed range and braking torque requested have to be selected. From these the gear (or gear ratio in case of CVT) that gives the maximum electric power is chosen as optimal one.

Figure 11-1 shows the comparison in simulation of the proposed algorithm with a classic approach of gear selection based on vehicle speed thresholds. In the example the considered vehicle is a SUV equipped



with a Turbo GDI engine of 280HP and 8 gears AT. In the NEDC, it can be observed that model based logic shifts the operating points of the engine towards lower BSFC conditions, leading to a fuel saving of approximately 2.2%. Nevertheless this benefit, the main advantage of the algorithm is the easy adaptation to the powertrain features, assuming their knowledge, that guarantees an optimal system behavior with lower tuning effort.

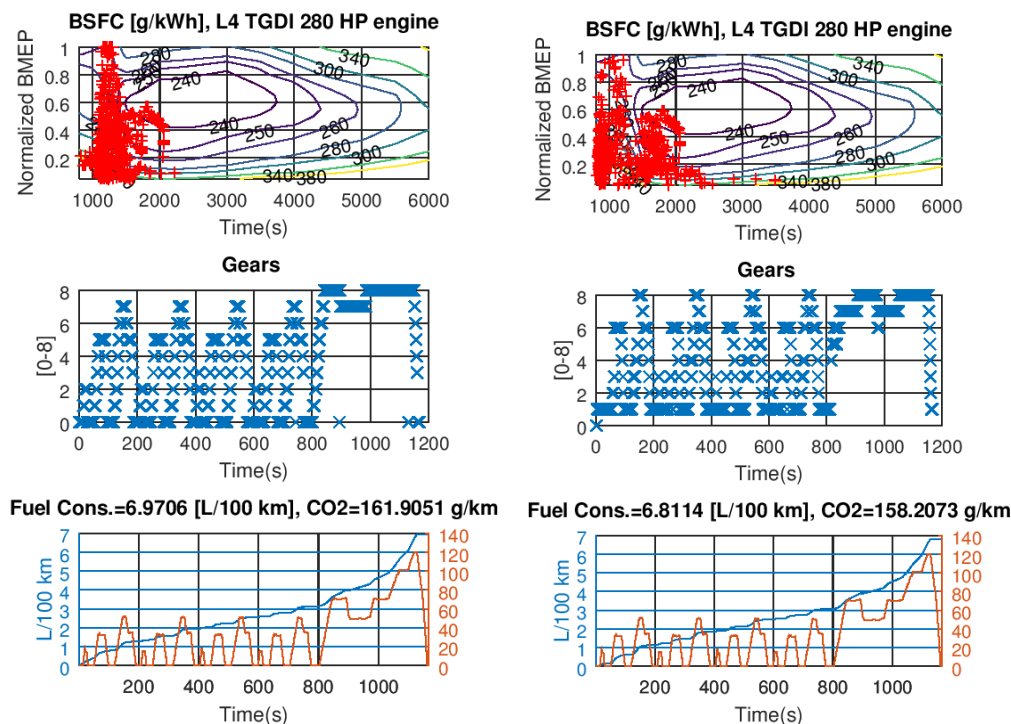


Figure 11-1 Comparison of Gear-shift logics in NEDC for a SUV with 280HP TGDI engine and 8 gears AT: classic approach (left) vs. model based logic (right)

## 11.2 Electric Hybrid Powertrain Energy Management

The energy management of a hybrid powertrain is key to maximize the benefits in terms of fuel consumption and vehicle performance.

Several control methods have been defined that can be classified in two main families:

- Rule Based (RB) strategies.
- Optimized Based (OB) strategies, among these the Dynamic Programming (DP) and Equivalent Consumption Minimization Strategy (ECMS).
- Combinations of control methods are possible. In [251] a comparison of the main strategies is presented and a hybrid method (RB-ECMS) is proposed, the last one on the right in the following Table 11-1. The analysis shows that the RB-ECMS is comparable with DP in terms of performance, but with advantage in the computation time.

In this PhD study two approaches have been employed, depending on knowledge or not of driving profile:

- *rule based logic*, when the mission profile is missing;
- *model based logic*, when the driving cycle is known in advance to the trip starting.

Table 11-1 Comparison of energy management strategies [251]

<i>DP</i>	<i>RB</i>	<i>ECMS</i>	<i>RB-ECMS</i>
+ globally optimal	– sub-optimal	– sub-optimal	– sub-optimal
– apparently unstructured result	– tuning of many parameters, threshold values	+ few calibration parameters	+ few calibration parameters
– long computation time	+ relatively simple, engineering intuition	+ short computation time	+ short computation time
– off line strategy	+ on-/off line strategy	+ on-/off line strategy	+ on-/off line strategy
+ handling nonlinear constraints	– specific rules depend strongly on the topology choice	– $\lambda(t)$ sensitive to $\xi(t)$ deviations	+ modes/rules independent on the topology choice

The proposed model based strategy can be considered an evolution of the methods presented in [251]. Both used logics define two thresholds of requested power to decide the electric motor and/or engine operations, as described in the Figure 11-2, the difference is in the manner the power thresholds are determined.

If the power request is below the iso-power blue line and the battery State of Charge (SOC) is above minimum value, the propulsion is pure electric otherwise the ICE is powered on and the electric motor is switched off. In the ICE propulsion area, the electric power generation can be performed by means of a PI controller that tracks a defined target of SOC. In case of powertrain architectures with two or more electric machines (e.g. power split, P0+P4, etc.) the electric power generation can be carried at same time with electric propulsion, if it is convenient.

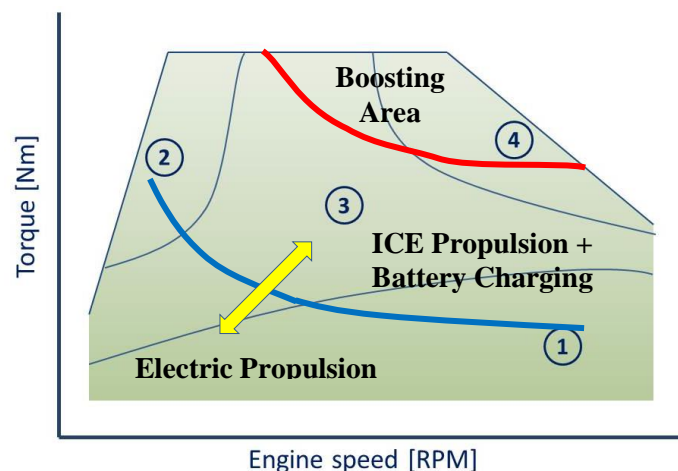


Figure 11-2 Powertrain operation areas

When the request of power is so high to overcome a second threshold, the red one in Figure 11-2, and the SOC is over a defined value, both the electric and thermal machines are turned on.

If the SOC level is close to the maximum level, for instance in case of subsequent events of braking energy recovery, the pure electric mode can be enabled also in the area between blue and red line until battery is discharged up to a lower level of SOC.

Assuming a defined electric hybrid architecture and battery charge sustaining operation, the power level to pass from electric to engine mode can be defined comparing the Equivalent Fuel Consumption rate  $E\dot{F}C$  of both driveline paths. The mechanical energy provided by the electric propulsion has to be converted in fuel to spend on recharging the battery at same level before the traction, according to the equation:

$$E\dot{F}C_{etd} = \frac{P_{trac}}{\eta_{trasm} \cdot \eta_{etd} \cdot \eta_{batd} \cdot \eta_{batc} \cdot \eta_{gen} \cdot \eta_{ice\ max}} \quad (11.8)$$

where  $\eta_{batd}$  and  $\eta_{batc}$  are the battery efficiencies in discharge and charge mode and  $\eta_{ice\ max}$  is the engine efficiency in best area of engine maps, with the hypothesis to recharge the battery in the best condition for the thermal engine.

The battery efficiencies can be considered equal to 1 in the architectures with double electric machines (e.g. power split, P0+P4, etc.) in case of hybrid series operation, because the generated energy doesn't pass through the battery storage. In case of engine propulsion the equivalent fuel propulsion rate is

$$E\dot{F}C_{ice} = \frac{P_{trac}}{\eta_{trasm} \cdot \eta_{ice}} \quad (11.9)$$

The Figure 11-3 can help to explain the equations (11.8) and (11.9).

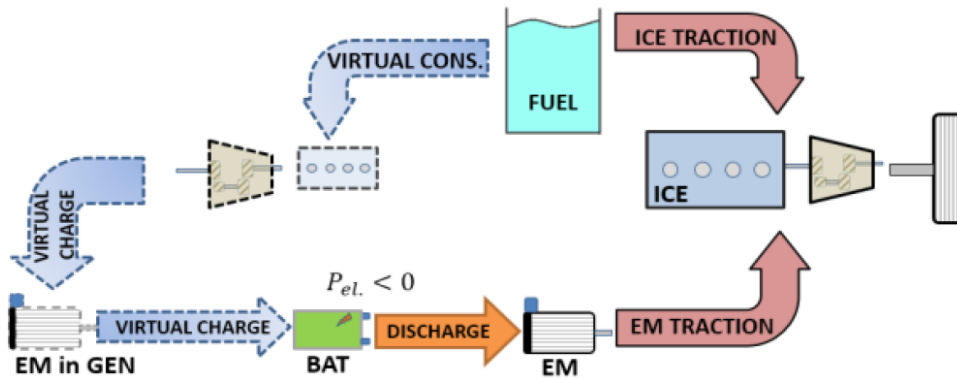


Figure 11-3 Energy flow comparison in a parallel hybrid vehicle in case of charge sustaining operation

The most convenient propulsion mode is selected evaluating the minimum between the  $E\dot{F}C$  of the engine and the electric drive:

$$\min(E\dot{F}C_{etd}, E\dot{F}C_{ice}) \quad (11.10)$$

It can be noted in (11.8) and (11.9) that the power level of blue curve significantly depends on the efficiency features of the motor, engine and transmission. Typically at engine low load, in the zone 1 of

engine map of the Figure 11-2,  $E\dot{F}C_{etd}$  has the minimum value. In case of rule based logic the blue line is set taking into account the previous considerations.

### 11.2.1 Model Based Energy Management

In case of driving cycle knowledge different and most effective management strategies can be used, for instance optimizing a cost function that takes into account the equivalent fuel consumption with  $\Delta SOC$  constraint or applying DP as presented in [251]. Both approaches are critical for the computational effort, both for ECU onboard implementation and for architecture optimization loops. For powertrain optimization, after the variation of the system parameters, the energy management strategy has to be updated in order to ensure the right evaluation of the architecture performances.

In this study an alternative way, named *model based* energy management, is proposed. It allows to define at beginning of the trip the power split between the ETDs and the ICE with aim to ensure in sustaining mode the SOC at end of trip close to initial one. The logic uses simplified physical models of the vehicle and the powertrain sub-components, that are updated in case powertrain architecture modification, allowing an “automatic” energy management adaptation. The computation time of this method is acceptable both for ECU implementation and for system optimization loops.

The main steps of the logic are following described and the work flow is illustrated in Figure 11-4:

- a. evaluation of instantaneous value of  $P_{trac}$  requested by means of a backward model of the vehicle, according to the equation (4.2), for the whole driving cycle;
- b. calculation of the kinetic energy that can be recovered during the trip;
- c. estimation of electric energy used by the auxiliary;
- d. after the estimation of the main components efficiencies in the powertrain, calculation of the  $E\dot{F}C_{etd}$  and  $E\dot{F}C_{ice}$  with the equation (11.8) and (11.9);
- e. split of the power for traction among the ETD systems and the ICE according to (11.10);
- f. evaluation of the energy used for electric propulsion during the trip;
- g. calculation of the energy harvested by a WHR system, if it is present;
- h. evaluation of the recovered useful energy, defined as difference between kinetic energy plus engine wasted energy recovered and electric auxiliary used energy;
- i. if the energy used by the motor at point (f) is lower than the recovered useful energy, the power level of electric propulsion area is increased until the energy balance is close to zero;
- j. if the electric propulsion energy at point (f) is higher than the useful recovered one, the delta has to be produced by the ICE to ensure the zero balance at end of the trip; if the time to recharge in optimal way the battery (high ICE efficiency) during the trip is not enough, a second loop reduces the power level for electric propulsion until achieving the energy balance.

The estimation error in each model can lead to a wrong final energy balance and not optimized use of the electric propulsion, with negative effect on fuel consumption or different SOC compared with the target. To prevent this problem a check on instantaneous value of SOC is performed during the trip, enabling or disabling the electric propulsion if the SOC overcomes an upper or lower threshold respectively. In future works an adaptive strategy to recover model errors will be developed.

Figure 11-5 presents WLTC simulations of a SUV equipped with a hybrid powertrain composed of P4+P2 48V-25/22kW electric drives and a 1.5L TGDI 140kW engine. On the left side of figure the optimization procedure is disabled and the energy saving in battery is higher than used one, leading to  $\Delta SOC$  different

from zero. In the right side, the optimization loop is active, thus the right energy balance is achieved with a  $\Delta$ SOC close zero.

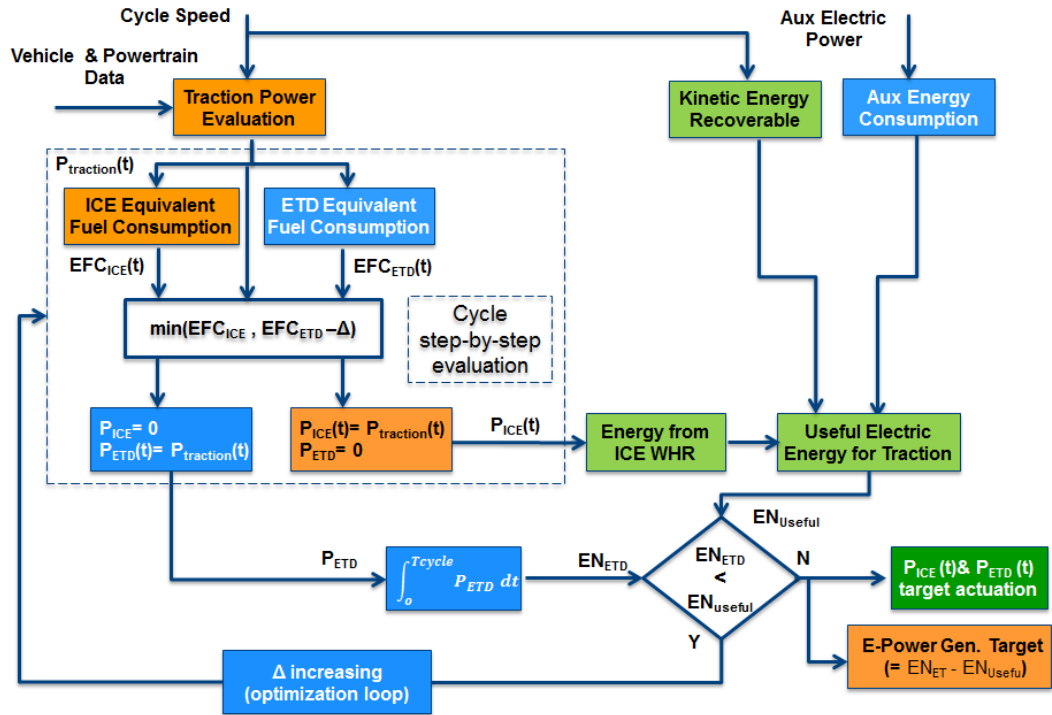


Figure 11-4 Workflow of model based powertrain energy management logic

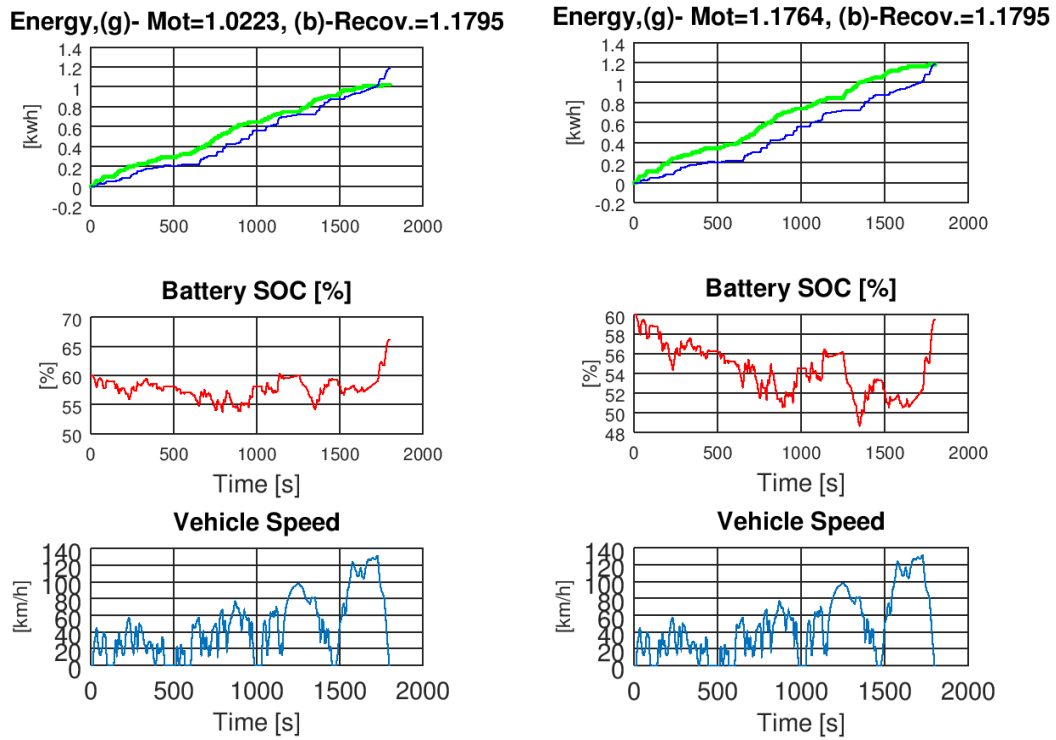


Figure 11-5 Model based powertrain energy management for a SUV with a hybrid powertrain composed of P4+P2 48V-25/22kW electric drives and a 1.5L TGDI 140kW engine: (Left) strategy disabled, (Right) strategy activated

## 11.3 Powertrain Control based on Acoustic Sensing

In the last years Magneti Marelli with the support of University of Bologna has developed an innovative multi-function sensor, that via acoustic is able to monitor many powertrain phenomena, for control and diagnosis purpose. Part of PhD research activities has been dedicated to improve some sensing functions and to develop control functions based on this novel sensing system. In particular the investigated functions have been Knock, Combustion Noise (CN) and the Turbocharger speed controls.

In this section, after a brief introduction of the acoustic sensor, the applications to the Boost, Knock and CN controls are presented. The Knock and CN controls were developed with a Rapid Control Prototyping (RCP) system applied to a GDI and Common Rail (CR) diesel engines respectively. Whereas the model based Turbocharged speed control has been designed and assessed by means of co-simulation Simulink-GT-Suite, considering a CR Diesel engine. Part of the activities with regard to CN control will be presented in the paragraph #11.4.3, whereas more details are available in the published works [210,222].

### 11.3.1 Features of Acoustic Sensing System

The acoustic sensing system is based on two main hardware solutions, see Figure 11-6:

- an acoustic probe with one or more MEMS microphones and without intelligence onboard;
- a smart device able to run the sensing algorithms, with ECU connection via CAN-BUS.

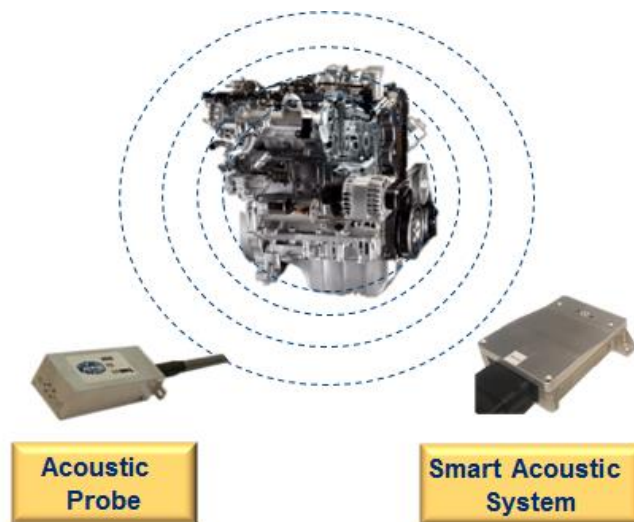


Figure 11-6 HW architectures of acoustic sensing system

The main possible functions are listed following, some of which are object of ongoing developments:

- Turbocharger Speed evaluation
- Knock & Misfire detection

- Combustion & Noise feedbacks
- Fuel Composition evaluation
- Valvetrain control
- Powertrain Failure detection and prevention.

It is import to remark the system capability to perform the contemporary sensing of many engine and powertrain phenomena, with obvious cost advantages.

### **11.3.2 Boost Pressure Control with support of Turbocharger Speed Sensing (Case Study)**

The new driving cycles require a greater focus on a wider engine operative area and especially in transient conditions, where a proper air path control is a challenging task for emission and drivability. In order to achieve this goal, turbocharger speed measurement can give several benefits during boost pressure transient and for over-speed prevention, allowing the adoption of a smaller turbocharger, that can further reduce turbo-lag, also enabling engine down-speeding.

So far, the use of turbocharger speed sensor was considered expensive and rarely affordable in passenger car applications, while it is used on high performance engines with the aim of maximizing engine power and torque, mainly in steady state, eroding the safe-margin for turbocharger reliability.

Thanks to the availability of a new cost effective turbocharger speed technology, based on acoustic sensing, turbocharger speed measurement has become affordably also for passenger car applications. In this study presented in [220], a new model-based boost pressure control employing the speed measurement is proposed. In particular, a cascade controller based on boost pressure, turbocharger speed and VGT position measurements has been developed. Furthermore, the open loop term and the speed target filtering have been calculated by means of a simplified physical model of the plant.

The control has been designed and validated by means of a 1-D model of a small turbocharged Diesel engine for passenger cars. The proposed control architecture performances will be shown, in a co-simulation environment built in Matlab/Simulink and GT-Suite, modelling a small diesel engine with a VGT, even though the same analysis could be carried in presence of a FGT and/or a spark ignition engine.

Moreover, realistic driving situations have been reproduced by means of a calibrated and validated model of engine, driveline and vehicle. The co-simulation technique allows exploitation of the best of the two design tools. The comparison between the standard production control without turbocharger speed feedback and the proposed was performed by the simulation of the same critical maneuvers, chosen to be representative of the real driving conditions. Moreover the achievable benefits have been analyzed.

#### **Turbocharger Speed Evaluation via acoustic**

The algorithm for the turbo-speed evaluation via acoustic has been already presented in different works [189,190] and summarized with block scheme in Figure 11-7. The main steps are the audio sampling, a model based filtering, the evaluation of blade frequency and finally the evaluation of the mean turbo speed.

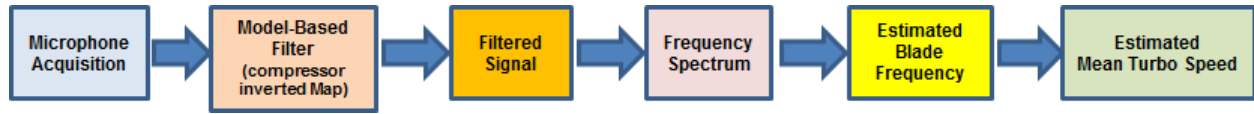


Figure 11-7 Work flow of Turbocharger Speed evaluation via acoustic sensing

The next Figure 11-8 illustrates the performance of the acoustic turbo speed evaluation during a load transient of a L0-Class Vehicle equipped with an EU6 1.3L CR Diesel engine. The reference sensor is the turbo SPEED DZ135 sensor by Micro-Epsilon.

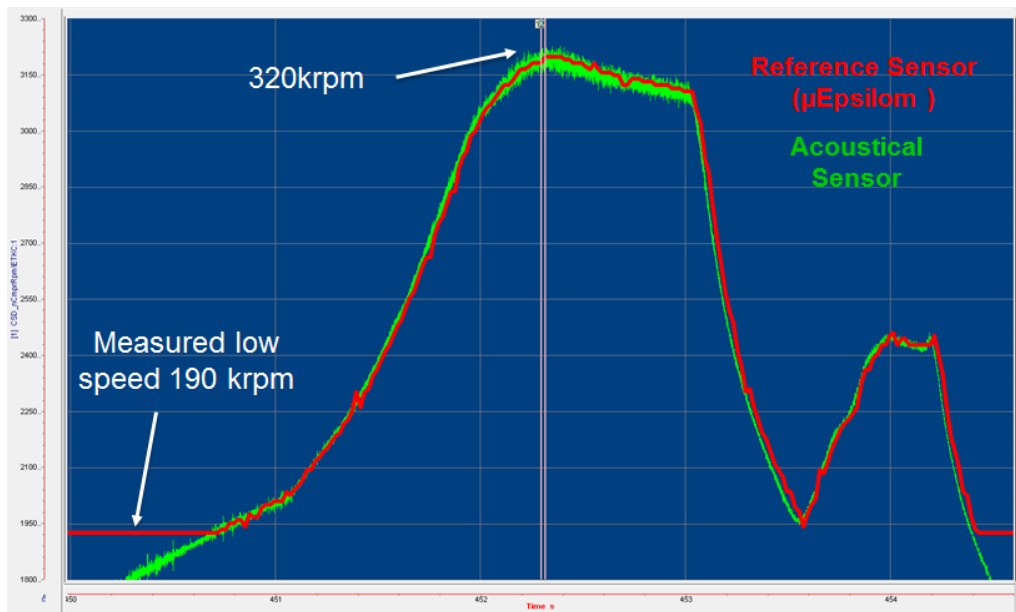


Figure 11-8 Performance of turbo speed evaluation via acoustic during a load transient

The acoustic based measurement is very good above 190 krpm, where the sound emitted by the turbocharged is prominent compared to surrounding noise.

## Engine Description and Experimental Set-Up

A general overview of the system is given in Figure 11-9. The engine is a 1.3L CR Diesel Engine (EU6 compliant) equipped with a HP-EGR circuit with cooler and an upstream throttle valve to obtain the desired EGR rates. The exhaust gas after-treatment system is composed by DOC, LNT and DPF. Moreover, the system is equipped with a VGT with a rack position sensor.

The experimental tests for the 1-D engine model validation have been carried out on a dynamic engine test bench. Furthermore, additional temperature and pressure sensors have been installed along the engine air path. An indicating acquisition system has been used to analyze the in-cylinder pressure sensors to evaluate IMEP, P<sub>MAX</sub>, CA<sub>10-90</sub> and MFB<sub>50</sub>, while turbocharger speed has been measured with the acoustic sensor developed.



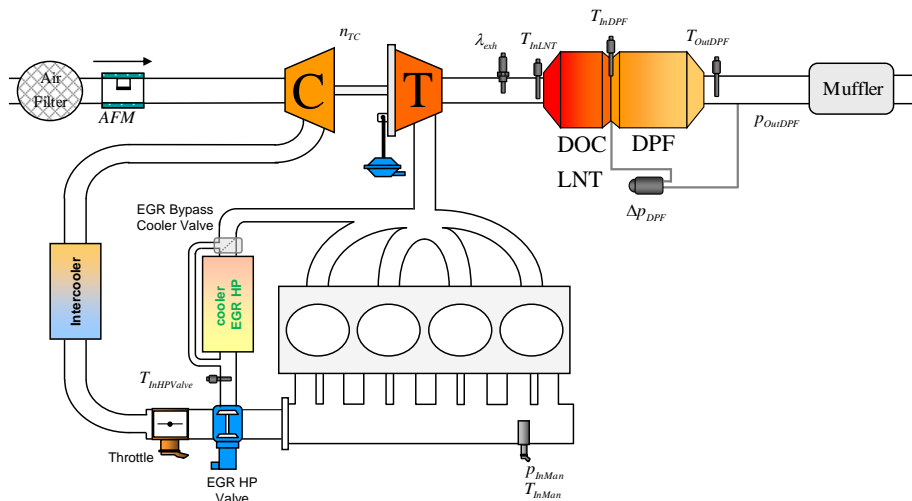


Figure 11-9 1.3L CR Diesel Engine layout

Furthermore, vehicle model has been fine-tuned and validated with experimental tests on a B-Class passenger car in real driving conditions. The cost-down parameters, which describe the rolling and aerodynamics resistances involved in the vehicle dynamics, have been evaluated on engine roll bench.

## Vehicle and Engine model description

A detailed vehicle and engine model, described in Figure 11-10, has been designed and validated against experimental data. The aim of the procedure was to obtain a tool to test in a virtual environment the performances of the new control architecture with less time and cost efforts.

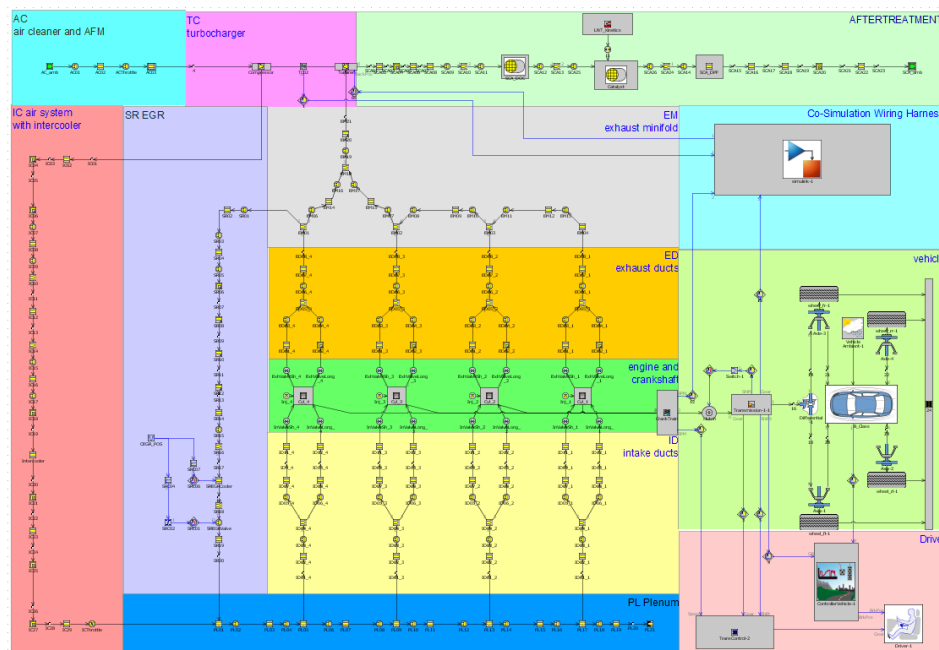


Figure 11-10 Engine, vehicle and driver model

## 1-D Engine Model

A 1-D model of the whole air path has been created in GT-Suite environment. Geometrical and material features of pipes were evaluated by inspection on the real engine. Turbocharger has been modelled with compressor and turbine manufacturer maps. In the following Figure 11-11 and Figure 11-12 an overview of the compressor maps is given. Reference pressure and temperature are respectively 1 bar and 288K.

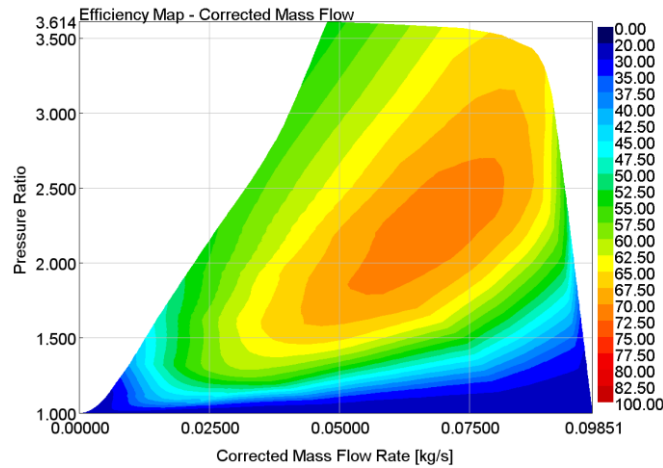


Figure 11-11 Compressor efficiency map

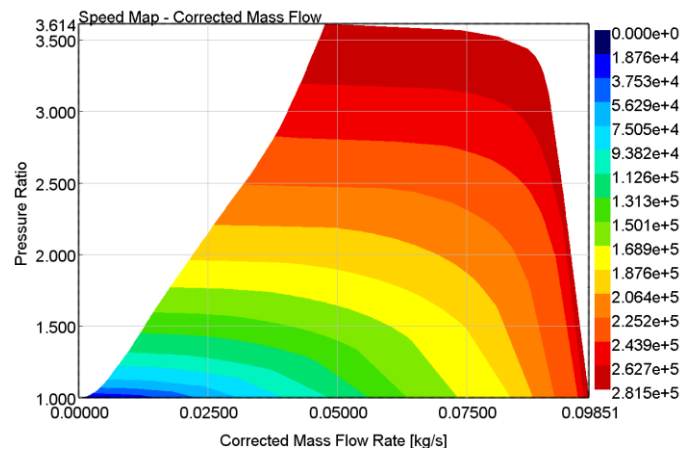


Figure 11-12 Compressor speed map

Additionally, a predictive combustion model has been used [293]. A detailed description of the approach is not given here, however, the calibration procedure can be summarized as follow:

- A reduced model with a cylinder and injector is extracted from the complete engine model. Fuel mass rate shape profile is given as input by a semi-empirical approach with parameters depending on ET (energizing time) and rail pressure. Air mass trapped inside cylinder and residuals has been imposed from experimental tests at the engine test bench. Heat losses were modeled by the Woschni approach.
- Eighteen points, as showed in
- Figure 11-13, with different EGR rates (0 to 45%), engine speeds and loads, injection patterns, lambda (1.05 to 4) have been considered.
- The predictive combustion model parameters have been optimized in order to fit the measured heat release rate curves obtained from the in-cylinder pressure data.

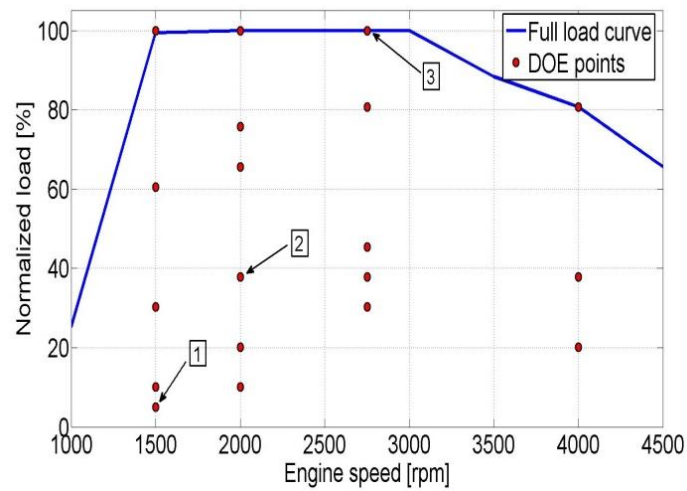


Figure 11-13 Design of Experiment (DOE) for model identification

Results are reported in Figure 11-14 in terms of predicted and measured MFB50 and CA10-90, which describes the burn duration. Errors in burn rate duration could be attributed to the convective heat transfer model or errors in turbulence modelling. This happens especially with more premixed combustions (with high pilot injection) when predictive combustion model shows lower accuracy.

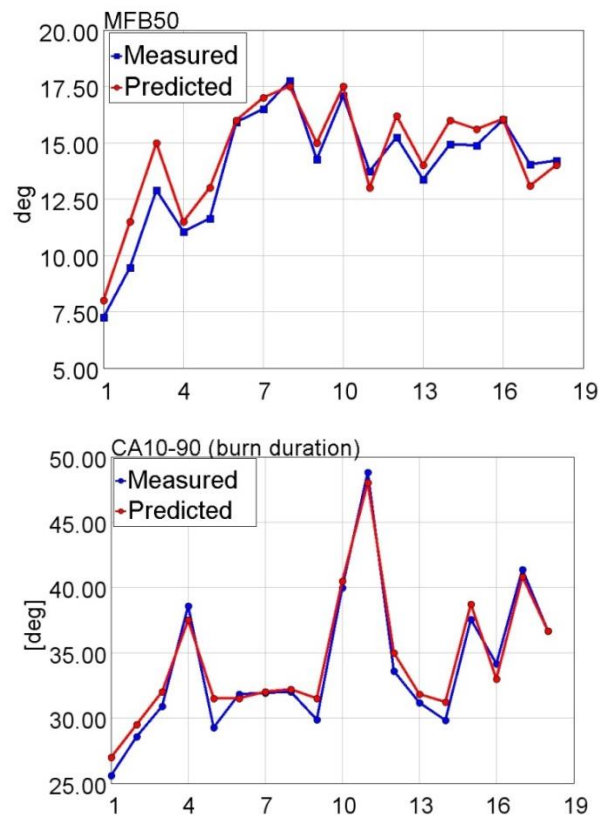


Figure 11-14 Model vs. experimental data, MFB50 and CA10-90

Globally, the accuracy of the model can be considered satisfactory for the purpose of this work which focuses mainly on the air and turbocharger dynamics.

Figure 11-15 shows the comparison between predicted and measured in cylinder pressure for the points 1, 2 and 3, taken as an example.

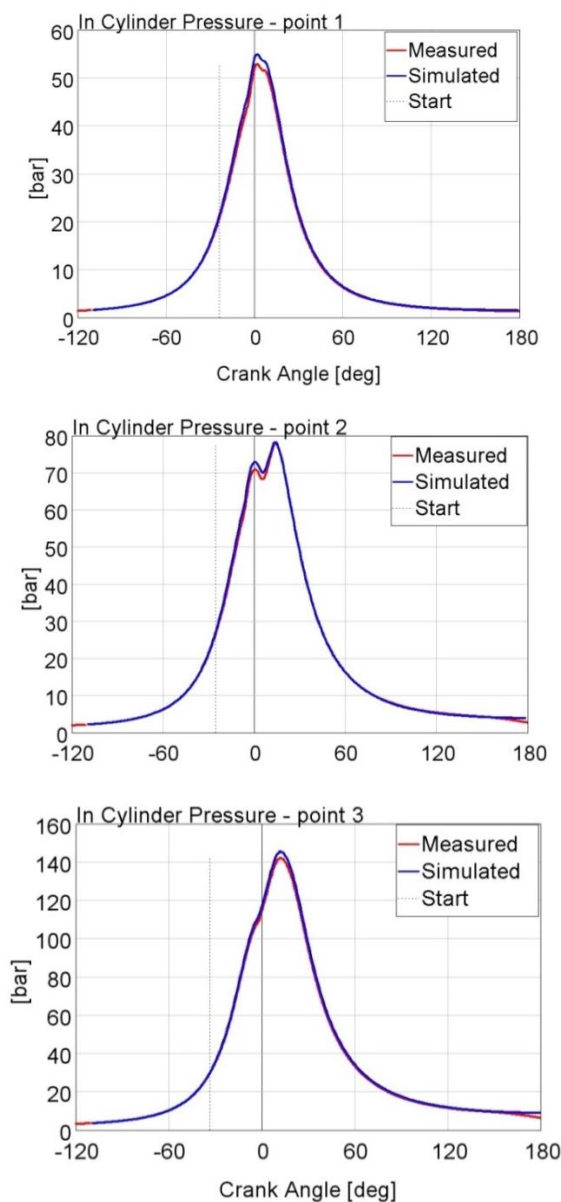


Figure 11-15 Predicted vs measured in cylinder pressure for the experimental points 1, 2 and 3

Figure 11-16 shows the relative error between the measured and simulated IMEP. The results demonstrate again an overall good agreement with data and an error below 4 % even at low loads. The air path model has been fine-tuned and validated with experimental data collected on engine test bench. Throttle and valves have been characterized by means of flushing tests. Pressure and temperature, logged during steady state tests, have been compared with the simulated signals and pressure drop along the pipes is adjusted.

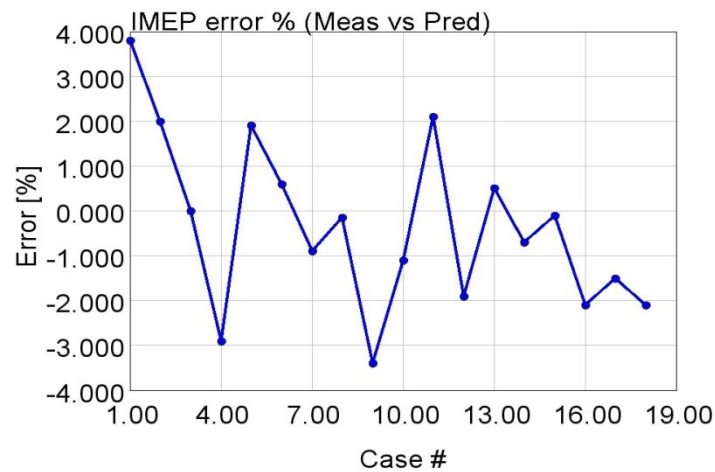


Figure 11-16 IMEP % error

The same signals logged during transient tests have been used to calibrate volume and thermal features of pipes, heat exchangers and manifolds. Intercooler and EGR coolers were characterized by means of semi-predictive approach considering the efficiency evaluated by experimental tests and imposing the downstream gas temperature. The same tests have been used for turbocharger calibration by means of inertia and map correction factors.

## Vehicle model

In addition, vehicle and driver behaviors have been modeled using proper templates featured with a real B-segment passenger car data. A gear shift law, depending on engine speed, has been added to simulate real driving conditions. The behaviors of simulated manifold pressure and turbocharger speed dynamics have been validated against experimental data collected on vehicle. In Figure 11-17, one of the transient maneuvers that have been used for the vehicle model validation has been summarized. In particular, a full load request from a middle load condition in third gear is shown.

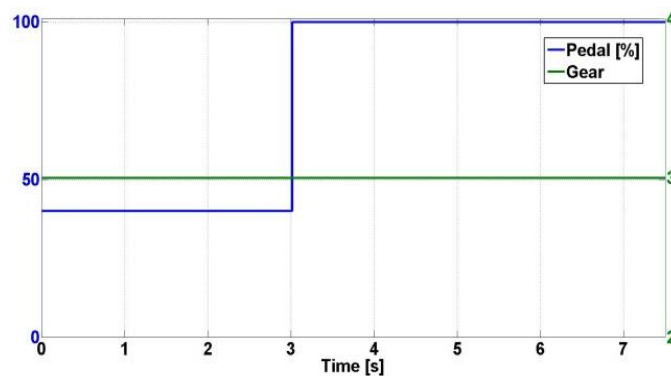


Figure 11-17 Reference vehicle maneuver

In Figure 11-18, a comparison between simulation and experimental measurement of the main signals has been showed. The coherence of the virtual model to the real system appears clearly, considering the vehicle as well as the air path dynamics.

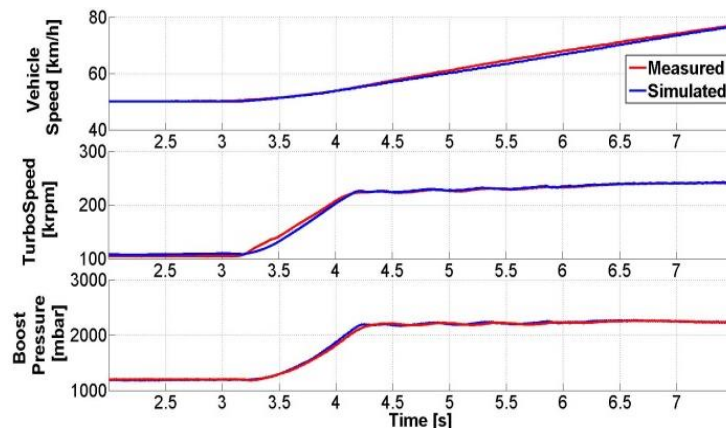


Figure 11-18 Comparison between simulated and measured signals of the vehicle and turbocharger during a transient

## Boost Pressure Control Architecture

The purpose of the boost pressure controller is to manage the intake manifold pressure level. In case of VGT, control modifies the efficiency of the turbocharger through an actuator that adjusts the deflector blades. This actuator changes the fluid-dynamic conditions of the flow at the turbine inlet, and modifies the operative point of the system. In this way, the air mass flow through the compressor is changed, and the boost pressure inside the intake manifold can be adjusted. Additionally, in order to have an accurate control of the intake manifold pressure level, which is based on torque request, emissions and fuel economy constraints, a pressure sensor is used as feedback. Turbocharger speed feedback is instead available only on heavy duty and high performance engines [294] due to the high cost of the sensor and it is not usually adopted in the standard boost control.

### Standard Boost Control

The standard boost controller architecture is composed of several sub-functions, as shown in Figure 11-19. The description of the main parts is the following:

- Boost Reference Pressure, it defines the intake boost pressure level target.
- Pressure Open Loop term, it defines the feed-forward contribution, in terms of actuator position. This block considers several engine and ambient parameters.
- Pressure Closed Loop term, this function guarantees that the pressure target is reached by the controller.
- Closed Loop VGT Actuator Control, in closed loop mode, it performs a faster position control of the turbine deflector blade, compensating the non-linearity of the actuator.

The open and closed loop parts of the boost controller can be enabled or disabled, in order to allow an effective turbocharger control over the entire engine operating range.

As matter of fact, Figure 11-19 represents a simplification of the real control which is adopted in automotive applications. The closed loop contribution ( $VGT_{pos} FB$ ) is often achieved by means of a PID controller and a complex gain scheduling, to take into account the non-linearities of the system. Boost target ( $P_{ref}$ ) is often filtered to reduce the wind-up of the integral term and to minimize the overshoot of the manifold pressure and the turbocharger over-speed, especially at high loads. Furthermore, the feed-

forward ( $VGT_{pos}FF$ ) contribution is quite complex and includes several maps based on engine and environmental conditions (e.g. atmospheric pressure and temperature). In addition, a dedicated management for transient conditions is needed. Finally, other auxiliary strategies are considered to manage some exceptional conditions.

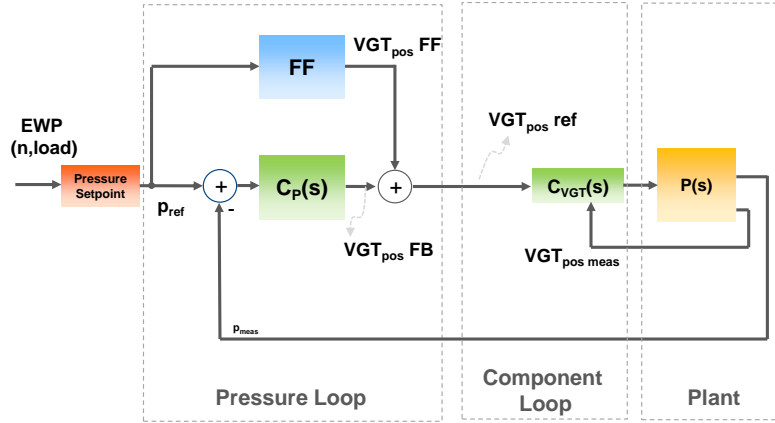


Figure 11-19 Standard boost pressure controller architecture

The calibration phase is even more complicated due to several maps, which require expensive experimental tests on the engine test bench and on vehicle in many environmental conditions to take into account altitude, hot and cold temperatures. Moreover, the safe margins, with respect to the over-speed, need to be chosen in order to ensure the integrity of the system. This, in conjunction with the components, system and engine production spread, leads to a sub-optimum calibration for certain engine operating points and conditions.

### New Boost Control Architecture

As mentioned before, the absolute intake manifold pressure is one of the main conditions that impact the behavior of the engine (torque, smoke, NOx engine out, etc.). Therefore, during the calibration phases, two aspects need to be considered: turbocharger over-speed events in all conditions and performances. These aspects lead to a trade-off analysis and a compromise must be reached. Thanks to the availability of a newly cost effective turbocharger speed technology, safety margins can be removed, avoiding over-speed events and obtaining best performances, as shown in [295]. Moreover, in transient conditions, the availability of the turbocharger speed measurement can be useful because it represents a state variable of the air path system, and provides transient information, which is important to reach the target faster.

Figure 11-20 shows a cascade control, which can be used with the turbocharger speed information. Compared to the standard control, a speed loop has been added whose target ( $NTC_{ref}$ ) is evaluated as sum of two terms. The first,  $nTCFF$ , is the feed-forward contribution whereas the second contribution ( $nTCFB$ ) compensates the pressure error ( $p_{ref} - p_{meas}$ ).

From now on, the actuator position control  $C_{VGT}(s)$  will be neglected. This control guarantees that the actuator position request is reached; its decoupling with the outside loops is ensured by the dynamics of pneumatic or electric actuator ( $t_{10-90} \leq 150$  ms). Different considerations should be made for the speed and pressure loops. In the plant, speed and pressure time response are comparable (same order of magnitude) and the interaction between the two control loops can be an issue. Giving a slower dynamic response to the  $C'_P(s)$  in the pressure loop, adjusting the PID parameters, can be a way to decouple the loops and avoid instability.  $C'_P(s)$  is indeed a slower PI controller with the main aim of adjusting possible errors in  $nTC_{ref}$ , assuring that the reference pressure is reached.

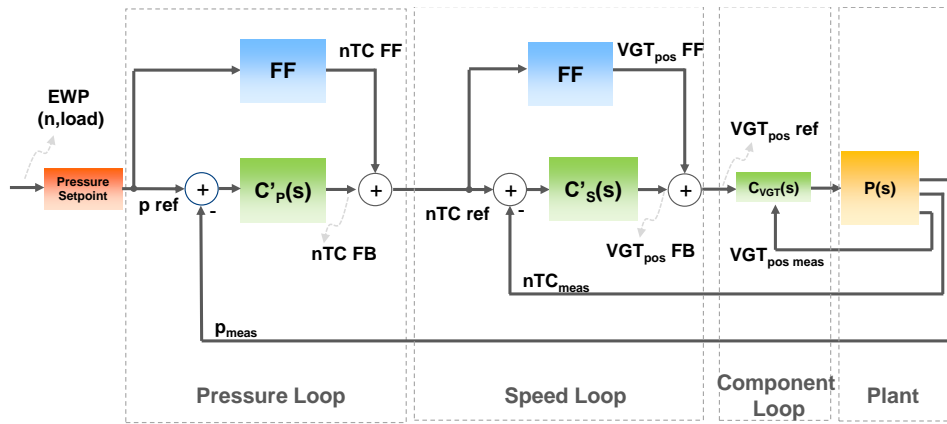


Figure 11-20 Turbocharger cascade control scheme

To maximize the benefits of turbocharger speed feedback and obtain other advantages, the control architecture has been improved and a physical based model has been implemented. In Figure 11-21, the new control architecture with the cascade control is described. A turbocharger physical model is implemented; it provides mainly two contributions: the feed-forward term ( $VGT_{pos} FF$ ) in the speed loop and the filtered reference ( $nTC_{filt}$ ) for feedback contribution of speed loop.

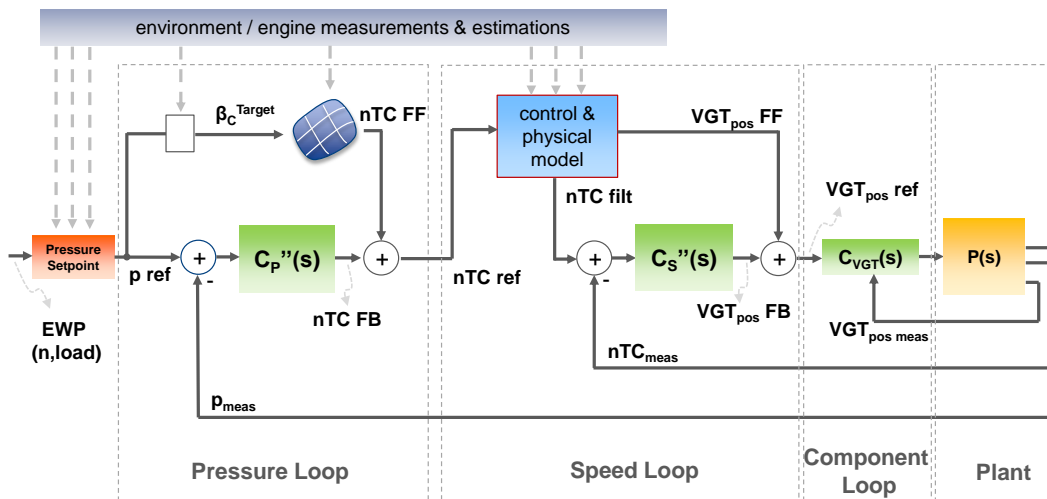


Figure 11-21 Model based control architecture

In addition, in the pressure loop, the feed forward contribution is given by a compressor inverse map. This map is obtained by the turbocharger component manufacturer data, and it gives turbocharger speed, mainly using the pressure ratio and air mass flow through the compressor.

## Turbocharger model

The main reasons for adopting a turbocharger physical direct model can be related to the severe effort required to build an inverse non-linear one. Building a direct-physical turbocharger model is instead easier because the physical direct equations, which are used to describe the system, assure the stability of the model. The issue of getting the command from the direct model is overcome by a controller based on physically-modeled speed, as shown in Figure 11-22.



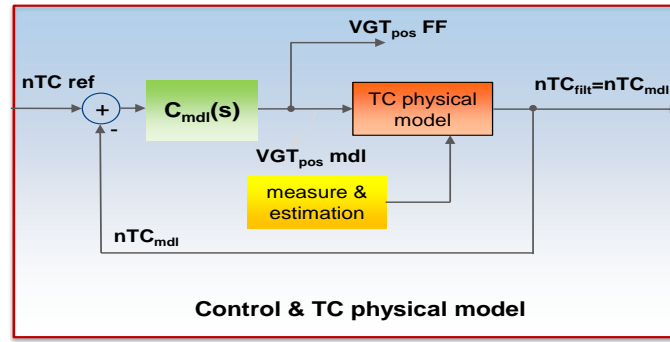


Figure 11-22 Turbocharger physical model and speed control

Figure 11-23 is an overview of the physical model; the main output is the modeled turbocharger speed ( $nTC_{mdl}$ ) evaluated in the power balance block, using the mechanical inertia as key parameter. Note that, only turbocharger inertia is considered; therefore air dynamics is not taken into account. This is a crucial aspect allowing  $C_{mdl}$  to be calibrated with higher dynamics than  $C_s''(s)$ , assuring model convergence.

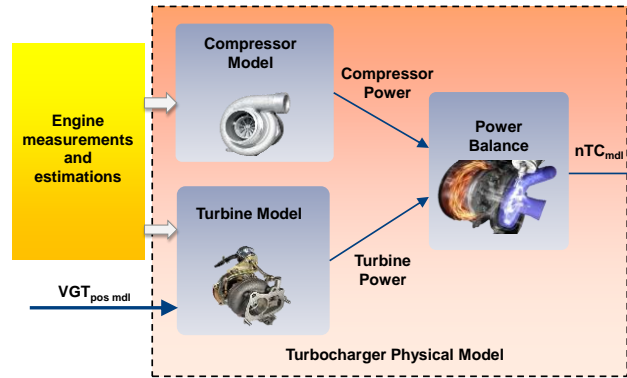


Figure 11-23 Overview of the model used in the new boost controller

Some maps are used to simulate the turbocharger behavior and evaluate the power of the turbomachines. Engine parameters estimations and measurements are used as inputs of the compressor and turbine blocks. Estimations are related to the upstream compressor, upstream and downstream turbine pressure, exhaust engine temperature. Measurements are related to the engine speed, the ambient air pressure and temperature.

The control variable, represented by  $VGT_{pos\_mdl}$ , is adjusted by a simple PI controller ( $C_{mdl}(s)$ ), without gain scheduling, whose input is the error between  $nTC_{mdl}$  and  $nTC_{ref}$ . The modeled rack position is used in the turbine model; it impacts on the efficiency and  $TFP$  (turbine flow parameter) which, in turn, influences the turbine power and therefore the power balance. Moreover,  $VGT_{pos\_mdl}$  is also the feed-forward contribution of the speed loop and therefore is equal to  $VGT_{pos\_FF}$ . In this way, a physical-based open loop of the actuator position request is obtained. The turbocharger modeled speed is also used as a filtered target for the feedback speed loop. In this way we obtain an achievable target, with real dynamic, avoiding unrealistic variations.

### Benefits of the new control architecture

The benefits of the cascade control, as already mentioned, are directly linked to the availability of the turbocharger speed measurement and can be summarized by the removal of the safety margin for the turbocharger over-speed event in steady state conditions assuring at the same time the convergence of both turbocharger speed and intake manifold pressure to the targets. In the following, the improvements will be

evaluated in different environmental conditions (low and high altitude), taking into account even the turbocharger production spread.

The advantages of the proposed model-based cascade control can be summarized as follow:

- By adopting the physical model for the feed forward contribution of the speed loop, the calibration effort can be reduced taking into account system non-linearities.
- The physical model allows to have an achievable speed target and to avoid a special management during transients, reducing the complexity of feedback controller and decreasing its calibration effort.
- The benefit of using the compressor map only, to obtain the feed forward contribution of the pressure loop, is the reduced calibration effort, with respect to a standard feed forward term, based on several maps.

Another advantage of adopting the compressor map is the possibility to adapt it during the engine working life since the relationship between the speed and pressure ratio is quite simple. With the availability of the turbocharger speed measurement it is instead possible to adjust the map and recover the system dispersions due to the production and component aging. Furthermore, after the adaptation, the feedback control contribution for the pressure loop is less significant and the dynamic of this loop can be slowed down. This helps to further achieve the cascade control frequency decoupling.

### Control Performance Analysis

The performances of the proposed control architecture, shown in the previous chapter, have been evaluated in a co-simulation environment by means of GT-Power and Matlab/Simulink tools. In this way, it has been possible to carry out the control design with a significant model of the plant which includes air-path dynamics, combustion behavior and vehicle dynamics. The description and validation of the 1-D model has been explained before, while, in Simulink environment, the standard and the new boost control architectures have been implemented. As shown in Figure 11-24, the 1-D model has been linked to the control model while they exchange signals simulating the real vehicle and ECU functions behavior.

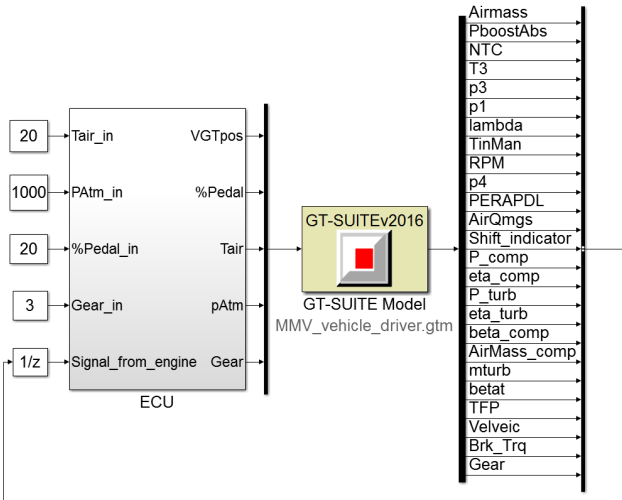


Figure 11-24 Co-simulation model overview, vehicle and control system

In the following table, the tests description is provided. The results have been evaluated in terms of time response, robustness against production spread of the turbocharger and safety from over-speed. Moreover, note that, in the investigated maneuvers (at high load conditions), EGR rate is low and the impact on the boost pressure controller can be neglected.

Table 11-2 Feasibility tests description

Test #	Test Description
1	Heavy full load step (50-80 km/h) in 3 <sup>rd</sup> gear at high altitude
2	Reference transient maneuver; robustness against turbocharger production spread
3	Reference maneuver at low altitude without safe margin for over-speed (higher pressure reference)
4	Heavy transient (20-50 km/h) with gear shift from 1 <sup>st</sup> to 2 <sup>nd</sup> at high altitude

### ***Test #1 – Heavy full load step (50-80km/h) in 3<sup>rd</sup> gear at high altitude***

As mentioned before, the aim of this kind of control architecture is the optimization of the transient behavior, even in critical atmospheric pressure and temperature conditions and with air system components dispersions, maintaining or even increasing the turbocharger reliability. For this reasons, heavy transient at high altitude, has been chosen to compare the results of the new boost control architecture against the standard. Specifically, as shown in Figure 11-25, a heavy full load request from steady state condition at 50 km/h, with third gear engaged, was chosen as the reference maneuver.

In Figure 11-26, the absolute intake manifold pressure and turbocharger speed dynamics, during the transient described above, are shown. In the top graph, the pressure targets ( $P_{ref}$ ) for the standard control at low and high altitude are described by green and magenta dotted lines, respectively. The blue dotted line is instead the pressure target at high altitude for the model based control. It is evident that, at high altitude, the standard control imposes a safeguard margin in manifold pressure, as presented also in [294], that can be avoided with the model based control. The dynamics of manifold pressure ( $p_{meas}$ ) for the standard control at low and high altitude are described by green and magenta lines, respectively. Pressure overshoot can be seen both for green and magenta lines. Turbocharger speed is shown in the middle graph revealing a dangerous over-speed at high altitude for the standard boost control due to the air path volume.

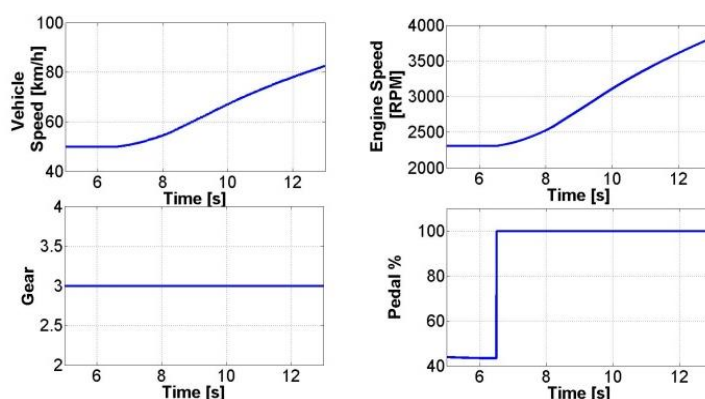


Figure 11-25 Reference transient maneuver

For this reason, a slower calibration, as shown with the brown line, is needed to provide reliability and accuracy in the intake air flow control penalizing the transient response in terms of air dynamics, smoke and torque. The model based control (blue line) provides instead better charging (higher manifold pressure) and avoids the overcoming of turbocharger maximum speed limit. Furthermore, rack position can be seen in the bottom graph.

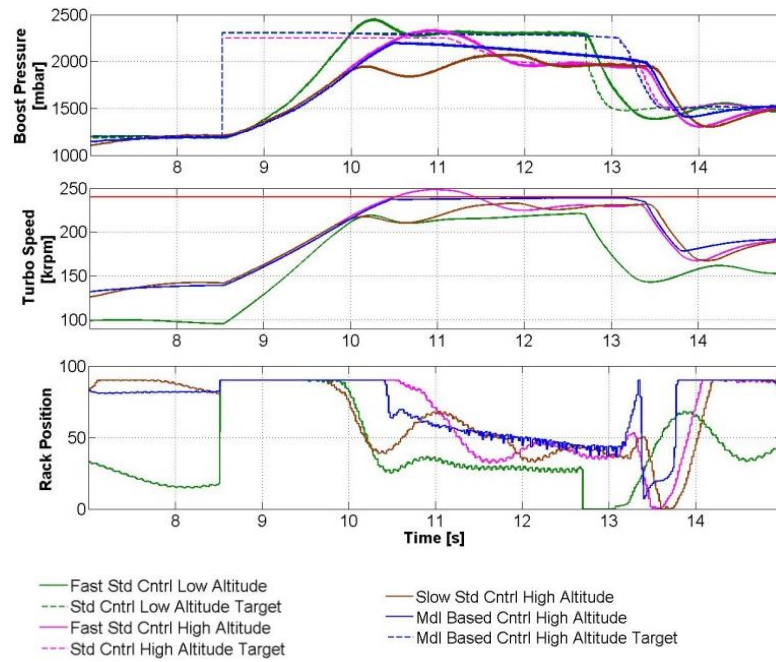


Figure 11-26 Comparison between fast standard, slow standard and model based boost control performance during reference transient under high altitude condition. Fast standard control performance under low altitude condition is shown to demonstrate limits of fast calibration also in this condition

In Figure 11-27 and Figure 11-28, the description of the proposed model based boost control is explained in details. A manifold reference pressure increase ( $p_{ref}$ ) leads to a turbocharger speed target ( $nTC_{ref}$ ) step calculated from the inverse compressor map ( $nTC_{FF}$ ) and the closed loop correction ( $nTC_{FB}$ ). In real behavior, the closed loop term correction is higher, due to the spread of air path component characteristics.

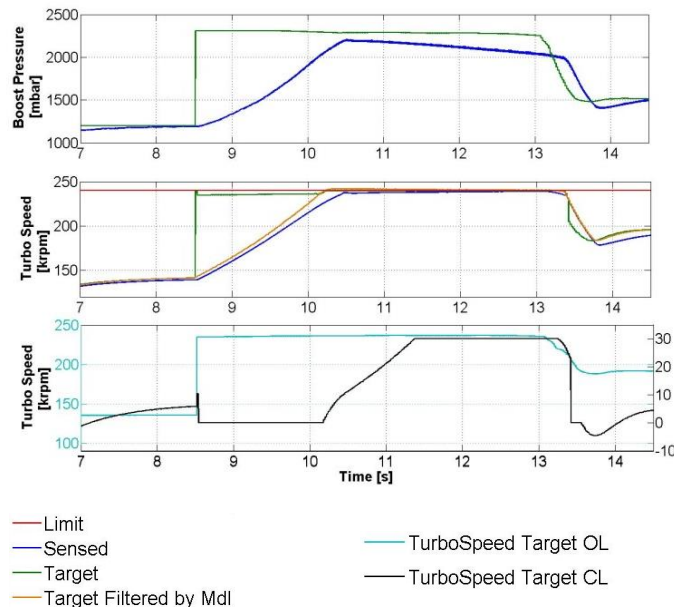


Figure 11-27 Detail of open loop ( $nTC_{FF}$ ) and closed loop ( $nTC_{FB}$ ) turbo speed target contributions given by model based pressure loop control during reference transient, under high altitude condition

However, using the reference model adaptation, this term can be reduced after few driving cycles, leading to a very faster control. The method to carry out the model adaptation will be presented in a future work. The speed

target is then filtered by means of the physical dynamic model of the air system (yellow line,  $nTC_{fil}$ ) in order to guarantee the attainability of the target, avoiding the excessive increasing of integral term in speed closed loop controller.

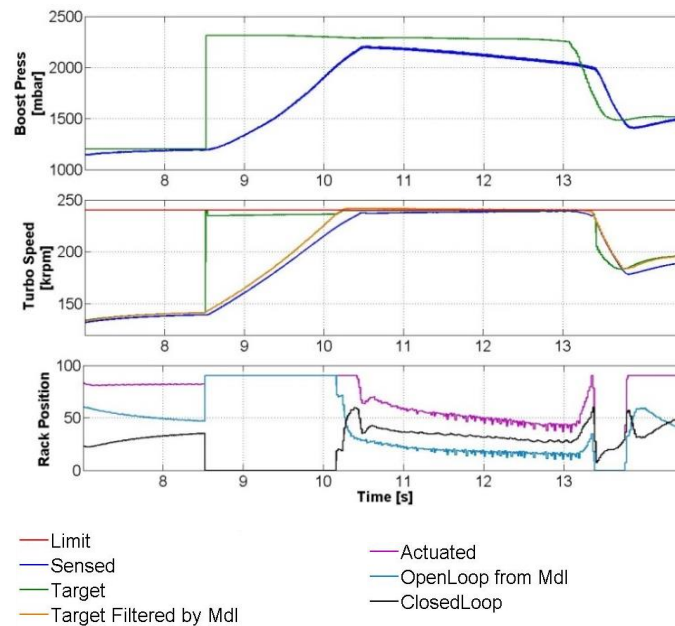


Figure 11-28 Detail of open loop (VGTpos FF) and closed loop (VGTpos FB) turbine rack position contributions given by model based control during reference transient, under high altitude condition

## ***Test #2 – Reference transient maneuver, robustness against turbocharger production spread***

Thanks to the simulation environment, the effects due to the turbocharger dispersions from the nominal characteristics have been studied. In particular, a bias of + 10% in compressor map has been simulated. In order to achieve this, the compressor map in 1-D model has been properly scaled by a speed multiplier. As it can be seen in Figure 11-29, in these conditions, the standard control system can lead the turbocharger to reach or even exceed its maximum speed if during the calibration phase a certain margin of safety is not maintained, with obvious repercussions on its reliability. On the contrary, a boost control based on the speed measurement feedback optimizes the performance of the turbocharger, leads it to work at higher speeds than standard control to ensure the achievement of the target pressure respecting the constraints on the maximum speed. Moreover, as it is shown in Figure 11-30, performances are not sacrificed; indeed, the pressure increasing is at the maximum rate because rack position is saturated at the maximum stop position.

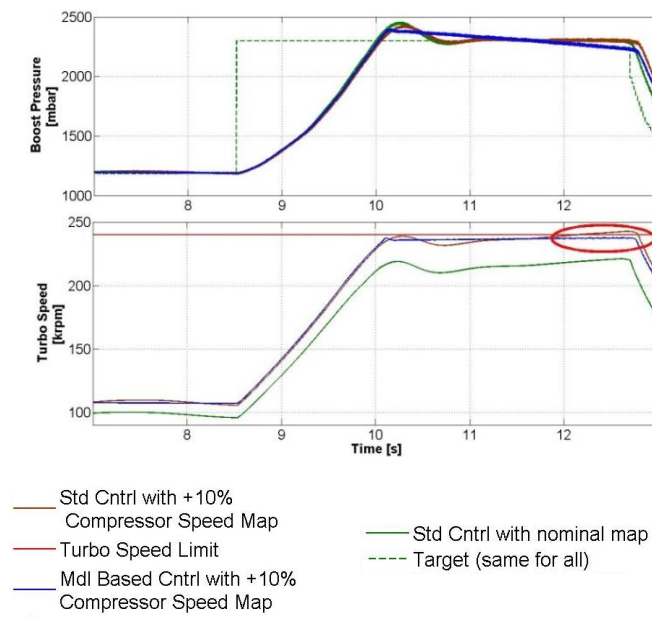


Figure 11-29 Comparison between standard and model based boost control in case of compressor speed map dispersion from nominal one. The red ellipse highlights the over-speed of turbocharger with standard boost control

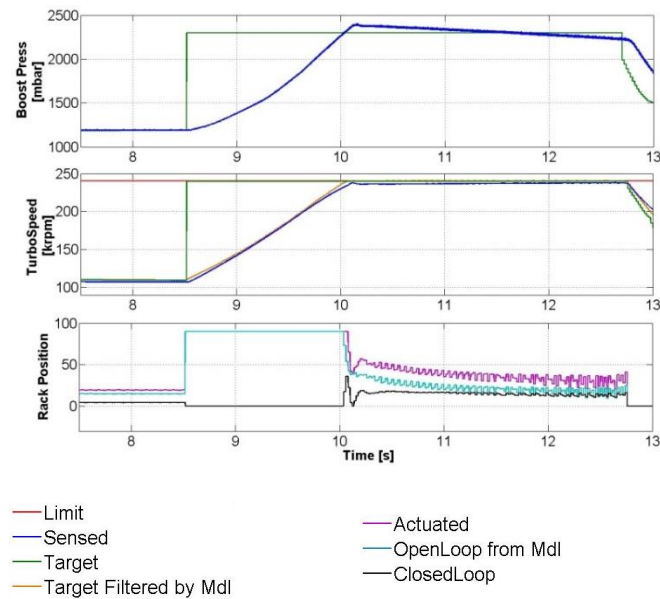


Figure 11-30 Detail of open loop and closed loop turbine rack position contributions given by model based inner loop control in case of compressor speed map dispersion

### ***Test #3 – Reference maneuver at low altitude without safe margin for over-speed (higher pressure reference)***

In the calibration phase of the standard control system, the maximum pressure is limited in a rather conservative way to take into account the dispersion of the air system components in production vehicles. In Figure 11-31, it is clear that the proposed control architecture does not require this margin of safety, allowing the optimization of performances of any compressor by using an higher  $P_{ref}$  without any risk of over-speed.



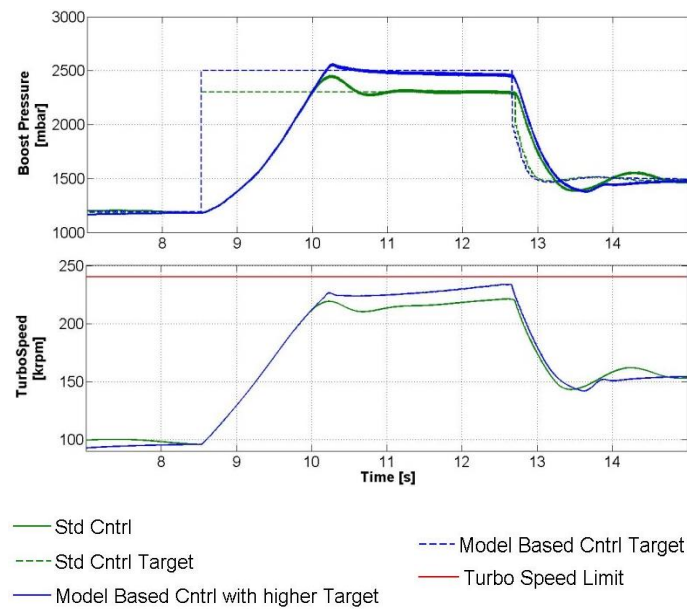


Figure 11-31 Comparison between standard control and model based control with pressure target increased, during reference transient

#### ***Test #4 – Heavy transient (20 to 50 km/h) with gear shift from 1<sup>st</sup> to 2<sup>nd</sup> gear at high altitude***

Lastly, the behavior at high altitude during a transition from 20 to 50 km/h with a gear shift from first to second has been analyzed. Although a significant reduction of the output torque and thus acceleration of the vehicle relative to the operating conditions at sea level has been shown in Figure 11-32, the proposed control ensures an overall higher torque with respect to the standard at high altitude, without the risk of overshoot. Indeed, the torque in a CR engine is limited by the air availability in order to limit smoke generation. With the proposed control, it is therefore possible to contain the air deficiency allowing a higher torque generation without smoke impact.

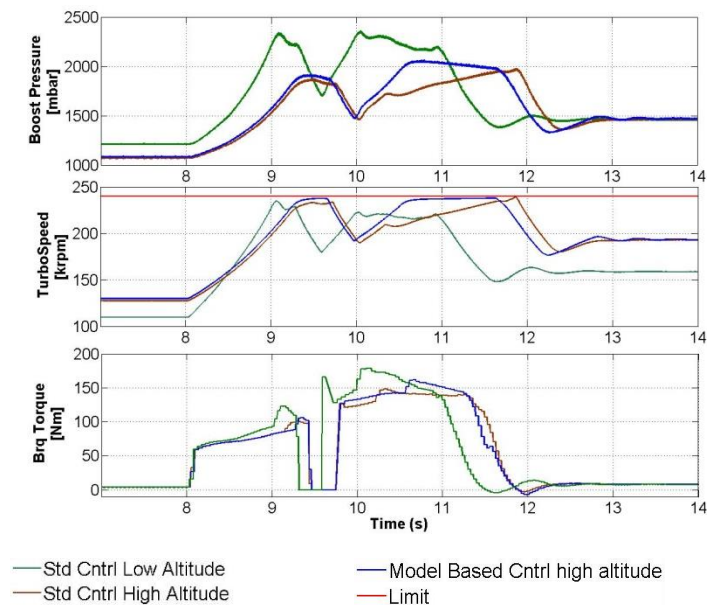


Figure 11-32 Comparison between fast standard, slow standard and model based boost control performance during fast transient with gear shifting under high altitude condition

### 11.3.3 Knock Control of GDI Turbocharged Engine (Case Study)

In modern GDI engines, knock represents one of the main constraints for the maximum thermal efficiency to be reached. Knock is one of the possible types of abnormal combustion that can occur in gasoline engines. After the spark discharge, the flame front propagates from the spark plug through the combustion chamber. While the flame front moves towards the cylinder walls, the fresh, end gas zone is compressed due to expansion of the burned gas, and heated by the flame front. When the unburned fresh charge reaches certain temperature and pressure levels, it may self-ignite. If the flame front does not reach the fresh gas before it self-ignites, the end gas gives rise to extremely rapid and uncontrolled combustions, called knock. Some of them produce extremely high temperature peaks and degenerate in pressure shock waves, thus possibly causing permanent thermo-mechanical damage to the combustion chamber components. Combustion chamber geometry, spark advance, fuel type, pressure and temperature levels are the main knock-related parameters. Limiting the spark advance with respect to the value that corresponds to maximum thermal efficiency, in an open loop control chain, it is possible to minimize the probability of knock onset. On the other hand, several uncontrolled parameters influence the detonation outset, as an example: fuel quality, intake pressure and temperature. To detect knocking combustions, a pressure sensor directly facing the combustion chamber provides the maximum information, but this type of technology does still not meet automotive constraints in terms of cost and reliability. To overcome these issues, alternative sensors have been developed. The most diffused knock detection systems are based on vibration sensors (accelerometer) screwed on the engine, in a specific position, or devices able to use the spark plug as a current sensor to detect the ion concentration variations inside the combustion chamber [191].

In this activity research a novel sensing system for knock detection based on acoustic has been developed and its performance has been evaluated in comparison with cylinder pressure sensor, assumed as reference. The acoustic sensing offers, at cost comparable with accelerometer, the capability to perform at same time more functions (e.g. turbocharger speed evaluation), as already explained.

The investigations on knock detection were carried with positive results in a 4 cylinders GDI engine for passenger car and in high speed 4 cylinders for motorbike. In the next section the focus is on car engine, showing the evaluation of the knock detection performance via acoustic and the results of closed loop control on engine test bench. More details of the whole research activity have been presented in specific works [211, 214, 215].

#### Experimental setup

All the experimental tests carried out during the research activity have been executed on a 4 cylinder 1.4L Turbocharged GDI engine, for passenger car applications. Its technical data are summarized in Table 11-3.

Table 11-3 Technical data of the engine used during the experimental tests

Displaced Volume	1390 cm <sup>3</sup>
Maximum Torque	220 Nm @ 1500-4000 rpm
Maximum Power	103 kW @ 6000 rpm
Architecture	L4, firing order 1-3-4-2
Number of valves	4 per cylinder
Intake system	Super and Turbo Charger
Injection system	GDI 180 bar
Bore	76.5 mm
Stroke	75.6 mm
Compression Ratio	10.1



The engine is managed by means of a Magneti Marelli ECU and a RCP system where run the new control functions based on acoustic sensing. Figure 11-33 shows the described experimental set-up.

The in-cylinder pressure of each cylinder has been measured by means of Kistler 6052A piezoelectric sensors. An acoustic probe, presented in a previous section, has been used for acquiring acoustic emissions.

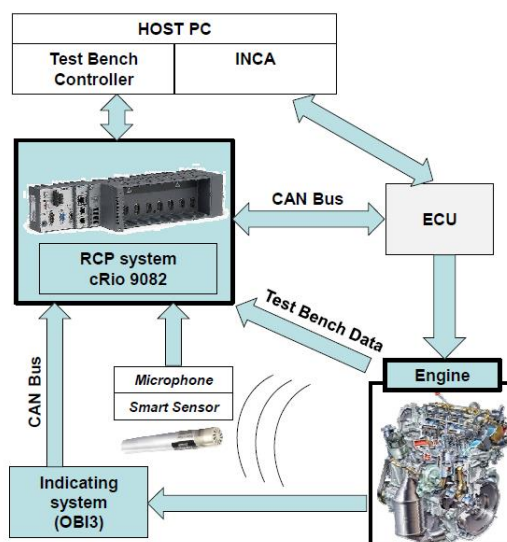


Figure 11-33 Experimental layout

To compare the results obtained by the sound analysis with the performance of the sensors, normally used for onboard application, the signal provided from the accelerometer already present on the production engine has also been acquired. The accelerometer was placed behind the volumetric compressor, between cylinders 2 and 3 (Figure 11-34). This type of sensor is a widespread solution adopted for knock onset detection in gasoline engines. The four in-cylinder pressure, accelerometer and acoustic emission signals have been acquired simultaneously at 200 kHz by means of an onboard indicating analysis system (OBI-M2) by Alma Automotive. A turbo SPEED DZ135 sensor by Micro-Epsilon, facing the compressor of the turbocharger, has been used to directly measure its rotational speed.

Moreover, the most important ECU and test bench variable have been acquired at low frequency using the ECU interface software INCA provide by ETAS and by means of the test bench management software.

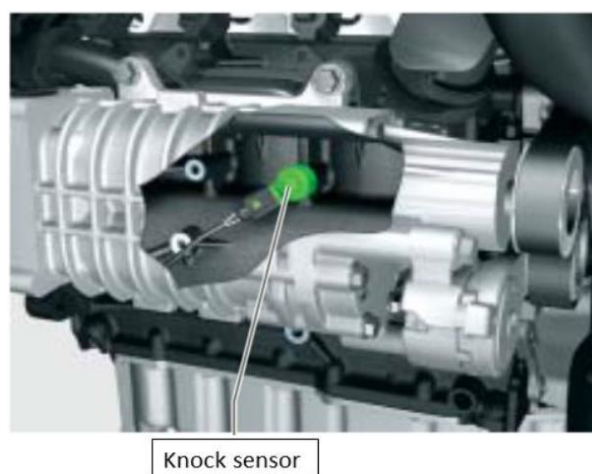


Figure 11-34 Installation of the production accelerometer sensor

## Knock Detection via Acoustic

In the first part of the study, a novel methodology to derive a knock index based on engine acoustic emissions has been carried out. Three engine operating points have been considered (Table 11-4).

Table 11-4 Engine operating points for knock testing

<i>Operating</i>	<i>Engine Speed</i>	<i>Intake Manifold</i>
1	2000 rpm	1300 mbar
2	2500 rpm	1500 mbar
3	3000 rpm	1500 mbar

One of the most important aspects that must be taken into consideration when performing an acoustic analysis is the microphone position. In fact, the acoustic waves emitted by a source may be partially or totally shielded by the presence of a barrier along their path, when diffusing through the surrounding environment. The acoustic sensor position has been defined after a preliminary investigation. Thirteen different locations around the engine have been tested during the experimental phase, to determine the ones that enable knocking clink, with constraint to sense at same time the turbocharger speed.

The placement with the highest signal to noise ratio has been identified in the intake side of the engine, under the intake manifold (Figure 11-35). Usually, onboard application requires a further optimization step for finding the best sensing position, but the signal to noise ratio is typically higher onboard the vehicle than in the test cell, due to noise absorption characteristics and shape of the engine compartment.

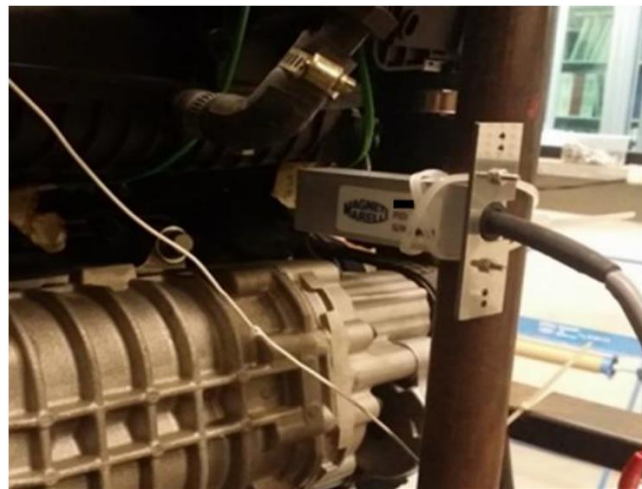


Figure 11-35 Positioning of the microphone based sensor

In the second part of activity the close loop control was assessed on real engine demonstrating that the audio-based algorithm is quite similar to accelerometer based implemented in standard MM ECU, allowing an essay switch between the two sensors.

## Combustion Chamber Vibration Modes

The combustion chamber can be considered as a bi-dimensional membrane that vibrates if excited by pressure waves. The vibration modes of the membrane are strictly correlated to the geometry of the

combustion chamber itself and to the thermal state of the trapped gas. The Draper's frequencies can be calculated by equation

$$fr = C_s \cdot \frac{\rho(r, c)}{\pi \cdot B} \quad (11.11)$$

where  $fr$  is the resonance frequency,  $C_s$  the sound speed,  $B$  the cylinder bore and  $\rho$  the wave number.

For the engine considered in this study, the first four vibration modes have been calculated using (11.11) and the values are listed.

Table 11-5 Combustion chamber resonant modes

$r, c$	$P$	$fr$
$[-]$	$[-]$	$[kHz]$
1,0	1.84	7.67
2,0	3.05	12.72
3,0	4.20	17.52
4,0	5.32	22.19

Preliminary experimental tests were performed by inducing knocking levels of different intensity (by acting on the Spark Advance), to verify whether the in-cylinder pressure signal was actually excited at the estimated resonant frequencies shown in Table 11-5, and whether such “signature” was observable also on the engine acoustic emission.

Figure 11-36 shows the Power Spectral Density (PSD) calculated for the in-cylinder pressure signal under non-knocking, light-knocking and heavy-knocking conditions (at a given engine speed), confirming the sensitivity of in-cylinder pressure to knock intensity, and the resonant frequencies values calculated by equation (11.11).

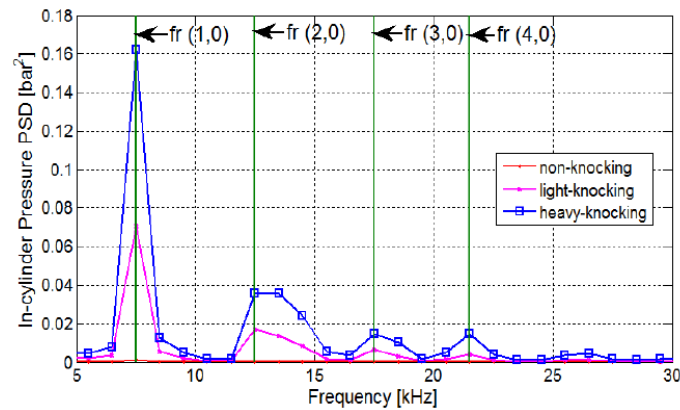


Figure 11-36 In-cylinder pressure signal energy distribution

The data shown in Figure 11-37 are related to the same tests of Figure 11-36, but in this case the PSD has been extracted from the acoustic emission signal, demonstrating that its frequency content is affected by knock in a similar way, and therefore proving that in principle the acoustic emission can be used to measure knocking intensity.

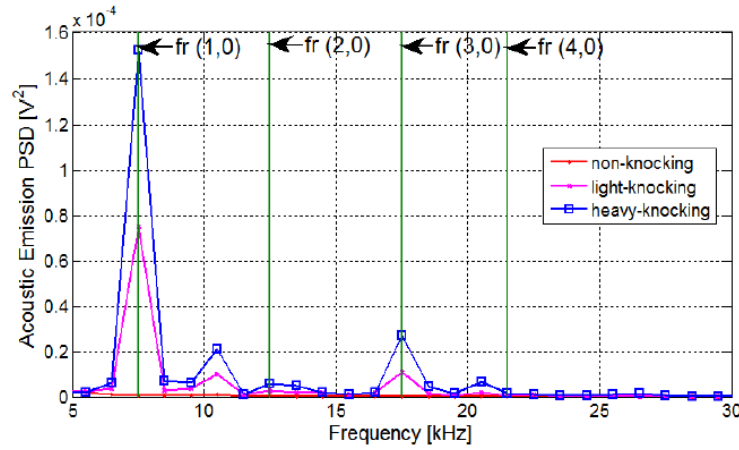


Figure 11-37 Acoustic emission signal energy distribution

Comparing the figures above, it may be noted that in both signals the same frequencies are excited during knocking combustions. Furthermore, the energy intensity in the acoustic emission spectrum increases in the same way as for the in-cylinder pressure signal. On the other hand, observing Figure 11-37, it is visible that the engine sound wave spectrum contains significant frequency components that are not correlated to knock intensity. This consideration suggests that the knock detection should be performed through an analysis of frequency bands close to combustion chamber natural modes, in order to avoid the influence of other acoustic sources.

Many types of knock indexes have been developed in the last decades. A detailed review of the main approaches has been presented in [193], and more recently in [195].

To assess the quality of the knocking information contained in the audio signal with respect to the one that can be extracted from the cylinder pressure, the first step of the study has been the definition of different knock intensity indexes based on acoustic emissions, and the comparison with an in-cylinder pressure based knocking index assumed as a reference. In particular, the Maximum Amplitude Pressure Oscillation (MAPO) defined by equation (11.12) has been considered as the reference pressure-based knocking index [194].

$$MAPO = \max(|P_{cyl_{filt}}|) \quad (11.12)$$

For MAPO evaluation, the in-cylinder pressure is high pass filtered at 5 kHz. MAPO values are strictly associated to the intensity of the pressure waves produced by the auto-ignition process, and therefore to the main knock-related damage mechanisms [28]. For sound based knock intensity, two different indexes have been considered [192], defined by equations (11.13) and (11.14):

$$Int = \frac{1}{\theta_2 - \theta_1} \cdot \int_{\theta_1}^{\theta_2} |Sound_{filt}| d\theta \quad (11.13)$$

$$SDBP = \max(|Sound_{filt\ 1}|) + \max(|Sound_{filt\ 2}|) + \max(|Sound_{filt\ 3}|) \quad (11.14)$$

For the *Int* index calculation, the acoustic emission signal (*Sound*) has been band-pass filtered between 7 and 8 kHz. This frequency band corresponds to the first vibration mode, which resulted as the most sensitive in both pressure and sound signals. The frequency bands corresponding to the first three vibration modes, which resulted more evident in the acoustic spectrum, have instead been chosen for the definition of *SDBP*. *Int* index represents the knocking index typically implemented within production ECUs for accelerometer-based knock-detection, and it is therefore particularly interesting to verify, in this study, the correlation level that may be achieved with in-cylinder pressure based knocking indexes using this type of algorithm.

The positions and widths of the angular windows used for knock evaluation for both in-cylinder pressure and sound emission are the same. Another aspect that should be considered, in sound analysis, is the transport time between sound emission and the moment that the sound wave reaches the microphone. By compensating this time delay, it is possible to maximize the signal to noise ratio and to assign the knocking event to the right cycle and cylinder. In the real time algorithm, the time delay has been initially estimated by measuring the air temperature and the distance between the microphone and each cylinder. The sound speed has been evaluated by means of its definition.

## Knock Detection Results

Knocking has been induced for the three engine operating conditions summarized in Table 11-4 and the sound was measured in each of the thirteen sensor positions. The complete engine operating range has not been explored because the goal of this first part of the study was the determination of the position with the best signal to noise ratio. For each operating condition, 500 subsequent engine cycles have been acquired and processed.

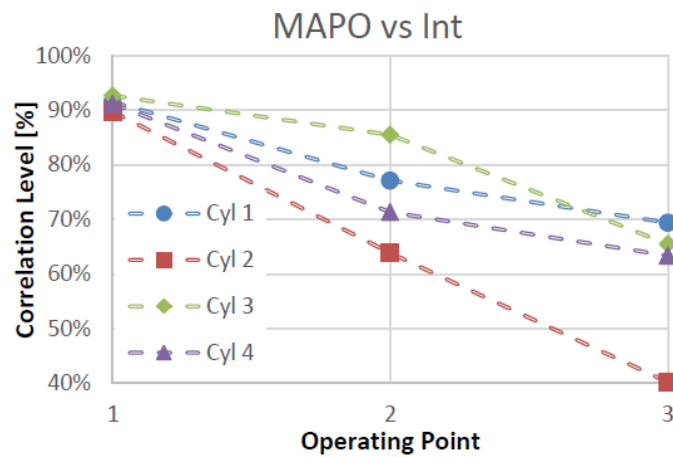
To evaluate the results, in terms of knock intensity detection, the Pearson's linear correlation coefficient has been calculated between MAPO and the two sound-based knocking indexes. The Pearson correlation coefficient is a statistical measure of the linear dependency between two variables  $x$  and  $y$  defined in equation (11.15). It can vary between +100% and -100%. A correlation level equal to 100% means that the two quantities change in the same way, therefore, the same information can be found in both signals.

$$r(x, y) = \frac{\sum_{i=1}^N (x_i - \bar{x}) \cdot (y_i - \bar{y})}{\sqrt{\sum_{i=1}^N (x_i - \bar{x})^2 \cdot \sum_{i=1}^N (y_i - \bar{y})^2}} \quad (11.15)$$

The experimental results, obtained in the position considered as optimal for the knock detection (intake engine side, with the acoustic sensor placed very close to the engine) are reported in the following Figure 11-38 and Figure 11-39.

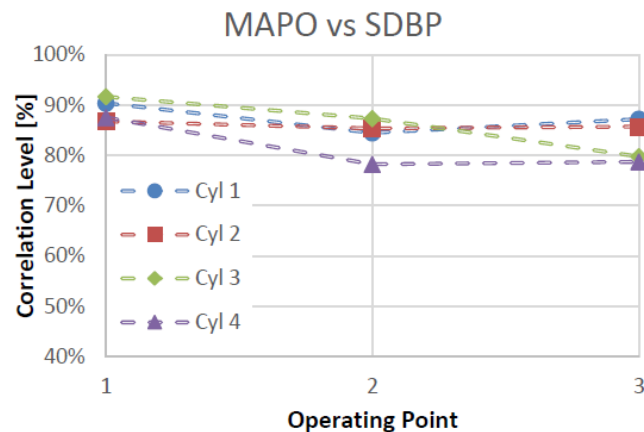
By analyzing the results reported below, it may be noted that *Int* knock index shows high correlation levels for the first operating point, but it highlights a decreasing trend when engine speed increases. On the other hand, the *SDBP* index presents a more stable behavior for the three operating conditions examined, and very high correlation levels.

Lee et al. [196] explain these two different trends by analyzing the behavior of the combustion chamber natural frequencies. When the engine runs at high speed, the contribution of the higher resonating modes becomes preponderant with respect to the resonances related to lower frequencies. As already clarified, *Int* index considers only one frequency band, whereas *SDBP* index takes into account also the natural frequencies that become more relevant when the engine runs at higher speeds. Based on such considerations, *SDBP* has been chosen as the sound-based knocking index to be implemented in the real-time knock control strategy.



Point #	rpm-mbar	Cyl. 1	Cyl. 2	Cyl. 3	Cyl. 4
1	2000-1300	91.54%	89.74%	92.66%	91.19%
2	2500-1500	77.12%	63.84%	85.52%	71.35%
3	3000-1500	69.41%	40.17%	65.49%	63.36%

Figure 11-38 Correlation levels between MAPO and Int audio knock index



Point #	rpm-mbar	Cyl. 1	Cyl. 2	Cyl. 3	Cyl. 4
1	2000-1300	91.82%	86.32%	92.60%	89.61%
2	2500-1500	82.30%	77.39%	86.98%	73.48%
3	3000-1500	84.58%	83.07%	78.15%	77.18%

Figure 11-39 Correlation levels between MAPO and Int audio knock index

It should finally be noted that the correlation levels presented in Figure 11-38 are particularly high. Slightly lower correlation levels were in fact obtained for the same data set by using the standard, production type accelerometer mounted on the engine for knock detection and control.

## Knock Control Strategy

In the previous paragraphs the feasibility of using the acoustic emission as knock information source has been proved and implemented in real time. In this part of the study, the possibility to switch from accelerometer to acoustic signal source only performing a recalibration of control strategy is

demonstrated. For the tests, the engine control has been managed by means of a Magneti Marelli standard ECU. The knock control strategy implemented in the ECU has been the same used in the standard accelerometer-based production system. Knock has been externally induced by applying controlled spark advance increments. The MAPO defined by equation (11.12) has been considered as the reference pressure-based knocking index, expressed in bar.

To maintain only the knock-related information contained in the in-cylinder pressure signal, it has been high-pass filtered at 5 kHz. The observation window adopted for MAPO evaluation starts from the Top Dead Center (TDC) and ends at 70 crankshaft angle degree (CAdeg) after Top Dead Center (ATDC), for all the tests that have been executed. In order to assess the ability of the audio-based knock system to maintain a light knock intensity, and to compare it to the standard accelerometer-based one, an empirical MAPO value limit considered as Light Knock Intensity Threshold (LKTH) has been set in bar, as shown by equation (11.16).

$$LKTH = \frac{Engine\ Speed}{2000} \quad (11.16)$$

Furthermore, a second MAPO limit, in this case as High Knock intensity Threshold (HKTH), has been defined by equation (11.17).

$$HKTH = \frac{Engine\ Speed}{1000} \quad (11.17)$$

In both expressions the *Engine Speed* is expressed in [rpm]. This distinction is useful to set an appropriate trade-off between performance and engine safe operating conditions. Table 11-6 collects the engine operating conditions and the corresponding MAPO limits for light and high knock.

The aim of this study is to demonstrate the possibility of substituting the accelerometer with an acoustic sensor as provider of knock intensity information in a standard engine management system, by only performing a knock detection strategy recalibration process. To evaluate the actual possibility to switch the standard knock control algorithm from vibration to sound, one of the hard constraints is that the structure of the knock index evaluated by the control system is to be the same for both signals.

Table 11-6 Engine operating conditions investigated during the tests

Engine speed [rpm]	Load	MAPO Light knock threshold (LKTH)	MAPO High knock threshold (HKTH)
2000	WOT	1.00 [bar]	2.00 [bar]
2500	WOT	1.25 [bar]	2.50 [bar]
3500	WOT	1.75 [bar]	3.50 [bar]

Recalibration procedure has involved only the parameters related to the knock observation windows (opening and closing crankshaft angles) and the ECU knock intensity thresholds. In particular, the mathematical structure of the Knock Index (KI) evaluated by the engine management system depends on the signal energy defined by equation (11.18), as presented in [197].

$$SignalEnergy = \frac{1}{N} \sum_{i=1}^N x(i)_{filt\ 6-16\ kHz}$$
(11.18)

Where  $N$  is the number of samples acquired in the angular period and band-pass filtered by the ECU is in the range between 6 to 16 kHz. Considerations regarding the dynamics of the average signal energy, its statistical distribution and the calibration efforts at the engine test bench, suggest realizing a logarithmic transformation by the following equation:

$$KI = \log(SignalEnergy) - \mu - KITH(rpm, load)$$
(11.19)

where  $\mu$  is the mean value of the statistical distribution estimated by a low pass filter applied to the current and previous estimated mean value, whereas  $KITH(rpm, load)$  is a threshold function of the engine operating point.

A detailed description of the algorithm implemented in the ECU can be found in a dedicated publication [197]. The main task that a knock controller should accomplish is the maximization of the engine performance (maximization of the combustion efficiency) while preserving the engine from damages caused by knocking combustion. Figure 11-40 illustrates the two typical operating regions of engine: the bottom area, indicated by “1”, is the non-knocking region, whereas the top area, labelled as “2”, is characterized by the onset of knocking combustions. The boundary line that divides the two regions represents the goal of the knock control strategy. When the engine runs at an operating condition located near the boundary line, it means that the maximization of the combustion efficiency has been achieved, while guaranteeing a non-damaging knock intensity level.

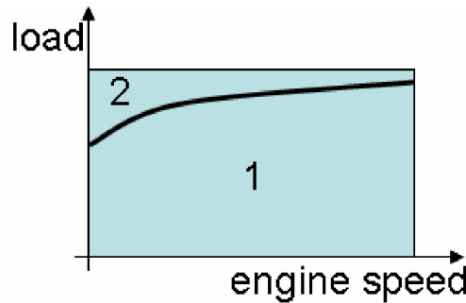


Figure 11-40 Main operating regions of engine: 1) non-knocking 2) knocking

After the knock controller tuning, a series of validation tests for each operating point have been performed. To assess the overall performance of the system, two types of tests have been performed. The first test has been performed in steady state conditions. Initially, knock is forced by adding a Spark Advance (SA) increment to the value calculated from the base map, thus enabling the knock controller to take action. The controller response is then observed and evaluated after steady-state conditions have been reached again. The SA increment has been the same for the test run with the accelerometer and the acoustic sensor, since the aim of this experiment is the assessment of the steady-state calibration procedure.



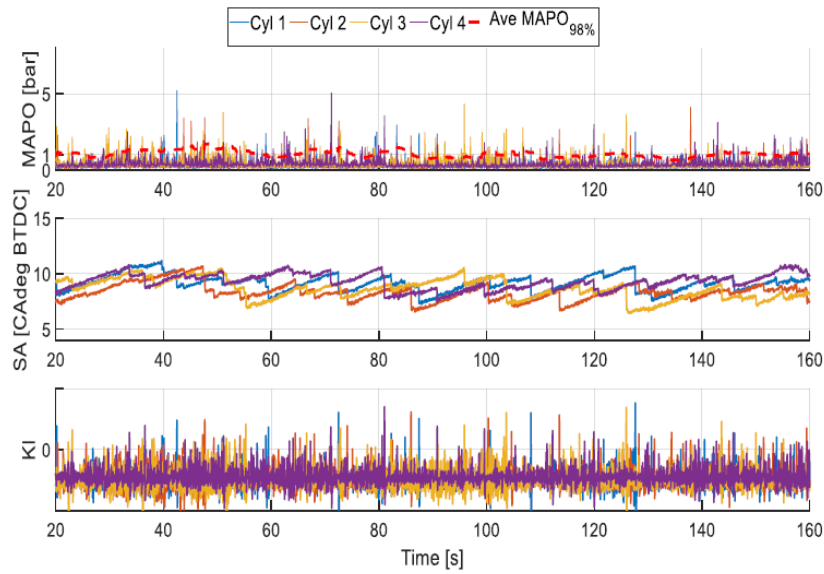


Figure 11-41 Results for steady state test runs at 2000 rpm WOT with accelerometer

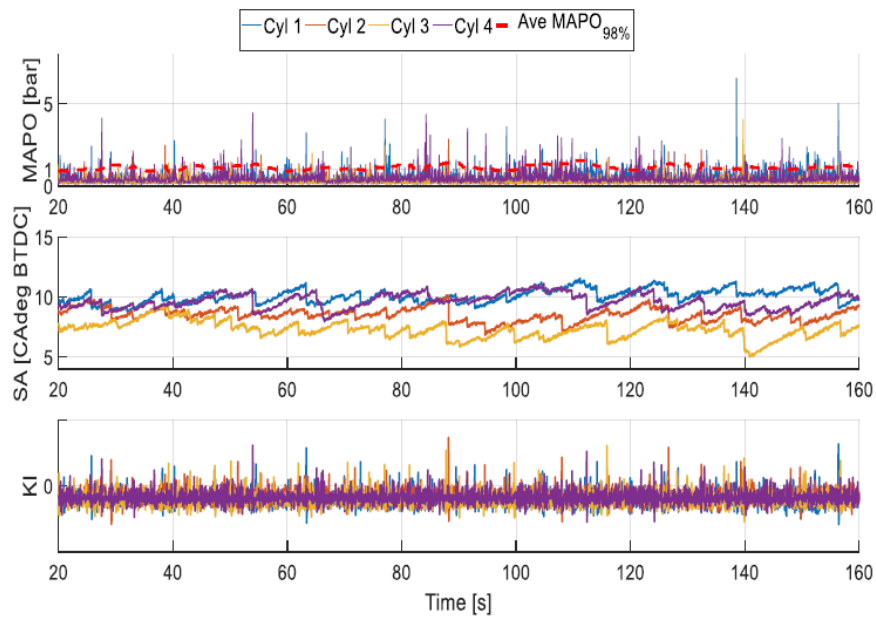


Figure 11-42 Results for steady state test runs at 2000 rpm WOT with acoustic probe

By the comparison of the couples of Figure 11-41 and Figure 11-42, which compare the same test performed using the accelerometer and sound signals, it can be appreciated as, for both signal sources, the control system has approximately the same behavior. For all the tests, the average MAPO percentile target has been reached. It is possible to see that the controller forces an oscillation of the MAPO percentile value around the target level (Table 11-6). The false positive percentages detected during the steady state tests have been calculated and collected in Table 11-7. Very few events are misinterpreted.

Table 11-7 Percentage of false positives occurred during the static test using accelerometer (top) and acoustic (bottom) sources.

	False Positives percentage			
	Cylinder 1	Cylinder 2	Cylinder 3	Cylinder 4
2000 rpm	1.28%	1.14%	0.72%	0.48%
2500 rpm	1.31%	0.96%	0.74%	0.15%
3500 rpm	0.40%	0.68%	0.37%	0.51%

	False Positives percentage			
	Cylinder 1	Cylinder 2	Cylinder 3	Cylinder 4
2000 rpm	1.45%	0.03%	1.99%	2.39%
2500 rpm	0.72%	0.91%	0.42%	0.34%
3500 rpm	0.41%	0.94%	0.81%	0.90%

Table 11-7 shows that the results obtained are similar for both the cases. The difference between the two detection methodologies is greater comparing cylinder 3 and 4 in the test at 2000 rpm, but the percentage values obtained are compatible with the standard production targets.

After the steady state validation, a transient test has been performed, with the purpose of comparing the stability and the reactivity of the controller. In this case, the test starts under light knock condition (the spark advance actuated is the same calculated from the spark advance base map), and after a few seconds a manual spark advance increment is forced. After reaching steady state condition, an instantaneous reduction of the spark advance angle w.r.t. the base map is forced. The aim of this test is the assessment of the ability of reaching (and maintaining) light knock conditions from two opposite directions. Because the aim of the knock controller is not only to safeguard the engine integrity, but to reach the maximum thermal efficiency while respecting the knock limit calibrated by the engine manufacturer. In this case, the knock threshold (Table 11-6) is not only a border line for the engine integrity, but at the same time, it is a thermal efficiency target, and as such the engine should work as close as possible to this limit.

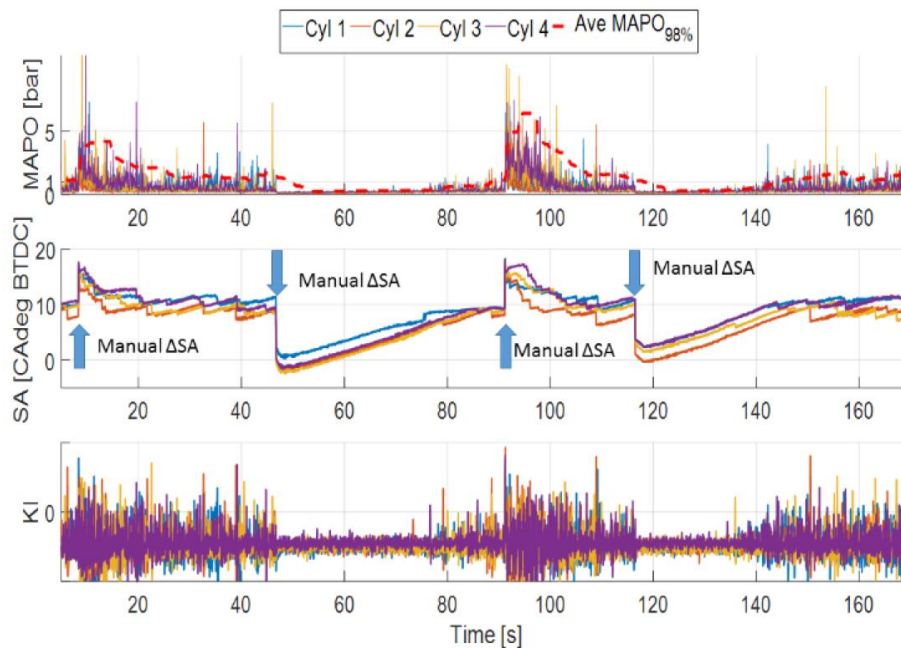


Figure 11-43 Results for transient state test runs at 2000 rpm WOT for vibration

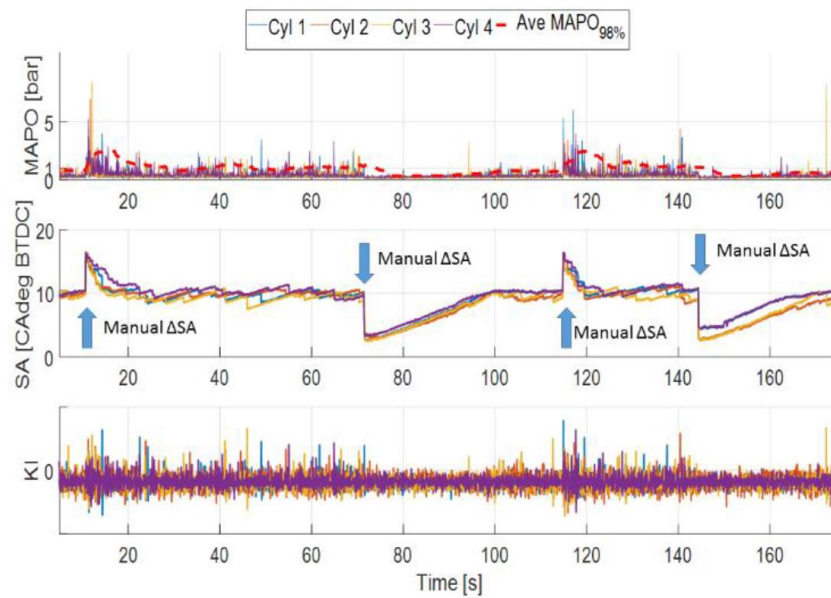


Figure 11-44 Results for transient state test runs at 2000 rpm WOT for acoustic probe

As in the previous case, the couple of Figure 11-43 and Figure 11-44 compares the same type of test performed during different engine operating conditions, using the accelerometer and sound sources. It is clearly emphasized how the control system tracks the light knock condition, keeping the engine in an oscillation around the MAPO percentage target similarly, both in the case of increment or decrement of the spark advance from the base condition, and for both acoustic and accelerometer-based systems. The time needed to recover a target condition (recovery time) is similar for the two systems based on different sensors, and the steady-state SA values (and the corresponding knocking levels) reached after rejecting the disturbance are also very similar, demonstrating the feasibility of a sound-based knock-controller based on the very same signal processing architecture as the production one, based on accelerometer sensors.

## 11.4 Virtual Sensor of Combustion Indexes (Case Study)

Due to the increasing request for pollutant emissions reduction in internal combustion engines, a large amount of research are ongoing to investigate advanced combustion methodologies presented in Chapter #6.4. In particular a significant reduction in both NO<sub>x</sub> and Particulate Matter added to an efficiency improvement can be achieved through Low Temperature Combustion approaches, usually characterized by high EGR rates and a highly premixed combustion portion.

Unfortunately, LTC operation is very sensitive to in-cylinder thermal conditions. Consequently, non-optimal combustion control can lead to combustion instability and cylinder-by-cylinder imbalance. In order to avoid such problem, closed-loop combustion control is necessary.

As a matter of fact, a significant improvement of combustion outputs can be achieved, also in conventional combustions of gasoline and diesel engines, through closed-loop combustion control based on the real-time processing of in-cylinder pressure signal [198,199,200]. This quantity provides crucial information about the way combustion takes place in the combustion chamber, such as indicated torque delivered by the engine, pressure peak location, start (SOC) and center of combustion (CA50). However, pressure sensors on-board installation is still uncommon, mainly due to problems related to reliability and cost. Therefore, over the past years, several remote combustion sensing methodologies have been

developed, the goal being to extract information about combustion through the real-time processing of signals coming from low-cost sensors (both standard and additional) mounted on the engine.

This section presents the research studies about overall remote combustion sensing methodologies that allows estimating many indicated quantities used in conventional and LTC closed-loop control strategies, such as:

- Indicated Torque delivered by the engine;
- Center of Combustion (CA50);
- Start of Combustion (SOC);
- Rate of Heat Released (ROHR) Peak location, corresponding to Pressure Peak location within the cycle;
- Combustion Noise (CN).

The presented virtual sensing approach is based on the analysis of engine vibration, engine speed fluctuation and engine acoustic emission, therefore the installation of cylinder pressure sensors is not required. Engine speed fluctuations can be derived from the same phonic wheel already mounted on-board for other control purposes (no extra hardware cost), while engine block acceleration and acoustic emission can be measured using an accelerometer mounted on the engine block and a proper acoustic probe (compared to the installation of pressure sensors, the additional hardware cost is much lower).

Previous works [201,202,203] demonstrate that CA50 (average value over one cycle) and indicated torque delivered by each cylinder can be determined through a proper processing of crankshaft speed fluctuations. Moreover the signal coming from the accelerometer mounted on the engine block can be used to determine start of combustion and pressure peak location within the engine cycle (one per cylinder), as presented in previous works [205,206,207], one of them by the author of this thesis [204]. In addition, a proper processing of the acoustic emission captured by a microphone-based device can be used to real-time control combustion noise.

The virtual sensors developed and presented in this study are general, therefore can be applied to engines with different architectures and combustions. The estimation algorithms have been implemented in a programmable Rapid Control Prototyping (RCP) system, used to real-time estimate the indicated quantities of interest during the operation of diesel and gasoline engines with different layouts (in terms of combustion order and angular spacing between combustions). In addition, to validate the algorithms for LTC strategies, one Compression Ignited (CI) diesel engine has been also operated in PCCI (diesel) and RCCI (dual fuel with diesel and gasoline) mode.

### ***Experimental Set-up***

In order to develop and validate the algorithms for the estimation of the above mentioned combustion indexes, a wide set of specifically designed tests have been run on a 1.3L Common Rail Diesel engine mounted in a test cell at the University of Bologna. The technical characteristics of the engine employed for the investigations are summarized in Table 11-8.

Table 11-8 Engine technical characteristics for the CI, PCCI and RCCI studies

Displaced Volume	1248 cm <sup>3</sup>
Bore	69.6 mm
Stroke	82 mm
Compression Ratio	16.8
Architecture	L4, firing order 1-3-4-2
Number of valves	4 per cylinder
Injection system	Common Rail Multi-Jet + PFI system
Maximum Torque	200 Nm @ 1500 rpm
Maximum Power	70 kW @ 3800 rpm

With regard to the analysis of PCCI combustion, this operating mode has been managed by simply modifying the EGR and the injection pattern and in such a way to obtain a highly premixed combustion portion (corresponding to the Pilot injection) and varying the Dwell Time (DT) between Pilot and Main injection.

Together with the PCCI operating mode, air and fuel path of the Diesel engine have been modified in order to be compatible with the RCCI operating mode. According to description in Chapter #6.4.5, a new intake manifold has been manufactured, and 4 gasoline PFI injectors have been installed on it, see Figure 11-45. These injectors have been connected to a rail filled with gasoline using a rotary fuel pump. Rail pressure has been kept constant at 5.5 bar using a pressure regulator.

In RCCI operating mode, the additional gasoline system allows injecting gasoline in the intake manifold, creating a gasoline-air mixture that enters the combustion chamber when the intake valve opens. Then, combustion activation is obtained through Diesel direct injection.

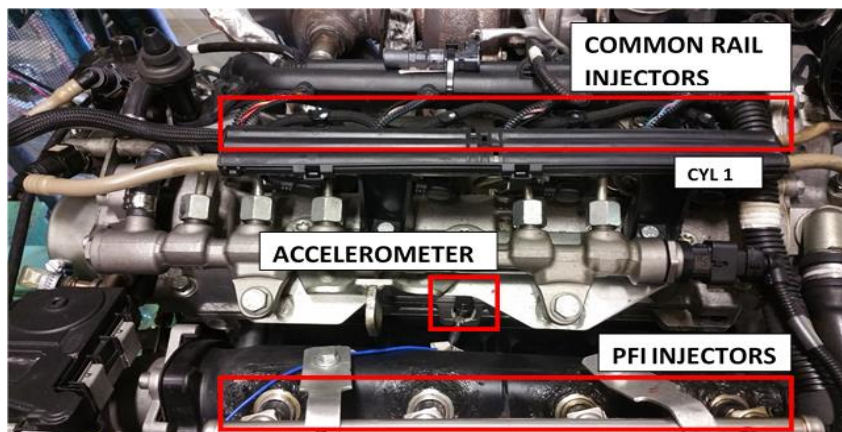


Figure 11-45 Fuel systems installation on engine employed for CI, PCCI and RCCI tests

The injection controller has been implemented in a Rapid Control Prototyping system based on a National Instruments cRio 9082, see Figure 11-46. The RCP samples at high frequency the signal coming from the crankshaft speed sensor (standard VRS), which allows the system to determine the instantaneous angular location within the engine cycle, engine block acceleration and the voltage signal coming from the microphone.

Once the angular position has been determined, the RCP outputs the logical commands for the PFI injectors, i.e. Energizing Time (ET<sub>gas</sub>) and Start of Injection (SOI<sub>gas</sub>). Then, a dedicated ECU converts

the logical commands and generates the corresponding electric commands for the PFI injectors. The RCP system is also suitable to manage Diesel injection. To do so, it communicates with the standard ECU via CAN bus (CAN0) to read and overwrite (when necessary) the injection parameters of interest, i.e. Energizing Time (ET) and Start of Injection (SOI).

The engine under investigation has been equipped with in-cylinder piezoelectric pressure sensors (Kistler 6058A), and one accelerometer (PCB Piezotronic 352C33) installed in a position in which the block acceleration due to the combustion process can be perceived with a high signal-to-noise ratio (the chosen position depends on the engine architecture taken into consideration). Finally, engine acoustic emission was measured using a microphone-based sensing device, developed by Magneti Marelli. Engine noise signal was also measured using a PCB Teds 378C01 microphone faced to the engine block and acquired at a sample frequency of 100 kHz, as a reference for the acoustic probe [210].

All the signals coming from standard sensors already present on-board for control purposes are monitored and acquired using INCA® software and ETAS® hardware. The non-standard sensors installed in the test cell are acquired using the test bench controller and stored in the Host PC. The scheme of the experimental layout is summarized in Figure 11-46.

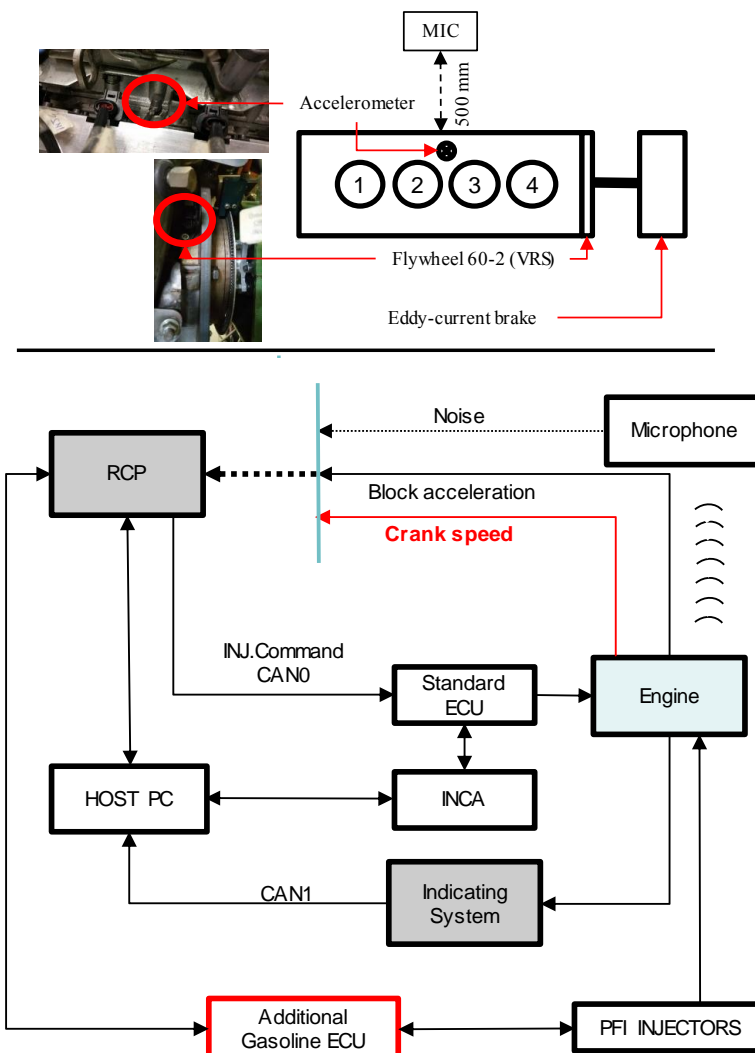


Figure 11-46 Scheme of the developed experimental setup for the management of CDC, PCCI and RCCI combustion

### 11.4.1 Indicated Torque and CA50 Evaluation via Crank-Shaft Speed Signal

According to previous works [260,261], the correlation existing between the generic  $k$ -th frequency components of engine speed and torque applied to the crankshaft can be expressed using a transfer function that only depends on the torsional characteristics of the engine-driveline system. The  $k$ -th harmonic component of torque delivered by the engine can be calculated as the difference between the corresponding harmonic components of indicated and reciprocating torque. Indicated torque fluctuation ( $T_{ind,k}$ ) can be directly calculated starting from cylinder pressure measurement, while reciprocating torque fluctuation ( $T_{r,k}$ ) can be calculated as a function of engine speed and reciprocating masses. With regard to the  $k$ -th harmonic component of engine speed ( $\dot{\theta}_k$ ), it can be calculated starting from engine speed measurement carried out using the same toothed wheel mounted on-board. Therefore, named  $H(j\omega)$  the transfer function, it can be expressed through equation (11.20).

$$H(j\omega) = \frac{T_{ind,k} - T_{r,k}}{\omega \cdot \dot{\theta}_k} \quad (11.20)$$

Since the value of the reciprocating masses is not always well known, the consequent errors in the evaluation of the transfer function might be not negligible. This problem has been overcome in previous works by the same authors [262] applying equation (11.20) to a test run in cutoff conditions (no fuel injected) at the same engine speed. The mathematical expression of  $H(j\omega)$  can be rearranged as follows:

$$H(j\omega) = \frac{T_{ind,k} - T_{ind\ cutoff,k}}{\omega \cdot (\dot{\theta}_k - \dot{\theta}_{cutoff,k})} \quad (11.21)$$

Here,  $T_{ind\ cutoff,k}$  and  $\dot{\theta}_{cutoff,k}$  represent the  $k$ -th harmonics of indicated torque and engine speed measured during an engine cycle run at the same engine speed but in cutoff conditions (no fuel injected). A detailed discussion of the methodology for the identification of the engine-driveline Transfer Function is beyond the scope of this work. However, the complete methodology is widely discussed in literature [201,202,203].

Once  $H(j\omega)$  has been determined, the transfer function can be calculated through the analysis of experimental data (torque and speed), but it is necessary to choose the proper  $k$ -th harmonic characteristic of the engine. The  $k$ -th harmonic of interest is the one at which torque and speed fluctuations show the highest amplitude, i.e. the one corresponding to the order characteristic of the engine. Since the engine used throughout this work performs 4 evenly-spaced combustions per cycle, the harmonic component of interest is  $k=4$ .

As a matter of fact, if all the cylinders behave the same way, i.e. produce the same torque waveform over crank angle, the only difference between the torque harmonic components will be a phase shift related to the firing order. Therefore, as it can be observed in Figure 11-47, if the 4 cylinders are perfectly balanced, the torque harmonic components ( $T_{ind,k}$ ) for  $k=1, 2, 3$  will be identically equal to 0.



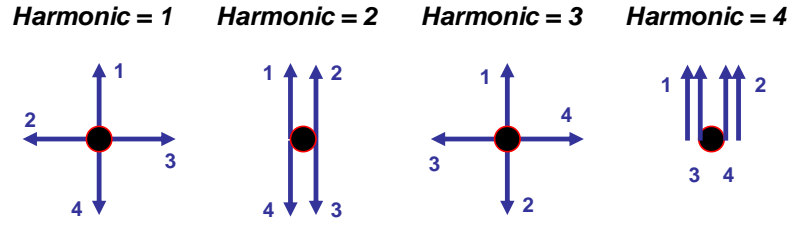


Figure 11-47 Torque harmonic components up to harmonic 4

Bearing in mind that only the harmonic component characteristic of the engine needs to be taken into account, the corresponding transfer function of the engine-brake system has been calculated from transient tests run in Conventioanl Diesel Combustion (CDC) mode. As reported in literature [262], only 3 engine speed ramps run at different load levels (cut-off conditions, medium load and full load) are necessary to calibrate the whole strategy. During the ramp tests, the whole speed range of the engine needs to be explored (from 1000 to approximately 4000 rpm for the 4-cylinder engine under study) to obtain a complete characterization of the transfer function. Amplitude and phase of the obtained transfer function are shown in Figure 11-48.

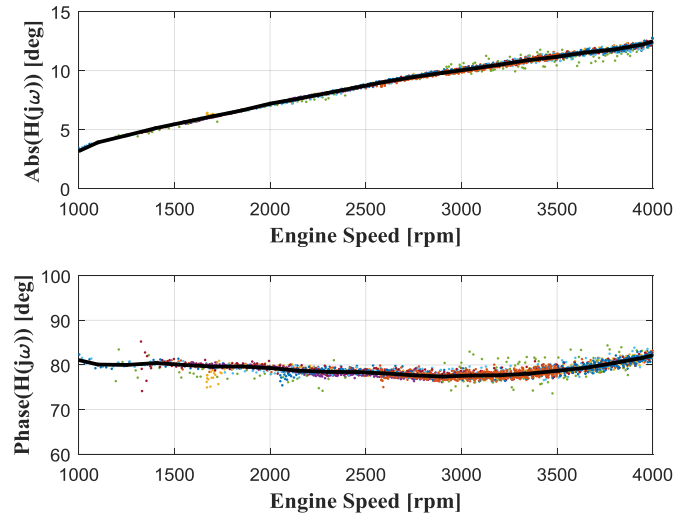


Figure 11-48 Transfer function characteristic of the CI engine-brake system

Once  $H(j\omega)$  has been determined, it can be used for real-time estimation of the indicated torque fluctuation during a generic operating condition simply rearranging equation (11.21) as follows:

$$T_{ind,k} = T_{ind\ cutoff,k} + H(j\omega) \cdot \omega \cdot (\dot{\theta}_k - \dot{\theta}_{cutoff,k}) \quad (11.22)$$

With regard to the quantities corresponding to the motored conditions,  $\dot{\theta}_{cutoff,k}$  can be measured during a cutoff and stored in a map as a function of engine speed, while  $T_{ind\ cutoff,k}$  can be estimated, as a function of manifold pressure and engine speed, through equation (11.23) [262] (both maps have been programmed in the RCP system).



$$\begin{aligned} abs(T_{ind\ cutoff,k}) &= c_0 + k_1 \cdot p_{man} + k_2 \cdot \dot{\theta}_0 \\ angle(T_{ind\ cutoff,k}) &= 90 [deg] \end{aligned} \quad (11.23)$$

It is important to highlight that the transfer function (and consequently the estimation of the torque harmonic component) is not affected by the combustion strategy (CDC, PCCI, RCCI, etc.), since it only depends on the torsional characteristics of the engine-driveline system under investigation [263].

## Conventional Diesel Combustion (CDC)

The calculated transfer function demonstrates that the indicated torque component of interest (amplitude and phase) can be estimated starting from the real-time processing of the crankshaft speed signal. Once the indicated torque fluctuation of interest has been determined, it can be used to estimate both indicated torque and center of combustion (CA50). As a matter of fact, previous works, where the author of the thesis was involved, demonstrate that it is possible to identify a strong correlation between torque fluctuation amplitude and its mean value over the engine cycle (together with the intake manifold pressure  $p_{man}$ ) as well as between torque fluctuation phase and CA50 (linear correlation) [202].

The above mentioned correlations have been determined offline, taking into account that both indicated torque and CA50 can be directly calculated starting from the acquired in-cylinder pressure signal. Indicated torque results to be correlated with the amplitude of its 4-th harmonic component and to the air quantity trapped inside the cylinder (therefore to intake pressure and engine speed), while a nearly linear correlation between CA50 and the phase of torque fluctuation can be set up.

With regard to CA50 has been determined as the angular position corresponding to 50% of the ROHR cumulated sum. As it is well known, net ROHR (that does not take into account the effects of “blow-by” and heat transfer through cylinder walls) can be directly calculated starting from in-cylinder pressure measurements through equation (11.24), from [86].

$$ROHR = \frac{1}{\gamma - 1} \cdot V \cdot \frac{dp}{d\theta} + \frac{\gamma}{\gamma - 1} \cdot p \cdot \frac{dV}{d\theta} \quad (11.24)$$

More details of this correlation analysis are not reported here, but it is fully discussed in literature. The main aspect to be underlined is that both torque delivered by the engine and the center of combustion can be estimated only through the analysis of crankshaft speed fluctuation (carried out using the same phonic wheel already mounted on-board).

The complete methodology for indicated torque and CA50 estimation has been implemented in the RCP and used to real-time estimate these quantities from engine speed measurement. The results obtained during transient tests run in CDC mode are reported in Figure 11-49. The estimation methodology proved to be very accurate in CDC mode, therefore the estimated indicated quantities might be used to feedback a closed-loop combustion control strategy.

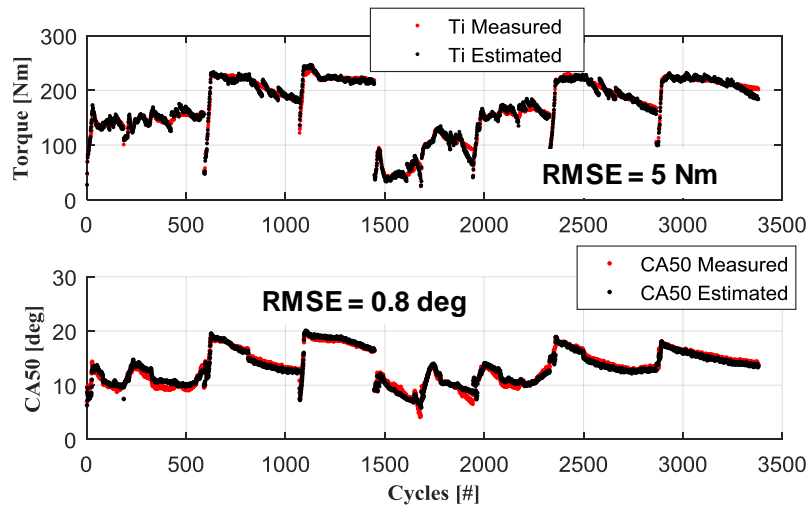


Figure 11-49 Indicated torque mean value and center of combustion in CDC mode, estimated vs measured

In this case, a closed-loop combustion control strategy has been also implemented in the RCP. Based on the estimated values of torque and center of combustion, such control strategy dynamically changes the energizing time of the Main injection ( $ET_{main}$ ) to keep torque constant while varying also the start of injection ( $SOI_{main}$ ) to keep nearly constant the center of combustion. To do so, when the engine is running, the controller reads via CAN bus the values of Start of Injection ( $SOI$ ) and Energizing Time ( $ET$ ) calculated by the engine control system for all the injections (Pilot, Pre and Main) of each combustion. Then, if the error between target and estimated indicated quantities remains below a calibrated threshold, the RCP system overwrites (via CAN bus) final  $SOI_{main}$  and  $ET_{main}$  with the same values calculated by the standard control (Standard injection pattern). Otherwise, if the error increases, the RCP system overwrites  $SOI_{main}$  and  $ET_{main}$  with new calibrations calculated by two separated PID controllers. Figure 11-50 reports a scheme of the whole developed controller.

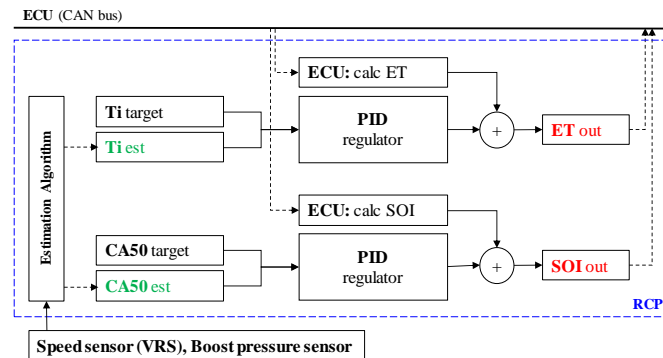


Figure 11-50 Scheme of the closed-loop combustion controller implemented and tested in this study; here, the estimated indicated quantities are the ones determined from the real-time processing of crankshaft speed fluctuations

To clarify how the developed controller works, Figure 11-51 shows the result obtained applying the closed-loop control strategy (that real-time varies the Main injection parameters) during a linear reduction of the amount of diesel injected in the Pilot injection (2-injections pattern).

As it can be observed in Figure 11-51, while the amount fuel injected in the Pilot injection is reduced (from 2.5 to nearly 0 mm<sup>3</sup>/stroke) the controller increases both  $ET_{main}$  and  $SOI_{main}$  to keep estimated torque and estimated CA50 at their target values. The experimental results demonstrate that the corrections based on the values of the estimated quantities also keep nearly at their target values the actual indicated quantities (calculated by the indicating system from in-cylinder pressure).

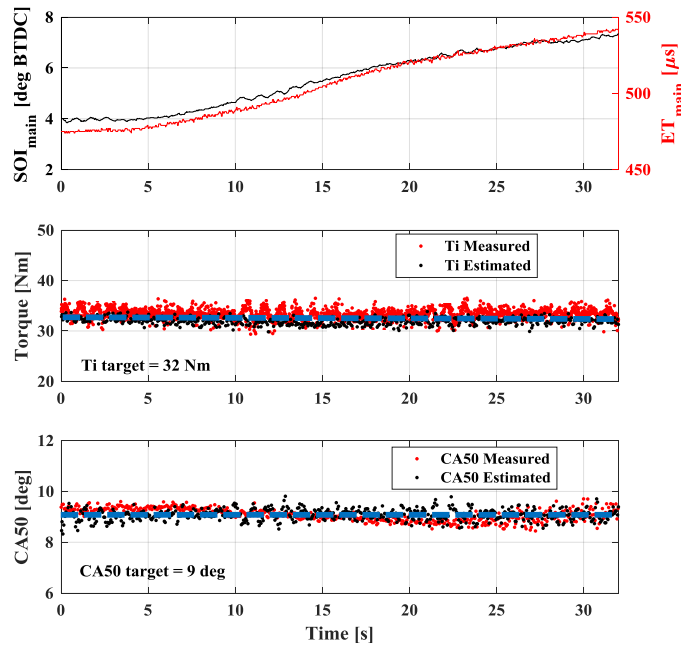


Figure 11-51 Closed-loop control of SOI<sub>main</sub> and ET<sub>main</sub> while reducing the amount of fuel injected in Pilot from 2.5 to nearly 0 mm<sup>3</sup>/stroke

Since the center of combustion estimation methodology proved to be effective for the closed-loop control of conventional diesel combustion, further investigations have been performed to extend the approach to other LTC strategy. To do so, the same CI engine has been modified to be operated in PCCI and RCCI mode.

### Pre-mixed Combustion Compression Ignition (PCCI)

PCCI combustions are diesel CI combustions mainly characterized by high EGR rates and highly premixed combustion portions. The combination of high ignition delays and EGR rates usually results in high sensitivity to cylinder thermal conditions; therefore closed-loop combustion control becomes crucial to guarantee combustion stability [41,306,307].

To validate the torque and CA50 estimation algorithm for PCCI diesel combustion, the standard injection pattern of the engine under investigation has been significantly modified. The number of injections has been set to 2 (Pilot, Main) and the amount of fuel injected in Pilot injection ( $Q_{pil}$ ) has been increased (up to 4 times the standard value) while reducing  $Q_{main}$  (to keep constant the overall fuel consumption). EGR rate has been also increased, the goal being to reduce combustion stability and increase cycle-to-cycle variability. As an example, starting from the standard injection pattern actuated by the ECU while running the engine at 2000 rpm and IMEP = 4 bar,  $Q_{pil}$  has been increased from 1 to 4 mm<sup>3</sup>/stroke and  $SOI_{pil}$  has been varied from nearly 14 up to 40 deg (while  $SOI_{main}$  has always been kept constant at 3.5 deg).

The variations applied to standard injection pattern significantly modify the way energy is released during the combustion process. Figure 11-52 shows an example of ROHR for an engine cycle in PCCI mode (red) compared to a baseline cycle run in CDC mode using the standard injection pattern (black).

For the cycle run in PCCI mode, the oscillations visible in the angular range corresponding to the Main combustion portion is caused by the impulsive energy release (more pre-mixed with respect to CDC), that occurs in a short angular range and produces high frequency oscillations captured by the in-cylinder pressure transducer.

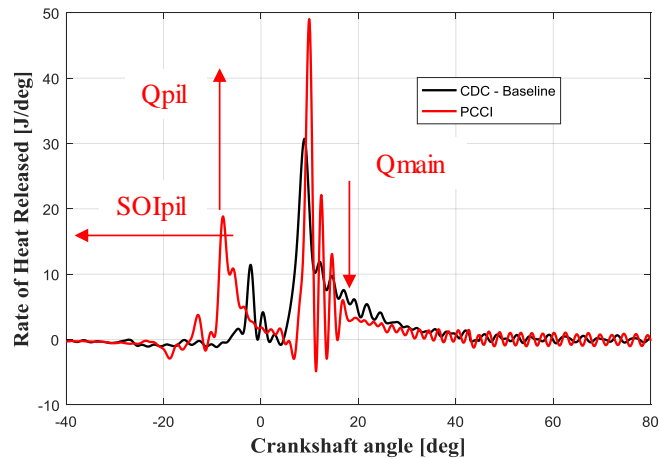


Figure 11-52 Comparison between ROHR in PCCI and CDC mode; tests run at 2000 rpm and IMEP = 4 bar

The whole PCCI combustion process can be often divided in 2 consecutive and partially overlapped combustion events. In this case, the calculated CA50 value becomes very noisy, and might also be unable to provide accurate information about combustion location within the cycle. To clarify this consideration, Figure 11-53 reports the cumulated (net) Rate of Heat Release for an engine cycle run in PCCI mode at 2000 rpm and IMEP = 4 bar. As it can be observed, identifying the angular position corresponding to the 50% of ROHR cumulated sum (CHR) can be critical, mainly due to the high dwell time (that leads to a non-monotonically increasing curve) between Pilot and Main injection. In some cases, this behavior makes CA50 a non-useful parameter for closed-loop combustion control.

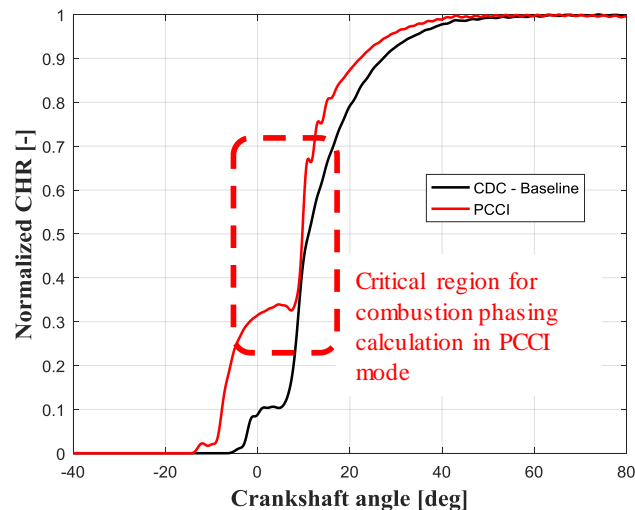


Figure 11-53 Normalized CHR curve for an engine cycle run at 2000 rpm and IMEP = 4 bar in PCCI mode

Although CA50 calculation might be critical for PCCI combustions, engine speed can still be used to estimate the indicated torque fluctuation of interest. Figure 11-54 reports the result obtained applying the torque fluctuation estimation methodology. As it can be observed, also in PCCI combustion, both amplitude (still strongly correlated with indicated torque mean value over the engine cycle) and phase of the indicated torque fluctuation can be accurately estimated. This quantity still provides important information about combustion location within the cycle, even if it is not always linearly correlated with CA50.

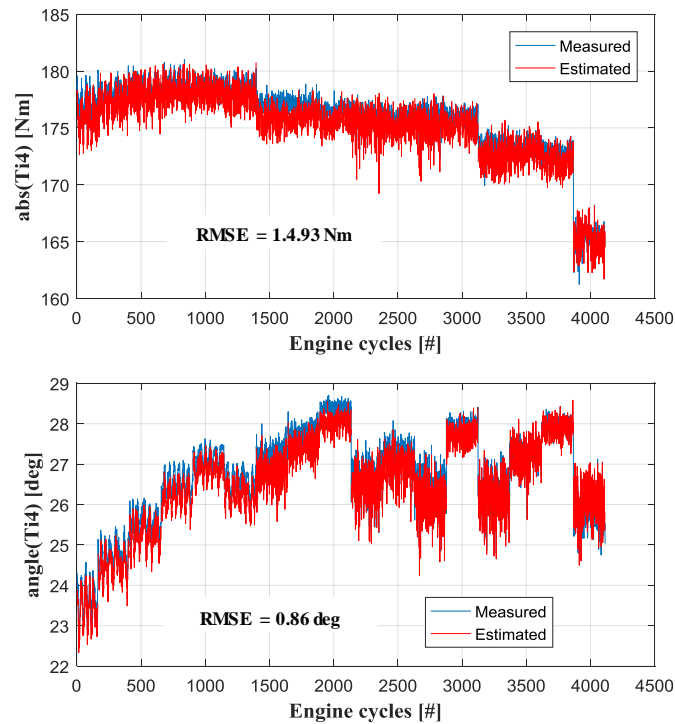


Figure 11-54 Measured vs Estimated Torque fluctuation (amplitude and phase) for the tests run in PCCI mode at 2000 rpm and IMEP = 4 bar (SOI variations)

## Reactivity Controlled Compression Ignition (RCCI)

As mentioned in the previous sections, the remote combustion sensing algorithm based on the analysis of crankshaft speed fluctuation has been also applied to the 1.3L Diesel engine run in RCCI mode.

To validate the methodology in RCCI mode, several tests have been run at 2000 rpm and IMEP = 4 bar investigating wide ranges of EGR (from 10% to 32%). In addition, 3 different gasoline/diesel target ratios have been tested: 55/45, 70/30 and 80/20 (the mass of each fuel has been corrected, with respect to the ratio, according to the differences between the lower heating values of the fuels). During all the tests, the base structure of the diesel injection pattern has been maintained in terms of number of injections and dwell time between injections, while combustion phasing has been modified varying *SOI<sub>main</sub>* (from 10° BTDC up to 45° BTDC). To achieve the mentioned gasoline/diesel target ratios maintaining constant the total amount of energy, the energy introduced with gasoline has been compensated equally reducing *Q<sub>main</sub>*.

Figure 11-55 shows 4-th harmonic component of Torque, respectively in terms of amplitude and phase, which results applying the estimation methodology during a test run in Dual Fuel mode with Gasoline/Diesel ratio equal to 80/20.

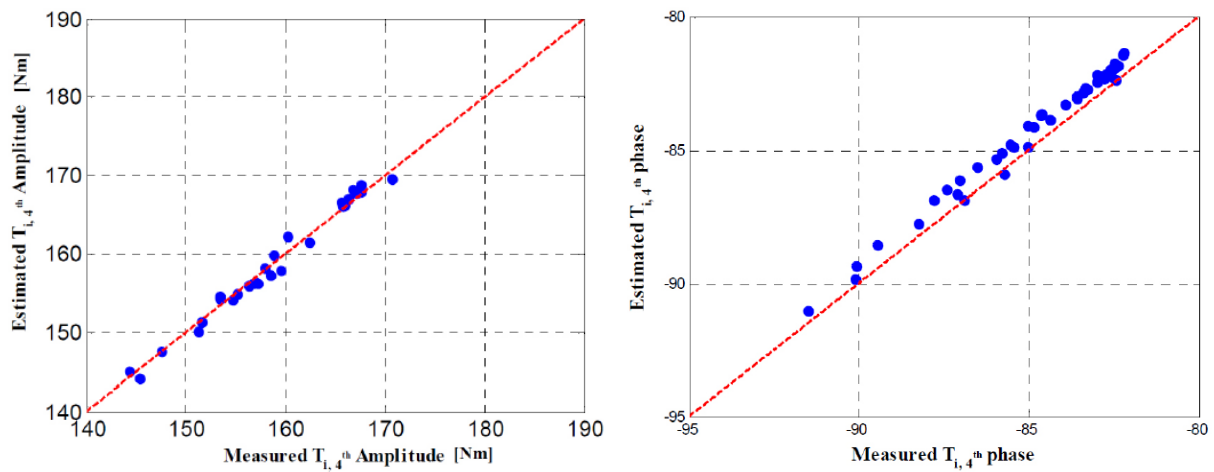


Figure 11-55 Amplitude (left) and Phase (right) of indicated torque fluctuation, measured vs estimated, for a test run at 2000 rpm, IMEP=4 bar, Gasoline/Diesel = 80/20, RMSE=3.6 Nm and RMSE=0.65°

Figure above proves that torque fluctuation can be properly estimated starting from the crankshaft speed fluctuations also in RCCI mode. Whereas Figure 11-56 shows the real-time application of the CA50 estimation algorithm to a steady-state test run with gasoline/diesel target ratio 55/45. During the test, *SOI<sub>main</sub>* has been varied from 5 to 0 deg BTDC (combustion retarded). As already mentioned, in this case the 3-injection pattern is simply shifted, because the Dwell Time between injections is kept constant. As a result, the average apparent heat release over the cycle (ROHR) varies as reported in the top subplot of Figure 11-56.

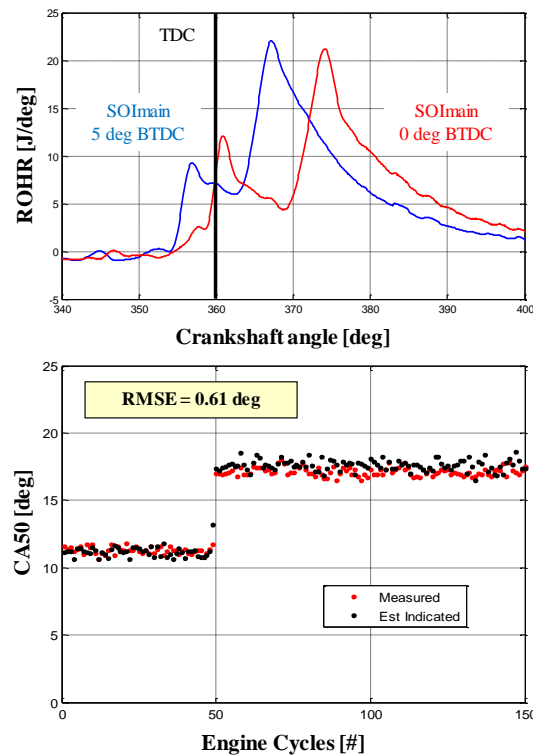


Figure 11-56 Measured and estimated center of combustion for a test run at 2000 rpm, IMEP = 4 bar, gasoline/diesel target ratio 55/45

Figure 11-57 shows, the results obtained applying the whole estimation procedure to the tests run with Gasoline/Diesel target ratios 70/30 and 80/20.

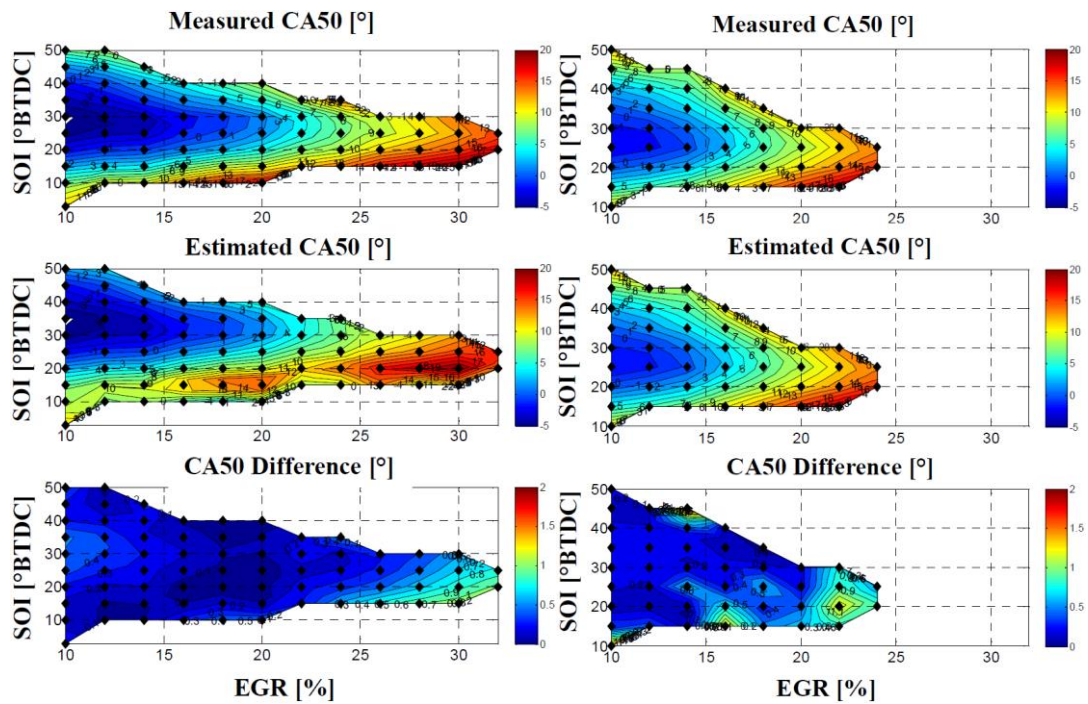


Figure 11-57 Estimated vs Measured CA50 and difference for Gasoline/Diesel 70/30 (left) and 80/20 (right)

Then, the estimated values of amplitude and phase of the torque fluctuation have been correlated to average indicated torque and CA50 respectively. Table 11-9 summarizes the accuracy of the obtained estimations for the 3 gasoline/diesel target ratios analyzed.

Table 11-9 Accuracy of torque and CA50 estimation for the tests run in RCCI mode

Fuel Ratio	Torque RMSE [Nm]	CA50 RMSE [deg]
Gasoline/Diesel 55/45	3.42	0.61
Gasoline/Diesel 70/30	3.60	0.65
Gasoline/Diesel 80/20	4.03	0.72

## 11.4.2 SOC, ROHR Position and CA50 Evaluation via Accelerometer

Another key source to sense ICE combustion is the engine block vibration sampled by means of an accelerometer. Prior studies [204, 209], where the authors of this research was involved, demonstrates that accelerometers mounted on the engine block can be used to extract useful information about combustion effectiveness. In this case, the accelerometer signal has been used to determine SOC and ROHR peak location.

In order to understand the nature of the correlation between engine block acceleration and the combustion process, Figure 11-58 (top) shows a comparison between the normalized accelerometer signal and the



corresponding normalized ROHR waveform. Both signals have been low-pass filtered in order to highlight the combustion information of interest. In this work, the correlations between engine block acceleration (measured using the accelerometer shown in Figure 11-45) and indicated quantities have been investigated for cylinder 1. The main idea behind the approach is that ROHR provides information about the way heat is released within the engine cycle, i.e. about combustion velocity. Due to this, it is reasonable to expect that acceleration signal might be strictly correlated to ROHR first derivative (NHRD) [205]. This consideration is confirmed by the comparison reported in Figure 11-58 (bottom).

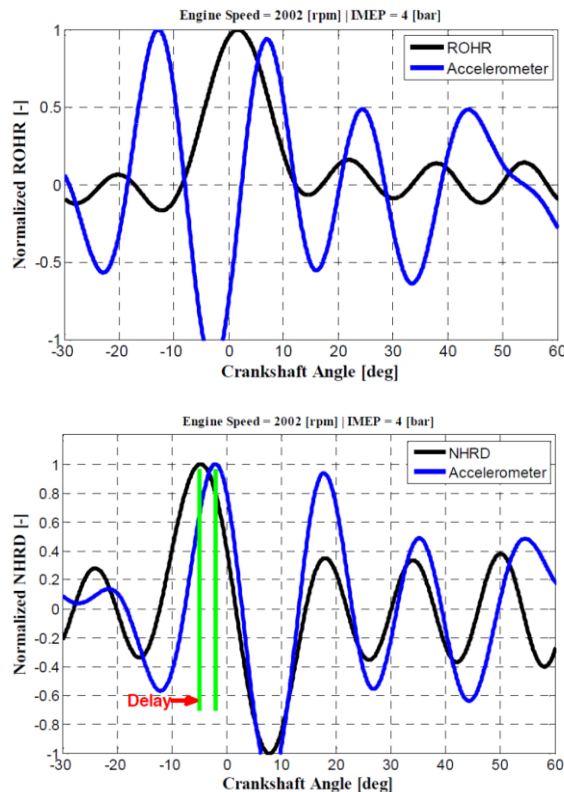


Figure 11-58 ROHR (top) and NHRD (bottom) compared with accelerometer signal for a test run in RCCI operating mode (2000 rpm, IMEP = 4 bar)

From the observation of previous figure arises that a strong similarity exists between ROHR derivate and the accelerometer signal. It is also interesting to notice the existence of a time delay between those two signals. Such delay depends of the accelerometer position, and it is equal to the time between the combustion event and the moment in which the effect is captured by the acceleration transducer. This delay is constant over time, but the angular delay might be variable, since it depends on crankshaft's angular velocity.

It is important to notice that accelerometer signal is the result of both combustion and mechanical forces. Therefore, in order to optimize the signal to noise ratio, the accelerometer needs to be properly windowed (in this case a Tukey window has been chosen). The window location within the engine cycle can be automatically determined using the information about combustion phasing obtained through the algorithm discussed in the previous section.

Compensating the mentioned accelerometer delay and using the appropriate window, NHRD and accelerometer normalized waveforms look very similar (Figure 11-59). In particular, the major accelerometer peak seems to be a good SOC estimator, while the following zero-crossing seems to be a



good estimator for angular location of ROHR peak and Cylinder Pressure peak. The identified correspondences have been used to set up an algorithm for real-time detection of SOC and Cylinder Pressure Peak location.

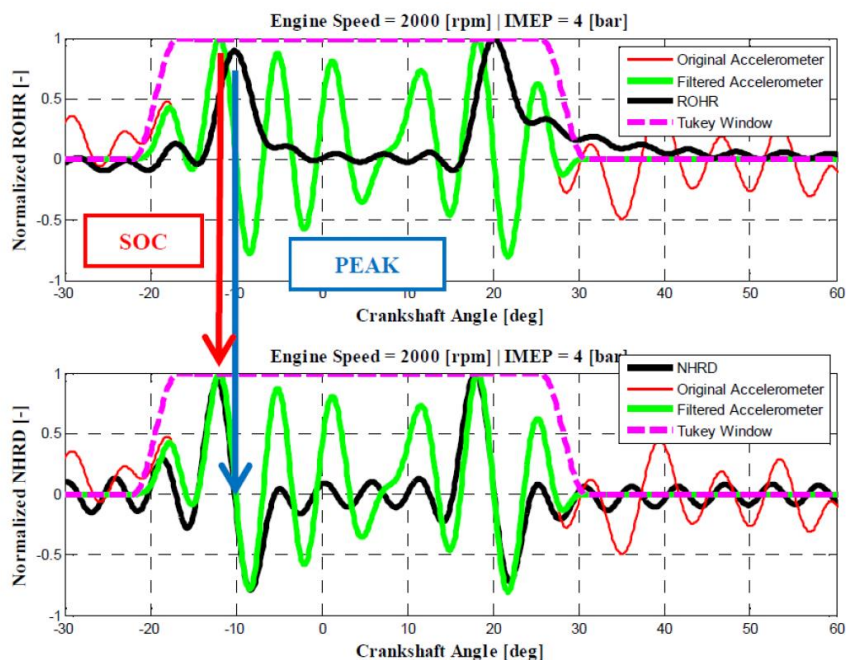


Figure 11-59 Overlap between the signals; SOC and RHOR Peak/Cylinder Pressure identification

## RCCI Results

This methodology has been applied to all the tests run in RCCI mode, and the results in terms of SOC and Cylinder Pressure Peak identification are shown in the following figure. In particular, Figure 11-60 reports the results obtained, in terms of SOC and ROHR peak location estimation, for the tests run with 70/30 Diesel/Gasoline ratio (each point in the figures corresponds to one engine cycle). The accuracy of the obtained results demonstrates that this methodology can be successfully applied to the analyzed RCCI combustion mode for the estimation of SOC and ROHR peak location (equivalent to Cylinder Pressure Peak position).

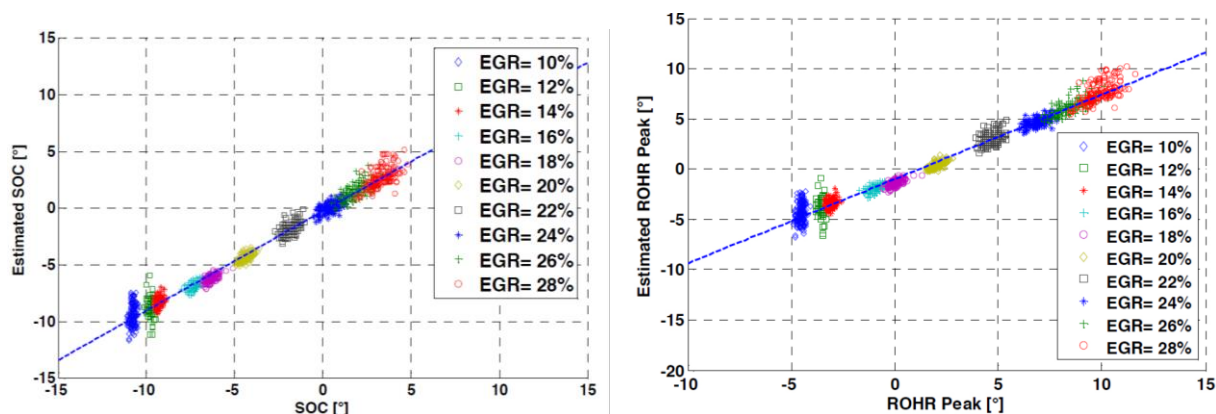


Figure 11-60 SOC Estimation (RMSE=1.68°) and ROHR Peak estimation (RMSE=0.89 deg) for different EGR values and SOIMain 20° BTDC Diesel/Gasoline 70/30.

After this first study the investigation of CA50 method has been extended to all 4 cylinders, implanting in RCP the aforementioned estimation algorithms. The methodology, implemented in the RCP system, filters the acquired accelerometer signal using a bandpass filter with cutoff frequencies equal to 0.3 kHz and 2.5 kHz. Then, the filtered signal is resampled in the angular domain and properly windowed around the top dead center (TDC) of each cylinder. Finally, the algorithm automatically detects, for each cylinder, the major peak of the windowed signal and the angular location of the following zero-crossing, that provides a reliable estimation of pressure peak position within the engine cycle. The Figure 11-61 illustrates in-cylinder pressure, cylinder pressure derivative and engine block acceleration (all normalized with respect to their maximum values) correlation, noting that the time delay of the accelerometer signal was characterized offline and compensated.

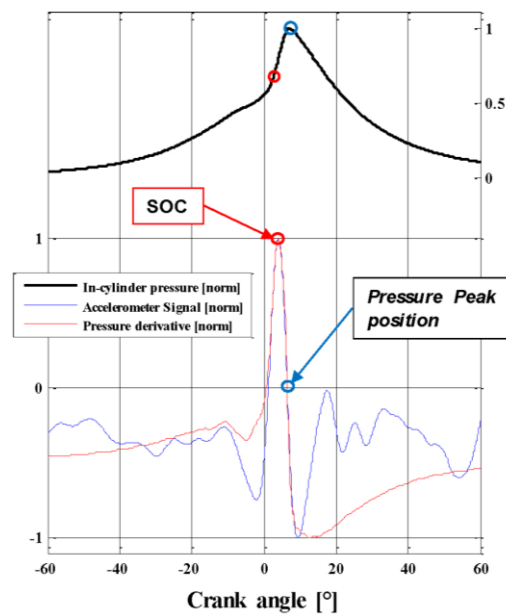


Figure 11-61 In-cylinder pressure, in-cylinder pressure first derivative and engine block acceleration (normalized with respect to their maximum) for a test run in RCCI mode at 2000 rpm, BMEP approximately 5 bar and CA50 = 9 deg.

The developed algorithm proved to be suitable for Pressure Peak location estimation in all the 4 cylinders. Figure 11-62.A reports the results obtained applying the estimation algorithm to all experimental during CA50 sweep performed with the closed loop control based on cylinder pressure measurement.

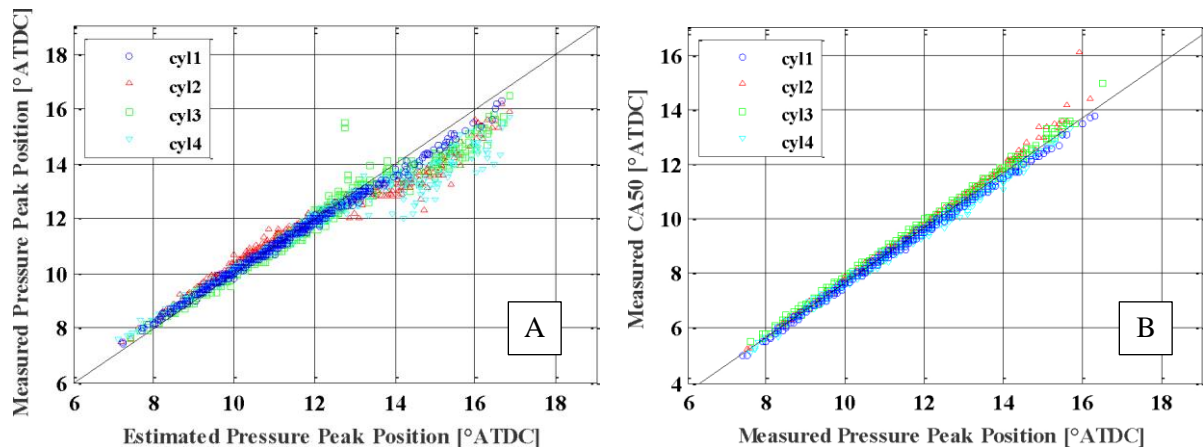


Figure 11-62 (A): Comparison between measured and estimated (from accelerometer signal processing) Pressure Peak location. (B): Correlation between measure CA50 and Pressure Peak location

The root mean squared error (RMS) between measured and estimated Pressure Peak location is equal to 0.47 deg. The estimated Pressure Peak location that calculates the RCP system corresponding to measure CA50 value shown in Figure 11-62.B

As reported in Figure 11-62.A a slight dispersion can be observed in the estimation of the latest peak pressure positions, mainly because retarded combustions (CA50 higher than 11 deg) usually produce acceleration signals characterized by a lower signal to noise ratio. This might also cause a reduction in the accuracy of CA50 estimation. However, the analyzed operating point the CA50 values of interest, i.e. the ones at which the efficiency of RCCI combustion is higher than CDC efficiency, are lower than 10 deg (around 8 deg).

## Conventional Diesel Combustion Results

The discussed algorithm proved to be effective for Pressure Peak location (strongly correlated with CA50, as swon in Figure 11-62 and [222]) and SOC estimation in all the engines under investigation. As an example, Figure 11-63 shows the results obtained during a transient test performed running the CI engine in CDC mode. The accuracy of the obtained results is high enough to feedback an algorithm for closed-loop combustion control.

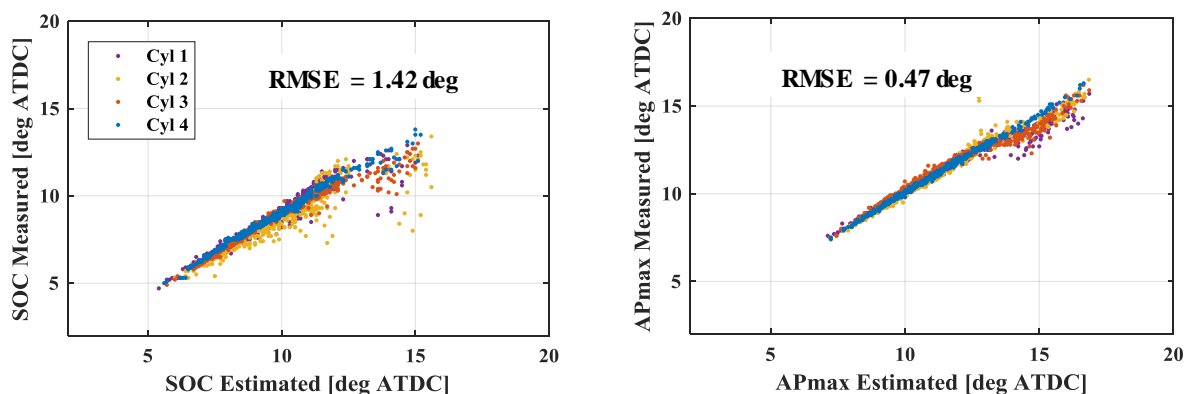


Figure 11-63 Estimation of Pressure Peak loaction and SOC during transient test run in CDC mode

## PCCI Results

Due to the highly pre-mixed portions, the approach needs to be slightly modified to properly manage PCCI combustions. As already discussed, the PCCI combustion process can be usually divided in 2 consecutive (partially overlapped) combustion events. As a result, the major peak in the accelerometer signal might be caused by both premixed and diffusive combustion portion. To manage this peculiar behavior, the algorithm has been modified to capture the maximum and the following zero-crossing of the 2 major peaks in the acceleration signal. To clarify this consideration Figure 11-64 shows the detection of the 2 peaks of interest for a test run at 2000 rpm and IMEP = 4 bar in PCCI mode.

It is important to highlight that the detection of combustion phasing based on accelerometer processing is not influenced by engine layout or combustion order, since the combustion process of each cylinder is windowed. In this case, the main limitation is the signal-to-noise ratio, that might be too low to guarantee

a robust estimation when the amplitude of mechanical vibrations is equal or higher than the amplitude of the vibrations caused by the combustion process.

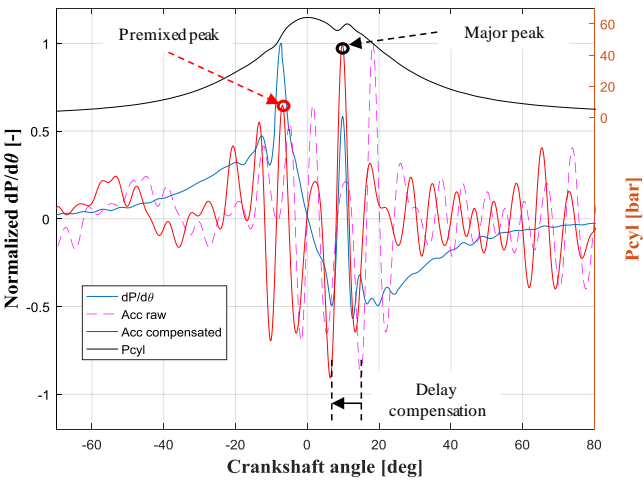


Figure 11-64 Application of the algorithm for the detection of accelerometer peaks location, engine cycle run in PCCI mode

The signal-to-noise ratio can be usually improved increasing the number of accelerometers applied to the engine block. However, the accuracy of the algorithm is usually low when in high speed (high amplitude of mechanical vibrations) or low load (low amplitude of combustion vibrations) conditions.

### 11.4.3Combustion Noise Control via Acoustic Emission Real-Time processing

The last part of this section describes a methodology for the calculation of engine noise, that provides a potential for the control of Common Rail Multi-Jet diesel engines.

As it well known, engine noise is usually monitored calculating the Combustion Noise (CN) index, that can be directly calculated from in-cylinder pressure trace. Many works [264,265,266] demonstrate that combustion noise is strongly influenced by the impulsiveness of the combustion process, because fast pre-mixed diesel combustions (with high ROHR peaks) are usually characterized by high CN values. To verify this, a set of experimental tests has been performed running the CI engine under study in CDC conditions. All the operating points (summarized in Table 11-10) have been run both using the standard injection pattern (3 injections) and switching off both Pilot and Pre injections (only one Main injection, with increased amount of fuel injected to compensate Pilot and Pre omission).

The set of experimental data confirms that CN, calculated using the algorithm proposed in [267], is strongly correlated to combustion impulsiveness, because it is well correlated with the maximum amplitude of cylinder pressure first derivative or with the maximum ROHR peak.

Table 11-10 Tests run in CDC mode for the analysis of the acoustic emission

Engine Speed	IMEP [bar]			
[Rpm]	3	6	9	12
1250	1	2	3	4
1500	5	6	7	8
2000	9	10	11	12
2500	13	14	15	16

As reported in Figure 11-65, for each operating point, the impulsive combustion (higher cylinder pressure derivative) is always characterized by a higher combustion noise.

Although CN shows a good correlation with pressure derivative and ROHR peak, the goal of the approach presented in this work is to provide an algorithm for the closed-loop control of engine noise based on the real-time processing of the signal coming from the acoustic probe faced to the engine block.

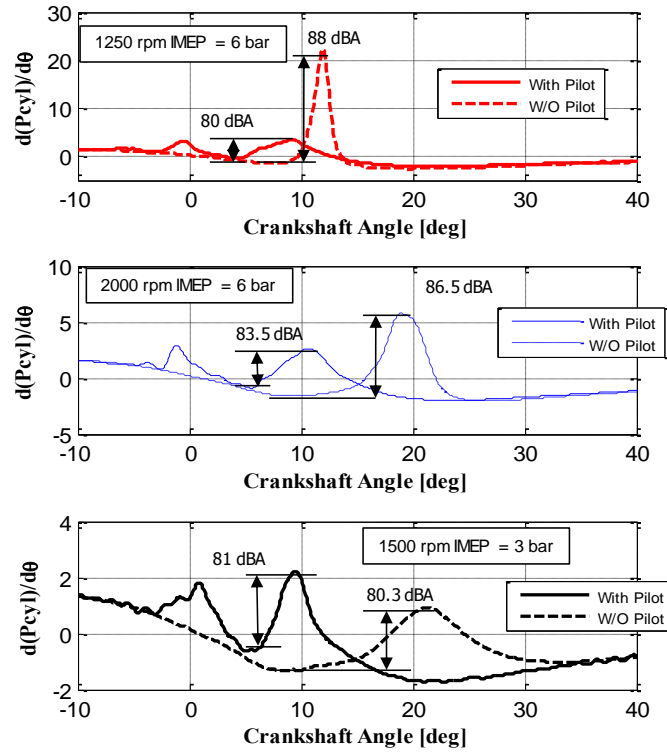


Figure 11-65 Comparison between cylinder pressure derivatives and corresponding Combustion Noise for engine cycles run in CDC mode with standard injection pattern (3 injections) and without pre-injections.

To do so, it is necessary to consider that the acoustic probe perceives the overall noise radiated by the engine, i.e. the sum of combustion noise (CN) and mechanical noise (MN). To quantify the overall noise radiated by the engine, equation (11.25) has been implemented in the RCP.

$$Noise = CN + MN = \log_{10} \left( \frac{\bar{E}}{\bar{E}_0} \right) \quad (11.25)$$

Here,  $\bar{E}$  is the mean energy level of the signal (evaluated from the spectrum of the acoustic emission signal), while  $\bar{E}_0$  is a standard reference value that corresponds to the energy level at 20  $\mu$ Pa, which is usually considered the threshold of human hearing at 1 kHz [266].

Since mechanical noise is produced by the mechanical components in motion, it is mainly influenced by the engine rotational speed. As a result, the overall noise is a function of both engine speed and combustion impulsiveness (ROHR peak). Figure 11-66 shows that the correlation between overall noise and ROHR peak is nearly linear. However, given a value of ROHR peak, the overall noise level rises with engine speed.

To highlight the effect of engine speed (mechanical noise) on the overall radiated noise, the linear fittings reported in Figure 11-66 are all characterized by the same slope, while a noise offset (mechanical noise variation) is applied to properly fit the experimental measurements.

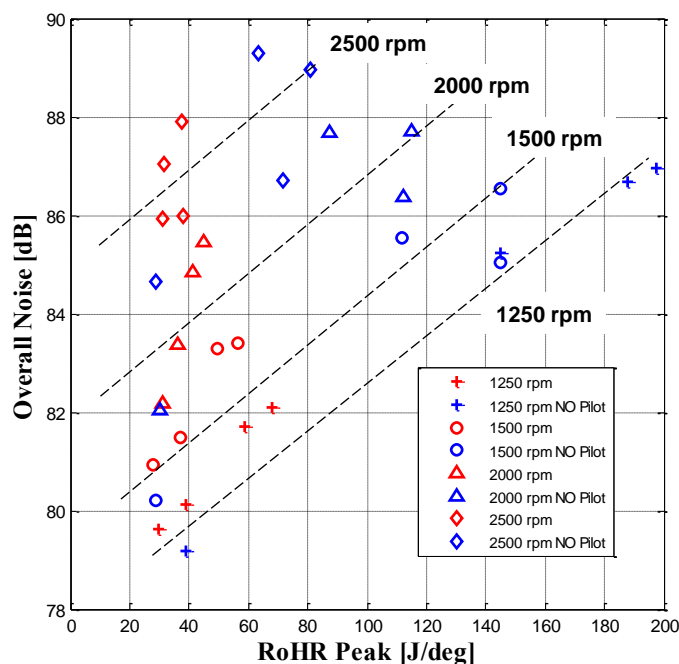


Figure 11-66 Correlation between overall noise radiated by the CI engine run in CDC mode (measured using the acoustic sensor) and ROHR peak; test run with standard injection pattern and omitting pre-injections

According to the discussed results, the use of an acoustic sensor allows the indirect calculation of CN. Once mechanical noise has been identified (mainly as a function of engine speed) the overall noise target needs to be set taking into consideration mechanical noise variations with engine speed.

In the research activity, presented in [210], it has been demonstrated that is possible to real-time control engine noise (overall), properly activating or omitting pre-injections (Pilot or Pre). The dynamic variation of the injection pattern (limited by the measured noise) provides a significant potential in the reduction of pollutant emissions, especially particulate matter [267], because while combustions performed without pre-injections are usually characterized by an unacceptable engine noise, soot emissions usually drop with respect to the corresponding operating conditions run with Pilot and Pre. The main idea behind the proposed approach is that the noise (and consequently pollutant emissions) can be controlled running the engine in an intermediate operating mode in which Pilot and Pre are removed only to a subset of the total number of combustions performed, according to a proper designed sequence of engine cycle over a generic  $N$ -cycles buffer [210]. The switching frequency between the two operating modes (standard with Pilot and Pre or modified activating only the Main injection) needs to be high enough to produce noise discontinuities that can be barely perceived by the driver. Once  $N$  is fixed,  $N+1$  options become available to properly design the sequence. Each sequence corresponds to an intermediate level between standard (3 injections) and modified (only one injection) injection patterns. To clarify this consideration, equation (11.26) reports a matrix that contains 8 injection sequences that can be designed for  $N = 7$ .

A noise control algorithm has been implemented in the RCP system and tested in dynamic conditions. This methodology real-time varies the sequence of standard and modified combustions based on the error between target and measured noise (calculated through equation (11.25) from the acoustic probe signal).

$$Sequences_{N=7} = \begin{bmatrix} 0000000 \\ 0001000 \\ 0010010 \\ 0101010 \\ 1010101 \\ 1101101 \\ 1110111 \\ 1111111 \end{bmatrix} \quad (11.26)$$

As it can be observed in Figure 11-67, the selection of the proper injection pattern (performed by a PID controller) always allows controlling the target noise level, except in the cases in which the noise target is higher or lower with respect to the reachable noise levels.

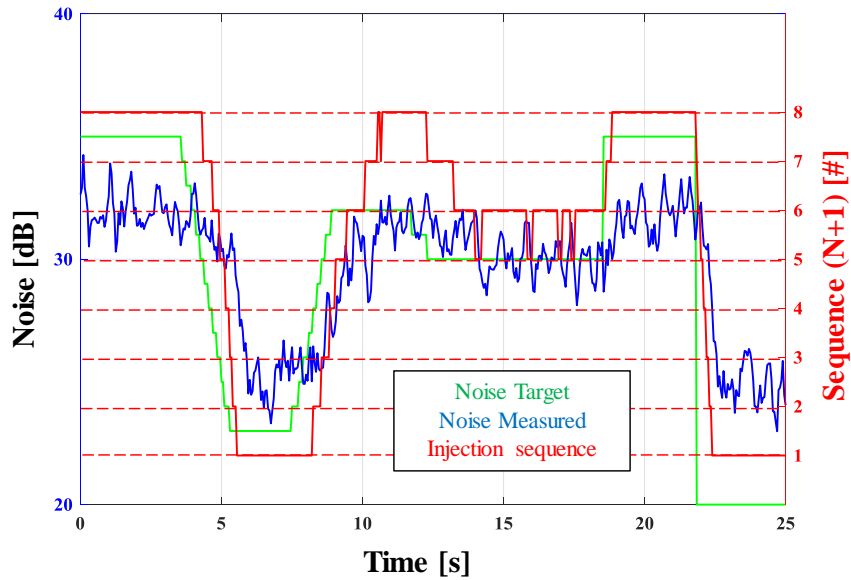


Figure 11-67 Noise produced by the engine (while activating the noise control algorithm) together with the selected injection sequence

## Summary

This paragraph summarizes algorithms for remote combustion sensing studied in the research activities. The discussed methodologies extract indicated quantities, usually directly calculated from in-cylinder pressure measurement, using virtual or low-cost sensors applied to the engine. In particular, to estimate torque, combustion phasing (center of combustion, pressure peak location and SOC) and combustion noise, the discussed procedures use the standard phonic wheel already present on-board for other control purposes, one additional accelerometer and one acoustic probe.

The complete remote combustion sensing methodology has been implemented in a programmable rapid control prototyping (RCP) system and applied to different combustion methodologies (both conventional and LTC) and engine architectures.



The proposed algorithms proved to be effective in all the analyzed cases, and the accuracy of the estimated combustion indexes seems to be accurate enough to feedback an algorithm for closed-loop combustion control, i.e. an algorithm that real-time varies the ignition/injection parameters to keep the estimated combustion feedbacks at the proper target value. For generic engine applications, the accuracy of the discussed algorithms cannot be defined a priori, because it will be strongly dependent on the signal-to-noise ratio characteristic of the specific application, i.e. on the capability of perceiving the effects of combustion using the analyzed low-cost sensors. However, this work clearly highlights the potential of the discussed approaches when implemented in a real-time system (RCP).

Additional work has been done to implement the developed algorithms in standard ECUs for on-board engine control, to prove that there is no limitation related to the on-board installation. Further studies are also being performed on an engine-dyno system to define the operating ranges in which a reliable combustion optimization can be guaranteed over time.

## 11.5 Advanced Combustion Control: the case of RCCI

As presented in Chapter #6.4.6 the RCCI combustion, despite the costs and complexity of two fuel systems, has many advantages than the other approaches to LTC. Indeed the possibility to define on-board the fuel proper reactivity allows to extend the operation area of the LTC combustion. However, the instability of the combustion remains an issue to be managed, like other LTC approach.

In this section a closed loop controller architecture is proposed and its behavior in a selected engine point is assessed by means of an RCP system. The engine is the same modified 1.3 L Diesel presented in Table 11-8 and the experimental set-up is the same illustrated in Figure 11-45 and Figure 11-46.

The investigation has been carried out in the engine operating point 2000 rpm and BMEP=6 bar, significant for the type approval cycle. Starting from conventional diesel combustion (CDC), a base calibration for RCCI operation has been defined with aim to reduce pollutant emissions (especially particulate matter and NO<sub>x</sub>) while keeping thermal efficiency equal or higher than the one obtained during standard diesel operation. The reference CDC test was performed with the standard injection pattern (3 injections per cycle, 2 Pre-injections and 1 Main injection). The main constraint for the calibration of RCCI mode was the limit of the Peak Pressure Rise Rate (PPRR), lower than 5 bar, considered a safe threshold to avoid knocking for the analyzed operating condition.

In Figure 11-68 the RCCI combustion parameters are summarized and the comparison between CDC and dual fuel RCCI at 2000 rpm and BMEP = 6 bar is illustrated, both in term of combustion performance and engine-out emissions. As it can be observed, compared to CDC, a significant reduction in the concentration of NO<sub>x</sub> and particulate matter can be obtained, together with a reduction of the overall fuel consumption. As expected, the RCCI operating mode suffers from a high concentration of unburned hydrocarbons. The set of parameters summarized in table of Figure 11-68 is the reference starting point for the activation of a closed-loop combustion control strategy, that needs to be tested and validated in operating conditions of interest, i.e. nearly optimal. Further optimizations of the set of injection parameters are beyond the scope of the work.



**Optimal set of combustion parameters identified for the RCCI operating mode at 2000 rpm and BMEP = 6 bar.**

SOI [° BTDC]	65
ET [μs]	490
SOI <sub>gas</sub> [° BTDC]	380
ET <sub>gas</sub> [μs]	2300
EGR rate [%]	0
Prail [bar]	500
Prail <sub>gas</sub> [bar]	5.5
Gasoline/diesel mass ratio	70/30
PPRR [bar/deg]	5
CA50 [deg ATDC]	8

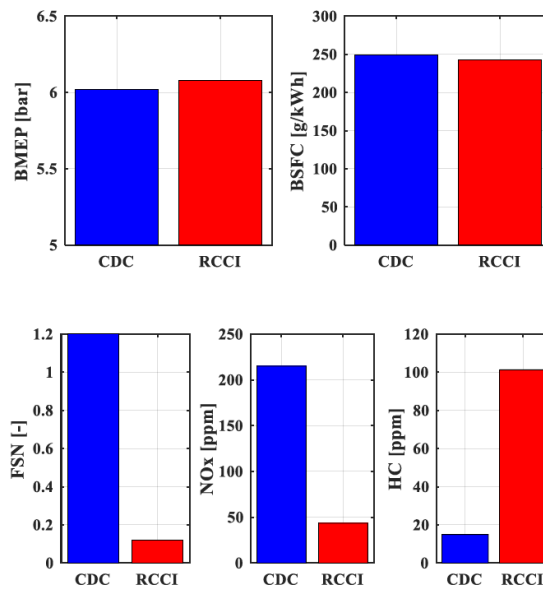


Figure 11-68 RCCI combustion parameters and Comparison between CDC and dual fuel RCCI at 2000 rpm and BMEP = 6 bar, both in term of combustion performance and engine-out emissions

### Closed-loop combustion control strategy

The closed-loop combustion controller proposed in this study keeps the CA50 of each cylinder at a proper target value. To control the center of combustion, the strategy varies the start of diesel injection (SOI<sub>main</sub>) to compensate the error between target and measured CA50. Due to the high cycle to cycle dispersion of CA50, the controller uses (as a feedback) the averaged center of combustion over the last 20 cycles. The real-time adjustment of diesel SOI<sub>main</sub> is performed using a PID controller that corrects injection phasing to meet the target CA50.

The critical aspects related to this kind of approach are mainly related to the limiting characteristics of RCCI combustion. The first limiting characteristic of RCCI operating mode is low combustion stability. As a matter of fact, the high cycle to cycle variability can easily lead to the occurrence of poor combustions and misfires. Misfiring cycles might be extremely critical for the closed-loop controller, since it is well known that, in such conditions, the calculated values of CA50 are strongly affected by the low signal to noise ratio in the calculation of energy release. Consequently, during very poor and misfiring combustions the calculated values of CA50 might be not correlated to the real behavior of the air/fuel mixture trapped in the combustion chamber. Experimental results clearly show that the frequency of misfiring cycles increases while retarding the center of combustion. Therefore, the real-time CA50 controller needs to monitor misfire occurrences and avoid unstable conditions advancing combustion.

To clarify the above considerations, Figure 11-69 reports the effects of CA50 variation on misfire frequency and PPRR during tests run at 2000 rpm, BMEP = 6 bar and reference gasoline/diesel ratio 70/30. For the presented experimental investigation, the maximum PPRR allowed was set to 9 bar/deg.

Another critical aspect to be addressed is that the selection of too advanced CA50 targets might result in a rapid increase of the peak pressure rise rate (PPRR), i.e. an increase of the mechanical load acting on piston and crankshaft. For this reason, to avoid reliability issues, the combustion controller needs to real-time monitor the pressure rise rate, retarding the CA50 target in case of impulsive combustions (PPRR over a calibrated threshold).

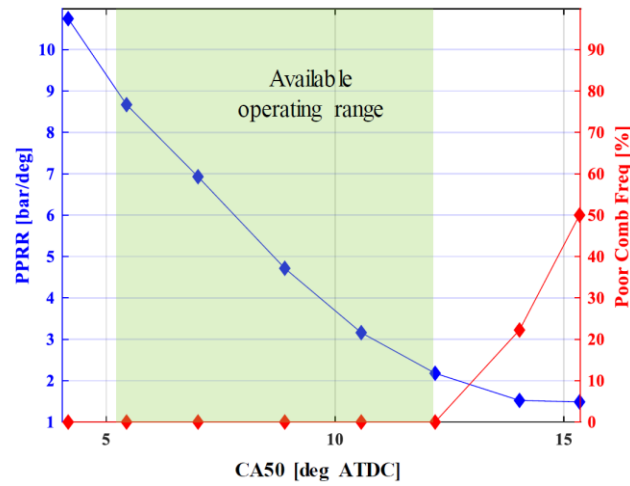


Figure 11-69 Effects of average CA50 variation on Misfire frequency and Peak Pressure Rise Rate; tests run at 2000 rpm and BMEP = 6 bar

The combustion control implemented in the RCP system allows controlling CA50 and respecting the limits established by misfire occurrence and maximum PPRR. The complete scheme of the strategy is reported in the next Figure 11-70.

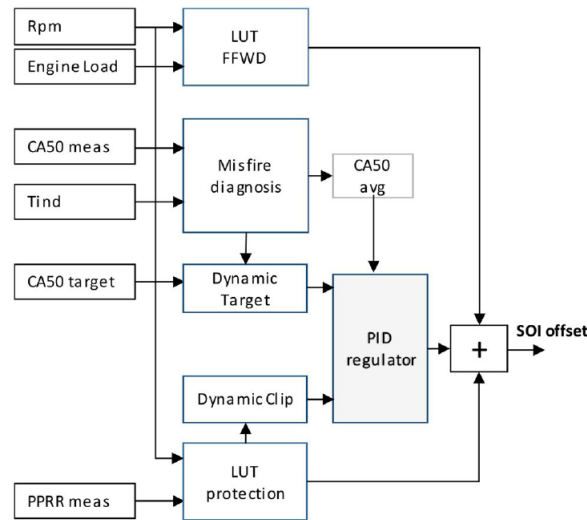


Figure 11-70 Scheme of the real-time injection controller implemented in the RCP system.

Here, the block termed “Misfire diagnosis” checks the discrepancy between indicated torque calculated by the indicating system ( $T_{ind}$ ) and expected indicated torque, evaluated as a function of total amount of fuel injected and  $SOI_{main}$  ( $T_{IndExp}$ ). The effect of  $SOI_{main}$  variation on torque is modeled as a variation of torque efficiency, as done for spark advance variation in standard SI engines [207]. When the difference between  $T_{ind}$  and  $T_{IndExp}$  exceeds a calibrated threshold, the corresponding CA50 is removed from the buffer for the calculation of  $CA50_{avg}$  and the base CA50 target is advanced. The *Pressure Rise Rate* limitation is managed in the block “LUT protection”, that automatically saturates the final contribution of the PID controller in case the measured PPRR exceeds the established limit. All the valid CA50 values (not excluded by the misfire check) are averaged over the last 20 combustions and used to calculate the combustion feedback for the PID controller ( $CA50_{avg}$ ).

The scheme reported in Figure 11-70 was implemented in the RCP system and used to control combustion starting from the base calibration reported in table of Figure 11-68. First, the closed loop controller was

activated using as inputs the indicated quantities (indicated torque, CA50 and PPRR) calculated by the indicated system and sent to the RCP system via CAN bus. Figure 11-71 reports the results obtained performing a sweep of target CA50 from 9.5 to 5.5 deg. As it can be observed, the controller is not able to reach the nominal target request in case of misfire occurrence or in case of activation of the protection due to high PPRR (the control retards CA50 with respect to the nominal target when PPRR exceeds the dotted threshold).

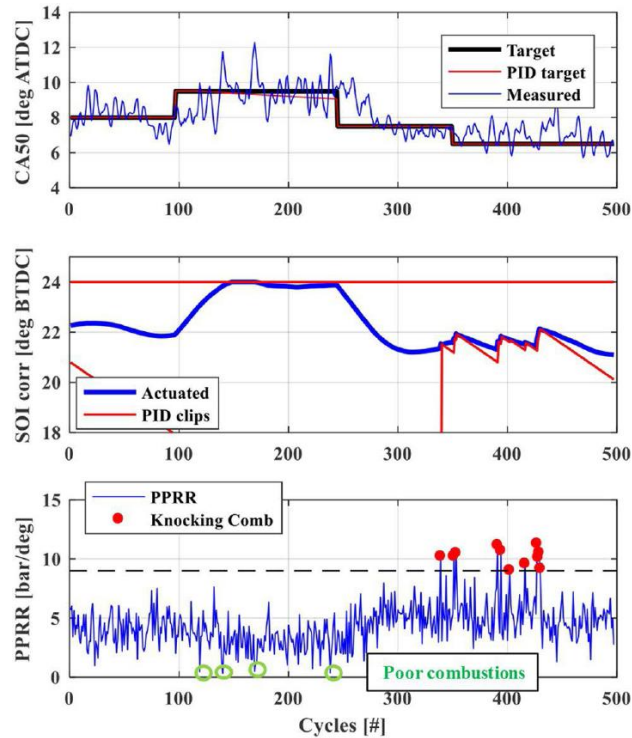


Figure 11-71 CA50 target sweep, results obtained for cylinder 1; tests run at 2000 rpm and BMEP = 6 bar

## Closed-Loop Combustion Control Based on Estimated Combustion Indexes

The results shown in previous section demonstrate that the proposed approach is suitable for closed-loop control of the center of combustion respecting the limitations from misfire occurrence and pressure rise rate. However, results were obtained using, as inputs, the indicated quantities provided by indicating system, therefore calculated from in-cylinder pressure measurement. The goal of the presented study is to replace the inputs coming from the indicating system with estimated quantities calculated from a proper processing of engine block acceleration.

The real-time methodology to estimated CA50 is already presented in the previous sections and it proved to be suitable for the estimation of pressure peak location in standard RCCI combustions, while it becomes extremely critical in case of poor combustions and misfires. In these cases, the amplitude of the major peak corresponding to cylinder pressure peak and the level of noise in the block acceleration signal might be similar. Consequently, the identified pressure might be unreliable or not representative of the real behavior of the air-fuel mixture in the combustion chamber.

To avoid the use of unreliable quantities in the control strategy, it is necessary to real-time detect misfires and poor combustions, the goal being to exclude the corresponding estimated pressure peaks from the control inputs. Thus a specifically designed integral index (*Kint*) for the detection of poor combustions was implemented. Such index is calculated as the integral of the filtered block acceleration signal,

windowed (for each cylinder) in the angular range  $0 \div 25$  degrees. To calculate the integral index, a specific band-pass filter was added. With regard to the chosen cut-off frequencies, block acceleration was band-pass filtered between 0.5 and 2.5 kHz. As shown in Figure 11-72, the occurrence of poor combustions seems to be strongly correlated to the chosen integral accelerometer.

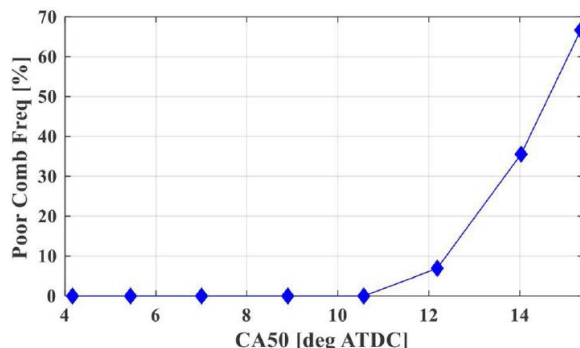


Figure 11-72 Frequency of poor combustions or misfires as a function of CA50 variation

Previous considerations explain how cylinder pressure peak estimation can be performed and validated through a proper processing of engine block vibration signal. Figure 11-73 (left) shows the results obtained applying the complete algorithm for pressure peak estimation to a set of experimental data acquired during a CA50 scan performed at 2000 rpm and BMEP = 6 bar. As it can be observed, the accuracy of the estimated peaks is very high, except for cycles characterized by poor combustions or misfires (highlighted with red circles), that can be identified using the above mentioned integral index (*Kint*).

The complete procedure for the estimation of pressure peak location and the detection of misfires and poor combustions was implemented in RCP system.

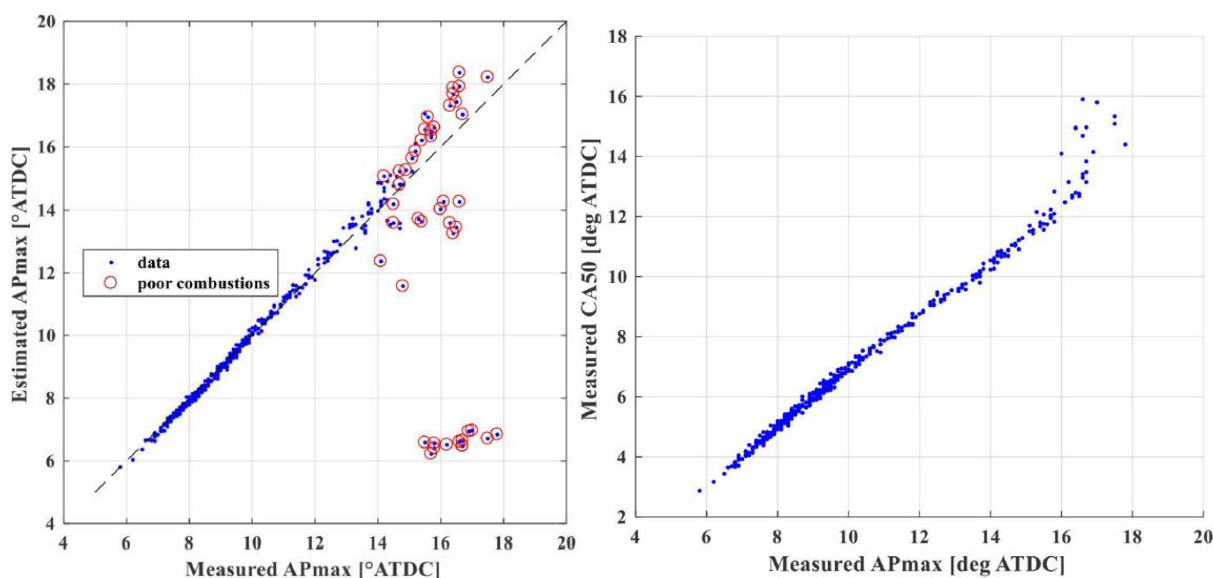


Figure 11-73 (Left): Comparison between measured and estimated pressure peak location. Tests run performing a CA50 target sweep from 5 to 10 degrees (closed loop combustion control based on cylinder pressure measurement). The red circles represent poor combustions and misfires discarded by the detections algorithm. (Right): Correlation between measure CA50 and pressure peak location.

Once the pressure peak location has been estimated, the RCP system calculates the corresponding CA50 value using the experimental linear correlation shown in Figure 11-73 (right). The results shown in Figure

11-73 also provides information about the maximum CA50 at which the engine can be run when combustion control is based on the accelerometer signal. As matter of fact, when the center of combustion is retarded up to approximately 10 degrees (corresponding to a pressure peak approximately at 14 degrees), the impulsiveness of combustion becomes very low (poor combustions). Consequently, the CA50 estimation performed using the acceleration signal becomes unreliable. Due to this limitation, the engine should be run (in the analyzed operating point) selecting CA50 targets lower than 10 degrees (combustion stability is the limiting factor).

Once the operating limitations related to combustion retard have been established, it is also necessary to take into account limitations in combustion advance, i.e. in the reduction of the target CA50. As already shown in Figure 11-69, reducing CA50 results in high PPRR values and knocking cycles, that increase mechanical load on the pistons and might lead to reliability issues over time.

To avoid reliability problems due to aggressive operating conditions (combustion too advanced) the combustion controller needs to limit SOI variations in case the maximum PPRR allowed (9 bar in this study) is exceeded. To control PPRR when only the accelerometer signal is available, an integral index similar to the one used for misfire detection was set up. This integral index (for PPRR estimation) was calculated from a band-pass filtered accelerometer signal. In this case, the selected cutoff frequencies of the filter are 0.6 and 3 kHz. The obtained index *Kint* PPRR results well correlated with the pressure rise rate calculated from in-cylinder pressure trace, therefore it can be used as a PPRR estimator. Figure 11-74 shows the correlation between measured and estimated PPRR for the same tests reported in Figure 11-73.

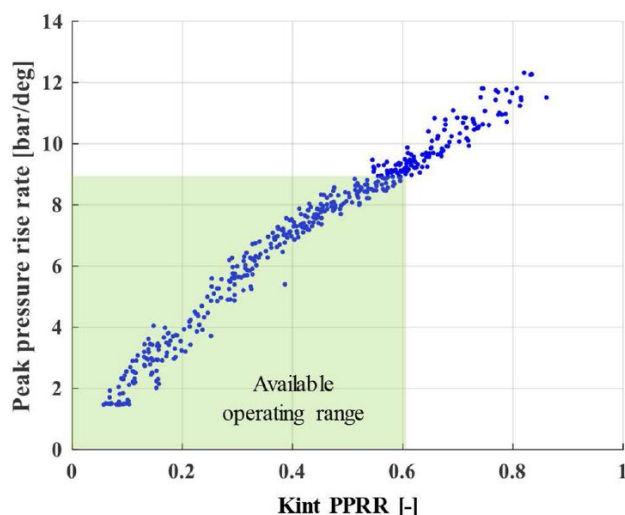


Figure 11-74 Peak pressure rise rate (PPRR), measured vs estimated. Tests run performing a CA50 target sweep from 5.5 to 10 degrees (closed loop combustion control based on cylinder pressure measurement).

The calculation of estimated PPRR was also implemented in the RCP system and used to complete the whole closed-loop combustion control strategy. All the combustion indexes estimated, using the discussed algorithms, from block acceleration processing (estimated CA50, *Kint* for poor combustions detections and estimated PPRR) can be used to replace the information provided by the indicated system.

The scheme of the complete combustion control methodology can be modified as reported in Figure 11-75. Here, in case of misfires due to excessive combustion retard, the CA50 target is automatically advanced, while in case *PPRR<sub>est</sub>* (i.e. PPRR estimated from block acceleration) exceeds the calibrated threshold, *SOI<sub>main</sub>* is limited by a proper dynamic clip (protection).

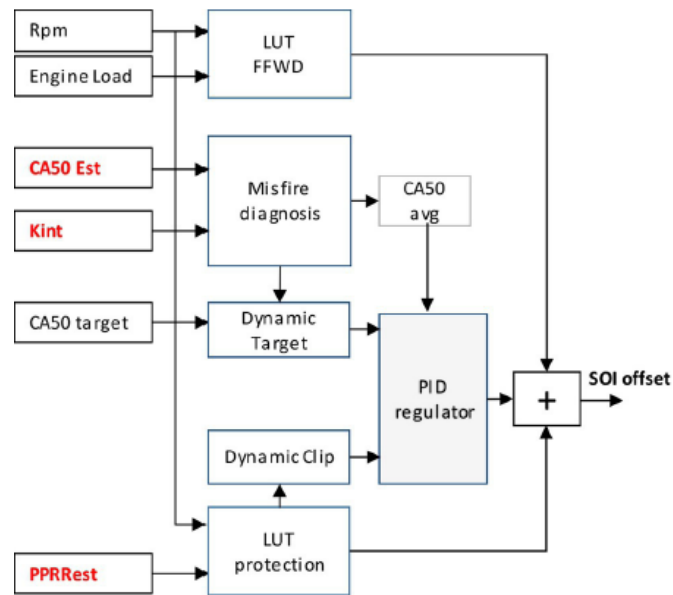


Figure 11-75 Scheme of the real-time injection controller implemented in the RCP system. All the combustion feedbacks used as inputs for the controller are estimated through a proper processing of engine block acceleration.

The discussed closed-loop combustion control strategy (schematized in Figure 11-75) was finally applied to control dual fuel RCCI combustion. To validate the methodology in steady operating conditions, a sweep of target CA50 from 9.5 to 5.5 deg was repeated. The sweep is similar to the one already shown in Figure 11-71.

As it can be observed in Figure 11-77, the controller allows correcting diesel *SOI<sub>main</sub>* to keep CA50 at the target value. It is interesting to observe that the base target is slightly corrected (advanced) in the first part of the test, to reduce the frequency of poor combustions/misfires. On the contrary, in the second part of the test, the target is reduced, down to 5.5 degrees. Combustion advance causes a significant increase of the estimated PPRR, that sometimes exceeds the threshold that triggers the activation of the protection strategy. The controller reacts clipping *SOI<sub>main</sub>* to stop further advancing the center of combustion. Consequently, the nominal target (5.5 deg) is not reached to avoid reliability problems.

The same methodology demonstrated to be suitable for closed-loop CA50 control in transient conditions. Figure 11-77, shows the results obtained running the engine at constant load (BMEP = 6 bar) and engine speed variable from 1800 to 2300 rpm. During the test, CA50 target was kept constant at 8 deg. As it can be observed, the controller keeps combustion stable at its target: due to a few poor combustions, in the first part of the ramp the target is slightly advanced, while in the last part of the test the SOI offset is limited by the dynamic clips, due to some high values of the estimated PPRR.

The experimental results clearly demonstrate the potential of the proposed methodology for the closed-loop control of RCCI combustion, avoiding both instabilities due to excessive combustion retard and undesired impulsive combustions (characterized by high values of the peak pressure rise rate). Due to the potential of the controller, further work is being performed to improve its robustness, mainly optimizing accelerometer location in the engine block, the goal being to maximize the signal to noise ratio and extend the operating range in which CA50 can be automatically identified (through the algorithm reported in Figure 11-61) for all the cylinders.

The control scheme is under study to manage the engine in Gasoline Compression Ignition (GCI) mode and will be the object of future presentations.



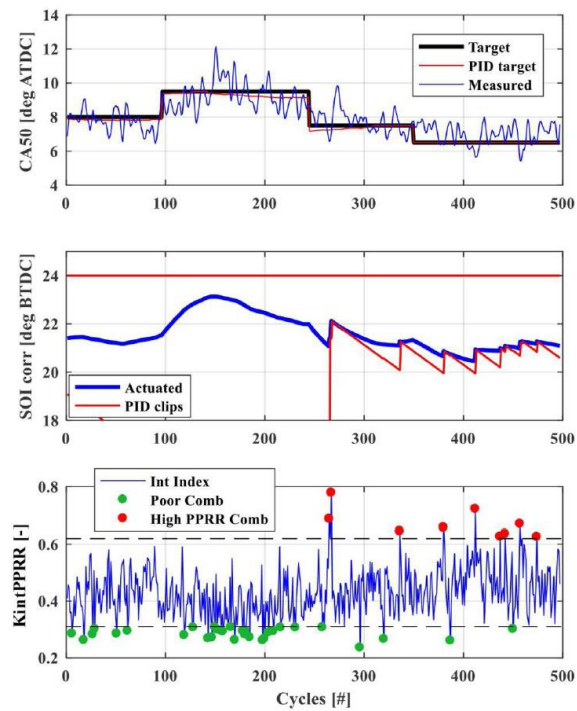


Figure 11-76 Closed loop RCCI combustion control based on estimated combustion indexes; test run at 2000 rpm and BMEP equal to 6 bar.

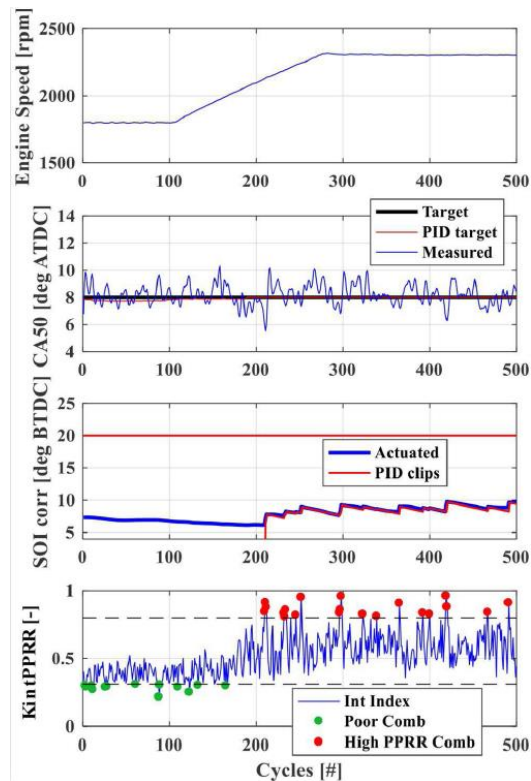


Figure 11-77 Closed loop RCCI combustion control based on estimated combustion indexes; test run at variable engine speed and BMEP approximately equal to 6 bar

## 12. Powertrain Architecture Definition and Selection

In this chapter examples of powertrain architecture definition and selection are illustrated, with aim of presenting technology pathways towards 2025 and post-2025 regulations.

The first section presents the conceptual design and the analytic assessment of electric hybrid powertrains to fulfill 2025 regulation, applying the methodology presented in the previous chapters.

The second section describes the comparison of different drivetrain technologies in terms of CO<sub>2</sub>-equivalent (CO<sub>2</sub>e) quantified over the WTW and total lifecycle paths.

### 12.1 Conceptual Design and Analytic Assessment of E-Hybrid Powertrains towards 2025 regulations (Case Study)

This section presents the conceptual design procedure and the analytic comparison of hybrid electric architectures, focusing on 48 Volt electric drive systems. As already introduced in the previous Chapter #8 these low voltage electric propulsion systems have a good trade-off between benefits and costs. In the considered timeframe up to 2025, this work will focus on powertrains designed for two different vehicles, C-Segment and SUV, covering the expected main market share [227,251]. In order to perform the right comparison, the design and control of the hybrid powertrains are optimized for each vehicle segment. The methodology applied is according to the steps presented in the previous chapters.

#### Powertrain Requirements

The definition and the deployment of vehicle and powertrain requirements have been carried out applying the multi-level QFD methodology presented in the Chapter #4.1. User's needs and their priority (1-low, 7-high), have been obtained from market researches [227,251] and they represent the inputs for QFD. Specifically, in HoQ1 (house of quality, level 1), driver's needs are evaluated in an objective way by means of engineering variables.

Table 12-1 shows the measurable requirements, which represent the inputs for the second level, coming from driver's point of view. Legislation requirements are clearly of great importance because the vehicle needs to fulfill them to be commercialized. They are not explicitly considered by the user, although their impact on customer's choice is becoming greater due to the driving bans imposed in many cities to the vehicles complying with old legislations. The constraints on CO<sub>2</sub> and pollutant emissions remain the main drivers of the technological change requested to new vehicles and powertrains.

The priorities and requirements targets in Table 12-1 depend on the vehicle segments, as describe in [227], legislation standards and the manufacturer positioning among the competitors.



Table 12-1 Measurable Powertrain Requirements and Priority from HoQ1 considering a C-segment vehicle and a SUV, considering emission standards at 2025

	Needs/ Requests		Measurable Needs and Request (from HoQ1, Vehicle Level)	MR Priority	Unit	C-Segment	SUV
End-User	Low Noise	1	Noise Emission Level	4	[dB]	< 75	< 75
	High Performance	2	Accel.Time 0 →100 km/h (HEV)	3	[sec]	< 9	< 6
		4	Max Vehicle Speed (ICE/EV)	3	[km/h]	195 /80	230 /100
	High Comfort	5	Accel. Time 0 →50 km/h (EV)	4	[sec]	< 4.5	< 4.5
		6	Gradability (ICE/EV)	4	%	>35% / >25%	>35% / >25%
		7	Time w/o acceleration during load Req.	4	[ms]	<150	<150
		9	Cabin Comfort (response and ambient Temp)	4	[sec] [°C]	< 5 -25/+50	< 5 -25/+50
	High Reliability	10	Mileage w/o failure	4	[1000 km]	150	150
	Easy to use	11	Energy Refilling autonomy	5	[km]	> 600 > 5	> 600 > 5
		12	Maintenance intervall	4	[kkm]	>25	>25
		13	Energy Refilling Time	4	[min]	< 5	< 5
	Low Fuel Consumption	14	Fuel Consumption	4	[L/100 km]	< 3.5	< 4.3
Standards	Low Emission	15	Toxic Emission according to Standard (WLTP and RDE)	7	[mg/km]	EU7	EU7
		16	EOBD/OBD2 compliance	7	[mg/km]	EU7	EU7
		17	CO2 according to Standard (NEDC)	7	[g/km]	< 80	< 100
	Safety	18	Mileage w/o critical event	7	[km]	life	life

In the HoQ2.1 of QFD level 2, the requirements and priorities for the powertrain, described in the previous Table 12-1 are mapped with their technical characteristics in Table 12-2, with appropriate specifications to effectively satisfy the requirements.

In Table 12-2, the priority specifications are reported. The relevance of the different powertrain characteristics is highlighted by the green histogram on the left and it is the result of driver's needs priority. Among all, the powertrain weight, including the contribution of the energy storage system, represents the most important factor in addition to the energy generation efficiency for the propulsion. Furthermore, among the technical characteristics with higher ranking, it must be noted that the energy refilling time is not so critical for a hybrid powertrain, in contrast to a pure electric one.

Clearly, emissions still have a crucial role. The reported powertrain characteristics and their specifications, determined following, are the inputs for the next phase of definition and selection of the powertrain architectures.

Table 12-2 Powertrain Technical Characteristics and relevance from HoQ2.2

Relevance histogram (HD)		Powertrain Characteristics (from HoQ2.2)	Relevance [0÷100]	Unit
	1	Powertrain Noise Level	10	[dB]
	2	Powertrain Time to Full Power	14	[s]
	3	Low-end Torque (at wheel)	19	[Nm]
	4	Speed Range of High Torque	16	[rpm]
	5	Maximum Power	20	[kW]
	7	Time w/o Torque delivery during load Req.	17	[ms]
	8	Powertrain Vibration	12	[dB]
	9	Tank to Wheel Maximum Efficiency	24	[%]
	10	Tank to Wheel Efficiency at part/low load	28	[%]
	11	NOx Emission according to RDE	13	[g/Kwh]
	12	HC/CO Emission according to RDE	15	[g/Kwh]
	13	Soot/PN according to RDE	14	[PN]
	14	CO2 on WLTC	22	[g/Kwh]
	15	Heating Power	4	[kW]
	17	Efficiency of Electric Power Gen.	20	[%]
	18	Energy Storage Capacity	14	[J]
	19	Energy Refilling Time	14	[min]
	25	% Braking energy recovered	22	[%]
	26	PWT Size	5	[Lit]
	27	PWT Weight	37	[kg]

## Evaluation of Powertrain Specifications to match Vehicle Requirements

In this section the focus is on quantitative powertrain specifications of Table 12-2 deduced from the end-user requirements in Table 12-1.

Solving the equation that describes the classical vehicle longitudinal motion, it is possible to define power and torque specifications of powertrain from vehicle performances for each vehicle segments object of study, in particular:

- maximum vehicle speed;
- acceleration (time to go from 0 to 100 kph);
- take-off capabilities (to move off the vehicle on a 25÷35% slope).

The requirements for CO<sub>2</sub> emission, fuel consumption and maximum vehicle range, especially in electric mode, are used to define the powertrain overall efficiency, the kinetic recoverable energy and the energy storage capacity. In particular, the electric energy storage system is specified to match with range requirement in electric mode.

User comfort and accessories, that influences the energy consumption of the vehicle, are considered constant in this in this work, whereas the pollutant requirements impact mainly on combustion mode and after treatment technologies.

The key formulas to define many powertrain parameters are derived from vehicle longitudinal model and mass or energy balance principles. They have been already introduced in the Chapter #4.5. For an easy reading, some equations of the procedure for the powertrain conceptual design applied to case study are reported again following. The powertrain traction power  $P_{trac}$  and the traction torque  $T_{trac}$  can be obtained with:

$$P_{trac} = M_V (a + C_r \cdot g + g \cdot p\%) \cdot V + \frac{1}{2} \cdot \rho \cdot C_x \cdot S_f \cdot V^3 \quad (4.2)$$

$$T_{trac} = (M_V (a + C_r \cdot g + g \cdot p\%) + \frac{1}{2} \cdot \rho \cdot C_x \cdot S_f \cdot V^2) \cdot r_w \quad (4.3)$$

To proceed with the calculation some vehicle parameters have to be assumed. For the baseline of case study they are the following:

Table 12-3 Vehicle parameters for powertrain power and torque evaluations

Vehicle Parameters	C-Segment	SUV
Chassis Mass	990	1340
Aerodynamic drag coefficient	0.27	0.32
Frontal Area [m2]	2.12	3.05
Wheel Rolling drag coefficient	0.009	0.0096
Wheel radius [m]	0.317	0.37055
Driver [kg]	75	75
First attempt Vehicle Mass [kg]	1325	1735

As anticipated, the vehicle mass has a huge impact on many vehicle performances and its value has to be refined during the sizing of powertrain after a first assumption to perform the preliminary calculation, according the design procedure presented in the workflow in Figure 4-5. For the evaluation of powertrain power and torque to reach the top vehicle speed target 1235kg and 1735 kg have been considered.

The powertrain power obtained from vehicle maximum speed requirement is typically the maximum needed and it depends little on weight, so the uncertainty in the mass doesn't introduce significant error in the calculation.

### ***Evaluation of Powertrain Features for Maximum Vehicle Speed***

Assuming zero acceleration in the equations (4.2) and (4.3) and considering the required vehicle speed  $V_{max}$  in Table 12-1, the powertrain traction power and torque can be calculated. Table 12-4 shows the power and torque needed to achieve different values of maximum speed for C-segment and SUV vehicles, in case of zero slope and  $p=5\%$ . In blue the relevant values for each vehicle type, considering the targets for ICE and EV mode. For the slope  $p=5\%$  lower vehicle speed targets than  $p=0$  are considered.

Table 12-4 Power and Torque to achieve maximum Vehicle Speed with slope  $p=0$ , slope  $p=5\%$

p=0 [%]	Vspeed [km/h]	C-Segment	SUV
<b>Power</b> [Kw]	80	6.4	10.1
	100	10.7	17.2
	195	61.0	102.1
	230	97.2	163.3
	250	123.3	207.7
<b>Torque</b> [Nm]	80	92	169
	100	122	229
	195	357	698
	230	482	947
	250	563	1108

p= 5 [%]	Vspeed [km/h]	C-Segment	SUV
<b>Power</b> [kW]	70	15.0	20.7
	90	21.3	30.3
	180	74.9	115.5
	220	117.4	185.3
<b>Torque</b> [Nm]	70	244	395
	90	271	449
	180	475	856
	220	609	1123.7

### Energy Storage Capacity for Vehicle Autonomy

Considering the vehicle speed profiles and the preliminary vehicle masses defined in the previous section, it is possible to define with equation (4.2) the power in the driving cycles to move and brake the vehicle and as consequence by means of an integration process the energies  $E_{MOV}$  needed to move the vehicle and dissipated  $E_{braking}$  for different standard cycles, see Table 12-5.

Table 12-5 Energy to move the vehicles  $E_{MOV}$  and dissipated  $E_{braking}$  in the case study, considering different standard cycles

	Cycle	Trip Distance	C-Segment		SUV	
		[km]	[MJ]	[kwh]	[MJ]	[kwh]
<b>Energy to move Vehicle</b> [MJ or (kwh)]	NEDC	10.8	3.9	1.08	5.3	1.47
	WLTC	23.29	10	2.78	13.6	3.78
	RTS95	12.74	7.6	2.11	10.2	2.83
	US06	12.81	6.9	1.92	9.3	2.58
<b>Braking Energy</b> [MJ or (kwh)]	NEDC	10.8	1.2	0.33	1.6	0.44
	WLTC	23.29	2.7	0.75	3.7	1.03
	RTS95	12.74	2.6	0.72	3.2	0.89
	US06	12.81	1.5	0.42	1.8	0.50

To evaluate the battery capacity as a function of electric autonomy requested in Table 12-1 the following equations can be used:

$$E_{trip} = \int_0^{t_{trip}} P_{bat} dt - E_{KER} = E_{MOV}/\eta + E_{aux} - E_{braking} \cdot \eta \quad (4.8)$$

$$E_{stored} = \frac{E_{trip}}{\alpha \cdot \beta} \cdot \frac{Requested\ Autonomy}{Trip\ Distance} \quad (4.9)$$

assuming  $\eta = 0.8$  the efficiency that takes into account the transmission and the electric traction drive losses. The electric energy  $E_{aux}$  consumed by the auxiliaries is calculated assuming a constant power  $P_{aux} = 280$  W during the trip.

The following Table 12-6 shows the energy need to move the vehicle in case of pure electric propulsion, including the electric load, and theoretical energy recovered during braking.

Table 12-6 Energy  $E_{trip}$  needed from the battery to move the vehicle in electric mode and recovered during braking

	Cycle	Trip Distance & Duration		C-Segment		SUV	
		[km]	[s]	[MJ]	[kwh]	[MJ]	[kwh]
Energy from Battery [MJ or (kwh)]	NEDC	10.8	1180	5.21	1.45	6.96	1.93
	NEDC	23.29	1800	13.00	3.61	17.50	4.86
	RTS95	12.74	889	9.75	2.71	15.94	4.43
	US06	12.81	596	8.79	2.44	14.53	4.04
Recoverd Energy in Battery [MJ or (kwh)]	NEDC	10.8	1180	0.96	0.27	1.28	0.36
	WLTC	23.29	1800	2.16	0.60	2.96	0.82
	RTS95	12.74	889	2.08	0.58	2.56	0.71
	US06	12.81	596	1.2	0.33	1.44	0.40

The battery capacity  $E_{SS}$ , see Table 12-7, is calculated with equation (4.9), in which  $E_{trip}$  is the value of NEDC in Table 12-6 with 20% of increasing, the  $\alpha$  and  $\beta$  factors are equal to 0.8.

The mass of battery pack is obtained with equation (4.10) considering the specific energy of 48V LiFePO cells around 130 Wh/kg and a packaging factor  $\gamma$  equal to 1.2.

$$M_{bat} = \frac{\gamma \cdot E_{ss}}{SE_{bat}} \quad (4.10)$$

Table 12-7 Battery capacity and weight

		C-Segment	SUV
Battery Capacity [kWh]	Cycle	HEV	HEV
	NEDC	1.43	2.20
Battery Mass [kg]	Cycle	HEV	HEV
	NEDC	13.2	20.3

### Vehicle Weight Evaluation

The preliminary vehicle mass  $M_v$  can be update with the equation:

$$M_v = M_{chas} + M_{pwt} + M_{ess} + M_{driver} \quad (4.11)$$

where the vehicle chassis mass, depending on vehicle segment is assumed from the values in Table 12-3. The estimation of energy storage delta mass due to electrification is obtained considering the battery mass  $M_{bat}$ , in Table 12-7.

The evaluation of powertrain mass is carried out considering the power to achieve top vehicle speed in Table 12-4 and typical value of the electric machine power density indicated in Chapter #8.2.3. The total mass of the two vehicles with electrification becomes 1350 kg and 1765 kg respectively.

### Evaluation of Powertrain Features to fulfill Vehicle Take-off Requirements

The powertrain traction power and torque to achieve vehicle take-off requirements can be calculated with the equations (4.2) and (4.3), where the acceleration is defined as  $a = 1.6 - 0.08(p-10)$ , linking the vehicle target acceleration to the slope  $p$  and vehicle speed is assumed equal to 10 km/h. A payload  $M_{load}$  of 400 kg is added to the vehicle mass. In the following Table 12-18 the power and the torque calculated with  $p=35\%$  for ICE mode and 25% for pure electric mode are reported.

Table 12-8 Power and Torque for Take-off in ICE and Electric mode

p= 35 [%]	Vspeed [km/h]	C-Segment	SUV
Power [kW]	10	12.7	15.7
Torque [Nm]	10	1445	2094

p= 25 [%]	Vspeed [km/h]	C-Segment	SUV
Power [kW]	10	10.4	12.9
Torque [Nm]	10	1191	1726

### Evaluation of Powertrain Performances for Vehicle Acceleration Requirements

The vehicle acceleration requirements are defined by criteria such as time interval to go from 0 to 100 kph, with targets defined in Table 12-1. Analytically the power requested can be obtained from the integration of equation (4.2). Assuming that the traction power  $P_{trac}$  of the powertrain is constant, the calculation of the duration  $t_f$  to go from zero speed to a final speed  $V_f$  can be done by resolving equation (4.16). The variation of the traction power as a function of acceleration time requirements (0 – 100 km/h) for the two segment vehicles (C-class and SUV) is illustrated in Figure 12-1 and in Table 12-9.

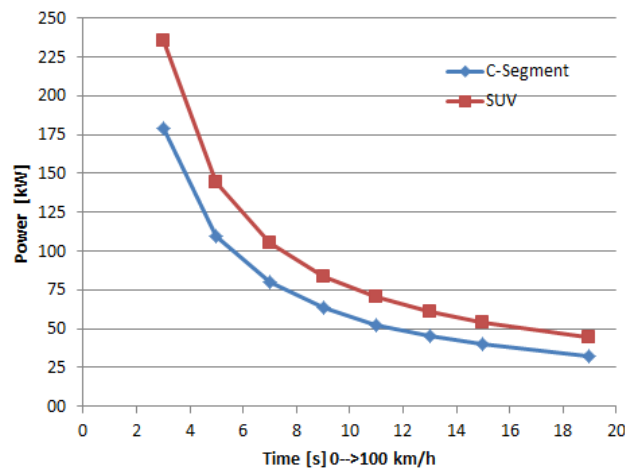


Figure 12-1 Traction power as a function of time from 0 - 100 kph requirement for a C-segment vehicle and for a SUV

Table 12-9 Power and Torque for Time 0→100 km/h

	t 0 → 100 km/h	C-Segment	SUV
Power [kW]	5	109.4	144.3
	7	79.6	105.4
	9	63.1	83.8
	11	52.5	70.0
Torque [Nm]	5	1248	1925
	7	909	1406
	9	720	1117
	11	600	934

Moreover the traction power as a function of the acceleration time requirements (0 – 50 km/h) for the two vehicle types with a payload of 150 kg is considered, taking into account an urban use of the vehicle in pure electric mode, see Table 12-10.

Table 12-10 Power and Torque for Time 0→50 km/h with payload 150kg

	t 0 → 50 km/h	C-Segment	SUV
Power [kW]	4.5	33.8	43.3
	5	30.5	39.2
	5.5	27.9	35.9
	6	25.7	33.1
Torque [Nm]	4.5	771	1156
	5	697	1047
	5.5	637	957
	6	587	883

### *Evaluation of Powertrain Features to Recover Vehicle Kinetic Energy*

One of the main advantages of an electric hybrid powertrain is the capability to recover the vehicle kinetic energy during the braking events. The maximum power can be evaluated using equation (4.16) where the initial vehicle speed is the current speed  $V_c$  and the final is zero or a lower level  $V_1$  and  $t_{braking}$  the braking duration. The maximum regenerative braking power has high impact on performance of battery too. Table 12-11 shows the maximum braking power  $P_{brake}$  in different standard cycles: it is higher in the cycles with frequently transients and for vehicle with higher mass.

Table 12-11 Maximum braking power  $P_{braking}$  for different standard cycles

	Standard Cycles	C-Segment	SUV
Maximum Braking Power [kW]	NEDC	22	32
	WLTC	28	38
	RTS95	60	82
	FIP-75	23	32
	US06	47	65

### Evaluation of Power and Torque for ICE and ETD Driveline

The powertrain maximum power  $P_{pwt}$  and torque  $T_{pwt}$  at vehicle wheels can be defined considering the maximum of the terms evaluated above, through the equations:

$$P_{pwt} = \max(P_{Vmax}, P_{take-off}, P_{acc}) \quad (4.20)$$

$$T_{pwt} = \max(T_{Vmax}, T_{take-off}, T_{acc}) \quad (4.21)$$

In Table 12-12 the results for the cases of study are highlighted in light blue. It can be observed that the power request is more demanding at the top vehicle speed, in accordance with the preliminary assumption, whereas the torque is maximum during the take-off with slope of 35% .

Table 12-12 Powertrain Maximum Power and Torque to fulfill requirements

	Requirements	C-Segment	SUV
Power [Kw]	Vspeed Max	61.0	163.3
	Vsp. Max @ 5% slope	74.9	185.3
	Take-off @ 35% slope	12.7	15.7
	0-100 km/h	63.1	105.4
Torque [Nm]	Vspeed Max	482	947
	Vsp. Max @ 5% slope	475	1124
	Take-off @ 35% slope	1445	2094
	0-100 km/h	720	1406

The equations (4.20) and (4.21) define the total outputs requested to the powertrain in ICE mode, considering the operation in hybrid mode only for the acceleration.

Taking into account the specific requirements for the electric propulsion mode and the requested power for kinetic energy recovery, the specifications for the Electric Traction Drive (ETD) system can be deduced, for the peak and continuous values:

$$P_{elect\ peak} = \max(P_{braking}, P_{e-take-off}, P_{e-acc}) \quad (4.22)$$

$$P_{elect\ cont} = P_{e-vmax} \quad (4.23)$$

Table 12-13 and Table 12-14 summarize the results of equations (4.22) and (4.23) for the cases of study, with assumption that the reference cycle for kinetic energy recovery is the WLTC. The maximum vehicle speed considered in electric mode is 80 km/h for the C-segment vehicle and 100 km/h for the SUV. With the slope  $p=5\%$  the top speed targets are lowered 70 and 90 km/h respectively.



Table 12-13 Electric Driveline system Peak Power and Torque to fulfill requirements

E-Driveline Peak P/T Specifications		Vehicles	
Peak	Requirements	C-Segment	SUV
Power [Kw]	Take-off @ 25% slope	10.4	12.9
	0-50 Km/h	33.8	43.3
	Braking	28.0	38.0
Peak Torque [Nm]	Take-off @ 25% slope	1191	1726
	0-50 Km/h	771	1156
	Braking	894	1236

It can be observed that the peak power request is more demanding for the acceleration, quite higher than energy recovery, whereas the maximum peak torque is for the take-off with slope of 25%. Instead the maximum continuous power and torque of the ETD are depending on the maximum vehicle speed in pure electric operation.

Table 12-14 Electric Driveline Continuous Power and Torque to fulfill requirements

E-Driveline Continuous P/T Specifications		Vehicles	
Continuous	Requirements	C-Segment	SUV
Power [Kw]	V. Speed Max	6.4	17.2
	V. Speed Max @ 5% slope	15.0	30.3
Torque [Nm]	V. Speed Max	92	229
	V. Speed Max @ 5% slope	244	449

### ***Transmission and ETD Specifications***

The previous quantities for power and torque are the values at wheel, to deduce the power and torque at engine and electric motor shafts, we need to consider the transmission that links the machines to the wheels, introducing the gear ratio  $\tau$ , defined with the equation (4.26), and the efficiency of transmission  $\eta_{trasm}$ .

The gear ratio and transmission efficiency depend on transmission type and hybrid powertrain architecture and the values of  $\tau$  have a significant impact on powertrain performance and energy consumption, because of the great influence on machine efficiency and sizing. The selected gearboxes for this study are a DCT for the C-segment and an AT for the SUV. The management of these automated gearbox are key for the ICE and ETD (in case of P2 architecture) operations and their control is performed with the logic presented in the Chapter #11.1.

From the maximum power values in Table 12-13 and Table 12-14 sensitivity versus the transmission ratio is performed to evaluate the torque to be requested to ETD system, both for peak and continuous operations, see the following Table 12-15.

The transmission global efficiency for the evaluation is assumed equal to 0.94, neglecting the dependence on gear ratio and temperature.

Table 12-15 Electric Driveline Power and Torque specifications as a function of Transmission Ratio

Transmission Ratio		6	10	12	18	6	10	12	18
Peak P/T Specifications		Vehicles							
Power [kW]	ETD Requirements	C-Segment				SUV			
	Take-off @ 25% slope	11.1	11.1	11.1	11.1	13.8	13.8	13.8	13.8
	0-50 km/h	36	36	36	36	46	46	46	46
	Braking	30	30	30	30	40	40	40	40
Torque [Nm]	Take-off @ 25% slope	211	127	105	70	306	183	153	102
	0-50 km/h	137	82	68	46	205	123	102	68
	Braking	158	95	79	53	219	131	109	73
	Take-off @ 25% slope	502	837	1005	1507	430	716	859	1289
Speed [rpm]	0-50 km/h	2512	4186	5023	7535	2149	3581	4297	6446
	Braking	1796	2993	3591	5387	1762	2937	3524	5286

Continous	ETD Requirements	C-Segment				SUV			
Power	Vsp. Max @ 5% slope	16	16	16	16	32	32	32	32
Torque		43	26	22	14	80	48	40	27
Speed		3516	5860	7032	10549	3868	6446	7735	11603

The transmission ratio has a positive effect on torque requested to the ETD system, lowering the torque and thus the current and the effect Joule losses. On the other hand motor speed increases with the risk to achieve the upper limit at high vehicle speed, despite the wide operation range of electric drives. The selection criteria of transmission ratio has to take into account also the efficiency of the electric drive, typically higher close the basic speed, for instance 3000÷5000 rpm for a 48V electric drive in the Figure 12-2.

In the second part of this section a sensitivity analysis of performance and fuel consumption/CO<sub>2</sub> by means of simulation will be presented, with the aim to define the better transmission ratio for the electric machine in each considered architecture.

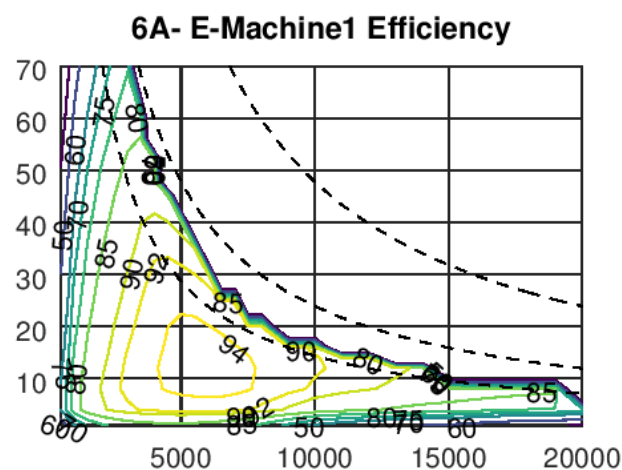


Figure 12-2 Efficiency map of 48V Electric Drive

### ***Powertrain Features to meet CO<sub>2</sub> and Pollution Requirements at 2025***

The targets are demanding both for CO<sub>2</sub> and pollutions, especially to take into account the realistic use of vehicles. The features of the baseline vehicles and powertrains, for the considered vehicle types, are

reported in the following Table 12-16. Both the engines are GDI turbocharged and compliant to EU6 regulation.

Table 12-16 Vehicle and Powertrain features of the vehicles considered as baseline

Vehicle Segment		C-Segment	SUV
Curb weight [kg]		1,325	1,735
Powered wheels		FWD	AWD
POWERTRAIN			
Architecture		S&S	S&S
Engine	Power	112 kW	204 kW
	Techs	L4 1.5L TGDI	L4 2.0L TGDI
Transmission	Type	DCT	AT
	Gears	7	8
Specifications		Baseline	Baseline
CO2 NEDC [g/km]		111.8	161.9
T acc. 0÷100 km/h [s]		8.4	5.5
Vmax Speed [km/h]		216	237

The efficiency improvement can be obtained with two main actions: the electrification, according to specifications defined in the previous paragraph, and the engine evolution.

The electrification by means of a proper architecture selection can lead to significant kinetic energy recovery and engine simplification, for instance, by reducing the number of cylinders. The applied approach will be discussed in the next paragraph.

Based on the engine technology prioritization in Chapter #6.7, the following technologies have been considered to improve the internal combustion engines:

- Extended Miller/Atkinson cycle;
- Compression Ratio increasing (+2);
- Water Injection systems;
- Cylinders reduction.

With focus on SUV, thanks to the first three technologies the CO<sub>2</sub> emission can be reduced about 4.5% in NEDC, maintaining the 4 cylinders, and up to 9% with 3 cylinder engine (140 kW).

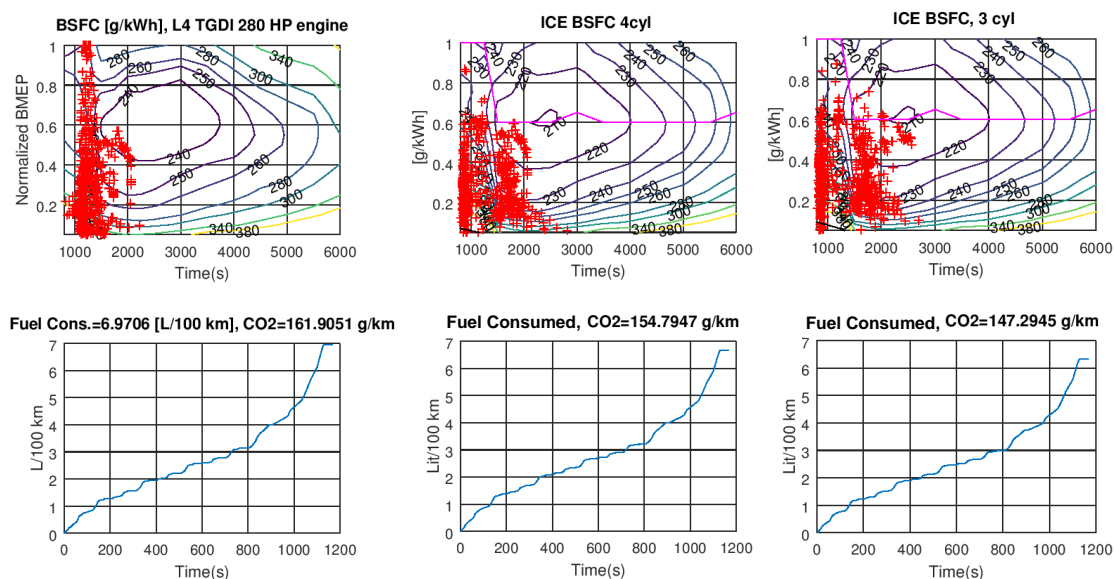


Figure 12-3 Simulation comparison of CO<sub>2</sub> emissions in NEDC cycle for baseline engine (left) and its evolution with 4 cylinders (central) and 3 cylinders (right)

To compensate the impact of displacement reduction at low speed, and thus maintaining the same vehicle acceleration, the boosting of an electric motor can be employed and an electric supercharger could be added.

The Water injection technology allows to mitigate the knock phenomena at low engine speed and to fulfil the EU7 emission requirement in RDE cycle, that forces engine to operate at  $\lambda=1$  combustion.

The other requirement to be managed is the major relevance of the cold condition ( $-7^{\circ}\text{C}$ ), that lead to introduce systems to accelerate powertrain warm-up. One of the most effective technologies illustrated in the previous chapter is the Fast Warm-up system. Its benefit on engine coolant warm-up time and fuel consumption/ $\text{CO}_2$  emission is illustrated in Figure 12-4. Thanks to faster friction reduction during the cycle, an improvement up to 3.6 of  $\text{CO}_2$  % can be achieved for the SUV. This system of energy recovery is also useful to compensate the intermittent operation in case of electric hybrid powertrain.

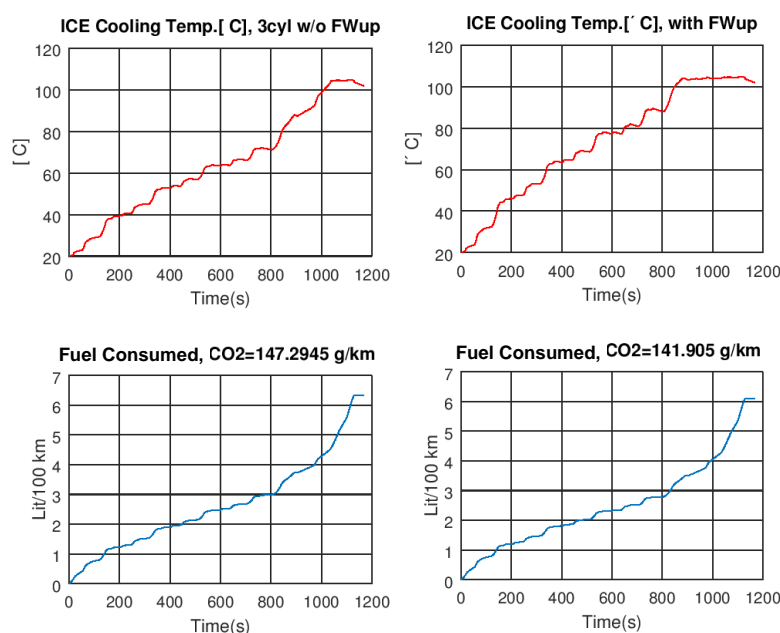


Figure 12-4 Comparison of engine warm –up with (right) and without Fast warm-up system (left) for the 3cylinder engine introduced above

Another key technology to face the cold starts is the Electric Heating Catalyst system. As already explained it ensures a faster catalyst light off with little fuel saving that in the case study is approximately 1% for both vehicles. The EHC technology can reduce the light-off time, useful especially in case of electric hybrid powertrain, characterized by the intermittent operation of the internal combustion engine.

## Definition of Electric Hybrid Powertrain Architecture

Starting from the architectures analysis and prioritization in Chapter #5.2 and #5.3 the preferred powertrain layouts are P2, P0+P4 and P2+P4 based on the 48V electric traction drives, Figure 12-5.

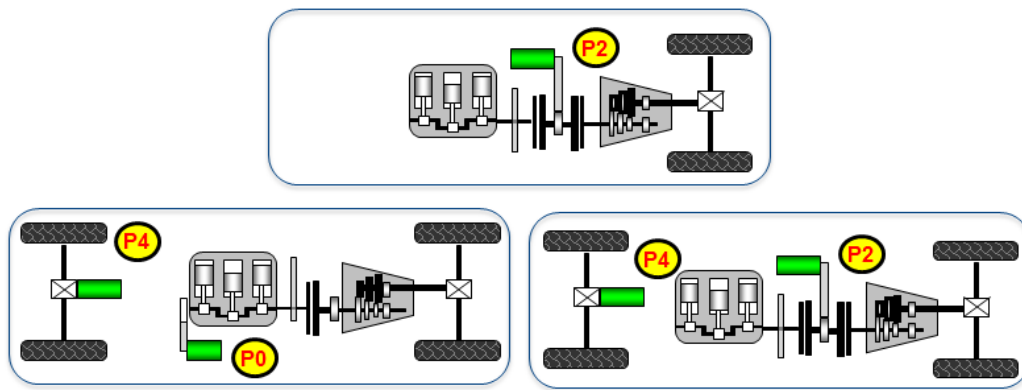


Figure 12-5 Preferred hybrid electric powertrain architectures for case study

Considering the specifications for the ETD systems in

Table 12-15 and the performance of 48V systems at the state-of-art (see

Table 8-4), the 48V architectures can fulfill the requested power, see Table 12-17. The total power is reported for each selected architecture.

48V electric drives with 22/25 kW maximum peak power have been chosen as a trade-off with costs. As benchmark a HV architecture has been also considered. Indeed during the architecture optimization by means of global vehicle simulation the LV architectures will be compared with the HV.

Table 12-17 Electric Traction Driver requirements vs Architecture solutions

Peak Spec. in [kW]		Vehicles		48V Solutions [kW]			HV Solution
Power [kW]	ETD Requirements	C-Segment	SUV	P2	P4+P0	P4+P2	P2
	0-50 Km/h	36	46	22/25	25+15	25+22	66
	Braking	30	40	25/27	27+17	27+25	72

## Sensitivity Analysis and optimization of E-Machines Transmission Ratio

In the previous section the importance of the right transmission ratio  $\tau$  between Electric Machine and wheels has been remarked. To obtain a correct comparison of the powertrain solutions, for each vehicle and powertrain architecture the transmission ratio has been optimized by means of model simulations, taking into account the CO<sub>2</sub> emission and performances (i.e. vehicle top speed , take-off, etc.).

To performe this kind of the optimization it has been fundamental the use of the model based gear-shit logic presented in Chapter #11.1, especially for the P0 and P2 machines, for which the operating points are highly influenced by the gear engaged in addition to transmission ratio between the electric machine and gearbox.

Figure 12-6 shows the sensitivity of CO<sub>2</sub> emissions, top speed and acceleration time versus transmission ratio of P4 48V 25kW electric motor in case of SUV with a Turbocharged GDI 1.5L engine. The electric hybrid architecture includes a P2 48V 22kW electric machine too.

In this example a sweep of  $\tau$  (x-axis of figure) was performed to define the optimal value. In this architecture the optimal value of transmission ratio is approximately 18.

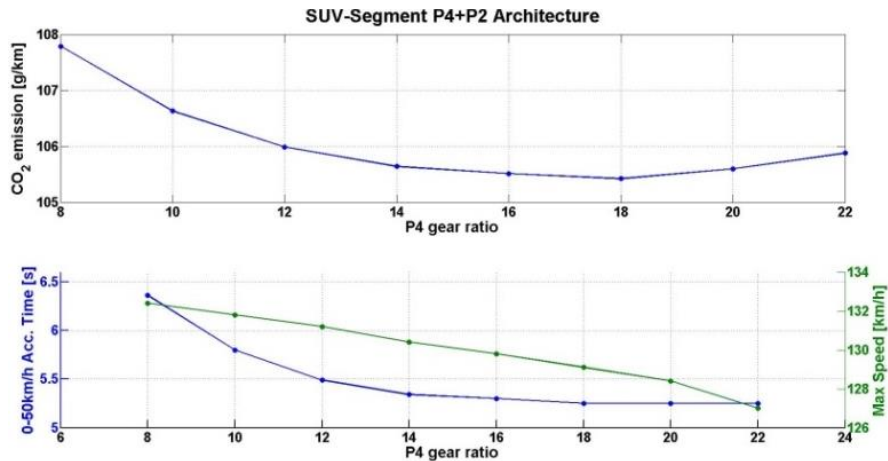


Figure 12-6 Sensitivity of P4 transmission ratio variation in SUV vehicle with P2+P4 48V 22kW/25kW electric motors and Turbocharger GDI 1.5L engine

## Analytic Assessment and Comparison of preferred Powertrain Architectures

After the preliminary design in previous sections, through the model of the vehicle and powertrain (see Chapter #10.2), the more promising configurations are evaluated to verify the capability of fulfilling the vehicle requirements defined in Table 12-1 (HoQ1). Moreover in addition to NEDC and WLTC, US06 and RTS 95 cycles were simulated, with the aim of verifying the behavior in more realistic conditions.

For each vehicle segment the 48V hybrid architectures previously selected with the preliminary design have been considered. The electric machines are Permanent Magnet Synchronous Motors with three rated peak power levels: 15, 22 and 25 kW.

For the C-segment vehicle two different engines were considered: Turbocharged GDI (TGDI) engines with 3 and 2 cylinders and VGT, for a maximum power of 112 kW and 83 kW, according to the baseline and specifications of Table 12-12, respectively.

At same time for the SUV two TGDI engines, with 4 and 3 cylinders and 204kW and 140 kW of output power respectively, have been evaluated.

In both engine families the following technologies were considered:

- Miller/Atkinson cycle ;
- Compression Ratio increase (+2);
- Water Injection system;
- Fast engine warm-up system;
- Electric Heating Catalyst system.

The transmission is a DCT with 7 gears for the C-segment vehicle and an AT with 8 and 10 gears for the SUV.

The electric energy storage is a 48V LiFePO<sub>4</sub> battery, air cooled, with a capacity of 1.4 kWh for the C-Segment vehicle and 2.2 kWh for the SUV.

## Comparison of Solutions for C-Segment Vehicle

Table 12-18 summarizes the performances achievable with the powertrain architectures pre-selected in the previous sections for the C-Segment vehicle. From simulation analysis, a 48V hybrid P2 powertrain

(SOL1 in the table) can guarantee performances quite similar to HV P2 system (SOL3) in NEDC, with the advantage of lower costs.

Table 12-18 Summary of C-Segment vehicle performances as a function of the analyzed powertrain architectures

Vehicle Segment		C-Segment					
VehicleC Parameters							Cx=0.24
Curb weight [kg]		1,325	1,350	1,381	1,401	1,369	1,239
Powered wheels		FWD	FWD	E-AWD	FWD	E-AWD	E-AWD
POWERTRAIN							
Architecture		S&S	P2	P4+P0	P2	P4+P0	P4+P0
Engine	Power	112 kW	83 kW			83 kW	
	Techs	1.5L TGD	L3, 1.12 L, CR+2, WI and Fast Wup			L2, 0.95 L	
Transmission	Type	DCT					
	Gears	7					
Electric Drive	Power	na	22kW	25+15	66kW	25+15	25+15
	Volatge	na	48V	48V	400V	48V	48V
	Battery	na	1.4 kWh				
Specifications	Target	Baseline	SOL1	SOL2	SOL3	SOL4	SOL5
CO2 NEDC [g/km]	80	111.8	90.7	90.2	90.5	85.5	75.7
(% reducruion vs. Baseline)			-18.9	-19.4	-19.1	-23.6	-32.3
CO2 WLTP [g/km]	na	119.9	93.2	90.2	90.8	87.7	77.6
(Delta Mass 250 kg)			-22.3	-24.8	-24.2	-26.9	-35.3
US06 [g/km]	na	136.3	114.22	106.92	104.84	103.29	91.07
[%]			-16.2	-21.6	-23.1	-24.2	-33.2
RTS 95 [g/km]	na	155.3	122.7	115.2	114.9	110.8	99.3
[%]			-21.0	-25.8	-26.0	-28.7	-36.0
(HEV) T acc. 0÷100 km/h [s]	9	8.4	8.04	6.59	5.68	6.56	5.89
(EV) T acc. 0÷50 km/h [s]	4.5	na	7.3	4.27	2.37	4.23	3.8
(ICE) Vmax Speed [km/h]	195	216	211	211	211	211	216
(EV) Vmax Speed [km/h]	80	na	108	134	160	134	142
Electric Autonomy [km]	>5	na	7	7	7	7.3	7.7
Additional Cost [€]			895	1350	1897	1350	1350
Techs Value [€/CO2 g/km]			42	62	89	51	37

The P2 LV is able to recover a significant part of kinetic energy in NEDC and the P2 HV offers negligible advantage in terms of CO<sub>2</sub> emission, despite better performances. The gap between P2 HV and LV systems increases considering cycles with many transients and high braking power peaks (e.g. RTS95), since in this case P2 LV recovers partially the kinetic energy of the vehicle.

The 48V P4+P0 architecture (SOL2) allows CO<sub>2</sub> emission similar to P2 HV, also in the more demanding driving cycles, with a limited gap in terms of performance. Considering the lower costs and the ability to fulfill all performance requirements the 48V P4+P0 architecture is the best solution. Another additional benefit of the P4+P0 layout compared with P2 HV is the All Wheel Driving operation.

The electrification compensates the engine power reduction due to engine downsizing, obtained with the reduction from 4 to 3 cylinders. However to reduce furtherer the CO<sub>2</sub> emission, the engine downsizing up to 2 cylinder (SOL5) is need. This step is compensated by means of the BMEP increasing, obtained with turbocharging system optimization.

However to fulfill the 2025 target of CO<sub>2</sub> emissions, without other expensive actions on the powertrain, an improvement of the vehicle aerodynamics (Cx=0.24) has also been introduced, allowing the achievement of less than 76 g/km of CO<sub>2</sub> ( ~ 3.27 L/100 km of fuel consumption) in NEDC. The costs of vehicle improvement are not considered, with assumption that they are included in a new vehicle design. The next Figure 12-7 shows, for the architecture 48V P4+P0 (SOL5) the operating points of the electric machines and of the engine in the WLTC cycle. Furthermore the SOC and cumulative fuel consumption [L/100/km] in comparison with the baseline engine are also depicted.



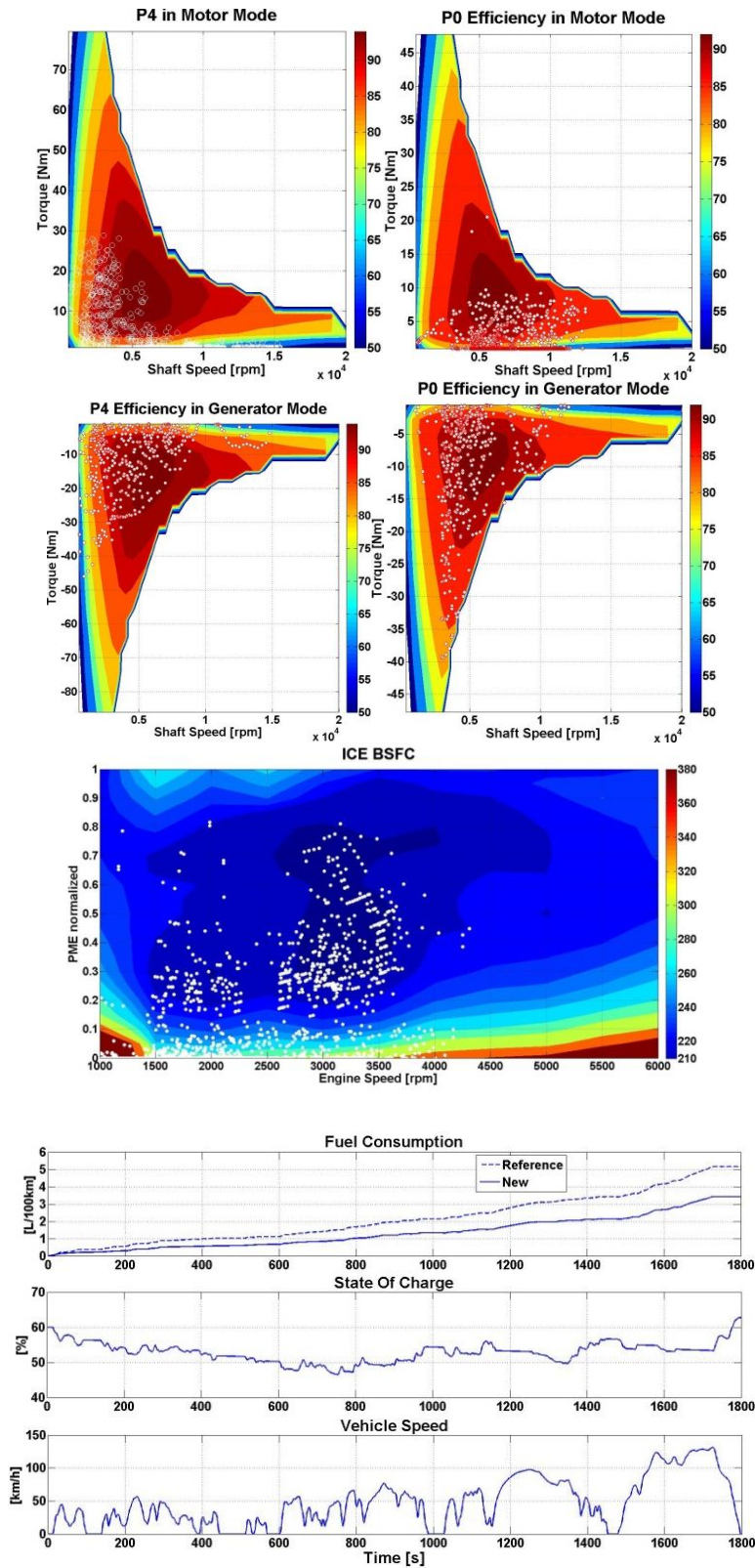


Figure 12-7 Operating points of Electric Machines and ICE in a WLTC cycle for C-Segment vehicle equipped with P4+P0 powertrain architecture (SOL5 of Table 12-18); the fuel consumption [L/100km] is shown in comparison with the baseline engine



Finally, the end-user's breakeven distance of the best powertrain architecture has been evaluated in comparison with the baseline engine, Figure 12-8. The cost estimations are derived from data in previous chapters and they include the battery. Its cost could be shared with the power net supply update to 48V, lowering the electrification cost. To consider the car manufacturer margin, the estimated costs were increased of 50%. Moreover a sensitivity analysis versus fuel price variation in [€] has been performed. The breakeven distance is in a range 85 000÷175000 km, for a fuel price variation between 1÷ 2 €.

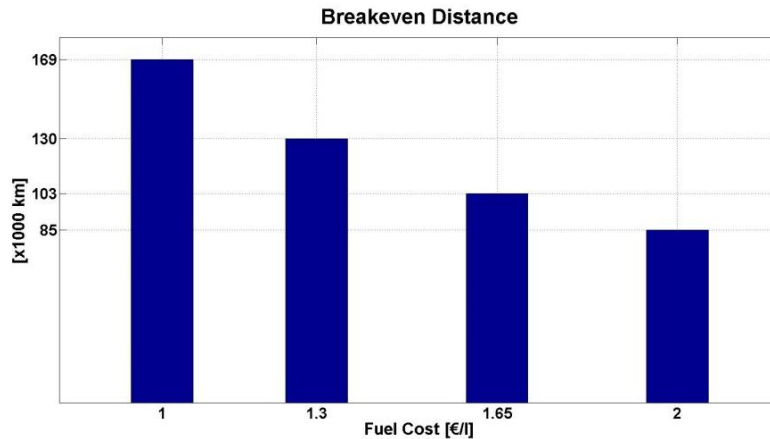


Figure 12-8 End-user 's breakeven distance compared with baseline for the C-Segment vehicle equipped with P4+P0 powertrain architecture (SOL5 of Table 12-18) and sensitivity analysis vs. fuel price variation in [€]

## Comparison of Solutions for SUV

A similar architecture analysis has been performed for the SUV and the results are presented in Table 12-19.

Table 12-19 Summary of SUV performances as function of the analyzed hybrid powertrain architectures

Vehicle Segment		SUV						
Curb weight [kg]		1,735	1,764	1,767	1,783	1,731	1,731	1,731
Powered wheels		AWD	E-AWD	E-AWD	AWD	E-AWD	E-AWD	E-AWD
Powertrain								
Engine	Power	204 kW				140 kW		
	Techs	L4 2.0L TGDl	CR+2, WI ,Fast Warm-up			L3, 1.5L		Cx= 0.24
Transmission	Type	AT						
	Gears	8					10	
Electric Drive	Power	na	25 + 15	25+22	66kW	25+22	25+22	25+22
	Volatge	na	48V	48V	400V	48V	48V	48V
	Battery	na	2.2 kW					
PWT Topology		S&S	P4+P0	P4+P2	P2	P4+P2	P4+P2	P4+P2
Specifications	Target	Baseline	SOL1	SOL2	SOL3	SOL4	SOL5	SOL6
CO2 NEDC [g/km] (% reduccion vs. Ref)	110	161.9	133.3	132.0	130.0	123.5	122.5	104.4
			-17.7	-18.5	-19.7	-23.7	-24.3	-35.5
CO2 WLTP [g/km] (Delta Mass 317 kg)	na	171.4	130.9	130.0	128.0	122.3	122.7	105.1
			-23.7	-24.2	-25.3	-28.7	-28.4	-38.7
US06 [g/km] [%]	na	199.6	161.2	157.1	155.0	153.6	154.7	128.2
			-19.2	-21.3	-22.3	-23.0	-22.5	-35.8
RTS 95 [g/km] [%]	na	213.9	165.3	158.7	157.2	156.9	156.0	133.8
			-22.7	-25.8	-26.5	-26.6	-27.1	-37.4
(HEV) T acc. 0÷100 km/h [s]	6	5.5	4.16	4.02	3.76	4.95	4.89	4.84
(EV) T acc. 0÷50 km/h [s]	4.5		5.46	4.55	2.99	4.46	4.45	4.4
(ICE) Vmax Speed [km/h]	230	237	239	239	239	215	215	238
(EV) Vmax Speed [km/h]	100	0	113	120	137	120	122	133
Electric Autonomy [km]	> 5	0	7	7	7	7.5	7.5	8.5
Additional Cost [€U]		0	2035	2555	2780	1495	1795	1795
Techs Value [€U/CO2 g/km]		na	71	85	87	39	46	31

The simulation demonstrates also for this vehicle the capability a 48V hybrid powertrain to fulfill all performance targets and a significant reduction of CO<sub>2</sub> emission. In addition to the electrification, engine technology improvements and downsizing are needed. The power reduction from 204 kW of baseline to 140 kW is compensated by the ETD system, but to reach the CO<sub>2</sub> target, also in this case aerodynamic improvement has been considered (SOL6).

As an example of performance evaluation for the SUV, with architecture 48V P4+P2 and engine 140 kW, the following Figure 12-9 shows the acceleration from 0 to 100 km/h in HEV mode and Figure 12-10 the acceleration from 0 to 80 km/h in EV mode.

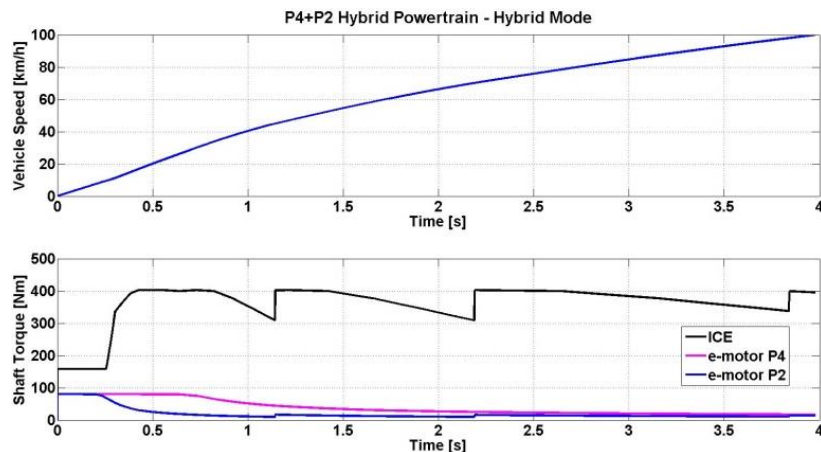


Figure 12-9 SUV acceleration from 0 to 100 km/h in HEV mode

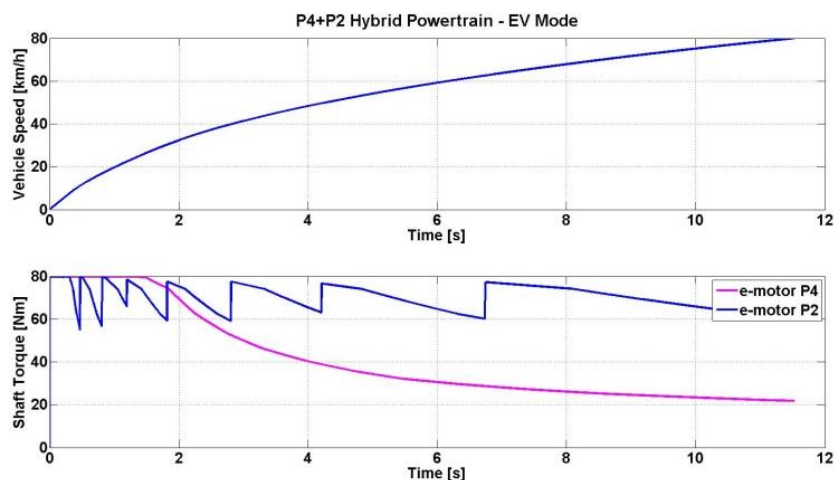


Figure 12-10 SUV acceleration from 0 to 80 km/h in EV mode

The capability of achieving the performance targets allows a comfortable operation of the SUV in pure electric mode, overcoming potential legislation restrictions in urban areas.

Also for the SUV, by means of the Total Cost of Ownership calculation, the breakeven distance compared with baseline has been evaluated: assuming the price of 1.65 € for the gasoline, the breakeven is in 45 000 km, see the following Figure 12-11.

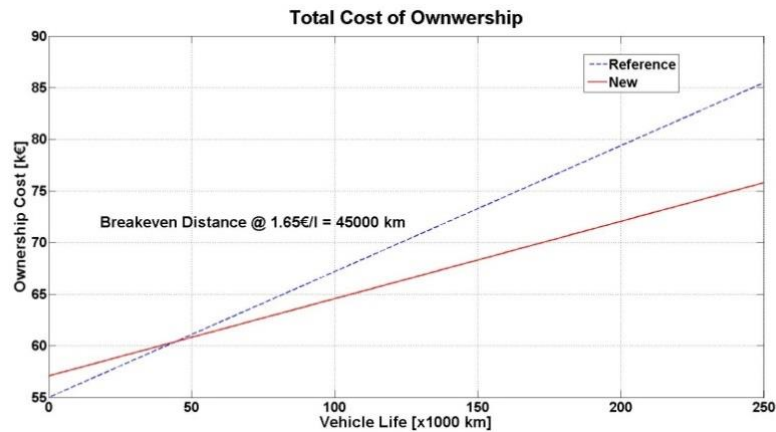


Figure 12-11 SUV Breakeven distance compared with baseline for the SUV equipped with 48V P4+P2 powertrain architecture, SOL6 of Table 12-19

### Rankine Cycle Advantage Evaluation in SUV

To lower further the CO<sub>2</sub> emission of the SUV, it has been investigated the introduction of a WHR system based on Rankine Cycle. In this case the RC integration is facilitated by the elimination of one engine cylinder and by the use of existent electric machine in P2 position as electric generator linked to the expander. The evaporator of RC is installed downstream the FastWarm-up (FWU) system. The RC sizing has been carried out using data from literature and according to methodology presented in Chapter #6.9.4. R123 is the working fluid and the expander is a scroll type. The heat sink is the external ambient, accepting a higher size of the condenser and the variability of ambient temperature, however assumed constant in the analysis. For a fast simulation in the standard cycles, the RC system has been modeled with a black box model that defines global efficiency as a function of engine exhaust gas flow rate and temperature.

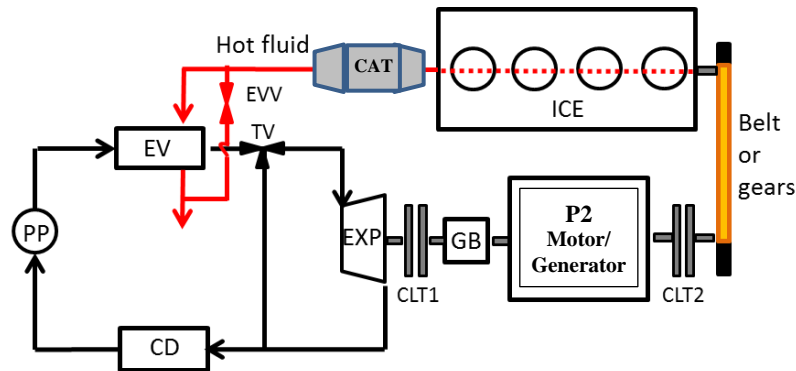


Figure 12-12 Principle scheme of RC integration in electrified powertrain

During the engine warm-up, when the FWU system is active the energy in the exhaust gas is too lower to permit an useful operation of the RC system. Thus the harvested energy by RC system is appreciable only when the by-pass valve of the FWU system is opened, that occurs when the engine coolant temperature overcomes the target of 85°C. For this reason during cold NEDC cycle, especially in case of electrified powertrains, the use of the RC system is limited.

Integrating the RC system in the better architecture of Table 12-19 (SOL6) the CO<sub>2</sub> decreases up to 102.9 g/km, obtaining a saving of approximately 1.4%. The RC system recovers energy mainly during the last part of NEDC (EUDC), where the electric motors and the FWU system are switched off. The following

Figure 12-13 shows the comparison of the inlet temperature of the RC evaporator and the generated power during the NEDC. The figure compares the behavior in ICE mode (left in figure) bypassing FWU system and the hybrid mode where the FWU is switched off after the engine warm-up. In the hybrid cycle the power harvested in the EUDC phase is higher because the available energy in the engine exhaust gas is higher due to the load increasing for battery recharging.

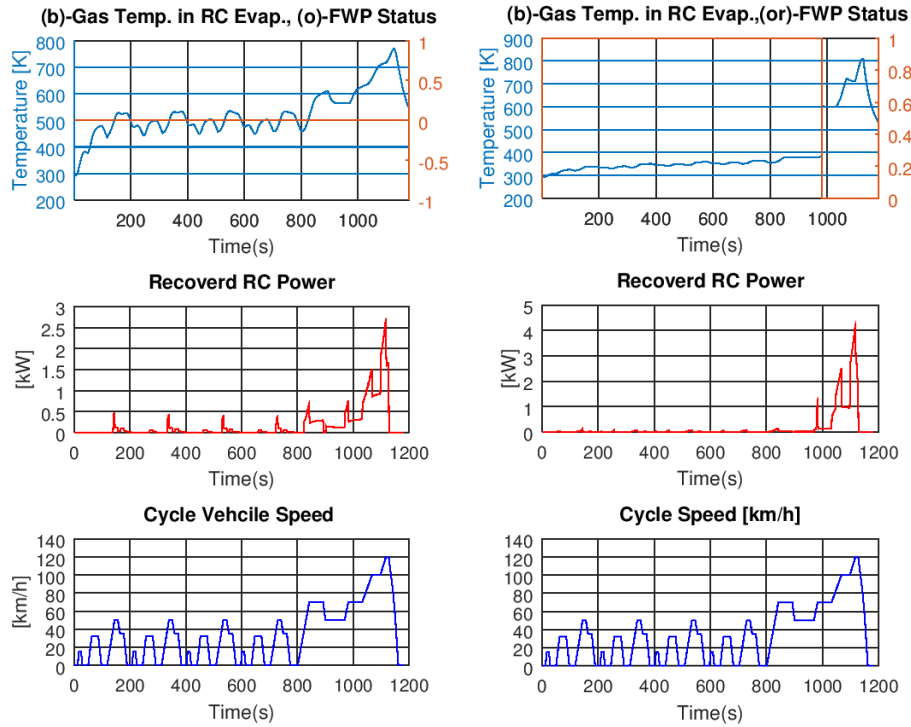


Figure 12-13 Comparison of RC Power recovered with and without activated FWU system: (left) in only ICE mode and (right) hybrid mode with use of the FWU.

The benefit of the RC system is higher in long driving profiles characterized by high load operation, where the warm up phase has a lower weight. For instance in WLTC, the energy  $\text{CO}_2$  saving can achieve approximately 3.2%. The Figure 12-14 illustrates the fuel consumption and the power harvested during in the aforementioned driving profile.

The fuel and  $\text{CO}_2$  saving increase up to 8% considering cruising driving profiles, typical of the highway, with vehicle speed in a range  $120 \div 140$  kph. In these conditions the hybrid powertrain operates in in ICE mode and the RC can provide the harvested power in parallel by means of the clutches CLT1 and CLT2 closing, see Figure 12-12. The following Figure 12-15 (left) shows the delivered mechanical power by the engine and the RC system during a driving cycle with three steps of vehicle speed. The RC power (difference between blue and red lines in the central picture) is in a range  $0.7 \div 3.1$  kW. Alternatively the recovered energy could be delivered through the electric pathway by means of P2 electric machine as generator and P4 as motor. In this case the saving is approximately 4 %, lower than the direct mechanical link due to loss in the energy conversion of the electric machines, see Figure 12-15(right).

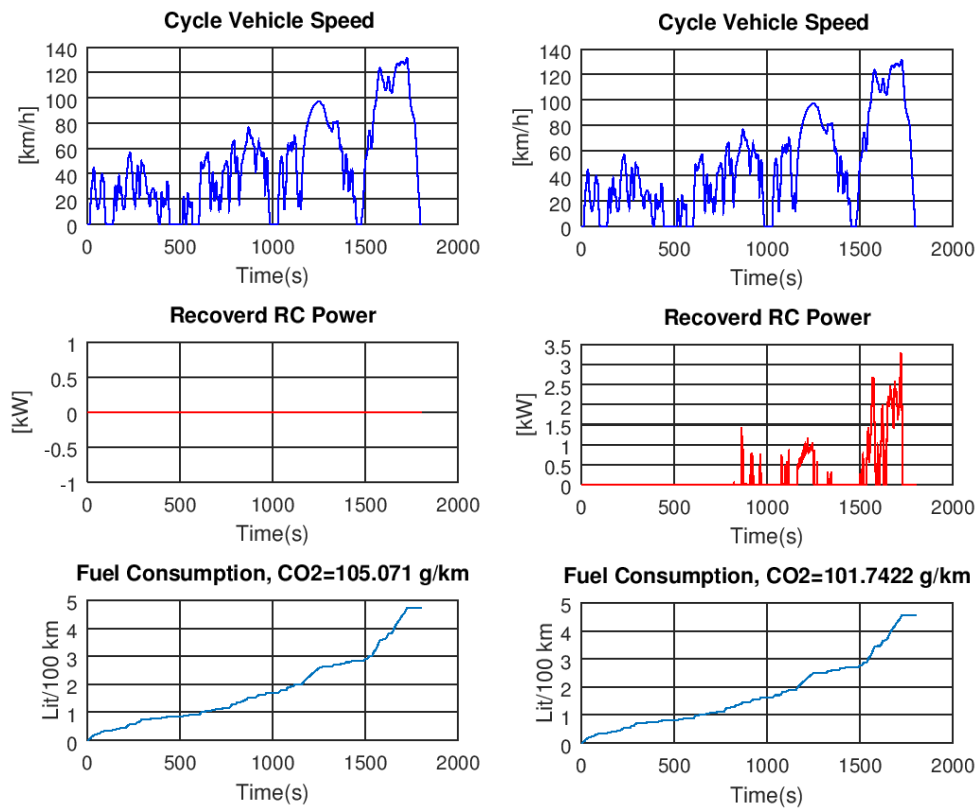


Figure 12-14 Comparison of power recovered with (right) and without (left) RC system in WLTC.

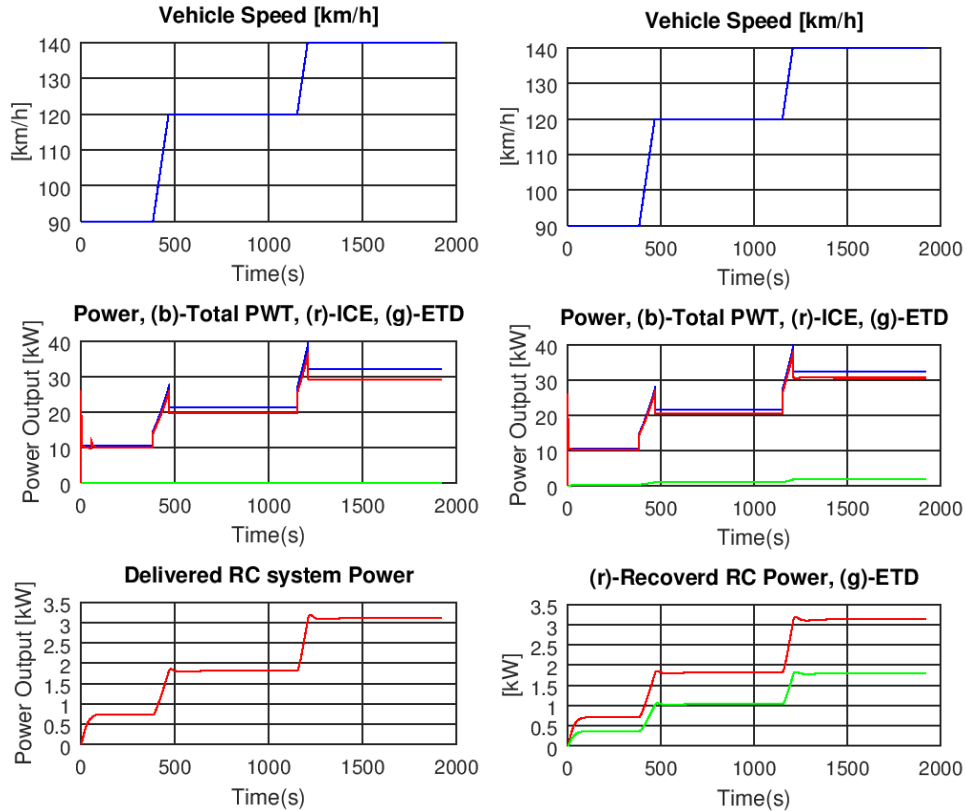


Figure 12-15 Hybrid powertrain behaviour in highway cruising condition with RC system: (left) mechanical actuation, (right) electric actuation

## Summary

Considering the emission standards in a timeframe up to 2025, with low voltage propulsion systems it is possible to achieve very low CO<sub>2</sub> emissions, close to the limits. However, for both vehicles considered in the analysis (Compact and SUV), further vehicle improvements are needed (e.g. aerodynamics and/or weigh reduction) to fulfill the targets. Alternatively blends with biofuels or synthetic fuels are needed.

The low voltage electric drives allow to implement full hybrid vehicles, without any limitations in comparison with high voltage systems, as a consequence they are a viable solution for the powertrain electrification at affordable costs.

The following Figure 12-16 and Figure 12-17 summarize the technologies paths for both the vehicles. In case of the C-segment vehicle, other options to the previous presented are proposed.

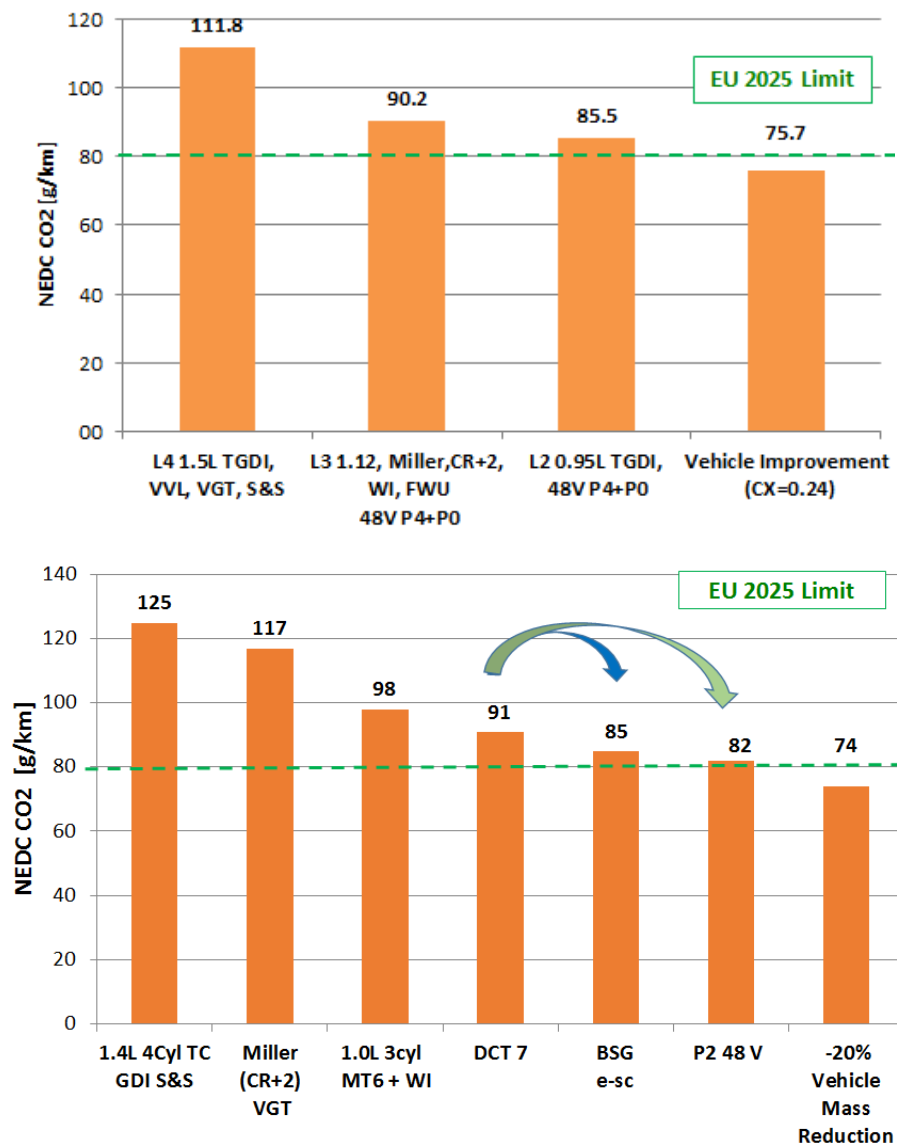


Figure 12-16 Technological paths for a C-Segment vehicle to face NEDC CO<sub>2</sub> requirements, without penalty on engine performance and emissions; the technologies are additive, excluding the path highlighted by the arrows where the adoption of BSG or P2 48 V layout are considered as an alternative

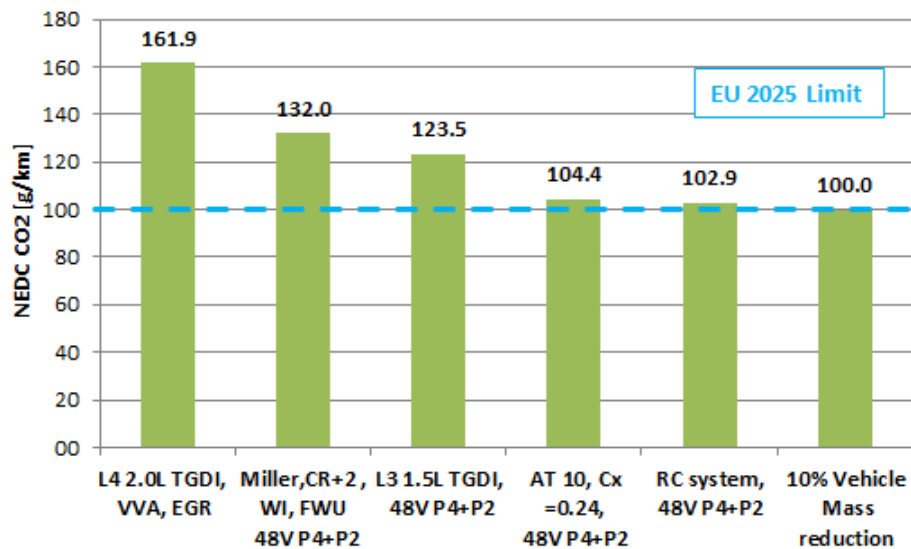


Figure 12-17 Technology paths to reduce NEDC CO<sub>2</sub> in a SUV

## 12.2 Vehicle WTW and LCA Analysis towards post 2025 regulations (Case Study)

Comprehensive objective evaluation of technologies can only be achieved under consideration of the entire product lifecycle, especially taking into account the GHG targets for transportation sector beyond 2030, see Chapter #2.1.

In this section, the resulting CO<sub>2</sub>-equivalent (CO<sub>2</sub>e) emissions of different drivetrain technologies are compared and quantified over the WTW and total lifecycle paths.

The evaluation considers a common vehicle body, technology and materials, and the provision of electric energy and fuel from fossil and renewable origins. However, the use phase has the major influence on the life cycle evaluation of vehicles. Determination and processing of data has been done by a combination of literature data and vehicle simulations.

This study treats a comparison of several powertrain concepts with different technologies. Considered technologies include different types of propulsion, energy forms and storage systems. In the use phase, electric energy and fuels are considered from different (fossil and renewable) sources.

### Steps of the Study

- A technology research has covered the determination of operation-relevant specifications (e.g. masses, efficiencies, future development potential) and production-relevant data for various components in the vehicle.
- Data regarding energy supply, production and end-of-life phases of the considered technologies has been taken from literature review, including environmental reports [4,17,230,231,232,233,258].
- The data combination and calculation of the entire balance have been performed by technical and economic models presented in Chapter #10.

## Reference Driving Cycle for TTW analysis

The reference driving cycle used to evaluate in simulation the TTW emissions and the energy consumptions is the NEDC and to take into account the gap with realistic use the values have been increased of 40%, according to data presented in Figure 2-7. For the PHEVs the CO<sub>2</sub> emission and energy consumption are measured applying the European legislation UN ECE R 101 [282]. It formulates specific rules for evaluating the fuel consumption and the emissions of plug-in vehicles with intermittent ICE operation, basing on the weighting of partial results in Charge Depleting (CD) and Charge Sustaining (CS) operation modes (for further details see Figure 2-10).

## Vehicle and Powertrain Architectures

The analysis has covered vehicles of Compact class with propulsion systems and energy forms listed in the following Table 12-20.

Table 12-20 Features of investigated Vehicle/Powertrain architectures

Vehicle Class	Propulsion System	Energy Storage	Energy Form
Compact (C)	Gasoline ICE	Fuel Tank	Gasoline
	Diesel ICE	Lion-battery	Diesel
	HEV Mild	H <sub>2</sub> Tank	Electric Energy (EU 28 mix)
	HEV Full		e-Fuels
	P-HEV		100% CO <sub>2</sub> neutral H <sub>2</sub>
	FCEV		100% Renewable Electricity
	BEV		

The Biofuel is not included in the energy forms, due to the low sustainability in term of land and water usage, as already explained in Chapter #9, only their blending in gasoline and diesel up to 5 and 10% respectively are considered. For each vehicle and powertrain architecture the performance targets in Table 12-21 have been assumed. They are defined taking into account market trend analysis and uniformity of performances, in order to carry out a proper comparison of powertrain alternatives. The requested pollutant regulation is at least EU7 level, whereas the CO<sub>2</sub> limit is according to proposal for 2025 in EU (80 g/km). However, in order to forecast the powertrain architecture footprint beyond 2025, the best of the powertrain technologies under development has been considered, without forgetting the costs.

The conceptual definition of the powertrains for HEVs, P-HEVs and BEV has been performed according to methodology presented in this thesis. For the FCEV the data is obtained from technical literature review, where many solutions have been presented [68].

Table 12-21 Performance requirements of investigated Vehicle/Powertrain architectures

		Powertrain Architecture			
		SI-ICE CI-ICE HEV	PHEV SI PHEV SI	FCEV	BEV
Minimum Vehicle Performance	Unit				
Time for acc. 0->100	[s]	9	9	9	9
Gradeability at 10 km/h	[%]	25	25	25	25
Minimum Top Speed	[km/h]	180	180	180	180
Minimum Top Speed (Electric Mode)	[km/h]	80	100	180	180
Minimum Driving Range in Electric Mode	[km]	0/5	50	500	500
Minimum Driving Range	[km]	500	500	500	500



The following Table 12-22, Table 12-23 and Table 12-24 illustrate the features of each powertrain with the outputs in terms of CO<sub>2</sub> and energy consumption. As anticipated, NEDC has been the used driving profile, increasing the cycle outputs of 40% to take into account the realistic use.

In 2025+ the electrification is not just seen as an add-on technology, but as an integrated system designed, where the ICE is optimized together with the electric motor (used for propulsion) in terms of combined system performance. Accordingly in case of the hybrid gasoline vehicles the ICEs are downsized and downrated (reduced in their maximum power), operate with a Miller cycle with increased compression rate. Hybrid Diesel ICEs are not downsized or downrated to prevent complex NO<sub>x</sub> after-treatment systems.

For the high benefit/cost ratio the 48V ETD systems are preferred (see Chapter #8.2.3), with different power rates from mild hybrid up to plug-in hybrid vehicles. P0+P4 and P2+P4 architectures have been preferred. They are quite less efficient than a power split architecture [298], but at same time they are less expensive, with possibility of electric All Wheel Drive (E-AWD) and Torque Vectoring functions. The transmissions are DCT types with 7 and 8 gears. Li-ion batteries of 1.4 kWh and 8 kWh have been selected for the HEVs and PHEVs respectively.

Table 12-22 Powertrain features of ICEs based vehicles and Mild HEVs

Powertrain					
Architecture		ICE-SI	ICE-CI	MildHEV-SI (P4+P0)	MildHEV-CI (P4+P0)
Engine	Power/Displacement	L3 , 1.0 L , 93 kW	L4 , 1.6 L , 80 kW	L2 , 0.95L , 83 kW	L4 , 1.6 L , 80 kW
	Techs	2stage TGDl, Miller , WI	LP EGR +LNT+SCRf	TGDl, Miller , WI	LP EGR +LNT+SCRf
Transmission	Type/Gears	DCT 7	DCT 7	DCT 7	DCT 7
	Powered wheels	FWD	FWD	E-AWD	E-AWD
Electric Drive	Power	na	na	25 kW+15 kW	25 kW+15 kW
	Volatge	na	na	48	48
	Battery Capacity	na	na	1.4 kWh	1.4 kWh
Electric Functions		S&S, eAux, SmartAlt	S&S, eAux, SmartAlt	S&S, eAux, KER, EV	S&S, eAux, KER, EV
Curb weight [kg]		1,237	1,267	1,240	1,303
CO2 TTW [g/km]		130	116	108	95
Energy TTW [MJ/100 km]		172	153	143	126

Table 12-23 Powertrain features of Full HEVs and P-HEVs

Powertrain					
Architecture		HEV-SI (P4+P2)	HEV-SI (P4+P2)	PHEV-SI (P4+P2)	PHEV-SI (P4+P2)
Engine	Power/Displacement	L2 , 0.93L , 93 kW	L4 , 1.6 L , 80 kW	L2 , 0.93L , 93 kW	L4 , 1.6 L , 80 kW
	Techs	2stage TGDl, Miller , WI	LP EGR +LNT+SCRf	2stage TGDl, Miller , WI	LP EGR +LNT+SCRf
Transmission	Type/Gears	DCT 8	DCT 8	DCT 8	DCT 8
	Powered wheels	E-AWD	E-AWD	E-AWD	E-AWD
Electric Drive	Power [kW]	25+25	25+25	25+25	25+25
	Volatge	48	48	48	48
	Battery Capacity	1.4 kWh	1.4 kWh	8 kWh	8 kWh
Electr. Functions		S&S, eAux, KER, EV	S&S, eAux, KER, EV	S&S, eAux, KER, EV	S&S, eAux, KER, EV
Curb weight [kg]		1,265	1,320	1,335	1,390
CO2 TTW [g/km]		100	90	36	32
ICE Energy TTW [MJ/100km]		133	118	136	121
ETD Energy TTW [MJ/100km]		0	0	56	59

The features of the FCEV vehicle have been adjusted from [68]. The fuel cell is a PEM with power up to 55kW. The battery is a LI-ion of 1.4 kWh of capacity and the H<sub>2</sub> tank is able to store up to 4kg of fuel.

In the case of BEV, to ensure a real autonomy up to 500 km, for the battery a capacity of 75 kWh is considered. In order to increase the efficiency a two gears transmission connects the 110 kW IPM motor to the wheels.

Table 12-24 Powertrain features of FCEV and BEV

Powertrain			
Architecture		FCEV	BEV-500
Fuel Cell	Power [kw]	55	
	Techs	PEM	
Transmission	Powered wheels	FWD	FWD
	Gears	Single speed	2-speed
Electric Drive	Power [kW]	110	110
	Volatge	400	400
	Battery Capacity	1.4 kWh	75 kWh
Electr. Functions		S&S, eAux, KER, EV	S&S, eAux, KER, EV
Curb weight [kg]		1,293	1,750
ETD Energy TTW [MJ/100km]		75.6	56

## Analysis of energy supply

The fuel and the electric energy provision foot prints (WTT) have been analyzed in different studies, among these the JRC analysis [230] was the most complete. The study was published in 2014 and for this reason the data have to be integrated with recently analysis [4,17,231,232,233,258].

The following table summarizes the WTT values for the energy forms considered in the evaluation. The values are a forecast in 2030. In case of electricity and hydrogen the value are significant lower than the values at 2014, 140 gCO<sub>2</sub>/MJ and 30 gCO<sub>2</sub>/MJ respectively.

Table 12-25 WTT CO<sub>2</sub> footprint for the energy forms considered in this study

Energy Form	WTT [gCO <sub>2</sub> /MJ]
Gasoline	14
Diesel	15.5
e-Fuels (for SI and CI engines)	5
Electric Energy (EU 28 mix)	50
Hydrogen	4

## Analysis of vehicle manufacturing footprint

As the energy WTT data, the literature is the source for the vehicle manufacturing footprint. Many LCA studies [17,231,232,234,235], including vehicle production and end of life disposal, have been published in US and EU. The results generally indicate that vehicle production and end of life disposal make a significant, but fairly constant contribution to the overall lifetime performance. For example, in a mid-sized car the GHG emission contribution is estimated beyond 2030 to be in a range 21÷27 g CO<sub>2</sub>eq/km for gasoline, diesel and hybrid vehicles. The fuel cell and battery vehicles GHG emissions for vehicle

production and disposal rise up to 50÷57 gCO<sub>2</sub>eq/km. In case of BEV a significant part of emissions is due to battery substitution, assuming a vehicle life time of 200 000 km. The following table summarizes the CO<sub>2</sub> footprint for the vehicle manufacturing considered in this analysis.

Table 12-26 CO<sub>2</sub> footprint for vehicle manufacturing considered in this study

Powertrain Architecture	VEH LCA [gCO <sub>2</sub> /km]
Gasoline ICE	21
Diesel ICE	22
HEV Mild (SI, CI)	24 ,25
HEV Full (SI, CI)	26 ,27
P-HEV (SI, CI)	37 ,38
FCEV	57
BEV	50

## Vehicle Life Cycle Results

Integrating the data in the previous tables, the complete LC impact for a C-segment vehicle with different powertrain architectures has been calculated, see Figure 12-18. The time frame is beyond 2025, but in dashed lines the footprint with the WTT values at 2014 for H<sub>2</sub> and electricity are added.

As expected the CO<sub>2</sub>e emissions decrease with electrification degree, also using the tailored 48V electric drives, due to global efficiency increase of powertrain. The substitution of the propulsion energy form with electricity improve furtherer the emissions. This is particularly true considering the prospective reduction of the WTT impact to produce the electricity, expected with the increasing of renewable energy production.

With current figures the global benefit of the PHEVs and BEVs is negligible versus the HEVs. For this reason and considering the costs of HEVs, they are preferable in a short term scenario. The cost aspect favorites the SI engines because the electrification reduce the gap with CI engines. In case of FCEVs, they offer advantages in a long term horizon, but the impact of vehicle manufacturing is the main drawback compared with PHEVs and BEVs. Naturally FCEVs are the unique alternative to BEVs to implement local zero emission vehicles, overcoming at same time the long re-fueling time of BEVs.

A further evaluation has been performed considering the use of 100% CO<sub>2</sub> neutral energy forms, see Figure 12-19, according to EU targets at 2050. In this case the electricity is considered produced by wind. As alternative energy carrier to the electricity the e-Fuels (for CI and SI engines) have been considered. The advantages and properties of these syntactic fuels have been already presented in the Chapter #9. With the adoption of the e-Fuels, produced with renewable electricity and CO<sub>2</sub> from air or renewable sources, the TTW footprint of the ICE based powertrains is zero. In this way the global CO<sub>2</sub> emission can become lower than BEVs and FCEVs, considering the forecast of their manufacturing footprints. The BEVs have to pay the impact of battery substitution, which impacts highly on manufacturing emission, and FCEVs need to improve production process in terms of CO<sub>2</sub> emission.

e-Fuel powered ICE vehicles are considered to be in co-existence with BEVs and FCEVs in the market. Though it is obvious that a transition to an alternative energy carrier such as battery or fuel cell electric vehicle will require a large additional investment in charging and refueling infrastructure, the additional invest in a nationwide new infrastructure is not yet considered at this time.

In this scenario, the electrification of the ICE based powertrain remains a key technology solution, because it improves the powertrain overall efficiency, with benefit on energy cost, reduces the urban combustion emissions and allows an easy implementation of the vehicle functions (Torque Vectoring,

AWD, etc.), even more requested by the end-user. To asses to viability of the e-Feul solutions, the cost of ownership has been evaluated and presented in the next paragraph.

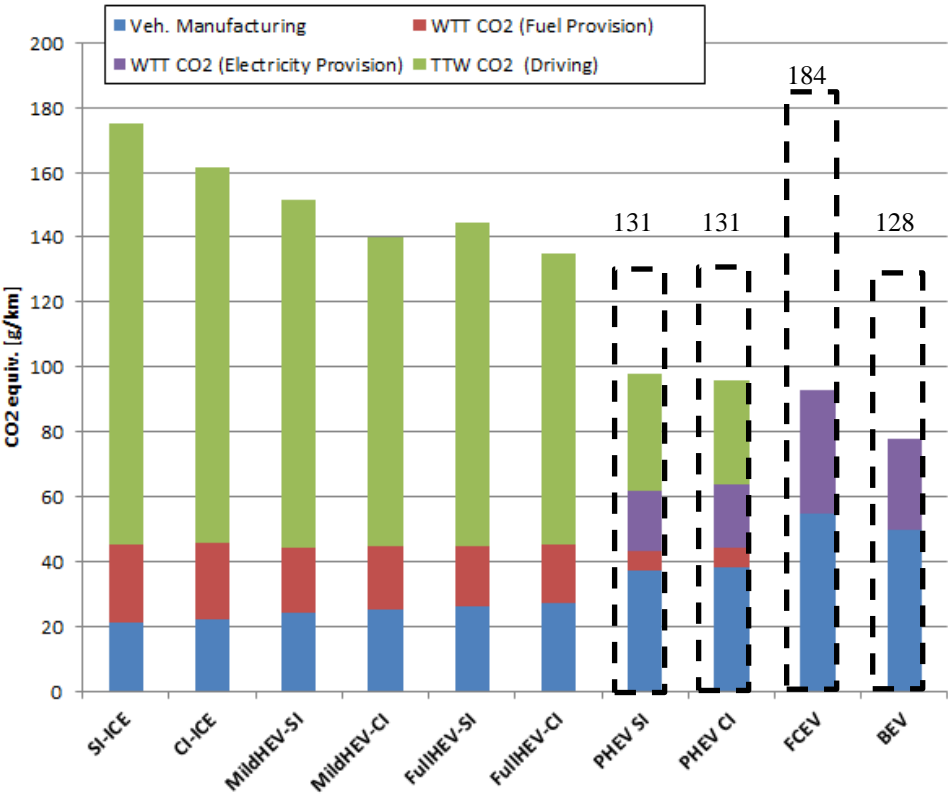


Figure 12-18 LCA of C-Segment Vehicle with different Powertrain Architectures

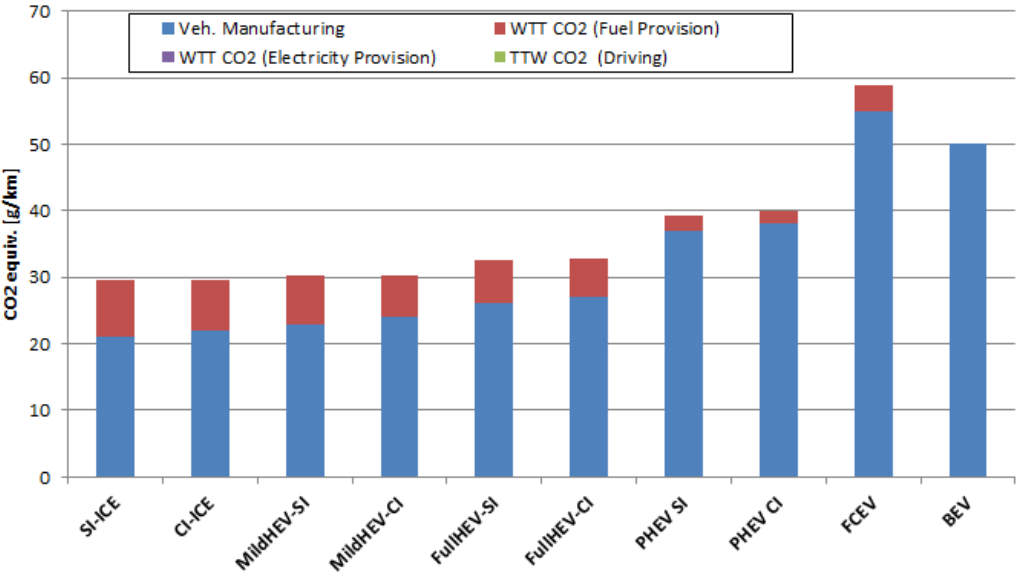


Figure 12-19 LCA of C-Segment Vehicle with different Powertrain Architectures in case 100% CO<sub>2</sub> neutral energy forms

## Total Cost of Ownership Comparison with Renewable Energy

At today's oil price, synthetic fuels are of higher costs than fossil fuel. Fossil fuels need to be replaced within the transport sector in the long term, so e-Fuels will have to compete economically with alternative powertrain concepts such as battery electric vehicles.

The following comparison is based on a simplified end customer total cost of ownership (TCO) including only vehicle price and fuel costs. The basis for the comparison is the same compact class vehicle used for LCA, with an end customer price of approximately 30.000 EUR and best in class ICE technology. The expected end customer range for a battery electric vehicle is over 450 km and requires a battery capacity of 75 kWh (with <15 kWh/100km and 90 % usable battery swing). The SI-ICE hybrid vehicle with the configuration presented in Table 12-23 has NEDC emission of approximately 70g/km and fuel consumption in real life condition of 4.2 liter/100km.

Vehicle manufacturer technology costs are derived by the analyses of the previous chapters and the target price increase in 2025 for the BEV is 9000 €, whereas the price increase for the hybrid ICE powertrain is 2500 €.

The electricity and e-Fuel price were obtained from [74]. A variation of 29÷39 €ct/kWh for electricity price is used to represent uncertainties in electricity cost. Pricing of e-Fuels at the gas station has two major tuning factors: blend rate of e-Fuel and taxation, taking into account that electricity has a significantly lower tax contribution within the traffic sector. For the TCO comparison a 100 percent e-Fuel is considered with a market price variation of 2.0÷2.5 € per liter, representing a low and high taxation scenario.

In order to be comparable in a well-to-wheel consideration with a BEV, a fossil-eFuel blend would still be justified resulting in lower fuel price at the gas station. Due to the lower vehicle price of a HEV, e-Fuels are more favorable up to 110÷165 thousand km, depending on pricing of the specific energy carriers, see Figure 12-20.

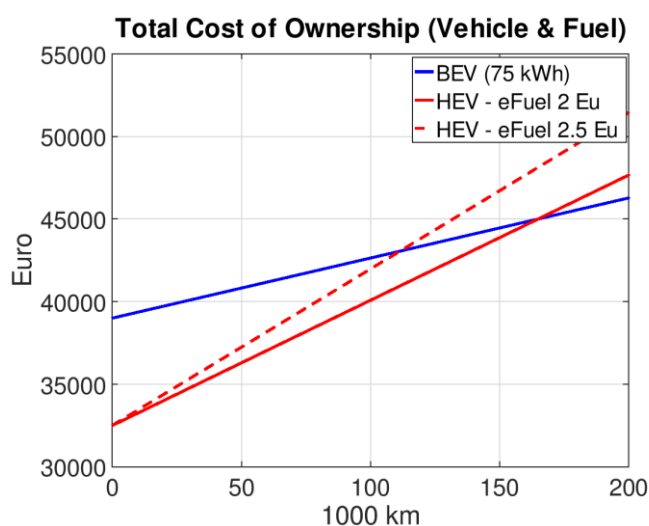


Figure 12-20 Breakeven distance of BEV vs. HEV with e-Fuel in case of C-Segment vehicle, considering e-Fuel price 2.0 and 2.5 €/L whereas electric energy 0.29 €/kWh

## 13. Summary & Outlook

Future emission standards represent a great challenge for the automotive industry, however, the definition of powertrain solutions has to take into account at the same time cost constraints and the end-user's requirements. The powertrain design is even more challenging because the legislations are focusing on the real use of vehicles. For these reasons new homologation procedures have been defined in USA and recently in Europe, with the introduction of WLTP and Real Driving Emission (RDE) procedures.

To fulfill the requirements coming from the end-users and legislations, several powertrain architectures and engine technologies are possible, such as Spark Ignition (SI) or Compression Ignition (CI) engines, with many new technologies, new fuels, and different degree of electrification.

The definition of the more promising powertrain architectures, with proper technology mix, and the assessment of benefits and costs must be accurately evaluated by means of objective procedures and tools in order to choose among the best alternatives.

Moreover, the impacts on Greenhouse Gas (GHG) or energy consumption should be evaluated in term of powertrain Well-to-Wheel or Life Cycle and not only evaluating the Tank-to-Wheel, as many legislations are considering.

The main achievements of this work have been:

- the definition of a structured methodology to link constraints and end-user's requirements to powertrain technical features, in order to perform a conceptual basic design and an objective comparison of architectures and technologies;
- the development of a conceptual design procedure of the powertrain architectures, with a proper technology mix, with the aim of reducing the analysis to the more promising solutions;
- the analytic comparison of the defined powertrain architectures and technologies, considering their effectiveness vs. regulations and end-user's requirements, the technological maturity and the impact on production costs;
- the analysis and investigations of the powertrain key technologies (e.g. Water Injection, Low Temperature Combustions, etc.);
- the definition of the possible powertrain technology pathways towards 2025 and a general forecast post-2025.

The methodology adopted for the conceptual design, the analysis and the comparison of the main powertrain architectures and technologies is according to a System Engineering approach, based on the listed tools and methodologies:

- a modified QFD approach for the deployment of technical requirements;
- deep technical literature analysis and experimental tests of the key technologies;
- vehicle and powertrain modelling with different level of detail to support design and analysis;
- technology cost analysis;

- technology selection and prioritizing methodologies.

The powertrain areas to be improved and possible technology paths have been defined (Figure 13-1):

- the Internal Combustion Engine, with particular focus on combustion, waste heat recovery technologies and controls;
- the reduction of fossil carbon contents in the fuel, with synthetic fuels produced by means of renewable energy and CO<sub>2</sub>;
- powertrain electrification, with several architectures and growing degree.

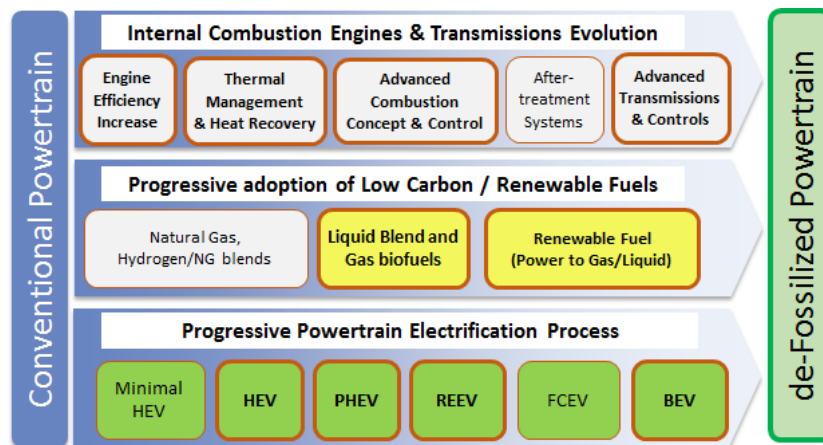


Figure 13-1 Technology options for Powertrain improvement

For each technology path the priority solutions have been identified, see Figure 13-1 (highlighted in red). The increase of electrification degree in powertrain enhances the requirement fulfillment, by means of the vehicle kinetic energy recovery and the shifting of ICE operation in highly efficiency areas. The electrification is also mandatory to provide new functions, which the end-user desires, such as Torque Vectoring and Electric All Wheels Driving.

The cost and packaging issues of the electric drives and the electric energy storage systems are the main concerns to be overcome in order to allow a large application of electric propulsion systems. Among the technologies under development the Low Voltage (48V) propulsion systems are very promising solutions with good trade-off between benefits and costs, allowing the implementation of real “electric full hybrid” vehicle. The application of these low voltage systems at affordable cost is also favored by the power net evolution towards high voltage than the current 12V.

An important pillar towards clean powertrain is the fuel de-fossilization, especially in a long term scenario beyond 2030. Among the alternatives to fossil fuels, together with the renewable electricity, the so called e-Fuels are very promising options. By means of a process named “Power-to-Liquids” synthetic fuels can be produced from water, electric energy and CO<sub>2</sub> (see Figure 13-2).

Using renewable electric energy and CO<sub>2</sub> extracted from the air the e-Fuels can significantly decrease the WTW CO<sub>2</sub> footprint of ICE based vehicles, taking into account a long term period, when the electric energy production is expected mainly from renewable sources, such as sun and wind. In this electric power generation scenario, the synthetic fuels are also promising options for large storage and simple local distribution of the energy, mitigating the discontinuity of the renewable sources. At same time the synthetic fuels can reduce up to four times the pollution production [PM/NO<sub>x</sub>] during the combustion

process, decreasing the gap vs. pure electric propulsion. The main advantages compared with BioFuels are the negligible water demand (1.4 lit for 1lit of e-fuel) and land use.

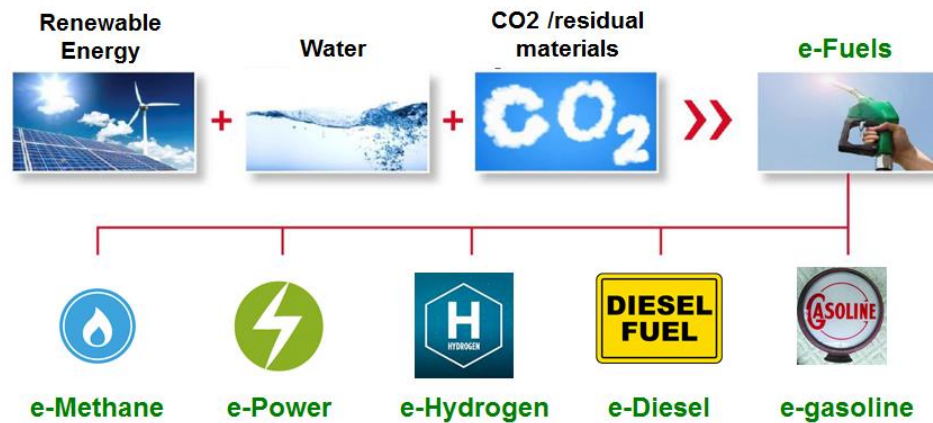


Figure 13-2 Various renewable fuels with different powertrain architectures

The cost is the main challenge, but recent studies forecast a price little higher than fossil fuel, considering future production technology improvements. Focusing on ICEs evolution, the main concerns to improve efficiency and emissions are:

- pumping losses at partial loads (SI engines);
- limited thermodynamic efficiency due to reduced compression ratio, to avoid knocking damages at high loads (SI engines);
- combustion chamber and exhaust system thermo-mechanical stresses at high loads (SI and CI engines);
- NOx production, expensive to be managed with catalyst (CI engines) and PM/PN (GDI and CI engines);
- waste heat in coolant and exhaust gas (SI and CI engines, higher in the first ones).

From prioritization based on QFD analysis the key technologies to face these limits are: Water Injection (WI) during the combustion, Low Temperature Combustions (LTCs) and Waste Heat Recovery Systems (WHRS), see Figure 13-3.

For the effectiveness of these technologies the proper control is fundamental. In some cases the state variables of the systems are not measurable, for cost and/or reliability of the sensors. This is the case of angular positioning of combustion for Low Temperature Combustions and engines adopting Water Injection. The use of virtual sensors based on grey-box models and sensors already presented in the engine management system is an effective solution as confirmed in this study. However a novel multifunction sensor has been developed. It is based on acoustic sensing and allows to implement at affordable cost the measurements of classic engine parameters (such as knock intensity and turbocharger speed) and new parameters (e.g. CN noise), for control and diagnosis purpose.



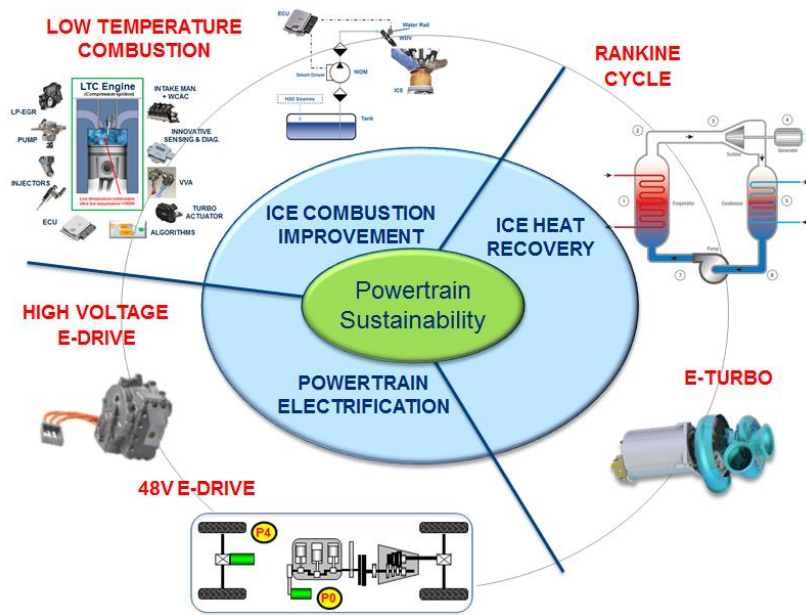


Figure 13-3 Key Powertrain technologies

Water injection (WI) is a cost-effective solution to minimize knocking in turbocharged downsized gasoline engines, allowing at the same time higher compression ratio. Furthermore the  $\lambda=1$  engine operation at high power is allowed, matching the new requirements of EU7 legislation, starting from 2023. For these reasons the WI can be exploited as a solution to reduce fuel consumption and CO<sub>2</sub> emissions, particularly at medium and high load, as well as to increase the engine power output. The benefits and constraints of Port Water Injection (PWI) technology have been investigated in experimental activities carried out on 1.4L Turbocharged GDI engine, installed on test bench in University of Bologna. The PWI system was retrofitted on the original engine and managed by a Rapid Control Prototyping system, that allows the functional by pass of Engine Control Unit. The effects on the combustion in significant engine points are according to the results obtained in literature. Increasing the ratio  $r$  between mass of water and fuel injected, the knocking tendency decrease, with a benefit on BSFC reduction of approximately 2%. Other activities were carried out to investigate the sensitivity of phenomena, varying engine points, water injection phase and pressure. Moreover preliminary control architecture has been defined.

The Low Temperature Combustion concept is a way to combine benefits of CI and SI engines, such as high efficiency and performance with easy pollution management, overcoming their specific limits. Different approaches are possible (e.g. PCCI, RCCI, GCI, etc.), but the main principle is to obtain a controlled homogeneous or partially homogeneous ignition of the air-fuel mixture, characterized by low local temperature and oxygen excess, that leads to high efficiency, low NO<sub>x</sub> and Soot generation. The main issue is the combustion instability, which can be overcome with a proper design of combustion, air and fuel systems, and the closed loop control of the combustion process.

In this study the focus was on the approaches PCCI (Premixed Combustion Compression Ignition) and RCCI (Reactivity Controlled Compression Ignition), applying these concepts to a 1.3L diesel engines, equipped with an additional multi-point gasoline injection system. In the PCCI approach only diesel fuel is used, with a proper pattern injection that increases the pre-mixed component of combustion. Whereas in the RCCI approach the combustion is performed using a dual fuel mixture of diesel and gasoline, with reactivity depending on the two fuels mass ratio. The gasoline injected in the intake manifold forms with air a homogeneous lean mixture, that doesn't burn easily due to low reactivity of gasoline. The ignition is ensured by the diesel injection, that operates has a sort of "spark plug". The investigated fuel mixtures were up to 80/20 gasoline/diesel mass ratio, with good results on consumption and emissions. In

comparison with a Conventional Diesel Combustion (CDC), RCCI has allowed up to 6% of fuel consumption reduction and a significant contemporary reduction of NO<sub>x</sub> and Soot, paying with the HCs increase, that can be managed with an oxidant catalyst present in current systems.

The engine management was performed by means of a RCP system, that has allowed the development of an innovative combustion control, based on virtual sensors, and the investigation of key aspects of this innovative combustion mode. The most important quantities used for the combustion control are the engine load (Indicated Mean Effective Pressure or delivered Torque) and the center of combustion (CA50), i.e. the angular position in which 50% of fuel burned within the engine cycle is reached. All these quantities can be directly evaluated starting from in-cylinder pressure measurement; however, the use of in-cylinder pressure sensors would significantly increase the cost of the engine management system, with reliability issues. As demonstrated in this study, alternatively these measurements can be performed through the magnetic pick-up facing the toothed wheel already present on-board and a low-cost accelerometer mounted on engine block. The information can be obtained observing with the first sensor the engine speed fluctuations and with the second one engine block vibration. Based on these feedbacks a Close Loop Combustion Control of RCCI has been implemented and tested on engine dyno. The control scheme is under study to manage the engine in Gasoline Compression Ignition (GCI) mode and will be the object of future presentations.

As well known, the majority of fuel energy in the ICEs is lost in heat. The Waste Heat Recovery technologies have the aim of harvesting this waste energy. The main systems are: Rankine Cycle system, Thermoelectric Generator and the integration of an Electric moto-generator in the Turbocharger (E-Turbo). Packaging and costs are the limits to be overcome. Taking into account the technology maturity, the amount of recoverable energy, that increases the benefit/cost ratio (gCO<sub>2</sub>/€), the Rankine Cycle systems are the most promising. The evaluations for this technology have been performed by means of simulation models, investigating the achievable benefits in term of fuel consumption/CO<sub>2</sub> in different driving cycles, that can be representative of the real conditions. Considering a conventional vehicle the fuel economy achievable is up to 4% in WLTP, whereas for an HEV (48V P2/P4 architecture) in highway cruising condition up to 8% can be obtained.

Finally, as case study, the concept methodology has been applied to define the powertrain architectures and the technology paths for a C-class vehicle and SUV, which cover a large range of vehicle features. To fulfill customer requirements and future European legislations for the emissions, without any performance penalty, the following technologies mix can be implemented (in case of C-Segment Vehicle):

- the 2020 regulations (95 g/km CO<sub>2</sub> and EU6d final) can be fulfilled with a low grade of electrification, employing technologies to improve the ICE combustion and the gearbox automatization;
- for the 2025 legislations (81 g/km CO<sub>2</sub> and EU7) a higher electrification degree is needed, but low voltage (48V) traction systems can be valid solutions to mitigate the cost increase;
- up to 2030 (61 g/km CO<sub>2</sub>), together with an higher electrification grade, vehicle weight reduction and further ICE improvements are needed, with the use of de-carbonized fuels (e.g. blend with bio-fuels or synthetic fuels over 20%).

In a long term scenario, considering the WTW CO<sub>2</sub> footprint and pollutants towards zero, the adoption of de-fossilized fuel cannot be avoided. The BEVs are not the only solution, valid alternative can be HEVs, PHEVs and RE-EVs propelled with e-Fuels, see Figure 13-4 .

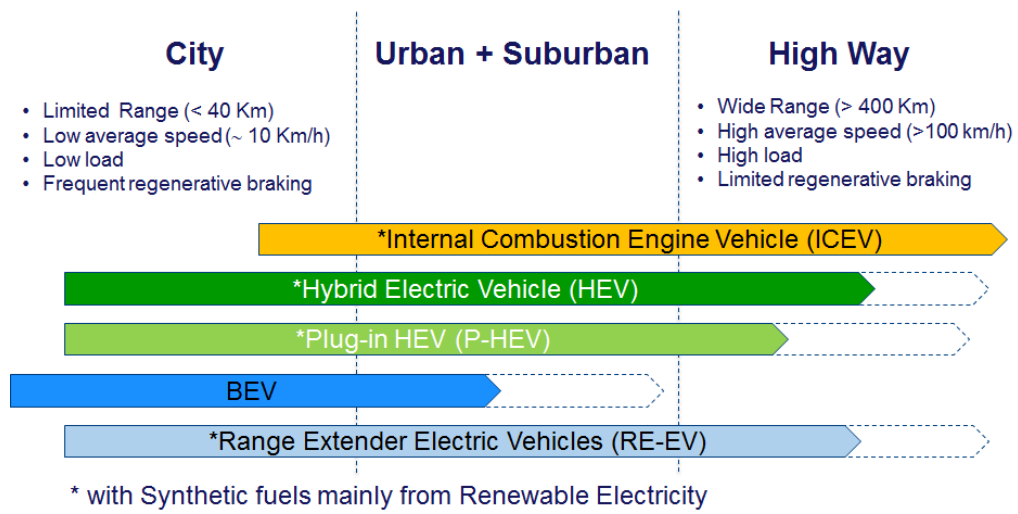


Figure 13-4 Application fields and Powertrain architectures

# References

1. P. Mock, et al., “The WLTP: How a new test procedure for cars will affect fuel consumption values in the EU”, ICCT Working Paper 2014-9, 29 October 2014
2. Haskins, C., INCOSE Systems Engineering Handbook. Version 3 (2006)
3. “Worldwide Emissions Standards Passenger Cars and Light Duty 2017-2018”, Delphi
4. P. Schmidt et al., “Power-to-Liquids, Potentials and Perspectives for the Future Supply of Renewable Aviation Fuel”, September 2016, German Environment Agency
5. Johnson, T. and Joshi, A., “Review of Vehicle Engine Efficiency and Emissions”, SAE Technical Paper 2018-01-0329, 2018, doi:10.4271/2018-01-0329.
6. Sugiyama M., “The new generation of Toyota Powertrain”, 25rd Aachen Colloquium Automobile and Engine Technology 2016
7. Johnson, V., “Fuel Used for Vehicle Air Conditioning: A State-by-State Thermal Comfort-Based Approach”, SAE Technical Paper 2002-01-1957, 2002, doi:10.4271/2002-01-1957.
8. Farrington, R., Rugh, J., “Impact of Vehicle Air-Conditioning on Fuel Economy, Tailpipe Emissions, and Electric Vehicle Range”, Earth Technologies Forum Washington, D.C., October 31, 2000
9. M. John et al., “A Comparison of Light-Duty Vehicle Emissions Over Different Test Cycles and in Real Driving Conditions”, F2014-CET-058, Fisita 2014
10. Bonnel P., Giechaskiel B., Vlachos G., Weiss M., et al., “The Euro 6 Real-Driving Emissions (RDE) procedure for light-duty vehicles: Effectiveness and practical aspects”, International Vienna Motor Symposium 2016
11. Favre C., Bosteels D., and May J., “Exhaust Emissions from European Market-Available Passenger Cars Evaluated on Various Drive Cycles”, SAE 2013-24-0154
12. F. An, R. Earley, L. Green-Weiskel, “Global Overview on Fuel Efficiency and Motor Vehicle Emission Standards: policy options and perspectives for international cooperation”, United Nations, Commission on Sustainable Development Nineteenth Session New York, 2-13 May 2011
13. ICCT, “Adjusting for vehicle mass and size in European post-2020 CO<sub>2</sub> targets for passenger cars”, August 2018
14. U. Tietge, P. Mock, J. German, A. Bandivadekar, N. Ligterink, “From Laboratory To Road - A 2017 update of official and ‘real-world’ fuel consumption and CO<sub>2</sub> values for passenger cars in Europe”, ICCT White Paper, November 2017
15. U. Tietge, S. Díaz, Z. Yang, P. Mock, “From Laboratory To Road International - A comparison of official and real-world fuel consumption and CO<sub>2</sub> values for passenger cars in Europe, the United States, China, and Japan”, ICCT White Paper, November 2017
16. J. J. Kasab, et al., “Technology Roadmap for Light-Duty Vehicle CAFE & GHG Emissions”, 2014 CRC Advanced Fuel and Engine Efficiency Workshop, 25-02-2014
17. C. Bauer, J. Hofer, H-J. Althaus, A. Del Duce, A. Simons, “The environmental performance of current and future passenger vehicles: Life Cycle Assessment based on a novel scenario analysis framework”, Applied Energy 2015
18. T. Hirai, et al., “Nissan’s Powertrain Strategy”, 26th Aachen Colloquium Automobile and Engine Technology 2017

19. "KPMG's Global Automotive Executive Survey 2014 Strategies for a fast-evolving market"
20. "Taxonomy and Definitions for Terms Related to On-Road Motor Vehicle Automated Driving Systems", Standard J3016\_201401 SAE International 2014
21. G. Fontaras, G. Zacharof, B. Ciuffo, "Fuel consumption and CO<sub>2</sub> emissions from passenger cars in Europe Laboratory versus real-world emissions", *Progress in Energy and Combustion Science*. 60 (2017) 97-131
22. Esposito, S., Hoppe, P., Kumagai, T., Mally, M., et al., "Model Based Development for Extreme Lean Burning Gasoline Powertrains- Combining Best Efficiency with Lowest Emissions", 2016 JSAE Congress, Sapporo, Japan, 19 Oct 2016 - 21 Oct 2016, 907-912.
23. Andersson, J., Keenan, M., Osborne, R., Rouaud, C., "Development of lean stratified turbocharged gasoline engines for 2018 SOP", SIA Technical paper, R-2013-06-22
24. Frost & Sullivan, "Strategic Analysis of the Global 48V Power-net Market", November 2016
25. B. Mohrmann, B. Hartmann, P. Schmitz, A. Warm, "High Performance Electrical Power Supply Systems – Requirements, Challenges and Design Concepts", 25th Aachen Colloquium Automobile and Engine Technology 2016
26. Johannes-Joerg Rueger, "Powertrain Trends and Future Potential", Panel "New Directions in Engine and Fuels" DEER Conference, Dearborn, August 4, 2009
27. Kawamoto, N., Naiki, K., Kawai, T., Shikida, T. et al., "Development of New 1.8-Liter Engine for Hybrid Vehicles", SAE Technical Paper 2009-01-1061, 2009, doi:10.4271/2009-01-1061.
28. J. Lee et al., "Development of Effective Exhaust Gas Heat Recovery System for a Hybrid Electric Vehicle", SAE Technical Paper 2011-01-1171, doi:10.4271/2011-01-1171
29. Hirota, Y., Iwata, R., Yamauchi, T., Orihashi, M. et al., "Development of a Compact Adsorption Heat Pump System for Automotive Air Conditioning System", SAE Technical Paper 2016-01-0181, 2016, doi:10.4271/2016-01-0181.
30. M. Verde, L. Cortes, J.M. Corberan, A. Sapienza, S. Vasta, et al., "Modelling of an adsorption system driven by engine waste heat for truck cabin a/c. Performance estimation for a standard driving cycle", *Applied Thermal Engineering*, Elsevier, 2010, 30 (13), pp.1511.
31. Masayoshi Mori et al. "Current Possibilities of Thermoelectric Technology Relative to Fuel Economy", SAE Technical Paper 2009-01-0170
32. R. Stobart, D. Milner, "The Potential for Thermo-Electric Regeneration of Energy in Vehicles", SAE Technical Paper 2009-01-1333
33. Legros Arnaud et al. "Comparison and Impact of Waste Heat Recovery Technologies on Passenger Car Fuel Consumption in a Normalized Driving Cycles", *Energies* 2014, 7, 5273-5290; doi:10.3390/en7085273
34. Arsie I., Cricchio A., Marano V., Pianese C., De Cesare M., "Modeling Analysis of Waste Heat Recovery via Thermo-Electric Generator for Fuel Economy Improvement and CO<sub>2</sub> Reduction for Small Diesel Engine", *SAE Int J. Passeng. Cars – Electron. Electr. Syst.* 7(1):246-255, 2014, doi:10.4271/2014-01-0663
35. "Roadmap ICT for the Fully Electric Vehicle", ICT4FEV. FP7 Grant Agreement Number 260116
36. M. De Cesare, M. Parotto, F. Covassin, "Electric Low Pressure Fuel Pump Control for Fuel Saving", SAE Technical paper 2013-01-0339, 2013
37. W. Lee et al., "Overview of Electric Turbocharger and Supercharger for Downsized Internal Combustion Engines", *ReserchGate* March 2017, DOI: 10.1109/TTE.2016.2620172

38. Arsie, I., Cricchio, A., Pianese, C., De Cesare, M., Nesci, W., "A Comprehensive Powertrain Model to Evaluate the Benefits of Electric Turbo Compound (ETC) in Reducing CO<sub>2</sub> Emissions from Small Diesel Passenger Cars", SAE Technical Paper 2014-01-1650
39. 2014.Terrence Alger, "Dedicated EGR - A Low Emission, High Efficiency Solution for SI Engines", SAE High Efficiency ICE, Detroit 2013
40. Saxena S, Bedoya, ID (2013), "Fundamental phenomena affecting low temperature combustion and HCCI engines, high load limits and strategies for extending these limits", Progress in Energy and Combustion Science 39: 457–488. Available: <http://dx.doi.org/10.1016/j.pecs.2013.05.002>.
41. Reitz R.D., Duraisamy G., "Review of high efficiency and clean reactivity controlled compression ignition (RCCI) combustion in internal combustion engines", Progress in Energy and Combustion Science (2014), <http://dx.doi.org/10.1016/j.pecs.2014.05.003>
42. Singh A.P., Agarwal A.K. (2018), "Low-Temperature Combustion: An Advanced Technology for Internal Combustion Engines". In: Srivastava D., Agarwal A., Datta A., Maurya R. (eds) Advances in Internal Combustion Engine Research. Energy, Environment, and Sustainability. Springer, Singapore, [https://doi.org/10.1007/978-981-10-7575-9\\_2](https://doi.org/10.1007/978-981-10-7575-9_2)
43. Scott Curran, Reed Hanson, Robert Wagner, Rolf Reitz, "Efficiency and Emissions Mapping of RCCI in a Light-Duty Diesel Engine", SAE 2013-01-0289, doi:10.4271/2013-01-0289
44. V. Prikhodko, Z. Gao, S. J. Curran, C. S. Daw, R. M. Wagner and J. E. Parks, "Modeling Emissions Controls for RCCI Engines", ERC-2013 Symposium June 5-6, 2013 University of Wisconsin, Madison
45. M. Sellnau, M. Foster, K. Hoyer, W. Moore, J. Sinnamon, and H. Husted, "Development of a Gasoline Direct Injection Compression Ignition (GDCI) Engine"
46. Sellnau, M., Hoyer, K., Moore, W., Foster, M. et al., "Advancement of GDCI Engine Technology for US 2025 CAFE and Tier 3 Emissions", SAE Technical Paper 2018-01-0901, 2018, doi:10.4271/2018-01-0901.
47. K. Fujiwara," Briefing on Mazda's Long-Term Vision for Technology Development - Technical Overview of SKYACTIV-X", 2017
48. Ellies, B., Schenk, C., and Dekraker, P., "Benchmarking and Hardware-in-the-Loop Operation of a 2014 MAZDA SkyActiv 2.0L 13:1 Compression Ratio Engine", SAE Technical Paper 2016-01-1007, 2016, doi:10.4271/2016-01-1007.
49. Curran Scott J, Hanson Reed M, Wagner Robert M, "Reactivity controlled compression ignition combustion on a multi-cylinder light-duty diesel engine", International Journal of Engine Research, Vol 13, Issue 3, pp. 216 - 225, First published date: April-26-2012.
50. Kokjohn S L, Hanson R M, ASplitter D, Reitz R D , "Fuel reactivity controlled compression ignition (RCCI): a pathway to controlled high-efficiency clean combustion", International Journal of Engine Research, Vol 12, Issue 3, pp. 209 - 226, First published date: June-22-2011, 10.1177/1468087411401548.
51. Del Vescovo, D., Kokjohn, S., and Reitz, R., "The Effects of Charge Preparation, Fuel Stratification, and Premixed Fuel Chemistry on Reactivity Controlled Compression Ignition (RCCI) Combustion", SAE Int. J. Engines 10(4):2017, doi:10.4271/2017-01-0773.
52. Gross, C. and Reitz, R., "Investigation of Steady-State RCCI Operation in a Light-Duty Multi-Cylinder Engine Using "Dieseline", SAE Technical Paper 2017-01-0761, 2017, doi:10.4271/2017-01-0761.

53. M. Hitomi, et al. "Development of a New Generation Clean Diesel Engine (2.2L) which Achieves both Driving Pleasure and Environmental Performance -Realization of a concept for ultra-low compression ratio of 14.0"
54. H. Sahara, et al., "Development of Model-Based Combustion Control to Ensure Robustness of Emissions, Fuel Consumption and Noise Performances in New Generation Diesel Engine", 7th IFAC Symposium on Advances in Automotive Control, Sept. 4-7, 2013. Tokyo, Japan
55. K. Yoshimoto, T. Onoyama, "Strategic Development Plan of Electrical Powertrain", 26th Aachen Colloquium Automobile and Engine Technology 2017
56. J. Merwerth, "The Hybrid-Synchronous Machine of The New BMW i3 & i8", 20.03.2014, Workshop University Lund
57. H. Sorger, "The Tailored Engine & Powertrain for 48 V", Future Powertrain Conference, Birmingham, 28-02-2018
58. K.M. Fritsch, C. Schmuelling, P. Wieske, "Designed by Power Demand: An Electric Drive System for Urban Mobility", 26th Aachen Colloquium Automobile and Engine Technology 2017
59. P. Firsching, T. Eckl, M. Rauch, M. Rohe, J. Kohlhoff, "48-Volt-Hybridisation of the Drive Train", 25th Aachen Colloquium Automobile and Engine Technology 2016
60. M. Hofer, T. Hackl, G. Schlager, "Magna's System Approach for 48 V Mild Hybrids", International Vienna Motor Symposium 2017
61. S. Sapsford, "Future Low Carbon Powertrains for High Performance Vehicles", Innovation in Automotive, 29-01-2012, Royal Academy of Engineering, Carlton House Terrace, London
62. U. Bünger et al., "Power-to-Gas in transport Status quo and perspectives for development", Federal Ministry of Transport and Digital Infrastructure (BMVI), June 2014
63. L. Grond, P. Schulze & J. Holstein, "Systems Analyses Power to Gas", Final Report, DNV KEMA Energy & Sustainability, Groningen, June 20, 2013
64. Frost&Sullivan, "Strategic Analysis of Future Battery Chemistries for Electric Vehicles in Europe and North America", MA77-18, December 2014
65. "Evolution-Electric vehicles in Europe: gearing up for a new phase?", Amsterdam round Table in collaboration with McKinsey & Company, April 2014
66. F. Badin et al., "Energy efficiency evaluation of a Plug-in Hybrid Vehicle under European procedure Worldwide harmonized procedure and actual use", EVS28 International Electric Vehicle Symposium and Exhibition, KINTEX, Korea, May 3-6, 2015
67. M. Contestabile, et al., "Battery electric vehicles, hydrogen fuel cells and biofuels. Which will be the winner?", ICEPT Working Paper, June 2011, Ref: ICEPT/WP/2011/008
68. R. Edwards, H. Hass, J.F. Larivé, L. Lonza, H. Maas, D. Rickeard, "Well-To-Wheels Report" (Version 4.a), JRC Technical Report 2014, Report EUR 26236 EN
69. Carl Berninghausen, "Power to Fuel, Sunfire – closing the carbon cycle", March 2012
70. Huei-Ru "Molly" Jhong, et al., "Electrochemical conversion of CO<sub>2</sub> to useful chemicals: current status, remaining challenges, and future opportunities", Current Opinion in Chemical Engineering 2013, Elsevier
71. J. Beck, "Electrochemical Conversion of Carbon Dioxide to Hydrocarbon Fuels", EME 580 Spring
72. A. Bocarsly "CO<sub>2</sub> Conversion to Fuels", A Progress Report on Liquid Light Inc., Columbia University, April 2014

73. S. Pischinger et al., "Fuel Design for Future Combustion Engines –A View from the Cluster Tailor-Made Fuels from Biomass", International Vienna Motor Symposium 2016
74. U. Schulmeister and S. Eppler "Roadmap to a de-fossilized powertrain", VDA Technical Congress 2017
75. H. Baumgarten et al., "Simulation-Based Development Methodology for Future Emission Legislation", International Vienna Motor Symposium 2016
76. T. Pauer, M. Frohnmaier, J. Walther, P. Schenk, A. Hettinger, S. Kampmann, "Optimization of Gasoline Engines by Water Injection", International Vienna Motor Symposium 2016
77. H. Müller, P. Gutruf, M. Martin, "Another future solution for long driving range at zero emission – Fuel Cell Range Extended EV", International Vienna Motor Symposium 2016
78. Brunner H., Hirz M., Fischer P., "CO<sub>2</sub> emissions of different technologies in passenger cars at real user scenarios in the product life cycle", International Vienna Motor Symposium 2016
79. Kirwan, J., Shost, M., Roth, G., and Zizelman, J., "3-Cylinder Turbocharged Gasoline Direct Injection: A High Value Solution for Low CO<sub>2</sub> and NO<sub>x</sub> Emissions", SAE Int. J. Engines 3(1):355-371, 2010, doi:10.4271/2010-01-0590.
80. Boggs, D., Dorobantu, M., German, J., A. Isenstadt, Watson, T., "Downsized, boosted gasoline engines", ICCT Working Paper 2016-21
81. Thewes, M., Baumgarten, H., Scharf, J., Birmes, G., et al., "Water Injection – High Power and High Efficiency Combined", 25th Aachen Colloquium Automobile and Engine Technology 2016.
82. C. Redtenbacher, et al. "Dual Fuel Combustion –A Promising Concept for Small to Large Engines?", International Vienna Motor Symposium 2016
83. Frost & Sullivan, "Role of Exhaust After-treatment Solution in Reducing Tailpipe Emissions 2016 and 2020 Global Outlook", August 2015
84. Frost & Sullivan, "Analysis of European Market Potential for Selective Catalytic Reduction (SCR) Technology for Passenger Vehicles", December 2014
85. Lenga, H., Hartmann, R., Hyouk Min, B., Grimm, J., Winkler, M., "Low Pressure EGR for Downsized Gasoline Engines", 23rd Aachen Colloquium Automobile and Engine Technology 2014
86. Heywood, J.B., Internal combustion engine fundamentals, New York, 1988
87. FEV-ICCT, "2025 Passenger Car and Light Commercial Vehicle Powertrain Technology Analysis", Final Report / September 2015
88. Martins, J., Uzuneanu, K., Ribeiro, B., and Jasasky, O., "Thermodynamic Analysis of an Over-Expanded Engine", SAE Technical Paper 2004-01-0617, 2004, doi:10.4271/2004-01-0617
89. Song, S., and Zhang, H., "Performance Study for Miller Cycle Natural Gas Engine Based on GT-Power", Journal of Clean Energy Technologies, Vol. 3, No. 5, September 2015
90. "2017 Audi A4 ultra with Millerized 2.0 TFSI offers 31 mpg combined; highest EPA-estimated fuel economy in competitive segment", Green Car Congress, accessed 17 August 2016, <http://www.greencarcongress.com/2016/08/20160817-audi.html>
91. Osborne, R., Downes, T., O'Brien, S., Pendlebury, K. et al., "A Miller Cycle Engine without Compromise - The Magma Concept", SAE Int. J. Engines 10(3):2017, doi:10.4271/2017-01-0642
92. Kyoung-Pyo Ha, Woo Tae Kim, In Sang Ryu, You Sang Son, "Development of Continuously Variable Valve Duration (CVVD) Engine", 25th Aachen Colloquium Automobile and Engine Technology 2016.



93. H. Sorger, W. Schöffmann, S. Lösch, A. Krobath, W. Unzeitig, G. Fraidl, P. Kapus, A. Fürhapter, "AVL's VCR System Modular and Cost Efficient CO<sub>2</sub> Reduction", AVL List GmbH, Graz, Austria, 2017-01-0634
94. Berger, J., Nowak, L., Pogam, M., Groupe, B. De Gooijer "PSA Gasoline Engine Next Generation: Gomecsys VCR Concept as a Solution?", 25th Aachen Colloquium Automobile and Engine Technology 2016.
95. Ferrey, P., Mieke, Y., Constensou, C., Collee V., "Potential of a Variable Compression Ratio gasoline SI Engine with very high Expansion Ratio and Variable Valve Actuation", Technical paper, SIA, 12/04/2013
96. Hoppe, F., Thewes, M., Baumgarten, H., Dohmen, J., "Water injection for gasoline engines: Potentials, challenges, and solutions", International Journal of Engine Research, 2015, doi: 10.1177/1468087415599867
97. Bevilacqua V., Jacobs E., Grauli G., Wüst J., "Future of Downsizing: Fuel Consumption Improvement in NEDC as well as in Customer Operating Conditions", SIA Technical paper 2013, R-2013-06-30
98. P.E. Kapus, C. Spanner, B. Graf, G.K. Fraidl "Cylinder Deactivation with 4 Cylinder Engines – An Alternative to 2 Cylinders?", International Vienna Motor Symposium 2011
99. Isenstadt A., German J., Dorobantu M., "Naturally aspirated gasoline engines and cylinder deactivation", ICCT Working Paper 2016-12
100. [www.delphi.com/manufacturers/auto/powertrain/gas/valvetrain/delphi-tula-dynamic-skip-fire-cylinder-deactivation-system](http://www.delphi.com/manufacturers/auto/powertrain/gas/valvetrain/delphi-tula-dynamic-skip-fire-cylinder-deactivation-system)
101. S. Ando, K. Takashima, "Highly efficient performance - The new Infiniti V6 Petrol Engine with Direct Injection and Turbocharging", International Vienna Motor Symposium 2016
102. T. Niizato et al., "Honda's New Turbo-GDI Engine Series for global application", International Vienna Motor Symposium 2016
103. M. Kliezt, P. Wilde, A. Kleczka, A. Rücker, M. Jung, "Hydrogen Fuel Cell Technology as a Key Element of the Energy Transition", International Vienna Motor Symposium 2016
104. T. G. Vlachos et al., "The Euro 6 Real-Driving Emissions (RDE) procedure for light-duty vehicles: Effectiveness and practical aspects", International Vienna Motor Symposium 2016
105. I. Hirose, "Mazda 2.5L SKYACTIV-G Engine with New Boosting Technology", International Vienna Motor Symposium 2016
106. Chadwell, C., Alger, T., Zuehl, J., and Gukelberger, R., "A Demonstration of Dedicated EGR on a 2.0 L GDI Engine", SAE Int. J. Engines 7(1):434-447, 2014, doi:10.4271/2014-01-1190
107. Durrieu D., Criddle M., Menegazzi P., Wu Y., "Electric supercharger: new electric and boosting architecture for downsizing and downspeeding", SIA Technical paper, R-2013-05-14
108. Stapelbroek, M., Birmes, G., Thewes, M., Espig, M. et al., "Fuel Consumption Reduction and Performance Improvement by Electric Driven Supercharger", 25th Aachen Colloquium Automobile and Engine Technology 2016
109. M. Görgen et al., "All lambda 1 gasoline powertrains", FEV Europe and RWTH Aachen University, Germany
110. Chang, J., Viollet, Y., Amer, A., and Kalghatgi, G., "Fuel Economy Potential of Partially Premixed Compression Ignition (PPCI) Combustion with Naphtha Fuel", SAE Technical Paper 2013-01-2701, 2013, doi:10.4271/2012-01-0677.

111. I. Hwang et al., "Hyundai-Kia's Highly Innovative 1.6L GDI Engine for Hybrid Vehicle", International Vienna Motor Symposium 2016
112. T. Heiduk, et al., "The new Audi V8 TDI engine", International Vienna Motor Symposium 2016
113. Ohta, Y., Fushiki, S., Matsuo, S., "The New PRIUS Powertrain: The New 1.8L ESTEC 2ZR-FXE Engine with the New Generation Hybrid System", International Vienna Motor Symposium 2016
114. Uwe Wagner et al., "48 V P2 Hybrid Vehicle with an Optimized Engine Concept – Optimum Drivability with Excellent Fuel Economy and Cost-Efficiency", International Vienna Motor Symposium 2016
115. E. Reichert, "Combustion Engine Development Utilizing Design for Six Sigma", FEV
116. Habs Moy, M., "Commercial Gas Turbine Engine Platform Strategy and Design", Master of Science In Engineering & Management, Massachusetts Institute of Technology, February 2000
117. Hirsch, R., Nase, A., Straschill, R., Will, P., "Connected and Automated Vehicles: New Degrees of Freedom to Improve the Powertrain", 25th Aachen Colloquium Automobile and Engine Technology 2016
118. "A Low Cost Vehicle Concept for the U.S. Market", University of Michigan
119. Göhlich, D., Gräbener, S., "Identification of User-Oriented Electric Commercial Vehicle Concepts with a Particular Focus on Auxiliaries", 25th Aachen Colloquium Automobile and Engine Technology 2016
120. J. Reeve, "LCVTP WS2: Electric Traction Motors, and guidance to their practical application"
121. T.Finken et al., "Comparison and design of different electrical machine types regarding their applicability in hybrid electrical vehicles", Paper ID 988, Proceedings of the 2008 International Conference on Electrical Machines
122. M. Zeraoulia et al., "Electric Motor Drive Selection Issues for HEV Propulsion Systems: A Comparative Study", IEEE VPPC'05, Sep 2005, Chicago, United States. pp.280-287, 2005.
123. "Overview of storage technologies", SENSIBLE Project funded by EU H2020, 22-01-2016
124. O. Imberdis, "Hybrid Electric Vehicles", 12th SIA–CNAM Conferences Series, March 8th 2011
125. Roman Virsik, Alex Heron, "Free piston linear generator in comparison to other range-extender technologies", EVS 27 Barcelona, Spain, November 17-20, 2013
126. Hugh Blaxill, "Near Term Spark Ignition Engine Technologies for Improved Fuel Economy", ERC 2011 Symposium 'Future Engines and their Fuels'
127. "Polaris Range EXtender Technology (REX)", National Defense Industrial Association, Joint Service Power Expo, Myrtle Beach, SC, May 5th, 2011
128. "Multi-fuel Range Extender with high efficiency and ultra-low emissions", FUEREX Project EU-FP7
129. Frost & Sullivan, "Market Assessment of Energy Conservation and Recovery Technologies for CO2 Reduction in Europe and North America", M7BC-18, March 2013
130. Hergott J., "Exhaust Waste Heat Recovery Systems Application to Rankine system", 17th Cycle of Conferences Cnam/SIA, 15/03/2016
131. J. Ringler, J., Seifert, M., Guyotot, V., and Hübner, W., "Rankine Cycle for Waste Heat Recovery of IC Engines", SAE Int. J. Engines 2(1):67-76, 2009, doi:10.4271/2009-01-0174

132. Zhou F. et al., "A review and future application of Rankine Cycle to passenger vehicles for waste heat recovery", *Renewable and Sustainable Energy Reviews* (2016), <http://dx.doi.org/10.1016/j.rser.2016.11.080>
133. Arsie, I., Cricchio, A., Pianese, C., Ricciardi, V. De Cesare, M., "Modeling and Optimization of Organic Rankine Cycle for Waste Heat Recovery in Automotive Engines", *SAE Technical Paper* 2016-01-0207, 2016, <https://doi.org/10.4271/2016-01-0207>
134. Gorbea Díaz C. E., "Vehicle Architecture and Lifecycle Cost Analysis In a New Age of Architectural Competition", PhD thesis, Technical University of Monaco 08/02/2011
135. Z. Dimitrova, F. Maréchalb, "Energy integration on a gasoline engine for a vehicular application", *Proceedings of ECOS 2017 - the 30th International Conference on Efficiency, cost, optimization, simulation and environmental impact of Energy Systems* July 2-July 6, 2017, San Diego, USA
136. G. Genta. *Motor vehicle dynamics – modeling and simulation*. World Scientific Publishing Co. Pte. Ltd, 1997.
137. A. Irimescu et al., "Automotive Transmission Efficiency measurement using a Chassis Dynamometer", *International Journal of Automotive Technology*, Vol. 12, No. 4, pp. 555–559 (2011), DOI 10.1007/s12239-011-0065-1
138. Jehlik, F., Iliev, S., Wood, E., and Gonder, J., "Investigation of Transmission Warming Technologies at Various Ambient Conditions", *SAE Technical Paper* 2017-01-0157, 2017, doi:10.4271/2017-01-0157
139. F. Vacca et al. "On the Energy Efficiency of Dual Clutch Transmissions and Automated Manual Transmissions", *Energies* 2017, 10, 1562; doi:10.3390/en10101562
140. M. A. Fayazbakhsh and M. Bahrami, "Comprehensive Modeling of Vehicle Air Conditioning Loads Using Heat Balance Method", *SAE Technical Paper* 2013-01-1507, doi:10.4271/2013-01-1507
141. Lee, S.D., Cherry, J., Safoutin, M., McDonald, J. et al., "Modeling and Validation of 48 V Mild Hybrid Lithium-Ion Battery Pack", *SAE Technical Paper* 2018-01-0433, 2018, doi:10.4271/2018-01-0433.
142. M. Hopp et al., "Thermal Conditioning and Efficiency Increase of Electric Vehicles Using a Heat Pump", *25th Aachen Colloquium Automobile and Engine Technology* 2016
143. J. R. Wagner et al., "Smart Thermostat and Coolant Pump Control for Engine Thermal Management Systems", *SAE Technical Paper* 2003-01-0272
144. P. Gaudino, et al., "Pseudo-Empirical Efficiency Model of a Gearbox for Passenger Cars, to Optimise Vehicle Performance and Fuel Consumption Simulation", *SAE Technical Paper* 2004-01-1617
145. Fiorani, P., Gambarotta, A., Lucchetti, G., Ausiello, F. De Cesare M., "A detailed Mean Value Model of the exhaust system of an automotive Diesel engine", *SAE Technical Paper* 2008-28-0027, 2008, doi:10.4271/2008-28-0027
146. F. Covassin, M. Preziuso, M. De Cesare, G. Serra, "A Mean Value Model of the Exhaust System with SCR for an Automotive Diesel Engine", *SAE Technical Paper* 2009-24-0131
147. L. Pace and M. Presti, "An Alternative Way to Reduce Fuel Consumption During Cold Start: The Electrically Heated Catalyst", *SAE Technical paper* 2011-24-0178, doi:10.4271/2011-24-0178
148. L. Pace and M. Presti, L. Poggio, V. Rossi, "Cold Start Thermal Management with Electrically Heated Catalyst: A Way to Lower Fuel Consumption", *SAE Technical paper* 2013-24-0158, doi:10.4271/2013-24-0158

149. Grimaldi, C., Poggiani, C., Cimarello, A., De Cesare, M. et al., "An Integrated Simulation Methodology of Thermal Management Systems for the CO<sub>2</sub> Reduction after Engine Cold Start", SAE Technical Paper 2015-01-0343, 2015, doi:10.4271/2015-01-0343
150. Brooker, A., Gonder, J., Wang, L., Wood, E. et al., "FASTSim: A Model to Estimate Vehicle Efficiency, Cost and Performance", SAE Technical Paper 2015-01-0973, 2015, doi:10.4271/2015-01-0973
151. A. Casavola, G. Gagliardi, W. Nesci, G. Prodi, "A quasi-static simulation tool for the design and optimization of hybrid powertrains", IAV- 2012
152. C.-c. Lin, Z. Filipi, Y. Wang, L. Louca, H. Peng, D. Assanis, and J. Stein, "Integrated Feed-Forward Hybrid Electric Vehicle Simulation in SIMULINK and its Use for Power Management Studies", SAE Technical Paper Series, (2001-01-1334), 2012
153. K. Wipke, M. Cuddy, and S. Burch, "ADVISOR 2.1: a user-friendly advanced powertrain simulation using a combined backward/forward approach", *IEEE Transactions on Vehicular Technology*, 48(6):1751–1761, 1999
154. De Cesare M., Covassin F., "Neural Network Based Models for Virtual NO<sub>x</sub> Sensing of Compression Ignition Engines", SAE Technical Paper 2011-24-0157, doi:10.4271/2011-24-0157
155. Arsie I., Pianese C., De Cesare M. et al., "A Methodology to enhance Design and on-board application of neural network models for virtual sensing of NO<sub>x</sub> emissions in Automotive Diesel Engines", SAE Technical Paper 2013-24-0138
156. Zuurendonk, B., "Advanced Fuel Consumption Emission Modeling using Willans Line scaling techniques for engines," DCT 2005.116, Traineeship report, Technische Universiteit Eindhoven, Department Mechanical Engineering, Dynamics and Control Technology Group, 2005.
157. Rizzoni, G., Guzzella, L. and Baumann, B.M., "Unified Modeling of Hybrid Electric Vehicle Drivetrains," *IEEE/ASME Transactions on Mechatronics*, Vol. 4, no. 3, September 1999.
158. Arsie, I., Pianese, C., Rizzo, G., Flora, R. et al., "A Computer Code for S.I. Engine Control and Powertrain Simulation," SAE Technical Paper 2000-01-0938, doi:10.4271/2000-01-0938, 2000.
159. Eichler, F., et al, "The New EA211 TSI® evo from Volkswagen", 37<sup>th</sup> International Vienna Motor Symposium, 2016
160. L. Guzzella and A. Sciarretta, "Vehicle Propulsion Systems", Springer Verlag, 3d edition, 2012
161. A. Baisden and A. Emadi, "ADVISOR-based model of a battery and an ultra-capacitor energy source for hybrid electric vehicles", *Vehicular Technology, IEEE* , 53(1):199–205, 2004
162. E. Surewaard and M. Tiller, "A Comparison of Different Methods for Battery and Supercapacitor Modeling", SAE Technical Paper Series, (2003-01-2290), 2012
163. Malaczynski, G., Roth, G., and Johnson, D., "Ion-Sense-Based Real-Time Combustion Sensing for Closed Loop Engine Control", *SAE Int. J. Engines* 6, n. 1 (2013): 267-277.
164. V. Johnson," Battery performance models in ADVISOR", *Journal of Power Sources*, 110(2):321–329, Aug. 2002
165. S. Boyd, J. Lee, and D. J. Nelson, "A Simplified Battery Model for Hybrid Vehicle Technology Assessment", SAE Technical Paper Series, 2007(2007-01-0301), 2012
166. V. Pop, H. J. Bergveld, P. H. L. Notten, and P. P. L. Regtien, "State-of-the-art of battery state-of-charge determination", *Measurement Science and Technology*, 16(12):R93–R110, Dec. 2005
167. S. Piller, M. Perrin, and A. Jossen, "Methods for state-of-charge determination and their applications", *Journal of Power Sources*, 96(1):113–120, June 2001.

168. M. Zolot, A. A. Pesaran, and M. Mihalic, "Thermal Evaluation of Toyota Prius Battery Pack", SAE Technical Paper Series, (2002-01-1962), 2002.
169. Shete, K., "Influence of Automotive Air Conditioning load on Fuel Economy of IC Engine Vehicles", International Journal of Scientific & Engineering Research, Volume 6, Issue 8, August-2015
170. Farrington, R., Rugh, J., "Impact of Vehicle Air-Conditioning on Fuel Economy, Tailpipe Emissions, and Electric Vehicle Range", Earth and Technologies Forum Washington, October 31, 2000, NREL/CP-540-28960
171. Ingersoll, J., Kalman, T., Maxwell, L., and Niemiec, R., "Automobile Passenger Compartment Thermal Comfort Model - Part I: Compartment Cool-Down/Warm-Up Calculation", SAE Technical Paper 920265, 1992, doi:10.4271/920265.
172. ASHRAE Handbook of Fundamental, American Society of Heating, Refrigerating, and Air Conditioning, Atlanta, GA, 1988
173. Fletcher, B., and Saunders, C., "Air Change Rates in Stationary and Moving Motor Vehicles", Journal of Hazardous Materials, 38:243-256, 1994.
174. Quoilin, S., "Sustainable Energy Conversion Through the Use of Organic Rankine Cycles for Waste Heat Recovery and Solar Applications", University of Liege, 2011.
175. Osborne S., Kopinsky J., Norton S.; Sutherland A. et al. "Automotive Thermal Management Technology", ICCT Working Paper 2016-18
176. Dimitrova Z., Maréchal F., "Techno-economic design of hybrid electric vehicles and possibilities of the multi-objective optimization structure", Applied Energy 161 (2016) 746–759
177. F. Schüppel, M- Schlüter, J. Gacnik, "Design of battery electric vehicles in accordance with legal standards and manufacturers' and customers' requirements", J. Liebl, Der Antrieb von morgen 2017, Proceedings, DOI 10.1007/978-3-658-19224-2\_2
178. Gianmario Pellegrino G., Vagati G., Boazzo B. and Guglielmi P., "Comparison of Induction and PM Synchronous motor drives for EV application including design examples", [IEEE Transactions on Industry Applications](#) (Volume: 48 , Issue: 6 , Nov.-Dec. 2012 ) doi: [10.1109/TIA.2012.2227092](#)
179. Finken T., Felden M. and Hameyer K., "Comparison and design of different electrical machine types regarding their applicability in hybrid electrical vehicles", Proceedings of the 2008 International Conference on Electrical Machines Paper ID 988
180. Juraschek S., Dipl. Buchner A., Schinnerl B., "The Electric Powertrain Technology of the BMW Group", 39th International Vienna Motor Symposium 2018
181. Aleo M., "Power Components in Electric Cars", Keynote Speech, Automotive- International Conference of Electrical and Electronic Technologies for Automotive, 04-07-2016, Torino.
182. Ehsani, M.; Emadi, A.; Gao, Y., "Modern electric, hybrid electric, and fuel cell vehicles: fundamentals, theory, and design", CRC Press 2009. ISBN: 1420053981.
183. Frost& Sullivan, "Strategic Analysis of Future Battery Chemistries for Electric Vehicles in Europe and North America Li-S to Emerge as a Top Alternative to Li-ion Post 2020", MA77-18, December 2014
184. Mueller C. "Battery Technology: Fueling the EV Hype", 9 November 2017, Motorworld Region Stuttgart, Germany
185. Kalhammer, F. R., Kopf, B. M., Swan, D., Roan, V. P., Walsh, M. P., "Status and Prospects for Zero Emissions Vehicle Technology", Report of the ARB Independent Expert Panel (2007)

186. Sudiro, M.; Bertucco, A., "Production of synthetic gasoline and diesel fuels by alternative processes using natural gas, coal and biomass: process simulation and economic analysis", *International Journal of Alternative Propulsion* Vol 2 (2008) No. 1
187. Ahmed S.; Kopasz J. P.; Russell B. J.; Tomlinson H.L., "Gas-to Liquids Synthetic Fuels for use in Fuel Cells: Reformability, Energy density and Infrastructure Compatibility", *Proceedings of the 3rd International Fuel Cell Conference*. Nagoya, Japan, Nov. 30 – Dec. 3, 1999
188. Yacobucci, B. D.; Schnepf, R. "Selected issues related to an expansion of the Renewable Fuel Standard (RFS)", *CRS Report for Congress*, 2007.
189. Cavina N., De Cesare M., Moro D., Serra G., "Exhaust Gas Turbocharger Speed Measurement Via Acoustic Emission Analysis", *SAE Technical Paper* 2008-01-1007
190. D. Moro; E. Corti; M. De Cesare; G. Serra, "Upgrade of a Turbocharger Speed Measurement Algorithm Based on Acoustic Emission", in: *Electronic Engine Controls*, 2009, WARRENDALE, PA, SAE International, 2009, 1, pp. 1 - 7 (atti di: SAE World Congress, Detroit, 20-23 Aprile 2009)
191. N. Cavina, L. Poggio, "Ion Current Based Spark Advance Management for Maximum Torque Production and Knock Control", *Proceedings of the 8th Biennial ASME Conference on Engineering Systems Design and Analysis*. New York: ASME International, 2006.
192. Cavina N., Sgatti S., Cavanna F., and Bisanti G., "Combustion Monitoring Based on Engine Acoustic Emission Signal Processing", *SAE Technical Paper* 2009-01-1024, 2009, doi:10.4271/2009-01-1024
193. Millo F. and Ferraro C., "Knock in S.I. Engines: A Comparison between Different Techniques for Detection and Control", *SAE Technical Paper* 982477, 1998, doi:10.4271/982477.
194. Brunt M., Pond C., and Biundo J., "Gasoline Engine Knock Analysis using Cylinder Pressure Data", *SAE Technical Paper* 980896, 1998, doi:10.4271/980896
195. Worret R., Bernhardt S., Schwarz F., and Spicher U., "Application of Different Cylinder Pressure Based Knock Detection Methods in Spark Ignition Engines", *SAE Technical Paper* 2002-01-1668, 2002, doi:10.4271/2002-01-1668
196. Lee, Jong-Hwa, Sung-Hwan Hwang, Jin-Soo Lim, Dong-Chan Jeon, e Yong-Seok Cho, "A New Knock-Detection Method using Cylinder Pressure, Block Vibration and Sound Pressure Signals from a SI Engine", *SAE Technical Paper*. SAE International, 1998
197. Pennese M., Damasceno C., Bucci A., and Montanari G., "Sigma® on knock phenomenon control of Flexfuel engines", *SAE Technical Paper* 2005-01-3990, 2005, doi:10.4271/2005-01-3990
198. Schten, K., Ripley, G., Punater, A., and Erickson, C., "Design of an Automotive Grade Controller for In-Cylinder Pressure Based Engine Control Development", *SAE Technical Paper* 2007-01-0774, 2007, doi:10.4271/2007-01-0774
199. Schnorbus, T., Pischinger, S., Körfer, T., Lamping, M. et Schnorbus, T., Pischinger, S., Körfer, T., Lamping, M. et al., "Diesel Combustion Control with Closed-Loop Control of the Injection Strategy", *SAE Technical Paper* 2008-01-0651, 2008, doi:10.4271/2008-01-0651
200. Willems, F., Doosje, E., Engels, F., and Seykens, X., "Cylinder Pressure-Based Control in Heavy-Duty EGR Diesel Engines Using a Virtual Heat Release and Emission Sensor", *SAE Technical Paper* 2010-01-0564, 2010, doi:10.4271/2010-01-0564
201. Moro, D., Cavina, N., Ponti, F., "In-Cylinder Pressure Reconstruction Based on Instantaneous Engine Speed Signal", *J. Eng. Gas Turbines Power*, 125(4), 1050-1058, doi:10.1115/1.1391430

202. Ponti, F., Ravaglioli, V., Serra, G., and Stola, F., "Instantaneous Engine Speed Measurement and Processing for MFB50 Evaluation", SAE Int. J. Engines 2(2):235-244, 2010, doi:10.4271/2009-01-2747
203. Ponti, F., Ravaglioli, V., and Serra, G., "Optimal Combustion Positioning Methodology Based on MFB50 On-Board Estimation", ASME 2010 Internal Combustion Engine Division Fall Technical Conference (ICEF2010), September 12-15, 2010, San Antonio, Texas, USA, doi:10.1115/ICEF2010-35166
204. Ponti F., Ravaglioli V., Cavina N., De Cesare M., "Diesel Engine Combustion Sensing Methodology Based on Vibration Analysis", ICEF2013, October 13-16, 2013, Dearborne, Michigan, USA
205. Taglialatela-Scafati, F., Lavorgna, M., and Mancaruso, E., "Use of Vibration Signal for Diagnosis and Control of a Four-Cylinder Diesel Engine", SAE Technical Paper 2011-24-0169, 2011, doi:10.4271/2011-24-0169
206. Arnone, L., Boni, M., Manelli, S., Chiavola, O. et al., "Block Vibration Measurements for Combustion Diagnosis in Multi-Cylinder Common Rail Diesel Engine", SAE Technical Paper 2009-01-0646, 2009, doi:10.4271/2009-01-0646
207. Polonowski, C., Mathur, V., Naber, J., and Blough, J., "Accelerometer Based Sensing of Combustion in a High Speed HPCR Diesel Engine", SAE Technical Paper 2007-01-0972, 2007, doi:10.4271/2007-01-0972
208. Poggiani C., Cimarello A., Battistoni M., Grimaldi C., Dal Re M. A., De Cesare M., "Optical Investigations on a Multiple Spark Ignition System for Lean Engine Operation", SAE Technical Paper 2016-01-0711, 2016, <https://doi.org/10.4271/2016-01-0711>
209. Ponti, F., Ravaglioli, V., De Cesare, M., Stola, F. et al., "Remote Combustion Sensing Methodology for PCCI and Dual-Fuel Combustion Control", SAE Technical Paper 2015-24-2420, 2015, <https://doi.org/10.4271/2015-24-2420>
210. Ponti, F., Ravaglioli, V., Stola, F., and De Cesare, M., "Engine Acoustic Emission Used as a Control Input: Applications to Diesel Engines", SAE Technical Paper 2016-01-0613, 2016, <https://doi.org/10.4271/2016-01-0613>
211. Cavina, N., Businaro, A., Mancini, G., De Cesare, M. et al., "Acoustic Emission Processing for Turbocharged GDI Engine Control Applications", SAE Int. J. Engines 8(4):1660-1668, 2015, <https://doi.org/10.4271/2015-01-1622>
212. Cavina N., Businaro A., Rojo N., De Cesare M., Paiano L., "Combustion and Intake/exhaust Systems Diagnosis Based on Acoustic Emissions of a GDI TC Engine", 71st Conference of the Italian Thermal Machines Engineering Association, ATI2016, 14-16 September 2016, Turin, Italy
213. Ponti F., Ravaglioli V., De Cesare M., "Real-time Processing of Engine Acoustic Emission for Diesel Injectors Diagnostic and Recentering", ICEF2016-9470, Proceedings of the ASME 2016 Internal Combustion Fall Technical Conference
214. Cavina, N., Businaro, A., De Cesare, M., Monti, F. et al., "Application of Acoustic and Vibration-Based Knock Detection Techniques to a High Speed Engine", SAE Technical Paper 2017-01-0786, 2017, <https://doi.org/10.4271/2017-01-0786>
215. Cavina, N., Businaro, A., De Cesare, M., and Paiano, L., "Knock Control Based on Engine Acoustic Emissions: Calibration and Implementation in an Engine Control Unit", SAE Technical Paper 2017-01-0785, 2017, <https://doi.org/10.4271/2017-01-0785>
216. De Cesare, M., Cavina, N., and Paiano, L., "Technology Comparison for Spark Ignition Engines of New Generation", SAE Int. J. Engines 10(5):2017

217. Cavina, N., Rojo, N., Businaro, A., Brusa, A., Corti, E., De Cesare, M., "Investigation of Water Injection Effects on Combustion Characteristics of a GDI TC Engine", SAE Int. J. Engines 10(4):2209-2218, 2017, doi:10.4271/2017-24-0052
218. Battistoni, M., Grimaldi, C., Cruccolini, V., Discepoli, G., De Cesare, M., "Assessment of Port Water Injection Strategies to Control Knock in a GDI Engine through Multi-Cycle CFD Simulations", SAE Technical Paper 2017-24-0034, 2017
219. Ravaglioli, V., Ponti, F., De Cesare, M., Stola, F. et al., "Combustion Indexes for Innovative Combustion Control," SAE Int. J. Engines 10(5):2017.
220. De Cesare, M., et al., "Boost Pressure Control in Transient Engine Load with Turbocharger Speed Sensing", SAE Technical Paper 2017-24-0049, 2017
221. De Cesare, M., "Technology Overview for future Powertrain", Keynote Speech, Automotive-International Conference of Electrical and Electronic Technologies for Automotive, 16-6-2017, Torino
222. Ravaglioli, V., Stola, F., De Cesare, M., Ponti, F. et al., "Injection Pattern Design for Real Time Control of Diesel Engine Acoustic Emission", SAE Int. J. Commer. Veh. 10(1):308-316, 2017, <https://doi.org/10.4271/2017-01-0596>
223. Ravaglioli, V., Carra, F., Moro, D., De Cesare, M. et al., "Remote Sensing Methodology for the Closed-Loop Control of RCCI Dual Fuel Combustion", SAE Technical Paper 2018-01-0253, 2018, doi:10.4271/2018-01-0253
224. De Cesare M., "Prospettive future del powertrain automobilistico", Giornata di Studio "Giorgio Minelli" sui Motori a Combustione Interna, Bologna, 20-04-2018
225. Zembi, M. Battistoni, F. Ranuzzi, N. Cavina and M. De Cesare "CFD Simulations of Port Water Injection Benefits in a GDI Engine un-der Knock-Limited Conditions", THIESEL 2018 Conference on Thermo- and Fluid Dynamic Processes in Direct Injection Engines
226. V. Ravaglioli, F. Ponti, F. Carra, M. De Cesare, "Heat Release Experimental Analysis for RCCI Combustion Optimization", Proceedings of the ASME 2018 Internal Combustion Fall Technical Conference ,ICEF2018, November 4-7, 2018, San Diego, CA, USA
227. M. Kratzsch, C. Danzer, T. Günther, G. Albrecht, M. Vallon, "Powertrain in 2025 – 75 g CO<sub>2</sub>/km, One Base Engine for the Entire Fleet?" 26<sup>th</sup> Aachen Colloquium Automobile and Engine Technology 2017
228. Deloitte, "Global Automotive Consumer Study Exploring consumers' mobility choices and transportation decisions", 2014
229. U.S. DRIVE Partnership, "Electrical and Electronics Tech Team Roadmap", June 2013
230. R. Edwards, H. Hass, J.F. Larivé, D. Rickeard, Werner Weindorf, "Well-To-Tank Report (Version 4.a)", JRC Technical Report 2014, Report EUR 26237 EN, doi:10.2790/95629
231. Schernus C., Schnorbus T., "From T2W to LCA –Zero-CO<sub>2</sub> Mobility Concepts and Their Different Shades of Green", Keynote SAE ICE2017, 2017-09-13
232. Möhring L., Andersen J., "CNG Mobility – Scalable, Affordable and Readily Available Solution for Environmental and Climate Challenges", 38th International Vienna Motor Symposium 2017
233. Severin C. et al., "Potential of Highly Integrated Exhaust Gas Aftertreatment for Future Passenger Car Diesel Engines", 38th International Vienna Motor Symposium 2017
234. Wang M., Elgowainy A., Han J. "Emissions Modeling: GREET Life Cycle Analysis ", The 2014 DOE Vehicle Technologies Office Annual Merit Review and Peer Evaluation Meeting, Washington, DC June 18, 2014



235. Brunner H., Hirz M., Fischer P., "CO<sub>2</sub>e-emissions of different technologies in passenger cars at real user scenarios in the product life cycle", 37th International Vienna Motor Symposium 2016
236. Curran S, Hanson RM, Wagner RM, "Effect of E85 on RCCI performance and emissions on a Multi-Cylinder light-duty diesel engine", SAE paper 2012; 2012-01-0376
237. M. Görgen et al., "Current and Future Trends of Gasoline Particulate Filter Technologies, Calibration Strategies and Aging Methods", 26th Aachen Colloquium Automobile and Engine Technology, 2017
238. E. Jean, "Just a DPF for Gasoline Engines?", 26th Aachen Colloquium Automobile and Engine Technology, 2017
239. Kunert S., "Integration of the three-way functionality into the Gasoline Particulate Filter – a new technology for the closed-coupled exhaust after-treatment", 39th International Vienna Motor Symposium 2018
240. Ehrhard J. et al., "Future Emission Legislation Requirements –Contribution of Electrically-Assisted Charging Systems", 25th Aachen Colloquium Automobile and Engine Technology, 2016
241. Münz S. et al. "eBooster-Design and performance of a innovative electrically driven charging system", BorgWarner Academy
242. Struzyna, R.; Span, R.; Eifler, W, "Utilization of waste heat through thermodynamic cycles", In Proceedings of 20th Aachen colloquium Automobile and engine technology, Aachen, Germany, 10–12 October 2011
243. Patterson, D.J.; Kruiswyk, R.W., "An engine system approach to exhaust waste heat recovery", In Proceedings of DEER Conference, Detroit, MI, USA, 13–16 August 2007
244. Morrison, O.; Seal, M.; West, E.; Connelly, W., "Use of a thermophotovoltaic generator in a hybrid electric vehicle", In Proceedings of Thermophotovoltaic Generation of Electricity: Fourth NREL Conference, Denver, CO, USA, 11–14 October 1999
245. M.Qinjun, "Gasoline Development Challenges & Solutions", AVL China 6 Emission Seminar, Wuhan, 2018.06.2018
246. Hartmann B., "Evolution of 48V Systems - Connecting the Domains of Powertrain and Power Supply", 48V Power Supply Systems, IQPC, November, 29th-30th, 2016, Berlin, Germany
247. Grams S., "Virtual Design and Optimization of Future Powertrain Architecture", 38th International Vienna Motor Symposium 2017
248. Akao, Y., "Quality Function Deployment", In Cambridge, MA: Productivity Press 1990, ISBN: 1563273136
249. Cohen, L., (1995), "Quality Function Deployment", Addison-Wesley, Reading
250. Dec J.E. and Yang Y., "Boosted HCCI for High Power without Engine Knock and with Ultra-Low NO<sub>x</sub> Emissions – using Conventional Gasoline", SAE 2010-01-1086, SAE Int. J. Engines ,Volume 3, Issue 1
251. Theo Hofman et al., "Rule-based energy management strategies for hybrid vehicles", Int. J. Electric and Hybrid Vehicles, Vol. 1, No. 1, 2007
252. "Pick-Up The ICCT, European vehicle market statistics", Pocketbook 2017/18
253. M. Kliezt et al., "Hydrogen Fuel Cell Technology as a Key Element of the Energy Transition", 37th International Vienna Motor Symposium 2016
254. Müller H. et al., "Another future solution for long driving range at zero emission Fuel Cell Range Extended EV", 37th International Vienna Motor Symposium 2016

255. Scharf et al., “Gasoline Engines for Hybrid Powertrains-High Tech or LowCost?”, 38th International Vienna Motor Symposium 2017
256. Gaëlle Hotellier, “PEM-Electrolysis – a technological bridge for a more flexible energy system”, [http://www.wissenschaft-frankreich.de/de/wp-content/uploads/2014/07/3\\_Hotellier\\_Siemens\\_online.pdf](http://www.wissenschaft-frankreich.de/de/wp-content/uploads/2014/07/3_Hotellier_Siemens_online.pdf)
257. ICCT, “China’s Stage 6 Emission Standard for New Light-Duty Vehicles (final rule)”, Policy Update, March 2017
258. Transport & Environment Report, “CNG and LNG for vehicles and ships - the facts”, October 2018
259. Alvarez R.A. et al., “Assessment of methane emissions from the U.S. oil and gas supply chain”, Science 21 June 2018, DOI: 10.1126/science.aar7204
260. Ponti, F., De Cesare, M., and Ravaglioli, V., "Development and Validation of a Methodology for Real-Time Evaluation of Cylinder by Cylinder Torque Production Non-Uniformities", SAE Technical Paper 2011-24-0145, 2011, doi:10.4271/2011-24-0145
261. Ponti, F., Ravaglioli, V., De Cesare, M., Stola, F., “Torque and Center of Combustion Evaluation Through a Torsional Model of the Powertrain”, ASME. J. Dyn. Sys., Meas., Control. 2015;137(6):061005-061005-9. doi:10.1115/1.4029195
262. Ponti, F., Ravaglioli, V., Moro, D., Serra, G., “MFB50 on-board estimation methodology for combustion control”, Control Engineering Practice, 2013, 21, pp. 1821 – 1829, doi:10.1016/j.conengprac.2013.05.001
263. Ravaglioli, V., Ponti, F., and Stola, F., "Torsional Analysis of Different Powertrain Configurations for Torque and Combustion Phase Evaluation", SAE Technical Paper 2011-01-1544, 2011, doi:10.4271/2011-01-1544
264. Busch, S., Zha, K., Miles, P., Warey, A. et al., "Experimental and Numerical Investigations of Close-Coupled Pilot Injections to Reduce Combustion Noise in a Small-Bore Diesel Engine", SAE Int. J. Engines 8(2):660-678, 2015, doi:10.4271/2015-01-0796.
265. Busch, S., Zha, K., Miles, P., Warey, A. et al., "Experimental and Numerical Investigations of Close-Coupled Pilot Injections to Reduce Combustion Noise in a Small-Bore Diesel Engine", SAE Int. J. Engines 8(2):2015, doi:10.4271/2015-01-0796
266. Ponti, F., Ravaglioli, V., Moro, D., and De Cesare, M., "Diesel Engine Acoustic Emission Analysis for Combustion Control", SAE Technical Paper 2012-01-1338, 2012, doi:10.4271/2012-01-1338
267. Shahlari, A., Hocking, C., Kurtz, E., and Ghandhi, J., “Comparison of Compression Ignition Engine Noise Metrics in Low-Temperature Combustion Regimes”, *SAE Int. J. Engines* 6(1):2013, doi:10.4271/2013-011659
268. Potteau S. et al., “Efficient Combination of Electric Supercharger, Cooled EGR and 12V Extended Stop Start for Future Boosted Gasoline Engines”, Technical Paper, R-2013-06-26 - SIA - 12/04/2013
269. D'Adamo, A., Berni, F., Breda, S., Lugli, M. et al., "A Numerical Investigation on the Potentials of Water Injection as a Fuel Efficiency Enhancer in Highly Downsized GDI Engines", SAE Technical Paper 2015-01-0393, 2015, <https://doi.org/10.4271/2015-01-0393>
270. Robert, A., S. Richard, O. Colin, and T. Poinot, "LES study of deflagration to detonation mechanisms in a downsized spark ignition engine", *Combustion and Flame* 162, no. 7 (2015): 2788-807. doi:10.1016/j.combustflame.2015.04.010

271. D'Adamo, A., Breda, S., Iaccarino, S., Berni, F. et al., "Development of a RANS-Based Knock Model to Infer the Knock Probability in a Research Spark-Ignition Engine", *SAE Int. J. Engines* 10(3):2017, doi:10.4271/2017-01-0551
272. Linse, D., A. Kleemann, and C. Hasse, "Probability density function approach coupled with detailed chemical kinetics for the prediction of knock in turbocharged direct injection spark ignition engines", *Combustion and Flame* 161, no. 4 (2014): 997-1014. doi:10.1016/j.combustflame.2013.10.025
273. Regulation (EC) No 333/2014 of the European Parliament and the Council of 11 March 2014 amending amending Regulation (EC) No 443/2009 to define the modalities for reaching the 2020 target to reduce CO<sub>2</sub> emissions from new passenger cars. <http://eur-lex.europa.eu/legal-content/EN/TXT/PDF/?uri=CELEX:32014R0333&from=EN>
274. Jan Dornoff et al., "The European Commission Regulatory Proposal for Post-2020 CO<sub>2</sub> Targets for Cars and Vans", ICCT, Berlin, 2018, <https://www.theicct.org/publications/ec-proposal-post-2020-co2-targets-briefing-20180109>
275. Nic Lutsey, "Transition to a Global Zero-Emission Vehicle Fleet: a Collaborative Agenda for Governments", ICCT White Paper September 2015
276. Bloomberg, "Electric Vehicle Outlook 2017", July 2017
277. International Energy Agency, "Global EV Outlook 2018", OECD/IEA 2018
278. EPA, "Final Determination on the Appropriateness of the Model Year 2022-2025 Light-Duty Vehicle Greenhouse Gas Emissions Standards under the Midterm Evaluation", EPA-420-R-17-001 January 2017
279. [https://www.arb.ca.gov/msprog/acc/mtr/acc\\_mtr\\_finalreport\\_full.pdf](https://www.arb.ca.gov/msprog/acc/mtr/acc_mtr_finalreport_full.pdf).
280. MIIT, "Parallel Management Regulation for Corporate Average Fuel Consumption and New Energy Vehicle Credits for Passenger Cars", 2017, <http://www.miit.gov.cn/n1146295/n1146557/n1146624/c5824932/content.html>.
281. Cui, H., "China's New Energy Vehicle Mandate Policy (Final Rule)", <https://www.theicct.org/publications/china-nevmandate-final-policy-update-20180111>.
282. UN ECE R101, <https://www.unece.org/trans/areas-of-work/vehicle-regulations/agreements-and-regulations/un-regulations-1958-agreement/un-regulations-addenda-to-the-1958-agreement/old-version-of-regulations-pages/regs-101-120.html>
283. Commission Regulation (EU) 2017/1151, June 1st, 2017, Official Journal of the European Union, L 175/1
284. Commission Regulation (EU) 2017/1153, June 2nd 2017, Official Journal of the European Union, L 175/679
285. Guinée JB et al., "Handbook on life cycle assessment – operational guide to the ISO standards", Dordrecht, The Netherlands, 2002
286. ISO. ISO 14040. Environmental management – life cycle assessment –principles and framework. International Organisation for Standardisation (ISO); 2006.
287. ISO. ISO 14044. Environmental management – life cycle assessment –requirements
288. Transport & Environment, "Cars with engines: can they ever be clean?", September 2018
289. Khalfan, A., Andrews, G., and Li, H., "Real World Driving: Emissions in Highly Congested Traffic", SAE Technical Paper 2017-01-2388, 2017, doi:10.4271/2017-01-2388

290. ICCT, "Remote-sensing Regulation for Measuring Exhaust Pollutants from in-Use Diesel Vehicles in China", Policy Update, September 2017
291. CARB, Jun. 2017, Public Webinar Workshop on Updates to CARB'S EMFAC2017 Model, [https://www.arb.ca.gov/msei/downloads/emfac2017\\_workshop\\_june\\_1\\_2017\\_final.pdf](https://www.arb.ca.gov/msei/downloads/emfac2017_workshop_june_1_2017_final.pdf).
292. ERTRAC, "European Roadmap Electrification of Road Transport", 3<sup>rd</sup> Edition, Version: 10, June 2017
293. Piano, A., Millo, F., Boccardo, G., Rafigh, M. et al., "Assessment of the Predictive Capabilities of a Combustion Model for a Modern Common Rail Automotive Diesel Engine", SAE Technical Paper 2016-01-0547, 2016, doi:10.4271/2016-01-0547
294. Ando S., Ishii H., Shikata A., Sui T., "The New VR30DDTT Engine from Infiniti – Outstanding Power and Response", 25th Aachen Colloquium Automobile and Engine Technology 2016
295. N. Cavina, M. De Cesare, V. Ravaglioli, F. Ponti, F. Covassin, "Full Load Performance Optimization based on Turbocharger Speed Evaluation via Acoustic Sensing", ICEF2014-5677
296. Subiantoro, Alison; Ooi, Kim Tiow; and Stimming, Ulrich, "Energy saving measures for automotive air conditioning (AC) system in the tropics" (2014), International Refrigeration and Air Conditioning Conference, July 14-17, 2014. Paper 1361. <http://docs.lib.purdue.edu/iracc/1361>
297. Sorrentino, M., Mauramati, F., Arsie, I., Cricchio, A. et al., "Application of Willans Line Method for Internal Combustion Engines Scalability towards the Design and Optimization of Eco-Innovation Solutions", SAE Technical Paper 2015-24-2397, 2015, doi:10.4271/2015-24-2397
298. Kapadia, J., Kok, D., Jennings, M., Kuang, M. et al., "Powersplit or Parallel - Selecting the Right Hybrid Architecture", SAE Int. J. Alt. Power. 6(1):2017, doi:10.4271/2017-01-1154
299. F. Le Berr, A. Abdelli and R. Benlamine, "Sensitivity Study on the Design Methodology of an Electric Vehicle", SAE Technical Paper 2012-01-0820
300. Department Of Energy, "Well-to-Wheels Greenhouse Gas Emissions and Petroleum Use for Mid-Size Light-Duty Vehicles", May 10, 2013
301. D. Di Battista, M. Mauriello, R. Cipollone, "Waste heat recovery of an ORC-based power unit in a turbocharged diesel engine propelling a light duty vehicle", Applied Energy 152 (2015) 109–120, <http://dx.doi.org/10.1016/j.apenergy.2015.04.088>
302. Thring RH, "Homogeneous-charge compression-ignition (HCCI) engines", SAE Technical paper 892068
303. Asad U., Zheng M., Ting DSK, Tjong J., (2015), "Implementation challenges and solutions for homogeneous charge compression ignition combustion in diesel engines", J Eng Gas Turbines Power 137:101505
304. Neely GD, Sasaki S, Leet JA, (2004), "Experimental investigation of PCCI-DI combustion on emissions in a light-duty diesel engine", SAE Technical paper 2004-01-0121
305. Landerl C. et al. , "The New 3- and 4-Cylinder Gasoline Engines of BMW Group – Modular Engine Family NEXT GENERATION", 26th Aachen Colloquium Automobile and Engine Technology 2017
306. Kanda, T., Hakozaiki, T., Uchimoto, T., Hatano, J. et al., "PCCI Operation with Early Injection of Conventional Diesel Fuel", SAE Technical Paper 2005-01-0378, 2005, doi:10.4271/2005-01-0378
307. Hardy, W. and Reitz, R., "A Study of the Effects of High EGR, High Equivalence Ratio, and Mixing Time on Emissions Levels in a Heavy-Duty Diesel Engine for PCCI Combustion", SAE Technical Paper 2006-01-0026, 2006, doi:10.4271/2006-01-0026

308. Manente V., Johansson B., Tunestal P., Cannella W., "Influence of inlet pressure, EGR, combustion phasing, speed and pilot ratio on high load gasoline partially premixed combustion", SAE paper 2010; 2010-01-1471
309. Olsson J-O, Tunestål P., Johansson B., Fiveland S., Agama R., Willi M. et al., "Compression ratio influence on maximum load of a natural gas fueled HCCI engine", SAE Technical paper 2002-01-0111
310. Horibe N, Harada S, Ishiyama T, Shioji M (2009), "Improvement of premixed charge compression ignition-based combustion by two-stage injection", *Int J Engine Res* 10:71–80
311. Torregrosa A, Broatch A, García A, Mónico L (2013), "Sensitivity of combustion noise and NOx and soot emissions to pilot injection in PCCI Diesel engines", *Appl Energy* 104:149–157
312. El Chammas, R. and Clodic, D., "Combined Cycle for Hybrid Vehicles", SAE Technical Paper 2005-01-1171, 2005, <https://doi-org.ezproxy.unibo.it/10.4271/2005-01-1171>
313. Endo, T., Kawajiri, S., Kojima, Y., Takahashi, K. et al., "Study on Maximizing Exergy in Automotive Engines", SAE Technical Paper 2007-01-0257, 2007, <https://doi-org.ezproxy.unibo.it/10.4271/2007-01-0257>
314. Kadota, M. and Yamamoto, K., "Advanced Transient Simulation on Hybrid Vehicle Using Rankine Cycle System", *SAE Int. J. Engines* 1(1):240-247, 2009, <https://doi-org.ezproxy.unibo.it/10.4271/2008-01-0310>.
315. Duparchy A. et al., "Heat recovery for next generation of hybrid vehicles: simulation and design of a Rankine Cycle system", in International Battery. In: Proceedings of hybrid and fuel cell electric vehicle symposium; 2009
316. Horst TA, et al., "Prediction of dynamic Rankine Cycle waste heat recovery performance and fuel saving potential in passenger car applications considering interactions with vehicles' energy management", *Energy Convers Management* 2014;78:438–51
317. Boretti A., "Recovery of exhaust and coolant heat with R245fa organic Rankine cycles in a hybrid passenger car with a naturally aspirated gasoline engine", *Appl Therm. Eng* 2012;36:73–7
318. Boretti AA., "Transient operation of internal combustion engines with Rankine waste heat recovery systems", *Appl Therm Eng* 2012;48:18–23
319. Domingues A, Santos H, Costa M., "Analysis of vehicle exhaust waste heat recovery potential using a Rankine cycle", *Energy* 2013;49:71–85
320. Eitel F., et al., "Potential and Challenges of Fuel Injection Pressure up to 50 MPa for Gasoline Direct Injection Engines", 26th Aachen Colloquium Automobile and Engine Technology 2017
321. Achleitner E., et al. "System Approach for a Vehicle with Gasoline Direct Injection and Particulate Filter for RDE", International Vienna Motor Symposium 2018
322. Prof. Kevin S. Jones, "State of Solid-State Batteries", <https://ceramics.org/wpcontent/uploads/2011/08/energy-ss-batteries-jones.pdf>
323. Ulvestad, A., "A brief review of current lithium ion battery technology and potential solid-state battery technologies", <https://arxiv.org/pdf/1803.04317>
324. Jones, K. S. et al. (2012), "The state of solid-state batteries", *American Ceramic Society Bulletin*, 91(2), pp. 26–31
325. De Cesare, M., Stola, F., Senni, C., Di Monte, A. et al., "Fuel Economy Optimization of Euro 6 Compliant Light Commercial Vehicles Equipped with SCR", SAE Technical Paper 2014-01-1356, 2014, <https://doi.org/10.4271/2014-01-1356>

326. Wang T, "Analysis of recoverable exhaust energy from a light-duty gasoline engine", *Applied Thermal Engineering* 53 (2013) 414-419
327. Galindo, J.; Ruiz Rosales, S.; Dolz Ruiz, V.; Royo Pascual, L.; Haller, R.; Nicolas, B.; Glavatskaya, Y., (2015), "Experimental and thermodynamic analysis of a bottoming Organic Rankine Cycle (ORC) of gasoline engine using swash-plate expander", *Energy Conversion and Management*. 103:519-532. doi:10.1016/j.enconman.2015.06.085

# List of Figures

Figure 1-1 Powertrain design challenges

Figure 1-2 Thesis structural overview

Figure 2-1 Automotive Technology Trends

Figure 2-2 Passenger Cars and Light Duty Vehicle Powertrain market scenario, IHS data base

Figure 2-3 Energy flow and functions in an ICE based vehicle

Figure 2-4 Comparison of global CO<sub>2</sub> regulations for new passenger cars

Figure 2-5 The major automotive regions will be requiring 3-6% reductions CO<sub>2</sub> per year, with Europe requiring the tightest standards

Figure 2-6 Best in Class Vehicle for CO<sub>2</sub> Emission in NEDC Cycle, status at May 2016

Figure 2-7 Divergence between real-world and manufacturers' type-approval CO<sub>2</sub> emission values (NEDC) for various on-road data sources, including average estimates for private cars, company cars, and all data sources

Figure 2-8 Divergence between official and real-world CO<sub>2</sub> emissions for new passenger cars in EU, United States, China, and Japan

Figure 2-9 Divergence between type-approval and Travelcard Nederland BV CO<sub>2</sub> emission values by power train type in build year 2016. Number of vehicles per category presented at the base of each bar

Figure 2-10 Evaluation of a PHEV fuel consumption based on the UN ECE R 101

Figure 2-11 Average CO<sub>2</sub> emission values and vehicle mass of major manufacturer groups in 2016; hypothetical 2021 targets are based on average 2016 mass; limit value curve for 2015 included for reference

Figure 2-12 Mass reduction in a mass-based CO<sub>2</sub> target system (left) and in a footprint-based

Figure 2-13 WTW, PTW and WTP definitions

Figure 2-14 Simplified scheme of the scope of the LCA

Figure 2-15 Criteria pollutants scenario

Figure 2-16 Comparison of NMOG/NMHC+NO<sub>x</sub> emission requirements in China, the European Union, and the United States during 1990–2025 [257]

Figure 2-17 Comparison of PM emission requirements in China, the European Union, and the United States during 1990–2025 [257]

Figure 2-18 Gap between type approval and real emission for NO<sub>x</sub> (g/km) in Diesel and Gasoline cars

Figure 2-19 Vehicle requirements from Market survey to QFD methodology

Figure 2-20 FEV forecast: connected vehicle penetration rate for EU market

Figure 2-21 Levels of automated driving (Source: [117])

Figure 2-22 FEV forecast: automated vehicle sales in EU per SAE level

Figure 2-23 End-user requirement variation in case of Autonomous Driving for two different users: ■ city driving with A-class vehicle; ♦ highway driving with C-Class vehicle (adapted from [117])

Figure 2-24 EU low-carbon economy road-map up to 2050 (source European Commission website)

Figure 2-25 Segmentation of electrical energy storage, adapted from [256]

Figure 3-1 Systems Engineering V-Model to Vehicle Development

Figure 3-2 Scheme of powertrain concept process adapted from [247]

Figure 3-3 Scheme of House of Quality, adapted from [249]

Figure 3-4 Multi-level QFD, from Needs/Wants of End-user to Powertrain Technical Characteristics, covers the first steps of V-Cycle

Figure 3-5 Simulation in the development process

Figure 3-6 The funnel of concept definition: focus on scoring

Figure 3-7 Technology selection process and Pugh Matrix structure

Figure 4-1 Conceptual sizing process of a Powertrain

Figure 4-2 Multilevel QFD: User and Standard requirements deployment to technical features of Vehicle and Powertrain sub-systems

Figure 4-3 Principle scheme and power flows of a hybrid electric powertrain

Figure 4-4 Example of Torque vs. Transmission Speed for an electric motor and combustion engine; Boosting function allows for additional torque for acceleration, especially when starting

Figure 4-5 Block diagram of the specification workflow (SP = specific power, SE = specific energy)

Figure 4-6 Pathway for a de-Fossilized Vehicle

Figure 4-7 Energy requirements for vehicle with gasoline engine in US combined Highway/Driving cycle (source: [www.fueleconomy.org](http://www.fueleconomy.org))

Figure 4-8 Energy flow and functions of an internal combustion engine in a vehicle

Figure 4-9 Strategic zones of improvements for SI Engine

Figure 4-10 Operating points of WLTC and RDE cycles in SI Engine maps

Figure 5-1 Propulsion energy pathways and vehicle powertrain architecture

Figure 5-2 Main Electrified Powertrain Architectures

Figure 5-3 Positioning of electrified vehicles in the space of Electric Range and Degree of Electrification

Figure 5-4 Electric machine positioning in HEVs

Figure 5-5 Powertrain Architectures by operating mode and positioning with energy flow

Figure 6-1 Engine requirements and issues of SI engines



Figure 6-2 Technologies to improve ICE based powertrain

Figure 6-3 Miller cycle: Early and Late Intake Valve Closing (IVC). (Source: FEV 2015)

Figure 6-4 Relationship between maximum BMEP and geometric compression ratio, series gasoline engines MY 2015/16 (Source: [93])

Figure 6-5 Description and comparison of possible implementations for a water injection system

Figure 6-6 External EGR System Layouts: 1. HP-EGR, 2. LP-EGR, 3. Dedicated EGR (Source SwRI)

Figure 6-7 2-Multistage air boosting systems: 2stage turbocharger and electric supercharger in addition to the turbocharger

Figure 6-8 Comparison of engine technologies for  $\lambda=1$  combustion for two different base engines

Figure 6-9 Comparison of the SI and CI combustion features

Figure 6-10 Lean concept operating modes in engine working points (Source: [22])

Figure 6-11 SI and Homogeneous Charge Compression Ignition (HCCI) combustion principles

Figure 6-12 Comparison of SI conventional combustion with lean (misfired) and HCCI combustion

Figure 6-13 Issues with the HCCI combustions

Figure 6-14 Low Temperature Combustion concepts

Figure 6-15 Low Temperature Combustion phases

Figure 6-16 Comparison of CDC and PCCI combustion in 1.3L diesel engine (Smoke [FSN] and CO [%vol] have been multiplied by 100)

Figure 6-17 Effect of EGR on HCCI combustion and emissions [302]

Figure 6-18 Architecture of GDCI engine

Figure 6-19 BSFC at 1500 rpm as a function of load for the three generations of the GDCI and comparison of the Gen.3 engine at 6 bar IMEP with various competitive engines

Figure 6-20 Engine Load-Speed Contour Plots with light naphtha + CR 14 piston configuration: High load line is limited by maximum pressure rise rate (5bar/°crank) and low load line is limited by COV of IMEP.

Figure 6-21 SPCCI basic concept

Figure 6-22 Comparison of output Torque curve for SPCCI engine of Mazda with previous generations

Figure 6-23 BTE comparison of Mazda's engine (SkyActiv-G) with other competitors and the BSFC evolution of new SkyActiv-X vs. SkyActiv-G

Figure 6-24 Comparison of BSFC curve for Mazda's SPCCI engine with conventional engine

Figure 6-25 Pressure and HRR in RCCI with gasoline (left), BTE for Gasoline and E85 compared to CDC (right)

Figure 6-26 NO<sub>x</sub> emission (left) and PM emission (right) in RCCI vs. CDC

Figure 6-27 CO emission (left) and HC emission (right) in RCCI vs. CDC

Figure 6-28 Exhaust gas temperatures in RCCI vs. CDC

Figure 6-29 GPF assembly and filtering scheme inside its channels

Figure 6-30 Overview of the possible positioning of the GPF with the integrated TWC functionality in the exhaust system

Figure 6-31 Comparison of primary energy used and resulting energy at the catalyst in the first 100s for identical emissions level using both heating processes [147]

Figure 6-32 Comparison of Technologies (Ranking and Technology Value Ratio)

Figure 6-33 Value Analysis of GDI engine Technologies [Cost/% CO<sub>2</sub> Saving]

Figure 6-34 Detail of the experimental setup: modified intake manifold (red arrow) and water rail (green arrow) are visible. Water injectors are highlighted with blue circles.

Figure 6-35 Images of water injector position in intake manifold and spray targeting

Figure 6-36 Effect of water injection on combustion phasing

Figure 6-37 Measured IMEP as a function of CA<sub>50%</sub>MFB, for different water quantities; larger markers identify maximum IMEP (and efficiency) points

Figure 6-38 Measured exhaust temperature reduction, depending on water ratio; bigger markers correspond to MBT. A reduction of about 50°C is achieved with 60% of water ratio

Figure 6-39 Comparison of knock intensity at different values of water/fuel mass; bigger markers correspond to MBT

Figure 6-40 Measured Brake Specific Fuel Consumption trends for different water ratio values

Figure 6-41 CFD engine model: geometry with injector locations (a); water and gasoline spray visualization (b); mesh (c)

Figure 6-42 (a) Spray angles definition; (b) Grid size effects on spray patterns and on tip penetration

Figure 6-43 Comparison of simulated and measured droplet diameters at various transverse locations at 15 mm from the tip

Figure 6-44 Timing and duration of each water injection case (a), and comparison of measured pressure vs. simulated in-cylinder pressure (b)

Figure 6-45 Dynamics of liquid water in the ports and runner, focus on case (c) and (f), see

Figure 6-46 Liquid water balance in the ports and runner; percentages refer to the injected water mass

Figure 6-47 Water effect on (a) peak pressure, (b) combustion phasing, and (c) charge cooling before spark, at -20 CAD aTDCf. Spark timing is fixed at SA = -14 CAD aTDCf

Figure 6-48 Effect of spark timing variation; Heat Release Rates at 3 bar injection pressure and water SOI = 360 CAD aTDCf (a). MAPO vs. SA at 3 bar and SOI = 0 CAD and 360 CAD aTDCf (b); in-cylinder pressure curves, with and w/o water, under the same knock margin (c)

Figure 6-49 In average conditions, about 2/3 of the energy stored in the fuel is lost through the exhaust and cooling system

Figure 6-50 Simplified energy balance in vehicle with GDI engine and waste recoverable energy [130]

Figure 6-51 Engine Heat Recovery

Figure 6-52 Description of Fast Warm-up operating modes

Figure 6-53 Scheme of an AHP system

Figure 6-54 Main layouts for the Electric Turbo-compound

Figure 6-55 TEG packaging and principle scheme of Seebeck cell

Figure 6-56 Rankine Cycle system components [130]

Figure 6-57 Energy utilization vs. package space of several heat recovery systems [131]

Figure 6-58 Weight to power ratio for different waste heat recovery technologies on a mobile application [33]

Figure 6-59 Architecture 1- the RC system utilizes the exhaust gas as the only heat source to evaporate the working fluid.

Figure 6-60 Architecture 2 of the RC in which a recuperator is added before the evaporator using the steam from the expander to preheat the working fluid

Figure 6-61 Architecture 3- in the RC system waste heat from the engine coolant is used to preheat the working fluid

Figure 6-62 Proposed RC system integration in electric hybrid powertrain

Figure 6-63 Example of Energy balance in RC System

Figure 6-64 Ideal vs. real RC cycle in TS diagram

Figure 6-65 Three types of working fluid: dry fluid, wet fluid, and isentropic fluid.

Figure 7-1 Expected impact of the Automated Driving on electric and electronic architectures [24]

Figure 7-2 Single Voltage and Single-Battery standard architecture (12V)

Figure 7-3 Dual Voltage architecture (12V/48V), typical of BSG (P0) application

Figure 7-4 Multi-Voltage architecture (12V/48V/HV)

Figure 7-5 Example of dual voltage 48V/12V electric power net architecture

Figure 8-1 Electric Propulsion System Architecture

Figure 8-2 Normalized Torque and Power characteristic vs. speed of an electric motor

Figure 8-3 Example of target specification for an electric vehicle adapted from [178]

Figure 8-4 Classification of electric motor types

Figure 8-5 Simplified cross sections of rotor for different motor types (red and green are the permanent magnets)

Figure 8-6 Comparison of different machine topologies for limited stator current, adapted from [56]

Figure 8-7 Exemplary efficiency maps of different machines with constant power [179]

Figure 8-8 Simplified scheme of 3-phase power Inverter with a DC/DC converter between it and the battery

Figure 8-9 Scheme of an Electric Traction Drive controller

Figure 8-10- Comparison of the cost relative by system power and supply voltage

Figure 8-11 Battery pack breakdown [184]

Figure 8-12 Specific Power vs. Specific Energy for various cell types from

Figure 8-13 Common chemistries of Lithium-ion battery electrodes and their open circuit voltage(top left); bottom tradeoff between voltage potential and capacity (bottom left); schematic of Lithium-ion battery structure (top right); example of standard cell open current voltage (OCV) potential (bottom right), from [134]

Figure 8-14 Mass of raw material used in Li-ion battery of two electrified vehicle from [184]

Figure 8-15 New battery requirements at 20025 [184]

Figure 8-16- Future battery chemistry

Figure 8-17 Specific Energy and Energy Density of new batteries in comparison with current Li-ion [183]

Figure 8-18- Comparative radar chart of new batteries in comparison with current Li-ion [183,322]

Figure 8-19 Battery Cycle Life comparison [134]

Figure 9-1 Pathways towards a de-fossilization of the powertrain: focus on de-fossilized fuels

Figure 9-2 Energy to vehicle powertrains pathways

Figure 9-3 Power-to-Liquids production, principle scheme from [4]

Figure 9-4 PtL production via Fischer-Tropsch pathway (high temperature electrolysis optional) [4]

Figure 9-5 PtL production via methanol pathway (high temperature electrolysis optional) [4]

Figure 9-6 PtL water demand compared to selected biofuels

Figure 9-7 Soot/NOx trade-off for different fuels at engine speed 2280 rpm and IMEP 9.4 bar

Figure 10-1 Scheme of 0-D model used for the powertrain system concept definition and analysis

Figure 10-2 Forces acting on a vehicle on a road grade, see [136]

Figure 10-3 QSS modeling physical causality of HEV components; (V) vehicle, (GB) gearbox, (TS) torque-split link, (M1/M2) EMGs, (P1/P2) power electronics/amplifier, (BT) battery, (C1,C2, CA and CWHR) clutches, (E) ICE, (WHR) Waste Heat Recovery system

Figure 10-4 Dynamic modeling physical causality of HEV components: (DC) Drive cycle, (V) vehicle, (GB) gearbox, (TS) torque-split link, (M) EMGs, (P1/P2) power electronics/amplifier, (BT) battery, (C1, C2, CA, CWHR) clutch, (E) ICE, (WHR ) Waste Heat Recovery, (EMT) electric motor transmission, (PMS) powertrain management system

Figure 10-5 Ford Fusion thermally sensitive simplified transmission model, gear efficiency as a function of lubricant temperature [138]

Figure 10-6 Sample of the experimentally measured DCT efficiency values as functions of input torque and different transmission temperature: (a)  $\omega_{in} = 1000$  rpm,  $T = 30$  °C; (b)  $\omega_{in} = 1000$  rpm,  $T = 70$  °C; (c)  $\omega_{in} = 2000$  rpm,  $T = 30$  °C; (d)  $\omega_{in} = 2000$  rpm,  $T = 70$  °C [139]

Figure 10-7 QSS schematic representation of a friction clutch element block

Figure 10-8 BSFC map of 1.4L Turbo GDI engine (baseline)

Figure 10-9 Linear relation between  $P_{out}$  and  $P_{in}$  at constant speed, adapted from [157]

Figure 10-10 BSFC evaluation for 1.4L Turbo GDI engine (baseline)

Figure 10-11 Correlation of BMEP and BSFC estimated vs. measured  
Figure 10-12 Simulated BSFC of 1.5L Turbo GDI with Miller cycle

Figure 10-12 Simulated BSFC of 1.5L Turbo GDI with Miller cycle

Figure 10-13 Measured BSFC map from [159] of the engine used for demonstrating the approach feasibility; the results are similar to the ones shown in Figure 10-12 obtained from the mode

Figure 10-14 ETD steady-state efficiency and max./min. torque maps

Figure 10-15 Equivalent resistive circuit of a battery, Kirchhoff law-based approach

Figure 10-16 Open Circuit Voltage ( $V_{oc}$ ) of LiFePO<sub>4</sub> Battery Cell at 23 °C [141]

Figure 10-17 Simplified scheme of heat flows between the vehicle and powertrain sub-systems

Figure 10-18 Schematic representation of thermal loads in a typical vehicle cabin

Figure 10-19 Example of thermal management system architecture for a spark ignition engine [143]

Figure 10-20 NEDC Simulation of SUV equipped with 2.0L TGDI engine

Figure 10-21 Results of Fuel mass flow rate simulation in a SUV equipped with 2.0L TGDI engine during NEDC

Figure 10-22 Results of Engine coolant simulation in a SUV equipped with 2.0L TGDI engine during NEDC

Figure 10-23 NEDC Simulation of C-Class BEV (Nissan Leaf) equipped with a 80 kW electric motor and a battery of 30 kWh

Figure 10-24 CO<sub>2</sub> evaluation on NEDC for different technology mix

Figure 10-25 Scheme of RC system utilizes the exhaust gas as heat source and integration with hybrid powertrain

Figure 10-26 Scheme of the Rankine Cycle plant model

Figure 10-27 Scheme of the countercurrent evaporator [133]

Figure 10-28 Validation results of the RC components models, with respect to literature experimental data: a) pump isentropic efficiency, b) evaporator power, c) expander power, d) condenser power

Figure 10-29 Qualitative representation of the RC on T-s diagram in nominal condition (black curve) against the cycles obtained with variation of overheating (red curve) and evaporation temperature (green curve) [133]

Figure 10-30 Scheme of the RC system control [133]

Figure 10-31 Scheme of model to evaluate vehicle Total Cost of Ownership

Figure 10-32 Simplified scheme of LCA scope adapted from [17]

Figure 10-33 Energy flow in different powertrain architectures (dashed line waste heat): (A) ICE vehicle, (B) Battery Electric Vehicle, (C) Range Extender Electric V

Figure 10-34 Workflow scheme for the LCA/WTW evaluation of Vehicle/Powertrain architectures, adapted from [17]

Figure 11-1 Comparison of Gear-shift logics in NEDC for a SUV with 280HP TGDI engine and 8 gears AT: classic approach (left) vs. model based logic (right)

Figure 11-2 Powertrain operation areas

Figure 11-3 Energy flow comparison in a parallel hybrid vehicle in case of charge sustaining

Figure 11-4 Workflow of model based powertrain energy management logic

Figure 11-5 Model based powertrain energy management for a SUV with a hybrid powertrain composed of P4+P2 48V-25/22kW electric drives and a 1.5L TGDI 140kW engine: (Left) strategy disabled, (Right) strategy activated

Figure 11-6 HW architectures of acoustic sensing system

Figure 11-7 Work flow of Turbocharger Speed evaluation via acoustic sensing

Figure 11-8 Performance of turbo speed evaluation via acoustic during a load transient

Figure 11-9 1.3L CR Diesel Engine layout

Figure 11-10 Engine, vehicle and driver model

Figure 11-11 Compressor efficiency map

Figure 11-12 Compressor speed map

Figure 11-13 Design of Experiment (DOE) for model identification

Figure 11-14 Model vs. experimental data, MFB50 and CA10-90

Figure 11-15 Predicted vs measured in cylinder pressure

Figure 11-16 IMEP % error

Figure 11-17 Reference vehicle maneuver

Figure 11-18 Comparison between simulated and measured signals

Figure 11-19 Standard boost pressure controller architecture

Figure 11-20 Turbocharger cascade control scheme

Figure 11-21 Model based control architecture

Figure 11-22 Turbocharger physical model and speed control

Figure 11-23 Overview of the model used in the new boost controller

Figure 11-24 Co-simulation model overview

Figure 11-25 Reference transient maneuver

Figure 11-26 Comparison between fast standard, slow standard and model based boost control performance during reference transient under high altitude condition. Fast standard control performance under low altitude condition is shown to demonstrate limits of fast calibration also in this condition

Figure 11-27 Detail of open loop (nTC FF) and closed loop (nTC FB) turbo speed target contributions given by model based pressure loop control during reference transient, under high altitude condition

Figure 11-28 Detail of open loop (VGTpos FF) and closed loop (VGTpos FB) turbine rack position contributions given by model based control during reference transient, under high altitude condition

Figure 11-29 Comparison between standard and model based boost control in case of compressor speed map dispersion from nominal one. The red ellipse highlights the over-speed of turbocharger with standard boost control

Figure 11-30 Detail of open loop and closed loop turbine rack position contributions given by model based inner loop control in case of compressor speed map dispersion

Figure 11-31 Comparison between standard control and model based control with pressure target increased, during reference transient

Figure 11-32 Comparison between fast standard, slow standard and model based boost control performance during fast transient with gear shifting under high altitude condition

Figure 11-33 Experimental layout

Figure 11-34 Installation of the production accelerometer sensor

Figure 11-35 Positioning of the microphone based sensor

Figure 11-36 In-cylinder pressure signal energy distribution

Figure 11-37 Acoustic emission signal energy distribution

Figure 11-38 Correlation levels between MAPO and Int audio knock index

Figure 11-39 Correlation levels between MAPO and Int audio knock index

Figure 11-40 Main operating regions of engine: 1) non-knocking 2) knocking

Figure 11-41 Results for steady state test runs at 2000 rpm WOT with accelerometer

Figure 11-42 Results for steady state test runs at 2000 rpm WOT with acoustic probe

Figure 11-43 Results for transient state test runs at 2000 rpm WOT for vibration

Figure 11-44 Results for transient state test runs at 2000 rpm WOT for acoustic probe

Figure 11-45 Fuel systems installation on engine employed for CI, PCCI and RCCI tests

Figure 11-46 Scheme of the developed experimental setup for the management of CDC, PCCI and RCCI combustion

Figure 11-47 Torque harmonic components up to harmonic 4

Figure 11-48 Transfer function characteristic of the CI engine-brake system

Figure 11-49 Indicated torque mean value and center of combustion in CDC mode, estimated vs measured

Figure 11-50 Scheme of the closed-loop combustion controller implemented and tested in this study; here, the estimated indicated quantities are the ones determined from the real-time processing of crankshaft speed fluctuations

Figure 11-51 Closed-loop control of SOI<sub>main</sub> and ET<sub>main</sub> while reducing the amount of fuel injected in Pilot from 2.5 to nearly 0 mm<sup>3</sup>/stroke

Figure 11-52 Comparison between ROHR in PCCI and CDC mode; tests run at 2000 rpm and IMEP = 4 bar

Figure 11-53 Normalized CHR curve for an engine cycle run at 2000 rpm and IMEP = 4 bar in PCCI mode

Figure 11-54 Measured vs Estimated Torque fluctuation (amplitude and phase) for the tests run in PCCI mode at 2000 rpm and IMEP = 4 bar (SOI variations)

Figure 11-55 Amplitude (left) and Phase (right) of indicated torque fluctuation, measured vs estimated, for a test run at 2000 rpm, IMEP=4 bar, Gasoline/Diesel = 80/20, RMSE=3.6 Nm and RMSE=0.65°

Figure 11-56 Measured and estimated center of combustion for a test run at 2000 rpm, IMEP = 4 bar, gasoline/diesel target ratio 55/45

Figure 11-57 Estimated vs Measured CA50 and difference for Gasoline/Diesel 70/30 (left) and 80/20 (right)

Figure 11-58 ROHR (top) and NHRD (bottom) compared with accelerometer signal for a test run in RCCI operating mode (2000 rpm, IMEP = 4 bar)

Figure 11-59 Overlap between the signals; SOC and RHOR Peak/Cylinder Pressure identification

Figure 11-60 SOC Estimation (RMSE=1.68°) and ROHR Peak estimation (RMSE=0.89 deg) for different EGR values and SOI<sub>Main</sub> 20° BTDC Diesel/Gasoline 70/30.

Figure 11-61 In-cylinder pressure, in-cylinder pressure first derivative and engine block acceleration (normalized with respect to their maximum) for a test run in RCCI mode at 2000 rpm, BMEP approximately 5 bar and CA50 = 9 deg.

Figure 11-62 (A): Comparison between measured and estimated (from accelerometer signal processing) Pressure Peak location. (B): Correlation between measure CA50 and Pressure Peak location

Figure 11-63 Estimation of Pressure Peak location and SOC during transient test run in CDC mode

Figure 11-64 Application of the algorithm for the detection of accelerometer peaks location, engine cycle run in PCCI mode

Figure 11-65 Comparison between cylinder pressure derivatives and corresponding Combustion Noise for engine cycles run in CDC mode with standard injection pattern (3 injections) and without pre-injections.

Figure 11-66 Correlation between overall noise radiated by the CI engine run in CDC mode (measured using the acoustic sensor) and ROHR peak; test run with standard injection pattern and omitting pre-injections

Figure 11-67 Noise produced by the engine (while activating the noise control algorithm) together with the selected injection sequence



Figure 11-68 RCCI combustion parameters and Comparison between CDC and dual fuel RCCI at 2000 rpm and BMEP = 6 bar, both in term of combustion performance and engine-out emissions

Figure 11-69 Effects of average CA50 variation on Misfire frequency and Peak Pressure Rise Rate; tests run at 2000 rpm and BMEP = 6 bar

Figure 11-70 Scheme of the real-time injection controller implemented in the RCP system.

Figure 11-71 CA50 target sweep, results obtained for cylinder 1; tests run at 2000 rpm and BMEP = 6 bar

Figure 11-72 Frequency of poor combustions or misfires as a function of CA50 variation

Figure 11-73 (Left): Comparison between measured and estimated pressure peak location. Tests run performing a CA50 target sweep from 5 to 10 degrees (closed loop combustion control based on cylinder pressure measurement). The red circles represent poor combustions and misfires discarded by the detections algorithm. (Right): Correlation between measure CA50 and pressure peak location.

Figure 11-74 Peak pressure rise rate (PPRR), measured vs estimated. Tests run performing a CA50 target sweep from 5.5 to 10 degrees (closed loop combustion control based on cylinder pressure measurement).

Figure 11-75 Scheme of the real-time injection controller implemented in the RCP system. All the combustion feedbacks used as inputs for the controller are estimated through a proper processing of engine block acceleration.

Figure 11-76 Closed loop RCCI combustion control based on estimated combustion indexes; test run at 2000 rpm and BMEP equal to 6 bar.

Figure 11-77 Closed loop RCCI combustion control based on estimated combustion indexes; test run at variable engine speed and BMEP approximately equal to 6 bar

Figure 12-1 Traction power as a function of time from 0 - 100 kph requirement for a C-segment vehicle and for a SUV

Figure 12-2 Efficiency map of 48V Electric Drive

Figure 12-3 Simulation comparison of CO<sub>2</sub> emissions in NEDC cycle for baseline engine (left) and its evolution with 4 cylinders (central) and 3 cylinders (right)

Figure 12-4 Comparison of engine warm –up with (right) and without Fast warm-up system (left) for the 3cylinder engine introduced above

Figure 12-5 Preferred hybrid electric powertrain architectures for case study

Figure 12-6 Sensitivity of P4 transmission ratio variation in SUV vehicle with P2+P4 48V 22kW/25kW electric motors and Turbocharger GDI 1.5L engine

Figure 12-7 Operating points of Electric Machines and ICE in a WLTC cycle for C-Segment vehicle equipped with P4+P0 powertrain architecture (SOL5 of Table 12-18); the fuel consumption [L/100km] is shown in comparison with the baseline engine

Figure 12-8 End-user 's breakeven distance compared with baseline for the C-Segment vehicle equipped with P4+P0 powertrain architecture (SOL5 of Table 12-18) and sensitivity analysis vs. fuel price variation in [€]

Figure 12-9 SUV acceleration from 0 to 100 km/h in HEV mode

Figure 12-10 SUV acceleration from 0 to 80 km/h in EV mode

Figure 12-11 SUV Breakeven distance compared with baseline for the SUV equipped with 48V P4+P2 powertrain architecture, SOL6 of Table 12-19

Figure 12-12 Principle scheme of RC integration in electrified powertrain

Figure 12-13 Comparison of RC Power recovered with and without activated FWU system: (left) in only ICE mode and (right) hybrid mode with use of the FWU.

Figure 12-14 Comparison of power recovered with (right) and without (left) RC system in WLTC.

Figure 12-15 Hybrid powertrain behaviour in highway cruising condition with RC system: (left) mechanical actuation, (right) electric actuation

Figure 12-16 Technological paths for a C-Segment vehicle to face NEDC CO<sub>2</sub> requirements, without penalty on engine performance and emissions; the technologies are additive, excluding the path highlighted by the arrows where the adoption of BSG or P2 48 V layout are considered as an alternative

Figure 12-17 Technology paths to reduce NEDC CO<sub>2</sub> in a SUV

Figure 12-18 LCA of C-Segment Vehicle with different Powertrain Architectures

Figure 12-19 LCA of C-Segment Vehicle with different Powertrain Architectures in case

Figure 12-20 Breakeven distance of BEV vs. HEV with e-Fuel in case of C-Segment vehicle

Figure 13-1 Technology options for Powertrain improvement

Figure 13-2 Various renewable fuels with different powertrain architectures

Figure 13-3 Key Powertrain technologies

Figure 13-4 Application fields and Powertrain architectures

# List of Tables

Table 2-1	Classic methodologies to determine future customer needs in the automotive industry from [134]
Table 2-2	Example of design requirements prioritization based on customer profile needs
Table 3-1	Example of space of solutions for powertrain design
Table 4-1	Example of HoQ1
Table 4-2	Measurable Vehicle Requirements and Priority, reported from HoQ1
Table 4-3	Example of House of Quality2.2
Table 4-4	Powertrain Technical Characteristics and relevance from HoQ2.2
Table 4-5	Maximum braking power $P_{braking}$ for different standard cycles
Table 4-6	Energy for vehicle moving and dissipated during braking, considering two different vehicles
Table 5-1	Functions in hybrid electric powertrains
Table 5-2	Selection Matrix of electric hybrid architectures
Table 6-1	Summary of technology impact from literature analysis
Table 6-2	Summary of Technology benefits and drawbacks for GDI engines
Table 6-3	Summary of Advanced Combustion technologies benefits and drawbacks
Table 6-4	Differences between GPF and DPF (Veng: engine displacement)
Table 6-5	Costs of analyzed technologies
Table 6-6	Selection Matrix of Technologies to ICE improvement (2025 timeframe)
Table 6-7	Specification of engine tested with PWI system
Table 6-8	Operating conditions for tests
Table 6-9	Comparison of the electric machines for Electric Turbo-compound
Table 6-10	Selection Matrix of Exhaust Heat Recovery Technologies
Table 6-11	Comparison among the RC architectures
Table 6-12	Comparison of different types of expanders for RC application to passenger vehicles
Table 6-13	Summary of the works about the application of Rankine Cycle to passenger vehicles
Table 6-14	Cost breakdown of RC system
Table 7-1	Vehicle electric load evaluation for conventional and new electric devices
Table 7-2	Powertrain impact of the new electrified devices
Table 7-3	Power –net evolution in the near future

Table 8-1	Key Features of Electric Traction Drives vs. powertrain architectures
Table 8-2	Selection Matrix with comparison of the electric motors for vehicle propulsion
Table 8-3	Comparison between SiC MOSFET and Si IGBT
Table 8-4	Comparison of High Voltage and Low Voltage (48V) Electric Traction Drive Systems
Table 8-5	Energy content for various energy sources by mass and volume [86,182,183]
Table 8-6	Chemical Reaction for a Lithium-Cobalt Oxide Battery (for $0 < x < 1$ )
Table 8-7	Properties and comparison of Li-ion batteries (0 means average performance, + advantage, - disadvantage)
Table 8-8	Comparative analysis of new batteries in comparison with current Li-ion, adapted from [183, 322]
Table 9-1	Energy carrier comparisons, based on research findings presented in this section (0 means average performance, + advantage, - disadvantage)
Table 9-2	PtL production efficiencies “gate-to-gate” (fuel output vs. electric input)
Table 10-1	Features of Model employed in this thesis
Table 10-2	ICE technologies and main parameters
Table 10-3	Vehicle and Powertrain Model validation with different vehicle/powertrain architectures
Table 10-4	Fuel benefit of ICE technologies vs. baseline engine estimated and from literature data
Table 11-1	Comparison of energy management strategies [251]
Table 11-2	Feasibility tests description
Table 11-3	Technical data of the engine used during the experimental tests
Table 11-4	Engine operating points for knock testing
Table 11-5	Combustion chamber resonant modes
Table 11-6	Engine operating conditions investigated during the tests
Table 11-7	Percentage of false positives occurred during the static test using accelerometer (top) and acoustic (bottom) sources.
Table 11-8	Engine technical characteristics for the CI, PCCI and RCCI studies
Table 11-9	Accuracy of torque and CA50 estimation for the tests run in RCCI mode
Table 11-10	Tests run in CDC mode for the analysis of the acoustic emission
Table 12-1	Measurable Powertrain Requirements and Priority from HoQ1 considering a C-segment vehicle and a SUV, considering emission standards at 2025
Table 12-2	Powertrain Technical Characteristics and relevance from HoQ2.2
Table 12-3	Vehicle parameters for powertrain power and torque evaluations
Table 12-4	Power and Torque to achieve maximum Vehicle Speed with slope $p=0$ , slope $p=5\%$

Table 12-5 Energy to move the vehicles  $E_{MOV}$  and dissipated  $E_{braking}$  in the case study, considering different standard cycles

Table 12-6 Energy  $E_{trip}$  needed from the battery to move the vehicle in electric mode and recovered during braking

Table 12-7 Battery capacity and weight

Table 12-8 Power and Torque for Take-off in ICE and Electric mode

Table 12-9 Power and Torque for Time 0→100 km/h

Table 12-10 Power and Torque for Time 0→50 km/h with payload 150kg

Table 12-11 Maximum braking power  $P_{braking}$  for different standard cycles

Table 12-12 Powertrain Maximum Power and Torque to fulfill requirements

Table 12-13 Electric Driveline system Peak Power and Torque to fulfill requirements

Table 12-14 Electric Driveline Continuous Power and Torque to fulfill requirements

Table 12-15 Electric Driveline Power and Torque specifications as a function of Transmission Ratio

Table 12-16 Vehicle and Powertrain features of the vehicles considered as baseline

Table 12-17 Electric Traction Driver requirements vs Architecture solutions

Table 12-18 Summary of C-Segment vehicle performances as a function of the analyzed powertrain architectures

Table 12-19 Summary of SUV performances as function of the analyzed hybrid powertrain architectures

Table 12-20 Features of investigated Vehicle/Powertrain architectures

Table 12-21 Performance requirements of investigated Vehicle/Powertrain architectures

Table 12-22 Powertrain features of ICEs based vehicles and Mild HEVs

Table 12-23 Powertrain features of Full HEVs and P-HEVs

Table 12-24 Powertrain features of FCEV and BEV

Table 12-25 WTT CO<sub>2</sub> footprint for the energy forms considered in this study

Table 12-26 CO<sub>2</sub> footprint for vehicle manufacturing considered in this study